

This file is part of the following work:

**van Gool, Bronwyn (2007) *Effects of blasting on the stability of paste fill stopes at Cannington Mine*. PhD Thesis, James Cook University.**

Access to this file is available from:

<https://doi.org/10.25903/wwvn%2Dzb47>

Copyright © 2007 Bronwyn Susan van Gool

The author has certified to JCU that they have made a reasonable effort to gain permission and acknowledge the owners of any third party copyright material included in this document. If you believe that this is not the case, please email

[researchonline@jcu.edu.au](mailto:researchonline@jcu.edu.au)

**James Cook University**  
**SCHOOL OF ENGINEERING**  
**CIVIL AND ENVIRONMENTAL ENGINEERING**

**Effects of Blasting on the Stability of Paste Fill  
Stopes at Cannington Mine**

Thesis Submitted by

**Bronwyn Susan van Gool BE(Hons)**

In September 2007

for the degree of Doctor of Philosophy

in the School of Engineering

James Cook University

## Statement of Access

I, the undersigned, the author of this thesis, understand that James Cook University will make it available for use within the University Library and, via the Australian Digital Theses network, for use elsewhere.

I understand that, as an unpublished work, a thesis has significant protection under the Copyright act and I do not wish to place any restriction on access to this work.

BS van Gool

10/9/07

Bronwyn van Gool

Date

## Statement of Sources Declaration

I declare that this thesis is my own work and has not been submitted in any form for another degree or diploma at any university or other institution of tertiary education. Information derived from the published or unpublished work of others has been acknowledged in the text and a list of references is given.

B van Gool

10/9/07

Bronwyn van Gool

Date

## **Statement on the Contribution of Others**

This thesis included the following contribution of others:

Grants: This work was supported by a grant from the Australian Research Council (#C00107460)

Supervision: Supervision for this thesis was provided by A/Prof W Karunasena and A/Prof N Sivakugan from James Cook University and Dr M Bloss from BHP Billiton's Cannington Mine

Editorial assistance: Assistance was provided by my supervisors

Project costs: BHP Billiton provided assistance to this work by covering the costs of the field instrumentation tests and the field monitoring conducted at Cannington Mine for this work.

Use of infrastructure external to JCU: Field monitoring and field instrumentation tests were carried out at BHP Billiton's Cannington Mine.

## **Acknowledgements**

I would like to thank the following people:

A/Prof Warna Karunasena and A/Prof Nagaratnam Sivakugan for their support, guidance and assistance in preparing this thesis.

BHP Billiton, Dr Martyn Bloss and Mr Dale Luke for their support.

Mr Warren O'Donnell and Mr Peter Grabau for their assistance with the laboratory tests.

Mr John Heilig for his assistance with the field tests

My family: my husband Shane, Mum and Dad for their endless support and encouragement throughout the years.

## **Abstract**

Paste fill is a cemented backfill used to fill the void left by mining to provide stability to the mine. It consists of tailings mixed with a small percentage of cement and water. As the mining sequence progresses and stopes adjacent to the fill are mined, the fill is subjected to blasting loads, and subsequently exposed. The purpose of this thesis was to study the effects of blast loading on paste fill, and the research consisted of experimental and numerical modelling components and some field work at Cannington mine.

The field work involved monitoring of paste fill during production blasts, in situ tests in paste fill at Cannington mine and laboratory tests on the paste fill samples. Triaxial geophones were installed in stope 4261 at Cannington Mine, which had previously been mined and filled with paste fill. These geophones were used to measure the velocity waveforms produced in the stope during the blasting in two adjacent stopes. The data collected as part of this field work resulted in the estimation of a peak particle velocity at which paste fill begins to fail.

The in situ tests involved monitoring the explosion of 9 blast holes in paste fill. Triaxial geophones were used to measure the velocity profile of each blast. The blast holes were detonated individually in order to obtain separate velocity profiles. The results were used to obtain a relationship between the peak particle velocity and the scaled distance from the blast.

The laboratory tests were conducted to measure the attenuation of a wave as it travels through a column of paste fill. Paste fill was poured into a 2.7 m long column in which 4 accelerometers were installed. A wave was induced in the column by striking the end of a column with a hammer and the particle acceleration was measured. The results were used to show the effect of paste fill mix on the attenuation of a wave.

The finite element method based numerical modelling package, ABAQUS/Explicit, was used to model the behaviour of paste fill due to adjacent blasting in an underground mine. The first numerical model consisted of a single column of explosive detonated in paste fill. The results of this model were validated against the data obtained in the field tests. Once validated, the model was run for different mixes of paste fill to observe the effect of cement and solids content of the paste fill on its behaviour. A model of a single column of explosive in rock was also developed and validated using the same method. The model was then extended to include a single column of explosive detonated in rock adjacent to a paste fill stope. This model was run for a variety of blasting conditions to observe the changes in paste fill behaviour due to different blasting conditions. These different blasting conditions included varying distances between the

explosive column and the rock/paste fill interface and various positions of the explosive column in relation to the paste fill stope. The model was finally extended to include a row of explosive columns parallel to the face of a paste fill stope. This model was run for a variety of blasting patterns and delay intervals to determine their effect on damage to paste fill. The model results showed that the peak particle velocity and therefore the damage to the paste fill reduced for increased cement contents of the fill. Similar results were observed for increased solids content, but to a lesser extent. The model results also indicated that the order of detonation and the delay time between the detonation of blast holes has little effect on the damage to the paste fill.



# Table of Contents

## *Title Page*

<i>Statement of Access</i>	<i>i</i>
<i>Statement of Sources Declaration</i>	<i>ii</i>
<i>Statement on the Contribution of Others</i>	<i>iii</i>
<i>Acknowledgements</i>	<i>iv</i>
<i>Abstract</i>	<i>v</i>
<i>Table of Contents</i>	<i>vii</i>
<i>List of Tables</i>	<i>xii</i>
<i>List of Figures</i>	<i>xiii</i>
<i>Nomenclature</i>	<i>xvi</i>
<b>1. Introduction</b>	<b>1</b>
<b>1.1. General</b>	<b>1</b>
<b>1.2. Problem Statement</b>	<b>1</b>
<b>1.3. Objectives</b>	<b>2</b>
<b>1.4. Relevance of Research</b>	<b>2</b>
<b>1.5. Thesis Overview</b>	<b>2</b>
<b>2. Literature Review</b>	<b>4</b>
<b>2.1. Blasting</b>	<b>4</b>
<b>2.2. Wave Propagation</b>	<b>4</b>
2.2.1. Types of Waves	4
2.2.2. Behaviour of Waves at Boundaries	6
<b>2.3. Peak Particle Velocity</b>	<b>7</b>
2.3.1. The Charge-Weight Scaling Law	8
2.3.2. Prediction of Peak Particle Velocity for a Column Explosion	8
2.3.3. Prediction of Damage using Peak Particle Velocity	10
<b>2.4. Cemented Backfill in Underground Mining</b>	<b>12</b>
2.4.1. Commonly Used Backfills	12
2.4.2. Paste Fill	12
2.4.3. Static Stability of Paste Fill	13
<b>2.5. Modelling an Explosive Blast</b>	<b>15</b>
2.5.1. The Concept of an “Equivalent Cavity”	15
2.5.2. Modelling a Cylindrical Charge	16
2.5.3. Applying the Blast Load	17
2.5.3.1. Applying a Blast Load to the Walls of an “Equivalent Cavity”	18
2.5.3.2. Applying a Blast Load to the Walls of the Blast Hole	19
2.5.3.3. Modelling the Chemical Reaction in a Blast Hole	20
2.5.4. Modelling Multiple Blast Holes	21
2.5.5. Modelling the Effects of a Blast on Cemented Backfill	21

2.6.	<b>Summary</b>	<b>23</b>
3.	<b><i>Monitoring of Stope 4261 During Nearby Blasting</i></b>	<b>25</b>
3.1.	<b>General</b>	<b>25</b>
3.2.	<b>Monitoring Equipment Used</b>	<b>25</b>
3.3.	<b>Location of Monitoring Equipment</b>	<b>26</b>
3.4.	<b>Type of Explosive Used in the Production Blasts</b>	<b>26</b>
3.5.	<b>Events Monitored</b>	<b>27</b>
3.5.1.	Stope 4760	27
3.5.2.	Stope 4763	30
3.6.	<b>Collected Data</b>	<b>31</b>
3.6.1.	Stope 4760	31
3.6.2.	Stope 4763	31
3.6.3.	Volume of Stopes	31
3.7.	<b>Analysis of Data</b>	<b>31</b>
3.7.1.	Volume of Failed Paste Fill	31
3.7.2.	Peak Particle Velocities Measured During Monitoring	34
3.7.2.1.	Stope 4760	34
3.7.2.2.	Stope 4763	44
3.7.2.3.	Summary	45
3.7.3.	Wave Transmission Across the Rock/Paste Fill Interface	45
3.7.4.	Estimation of the Peak Particle Velocity at which Failure of Paste Fill Occurs	47
3.7.5.	Fourier Analysis	50
3.7.6.	Damage to Walls of Tunnel in Paste Fill	51
3.8.	<b>Summary</b>	<b>51</b>
4.	<b><i>Field Instrumentation Tests</i></b>	<b>53</b>
4.1.	<b>Introduction</b>	<b>53</b>
4.2.	<b>Location of the Blast Holes and Geophones</b>	<b>53</b>
4.3.	<b>Type of Explosive Used in the Test</b>	<b>55</b>
4.4.	<b>Test Methodology</b>	<b>56</b>
4.5.	<b>Collected Data</b>	<b>57</b>
4.6.	<b>Analysis of Results</b>	<b>58</b>
4.6.1.	Calculation of Peak Particle Velocity	58
4.6.2.	Equation for Predicting Peak Particle Velocity in Paste Fill	58
4.6.3.	Effect of the Paste Fill/Rock Interface	62
4.6.4.	Predicting ppv in Paste Fill from Blast in Adjacent Rock	65
4.6.5.	Damage to Paste Fill During Field Instrumentation Tests	67
4.6.6.	Fourier Analysis of Data	68
4.7.	<b>Summary</b>	<b>68</b>
5.	<b><i>The Study of Blast Attenuation in Paste Fill using Laboratory Tests</i></b>	<b>71</b>
5.1.	<b>General</b>	<b>71</b>
5.2.	<b>Seismic Attenuation and Dispersion</b>	<b>71</b>

<b>5.3.</b>	<b>Apparatus</b>	<b>73</b>
5.3.1.	General	73
5.3.2.	Accelerometers	74
5.3.3.	Pipe	76
5.3.4.	Measuring Device	77
5.3.5.	Hammer	77
<b>5.4.</b>	<b>Test Methodology</b>	<b>78</b>
5.4.1.	Preparation of Paste fill	78
5.4.2.	Pouring of Columns	79
5.4.3.	Test Procedure	80
<b>5.5.</b>	<b>Calibration of the Accelerometers</b>	<b>82</b>
5.5.1.	Method of Calibration	82
5.5.2.	Calibration Factors	84
<b>5.6.</b>	<b>Analysis of Results</b>	<b>84</b>
5.6.1.	Reproducibility of Results	84
5.6.2.	Transmission of a Wave through a Column of Paste Fill	85
5.6.3.	Effect of Curing Age on Attenuation	88
5.6.4.	Effect of Paste Fill Mix on Attenuation	88
<b>5.7.</b>	<b>Summary</b>	<b>90</b>
<b>6.</b>	<b><i>Applying a Blast Load</i></b>	<b>92</b>
<b>6.1.</b>	<b>Introduction</b>	<b>92</b>
<b>6.2.</b>	<b>What Happens When an Explosive Detonates?</b>	<b>92</b>
<b>6.3.</b>	<b>Measuring Blast Damage</b>	<b>94</b>
<b>6.4.</b>	<b>Prediction of Peak Particle Velocity</b>	<b>94</b>
<b>6.5.</b>	<b>How Can Blast Loads be Applied in ABAQUS/Explicit</b>	<b>96</b>
6.5.1.	Applying a Time Varying Pressure to the Walls of the Blast Hole	96
6.5.2.	Applying a Time Varying Pressure to the Walls of an “Equivalent Cavity”	96
6.5.3.	Incident Wave Field	97
6.5.4.	Modelling the Chemical Reaction using the Jones-Wilkens-Lee Equation of State Material Model	97
6.5.5.	Discussion of Blast Loading Methods	98
<b>6.6.</b>	<b>Concept of an “Equivalent Cavity”</b>	<b>98</b>
<b>6.7.</b>	<b>Explosives Being Modelled</b>	<b>100</b>
<b>6.8.</b>	<b>Form of the Loading Function</b>	<b>101</b>
6.8.1.	Calculating the Initial Peak Pressure	107
<b>6.9.</b>	<b>Validation of the Loading Function</b>	<b>108</b>
<b>6.10.</b>	<b>Variables Which Affect Blast Loading</b>	<b>111</b>
6.10.1.	Types of Explosives	111
6.10.2.	Rock Properties	112
6.10.3.	Mining Methods	112
6.10.4.	Blasting Pattern	113
6.10.5.	Initiation Patterns	116
6.10.6.	Delay Intervals	116

6.10.7.	Blast Size	117
6.10.8.	Velocity of Detonation	117
<b>6.11.</b>	<b>Summary</b>	<b>117</b>
<b>7.</b>	<b><i>Development of the Finite Element Model</i></b>	<b>118</b>
<b>7.1.</b>	<b>Finite Element Analysis</b>	<b>118</b>
7.1.1.	General	118
7.1.2.	ABAQUS	118
7.1.2.1.	ABAQUS/Standard	119
7.1.2.2.	ABAQUS/Explicit	120
7.1.2.3.	ABAQUS/CAE	121
7.1.2.4.	ABAQUS/Viewer	122
<b>7.2.</b>	<b>The ABAQUS input file</b>	<b>122</b>
7.2.1.	Model Data	122
7.2.2.	History Data	123
7.2.3.	Data Definitions	124
<b>7.3.</b>	<b>Problem Definition</b>	<b>124</b>
7.3.1.	General	124
7.3.2.	Stage 1 Model: Single Column of Explosive in Paste Fill	125
7.3.3.	Stage 2 Model: Single Column of Explosive in Rock	128
7.3.4.	Stage 3 Model: Columns of Explosive in Rock Adjacent to Paste Fill	130
<b>7.4.</b>	<b>Simplifications and Assumptions</b>	<b>135</b>
<b>7.5.</b>	<b>Model Parameters</b>	<b>135</b>
7.5.1.	Material Properties	135
7.5.1.1.	Constitutive Models	135
7.5.1.2.	Mohr Coulomb Material Model	136
7.5.1.3.	Material Models to apply in ABAQUS/Explicit	137
7.5.1.4.	Drucker Prager Plasticity Model	137
7.5.1.5.	Matching Mohr-Coulomb Parameters to the Drucker-Prager Model	139
7.5.1.6.	Damping	140
7.5.2.	Interface between Paste Fill and Rock	142
7.5.3.	Boundaries	143
7.5.4.	Element Definitions	143
7.5.4.1.	Element Types	143
7.5.4.2.	Element types used in Models	146
7.5.5.	Loading of Model	147
7.5.6.	Outputs	147
<b>8.</b>	<b><i>Numerical Model Results and Discussion</i></b>	<b>149</b>
<b>8.1.</b>	<b>Stage 1 Model: Single Column of Explosive in Paste Fill</b>	<b>149</b>
8.1.1.	Stage 1 Model Scenarios	149
8.1.2.	Stage 1 Model Results and Discussion	150
8.1.2.1.	Comparison of Model Results and Field Data	150
8.1.2.2.	Damage to Paste Fill	151
8.1.2.3.	Effect of Cement Content on Peak Particle Velocity	151
8.1.2.4.	Effect of Solids Content on Peak Particle Velocity	154
8.1.2.5.	Comparison between Effect of Cement and Solids Content	154

<b>8.2. Stage 2 Model: Single Column of Explosive in Rock</b>	<b>156</b>
8.2.1. Scenarios Modelled	156
8.2.2. Results and Discussion	157
8.2.2.1. Comparison of Results against Peak Particle Velocity Prediction Equation	157
8.2.2.2. Effect of Rock Parameters on Peak Particle Velocity	158
<b>8.3. Stage 3 Model: Column of Explosive in Rock Adjacent to Paste Fill</b>	<b>159</b>
8.3.1. General	159
8.3.2. Scenario 1: Single Borehole Detonated Adjacent to the Centreline of a Paste Fill Stope	159
8.3.2.1. Effect of Rock/Paste Fill Interface	160
8.3.2.2. Internal Reflections Within Paste Fill	165
8.3.2.3. Effect of Distance of Borehole from Paste Fill on Peak Particle Velocity	172
8.3.2.4. Effect of Borehole Diameter on Peak Particle Velocity	174
8.3.3. Scenario 2: Single Borehole Offset from the Centreline of the Paste Fill Stope	176
8.3.3.1. Effect of Location of Borehole Relative to Paste Fill	176
8.3.4. Scenario 3: Detonation of a Row of Boreholes Parallel to a Face of the Paste Fill Stope	178
8.3.4.1. Comparison of Single Borehole Versus Multiple Boreholes	179
8.3.4.2. Comparison of Detonation Patterns	181
8.3.4.3. Effect of Delay Time on Peak Particle Velocity	183
<b>8.4. Summary</b>	<b>184</b>
8.4.1. Stage 1 Model	184
8.4.2. Stage 2 Model	185
8.4.3. Stage 3 Model	185
<b>9. Summary, Conclusions and Recommendation for Future Work</b>	<b>187</b>
<b>9.1. Summary and Conclusions</b>	<b>187</b>
<b>9.2. Recommendations for Future Work</b>	<b>190</b>
<b>10. References</b>	<b>191</b>
<i>Appendix A - Plan of Stopes in Monitoring Program</i>	<i>196</i>
<i>Appendix B - Stope 4760</i>	<i>197</i>
<i>Appendix C - Stope 4763</i>	<i>198</i>
<i>Appendix D – Field Instrumentation Tests</i>	<i>199</i>
<i>Appendix E – Waveforms Recorded in Laboratory Tests</i>	<i>200</i>
<i>Appendix F – Electronic Copy of Finite Element Model Input Files</i>	<i>201</i>

## List of Tables

<i>Table 2.1 Peak Particle Velocity – Damage Correlation (Persson et al. 1994)</i> .....	11
<i>Table 3.1 Properties of Powerbulk VE</i> .....	27
<i>Table 3.2 Monitoring Data Collected During Blasting of Stope 4760</i> .....	29
<i>Table 3.3 Details of Stope 4763 Blast Event Monitored</i> .....	30
<i>Table 3.4 Failure Observed During Blasting of Secondary Stopes</i> .....	34
<i>Table 3.5 Results for Blast 904064</i> .....	37
<i>Table 3.6 Blast 904068 Delay Times</i> .....	40
<i>Table 3.7 Results for Blast 904068</i> .....	41
<i>Table 3.8 Delay Times for Blast 904072</i> .....	42
<i>Table 3.9 Results for Blast 904072</i> .....	44
<i>Table 3.10 Transmission of Blast Wave Across Rock/Paste Fill Interface</i> .....	46
<i>Table 3.11 Characteristic Impedance of Rock and Paste Fill at Cannington Mine</i> .....	47
<i>Table 3.12 Peak Particle Velocity at which Failure Occurs in Paste Fill</i> .....	49
<i>Table 4.1 Distance Between Explosives and Geophones</i> .....	55
<i>Table 4.2 Properties of Explosive Used in Field Instrumentation Tests</i> .....	55
<i>Table 4.3 Effect of Paste Fill/Rock Interface on Transmission of p-Wave</i> .....	64
<i>Table 4.4 Results of Fourier Analysis</i> .....	69
<i>Table 5.1 Paste Fill Mixes used in Laboratory Tests</i> .....	79
<i>Table 5.2 Calibration for Reference Accelerometer</i> .....	83
<i>Table 5.3 Calibration of Accelerometers</i> .....	84
<i>Table 5.4 Quality Factors for Paste Fill Obtained in Laboratory Test</i> .....	87
<i>Table 6.1 Blast Parameters for Stope 4760</i> .....	95
<i>Table 6.2 Advantages and Disadvantages of Methods of Applying a Blast Load</i> .....	99
<i>Table 6.3 Loading Functions found in Literature</i> .....	102
<i>Table 7.1 Paste Fill Mixes used in the Stage 1 Model</i> .....	127
<i>Table 7.2 Material Properties used for Paste Fill</i> .....	127
<i>Table 7.3 Rock Types Used in the Stage 2 Model</i> .....	129
<i>Table 7.4 Material Properties used for Rock</i> .....	130
<i>Table 8.1 Expected Failure of Paste Fill from Single Column of Explosive in Nearby Rock</i> .....	176
<i>Table 8.2 Expected Failure of Paste Fill from Multiple Boreholes in 2.5 m from Paste Fill</i> .....	180

## List of Figures

<i>Figure 2.1 – Reflection of a p-wave at a Free Boundary</i>	6
<i>Figure 2.2 – Reflection and Refraction of a p-Wave at a Boundary Between Two Media</i>	7
<i>Figure 2.3 – Geometry of a Blast Hole Loaded With Explosives</i>	9
<i>Figure 2.4 – Typical Extraction Sequence Around a Backfilled Stope</i>	13
<i>Figure 3.1 – Layout of Stopes Used in Monitoring Program</i>	26
<i>Figure 3.2 – Location of Geophones G3 to G6</i>	27
<i>Figure 3.3 – Location of Geophone G7</i>	28
<i>Figure 3.4 – Winze Blast Hole Layout for Stope 4760</i>	29
<i>Figure 3.5 – Failure at Intersection of Stope 4261 and 4760</i>	32
<i>Figure 3.6 – Failure at Intersection of Stope 4261 and 4763</i>	33
<i>Figure 3.7 – Location of Blast 904064 Boreholes</i>	35
<i>Figure 3.8 – Velocity Profiles Measured During Blast 904064</i>	36
<i>Figure 3.9 – Location of Blast 904068 Boreholes</i>	38
<i>Figure 3.10 – Velocity Profiles Measured During Blast 904068</i>	39
<i>Figure 3.11 – Location of Blast 904072 Boreholes</i>	42
<i>Figure 3.12 – Velocity Profiles Measured During Blast 904072</i>	43
<i>Figure 3.13 – Frequency Spectrum for Blast 904064, Wave Arrival 1 Recorded at Geophone G3 in Rock</i>	51
<i>Figure 4.1 – Plan View of Blast Holes and Geophones within Stope 4261</i>	54
<i>Figure 4.2 – Waveforms Recorded at Geophone G1 for Blast Cann#1 and the Velocity Magnitude for this Blast</i>	59
<i>Figure 4.3 – Peak Particle Velocity in Paste Fill</i>	61
<i>Figure 4.4 – Equivalent Distances for Blast in Rock Adjacent to Paste Fill</i>	66
<i>Figure 5.1 – Accelerometer Connected to Circuit Board</i>	74
<i>Figure 5.2 – Accelerometer Installed in Casing Prior to Pouring Resin</i>	75
<i>Figure 5.3 – Accelerometer Installed in Pipe Joiner</i>	76
<i>Figure 5.4 – Apparatus for Preliminary Test</i>	77
<i>Figure 5.5 – Apparatus for the Full Test Stage</i>	77
<i>Figure 5.6 – Hammer used to Initiate Waves in Laboratory Tests</i>	78
<i>Figure 5.7 – Paste Fill Being Mixed in the Cement Mixer as Cement is Added</i>	79
<i>Figure 5.8 – Paste Fill Column Filled to the First Accelerometer</i>	80
<i>Figure 5.9 – Finished Paste Fill Column</i>	81
<i>Figure 5.10 – Columns Ready For Testing</i>	81
<i>Figure 5.11 – Apparatus used to Calibrate Accelerometers</i>	83
<i>Figure 5.12 – Waveforms Recorded for Column 6 After 14 Days Curing Time</i>	86
<i>Figure 5.13 – Comparison of Waveforms Recorded for Column 6 After 14 Days Curing Time</i>	87
<i>Figure 5.14 – Frequency Spectrum for Waveforms Recorded for Column 6 After 14 Days Curing Time</i>	87
<i>Figure 5.15 – Comparison of Waveforms Recorded for Different Curing Times</i>	89
<i>Figure 5.16 – Comparison of Waveforms Recorded for Different Cement Contents</i>	91
<i>Figure 6.1 – Fragmentation Zones Around a Blast Hole in Rock</i>	93
<i>Figure 6.2 – Unit Loading Amplitude Applied to ABAQUS/Explicit Models</i>	106
<i>Figure 6.3 – ppv Versus Pressure for 2 m Long Explosive Column in Rock</i>	109
<i>Figure 6.4 – Validation of the Stage 1 Model - Cartridge of Explosive in Paste Fill</i>	110
<i>Figure 6.5 – Validation of Stage 2 Model - Explosive Column in Rock</i>	110

<i>Figure 6.6 – Blasting Methods Used in Underground Metal Mines</i>	114
<i>Figure 6.7 – Ring Blasting (Sen, 1995)</i>	115
<i>Figure 6.8 – Vertical Crater Retreat Blasting (Sen, 1995)</i>	116
<i>Figure 7.1 – ABAQUS Modelling Process</i>	119
<i>Figure 7.2 – Scenario Represented in Stage 1 Models (Not to Scale)</i>	125
<i>Figure 7.3 – Finite Element Mesh for the Stage 1 Model</i>	126
<i>Figure 7.4 – Scenario Represented in Stage 2 Model (Not to Scale)</i>	128
<i>Figure 7.5 – Finite Element Mesh for Stage 2 Model</i>	129
<i>Figure 7.6 – Scenario Represented in the Stage 3 Model</i>	132
<i>Figure 7.7 – Scenario Represented by Stage 3 Model (Plan View)</i>	133
<i>Figure 7.8 – Finite Element Mesh for Stage 3 Model</i>	134
<i>Figure 7.9 – Mohr Coulomb Stress Conditions at Failure (Craig 1997)</i>	136
<i>Figure 7.10 – Drucker-Prager Yield Surface in the Meridional Plane</i>	138
<i>Figure 7.11 – Typical Stress-Strain Curve for a Ductile Material</i>	139
<i>Figure 7.12 – Comparison of Mohr-Coulomb and Drucker-Prager Models in the Deviatoric Plane (ABAQUS 2003)</i>	139
<i>Figure 7.13 – Typical Axisymmetric Element (ABAQUS 2003)</i>	144
<i>Figure 7.14 – Node Numbering on 4 node Axisymmetric Element (ABAQUS 2003)</i>	144
<i>Figure 7.15 – Node Numbering on 4 node Plane Strain Element (ABAQUS 2003)</i>	145
<i>Figure 7.16 – Node Numbering on 4 Infinite Element (ABAQUS 2003)</i>	146
<i>Figure 8.1 – Stage 1 Model Results and Field Instrumentation Test Data</i>	150
<i>Figure 8.2 – Stress in the Region of the Blast Load</i>	152
<i>Figure 8.3 – Stage 1 Model Results for Paste Fill with 76% Solids Content</i>	152
<i>Figure 8.4 – Stage 1 Model Results for Paste Fill with 78% Solids Content</i>	153
<i>Figure 8.5 – Stage 1 Model Results for Paste Fill with 80% Solids Content</i>	153
<i>Figure 8.6 – Stage 1 Model Results for Paste Fill with 6% Cement Content</i>	154
<i>Figure 8.7 – Stage 1 Model Results for Paste Fill with 4% Cement Content</i>	155
<i>Figure 8.8 – Stage 1 Model Results for Paste Fill with 2% Cement Content</i>	156
<i>Figure 8.9 – Stage 1 Model Results for Different Paste Fill Mixes</i>	156
<i>Figure 8.10 – Stage 2 Model Results Versus Peak Particle Velocity Predictions</i>	158
<i>Figure 8.11 – Stage 2 Model Peak Particle Velocities for Different Rock Types</i>	159
<i>Figure 8.12 – Particle Velocity 0.005 s After Detonation</i>	161
<i>Figure 8.13 – Particle Velocity 0.020 s After Detonation</i>	162
<i>Figure 8.14 – Particle Velocity 0.045 s After Detonation</i>	163
<i>Figure 8.15 – Particle Velocity 0.090 s After Detonation</i>	164
<i>Figure 8.16 – Particle Velocity 0.049 s After Detonation</i>	166
<i>Figure 8.17 – Particle Velocity 0.098 s After Detonation</i>	167
<i>Figure 8.18 – Particle Velocity 0.147 s After Detonation</i>	168
<i>Figure 8.19 – Particle Velocity 0.196 s After Detonation</i>	169
<i>Figure 8.20 – Particle Velocity 0.245 s After Detonation</i>	170
<i>Figure 8.21 – Particle Velocity 0.294 s After Detonation</i>	171
<i>Figure 8.22 – Particle Velocity in the x-Direction</i>	172
<i>Figure 8.23 – Velocity in the y-Direction</i>	172
<i>Figure 8.24 – Centreline of Paste Fill Along Which the Results Have Been Analysed</i>	173
<i>Figure 8.25 – Comparison of results from a Single Borehole at Various Locations Relative to the Paste Fill</i>	174
<i>Figure 8.26 – Location of 76 mm Diameter Blast Holes, Blast 904064</i>	175
<i>Figure 8.27 – Comparison of Results from a 89 mm and 76 mm Diameter Blast Holes</i>	175
<i>Figure 8.28 – Stage 3 Model, Scenario 2</i>	177



<i>Figure 8.29 – Line Along which Results were Analysed for Stage 3 Model, Scenario 2</i>	177
<i>Figure 8.30 – Peak Particle Velocities Along Paste Fill Face Due to a Single Column of Explosive</i>	178
<i>Figure 8.31 – Borehole Numbering for Stage 3 Model, Scenario 3</i>	179
<i>Figure 8.32 – ppv Predicted along the Centreline of a Paste Fill Stope</i>	180
<i>Figure 8.33 – ppv Predicted Along the Face of a Paste Fill Stope</i>	181
<i>Figure 8.34 – ppv Predicted Along the Centreline of a Paste Fill Stope for Different Detonation Patterns</i>	182
<i>Figure 8.35 – ppv Predicted Along the Face of a Paste Fill Stope for Different Detonation Patterns</i>	182
<i>Figure 8.36 – ppv Predicted Along the Centreline of a Paste Fill Stope for Different Delay Times</i>	183
<i>Figure 8.37 – ppv Predicted Along the Face of a Paste Fill Stope for Different Delay Times</i>	184

## Nomenclature

a	Attenuation coefficient
$b_1$	Damping coefficient
$b_2$	Damping coefficient
c	Wave velocity
$c_p$	Velocity of a p-wave
$c_s$	Velocity of a s-wave
d	Cohesion
$e_{mo}$	Initial energy per mass unit
f	Frequency
g	A deviatoric stress measure
h	Height
i	The increment number
j	The third invariant of deviatoric stress
k	A site specific constant for the charge-weight scaling law
$l_e$	An element characteristic length
m	The equivalent pressure stress
n	An integer
p	Pressure
$p_{bv1}$	Bulk viscosity pressure in the form of damping of the “ringing” in the highest element frequency
$p_{bv2}$	Bulk viscosity pressure in the form of damping in solid continuum elements
ppv	Peak particle velocity
q	The Mises equivalent stress
r	Pulse travel distance
$s_1$	The gain of the reference accelerometer
$s_2$	The gain of the accelerometer being calibrated
t	Time

$u^N$	A degree of freedom (displacement or rotation component)
$\dot{u}$	Velocity
$\ddot{u}$	Acceleration
$v$	The magnitude of the resultant particle velocity
$v_{\text{radial}}$	The particle velocity in the radial direction
$v_{\text{transverse}}$	The particle velocity in the transverse direction
$v_{\text{vertical}}$	The particle velocity in the vertical direction
$w$	Strike length
$A$	Amplitude
$B$	Material constant for the JWL equation of state
$C$	Constant, experimentally estimated to be $0.53 \pm 0.04$
$D$	Distance between hanging wall and foot wall
$E$	Young's Modulus
$F$	The discrete Fourier transform output
$G$	Yield criteria
$H$	The height of the explosive in the blast hole
$I^J$	The internal force vector
$J$	Material constant for the JWL equation of state
$K$	The ratio of the yield stress in triaxial tension to the yield stress in triaxial compression
$L$	Linear charge density
$M^{NJ}$	The mass matrix
$N$	The total number of discrete samples taken in the time domain
$P^J$	The applied load vector
$Q$	Quality factor
$R$	Distance
$S1, S2$ and $S3$	The principal stresses on the deviatoric plane
$T$	Total sampling time

$U_1$	the output of the reference accelerometer
$U_2$	The output of the accelerometer being calibrated
$W$	Weight
$\alpha$	Site specific constant for the charge-weight scaling law
$\beta$	Site specific constant for the charge-weight scaling law
$\chi_R$	Factor for mass proportional damping
$\delta_R$	Factor for stiffness proportional damping
$\varepsilon$	Strain
$\dot{\varepsilon}_{vol}$	Volumetric strain
$\phi$	Friction angle
$\gamma$	Unit weight
$\eta$	The slope of the linear yield surface in the p-t stress plane commonly referred to as the friction angle of the material
$\varphi$	Decay factor
$\kappa$	Geometric attenuation exponent
$\lambda$	Lame's Constants
$\mu$	Lame's Constants
$\nu$	Poisson's Ratio
$\theta$	Angle of failure plane from horizontal = $45+\phi/2$
$\rho$	Density
$\sigma$	Stress
$\tau_f$	Shear strength
$\omega$	The angle for the column version of the charge-weight scaling law (see Figure 2.3)
$\omega$	Natural frequency
$\xi$	Fraction of critical damping
$\psi$	The dilation angle in the p-t plane
$\Phi$	Factor of Safety

- $\Theta$  Material constant for the JWL equation of state
- $\Omega$  The pulse rise time
- $\Psi_1$  Material constant for the JWL equation of state
- $\Psi_2$  Material constant for the JWL equation of state

# 1. Introduction

## 1.1. General

Cannington Mine is an underground lead-silver-zinc mine that is located in north-west Queensland, approximately 220 kilometres south-east of Mount Isa. The mine, which is the world's largest single mine producer of silver, is owned and operated by BHP Minerals. Cannington is the first mine in Australia to use the open stoping mining method with post-placed paste fill. The ore is mined in sections, referred to as 'stopes'. Once the ore from a stope is removed, the stope is filled with paste fill to give support to the mine. Paste fill consists of mine tailings with a typical effective grain size of 5  $\mu\text{m}$  mixed with a small percentage of cement binder.

## 1.2. Problem Statement

Paste fill is used in mines to fill the voids left by mining and to provide stability during the remaining mining sequence. As the mining sequence progresses, and stopes adjacent to the fill are mined, the fill is subjected to blasting loads, and subsequently exposed. This may happen several times during the mining sequence as additional stopes are mined in the area. During this time, the fill must remain stable as it provides local and regional support to the mine. If the fill fails and falls into the void left by the mining, the processing cost increases, as additional material must be processed, with no additional materials produced. The stability of the fill is also a serious safety issue for the mine as failure of the fill could potentially result in the loss of life.

Cement is added to the paste to increase the strength of the material, with strength increasing as cement content increases. However, the cost of adding cement to the fill is high, with filling of the stopes costing 20 % of the entire mining operations. If the cement content could be reduced by 1 %, it would result in a saving of approximately one million dollars per year. It is therefore necessary to optimize the cement content of the paste, ensuring that adequate cement is added to maintain stability while minimizing the cost.

As a result of research on the static stability of cement-based fills, the cement content of such fills has been reduced. However, as the cement content is reduced, a concern arises over the stability of the fill during dynamic events it is exposed to such as blasting. More research is necessary into the dynamic aspects of cemented backfill to ensure that these fills will remain stable. One of the reasons research may be limited is due to the complexity of the mechanics of transfer of explosive energy to rock and to paste, and the resulting stress wave field.

Several numerical models of blasting have been created, however the majority of these models consist of a single blast hole located in a uniform mass of rock. A few researches have modelled the effects of an explosive blast on cemented backfill (refer to section 2.5.5), however, these studies have not considered the effects of multiple blasts on the backfill. During a production blast in a mine, multiple blast holes are detonated with small delays between detonations. The blast wave from each blast hole is transmitted to the backfill material, and due to the effects of reflection of the waves within the backfill, these waves can combine to produce larger peak particle velocities within the backfill than would be created by a single blast hole. Therefore, the effects of multiple blast holes must be considered when predicting the effect of blasting on nearby backfill material.

### ***1.3. Objectives***

The objectives of this thesis are to:

- Develop a computer-aided model to predict dynamic response of paste fill due to blast loading using commercially available finite element software packages;
- Measure blast response in paste fill and verify developed computer models using these measurements; and
- Estimate the blast damage using predicted response for different scenarios and assess the stability of paste fill stopes during and after blasting

### ***1.4. Relevance of Research***

The cost of backfilling the mine is the single greatest expense at Cannington Mine, contributing to 20 % of the total costs. As the cost of adding cement to the tailings contributes to a great proportion of this cost, it is necessary to minimize the amount of cement added to the paste fill. However, the strength of the paste fill is dependent on the amount of cement added to the fill. It is therefore necessary to determine the amount of cement required to maintain the stability of the mine. As a result of research into the static stability of paste fill, the cement content of paste fills has been reduced. However, the paste fill is also subjected to blast loadings from mining adjacent to the fill, leading to concern over the stability of fills with reduced cement content. Little research has been conducted to determine the effects of blast loading on paste fill, and such research will be relevant to the mines around the world.

### ***1.5. Thesis Overview***

This chapter introduced the research problem and the objectives of this research and has identified the relevance of the research. Chapter 2 reviews previous research that has been conducted into paste fill. Previous numerical modelling of blasting is also covered in this

extensive literature review. This review also covers the various factors involved with the static and dynamic analysis of cemented backfills.

Chapter 3 describes the field monitoring that was undertaken at Cannington Mine during blasting carried out adjacent to an instrumented paste fill stope. The data obtained from the monitoring are analysed and the conclusions drawn from these data are presented, including observed behaviour of the blast waves travelling through the boundary between ore and paste fill and peak particle velocities at which damage to the paste fill is observed to occur. Chapter 4 presents the results of a set of field tests in which a number of blasts were monitored in a paste fill stope. The data obtained from these tests were used to obtain a relationship between the peak particle velocity and distance from a blast in paste fill, to determine a blast loading function to apply in a numerical model, and to validate the numerical models. Chapter 5 covers a laboratory testing program in which stress waves were produced in columns of paste fill. Effects of curing age, cement content and solids content of the paste fill on wave propagation were analysed.

Chapter 6 outlines methods for numerically modelling blasting in the scale required for this research, and identifies the need for a Blast Loading Function. The development of the loading function is presented in this chapter. The development of a finite element model to study the effects of blasting in an underground mine is presented in Chapter 7. This chapter includes a general overview of finite element modelling, including the capabilities of the numerical modelling program ABAQUS/Explicit which was used for this research. An overview of the models used in this research is given, and the model parameters used in each model are presented. Chapter 8 presents results of the numerical models. Chapter 9 provides a summary and conclusions of the research and some recommendations for future research.



## **2. Literature Review**

The following chapter reviews previous research that has been conducted into modelling of blasting, and studies of paste fill. This review also covers the various factors involved with the static and dynamic analysis of cemented backfills.

### ***2.1. Blasting***

Before the effects of blasting can be modelled, the mechanics of an explosive blast must be known. Experiments have indicated that when an explosive detonates in a blast hole in rock, the chemical reaction produces a gas at a very high temperature and pressure. This gas exerts a very high pressure on the blast hole walls, pushing the walls outwards and shattering the rock surrounding the blast hole. The high pressure sends a stress wave through the rock, which expands cylindrically from the blast hole. The tangential stress from this wave causes radial cracks to occur around the blast hole. The gases then expand into the cracks surrounding the blast hole, opening up the cracks and reducing the pressure of the gas. If the stress wave encounters a free boundary, the compressional wave is reflected back as a tensional wave, and cracking known as spalling may occur at the boundary if the tensile stress of the wave is larger than the tensile strength of the rock (Atchison 1968).

Damage to the rock structure during blasting occurs as a result of the stress wave, and the explosion gas. Experimental study has shown that the stress waves causes cracks in the rock, and the explosion gases separate this crack pattern (Liu and Katsabanis 1997). The diameter of the fraction zone was found experimentally to approach 6 hole diameters for a spherical charge and 9 hole diameters for a cylindrical charge (Kutter and Fairhurst, 1971).

### ***2.2. Wave Propagation***

When a column of explosive detonates in a rock mass, stress waves are generated and travel through the solid. It is therefore necessary to have an understanding of these stress waves and how they behave in order to model such waves. The behaviour of such waves is complex, particularly near borders between two media.

#### **2.2.1. Types of Waves**

Three separate groups of waves can be identified from seismographic records. The first group of waves to arrive are dilatation waves which have the highest velocity, followed by distortion waves. Finally, the surface waves, or Rayleigh waves arrive. These waves have a larger amplitude than either dilation or distortion waves (Kolsky, 1963).

There are two types of waves that can be propagated through an elastic solid, p-waves and s-waves. The particle motion of p-waves, which are also known as dilatational or compressional waves or longitudinal waves, is in the direction of propagation, and the particle motion of a s-wave, which is also known as a distortional or shear wave, is perpendicular to the direction of propagation. Other types of waves can also be propagated if the solid has a boundary. Rayleigh waves can be at a free surface, and in a similar fashion, Love waves can be propagated at a surface boundary between two surface boundaries.

For an isotropic elastic solid, p-waves travel at the velocity given by:

$$c_p = \sqrt{\frac{\lambda + 2\mu}{\rho}} \quad (2.1)$$

where,

$c_p$  = speed of the p-wave

$\rho$  = density of the solid

$\lambda$  and  $\mu$  = Lamé's Constants

The motion of these waves is along the direction of propagation, and these waves involve no rotation (Kolsky 1963). For an isotropic elastic solid, s-waves travel at the velocity given by the following equation. The motion of these waves is transverse and parallel to the wave front (Kolsky 1963).

$$c_s = \sqrt{\frac{\mu}{\rho}} \quad (2.2)$$

where,

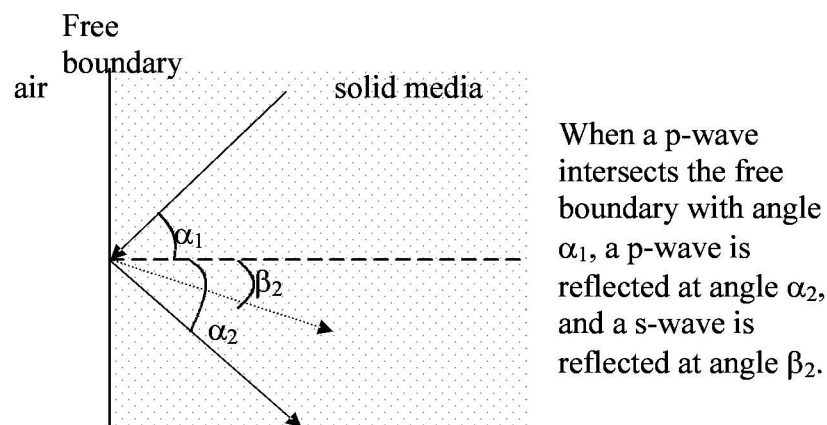
$c_s$  = speed of the s-wave

Rayleigh waves are elastic surface waves that can occur when a bounding surface is present. The velocity of propagation of Rayleigh waves is smaller than that of dilatation or distortion waves. The effect of a Rayleigh wave decreases rapidly with depth, although there is no finite depth at which motion in a direction normal to the surface vanishes. Rayleigh waves of high frequency will be attenuated more rapidly with depth than those of low frequency. There are both horizontal and vertical components of Rayleigh waves, and in theory the vertical component should dominate (Kolsky, 1963).

### 2.2.2. Behaviour of Waves at Boundaries

When either a p-wave or an s-wave intersects with a boundary, both reflection and refraction of that wave occur. The reflected and refracted waves generally consist of waves of both types, with a total of four waves leaving the boundary, two reflected and two refracted waves.

When a wave intersects with a boundary between a solid media and a vacuum, there are no refracted waves. Similarly, at a boundary between a solid and air, it can be assumed that there are no refracted waves. The reflection of a p-wave at a free boundary is shown in Figure 2.1. The solid lines in the figure represent p-waves and the dashed line represents an s-wave.

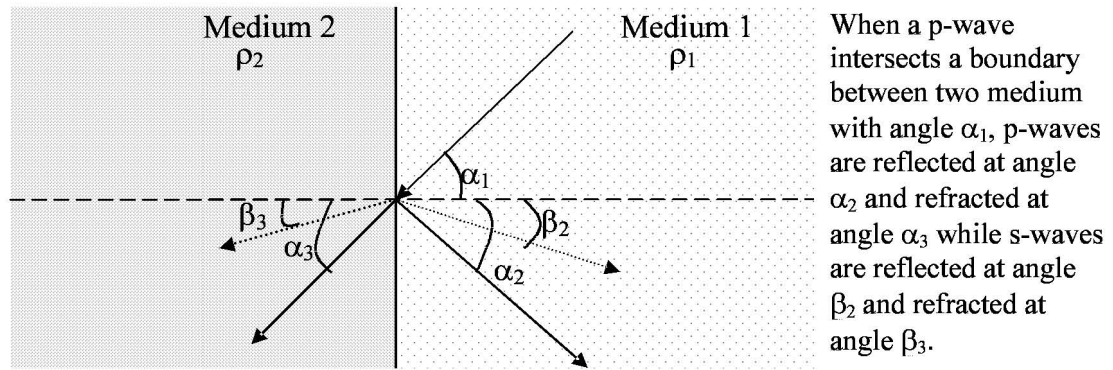


**Figure 2.1 – Reflection of a p-wave at a Free Boundary**

If the incident wave is at right angles to the boundary, there is no distortion wave, and therefore the amplitude of the reflected wave is equal to the amplitude of the incident wave. The reflection of an s-wave at a free boundary is very similar.

When a wave intercepts an interface between two media, reflection occurs similar to that at a free surface, and two waves are refracted, as shown in Figure 2.2. The solid lines in this figure represent s-waves and the dashed lines represent p-wave. When the incident dilatation wave intersects the boundary at right angles, only dilatation waves are generated. When an s-wave intersects with a boundary between two media, reflection and refraction occur in a similar manner.

The amplitude of the reflected stress wave depends on the characteristic impedance of the medium,  $\rho c$ . No wave will be reflected at normal incidence when the product of the density and velocity is the same for the two media.



**Figure 2.2 – Reflection and Refraction of a p-Wave at a Boundary Between Two Media**

### 2.3. Peak Particle Velocity

As discussed in section 2.1, upon the detonation of an explosive, the reaction produces gaseous products which are under high pressure. These gases expand, causing the borehole walls to move outwards and creating a dynamic stress field in the surrounding rock. An expanding stress field is set up in the rock mass as the gas continues to expand. The motion spreads in the form of waves: p-, and s-waves, each of which has a characteristic propagation velocity in a given material. These stress waves expand through the solid causing ground vibration. This ground vibration causes the particles in the rock mass to run through an elliptical motion, and the highest velocity experienced by the particle is known as the peak particle velocity (ppv) (Holmberg and Persson, 1979). Experimental evidence has shown that the peak particle velocity of the wave decreases with distance from the charge. The propagation velocity of the p- and s-waves and their behaviour at boundaries between two different materials was discussed in section 2.2.

The peak particle velocity, which can be measured experimentally with geophones, has been observed in studies of blast vibration. The focus of many of these studies has been on the blast vibration occurring in the material located at a distance from the explosive source, which is known as the far field. The far field is the name given to the region that is located at a sufficient distance from the explosive source that the explosive source can be treated as a point source. As a result of these studies, theories of blast vibration in the far field have been reasonable well established (Yang et al. 1994), and have resulted in the observation of the charge-weight scaling law, which is discussed in section 2.3.1.

The peak particle velocity has been used to estimate blast damage, as Holmberg and Persson (1979) showed that at a critical level of peak particle velocity, permanent damage to the rock mass occurs. This concept is discussed further in section 2.3.3.

### 2.3.1. The Charge-Weight Scaling Law

Holmberg and Persson (1979) studied the peak particle velocities experienced at a distance from an explosive charge. The study showed that the peak particle velocity decreases with distance from the explosive source, and can be predicted by the following equation, which is known as the charge-weight scaling law.

$$ppv = \frac{kW^\alpha}{R^\beta} \quad (2.3)$$

where ppv = peak particle velocity

W = charge weight

R = distance

k,  $\alpha$ ,  $\beta$  = constants specific to the site

The constants depend on the material properties of the rock mass at the site, and on the units the charge weight, distance and peak particle velocity are specified with. Equation 2.3 was developed from data mainly from far-field vibration measurement (Yang et al. 1994), and is suitable for prediction of the peak particle velocity in the far field or from a point source.

### 2.3.2. Prediction of Peak Particle Velocity for a Column Explosion

Equation 2.3 can be used to predict the peak particle velocity in the far field or from a point source. However, studies have shown that this equation does not accurately predict peak particle velocities in the near field (Yang et al. 1994). Figure 2.3 shows a typical blast hole arrangement consisting of a blast hole is filled with explosive, and ‘stemmed’ with an inert material. In this situation, equation 2.3 is only valid when the distance from the charge is large in comparison to the charge length and the charge can be treated as concentrated (Holmberg and Persson, 1979). Holmberg and Persson modified equation 2.3 by integrating the equation over the length of the explosive column to predict the peak particle velocity from a blast hole loaded with explosives in the near field, resulting in the following equation:

$$ppv = kL^\alpha \left[ \int_0^H \frac{dx}{\left[ R_0^2 + (R_0 \tan \varpi - x)^2 \right]^{\beta/2\alpha}} \right]^\alpha \quad (2.4)$$

where, ppv = peak particle velocity, (m/s)

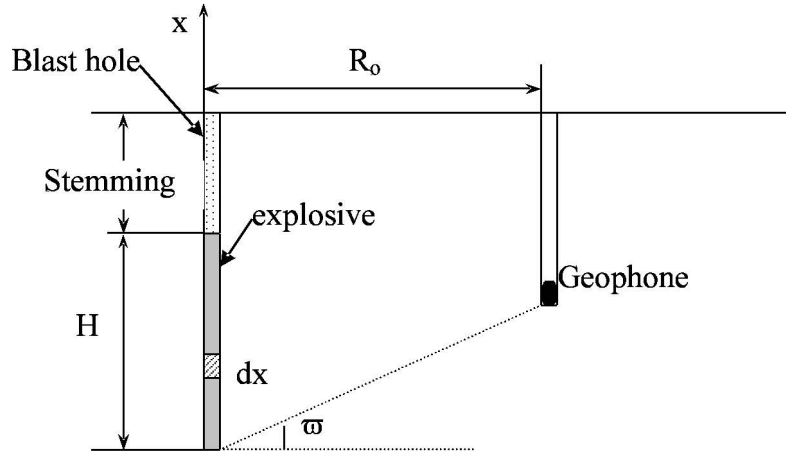
$L$  = linear charge density, (kg/m)

$k$ ,  $\alpha$ ,  $\beta$  are site specific constants

$R_0$  = the horizontal distance between the explosive and the geophone (m)

$\varpi$  = the angle shown in Figure 2.3 (radians)

$H$  = the height of the explosive in the blast hole (m)



**Figure 2.3 – Geometry of a Blast Hole Loaded With Explosives**

For blast waves in rock,  $\beta$  is often approximately equal to  $2\alpha$ , for example, for hard bedrock  $k = 700$ ,  $\alpha = 0.7$  and  $\beta = 1.5$  if  $W$ ,  $R$  and  $ppv$  are measured in the units given with equation 4.2 (Holmberg and Persson, 1979). Equation 2.3 has an analytical solution for the case when  $\alpha = \frac{1}{2}\beta$ , (Persson et al. 1994, Sartor 1999) which is of the form:

$$ppv = k \left[ \frac{L}{R_0} \right]^{\beta/2} \left[ \varpi - \arctan \left( \frac{R_0 \tan \varpi - H}{R_0} \right) \right]^{\beta/2} \quad (2.5)$$

Sartor (1999) used this equation to model the vibration induced damage from blasting at Cannington Mine. Data such as the timing and amplitude of the peak particle velocity were measured, using a set of geophones, and a site-specific vibration equation for Cannington Mine was developed. The constants in the equation were found to be:  $k = 2938$ ,  $\alpha = \frac{1}{2}\beta = 0.66$ .

The column version of the charge-weight scaling law (equation 2.5) can predict the peak particle velocity in the near field, however the user must be aware that it has the limitations listed below. Despite these limitations, the charge-weight scaling law is widely used.

- In order to the equation to predict realistic values, the constants must be obtained specific to the site. Yang et al. (1994) demonstrated this by estimating values of peak

particle velocity by equation 2.3, using site parameters for the equation 2.3 typical of the value recommended for many far-field vibration predictions ( $k = 700$ ,  $\alpha = 0.7$ ,  $\beta = 1.5$ ), integrated over the charge length (i.e. the process used to obtain equation 2.5). These values were compared against the monitored blast vibration and its attenuation in the near-field of a 2.4 m long column of emulsion explosive. The values predicted with the equation were found to be significantly lower than the measured values in the near field.

- Although equation 2.5 can give some acceptable predictions is calibrated to the site, it cannot provide any understanding of the wave propagation (Yang et al., 1994).
- The charge-weight scaling laws (equations 2.3, 2.4 and 2.5) do not provide an insight into any blast mechanisms and do not predict vibration variations with time. They only provide a simple engineering method of estimating peak particle velocity measured as a function of charge weight and distance (Blair and Minchinton, 1996).
- The charge-weight scaling laws do not take into account the effect of any joints or other discontinuities in the rock. If such discontinuities occur, the vibration response from a blast hole becomes complicated due to wave reflection and refraction (Blair and Jiang, 1995).

Due to the limitations of the charge-weight scaling law, numerical modelling has been used by numerous authors to predict the effects of blasting on the surrounding area. This is discussed in section 2.5.2.

### **2.3.3. Prediction of Damage using Peak Particle Velocity**

Prediction of damage due to an explosive blast is complicated and depends on a number of factors including the strength of the rock mass in which the blast hole is located, the presence of any joints and fissures in the rock mass, the charge size and the spacing between blast holes. However, the peak particle velocity has been used to make reasonably reliable predictions of where rock damage will occur from an explosive charge and of the degree of fragmentation that will occur in the near field (Persson et al., 1994). This method has been used for a number of purposes including quantitative predictions of fragmentations for different blast hole arrangements and for predicting damage to the remaining rock. In order to use this method, the peak particle velocity is correlated to levels of damage found through experiments. For example, the peak particle velocities characteristic of different levels of damage for hard Scandinavian granitic or gneiss bedrock is given in Table 2.1 (Persson et al., 1994).

The estimation of damage from peak particle velocity is based on the assumption that stress, and therefore damage, is proportional to peak particle velocity. This relationship between peak particle velocity and stress is implied by the following simple equation for stress caused by a stress wave in a bar:

$$\sigma = \frac{ppv}{c} E \quad (2.6)$$

where  $\sigma$  = stress

ppv = peak particle velocity

c = the wave propagation speed

E = Young's Modulus

**Table 2.1 Peak Particle Velocity – Damage Correlation (Persson et al. 1994)**

<b>Peak Particle Velocity (m/s)</b>	<b>Characteristic Level of Damage for Hard Scandinavian Granitic Bedrock</b>
0.7 to 1	Slight swelling and slightly decreased shear strength
2.5	Fragmentation begins to become marginal
5	Very good fragmentation mainly along planes of weakness
15	Crushing of the granite

A similar relationship was used by Baylot (1993) who predicted the stresses impacting on under reinforced concrete structures from explosives. Baylot (1993) estimated the peak stress in the soil mass by multiplying the peak particle velocity by the acoustic impedance using the following equation:

$$\sigma = ppv \times \rho c \quad (2.7)$$

where  $\rho$  = density



The method of predicting peak particle velocity to predict damage is useful where an indication of where damage might occur is needed, such as in a situation where different blast hole layout patterns are to be compared. However, this method cannot give exact calculations of where damage will occur as it does not take into consideration many factors which affect blast damage, including:

- The shape of the waveform and the duration of the dynamic loading. These factors are important as if the duration of the stress is too short, the stress from the blast wave may exceed the material strength and not cause damage.
- The presence of any joints in the rock mass and their effect on blast damage are not taken into account.
- The velocity of detonation of the explosive material is not taken into account.
- The presence of any free surfaces in the vicinity must be taken into account. These free surfaces were considered in the predictions given in Table 2.1.

## ***2.4. Cemented Backfill in Underground Mining***

### **2.4.1. Commonly Used Backfills**

A variety of different types of backfills are available for use in underground mines. Some of the commonly used backfills are as follows:

- Hydraulic Fill: the product resulting from the partial dewatering of the tailings (Cowling et al., 1983)
- Cemented Hydraulic Fill (CHF): produced by mixing hydraulic fill and cementing agents. (Cowling et al., 1983)
- Rockfill: crushed rock. At Mount Isa Mines, the rock is crushed to 300 mm and screened at 25 mm. (Cowling et al., 1983)
- Cemented Rockfill: produced by mixing rockfill and cemented hydraulic fill. (Cowling et al., 1983)
- Pastefill: mine tailings with a typical effective grain size of 5  $\mu\text{m}$  mixed with a small percentage of cement binder.

### **2.4.2. Paste Fill**

Cannington Mine uses the open stoping mining method in conjunction with post-placed backfill. The ore body is divided into a series of stopes, which are volumetric units in the shape of a rectangular prism. These stopes are mined systematically over time, and the void is filled with

backfill. The type of backfill used at Cannington mine is known as paste fill, which consists of mine tailings, water and approximately 4 % of cement.

Paste fill is a relatively new technology that is used to fill the voids left by mining. There are a number of benefits in the use of paste fills, including an effective means of tailings disposal, improvement of local and regional rock stability, greater ore recovery and reduced environmental impacts. Paste fill is also used in a number of mines in Canada.

### 2.4.3. Static Stability of Paste Fill

Bloss et al. (1993) reported the results of a number of investigations conducted at Mount Isa Mines. The distribution of the fill material within the stope was predicted, and the stability of the stope was modelled using TVIS, a three-dimensional elasto-plastic finite-element program. Most of the model predictions were conservative. The few cases where the fill was predicted to be stable and failure occurred were thought to be due to the effects of blasting or weak fill, which were not considered in this model.

In order to model the static stability of the stope, the complete extraction and filling process around a given stope was modelled. This extraction sequence is shown in Figure 2.4. One of the major conclusions drawn by Bloss et al. (1993) was the importance of simulating the extraction and filling of adjacent stopes in a systematic manner in order to accurately model the stresses in the fill.

5	4	3
2		1
8	7	6

**Figure 2.4 – Typical Extraction Sequence Around a Backfilled Stope**

Bloss and Greenwood (1998) reported on further study conducted with the TVIS model. Improvements to the model showed that the original model had underestimated the confining stresses on the middle stope, which resulted in overestimating the vertical stress and the instability. This new set of modelling reported by Bloss and Greenwood (1998) found that the arching mechanism was dominant in stabilising the fill.

A series of laboratory tests was carried out to determine the behaviour of paste fill from Cannington Mine. Total stress parameters were obtained from the paste fill under unconfined compression, confined triaxial compression and tension (Rankine et al., 2001). The results of the laboratory tests were used as input parameters to a stability analysis. Rankine (2000) developed a model of the extraction, filling and curing of an idealized nine-stope arrangement

using FLAC<sup>3D</sup>, a finite difference numerical modelling package. The idealised nine-stope arrangement used by Bloss et al. (1993) was used to simplify the complex mining sequence.

The results of this model showed that the primary stope was most stable when completely surrounded by rock. As the surrounding stopes were excavated and filled, the vertical stresses in the primary stope increased due to the progressive loss of arching.

A number of mines in Canada use paste fill instead of other alternatives such as slurry or cemented rock fill systems. This use of pastefill has sparked some research into the behaviour of the paste fill. The Golden Giant Mine in Canada began using paste fill in 1996. As a result of this change to paste fill, Pierce et al. (1998) conducted laboratory testing and stability analysis of paste backfill. The laboratory tests involved unconfined and triaxial compression tests, and confined compression tests on samples with a solids density of 75 %, and cement binder contents of 3, 5, and 7 % by dry weight. The cement content consisted of a 50:50 mix of Portland cement and type C fly ash. A stability analysis was conducted for mining by blast hole open stoping methods, with cemented backfills. Safety factors against failure of the fill were obtained using limit equilibrium methods and the stability was then modelled numerically using FLAC<sup>3D</sup>.

For this model, a confined block failure mechanism proposed by Mitchell et al. (1982) was assumed. The factor of safety against failure for this failure mechanism is given by:

$$\Phi = \frac{W_n \cos \theta \tan \phi + dDw / \cos \theta}{W_n \sin \theta} \quad (2.8)$$

where  $\Phi$  = factor of safety

$W_n$  = net weight of sliding block

$\theta$  = angle of failure plane from horizontal =  $45 + \phi/2$

$\phi$  = fill friction angle

$d$  = fill cohesion

$D$  = distance between hanging wall and foot wall

$w$  = strike length

The net weight of sliding block without surcharge is:

$$W_n = \gamma D w h^* \left[ 1 - \frac{2d}{\gamma D} - \frac{1}{2} \left( 1 - \frac{D}{h} \times (\theta - 2K_0 \tan \phi) \right) \right] \quad (2.9)$$

where  $h$ =fill height

$h^*$ =effective sliding block height =  $H - (w \tan \alpha)/2$

$\gamma$  = fill unit weight

$K_0 = 1 - \sin \phi$

From these equations, it was found that the factor of safety decreases with increased stope width for a given binder content and curing time. As the binder content and curing time increases, the factor of safety also increases.

## 2.5. Modelling an Explosive Blast

Numerical modelling has been used to model explosive blasts in order to improve understanding of the mechanics of a blast. The development of computer codes has allowed the use of numerical modelling packages to be used to improve the models of blasting. This has allowed a much more detailed prediction of blast damage than is possible with the use of the charge-weight scaling laws (equations 2.3 and 2.5), as the numerical models are not limited by all of the same assumptions and simplifications on which the charge-weight scaling laws are based. The influence of factors such as the material properties of the surrounding rock mass, the velocity of detonation of the explosive and the effect of nearby free surfaces can be included in the model. This allows an understanding of the effect of each of these factors on the transmission of the blast wave through the rock mass to be studied.

### 2.5.1. The Concept of an “Equivalent Cavity”

One of the earliest models was produced by Sharpe (1942) who developed a solution for stress distribution around a spherical explosive source. Sharpe (1942) modelled the explosive source by applying a transient cavity pressure to the wall of a spherical cavity. The pressure function used was applied to the walls of an “equivalent cavity” instead of the physical walls of the blast-hole itself. The radius of the cavity was set a distance from the blast hole wall that ensured that the strength of the material is greater than the stresses experienced from the shock wave. Outside this “equivalent cavity” elastic wave propagation only is expected to occur. Sharpe (1942) showed that vibration predictions based upon pressure functions applied to the walls of an equivalent cavity gave reasonable agreement with blast vibration field measurements. This concept has been used by many authors since Sharpe (1942) developed it.

The radius to use for an “equivalent cavity” was obtained by Kutter and Fairhurst (1971). Kutter and Fairhurst (1971) studied the fracture process in blasting with experiments and numerical modelling. The concept of an “equivalent cavity” as proposed by Sharpe (1942) was used in the numerical modeling. Through experimental work, the diameter of the fractured zone around an explosion was found to approach 6 hole diameters for a spherical charge and 9 hole diameters for a cylindrical charge. The stress field generated by the pressurized gas in this star-cracked cavity was shown to be identical to that of a pressurized and uncracked ‘cavity’ whose diameter is equal to that of the fractured zone. An explosive charge was modelled by applying a pressure to the walls of an “equivalent cavity”. In order to avoid modeling the cracking process, the cavity was sized so that no crushing occurs around the blast hole. Cracks in the rock are generated when the pressure experienced by the rock is higher than the dynamic compressive strength of the rock. Therefore, at the point where new cracks are no longer initiated, the peak wall pressure is equal to the dynamic compressive strength of the rock. This point was found to occur at approximately 4 times the cavity radius for a spherical charge and approximately 6 times the blast hole radius for a cylindrical charge. A higher radius is required for a cylindrical charge because the rate of attenuation of the blast wave is smaller than for a spherical charge.

### **2.5.2. Modelling a Cylindrical Charge**

The model produced by Sharpe (1942) was for a spherical blast. However, in applying the modelling to a blast hole, a model of a cylindrical charge was required. Starfield and Pugliese (1968) modelled a cylindrical charge by discretising the charge into a set of charge segments, each of which was represented by a spherical charge. The blast load was modelled by applying a pressure with a sine wave function to the walls of the cavity. The strains and stresses at any point could then be determined numerically. The model predictions from this model were generally found to be in good agreement.

The method of using a stack of spherical charges to model a cylindrical charge was also used by Harries (1990) and Zou (1990). Zou (1990) considered a cylindrical charge as the superposition of spherical charges. Using the stress wave theory in the spherical coordinate system and the superposition principle, the 3-D distribution of average energy densities of the stress wave in the rock mass was calculated.

Harries (1990) simulated a cylindrical charge by using a string of spheres. He calculated the radial stress, tangential stress, axial stress, strain energy per unit length and displacement expected by a string of spherical charges and compared the results against that expected for an infinitely long cylinder. He found that the stress distribution around a cylinder can be simulated

by a string of spheres, if the spheres have the same radius as the cylinder, and the centre of the spheres are spaced one radius apart.

The dynamic case was modelled by superimposing the results of spherical charges spaced one radius apart with a time delay between each sphere corresponding to the velocity of detonation of the explosive. Harries (1990) found that in order to correctly model a dynamic blast, attenuation and dispersion must be taken into account. This was achieved using the constant Q model of proposed by Kjartansson (1979). By using a value of  $Q = 4.5$ , good agreement was found between theory and experimental results.

Work by other authors suggested that the radiation from a vertical cylindrical source in an infinite half-space cannot be accurately represented by a model of stacked spheres (Blair and Jiang, 1995). Blair and Jiang (1995) found the use of a finite element model to produce more acceptable results. They modelled a single blast hole using an axisymmetric model and applying a blast load as a time-varying pressure applied to the walls of an “equivalent cavity” as proposed by Sharpe (1942). This model was used to study the influence of charge length upon blast vibrations, assuming that the explosives have an infinite velocity of detonation (i.e. the entire column of explosive detonates simultaneously). The results showed that when the charge length was greater than a critical value, the peak particle velocity experienced in the surrounding rock mass did not increase. This is because the charge weight in the borehole is proportional to the charge length. This finding shows why the weight/length value is used in the charge weight scaling laws for column charges.

### **2.5.3. Applying the Blast Load**

One of the first considerations in creating a numerical model of an explosive blast is applying a blast load to the model. The method of applying the blast load that is most appropriate for a model depends on the purpose of the model. Rock damage and fragmentation from blasting is caused by stress waves and gas penetration. It is very difficult to model both of these mechanisms in a combined model (Yang et al., 1996). Generally, only one of these mechanisms is modelled, and the appropriate mechanism is dependent on the purpose of the model. If the rock damage caused by the stress wave is of interest, appropriate blast loading methods include applying a time varying pressure to the walls of an “equivalent cavity”. If the fragmentation caused by the gas penetration is of interest, appropriate blast methods include applying a time varying pressure to the walls of the blast hole column and modelling the chemical reaction in a blast hole using the Jones-Wilkens-Lee (JWL) Equation of State Material Model.

### 2.5.3.1. *Applying a Blast Load to the Walls of an “Equivalent Cavity”*

The advantages of this method are that it accurately models the effects of a blast load to the rock mass surrounding the cracked region and is numerically efficient which means that the model will often solve in a reasonably short time frame. The disadvantages are that this method does not provide accurate model results in the cracked region surrounding the blast hole and is therefore not suitable for some applications. This method is typically used to model the transmission of the shock wave through the material when the effect of the rock mass or structures within the rock mass is of interest.

In order to use this method, it is necessary to determine an appropriate pressure load to apply. The load is applied as a time-varying load which typically increases in magnitude very quickly to a maximum value and decreases to zero. A variety of different pressure loads have been used by different authors. A summary of the most commonly used pressure loads is given below.

Several authors including Jiang et al. (1995), Minchinton and Lynch (1996), Blair and Minchinton (1996) and Blair and Jiang (1995) used a loading function of the form:

$$p(t) = p_0 t^n e^{-\phi t} \quad (2.10)$$

where  $p(t)$  = pressure as a function of time

$p_0$  = maximum pressure

$t$  = time

$\phi$  = decay factor

$n$  = integer

Jiang et al. (1995) used this source function to model a spherical source in an elastic and viscoelastic material, while Blair and Jiang (1995) modelled the surface vibrations caused by a vertical column of explosive by applying this pressure function to the walls of an “equivalent cavity” as defined by Sharpe (1942). The effect of the source parameters  $n$  and  $\phi$  were investigated. Peak particle velocity was found to increase with  $\phi$  for  $n=1$ , and to decrease with  $n$  for  $\phi = 2000$ . Small values of  $n$  were used in both of these cases.

Olofsson et al. (1999) modelled ground shock wave propagation using FLAC, a two-dimensional finite-difference numerical modelling package. The purpose of this modelling was to consider the effect of explosive loads from bombing in the design of underground civil

defence structures. A spherical explosive source was assumed for this scenario. The computer program CONWEP was used to estimate the explosion effects from a conventional bomb and to estimate crater dimensions and peak particle velocities at a set number of points. These peak particle velocities were used to obtain a pressure load that was applied to the crater boundary using the crater dimensions estimated by the computer program CONWEP. The load was normal to the crater boundary and uniformly distributed along the crater boundary. Olofsson et al. (1999) support the method of applying loads at the boundary of the crater created by blasting, particularly when the numerical modelling code is not well suited to modelling the detonation and formation of a crushed zone.

O'Hearn and Swan (1989) modelled the response of a sill mat of cemented hydraulic fill to blast loads using UDEC, a explicit, time marching, distinct element code. The blast, a sinusoidal pulse with a duration of 10 ms and a frequency of 100 Hz, was applied to one side of the model. Several other authors have also used sinusoidal pulses, including Todo and Dowding (1984).

Sarracino and Brinkmann (1990) conducted experiments to determine which mechanisms participate in production blasting. The results of these experiments demonstrate that the use of an “equivalent cavity” to model blasting produces reasonable results. As discussed in section 2.1, blast damage is caused by two different energy sources: stress wave and gas penetration. These sources act almost instantaneously, making it difficult to resolve their effects. Sarracino and Brinkmann (1990) studied only the stress loading on the rock experimentally by preventing the gases from penetrating the surrounding rock by lining the blast hole with a metal tube which was closed at the bottom. The acceleration and strain measurements were compared against measurements for normal blast holes and showed that the character of the shock transmitted to the rock was the same. The results of this experiment indicate that a numerical model which models only the effects of the stress wave will produce acceptable results if the user is not interested in the crushing caused by the gas penetration. Sarracino and Brinkmann (1990) modelled this explosive column in DYNA2D, an explicit two-dimensional finite element code.

### ***2.5.3.2. Applying a Blast Load to the Walls of the Blast Hole***

The advantages of this method are that this method accurately models the effects of a blast load to the rock mass surrounding the blast hole, including the cracked region. The disadvantages are that this method is numerically expensive due to complex cracking models and the small mesh sizes that are required. This method is typically used to model the cracking in the region immediately surrounding the blast hole. It is not generally used for large scale models.

In order to use this method, it is necessary to determine an appropriate pressure load to apply. As for blast loads applied to the walls of an “equivalent cavity”, the load is applied as a time-



varying load which typically increases in magnitude very quickly to a maximum value and decreases to zero. The form of the pressure load is used for both cases. A summary of the most commonly used pressure loads is given in section 2.5.3.1.

### ***2.5.3.3. Modelling the Chemical Reaction in a Blast Hole***

A third method of applying a blast load to a numerical model is to model the blast load. The Jones-Wilkens-Lee (JWL) equation of state material model (Lee et al., 1973) has been used by several authors for this purpose, including Liu and Katsabanis (1996), Thorne et al. 1990 and Yang et al. (1996). The advantages of this method are that it accurately models the explosion in the blast hole, the loading on the rock mass surrounding the blast hole and the cracking surrounding the blast hole. The disadvantages are that this method is numerically expensive due to the complex reactions that occur in the blast hole and the complex cracking model and small mesh sizes that are required. This method is typically used to model the cracking in the region immediately surrounding the blast hole. It is not generally used for large scale models. The JWL equation of state material model is discussed in section 6.5.4. Some cases where the JWL equation of state material model have been used are described below.

Daehnke et al. (1996) used a coupled solid, fluid and fracture mechanics numerical model to analyse the gas driven fracture propagation phase, to predict propagation rates and to give insights into the pressure profiles and gas velocities within the fractures. The results of the numerical modelling showed that dynamic material properties significantly influence propagation rates and need to be incorporated in the numerical analyses. The results from the numerical model were found to give similar results to laboratory experiments conducted as part of this research.

Yang et al. (1996) presented a constitutive model for blast damage resulting from impulsive loading from stress waves. ABAQUS/Explicit was used to model confined blast, axisymmetric model, with an axis of symmetry down centre of borehole. The blast load was applied by modelling the explosion using the JWL Equation of State model. A user-defined subroutine was used for the material model. This model was validated by reproducing the observed cratered shape from field experiments of single hole blasts. The model results indicated that comparisons between measured and calculated vibration waveforms provide one approach to the development and verification of numerical models for damage prediction.

Liu and Katsabanis (1997) modelled rock fragmentation from blasting by developing a continuum damage model. Once the model was developed, the dynamic finite element program ABAQUS/Explicit (version 5.3) was used to solve the problem. The system of equations developed in the model was coded into ABAQUS through user-defined subroutines. Liu and

Katsabanis (1997) solved several problems, demonstrating the suitability of their damage model for blasting analysis. These problems were run in three-dimensional space, however, they were small scale models, as full-scale modelling would have required extreme computer resources. The element size close to the explosive was 80mm x 80 mm x 100 mm. Therefore, applying such a model to the full sized stopes with heights of up to 100 metres would require a lot of computer resources.

#### **2.5.4. Modelling Multiple Blast Holes**

Many studies were found where blast holes were modelled. However, the majority of these studies consisted of axisymmetric models with the centre line along the centre of the blast hole. Few of these studies included multiple blast holes, or three-dimensional models. One of the few studies to include multiple blast holes was by Preece and Thorne (1996). Preece and Thorne (1996) modelled the detonation of two blast holes located 3 m apart using the dynamic finite element computer program PRONTO-3D, a numerical modelling package developed at Sandia National Laboratories. The model was produced to model the effect of detonation timing on fragmentation, and used a damage constitutive model to simulate the dynamic fracture of rock. This damage constitutive model was based on tensile failure and was unable to predict damage in compression. The explosive detonation was modelled with detonation beginning at the bottom of each explosive column and was modelled with a controlled burn based on a specified detonation velocity. Although this model produced acceptable results for the two blast holes, the complexity of model required approximately 4 days of CPU time to solve. Therefore, this approach would not be suitable to model the number of explosive columns used in a production blasts due to the time that would be required to solve the model.

#### **2.5.5. Modelling the Effects of a Blast on Cemented Backfill**

Many researches have modelled the effects of an explosive blast on cemented fill, using both physical models and numerical modelling. A summary of these studies is given in the following section.

O'Hearn and Swan (1989) modelled the stability of cemented hydraulic fill. A numerical model was produced of a sill mat composed of cemented hydraulic fill. A sill mat is a thin bedded plug that is situated below weaker backfill and used to support the overlying fill when mining underneath the stope. As seismic events in the region were known to cause failure, O'Hearn and Swan (1989) produced a model in the numerical modelling package UDEC, an explicit, time marching, distinct element code, to study the response of the cemented fill to seismic events. The blast load was applied as a sinusoidal pressure pulse with a duration of 10 ms and a frequency 100 Hz. From this project, it was found that peak particle velocities between 200 and

300 mm/s in the fill, caused the collapse of the overlying fill. This study focused on seismic events occurring in the far field, with the nearest blast 20 m from the fill.

In another study, Lilley (1994) researched the near field effects of blasting on cemented hydraulic fill, and developed a mathematical model to determine the effects of blasting on cemented hydraulic fill (CHF). Lilley and Chitombo (1998) continued this research, improving the model. A transmission of blast vibrations was modelled from the source, through ore, across the ore/CHF interface, and into the CHF mass using a vibration transfer model. A number of assumptions were made to simplify the model.

The results demonstrated the dependence of the model on the source. The source was assumed to be a point in the model produced by Lilley, while Lilley and Chitombo (1998) assumed a cylindrical source. As a result, Lilley's model predicted a low likelihood of damage, while Lilley and Chitombo's model predicted plastic deformation in the CHF, near the interface for a source located 5 metres from the ore/CHF interface with a peak particle velocity of 1500 mm/s at the source, a velocity typical from blasting in hard rock (Pierce 2001).

In one another study, Itasca (Pierce 2001) used the numerical modelling package FLAC, the two-dimensional version of FLAC<sup>3D</sup>, to simulate blast and impact loadings on fill. A two dimensional model was used, and the blast was simulated by applying a velocity pulse at the centre of the pillar. A number of assumptions and simplifications were used in the development of this model; however, this model was useful for an initial assessment of the stability of fill under blasting loads.

Physical models have also been used to predict the effect of blasting on nearby cemented backfill. Nnadi (1990) used scale models to determine the stability of cemented backfills under dynamic loading. Nnadi (1990) found that centrifuge modelling with increased gravity loadings was required to obtain accurate results from scale models. Nnadi and Mitchell (1991) reported the results of centrifuge models used to simulate blast loadings and predict the response of cemented mine backfills, using impact loading to simulate a blast. This experiment proved centrifuge modelling to be a useful tool for blast studies, although the impact load could not easily be correlated to a given blast energy in the field.

Mitchell and Nnadi (1994) continued the centrifuge study, using a centrifuge model to evaluate the effect of dynamic loads caused by ring blasting on the stability of an exposed face of tailings. The loads induced no static failures. This experiment indicated that the probability of ring blasting producing ore dilution from this type of backfill is low.

## ***2.6. Summary***

Much research has been conducted on the processes involved in blasting and in modelling an explosive blast. This research has shown that the damage to a rock structure due to blasting results from two mechanisms, the effects of the explosion gas and the transmission of a stress wave. Experimental study indicates that the stress wave causes cracks in the rock which the explosion gases expand into and separate the crack pattern.

The motion from a blast spreads in the form of waves which expand through the solid causing ground vibration. The highest velocity experienced by a particle is known as the peak particle velocity. The peak particle velocity of the wave decreases with distance from the explosive source. The peak particle velocity can be used to estimate blast damage, as experiments have shown that permanent damage to the rock occurs at a critical peak particle velocity. This is based on the assumption that stress, and therefore damage, is proportional to peak particle velocity.

Equations 2.3 and 2.5 have been developed to predict the peak particle velocity in the far field and the near field respectively. These equations contain constants which are specific to a given site. Sartor (1999) used equation 2.5 to determine the constants for these equations for rock at Cannington Mine. The constants for these equations for paste fill at Cannington Mine are presented in this chapter 4 of this dissertation.

Equations 2.3 and 2.5 have several limitations in predicting the peak particle velocity in a realistic rock mass. For example, these equations do not predict vibration variations with time, and they do not take into account the effect of any joints, discontinuities or free surfaces in the rock. For this reason, numerical modelling has been used to predict the effects of blasting on the surrounding area. Some of the models that have been created include the following:

- Modelling a spherical explosive charge. One of the earliest models was created by Sharpe (1942). Sharpe (1942) modelled the spherical explosive charge by applying a pressure to the wall of an “equivalent cavity”, rather than to the physical walls of the physical cavity. This ensured that the elastic wave propagation only had to be modelled. Kutter and Fairhurst (1971) later determined that the radius of the equivalent cavity should be approximately 4 times the cavity radius for a spherical charge and approximately 6 times the cavity radius for a cylindrical charge.
- Modelling a column explosive charge. The earliest models of a cylindrical charge involved modelling the charge as a stack of spherical charges (Starfield and Pugliese, 1968; Harries, 1990; and Zou, 1990). However, work by other authors found that the

use of a finite element model produced more acceptable results (Blair and Jiang, 1995). Many authors have produced numerical models of a single column of explosive in a uniform material. This has allowed simplifications such as the use of axisymmetric models to be used in order to reduce the computing time of the model. While this approach is useful for studying the effects of blasting surrounding a single blast hole, this method is not able to predict the effect of production blasting in rock on nearby fill.

- Modelling multiple blast holes. While the majority of the studies consisted of models of a single blast hole, a few studies included multiple blast holes. One such example was Preece and Thorne (1996) who modelled two blast holes located 3 m apart using a 3-dimensional model. This model was reported to produce acceptable results, however the complexity of the model required approximately 4 days of CPU time to solve. The solving time makes the production of larger models consisting of many blast holes impractical.
- Modelling the effects of a blast on cemented backfill. A number of studies were found where the effects of an explosive blast were modelled. O’Hearn and Swan (1989) modelled the effects of blasting on a sill mat composed of cemented hydraulic fill. A model of the sill mat and the overlying weaker backfill was produced and the blast load was applied to the side of the model to simulate the blast loading expected in the far field, with the nearest blast load 20 m from the fill. Lilley (1994) modelled the near field effects of blasting on cemented hydraulic fill, and the work was continued by Lilley and Chitombo (1998). A transmission of blast vibrations was modelled from the source through the ore and across the interface into the cemented hydraulic fill. Pierce (2001) used a two dimensional model to study blast and impact loadings on fill. In this model the blast was simulated by applying a velocity pulse at the centre of the pillar.

Although a large number of numerical models of blast loads have been produced, few of these models consider the effect of blasting in rock on nearby backfill and none of these models predict the effect of the detonation of multiple blast holes in rock on nearby backfill. A production blast in a mine involves the detonation of multiple blast holes with small delays between each blast. The blast wave from each blast hole is transmitted to the backfill material, and due to the effects of reflection of the waves within the backfill, these waves can combine to produce larger peak particle velocities within the backfill than would be created by a single blast hole. Therefore, it is important to consider the effects of multiple blast holes. The objective of this thesis involve the development of a computer-aided model to predict the dynamic response of paste fill due to blast loading from one or more blast holes located in nearby rock.

### **3. Monitoring of Stope 4261 During Nearby Blasting**

#### ***3.1. General***

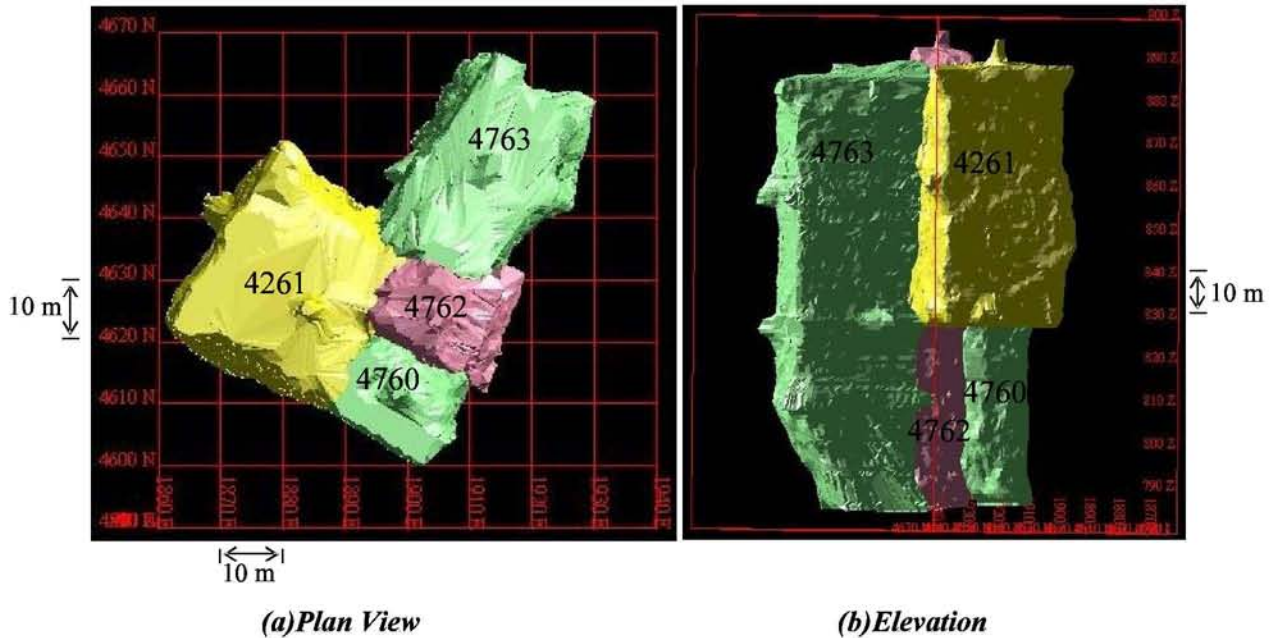
A monitoring program was put into place at Cannington Mine to measure the velocities experienced in a backfilled stope during extraction of adjacent secondary stopes. Stope 4261 was chosen for this monitoring program. The stope had been backfilled with a combination of rock and paste fill after its extraction. The paste fill consisted of 76 % solids and 3.8 % cement. The rock pieces were found to be concentrated towards the centre of the stope and almost non-existent towards the edges of the stope. Stope 4261 is 60 m high, 30 m wide and 30 m long and extends from the 375 m level down to 425 m level. One secondary stope adjacent to 4261 had been mined and backfilled prior to monitoring program. This was stope 4762, which had dimensions of 15 m wide by 15 m long by 100 m high, and extended from 375 m level to 475 m level.

A horizontal tunnel was excavated two thirds of the way through stope 4261 at the 400 m level, which was at the mid height of the stope. Monitoring equipment was installed in boreholes drilled from this tunnel. Stope 4261 was monitored during blasting of adjacent stopes 4760 and 4763. Stope 4760 had dimensions of 100 m high, 15 m wide and 15 m long and extended from 375 m level to 475 m level. Blasting occurred in 8 stages between the 14<sup>th</sup> September and 9<sup>th</sup> October 2001. Stope 4763 had dimensions of 104 m high, 30 m wide, 27.5 m long at the base and 36.5 m long at the top and extended from 375 m level to 475 m level. Blasting occurred in 8 stages between during May 2002. The positions of stopes 4760, 4261, 4762 and 4763 relative to one another can be seen in Figure 3.1 and plans of the stopes are given in Appendix A.

#### ***3.2. Monitoring Equipment Used***

The monitoring program involved the installation of 5 triaxial geophones in the backfilled stope 4261. During blast events, the geophones were connected to a Blastronics BMX Blast monitor. Triaxial geophones measure velocities in three directions, which are perpendicular to one another. The velocity at that point can then be obtained by calculating the vector sum of these velocity records.

Upon the complete extraction of each adjacent stope, the inside of the cavity was scanned and input into a computer program which was used to provide an accurate representation of the size of the cavity. The volume of paste fill which failed during the removal of the secondary and tertiary stopes was calculated from this information.



**Figure 3.1 – Layout of Stopes Used in Monitoring Program**

### **3.3. Location of Monitoring Equipment**

A total of 5 triaxial geophones were installed from boreholes drilled from a tunnel that was excavated 20 metres into the paste fill stope 4261. A borehole was drilled from the end of this tunnel towards the adjacent rock at an angle of  $33^\circ$  to the horizontal. Four triaxial geophones, G3, G4, G5 and G6, were positioned in this borehole, as shown in Figure 3.2. The fifth geophone, G7, was installed in a borehole drilled into the side wall of the tunnel, as shown in Figure 3.3. As can be seen, geophone G3 was installed in the rock, while the remaining geophones were installed in paste fill. The distances of G3, G4, and G5 from the end of the drive are shown in Figure 3.2.

### **3.4. Type of Explosive Used in the Production Blasts**

The emulsion type explosive Powerbulk VE, at a density of approximately  $1.0 \text{ g/cm}^3$ , was used in the production blasts at Cannington Mine. Powerbulk VE is a primer sensitive bulk emulsion explosive that has been designed for used in underground blasting applications. Powerbulk VE is a fluid with a viscosity similar to that of heavy grease. It is pumped into boreholes and can be used for boreholes of up to 35 m length. The explosive can be detonated using either a primer or a Powergel packaged explosive cartridge in conjunction with a detonator. Information about this explosive, which was supplied by Orica, is given in Table 3.1.

**Table 3.1 Properties of Powerbulk VE**

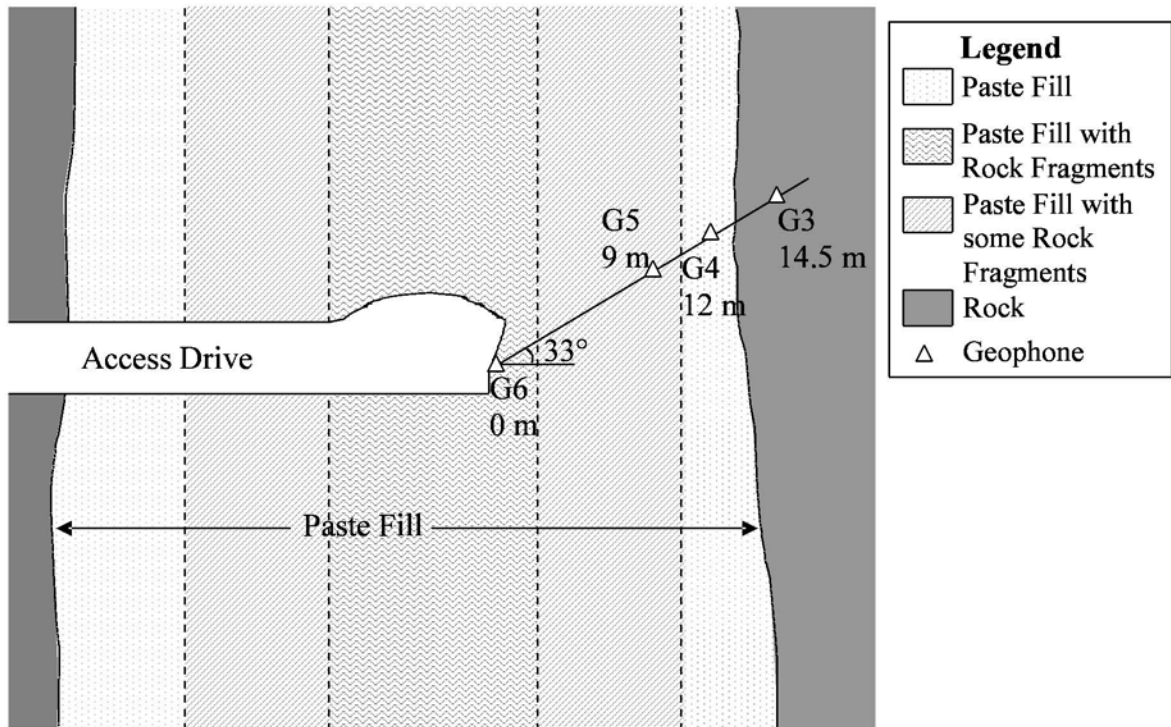
Density (g/cm <sup>3</sup> )	0.8	1.0	1.2
Calculated Velocity of Detonation (km/s)	4.3	5.3	6.2

### 3.5. Events Monitored

Monitoring data was collected during the blasting of stopes 4760 and 4763. The blast events for which occurred during this blasting and the blast events for which monitoring data was available for analysis is discussed in this section.

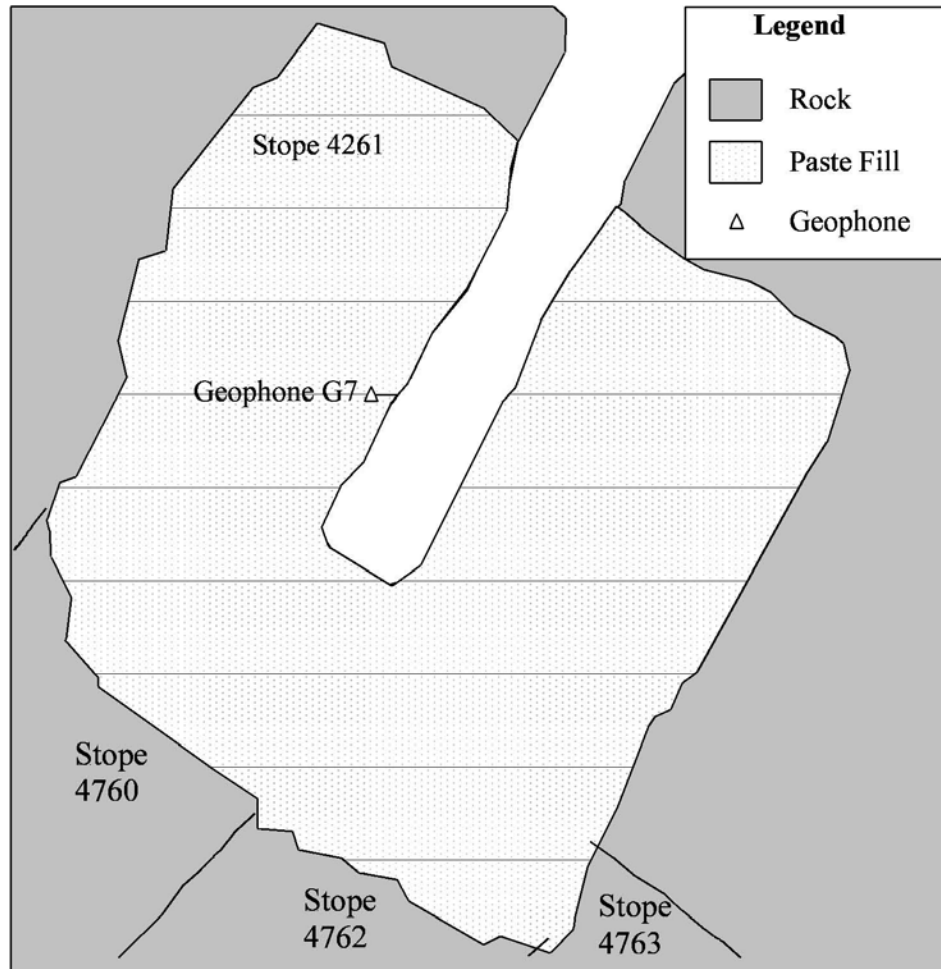
#### 3.5.1. Stope 4760

Stope 4760 is a secondary stope with two paste fill exposures. The first paste fill exposure is stope 4261, which is to the west, and involves an exposure between the 375 m level and the 425 m level. The second paste exposure, stope 4762, is to the north, and extends from the 375 m level to the 475 m level. Stope 4760 also extends from the 375 m level to the 475 m level.



**Figure 3.2 – Location of Geophones G3 to G6**





**Figure 3.3 – Location of Geophone G7**

Blasting was carried out over a 3 ½ week period, with a total of 8 separate blast events. Table 3.2 lists the blast events for which data was collected. Blast plans and delay times for these events are given in Appendix B.

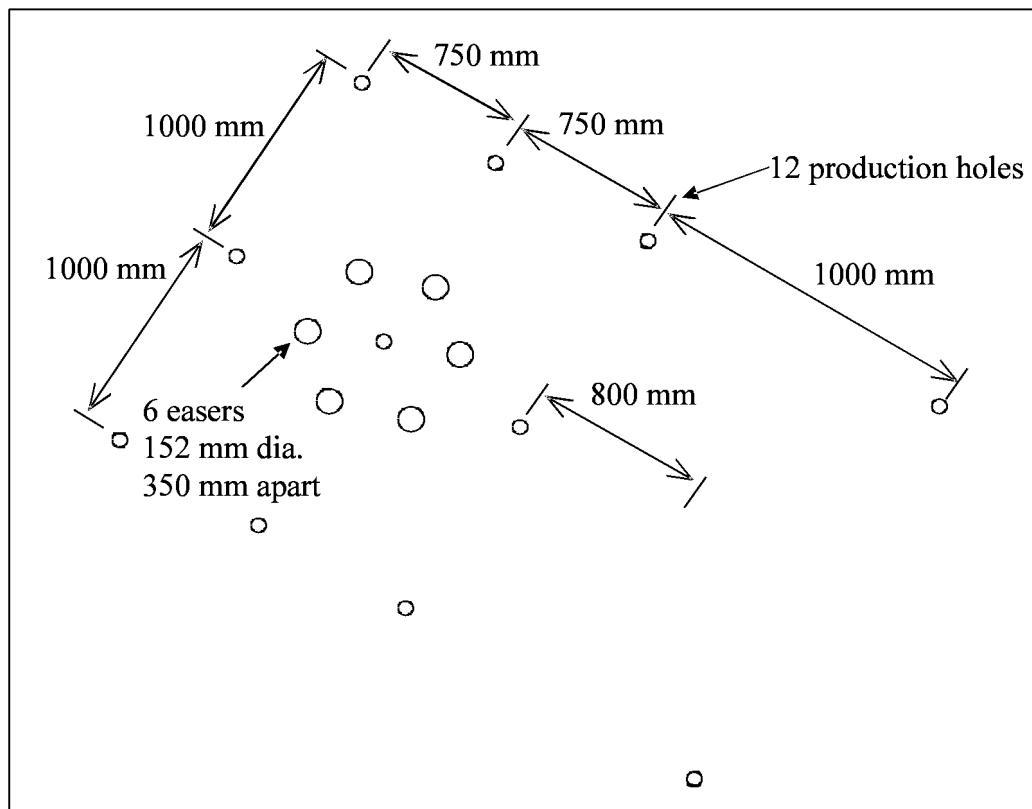
The ring types given in Table 3.2 refer to the different types of blast hole patterns used in the production blasts that were monitored. The following three types of blast hole patterns were used in the production blasts that were monitored:

- Winze

The winze is a vertical shaft that is excavated at the beginning of the mining sequence for a given stope. The winze monitored in this production blast consisted of 12 production blasts with a 69 mm diameter and 6 easers with a 152 mm diameter. The easers are boreholes drilled into the rock to allow room for the crushed rock to expand into during blasting. The layout of the winze blast monitored for stope 4760 is shown in plan view in Figure 3.4. All blast holes were vertical.

**Table 3.2 Monitoring Data Collected During Blasting of Stope 4760**

File Name	Blast Number	Level (m)	Ring Type	Mass of Explosive (kg)	Date	Metres Charged (m)	Comments
BHP#13	904064	425	Winze	893	18/9/01	143.5	Data OK
Table 3.4							
09281751	904068	475	COS, Rings 1,2,3,4	3204	22/9/01	576	Data OK
Table 3.6							
09291749	904072	425	COS, Rings 1,2,3,4	3902	25/9/01	727	Saturation on most channels
Table 3.8							
09301747	904078	400	COS, Rings 1,2,3,4	9645	9/10/01	1531	Disk full – data lost



**Figure 3.4 – Winze Blast Hole Layout for Stope 4760**

- COS

The COS blast pattern consisted of rows of vertical blast holes with a diameter of 89 mm.

- Rings

The ring blast pattern consisted of a set of blast holes drilled in a radial pattern. The blast holes in the rings had diameters of 76 mm for rings close to the paste fill face of stope 4760, and diameters of 89 mm for the rings in the main body of the stope.

### 3.5.2. Stope 4763

Stope 4763 is a secondary stope with one paste fill exposure composed of fill masses from stopes 4261 and 4762, on the south side. The paste fill exposure of stope 4261 involves an exposure between the 375 m level and the 425 m level while the paste fill exposure of stope 4762 involves an exposure between the 375 m level to the 475 m level. Stope 4763 extends from the 375 m level to the 475 m level. Blasting was carried out with a total of 8 separate blast events. The southern most rings were fired together from the bottom up, allowing the paste to be exposed last to reduce the chance of damage to the paste fill mass. Data was collected during the firing of the southern main rings between the 475 m level and the 375 m level. This blast involved approximately 30000 kg of emulsion explosive installed in 89 mm boreholes. Table 3.3 lists the details of this blast event. Blast plans and delay times for these events are given in Appendix C.

**Table 3.3 Details of Stope 4763 Blast Event Monitored**

<b>File Name</b>	<b>Blast Number</b>	<b>Level (m)</b>	<b>Ring Type</b>	<b>Mass of Explosive (kg)</b>	<b>Date</b>	<b>Metres Charged (m)</b>
09051801	904186	375	Rings 5, 6, 7, 8, 9, 10	10140	9/5/02	1630.2
	904187	425	Rings 5, 6, 7, 8, 9	12809	9/5/02	2059.4
	904188	450	Rings 5, 6, 7, 8	2894.8	9/5/02	465.4
<b>Total</b>				<b>25844</b>		<b>4155</b>

### **3.6. Collected Data**

Each geophone recorded a set of 3 velocity versus time profiles for each blast event that was monitored. The overall velocity profile for each geophone was obtained by calculating the vector sum of these three records.

#### **3.6.1. Stope 4760**

Records were collected for all 5 geophones during the first 3 blast events for stope 4760 listed in Table 3.2. However, the monitor failed to record the data for the fourth blast event, blast number 904078, as the disk on the Blastronics BMX blast monitor was full. The velocity profiles measured during each blast are given in Appendix B

#### **3.6.2. Stope 4763**

The geophones were tested prior to blasting stope 4763. During this test, geophones G3 and G4 tested dead. These geophones were the closest geophones to the blast of stope 4760, and were most likely to be damaged during the blast. As a result, velocity records for only geophones G5, G6 and G7 were recorded during the southern main ring blast of stope 4763. Results consisted of an 11000 ms duration sample for G5 (sample interval 200  $\mu$ s), a 2750 ms duration sample for G6 (sample interval 50  $\mu$ s), and an 1100 ms duration sample for G7 (sample interval 20  $\mu$ s). The distance between the geophones and the main ring ranged between 19 m and 83 m.

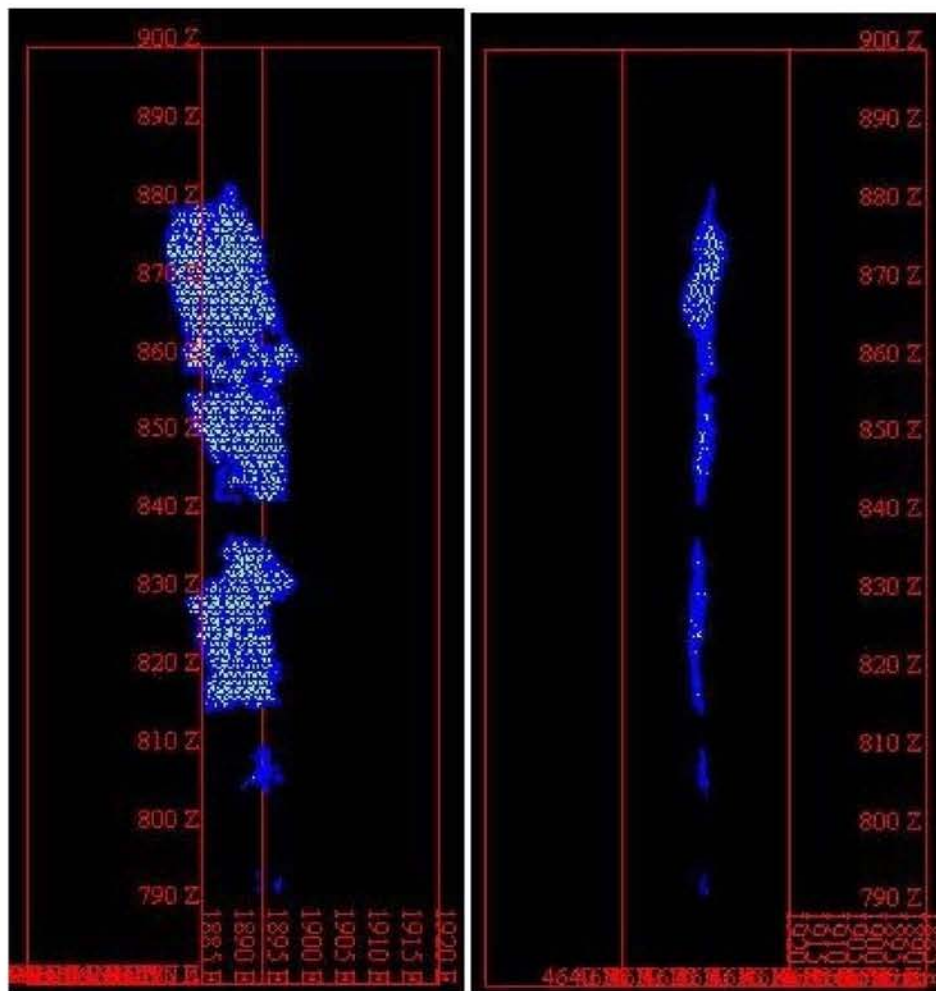
#### **3.6.3. Volume of Stopes**

In addition to the blast records, the cavity of each stope was scanned. The volume of paste fill that failed was determined by comparing the cavity extracted for each stope. These volumes are shown in Figure 3.5 and Figure 3.6.

### **3.7. Analysis of Data**

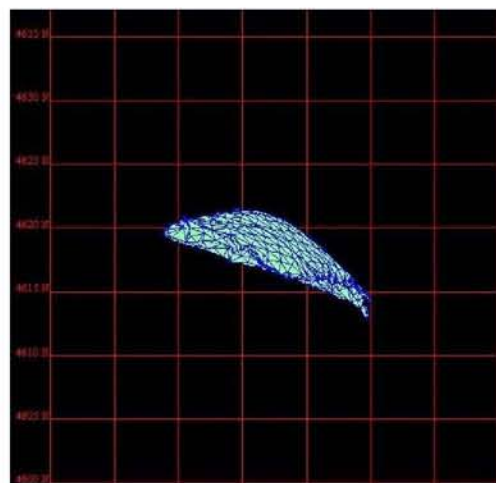
#### **3.7.1. Volume of Failed Paste Fill**

The volume of failed paste fill for each blast was obtained through a comparison of the volume of the cavity extracted with each stope. Once a stope is extracted, the inside of the cavity is scanned. The volume that overlapped between the cavity of stope 4261 and the adjacent stopes represents the volume of paste fill that failed during the extraction of the adjacent stopes. Computer software used by Cannington Mine was used to calculate the volume of the intersection between the stopes, and to plot images of this volume. The failure at the interface of stopes 4261 and 4760 is shown in Figure 3.5, and the failure at the interface between stopes 4261 and 4763 is shown in Figure 3.6. The volume of failure for each interface is given in



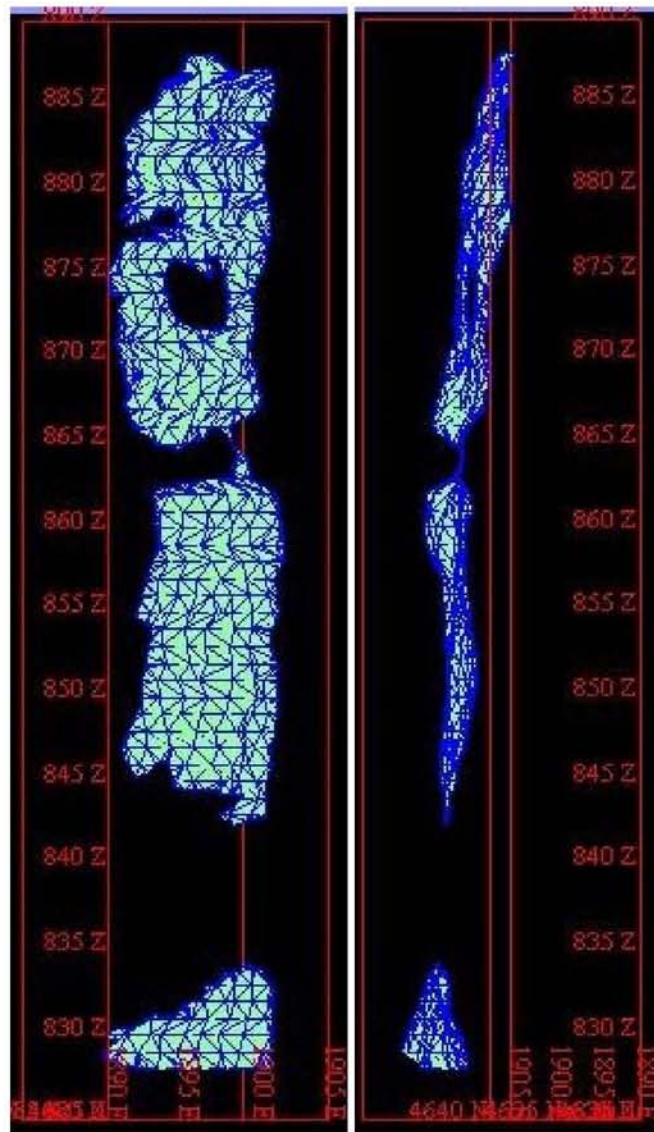
*(a) Front View*

*(b) Side View*



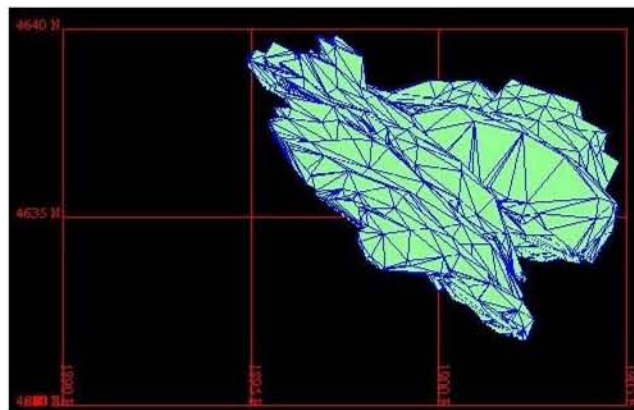
*(c) Plan View*

*Figure 3.5 – Failure at Intersection of Slope 4261 and 4760*



(a) Front View

(b) Side View



(c) Plan View

Figure 3.6 – Failure at Intersection of Slope 4261 and 4763

Table 3.4. The average thickness of failure in the paste fill estimated from this data is also given. As can be seen, generally the average of thickness of failure of paste fill was approximately 1 to 1.5 m.

**Table 3.4 Failure Observed During Blasting of Secondary Stopes**

<b>Interface of Stopes</b>	<b>Volume of Failure (m<sup>3</sup>)</b>	<b>Estimated Percent of face failed (m)</b>	<b>Estimated Height of Failure (m)</b>	<b>Estimated width of failure (m)</b>	<b>Average Thickness of failure (m)</b>
4261 & 4762	4674.8	100 %	60	15	5.2
4261 & 4760	463.1	50 %	60	15	1.0
4261 & 4763	631	60 %	60	12	1.5
4762 & 4760	520.6	60 %	90	12	0.8

### **3.7.2. Peak Particle Velocities Measured During Monitoring**

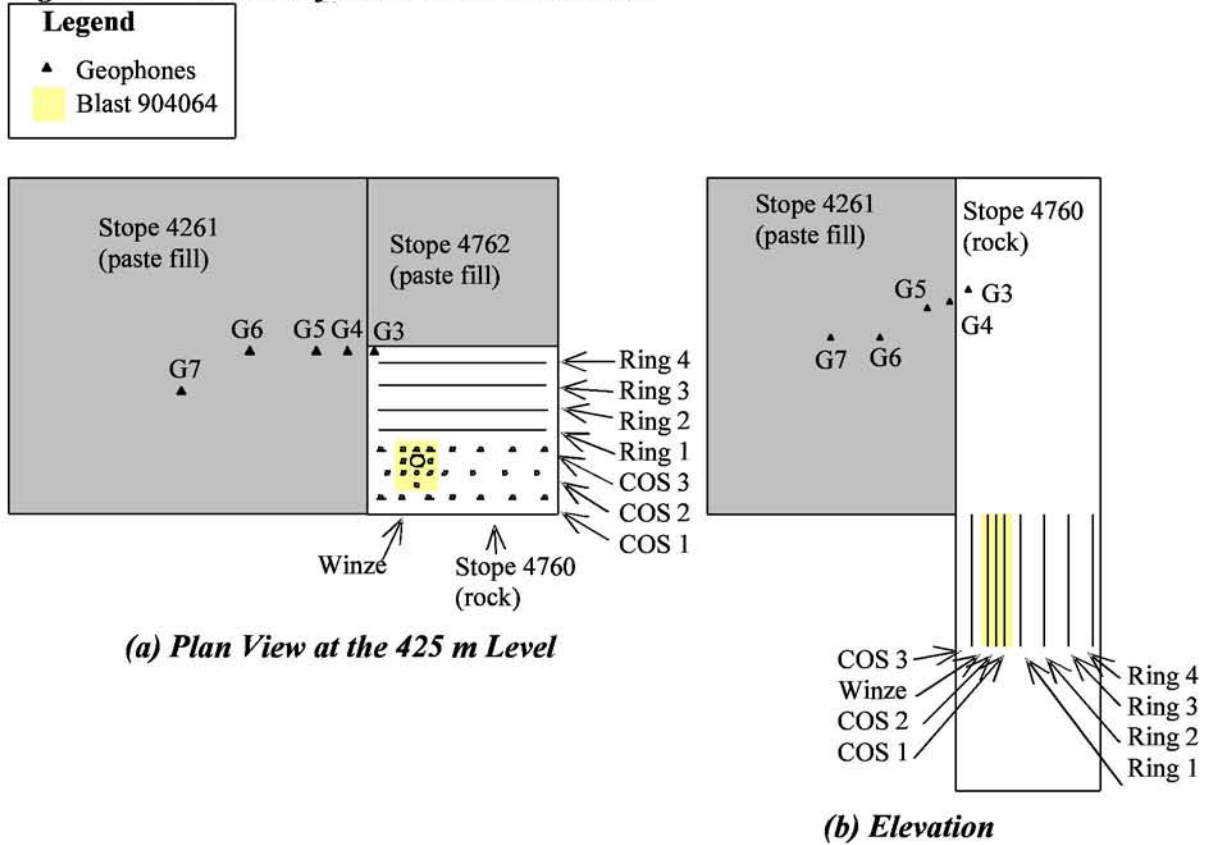
#### **3.7.2.1. Stope 4760**

##### ***Blast 904064***

Blast 904064 consisted of a winze that extended down from the 425 m level. This blast consisted of 9 production holes with a diameter of 69 mm surrounding a 152 mm diameter easer borehole. A total of 893 kg of explosive was used, over a total blast hole length of 143.5 m. The location of the boreholes detonated in blast 904064 are shown in Figure 3.7.

Velocity profiles measured at each geophone are given in Figure 3.8. These profiles show the arrival of several waves. The blast consisted of 9 blast holes which are shaded yellow in Figure 3.7. The arrival of these blasts can be identified by the delay time used for each blast hole. In some cases, more than 9 wave arrivals can be identified. This may be due to reflections within the paste fill from the first blast holes interfering with the waves from the later blast holes. The peak particle velocity for each wave is given in Table 3.5.

**Figure 3.7 – Location of Blast 904064 Boreholes**



Comparison of records from Geophone G3, situated in the rock, and geophone G4, situated in the paste fill adjacent to geophone G3, show a reduction in peak particle velocity which can be attributed to losses experienced at the rock/paste fill interface. Comparison of Geophones G4, G5, G6 and G7 generally show the peak particle velocity decreasing with distance from the blast as expected. However in a number of cases, the peak particle velocity increased with distance. This increase in peak particle velocity may be due to the reflection of waves from the paste fill/rock interface. The waveforms given in Figure 3.8 show a relatively slow attenuation of the velocity which also suggest that a significant amount of the wave is being reflected within the paste fill.



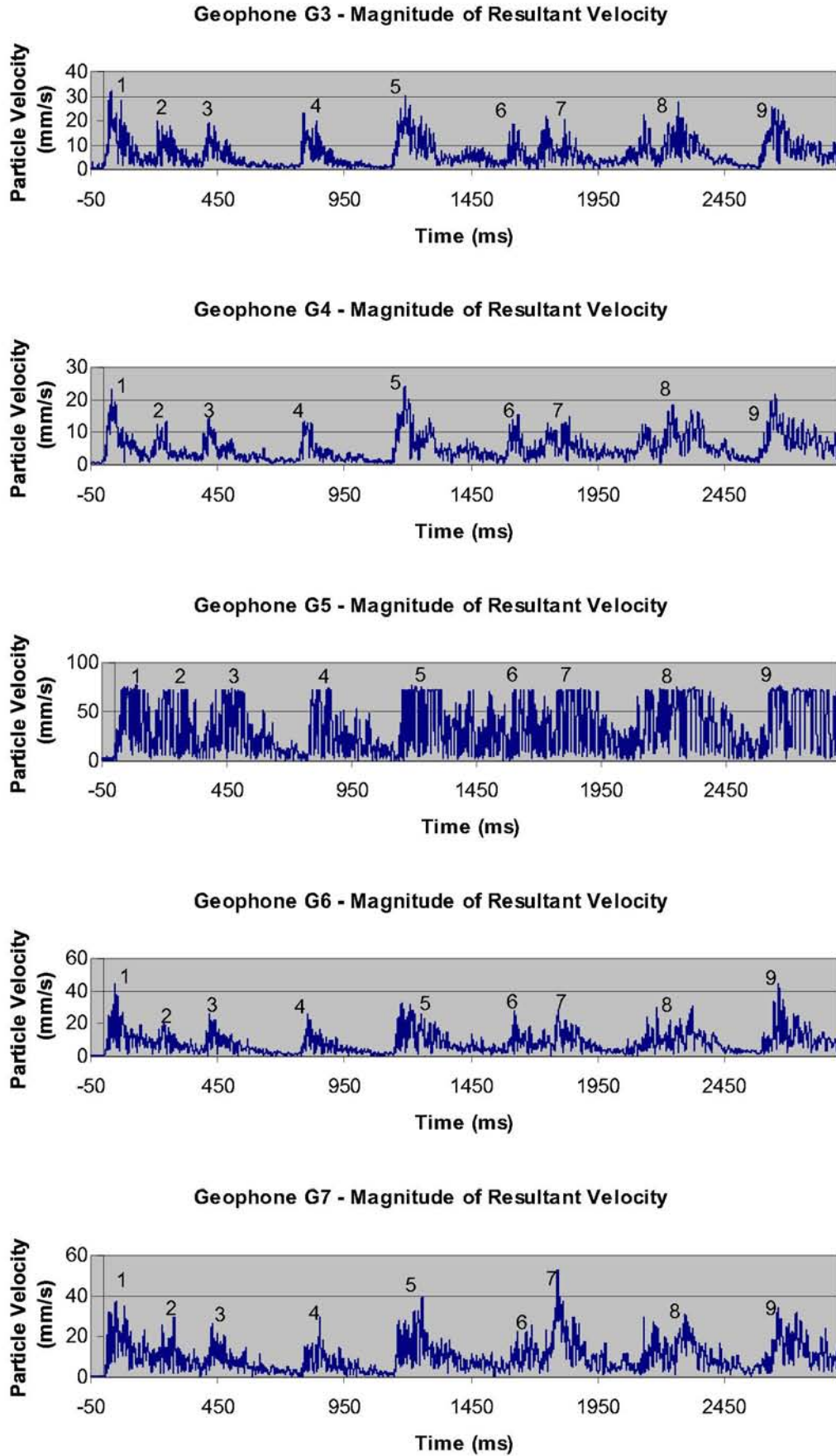


Figure 3.8 – Velocity Profiles Measured During Blast 904064

**Table 3.5 Results for Blast 904064**

<b>Geophone</b>	<b>G3</b>	<b>G4</b>	<b>G5</b>	<b>G6</b>	<b>G7</b>
Min Distance from Blast (m)	32.2	30.9	29.6	27.4	24.2
Max Distance from Blast (m)	54.9	53.8	52.6	50.1	47.3
Material at Geophone Location	Rock	Paste	Paste	Paste	Paste
Wave 1 ppv (mm/s)	32.5	23.2	78.1	44.6	37.2
Wave 2 ppv (mm/s)	20.2	13.6	73.9	21.0	29.8
Wave 3 ppv (mm/s)	19.2	14.6	74.5	26.4	26.1
Wave 4 ppv (mm/s)	23.0	13.3	74.8	26.4	29.5
Wave 5 ppv (mm/s)	30.1	24.3	76.3	32.4	39.6
Wave 6 ppv (mm/s)	22.0	15.7	73.5	28.3	26.1
Wave 7 ppv (mm/s)	20.3	15.0	75.7	29.3	53.0
Wave 8 ppv (mm/s)	27.5	18.4	76.3	30.6	31.0
Wave 9 ppv (mm/s)	25.6	21.8	77.9	44.1	34.0

***Blast 904068***

Blast 904068 consisted of the detonation of the 475 m level COS upholes and Rings 1, 2, 3 and 4. A total of 8 vertical COS boreholes of 89 mm diameter were detonated in this blast. Each Ring consisted of between 12 and 14 boreholes of 89 mm diameter drilled radially from the 475 TA63 DS tunnel. A total of 3204 kg of emulsion explosive was used; over a total blast hole length of 576 m. The location of the boreholes detonated in blast 904068 are shown as the yellow shaded section in Figure 3.9.

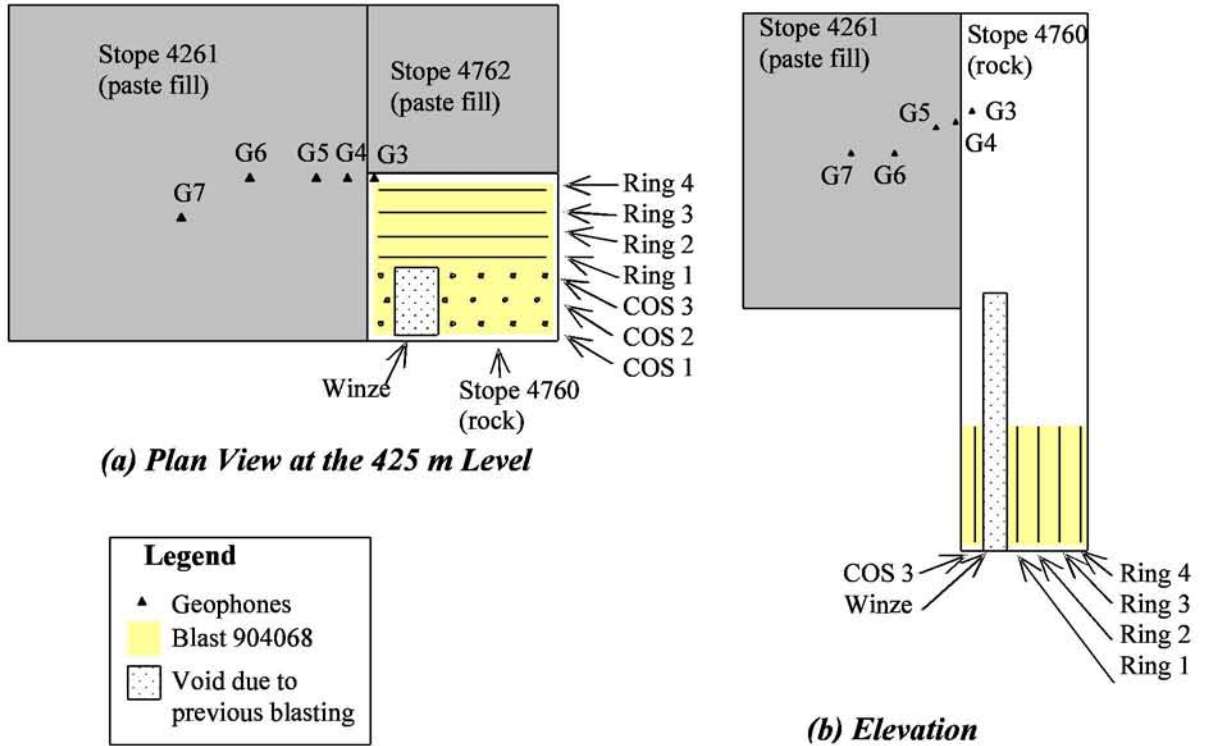


Figure 3.9 – Location of Blast 904068 Boreholes

Velocity profiles measured at each geophone are given in Figure 3.10. The record lasts for 3 seconds, and shows the velocities experienced during the first half of the production blast. These profiles show the arrival of 5 waves. These waves were compared against delay times identified in the firing plans to identify the blast holes responsible for each wave as shown in Table 3.6.

As can be seen, individual wave arrivals could not be identified for several blast holes. In some cases (COS 1 holes 4 and 5, and COS 3 holes 4 and 5) this may be attributed to the reduction of the signal due to travelling through broken rock as a result of previous detonation. In the remaining cases, the absence of an arrival wave indicated the misfiring of the blast hole. The peak particle velocity for each wave is given in Table 3.7.

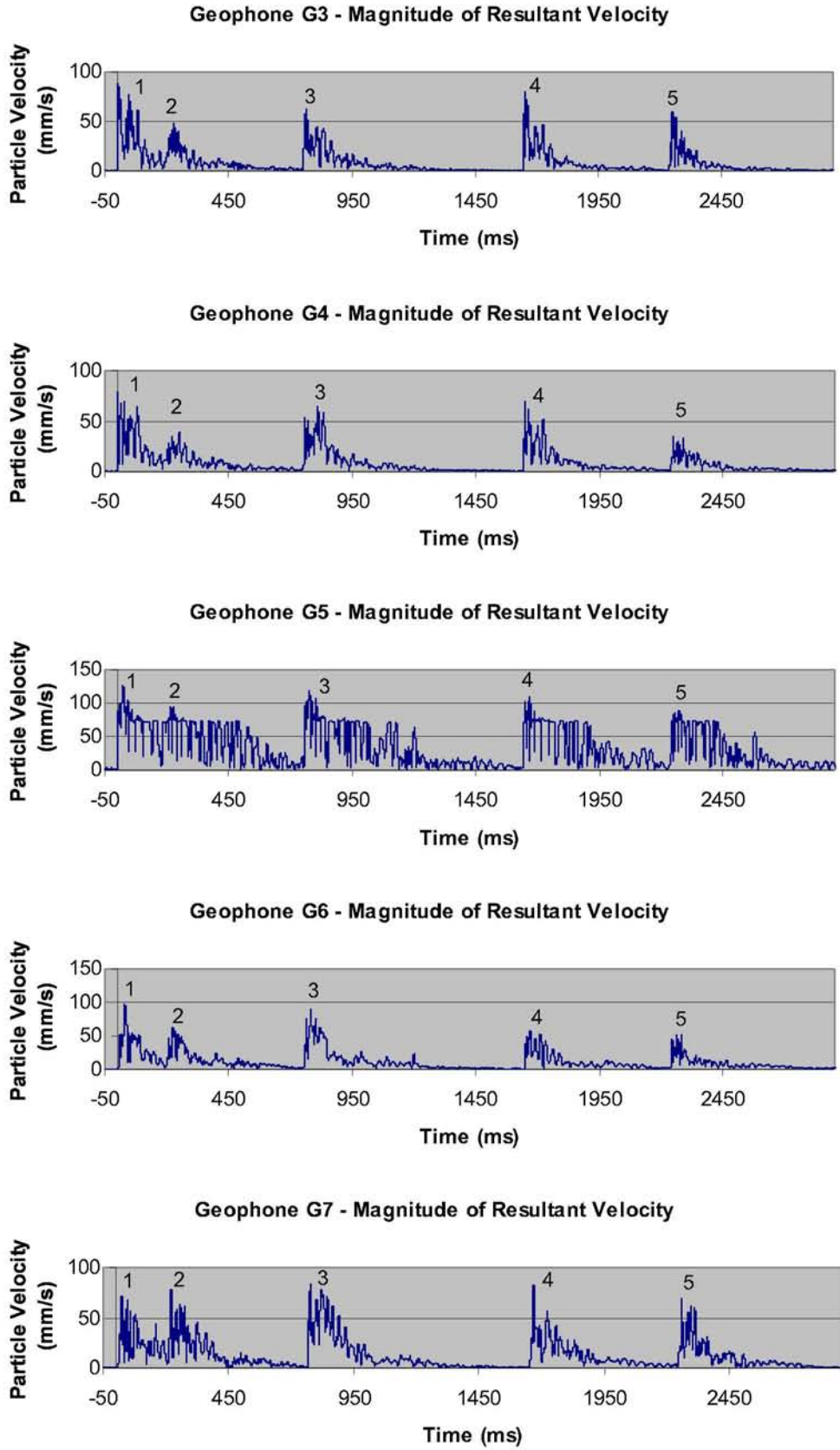


Figure 3.10 – Velocity Profiles Measured During Blast 904068

**Table 3.6 Blast 904068 Delay Times**

<b>Blast Type</b>	<b>Blast Hole</b>	<b>Delay (ms)</b>	<b>Delay (s)</b>	<b>Arrival number</b>
COS 1	3	200	0.2	1
COS 3	3	200	0.2	1
COS 2	4	400	0.4	2
RING 4	3	450	0.45	2
RING 4	1	500	0.5	2
COS 1	4	600	0.6	NO ARRIVAL IN SIGNAL
COS 3	4	600	0.6	NO ARRIVAL IN SIGNAL
COS 2	5	1000	1	3
COS 1	5	1400	1.4	NO ARRIVAL IN SIGNAL
COS 3	5	1400	1.4	NO ARRIVAL IN SIGNAL
RING 1	8	1400	1.4	NO ARRIVAL IN SIGNAL
RING 1	7	1675	1.675	NO ARRIVAL IN SIGNAL
RING 1	9	1675	1.675	NO ARRIVAL IN SIGNAL
RING 1	6	1800	1.8	4
RING 1	10	1800	1.8	4
RING 1	5	1950	1.95	4
RING 1	11	1950	1.95	4
RING 1	4	2275	2.275	NO ARRIVAL IN SIGNAL
RING 1	12	2275	2.275	NO ARRIVAL IN SIGNAL
RING 1	3	2400	2.4	5
RING 2	8	2400	2.4	5

**Table 3.7 Results for Blast 904068**

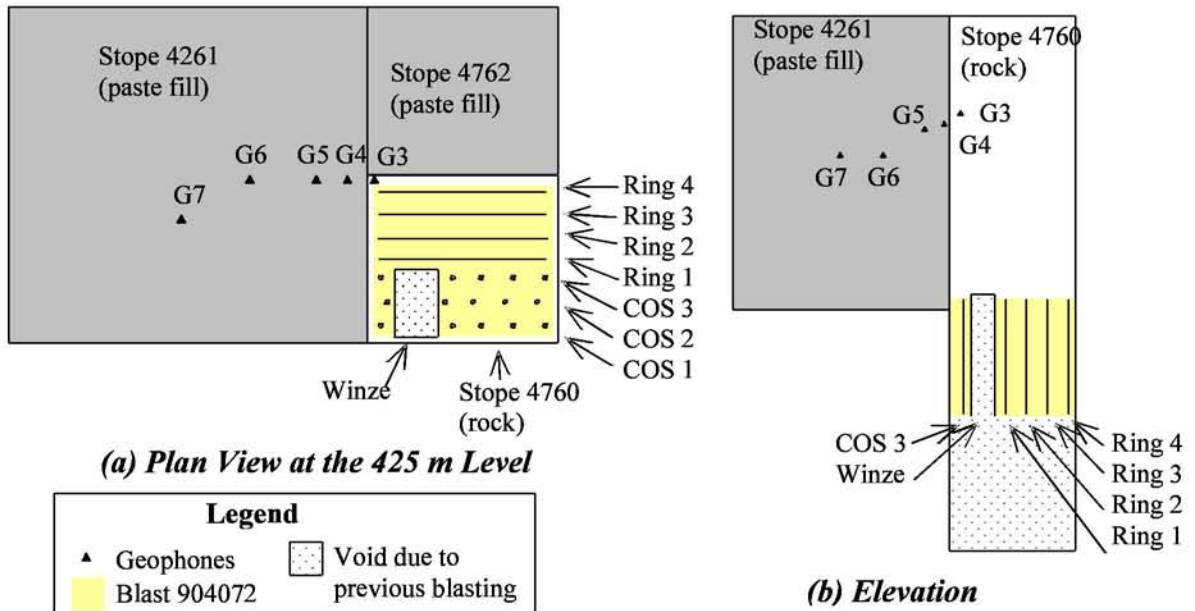
<b>Geophone</b>	<b>G3</b>	<b>G4</b>	<b>G5</b>	<b>G6</b>	<b>G7</b>
Min Distance from Blast (m)	30.9	29.6	28.2	25.9	23.6
Max Distance from Blast (m)	56.6	55.9	55.3	54.2	50.1
Material at Geophone Location	Rock	Paste	Paste	Paste	Paste
Wave 1 ppv (mm/s)	88.6	39.7	124.6	97.3	71.9
Wave 2 ppv (mm/s)	48.6	39.0	94.1	63.0	78.0
Wave 3 ppv (mm/s)	63.2	65.2	117.8	89.4	83.8
Wave 4 ppv (mm/s)	80.4	70.6	108.0	57.5	83.0
Wave 5 ppv (mm/s)	60.4	34.6	86.9	52.3	70.1

Comparison of records from Geophone G3, situated in the rock, and geophone G4, situated in the paste fill adjacent to geophone G3, show a reduction in peak particle velocity that can be attributed to losses experienced at the rock/paste fill interface. Comparison of Geophones G4, G5, G6 and G7 generally show the peak particle velocity decreasing with distance from the blast as expected. However, as observed in the results for blast 904064, in a number of cases, the peak particle velocity increased with distance. This increase in peak particle velocity may be due to the reflection of waves from the paste fill/rock interface. The waveforms given in Figure 3.10 show a relatively slow attenuation of the velocity which also suggest that a significant amount of the wave is being reflected within the paste fill.

### ***Blast 904072***

Blast 904072 consisted of the detonation of the 425 m level COS downholes and Rings 1, 2, 3 and 4. A total of 8 vertical COS holes were detonated in this blast. Each Ring consisted of between 13 and 16 blast holes drilled radially from the 425 TA63 DS tunnel. Each blast hole was 89 mm in diameter. A total of 3902 kg of emulsion explosive was used; over a total blast hole length of 727 m. The location of the boreholes detonated in blast 904072 are shown as the area shaded yellow in Figure 3.11.

Velocity profiles measured at each geophone are given in Figure 3.12. The record lasts for 3 seconds, and shows the velocities experienced during the detonation of the COS holes and the initial 3 blast holes of Ring 1. These profiles show the arrival of 5 waves.



**Figure 3.11 – Location of Blast 904072 Boreholes**

These waves were compared against delay times identified in the firing plans to identify the blast holes responsible for each wave as shown in Table 3.8. The peak particle velocity for each wave is given in Table 3.9.

**Table 3.8 Delay Times for Blast 904072**

Blast Type	Blast Hole	Delay (ms)	Delay (s)	Arrival Number
COS 1	3	200	0.2	1
COS 3	3	200	0.2	1
COS 2	4	400	0.4	2
COS 1	4	600	0.6	2
COS 3	4	600	0.6	3
COS 2	5	1000	1	4
COS 1	5	1400	1.4	5
COS 3	5	1400	1.4	5
RING 1	3, 4 and 5	1400	1.4	5

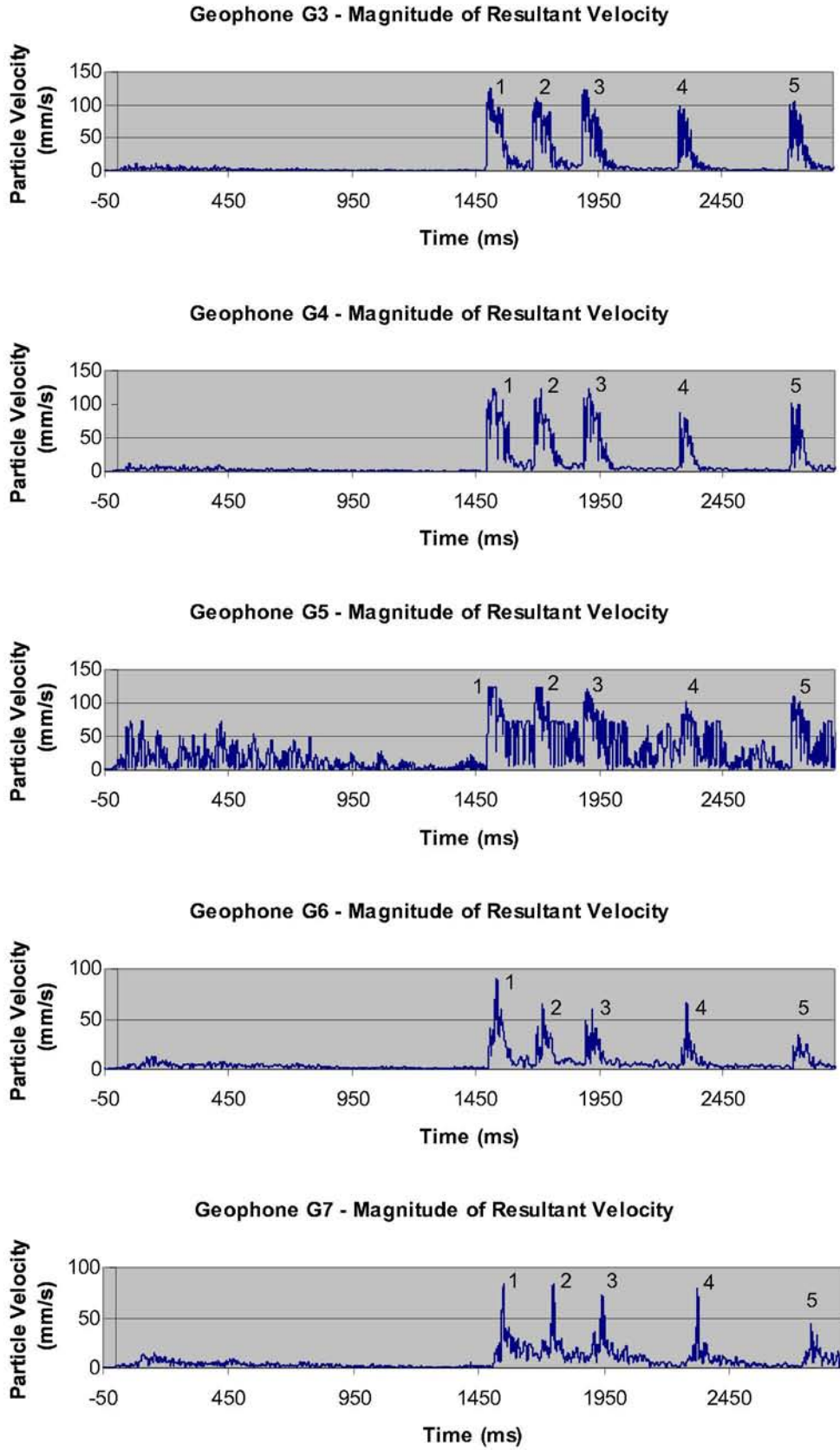


Figure 3.12 – Velocity Profiles Measured During Blast 904072



**Table 3.9 Results for Blast 904072**

<b>Geophone</b>	<b>G3</b>	<b>G4</b>	<b>G5</b>	<b>G6</b>	<b>G7</b>
Min Distance from Blast (m)	52.9	51.5	50.1	46.7	45.3
Max Distance from Blast (m)	80.5	79.5	78.6	76.4	73.4
Material at Geophone					
Location	Rock	Paste	Paste	Paste	Paste
Wave 1 ppv (mm/s)	126.2	124.8	123.7	90.5	84.4
Wave 2 ppv (mm/s)	111.5	124.8	123.7	64.6	83.6
Wave 3 ppv (mm/s)	123.4	124.8	122.4	61.1	73.1
Wave 4 ppv (mm/s)	99.7	88.3	100.9	67.0	79.6
Wave 5 ppv (mm/s)	105.4	103.4	109.9	34.1	44.6

As can be seen, the results observed for blast 904072 were similar to those observed for blasts 904064 and 904068.

### ***Blast 904078***

The blast monitor failed to record any data during this blast as the disk was full. Therefore, no analysis could be conducted for this blast.

### ***3.7.2.2. Stope 4763***

Stope 4763 was detonated after stope 4760. During testing of the geophones prior to detonating stope 4763, geophones G3 and G4 tested dead. As a result, velocity records were only recorded for geophones G5, G6 and G7. The velocity records for these geophones showed similar results as those seen during the blasting of stope 4760. The peak particle velocities were generally seen to reduce with distance, but in some cases these peak particle velocities increased. This increase in peak particle velocity may be due to the reflection of waves from the paste fill/rock interface.

As shown in Figure 3.2, geophones G3 and G4 were located on either side of the rock/paste fill interface. Since these geophones did not record any data during these blasts, the transmission of the wave across the interface could not be analysed. Therefore, these waveforms were not analysed further.

### **3.7.2.3. Summary**

Stope 4261 was monitored during the extraction of adjacent stopes 4760 and 4763. In all cases, comparison of peak particle velocities recorded at geophone G3, situated in the rock, and geophone G4, situated in the paste fill adjacent to geophone G3, show a reduction in peak particle velocity which can be attributed to losses experienced at the rock/paste fill interface. Comparison of peak particle velocities recorded at geophones G4, G5, G6 and G7 generally show the peak particle velocity decreasing with distance from the blast as expected. However in a number of cases, the peak particle velocity increased with distance. Results from field instrumentation tests discussed in Chapter 4 indicate that approximately 90 % of the pressure wave is reflected at the paste fill/rock boundary. Therefore, the increase in peak particle velocity observed in the blast monitoring can be attributed to the reflection of waves from the paste fill/rock interface. The relatively slow attenuation of the velocity observed in the waveforms also suggests that a significant amount of the wave is being reflected within the paste fill.

### **3.7.3. Wave Transmission Across the Rock/Paste Fill Interface**

The peak particle velocities measured at geophones G3 and G4 were used to examine the effect of the rock to paste fill interface on the transmission of the wave generated from the explosion. Geophone G3 was located in the rock and geophone G4 was located in the paste fill. The geophones were 2.5 m apart. The percentage of the wave that was refracted through the interface into the rock was calculated as the percentage of the peak particle velocity measured at geophone G4 compared to the peak particle velocity measured at geophone G3.

The results of the analysis are given in Table 3.10. As can be seen, the percentage of refraction into the paste fill varies considerably. This is due to a number of factors including the geometry of the boreholes in comparison to the geophone locations, and the reflection of waves within the paste fill from previous blasts interfering with the peak particle velocity measured at geophone G4. A field instrumentation test of blasts in paste fill indicated that the paste fill/rock boundary reflects approximately 90 % of the blast wave back into the paste fill. Therefore, during a production blast involving the detonation of numerous boreholes with millisecond delays between each blast, a large amount of reflection would occur. The peak particle velocities measured at geophone G4 is the peak particle velocity experienced at this location as a sum of all waves present at that time. Therefore, the peak particle velocities measured at geophone G4 may be much higher than the peak particle velocities that would be experienced if a single explosive were detonated. As can be seen in Table 3.10, in some cases the large amount of reflection of pressure waves within the paste fill produced peak particle velocities in the paste fill that were larger than those measured in the rock. The results from this analysis indicate that

**Table 3.10 Transmission of Blast Wave Across Rock/Paste Fill Interface**

<b>Blast Number</b>	<b>Wave Number</b>	<b>Ppv Measured</b>	<b>ppv Measured</b>	<b>Percentage of</b>	<b>Percentage of</b>
		<b>at Geophone G3 in Rock (mm/s)</b>	<b>at Geophone G4 in Paste Fill (mm/s)</b>	<b>Pressure Wave Refracted into Paste Fill</b>	<b>Pressure Wave Reflected into Rock</b>
904064	1	32.5	23.2	71.5 %	28.5 %
904064	2	20.2	13.6	67.3 %	32.7 %
904064	3	19.2	14.6	75.9 %	24.1 %
904064	4	23.0	13.3	57.6 %	42.4 %
904064	5	30.1	24.3	80.5 %	19.5 %
904064	6	19.0	15.7	82.7 %	17.3 %
904064	7	22.0	13.0	59.3 %	40.7 %
904064	8	20.3	15.0	73.8 %	26.2 %
904064	9	22.7	12.7	55.8 %	44.2 %
904064	10	27.5	18.4	66.7 %	33.3 %
904064	11	25.6	21.8	85.3 %	14.7 %
904068	1	88.6	79.3	89.5 %	10.5 %
904068	2	48.6	39.0	80.1 %	19.9 %
904068	3	63.2	65.2	103.2 %	0 %
904068	4	80.4	70.6	87.8 %	12.2 %
904068	5	60.4	34.6	57.3 %	42.7 %
904072	1	126.2	124.8	98.9 %	1.1 %
904072	2	111.5	124.8	111.9 %	0 %
904072	3	123.4	124.8	101.1 %	0 %
904072	4	99.7	88.3	88.6 %	11.4 %
904072	5	105.4	103.4	98.0 %	2.0 %

a large proportion of the stress wave is refracted from the rock into the paste fill, with a minimum of 55 % of the wave observed to be refracted.

The refraction and reflection of waves at a boundary between two different materials is complicated and the amplitude of each of the waves generated at the boundary is dependent on the characteristic impedance of the materials, where the characteristic impedance is a material property which affects the transmission of waves through an elastic medium. The characteristic impedance is the product of the p-wave velocity and the density. When two different materials have the same characteristic impedance, the wave will be fully refracted through an interface of the two materials. When the characteristic impedance of the second material is greater than the characteristic impedance of the first material, the majority of the wave will be reflected back into the first material at an interface between the two materials. Similarly, when the characteristic impedance of the second material is less than the characteristic impedance of the first material, the majority of the wave will be refracted from the first material to the second material at an interface between the two materials.

The p-wave velocity, density and characteristic impedance of rock and paste fill at Cannington Mine is shown in Table 3.11. As can be seen, the characteristic impedance of rock is much larger than the characteristic impedance of paste fill. It is not surprising then that the majority of the wave will be refracted from the rock into the paste fill. In a similar manner, in the case of a wave travelling through the paste fill towards a paste fill/rock interface it is expected that the majority of the wave would be reflected back into the paste fill.

**Table 3.11 Characteristic Impedance of Rock and Paste Fill at Cannington Mine**

<b>Material</b>	<b>P-Wave Velocity (m/s)</b>	<b>Density (kg/m<sup>3</sup>)</b>	<b>Characteristic Impedance (Ns/m<sup>3</sup>)</b>
Rock	2330	3950	9203562
Paste Fill	176	2003	353031

#### **3.7.4. Estimation of the Peak Particle Velocity at which Failure of Paste Fill Occurs**

The peak particle velocities at which the paste fill failed could not be calculated from the monitoring data, as useable data was not obtained during the blasting of the sections of the adjacent stopes that were the closest to the geophones. The recordings taken during these blasts were “saturated”, i.e. the velocities experienced at the geophones during these blasts were much higher than the levels at which the geophones were set to record. Geophones G3 and G4 were either lost or damaged beyond use during these blasts.

The peak particle velocity that causes failure in the paste fill was estimated using data from the following sources:

- The blast plans for stope 4760
- The volume of paste fill that failed, particularly the thickness of the failed section, discussed in section 3.7.1
- Equations for predicting peak particle velocities using constants previously reported for rock at Cannington Mine (Sartor, 1999) and constants for paste fill obtained during field instrumentation tests (see Chapter 4).

The peak particle velocity experienced at the failure plane in the paste fill was estimated using the following method:

1. Determine the location of the nearest borehole to the rock/paste fill interface.
2. Estimate the peak particle velocity in the rock immediately prior to the rock/paste fill interface using equation 2.5.  
The values of the constants for rock at Cannington Mine were obtained from work by Sartor (1999). These values are  $k = 2938$  and  $\beta/2 = 0.66$ .
3. The peak particle velocity in the paste fill immediately after the rock/paste fill interface was estimated by assuming that 50 % or 90 % of the wave will be refracted across the interface, as calculated in section 3.6.3.
4. Equation 2.5 and the site specific constants for paste fill presented in Chapter 4 ( $k = 1000$  and  $\beta = 1.02$ ) were used to calculate the equivalent distance a wave would have travelled in paste fill to result in the same peak particle velocity.
5. Equation 2.5, the site specific constants for Cannington Mine paste fill and the equivalent distance of the failure plane from an explosive source in paste fill were used to estimate the peak particle velocity at the failure plane.

The results from this calculation are given in Table 3.12. From these results it can be seen that failure of paste fill is expected to occur when peak particle velocities over 2.5 m/s are experienced.

**Table 3.12 Peak Particle Velocity at which Failure Occurs in Paste Fill**

Interface	Average Thickness of Paste Fill Failure (m)	Diameter of Borehole (mm)	Linear Charge Density (kg/m)	Distance from Interface (m)	ppv at interface in rock (mm/s)	ppv at interface in paste fill (mm/s)		Equivalent Distance from Source to Interface if Explosive is in Paste Fill		ppv at Failure Plane	
						50% *	90%*	50%*	90%*	50%*	90%*
4261– 4760	1	89	6.22	2	12328.93	4418	7230	0.52	0.20	2.51	2.85
4762– 4760	0.8	76	4.54	1.4	12943.39	4597	7522	0.35	0.14	2.48	2.76

Note: \*The percentage of the wave assumed to be refracted through the rock/paste fill interface as calculated in section 3.7.3.

### 3.7.5. Fourier Analysis

The fast Fourier transform of each waveform was calculated in order to analyse the frequency content of the waveforms. The fast Fourier transform is a method used by computer programs such as Microsoft Excel to calculate the discrete Fourier transform of a signal. The discrete Fourier transform is defined as:

$$F(i\Delta f) \equiv \sum_{n=0}^{N-1} f(n\Delta t) e^{-i(2\pi i\Delta f)(n\Delta t)} \text{ for } i = 0, 1, 2, \dots, N-1 \quad (3.1)$$

where  $N$  = the total number of discrete samples taken in the time domain

$$\Delta t = \text{the time increment between samples } \Delta t = \frac{T}{N}$$

$T$  = total sampling time

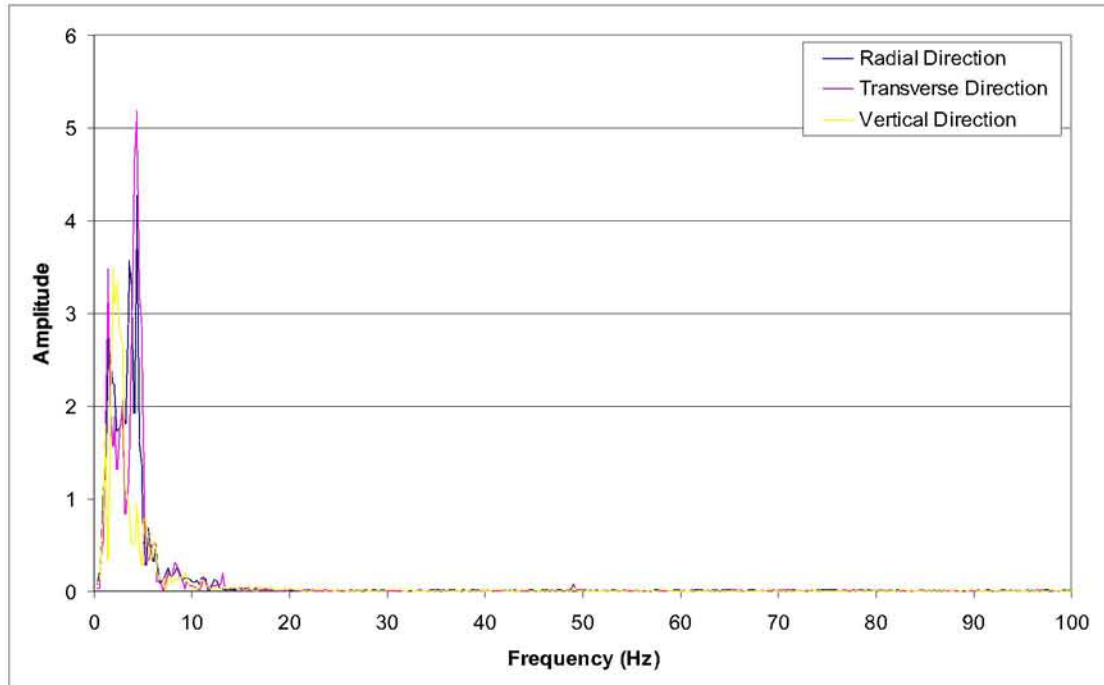
$$f_s = \text{the sampling frequency } f_s = \frac{1}{\Delta t} = \frac{N}{T}$$

$\Delta f$  = the frequency increment for the output in the frequency domain

$F(i\Delta f)$  = the discrete Fourier transform output

The discrete Fourier transform output is given as one complex number for each discrete frequency and provides information about the relative contribution of each discrete frequency to the signal. The magnitude of the complex number calculated by the fast Fourier transform is used to compare the relative contribution of the different frequencies.

An example of the frequency spectrum generated for one of the velocity waveforms is shown in Figure 3.13. Similar frequency spectrums were obtained for all other waveforms. In all cases, the frequency spectrums indicate that it is the lower frequencies that contribute to the waveform. This is likely due to the higher frequencies attenuating prior to the waves reaching the geophones. No significant difference was seen between the contribution of the frequencies at the geophone in rock compared to the geophones in paste fill.



**Figure 3.13 – Frequency Spectrum for Blast 904064, Wave Arrival 1 Recorded at Geophone G3 in Rock**

### 3.7.6. Damage to Walls of Tunnel in Paste Fill

During the production blasts of stopes adjacent to stope 4261, minimal damage to the walls of the tunnel in the paste fill was observed. The vibrations from the nearby blasts appeared to simply shake the dust off the walls. This indicates that the peak particle velocities experienced in the general mass of paste fill are less than required to damage the paste fill.

## 3.8. Summary

The paste fill stope 4261 at Cannington Mine was monitored during the extraction of adjacent stopes. A total of five geophones were used for the monitoring program, 4 of which were installed in paste fill and one of which was installed in rock.

The following observations were made during the field monitoring:

1. Higher than expected peak particle velocities were observed in the paste fill when compared to those observed in the rock. This indicates a large proportion of the waves that enter the paste fill are reflected back into the paste fill at the paste fill/rock boundary. This results in the slow attenuation of the wave within the paste fill. This slow attenuation was also observed in the velocity profiles measured during the field monitoring exercise.



### Chapter 3 – Monitoring of Stope 4261 During Nearby Blasting

2. The majority of the blast wave was refracted from the rock into the paste fill at the rock/paste fill interface.
3. The peak particle velocity at the failure plane in paste fill was estimated to be 2.5 m/s.
4. Damage to the paste fill was not visible at the tunnel wall due to the attenuation of the blast wave prior to reaching the centre of the paste fill stope.
5. A Fourier analysis of the data indicated that the higher frequencies had attenuated before the blast waves reached the geophones.

## **4. Field Instrumentation Tests**

The monitoring of production blasts discussed in Chapter 3 was useful to obtain information on how blast waves travel from a blast hole through the rock and into the paste fill. However, in order to obtain a relationship that describes the travel of a wave through paste fill, it was necessary to record the transmission of a blast wave originating within the paste fill. Therefore, field instrumentation tests which involved detonating blast holes within paste fill was conducted at Cannington Mine. These field instrumentation tests are discussed in the following chapter.

### ***4.1. Introduction***

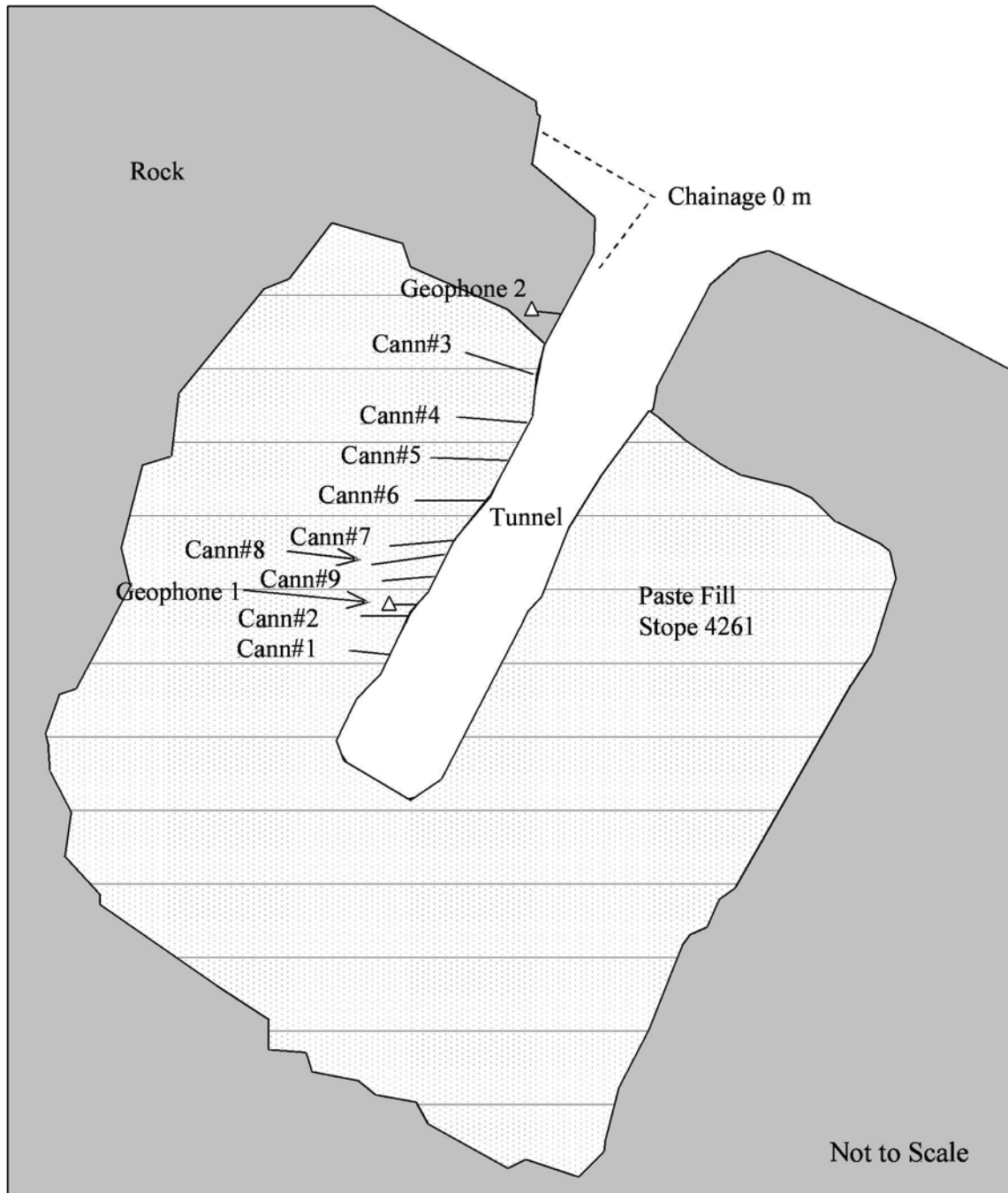
A blast monitoring exercise was conducted at Cannington Mine on the 12<sup>th</sup> and 13<sup>th</sup> of September, 2002. The field instrumentation tests were conducted with the help of Mr. Dale Luke from Cannington Mine and Mr. John Heilig, a consulting engineer from Heilig and Partners. In this exercise, two geophones were used to measure velocity waveforms produced by a series of explosions. The tests were carried out in stope 4261, which has previously been mined and backfilled with paste. The purpose of this exercise was to obtain a representative waveform caused by the detonation of a single explosive. This waveform was used to develop a blast loading function for use in the numerical models, as described in Chapter 6. Another aim of this exercise was to observe the response of the paste to the explosives. Nine separate blasts were monitored by two geophones, one of which was situated in the rock, while the other was situated in the paste fill.

### ***4.2. Location of the Blast Holes and Geophones***

The field instrumentation tests were conducted in stope 4261, at the 400 m level. Ten blast holes with a diameter of 44 mm and a length of approximately 3 m were drilled into the wall of the tunnel leading into the paste fill stope, as shown in Figure 4.1. The orientation of each blast hole is shown in Figure 4.1 and the chainage at which each blast hole was drilled is listed in Table 4.1. Two geophones were installed into this wall, one geophone installed in paste fill, and the other geophone installed in rock, approximately 1 m beyond the paste fill/rock interface. The blast holes were loaded with Orica 200 mm by 32 mm powergel plugs. Each powergel plug was initiated separately using a detonation cord. The geophones were connected to a Blastronics BMX blast monitor that was used to record the velocity waveforms resulting from each blast. As each blast hole was fired individually, a separate waveform was recorded for each blast.

The position of each blast hole was measured prior to the blasting exercise, and the depth of each blast hole was measured. This information was used to calculate the distance from the

centre of each explosive to each geophone. These distances and the depth of the blast holes are listed in Table 4.1. The explosives are labelled by the name of the waveform file that recorded the detonation of that explosive, and the chainage at which the hole was drilled. The chainage was measured from the entrance of the tunnel. The explosives were fired in the order they are listed in Table 4.1.



**Figure 4.1 – Plan View of Blast Holes and Geophones within Stope 4261**

**Table 4.1 Distance Between Explosives and Geophones**

<b>Chainage (m)</b>	<b>Waveform File Name</b>	<b>Blast Hole Length (m)</b>	<b>Distance from Geophone 1 (m)</b>	<b>Distance from Geophone 2 (m)</b>
25	Cann#1	1.97	3.48	17.27
23	Cann#2	2.45	1.96	15.55
11	Cann#3	3.20	10.96	3.66
13	Cann#4	3.37	8.19	5.97
15	Cann#5	3.30	6.25	7.90
17	Cann#6	3.15	4.11	10.02
19	Cann#7	3.25	2.12	12.26
20	Cann#8	3.34	1.56	13.15
21	Cann#9	2.69	0.95	13.84

### ***4.3. Type of Explosive Used in the Test***

Cartridges of the emulsion explosive Powergel Powerfrag supplied by Orica were used for the field instrumentation tests. The high strength, water resistant packaged explosive has the properties listed in Table 4.2. Powergel Powerfrag is initiated through the use of a detonator and is designed for priming applications and as a medium density column explosive in mining and general blasting work. The explosive is suitable for use in blast holes of any depth, as long as the depth of any water in any holes does not exceed 20 m.

**Table 4.2 Properties of Explosive Used in Field Instrumentation Tests**

<b>Diameter (mm)</b>	<b>Nominal Length (mm)</b>	<b>Density (g/cm<sup>3</sup>)</b>	<b>Nominal Mass (g)</b>	<b>Typical Velocity of Detonation (km/s)</b>
32	200	1.18	170	4.0

#### ***4.4. Test Methodology***

The following methodology was used for the field instrumentation tests:

1. A tunnel was excavated two-thirds of the way through the paste fill stope 4621 at the 400 m level. This was at the mid-height of the stope.
2. A total of 12 boreholes of 44 mm diameter were drilled into wall of tunnel. One of these boreholes was drilled into the rock, while the remaining 11 boreholes were drilled into the paste fill. These boreholes had an average depth of 2 to 3.5 m. Two of these boreholes were to be used for the installation of geophones and the remaining 10 were intended for use as blast holes. However, one hole became blocked and could not be used as a blast hole.
3. A triaxial geophone was installed into the borehole in the rock and another triaxial geophone was installed into one of the boreholes in the paste fill. The geophone installed in the paste fill was also used for the monitoring discussed in Chapter 3. Geophone 1 was located in the paste fill, while geophone 2 was located in the rock. Geophone 2 was approximately 1 m from the paste fill/rock interface.
4. The position and alignment of each borehole and the geophones were measured to ensure that the distance between each explosive and geophone could be accurately determined.
5. The boreholes that the geophones were installed in were backfilled with a cemented mixture.
6. On the day of the field instrumentation tests, each of the boreholes was cleared of debris. At this point, one borehole was found to be blocked and therefore unusable.
7. The geophones were tested and prepared for use.
8. Each of the 9 usable boreholes was loaded with one cartridge of Powergel Powerfrag emulsion explosive supplied by Orica, and each explosive cartridge was connected to detonation cord.
9. The depth of each borehole from the tunnel wall to the location of the explosive was measured to find the position of each explosive cartridge.
10. “Before” photographs were taken of each borehole that had been loaded with explosive.
11. A blastronics BMX blast monitor, supplied by Mr John Heilig, was set up, connected to each geophone and prepared to record the first explosive blast. The velocities measured by each geophone were monitored by the blastronics BMX blast monitor, and, once a trigger value was reached the monitor recorded the data from the geophone. The trigger values were based on the velocities detected by the geophones prior to each blast and were therefore re-set prior to each blast.

12. The first explosive cartridge, “Cann#1” was wired ready to fire and fired once all personnel had cleared the area.
13. Once the dust had settled in the area, an “after” photograph was taken of the first borehole, however due to the lack of visible damage to the walls, it was decided that “after” photographs would not be taken of the remaining boreholes. The lack of damage apparent of the wall of the tunnel was due to the use of only one cartridge in each blast hole. It was necessary to use such a small amount of explosive to ensure that the tunnel walls did not become unstable during the field instrumentation tests as this would have been unsafe for the people entering the tunnel during and after the tests. A much larger amount of explosive is generally used in each blast hole when blasting in rock.
14. The BMX blast monitor was checked to ensure that it had recorded a waveform and set up to record the next shot while the next explosive was wired ready to fire.
15. The next shot was fired once the area was clear.
16. Steps 14 and 15 were repeated until all shots were fired.
17. At the completion of the field tests, the measured waveforms were checked by Mr John Heilig to ensure that realistic results had been obtained. The waveforms recorded by the BMX blast monitor were converted from the Blastronics software format to Microsoft Excel format in order to allow analysis of the results.

#### ***4.5. Collected Data***

A set of three velocity waveforms was measured at each geophone during each explosive blast of the field instrumentation tests. These waveforms represent the velocity at the geophone in three mutually perpendicular directions. Velocity waveforms were not recorded at either geophone during the detonation of the explosive in borehole Cann#2 and geophone 1 did not record a velocity waveform during the detonation of the explosive in borehole Cann#4. This was due to the trigger value set for these geophones for these blasts being observed prior to the blast occurring. Velocity waveforms were recorded at both geophones during the detonation of all other explosives.

The data was converted from the format used by the Blastronics software of the BMX blast monitor to Microsoft Excel format to allow analysis of the data. The three waveforms recorded at geophone G1 for one explosive blast (Cann#1) is given in Figure 4.2.

## 4.6. Analysis of Results

### 4.6.1. Calculation of Peak Particle Velocity

Each geophone recorded velocity waveforms for the radial, transverse and vertical directions. These velocities are the particle velocities experienced in mutually perpendicular directions at the location of the geophone. In order to calculate the peak particle velocity, the magnitude of the resultant velocity was calculated using the following formula:

$$v = \sqrt{v_{radial}^2 + v_{transverse}^2 + v_{vertical}^2} \quad (4.1)$$

where  $v$  is the magnitude of the resultant particle velocity

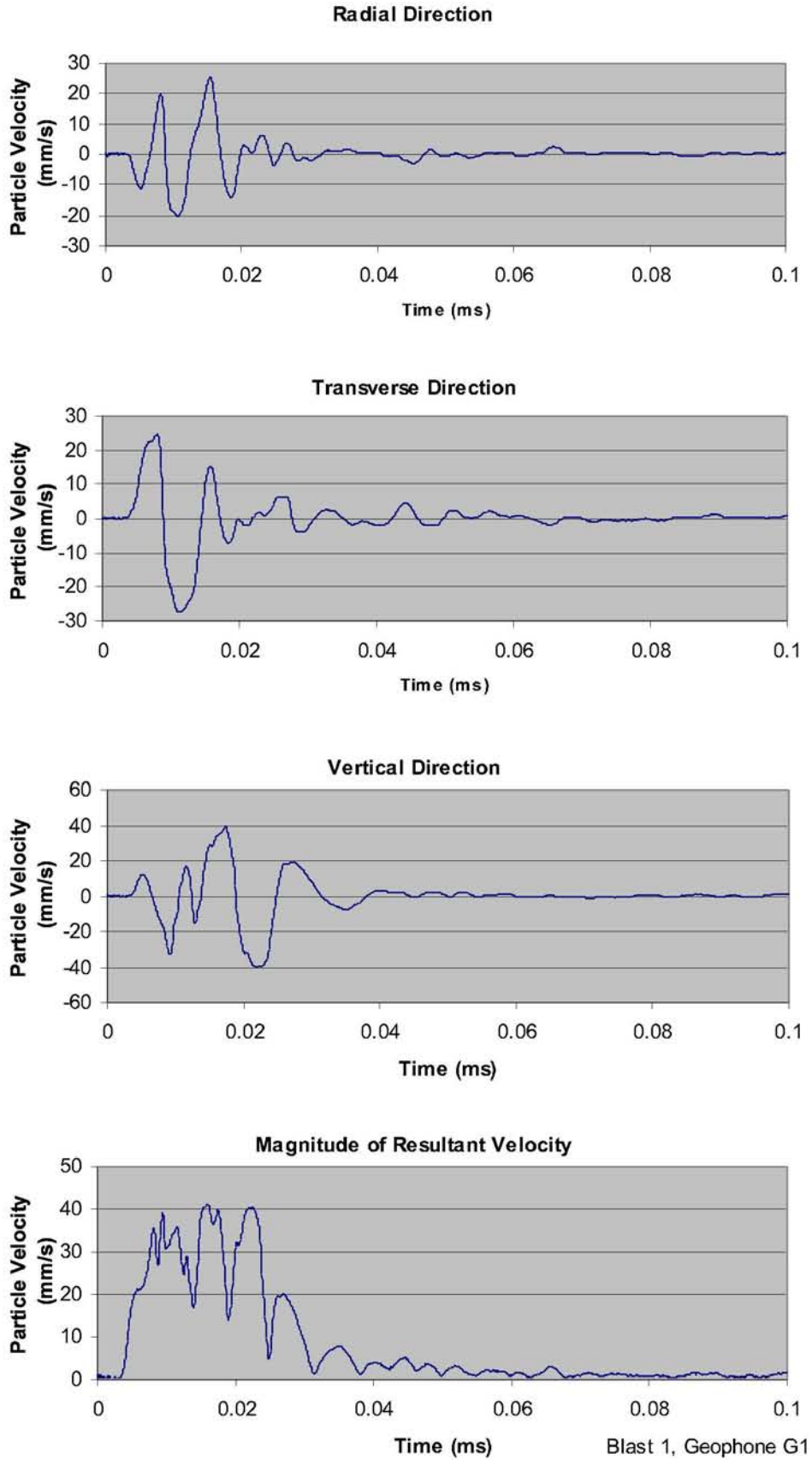
$v_{radial}$ ,  $v_{transverse}$  and  $v_{vertical}$  are the particle velocities in the radial, transverse and vertical directions respectively

The magnitude of the resultant velocity was calculated for each time step in order to obtain a resultant velocity magnitude waveform. The peak particle velocity, which is the maximum resultant velocity magnitude experienced due to the blast, could then be observed from the resultant velocity magnitude waveform. The values of peak particle velocity obtained from the resultant velocity waveforms were used for the analysis of the field instrumentation test data. The waveforms recorded at geophone 1 during the detonation of the explosive in borehole Cann#1 is given in Figure 4.2 along with the resultant velocity magnitude waveform.

The waveforms recorded at each geophone for each blast are given in Appendix D.

### 4.6.2. Equation for Predicting Peak Particle Velocity in Paste Fill

The peak particle velocities measured at Geophone 1 were used to determine the constants of the equation used to predict peak particle velocities in paste fill. The mechanics of what happens in the material surrounding a borehole when an explosive detonates is discussed in detail in Section 6.2. The detonation of an explosive charge in a borehole produces an initial shock wave in the surrounding material. This shock wave quickly decays into a stress wave. If the pressure of the initial shock wave is greater than the strength of the material, crushing of the material will occur as discussed in Section 6.2. As the wave moves out from the borehole, the pressure decreases and the wave becomes an elastic compressive wave known as a p-wave. The different types of waves are discussed in section 2.3.3. The wave strength in this region can be expressed in terms of the peak particle velocity (Holmberg and Persson, 1979). The peak particle velocity can be predicted by equation 2.3.



**Figure 4.2 – Waveforms Recorded at Geophone G1 for Blast Cann#1 and the Velocity Magnitude for this Blast**



For blast waves in rock,  $\beta$  is often approximately equal to  $2\alpha$ , for example, for hard bedrock  $k = 700$ ,  $\alpha = 0.7$  and  $\beta = 1.5$  if  $W$ ,  $R$  and  $ppv$  are measured in the units given with equation 2.3 (Holmberg and Persson, 1979). If it is assumed that  $\beta = 2\alpha$ , equation 2.3 reduces to the following:

$$ppv = k \left( \frac{\sqrt{W}}{R} \right)^\beta \quad (4.2)$$

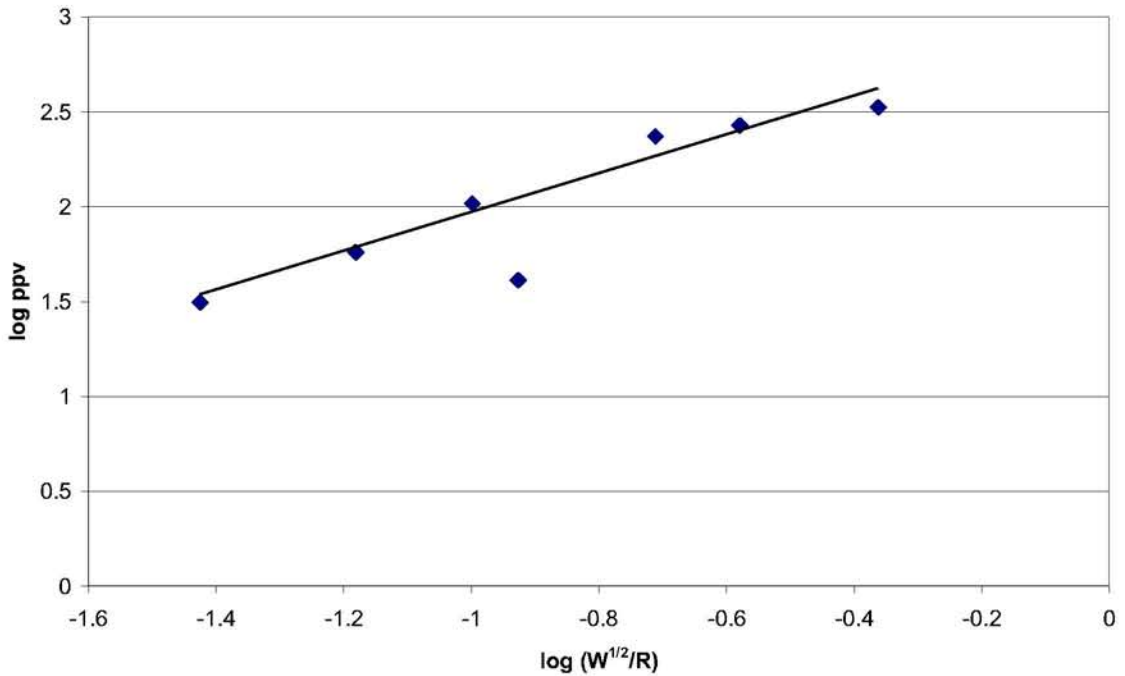
Taking the logarithm of each side of equation 4.2 produces the following relationship:

$$\begin{aligned} \log ppv &= \log \left[ k \left( \frac{\sqrt{W}}{R} \right)^\beta \right] \\ \log ppv &= \log k + \beta \log \frac{\sqrt{W}}{R} \end{aligned} \quad (4.3)$$

The logarithm of the peak particle velocity measured at geophone 1 during each blast was plotted against the logarithm of the term  $\frac{\sqrt{W}}{R}$  as shown in Figure 4.3 to obtain values of  $k$  and  $\beta$  for paste fill.

The line of best fit was calculated, and had the following relationship:

$$\log ppv = 3.00 + 1.02 \log \frac{\sqrt{W}}{R} \quad (4.4)$$



**Figure 4.3 – Peak Particle Velocity in Paste Fill**

The values of  $k$  and  $\beta$  calculated from equation 4.4 were  $k = 1000$  and  $b = 1.02$ , which produces the following peak particle velocity equation for paste fill:

$$ppv = 1000 \left( \frac{\sqrt{W}}{R} \right)^{1.02} \quad (4.5)$$

Equation 4.5 is valid when the entire wave propagation is within paste fill. The following items must be considered when estimating the peak particle velocity in paste fill from a blast in rock:

- The peak particle velocity equation for paste fill (Equation 4.5)
- The peak particle velocity equation for Cannington Mine Rock previously calculated by Sartor (1999)
- The percentage of the blast wave observed to cross the rock/paste fill boundary (section 3.7.3)

A proposed method to estimate the peak particle velocity in paste fill from a blast in rock is shown in section 4.6.4. A similar method was used in section 4.6.3 to assess the effect of the paste fill/rock interface on the transmission of the blast wave.

### 4.6.3. Effect of the Paste Fill/Rock Interface

The peak particle velocities measured at Geophone 2 were used in conjunction with the constants calculated for equation 4.2 to examine the effect of the paste fill to rock interface on the transmission of the wave generated from the explosion. Geophone 2 was located in the rock, approximately 1 m from the paste fill/rock interface.

The methodology presented in the following steps was used for this analysis. The calculations for the blast wave from Cann#1 are given as an example below.

1. The peak particle velocity in the paste fill at the interface was estimated using equation 4.5.
2. The peak particle velocities measured at Geophone 2 were used to calculate the equivalent distance between the geophone and an explosive source that would give the same peak particle velocity if the explosive and the geophone had both been located in rock. Equation 2.3 was used for this calculation, along with values of the constants  $k$  and  $\beta$  calculated for Cannington Mine Rock by Sartor (1999). The values of the constants are  $k = 2938$  and  $\beta = 1.32$ .
3. The equivalent distance from an explosive source in rock to the interface was calculated based on the equivalent distances calculated in Step 2 and the fact that geophone 2 was located in the rock 1 m from the paste fill/rock interface.
4. The peak particle velocity in the rock at the interface was estimated using equation 4.2 and the constants for Cannington Mine rock reported by Sartor (1999).
5. The percentage of the wave which was refracted through the interface into the rock was calculated.

An example calculation is given below:

***Example 4.1 Calculation of the effect of interface on blast Cann#1***

*Step 1*

*R = distance from blast to paste fill/rock interface = 16.3 m*

*W = 0.17 kg*

*Peak particle velocity in the paste fill at the interface is:*

$$\begin{aligned}
 ppv &= 1000 \left( \frac{\sqrt{0.17}}{16.3} \right)^{1.02} \\
 &= 23.1 \text{ mm/s}
 \end{aligned}$$

*Step 2*

*At Geophone 2, ppv = 0.93 mm/s, W = 0.17 kg*

$$0.93 = 2983 \left( \frac{\sqrt{0.17}}{R} \right)^{1.32}$$

$$R = \sqrt{0.17} \left( \frac{2938}{0.93} \right)^{1/1.32}$$

$$= 185 \text{ m}$$

*Where R = the equivalent distance between explosive source and geophone G2 if the blast had occurred in rock.*

*Step 3*

*The equivalent distance between explosive source and geophone G2 if the blast had occurred in rock = 185 m*

*The distance from geophone G2 to the paste fill/rock interface = 1 m*

*Therefore, the equivalent distance between the explosive source and the location of the interface = 184 m*

*Step 4*

*The peak particle velocity in the rock at the interface is estimated as follows:*

$$ppv = 2938 \left( \frac{\sqrt{0.17}}{184} \right)^{1.32}$$

$$= 0.94 \text{ mm/s}$$

*Step 5*

*ppv on paste fill side of interface = 23.1 mm/s*

*ppv on rock side of interface = 0.94 mm/s*

*Therefore, the percentage of wave which refracted through the interface*

$$= \frac{0.94}{23.1} \times 100\%$$

$$= 4.0\%$$

The results of the analysis are given in Table 4.3. The analysis indicated that between 4 % and 10 % of the wave was refracted through the interface into the rock, while the remaining 90 % of the wave was reflected back into the paste fill. The tendency of the paste fill/interface to reflect the majority of the pressure wave back into the paste fill indicates that once a pressure wave enters a paste fill stope, it will be transmitted back and forth within the stope until the wave attenuates. This result agrees with observations made during the blast monitoring discussed in Chapter 3 where it was observed that once the wave entered the paste fill, it seemed to bounce around within the paste fill and take a long time to leave the material.

**Table 4.3 Effect of Paste Fill/Rock Interface on Transmission of p-Wave**

<b>Blast Number</b>	<b>Distance from Explosive to Geophone 2 (m)</b>	<b>ppv measured at Geophone 2 (mm/s)</b>	<b>Distance from Explosive to Interface (m)</b>	<b>ppv on Paste Fill side of Interface (mm/s)</b>	<b>Equivalent Distance: Explosive to Geophone, both in Rock (m)</b>	<b>Equivalent Distance: Explosive to Interface, both in Rock (m)</b>	<b>ppv on Rock side of Interface (mm/s)</b>	<b>Percent of Pressure Wave Refracted into Rock</b>	<b>Percent of Pressure Wave Reflected into Paste Fill</b>
Cann#1	17.27	0.93	16.27	23.14	184.6	183.6	0.94	4.1 %	95.9 %
Cann#3	3.66	10.77	2.66	147.82	28.9	27.9	11.28	7.6 %	92.4 %
Cann#4	5.97	3.99	4.97	77.85	61.2	60.2	4.08	5.2 %	94.8 %
Cann#5	7.90	3.72	6.90	55.65	64.6	63.6	3.80	6.8 %	93.2 %
Cann#6	10.02	4.13	9.02	42.34	59.7	58.7	4.22	10.0 %	90.0 %
Cann#7	12.26	2.78	11.26	33.74	80.6	79.6	2.82	8.4 %	91.6 %
Cann#8	13.15	2.19	12.15	31.19	96.4	95.4	2.22	7.1 %	92.9 %
Cann#9	13.84	1.06	12.84	29.48	167.7	166.7	1.06	3.6 %	96.4 %

#### 4.6.4. Predicting ppv in Paste Fill from Blast in Adjacent Rock

The following steps can be used to predict the peak particle velocity in paste fill resulting from a blast in rock:

1. Estimate the peak particle velocity in the rock at the rock/paste fill interface using equation 4.2 and the constants  $k$  and  $\beta$  calculated for Cannington Mine rock by Sartor (1999). The values of the constants are  $k = 2938$  and  $\beta = 1.32$ .

$$ppv_{\text{int}} = 2938 \left( \frac{\sqrt{W}}{R_{\text{int}}} \right)^{1.32}$$

where  $ppv_{\text{int}}$  is the peak particle velocity in the rock at the rock/paste fill interface (mm/s)

$R_{\text{int}}$  is the distance from the explosive source to the rock/paste fill interface (m)

2. Estimate the peak particle velocity in the paste fill at the rock/paste fill interface assuming that between 50 % and 90 % of the amplitude of the blast wave will be refracted from the rock into the paste fill as occurred in the production blasts that were monitored at Cannington Mine (refer to section 3.7.3).

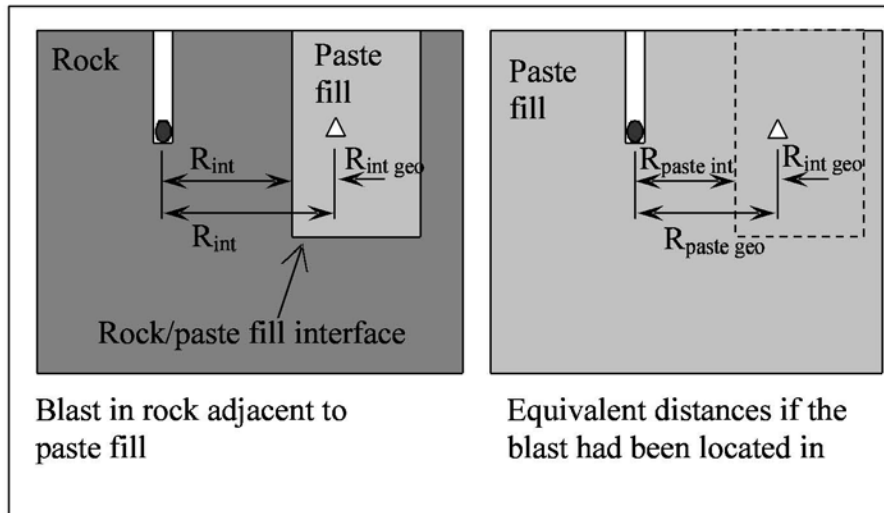
$$ppv_{\text{paste int}} = 0.5 ppv_{\text{int}}$$

where  $ppv_{\text{paste int}}$  is the peak particle velocity in the paste fill at the rock/paste fill interface (mm/s)

3. Calculate the equivalent distance between the interface and an explosive source that would give the same peak particle velocity in the paste fill at the location of the interface if the explosive and the geophone had both been located in paste fill. This concept is shown in Figure 4.4.

$$R_{\text{paste int}} = \sqrt{W} \left( \frac{1000}{ppv_{\text{paste int}}} \right)^{1/1.02}$$

where  $R_{\text{paste int}}$  is the equivalent distance between an explosive source in paste fill and the interface (m)



**Figure 4.4 – Equivalent Distances for Blast in Rock Adjacent to Paste Fill**

4. Calculate the equivalent distance between the geophone and an explosive source that would give the same peak particle velocity in the paste fill at the location of the geophone if the explosive and the geophone had both been located in paste fill.

$$R_{paste\ geo} = R_{paste\ int} + R_{int\ geo}$$

where  $R_{paste\ geo}$  is the equivalent distance between an explosive source in paste fill and the geophone (m)

$R_{int\ geo}$  is the distance between the rock/paste fill interface and the geophone (m)

5. Estimate the peak particle velocity in paste fill using equation 4.5 and  $R_{paste\ geo}$ .

$$ppv_{paste} = 1000 \left( \frac{\sqrt{W}}{R_{paste\ geo}} \right)^{1.02}$$

where  $ppv_{paste}$  is the peak particle velocity in the paste fill due to the blast in the rock (mm/s)

An example calculation is given below:

**Example 4.2 Estimation of ppv in paste fill due to blast in nearby rock**

*Problem:*

*20 kg of explosive is detonated in rock 5 m from a rock/paste fill interface.*

*Estimate the peak particle velocity measured at a geophone located 2 m beyond the*

*rock/paste fill interface.*

*Calculation:*

$$W = 20 \text{ kg}, R_{\text{int}} = 5 \text{ m}, R_{\text{int geo}} = 2 \text{ m}$$

*Step 1*

$$\begin{aligned} ppv_{\text{int}} &= 2938 \left( \frac{\sqrt{20}}{5} \right)^{1.32} \\ &= 2535 \text{ mm/s} \end{aligned}$$

*Step 2*

$$\begin{aligned} ppv_{\text{paste int}} &= 0.5 \times 2535 \\ &= 1267 \text{ mm/s} \end{aligned}$$

*Step 3*

$$\begin{aligned} R_{\text{paste int}} &= \sqrt{20} \left( \frac{1000}{1267} \right)^{1/1.02} \\ &= 3.5 \text{ m} \end{aligned}$$

*Step 4*

$$\begin{aligned} R_{\text{paste geo}} &= R_{\text{paste int}} + R_{\text{int geo}} \\ &= 3.5 + 2 \\ &= 5.5 \text{ m} \end{aligned}$$

*Step 5*

$$\begin{aligned} ppv_{\text{paste}} &= 1000 \left( \frac{\sqrt{20}}{5.5} \right)^{1.02} \\ &= 803 \text{ mm/s} \end{aligned}$$

*Therefore, a peak particle velocity of approximately 800 mm/s would be expected at the geophone.*

#### **4.6.5. Damage to Paste Fill During Field Instrumentation Tests**

During the field instrumentation tests, “before” photographs were taken of the tunnel wall at each borehole location and an “after” photograph was taken of borehole Cann#1. “After” photographs were not taken of the remaining boreholes as there was no visible damage to the tunnel walls. This is due to the use of a single cartridge of explosive in each borehole. The boreholes were all between 2 and 3 m deep. Using equation 4.2, the peak particle velocity predicted 2 m from the explosion of a single 170 g cartridge of explosive is 198 mm/s. This is much less than the 2.5 to 3.5 m/s required in order to cause damage to paste fill observed in the field monitoring discussed in Chapter 3.



The maximum peak particle velocity observed during the field instrumentation tests was 335 mm/s. This was recorded at geophone 1 during the explosion of borehole Cann#9 which was located 0.95 m from the geophone. Based on these results and the lack of visible damage, it is expected that the paste fill was only damaged in the immediate vicinity of the explosive material.

#### **4.6.6. Fourier Analysis of Data**

The fast Fourier transform of each waveform was calculated in order to analyse the frequency content of the waveforms, using the method presented in section 3.6.5. The analysis showed that the maximum frequencies contributing to a waveform generally decreased with distance. This indicates that the higher frequencies are attenuated prior to lower frequencies from a blast wave. The results of the analysis are given in Table 4.4.

### **4.7. Summary**

A set of field instrumentation tests were conducted on stope 4261, a paste fill stope at Cannington Mine. These tests involved the installation of two geophones, one in paste fill and one in rock, to measure velocities during the detonation of 9 boreholes. The boreholes were all located in the paste fill and each borehole was loaded with one cartridge of the emulsion explosive Powergel Powerfrag.

The following observations were made as a result of these field instrumentation tests:

1. The peak particle velocity can be predicted through the use of equation 4.2. The constants for this equation were measured to be  $k = 1000$  and  $\beta = 1.02$  for paste fill at Cannington Mine. For rock,  $k = 2938$  and  $\beta = 1.32$  as reported by Sartor (1999).
2. Approximately 90 % of the blast wave is reflected back into the paste fill at the paste fill/rock interface.
3. Damage to the paste fill was not visible at the tunnel wall due to the small mass of explosives used in the field tests. The lack of damage apparent of the wall of the tunnel was due to the use of only one cartridge in each blast hole. It was necessary to use such a small amount of explosive to ensure that the tunnel walls did not become unstable during the field instrumentation tests as this would have been unsafe for the people entering the tunnel during and after the tests. Despite the small volume of explosive used in these tests there was still sufficient data to meet the aims of the field instrumentation tests.

**Table 4.4 Results of Fourier Analysis**

Borehole	Distance from Geophone 1 (m)	Geophone 1 Maximum Frequency (Hz)			Distance from Geophone 2 (m)	Geophone 2 Maximum Frequency (Hz)		
		Radial	Transverse	Vertical		Radial	Transverse	Vertical
Cann#1	3.48	550	650	660	17.27	140	220	200
Cann#3	10.96	720	670	580	3.66	1090	870	1330
Cann#4	8.19	N/A <sup>1</sup>	N/A	N/A	5.97	640	730	1270
Cann#5	6.25	720	720	2050	7.90	600	560	570
Cann#6	4.11	1640	1330	2200	10.02	500	550	500
Cann#7	2.12	2110	2090	2200	12.26	340	430	540
Cann#8	1.56	1700	2100	2110	13.15	360	360	400
Cann#9	0.95	2240	2120	2490	13.84	290	240	280

<sup>1</sup> The blast monitor did not record a useable signal at geophone 1 for blast Cann#4

4. Higher frequencies attenuate faster than lower frequencies during the transmission of the blast wave.

## **5. The Study of Blast Attenuation in Paste Fill using Laboratory Tests**

A set of laboratory tests was conducted to study the attenuation of a longitudinal wave travelling through a column of paste fill. These tests are discussed in this chapter.

### ***5.1. General***

Work on determining the strength parameters of Cannington Mine paste fill has shown that the strength of paste fill changes with curing age, and the cement and solids content of the fill (Rankine, 2004). Since the strength of the material changes, it was decided to see if the attenuation of waves travelling in paste fill would show similar changes with curing age and paste fill mix. Therefore, a set of laboratory tests were conducted to study the transmissions of longitudinal waves through a column of paste fill. The aims of this experiment were to:

- Measure the attenuation of a longitudinal wave travelling through a column of paste fill;
- Study the effects of cement content on the attenuation of a longitudinal wave in paste fill;
- Study the effects of solids content on the attenuation of a longitudinal wave in paste fill; and
- Study the effects of curing age on the attenuation of a longitudinal wave in paste fill.

This experiment involved measuring the transmission of a longitudinal wave in a column of paste fill using accelerometers. The paste fill was cured in 2.7 metre lengths of pvc pipe, and accelerometers were placed at several locations along the column. The wave was induced in the column by a hammer strike to the end of the column.

### ***5.2. Seismic Attenuation and Dispersion***

Attenuation is the weakening of a stress wave as it travels through a medium. It occurs due to two main mechanisms, geometric spreading and energy loss. Geometric attenuation occurs when waves are radiated from a source such as an explosive blast. When waves radiate from a source, the energy of the wave is spread over the area of the wave front, which increases with distance from the source. The energy per unit area therefore decreases as the distance from the wave source increases. The amplitude of the wave is proportional to the square root of energy per unit area, and hence the amplitude decreases with distance from the source (Sharma, 1997). Geometric attenuation can be expressed as:

$$A = A_0 \frac{1}{r^\kappa} \quad (5.1)$$

where  $A$  = Amplitude (m/s)

$A_0$  = initial amplitude where  $r = 0\text{m}$  (m/s)

$r$  = pulse travel distance (m)

$\kappa$  = geometric attenuation exponent.

Values of  $\kappa$  depend on the type of waves, where  $\kappa$  is 0 for plane waves, 0.5 for cylindrical waves, and 1.0 for spherical waves.

Other energy losses also occur, in the form of frictional dissipation of the elastic energy into heat. These losses are known as internal friction and can be expressed as shown in equation 5.2. The frequency of the wave affects the attenuation characteristics, with higher frequencies attenuating more rapidly than low frequencies, as the energy loss in higher frequencies is more rapid. The combined effect of both methods of attenuation is given by the relationship given in equation 5.3.

$$A = A_0 e^{-\frac{\pi f}{Qc} r} \quad (5.2)$$

where  $f$  = frequency

$c$  = wave velocity

$Q$  = quality factor

$$A = \frac{A_0 e^{-ar}}{r^\kappa} = \frac{A_0 e^{-\frac{\pi f}{Qc} r}}{r^\kappa} \quad (5.3)$$

where  $a$  = attenuation coefficient

Attenuation is commonly measured using the rock quality factor,  $Q$ , which is defined by the following relationship:

$$a = \frac{\pi f}{Qv} \quad (5.4)$$

The quality factor can found using the rise time relation, as follows:

$$\Omega = \Omega_0 + \frac{Ct}{Q} \quad (5.5)$$

where  $\Omega$  = the pulse rise time (s)

$\Omega_0$  = the initial pulse rise time at  $t = 0$  (s)

$t$  = the time of pulse propagation (s)

$C$  = constant, experimentally estimated to be  $0.53 \pm 0.04$

### **5.3. Apparatus**

The apparatus used for the laboratory experiment is described in the following section.

#### **5.3.1. General**

The laboratory tests were conducted in two stages. The first stage consisted of a preliminary test to measure the waves that can be induced in a column of paste fill with a hammer strike and to determine the most appropriate instrumentation to use to measure the wave. The preliminary test was also used to determine whether or not accelerometers could be recovered from the column on completion of the test. The preliminary test was conducted on paste fill set in a 2.5 m long column which had two accelerometers installed in the column. The accelerometers were connected to an oscilloscope to measure the waveforms produced during the test.

On the completion of the preliminary test, a measuring device was purchased to enable the use of 4 accelerometers in each column in the full test stage of tests. The paste fill was poured in columns that were 2.7 m long and had 4 accelerometers installed in the column. In both stages of the laboratory tests, a steel plate was attached to the paste fill at the end of the column to ensure that the load was applied evenly across the paste fill and to protect the paste fill from damage from repeated hammer strikes to the same spot. Waves were induced in the column with a hammer strike.

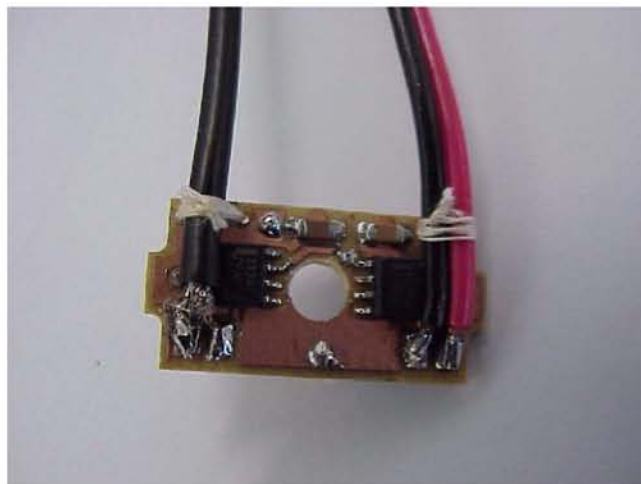
The apparatus for the experiment consisted of the following items:

- Accelerometers;
- Short lengths of 100 mm diameter pvc pipe. These pipe sections were between 0.5 and 0.7 m long;
- 4 pipe joiners for each column;

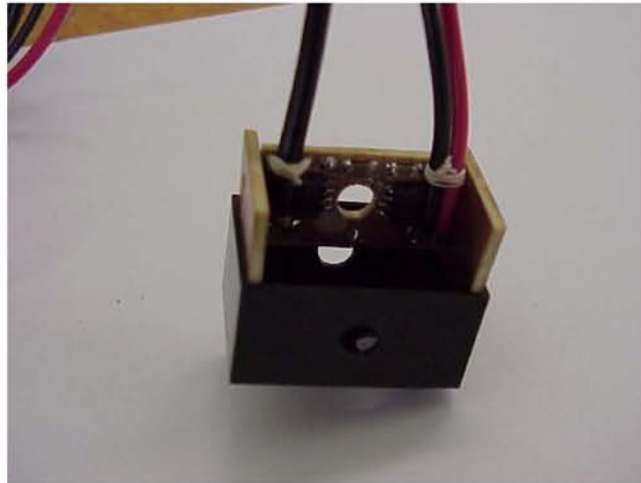
- An end cap for each column;
- Two steel plates for each column;
- An oscilloscope for the preliminary tests;
- A USB 26  $\mu$ DAQ analog data acquisition device;
- Two hammers of different lengths and weights;
- A stand to hold the hammers; and
- A protractor to measure the angle the hammers were raised to before striking the paste fill.

### 5.3.2. Accelerometers

The accelerometers were made by Dr Peter Grabau, from the Electrical and Computer School of Engineering. They consisted of an Analog Devices ADXL202E low-power 2-axis accelerometer connected to a circuit board as shown in Figure 5.1, and encased in resin inside a small black box as shown in Figure 5.2. The purpose of the resin was to protect the accelerometers when they were placed into the paste fill column, as the moisture present during the pouring of the column would have destroyed an unprotected accelerometer. The accelerometers are capable of measuring both dynamic accelerations such as vibration and static acceleration such as gravity. The accelerometers can measure acceleration on 2 axes. The output is a voltage whose duty is proportional to acceleration.



*Figure 5.1 – Accelerometer Connected to Circuit Board*



***Figure 5.2 – Accelerometer Installed in Casing Prior to Pouring Resin***

A problem faced early in the test process was identifying a method of placing the accelerometers into the paste fill column in such a way that the following criteria were met:

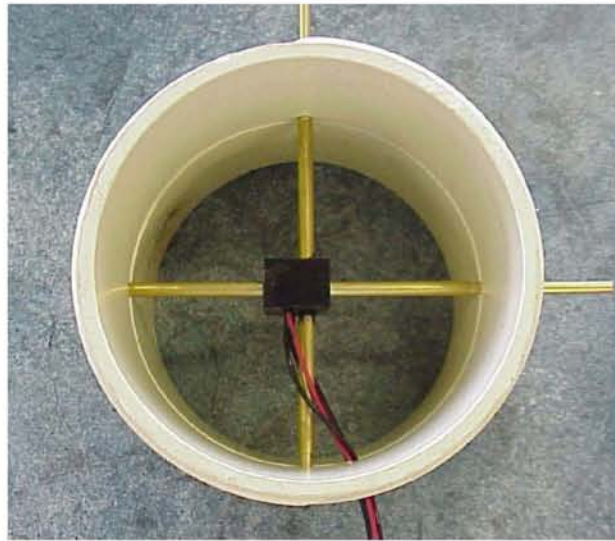
- The accelerometer was not damaged during the pouring and curing of paste fill;
- The accelerometer had good contact with the surrounding paste fill;
- The accelerometer was orientated correctly; and
- The exact location of the accelerometer was known.

In order to protect the accelerometers from damage due to moisture in the paste fill, the accelerometers were encased in a small black box full of resin. In order to allow the accelerometer to be set in the centre of the pipe and in the correct orientation, brass tubes were placed in the black box (see Figure 5.3) during the pouring and setting of the resin. These tubes were used to locate the accelerometer in the centre of the column. Holes were drilled through the pvc pipe joiners and the accelerometers were held in place in the centre of the pipe joiner by placing brass poles through the holes and the brass tubes. Once the paste fill was poured into the column and had set, the brass poles were removed, ensuring that the accelerometer was in contact with only the paste fill, not the pipe. By placing the accelerometers into the paste fill as it was poured, the paste fill set to the accelerometer as it cured, providing good contact between the accelerometer and the paste fill. The holes that were drilled into the wall of the pvc pipe joiner could then be measured to determine the exact location of the accelerometer along the length of the column.

The final problem was setting the accelerometers in the desired location along the length of the pipe. Since a 2.7 m long pipe was used, it would be difficult to reach into the pipe to set an



accelerometer into the middle of the pipe, so an alternative was required. Short lengths of pipe, varying in length between 0.5 m and 0.7 m were used instead, connected with pipe joiners. The accelerometers were placed in the pipe joiners, every 0.5 m along the length of the pipe. The advantage of this system was that it allowed the accelerometers to be placed in the desired location, while eliminating damage to the accelerometers during the compaction of the paste fill. The paste fill was poured in 0.5 m sections and compacted. The joiner containing an accelerometer was then added, before the next pipe section was added, and more paste fill was poured and compacted.

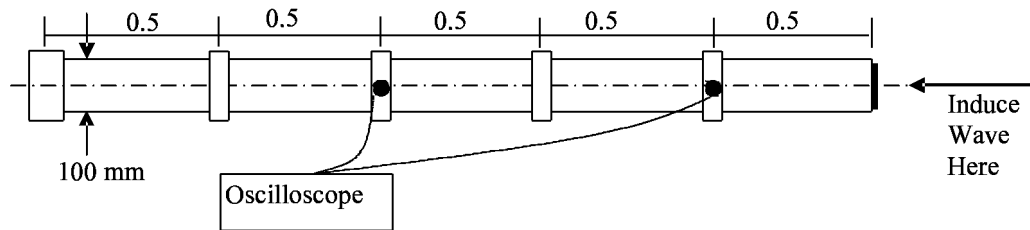


*Figure 5.3 – Accelerometer Installed in Pipe Joiner*

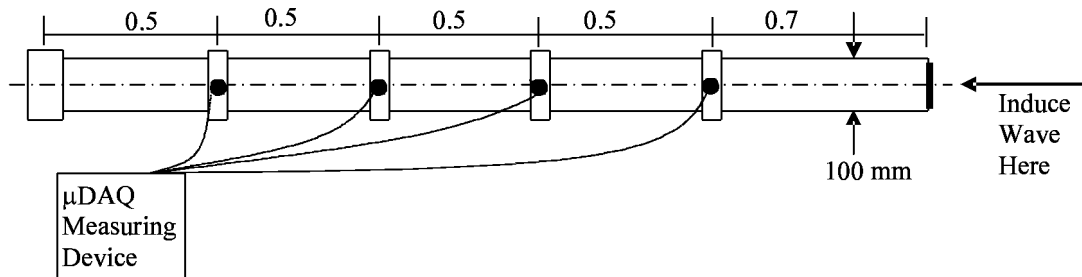
### 5.3.3. Pipe

Rather than set the paste fill into a single long pipe, short sections of pipe were used and joined together using pipe joiners. These pipes varied between 0.5 and 0.7 m in length. This not only allowed the accelerometers to be placed in the correct orientation, but it also allowed the paste fill to be correctly poured and compacted. Steel plates were used on each end of the paste fill column to allow the ends to be hit with a hammer without damaging the paste during testing. By placing the steel plates on the ends during pouring, the plates were set in place as the paste fill cured, eliminating the need to use an adhesive. During pouring, the paste fill was compacted using a steel rod. This was done in order to simulate the paste fill found in stopes in Cannington Mine, where the huge distance the paste fill falls to the stope acts to compact the wet material.

For the preliminary test, 0.5 m lengths of pipe were joined together to form a 2.5 m long pipe, and the accelerometers were placed 1 m apart, 0.5 m from one end of the pipe. Steel plates were used to cover the end of the pipe, so that when a wave was induced with a hammer, it was uniformly distributed over the end surface, and the paste fill ends were not damaged. The apparatus for the preliminary test is shown in Figure 5.4.



**Figure 5.4 – Apparatus for Preliminary Test**



**Figure 5.5 – Apparatus for the Full Test Stage**

For the full test stage, four 0.5 m long pipe sections and one 0.7 m long pipe section were joined together to form a 2.7 m long pipe. Four accelerometers were placed in the column, 0.5 m apart and 0.5 m from one end of the pipe. Steel plates were used to cover the end of the pipe, so that when a wave was induced with a hammer, it was uniformly distributed over the end surface, and the paste fill ends were not damaged. The apparatus for the stage 2 tests is shown in Figure 5.5.

### 5.3.4. Measuring Device

An oscilloscope was used to measure the acceleration during the preliminary test and the calibration of the accelerometers. The oscilloscope however could not be used to measure signals from more than two accelerometers at any one time. For this reason, an Eagle Technology USB 26  $\mu$ DAQ analogue data acquisition device was used for the full test. The  $\mu$ DAQ has 16 analogue input channels. Data measured from the  $\mu$ DAQ software was converted into Microsoft Excel format to allow analysis of the waveforms.

### 5.3.5. Hammer

A hammer was used to induce a wave in the paste fill by striking the end of the column. In order to supply a consistent force each time to the column, the hammer was set up so that it swung on a pivot point, striking the paste fill column as it reached the vertical position. A protractor was used to measure the angle the hammer was lifted to. The hammer was raised to a set angle and then allowed to fall. Two different sized hammers were used to induce waves of varying magnitude in the paste fill. The hammer apparatus is shown in Figure 5.6.



*Figure 5.6 – Hammer used to Initiate Waves in Laboratory Tests*

#### **5.4. Test Methodology**

The test methodology is described in the following section.

##### **5.4.1. Preparation of Paste fill**

Several drums of tailings were provided by Cannington Mine for use in the laboratory tests. The tailings in these drums were found to have quite a high water content, so they were allowed to dry until the water content was reduced to below the water content required for the laboratory tests. The water content of the partially dried tailings was determined to allow calculation of the quantities of cement and water to be added to the fill to create the appropriate mix. The following steps were followed to prepare the paste fill:

1. The water content of the tailings provided by Cannington Mine was determined.
2. The tailings were allowed to air dry.
3. The water content of the dried tailings was determined.
4. The quantity of tailings, water and cement required to produce the desired mixture of paste fill was calculated.
5. The tailings required for the mixture was measured and placed into the cement mixer.

6. The water and cement required for the paste fill mixture was measured. The cement mixer containing the tailings was turned on and the water and cement powder were added to the cement mixer, as shown in Figure 5.7.
7. The cement mixer was left running for half an hour to ensure that the paste fill was uniformly mixed.
8. The columns were poured with paste fill.

The paste fill mixtures used for the laboratory tests are given in Table 5.1.



*Figure 5.7 – Paste Fill Being Mixed in the Cement Mixer as Cement is Added*

**Table 5.1 Paste Fill Mixes used in Laboratory Tests**

Column	Preliminary	1	2	3	4	5	6
Cement content (%)	4	3	4	3	4	4	2
Solids Content (%)	74	77	77	79	79	77	79

#### **5.4.2. Pouring of Columns**

The pouring method consisted of the following steps:

1. Prepare paste fill as outlined in section 5.4.1.
2. Place end cap onto a length of pipe and sit steel plate within the pipe inside the end cap. Pour in paste fill while pipe is standing upright. Compact with a steel rod.
3. Place a pipe joiner containing an accelerometer on to pipe. A paste fill column poured and compacted to the first pipe joiner is shown in Figure 5.8.



*Figure 5.8 – Paste Fill Column Filled to the First Accelerometer*

4. Place next section of pipe into pipe joiner. Pour in paste fill and compact.
5. Repeat Steps 3 and 4 three times, ensuring that the accelerometer in each new pipe joiner is aligned the same way as the first accelerometer.
6. Place steel cap on the top of the pipe. Cure upright for 7 days. A finished paste fill column is shown in Figure 5.9.
7. Relocate paste fill column to sit horizontally on a long bench to allow for testing. Three columns are shown in Figure 5.10.

### **5.4.3. Test Procedure**

The columns were tested at curing ages of 7, 14 and 28 days. The following methodology was followed for the testing of the columns:

1. The hammer was positioned on the stand so that the tip of the hammer lined up with the centre of the steel plate, which was marked on the plate. The hammer stand was positioned in front of the steel plate so that the tip of the hammer touched the steel plate when the hammer hung freely from the hammer stand.
2. The hammer was positioned on the stand so that the tip of the hammer lined up with the centre of the steel plate, which was marked on the plate. The hammer stand was positioned in front of the steel plate so that the tip of the hammer touched the steel plate when the hammer hung freely from the hammer stand.



*Figure 5.9 – Finished Paste Fill Column*



*Figure 5.10 – Columns Ready For Testing*

3. The accelerometers were connected to the monitoring device, which was connected to the computer. The monitoring program was set up to record.
4. The hammer was raised to an angle of 15 degrees and then allowed to swing and strike the steel plate at the end of the column.

5. After each hammer strike, the recorded waveforms were checked to ensure that the waveform had been captured and the waveforms were saved to disk. The monitoring program was then set up to record the waveform from the next hammer strike.
6. Steps 3 and 4 were performed twice for each measurement required to ensure that the waveforms obtained were reproducible.
7. The hammer stand was then positioned in front of the steel plate at the opposite end of the column and steps 3 and 4 were repeated.

Waveforms were induced and measured from both ends of the column, and for curing ages of 7, 14 and 28 days.

### ***5.5. Calibration of the Accelerometers***

Prior to using the accelerometers in the laboratory tests, they required calibration. The calibration process was used to obtain the gain of the accelerometer. The accelerometers were calibrated in the mechanical vibrations lab at James Cook University by comparing the accelerometers against a reference accelerometer using a method similar to that outlined in International Standard ISO 16063-1:1998(E) section 5.3. The method used to calibrate the accelerometers and the calibration factors obtained are discussed in the following section.

#### **5.5.1. Method of Calibration**

The accelerometers were calibrated against a reference accelerometer for which the calibration is known. In this method of calibration, both accelerometers are subjected to the same input motion and their outputs are measured. The gain of the new accelerometer can then be calculated from the following equation:

$$s_2 = \frac{U_2}{U_1} s_1 \quad (5.6)$$

where  $s_1$  = the gain of the reference accelerometer

$s_2$  = the gain of the accelerometer being calibrated

$U_1$  = the output of the reference accelerometer

$U_2$  = the output of the accelerometer being calibrated

The input motion was applied to the accelerometers through the use of a shaker table. The shaker table consisted of a shaker which was suspended above an aluminium plate so that the

needle from the shaker is touching the plate as shown in Figure 5.11. The shaker was used to apply sinusoidal motion to the aluminium plate. A frequency analyser connected to the shaker was used in order to vary the frequency of this motion. The accelerometers were attached to the aluminium plate using an adhesive and an oscilloscope was used to measure the output of the accelerometers. The output of the accelerometers was measured for frequencies ranging between 250 Hz and 1000 Hz, which was the range of frequencies expected to be encountered in the laboratory tests. The reference accelerometer was a Bruel & Kjaer accelerometer type 4384 which had the calibration given in Table 5.2.



*Figure 5.11 – Apparatus used to Calibrate Accelerometers*

**Table 5.2 Calibration for Reference Accelerometer**

Description	Value
Charge Sensitivity (pC/g)	983
Voltage Sensitivity (mV/g)	7.85
Capacitance (pF)	1253



### 5.5.2. Calibration Factors

The gain for each accelerometer was calculated using equation 5.6. The results obtained are given in Table 5.3.

**Table 5.3 Calibration of Accelerometers**

Accelerometer Number	Gain (mV/g)
1	271.6
2	344.9
3	78.9
4	226.8
5	228.4
6	342.6
7	426.0
8	265.9
A	341.5
B	485.0

## 5.6. Analysis of Results

A set of acceleration waveforms was obtained from the Laboratory Tests. These waveforms were converted to velocity waveforms and analysed. The results of the laboratory tests are given in the following section.

### 5.6.1. Reproducibility of Results

In order to ensure that the data obtained from this experiment was reproducible, each measurement was repeated. The two waveforms obtained from each measurement were then compared. Waveforms recorded in column 6 at a curing time of 14 days are shown in Figure 5.12. As can be seen, the waveforms have the same shape and the same peak particle velocities.

This was seen for all waveforms which were recorded. These waveforms demonstrate that the method used for the laboratory tests produced reproducible results.

### **5.6.2. Transmission of a Wave through a Column of Paste Fill**

Waveforms were measured at four locations along the column for each hammer strike. A comparison of waveforms measured at 0.5, 1.0, 1.5 and 2.0 m from the location of the hammer strike is shown in Figure 5.13. These are the waveforms measured at column 6 when it had been cured for 14 days. The waveforms for columns 1 to 5 are given in Appendix E. As can be seen, the wave measured at a distance of 0.5 m from the source has a high amplitude and a short wavelength whereas the wave measured at a distance of 2.0 m from the source has a low amplitude and a long wavelength. The reduction of amplitude as the wave travels through the paste fill corresponds to a reduction in peak particle velocity with distance from the source. This result is consistent with the results of the field instrumentation tests (see chapter 4), and the peak particle velocities predicted by the charge weight scaling law (see equation 2.3).

A comparison between the waveforms measured at different locations along the column shows the wavelength increasing and the frequency decreasing with distance from the source. This result indicates that the higher frequencies attenuate before the lower frequencies. This result was observed for each column at each curing age tested. The fast Fourier transform of each waveform was calculated in order to analyse the frequency content of the waveforms. A brief description of the fast Fourier transform method is given in section 3.7.5. The frequency spectrum generated for the velocity waveforms measured in column 6 at a curing age of 14 days is given in Figure 5.14. This figure shows that for the waveform recorded at 0.5 m from the source, some high frequencies are present. These high frequencies are dramatically reduced in the waveforms recorded at 1.0 m from the source and the waveforms recorded at 1.5 m and 2.0 m from the source do not contain any high frequencies. Similar frequency spectrums were obtained for the waveforms recorded in the other columns. In all cases, the frequency spectrums showed that the higher frequencies attenuate faster than lower frequencies in paste fill.

In order to provide a measure of attenuation, the quality factor discussed in section 5.2 was obtained for the paste fill in each column for each curing time. The quality factor was obtained from the relationship between the pulse rise time and the time of pulse propagation which was given in equation 5.5. The pulse rise time and the time of pulse propagation was determined for each measured waveform and plotted. A linear trendline was obtained, from which the slope of the line was equal to  $c/Q$ . The quality factor was then obtained using a value of  $c = 0.53$ .

The quality factors obtained from the laboratory tests are summarised in Table 5.4.

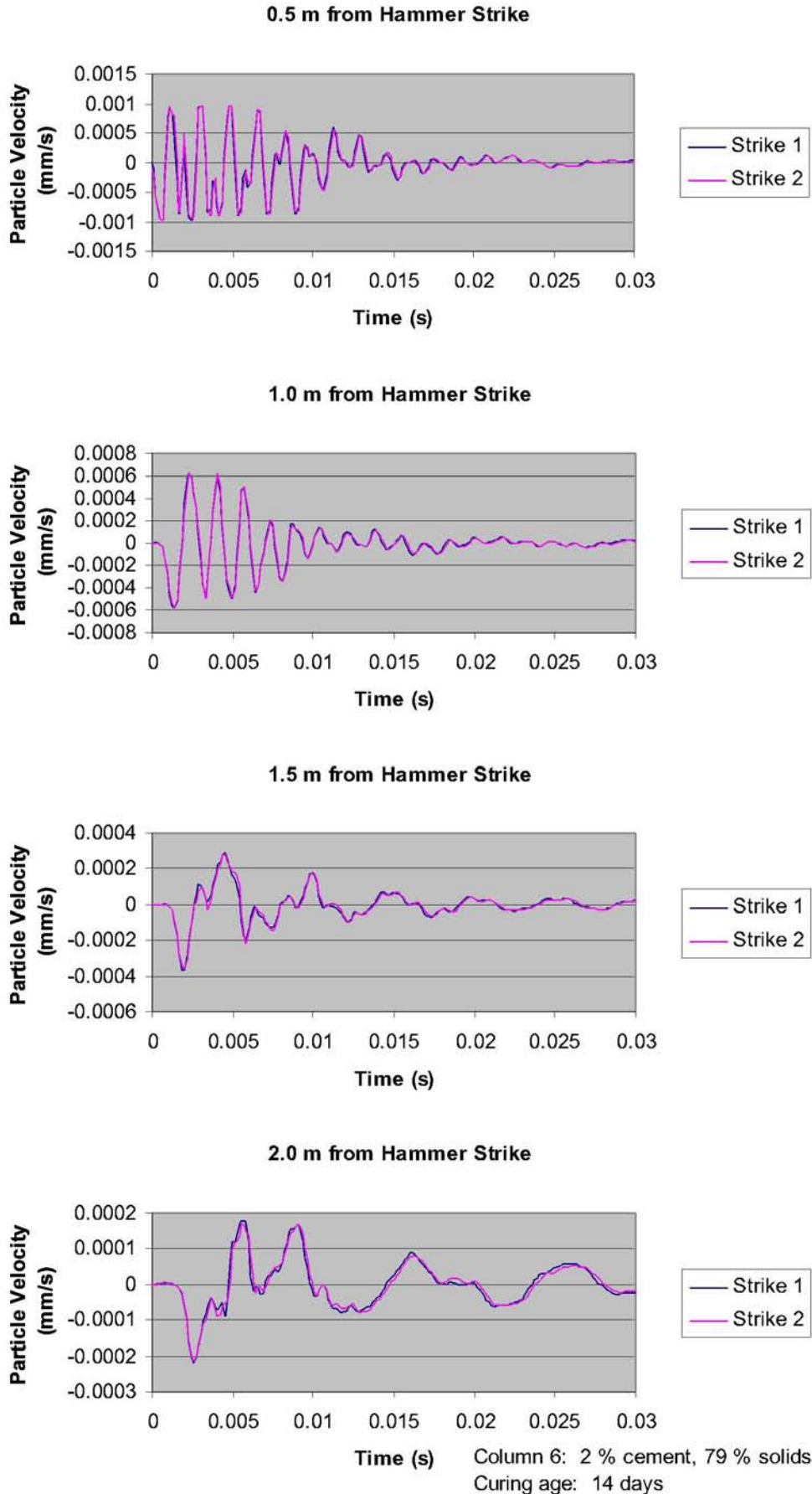
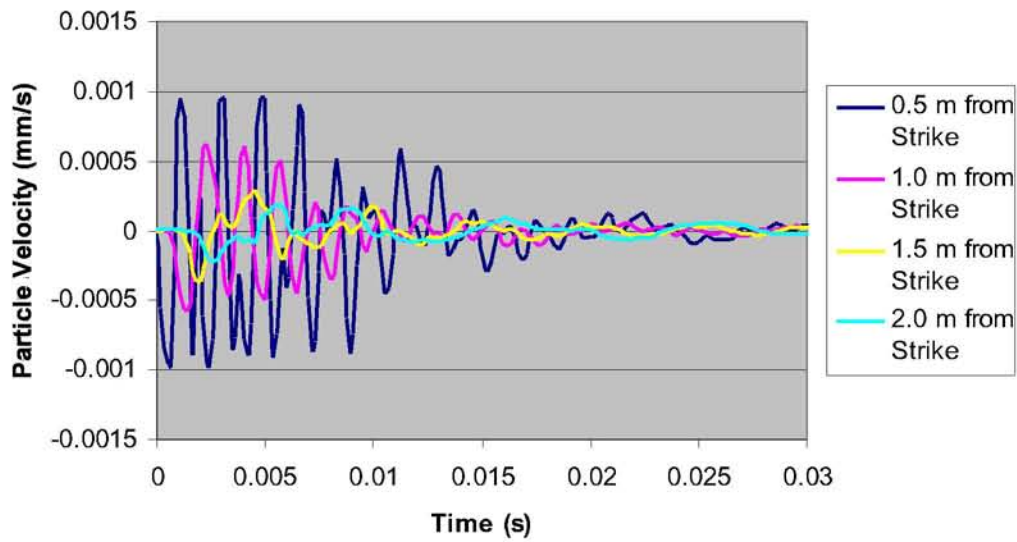
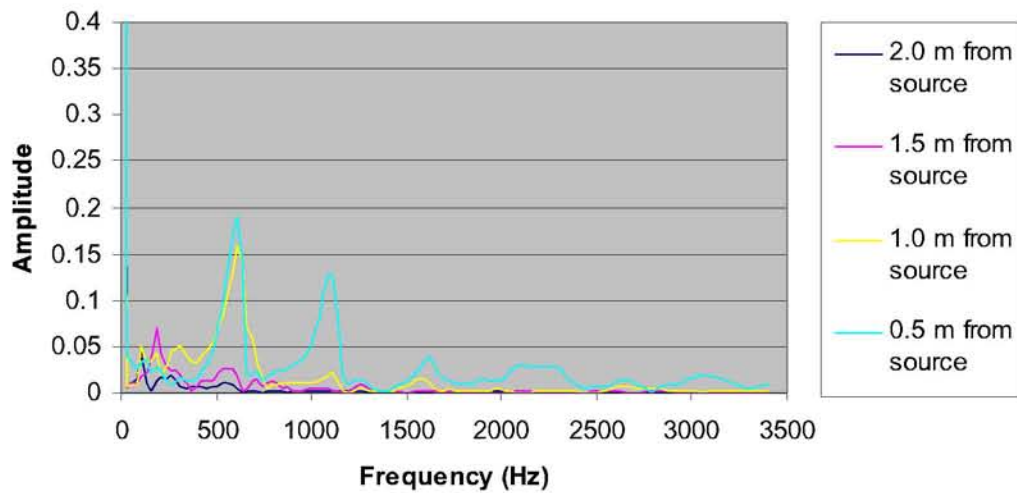


Figure 5.12 – Waveforms Recorded for Column 6 After 14 Days Curing Time



*Figure 5.13 – Comparison of Waveforms Recorded for Column 6 After 14 Days Curing Time*



*Figure 5.14 – Frequency Spectrum for Waveforms Recorded for Column 6 After 14 Days Curing Time*

**Table 5.4 Quality Factors for Paste Fill Obtained in Laboratory Test**

Column	1	2	3	4	5	6
Quality Factor	N/A*	0.78	2.40	0.76	1.06	1.50

\*Insufficient data was obtained to calculate Q as one of the accelerometers was faulty.

### **5.6.3. Effect of Curing Age on Attenuation**

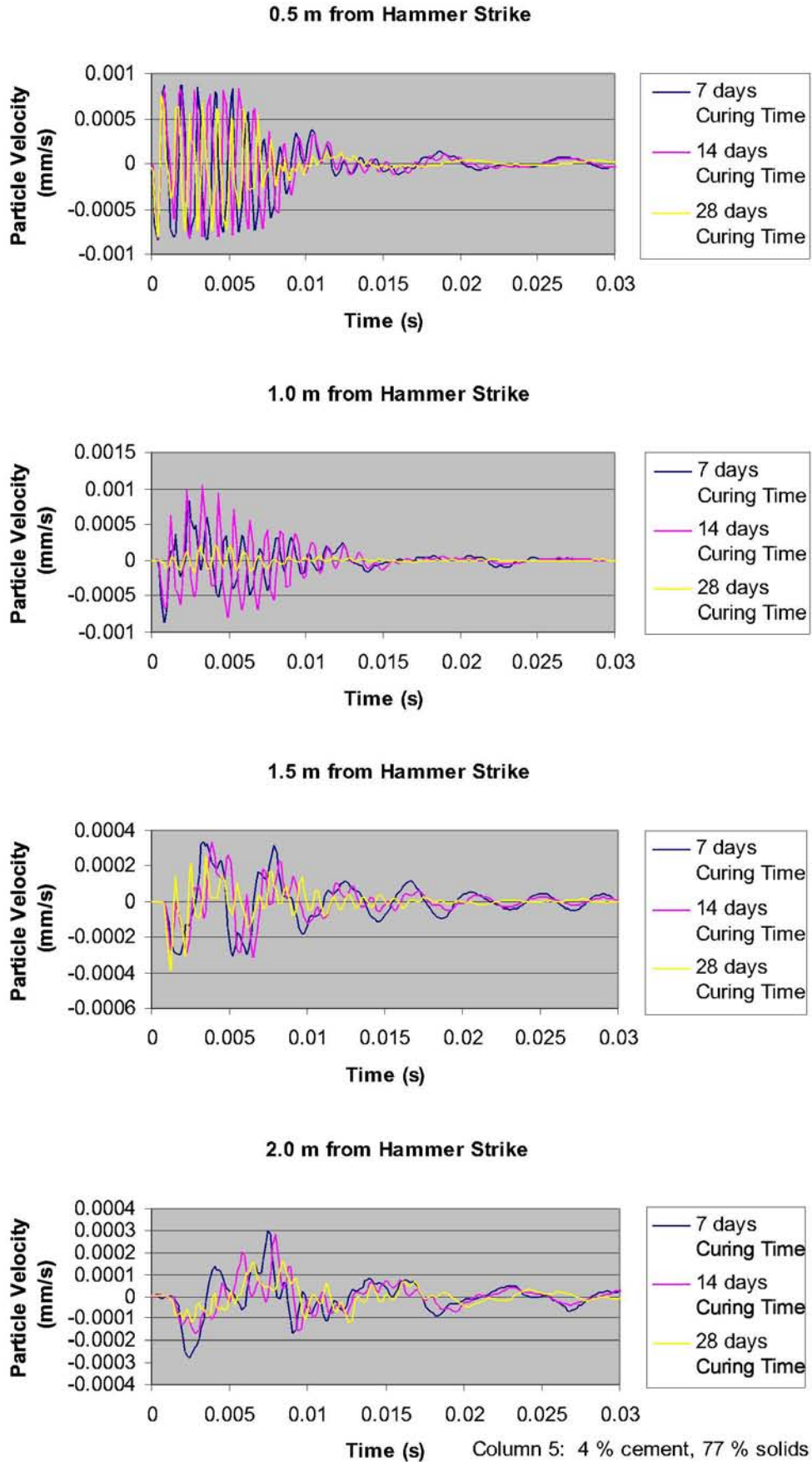
The columns were tested for curing ages of 7, 14 and 28 days. The waveforms recorded at the different curing ages were then compared to determine whether the curing age has an effect on the transmission of a wave through paste fill. A comparison of the waveforms recorded for column 5 is shown in Figure 5.15.

The waveforms recorded for the 7 day and 14 day tests were very similar. As can be seen in Figure 5.15, similar peak particle velocities were recorded at all locations along the column. A slight increase in wavelength was observed between the 7 day and the 14 day tests, with the increase in wavelength becoming more pronounced with distance from the source. The waveforms recorded for the 28 day tests were similar in shape to the waveforms recorded in the 7 and 14 day tests. However, the peak particle velocities from the 28 day waveforms were less than those for the 7 and 14 day tests. A slight increase in wavelength was also observed for the 28 day tests.

These results show that the wave attenuated faster in the paste fill once it had fully cured. The paste fill reaches its full strength when it is just fully cured. Therefore, the results show that as the strength of the material increases, waves attenuate faster within the material. This indicates that waves of a level capable of causing failure of the material are likely to penetrate deeper into a weaker material, resulting in greater failure of that material. Similar observations were made for the other columns analysed. These results indicate that in order to reduce the damage observed in the paste fill during blasting, the paste fill should be allowed to fully cure before it is exposed to nearby blasting.

### **5.6.4. Effect of Paste Fill Mix on Attenuation**

The columns were tested for a number of different paste fill mixes, which are listed in Table 5.1. The waveforms recorded in columns of different paste fill mix were then compared to determine whether the cement or solids content had an effect on the transmission of a wave through paste fill. A comparison of the waveforms with a solids content of 77 % and cement contents of 2 %, 3 % and 4 % is shown in Figure 5.16. As can be seen, waveforms of similar shape were recorded for distances of 1.5 m and 2.0 m. At distances of 0.5 m and 1.0 m, the amplitude in the waveforms recorded in the column with 2 % cement is seen to attenuate much slower than the waveforms recorded in the columns with 3 % and 4 % cement content. This reflects the observations made with the effect of curing time, where the waveforms attenuate slower in the weaker material.



*Figure 5.15 – Comparison of Waveforms Recorded for Different Curing Times*

In Figure 5.16, peak particle velocities and wavelengths were similar in the waveforms recorded at distances of 1.5 m and 2.0 m from the source. Similar observations were made when the waveforms of two different solids contents were compared. As the strength of the paste fill changes with solids and cement content, a greater effect of the material composition on attenuation was expected than that measured. These waveforms were induced from very small loads, resulting in waveforms with very small amplitudes. In order to study the effect of paste fill composition, a greater variety of paste fill mixes and larger loads may be required.

### ***5.7. Summary***

A set of laboratory tests was conducted to study the attenuation of a longitudinal wave travelling through a column of paste fill. These tests involved the generation of a longitudinal wave in a column of paste fill. Accelerometers installed along the length of the column were used to measure the acceleration at four locations along the column, from which the attenuation of the wave within the paste fill could be determined.

The following observations were made as a result of these laboratory tests:

1. Peak particle velocity was observed to decrease with distance from the source.
2. Wavelength was observed to increase with distance from the source.
3. Higher frequencies were observed to attenuate faster than lower frequencies.
4. The wave attenuated faster in the paste fill once it had fully cured and reached its full strength. Therefore, in order to reduce the damage observed in paste fill during blasting, the paste fill should be allowed to fully cure before it is exposed to nearby blasting.
5. As the strength of the material increases, waves attenuate faster within the material.

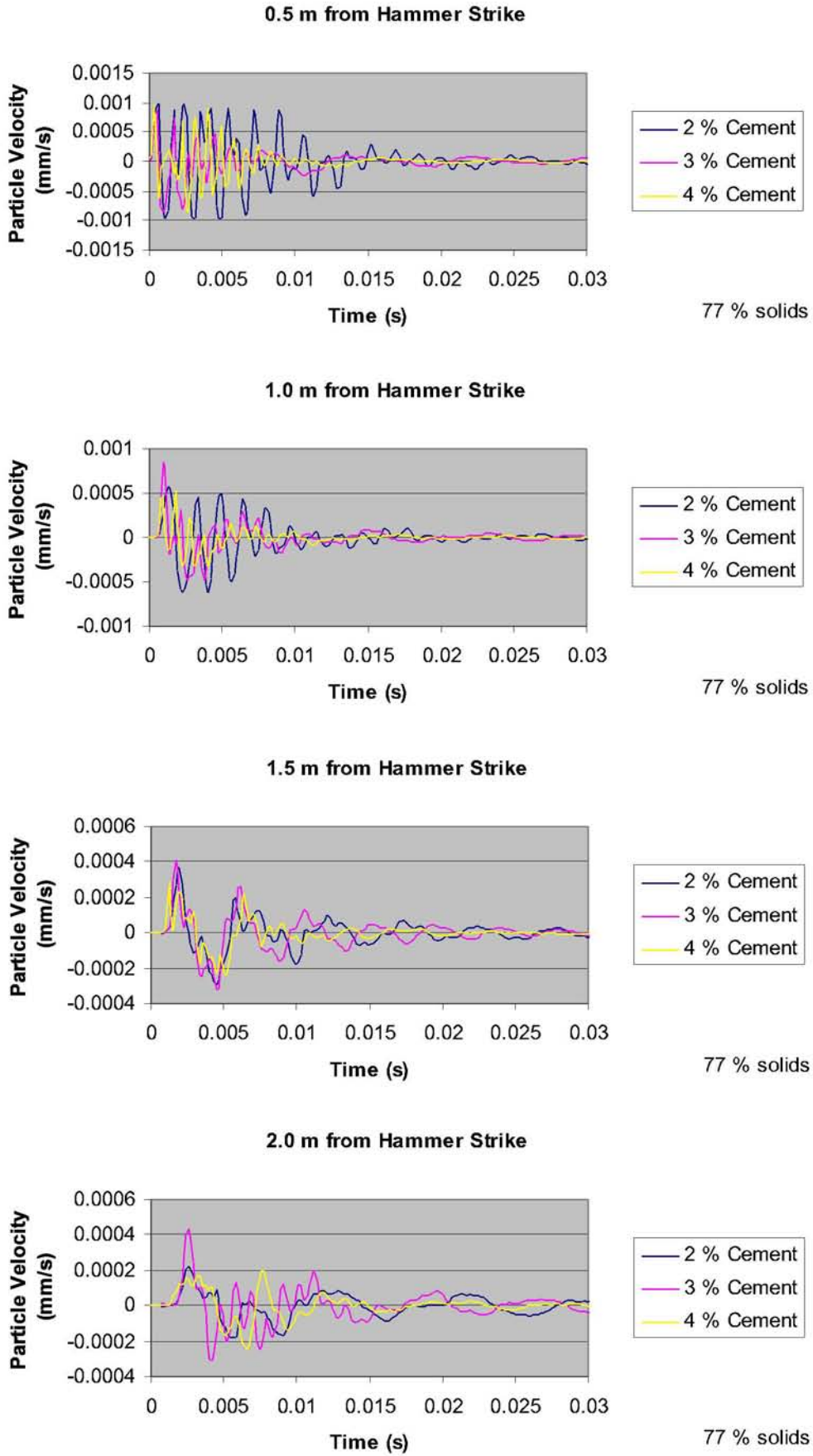


Figure 5.16 – Comparison of Waveforms Recorded for Different Cement Contents



## 6. Applying a Blast Load

### 6.1. Introduction

One of the most important aspects of building a numerical model to estimate the effects of blasting on paste fill is to ensure that a representative blast load is applied to the model. A number of methods of applying a blast load are available. The most suitable method of applying a blast load to a numerical model is dependent on the purpose of the model. For this project, it is necessary that the blast loading function is representative of loads applied to the blast hole walls during a blast, and is numerically efficient. The different methods of applying blast loads available in ABAQUS/Explicit and the method chosen for this project are discussed in this chapter.

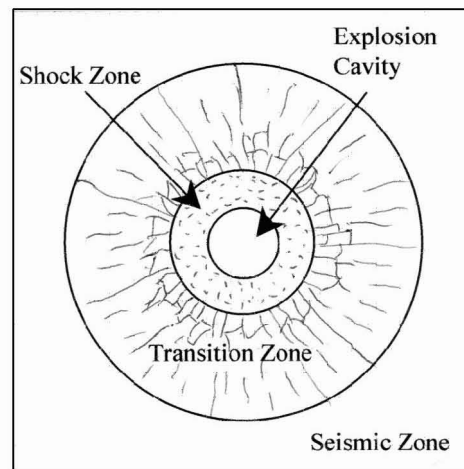
### 6.2. What Happens When an Explosive Detonates?

When an explosive detonates in a blast hole in rock, the chemical reaction produces a gas at a very high temperature and pressure. This gas exerts a very high pressure on the blast hole walls, pushing the walls outwards and shattering the rock surrounding the blast hole. The high pressure sends a stress wave through the rock, which expands radially from the blast hole. The tangential stress from this wave causes radial cracks to occur around the blast hole. The gases then expand into the cracks surrounding the blast hole, opening up the cracks and reducing the pressure of the gas. The response of the material surrounding the blast hole to loading from the detonation of an explosion can be categorized into the following three zones (Brady and Brown, 1993):

1. Shock zone or crushed zone: In the immediate vicinity of the blast hole, the rock behaves mechanically as a viscous solid and the stress wave causes the material to be crushed or extensively cracked. The radius of the shock zone is approximately twice the radius of the blast hole.
2. Transition zone: The transition zone is immediately outside the shock zone. The rock behaves as a non-linear elastic solid subject to large strain in this region. New cracks are initiated in the radial direction in this zone by interaction of the stress wave with the crack population. The radius of this zone is approximately 4 to 6 times the radius of the blast hole.

3. Seismic Zone: Beyond the transition zone, the rock behaves linearly elastically and rock behaviour can adequately be explained by elastic fracture mechanics theory. Crack propagation in this region occurs by extension of the longest cracks in the transition zone.

These zones are shown in Figure 6.1. During blasting in the mine, the paste fill is always located within the seismic zone and never within the shock or transition zone. Therefore the interest in the numerical modelling is mainly with the seismic zone. This can be clearly seen from the field monitoring discussed in Chapter 3. The production blasts monitored consisted of 89 mm diameter boreholes, with a transition zone radius of 0.18 to 0.27 m. The nearest borehole was located 2 m from the paste fill.



**Figure 6.1 – Fragmentation Zones Around a Blast Hole in Rock**

If the stress wave encounters a free boundary, the compressional wave is reflected back as a tensional wave, and cracking known as spalling may occur at the boundary if the tensile stress of the wave is larger than the tensile strength of the rock (Atchison 1968).

As these two energy sources, shock wave and gas penetration, occur both simultaneously and almost instantly, it is difficult to determine which explosive effects occur from each source. A look at the literature shows that authors are divided over which energy source has the greatest effect, and shows that in order to accurately model the damage to the blast hole walls, both effects must be considered. Sarracino and Brinkmann (1990) compared the damage caused by explosives enclosed in metal tubes to prevent gas penetration and normal blast holes. The acceleration and strain measurements showed that the character of shock transmitted from both were the same. Although there is some disagreement between researchers over the effects of the shock wave and the gas penetration, many authors agree that the shock wave stresses and causes acceleration to the surrounding material, while

the majority of fracturing is caused by gases penetrating into crack surrounding the blast hole (Sarracino and Brinkmann, 1990; Daehnke et al., 1996; Liu and Katsabanis, 1997).

The gases produced during the explosion provide the load to the surrounding rock. During detonation, the gases are produced quickly, and so the load would be expected to increase from zero to the maximum load over a very short period of time. When the rock immediately surrounding the blast hole is shattered, the gas expands into the new volume available, reducing the pressure and therefore the blast load. The gas pressure continues to reduce as the gas expands into the cracks produced by the shock waves. This reduction in pressure would be gradual due to the time required for the gas to expand into the cracks. Therefore, the expected shape of the load curve relative to time is a sudden, almost instantaneous increase from zero to maximum load, followed by a gradual decrease.

### ***6.3. Measuring Blast Damage***

In order to model the effect of blasting on paste fill, a measure of blast damage is required. When an explosive detonates, stress waves are generated and travel through the solid, causing ground vibration. This ground vibration causes the particles in the rock mass to run through an elliptical motion, and the highest velocity experienced by the particle is known as the peak particle velocity (ppv). Persson et al. (1994) were able to make reliable predictions of rock damage based on the vibration particle velocities in the rock. Field monitoring results presented in chapter 3 indicate that damage is observed in paste fill when peak particle velocities of the order of 2.5 m/s are experienced.

### ***6.4. Prediction of Peak Particle Velocity***

As discussed in Section 2.3, when an explosive detonates, stress waves are generated and travel through the solid, causing ground vibration. This ground vibration causes the particles in the rock mass to run through an elliptical motion, and the highest velocity experienced by the particle is known as the peak particle velocity (Holmberg and Persson, 1979). The peak particle velocity decreases with distance from the charge, and can be predicted by equation 2.3 for a spherical explosive.

However, explosives are commonly loaded into blast holes, as shown in Figure 2.3. In this figure, the bottom of the blast hole is filled with explosive, and the blast hole is 'stemmed' with an inert material. Holmberg and Persson (1979) modified equation 2.3 to predict the peak particle velocity for

blast waves resulting from columns of explosive, resulting in equation 2.5 which is valid when  $\beta$  is equal to  $2\alpha$ , which is often seen in rock.

As discussed in Section 2.3, Sartor (1999) used this equation to model the vibration induced damage from blasting in rock at Cannington Mine. The constants in the equation were found to be:  $k = 2938$ ,  $\alpha = \frac{1}{2}\beta = 0.66$ . Field tests conducted in paste fill described in Chapter 4 were used to develop a site specific equation for the paste fill at Cannington Mine. The constants were found to be  $k = 1000$  and  $\beta = 1.02$ .

Equation 2.5 can be used to determine the peak particle velocity a loading function should produce at various distances from the charge. This can be used to validate the loading function. The average linear charge density and blast hole length for a set of mass blasts monitored at Cannington Mine is given below in Table 6.1.

**Table 6.1 Blast Parameters for Stope 4760**

<b>Blast Number</b>	<b>Average Blast Hole Length (m)</b>	<b>Average Linear Charge Density (kg/m)</b>
904061	15.7	6.217
904064	2.0	6.223
904065	15.5	6.213
904066	14.7	6.212
904068	20.6	5.563
904072	20.0	5.367
904077	20.1	8.611
904078	20.7	6.300

## **6.5. How Can Blast Loads be Applied in ABAQUS/Explicit**

A literature search including the ABAQUS (2003) manuals revealed the following four methods of applying blast loads in numerical modelling, which are discussed in detail in the following sections:

- Applying a time varying pressure to the walls of the blast hole column;
- Applying a time varying pressure to the walls of the zone in which cracks occur during a blast;
- Applying an incident wave field; and
- Modelling the detonation of the explosive using the Jones-Wilkens-Lee (JWL) Equation of State (EOS) material model.

### **6.5.1. Applying a Time Varying Pressure to the Walls of the Blast Hole**

Perhaps the simplest method of applying a blast load in the numerical model is to apply a pressure to the walls of the blast hole column. IN ABAQUS, the pressure can be applied as a surface load using the \*DSLOAD command in conjunction with the \*AMPLITUDE function to vary the pressure with time. Since the pressure is applied to the walls of the blast hole, the cracking region adjacent to the blast hole must be modelled. This results in the use of a complex material model and cracking model which causes the model to take much longer to solve. This method is appropriate for situations where the cracking pattern or damage adjacent to the blast hole is required, but is not practical for use in a large scale model due to the time required to solve such a model. An example where this method has been used is seen in the work by Grady and Kipp (1980) who used a combination of experimental work and numerical modelling to develop a fracture model for rock incorporating both rate sensitive features of the fracture process and material wave propagation characteristics.

### **6.5.2. Applying a Time Varying Pressure to the Walls of an “Equivalent Cavity”**

This method involves applying the blast load as a time varying pressure using the \*DSLOAD and \*AMPLITUDE commands as discussed above, however the load is applied at a boundary beyond the cracking zone of the blast hole. This enables simpler material models to be used for the analysis which reduced the computation time for the model. Examples where this method has been used include Jiang et al. (1995), Minchinton and Lynch (1996), Blair and Minchinton (1996), Blair and Jiang (1995) and Potyondy et al. (1996). The applications of these models included studying the

damage zone around a blast hole (Blair and Minchinton 1996) and studying surface vibrations due to a vertical column of explosive (Blair and Jiang 1995).

### 6.5.3. Incident Wave Field

The \*INCIDENT WAVE option is used in ABAQUS to apply incident wave loads such as those experienced due to an underwater explosion or a blast in air. This method is designed to model loads due to external wave sources, which occur in a fluid external to the structure of interest. This fluid is often air or water. Different methods are available depending on whether the user wishes to model the wave in the fluid and the structure, or the wave only in the structure (ABAQUS 2003). Since blasting in an underground mine involves explosives detonated in the rock mass, and not in a fluid, the \*INCIDENT WAVE option was not considered a feasible option for loading the numerical model. Applications of this method include modelling the impact of air blasts or underwater explosions on nearby structures.

### 6.5.4. Modelling the Chemical Reaction using the Jones-Wilkens-Lee Equation of State Material Model

Jones-Wilkens-Lee (JWL) equation of state material model (Lee et al., 1973) is used to model the detonation of non-ideal detonation. It was developed to allow fitting to pressure data obtained using the cylinder expansion test, and has been used in the design of explosive devices and in the modelling of non-ideal detonations (Persson et al., 1994).

This method involves modelling the generation of pressure as the explosive detonates by assigning the JWL material model to the explosive elements and defining detonation points in the explosive. The material model is defined using the \*DENSITY, \*EOS, TYPE=JWL and \*DETONATION POINT keywords. The JWL equation of state used in ABAQUS can be written in terms of the initial energy per unit mass as follows (ABAQUS 2003):

$$p = J \left( 1 - \frac{\Theta \rho}{\Psi_1 \rho_0} \right) e^{-\Psi_1 \frac{\rho}{\rho_0}} + B \left( 1 - \frac{\Theta \rho}{\Psi_2 \rho_0} \right) e^{-\Psi_2 \frac{\rho}{\rho_0}} + \frac{\Theta \rho^2}{\rho_0} e_{m_0} \quad (6.1)$$

where  $J$ ,  $B$ ,  $\Psi_1$ ,  $\Psi_2$  and  $\Theta$  are material constants

$e_{m_0}$  is the initial energy per mass unit

$\rho_0$  is the density of the explosive

$\rho$  is the density of the detonation products

The arrival time of the detonation wave at a material point is calculated as the distance from the material point to the nearest detonation point divided by the detonation wave speed, and takes into account the detonation delay of the given detonation point (ABAQUS 2003).

This method was used by Yang et al. (1996), Liu and Katsabanis (1996) and Thorne et al. (1990). Applications included the development of constitutive models for blast damage (Yange et al. 1996, Liu and Katsabanis 1996) and investigation of the fundamental mechanisms of cratering (Thorne et al. 1990).

### **6.5.5. Discussion of Blast Loading Methods**

The advantages and disadvantages of the methods discussed above are given in Table 6.2. The method of blast loading to choose for any project depends on the purpose of the modelling and the desired results. The purpose of this project is to assess the effects of blast loads on nearby paste fill material. The blast holes are located in the rock, and the paste fill material is located near by but outside the cracking zone of the blast hole. The lack of symmetry in the region of interest requires the full paste fill stope to be included in the model, resulting in large scale models in 3-dimensions. Due to the large scale of the model, a blast loading method that is numerically efficient is required to ensure that the model can be solved within a reasonable time frame. The results of interest are the velocities experienced in the nearby paste fill as a result of the blast. Therefore, the blast loading method for this project must provide reliable results in the paste fill at a distance from the blast source, but reliable results within the cracked zone are not necessary. The method of applying a pressure to the walls of the zone in which cracks occur (see section 6.5.2) was found to satisfy these requirements.

### **6.6. Concept of an “Equivalent Cavity”**

A cylindrical “equivalent cavity” was used in order to model only the seismic zone, in which elastic wave propagation is expected to occur. This method avoids modelling the region where new cracks in the material are initiated from the shock wave during an explosion. The concept of an “equivalent cavity” was first proposed by Sharpe (1942). Sharpe’s work, and work by other authors (Kutter and Farihurst, 1971; Blair and Jiang, 1995) have shown that the use of an “equivalent cavity” gives reasonable agreement with field measurements. When this concept is used, the blast pressure is applied to the walls of the “equivalent cavity” instead of the walls of the blast hole. The radius of the

**Table 6.2 Advantages and Disadvantages of Methods of Applying a Blast Load**

<b>Method</b>	<b>Advantages</b>	<b>Disadvantages</b>	<b>Typical Use</b>
Applying a time varying pressure to the walls of the blast hole column (see section 6.5.1)	Accurately models the effects of a blast load to the rock mass surrounding the blast hole, including cracking	Numerically expensive due to complex cracking models and small mesh sizes required.	Generally used for modelling the cracking in the region immediately surrounding the blast hole. Not generally used for large scale models.
Applying a time varying pressure to the walls of the zone in which cracks occur during a blast (see section 6.5.2)	Accurately models the effects of a blast load to the rock mass surrounding the cracked region  Numerically efficient	Does not provide accurate model results in the cracked region surrounding the blast hole	Used to model the transmission of the shock wave through the material
Applying an incident wave field (see section 6.5.3)	Models the loading on structures due to explosives blasts in a “fluid” external to the structure	Not applicable for cases where the blast occurs within the structure of interest.	Generally used for loading due to underwater explosions on structures or airblast loading on structures
Model the chemical reaction in a blast hole using the JWL Equation of State Material Model (see section 6.5.4)	Accurately models the explosion in a blast hole and the loading on the rock mass surrounding the blast hole, including cracking	Numerically expensive due to complex reactions in the blast hole and complex cracking model and small mesh sizes required.	Generally used for modelling the cracking in the region immediately surrounding the blast hole. Not generally used for large scale models.



cavity is set a distance from the blast hole wall that ensures that the strength of the material is greater than the stresses experienced from the shock wave, which is typically thought to occur between 3 and 9 times the blast hole radius (Kutter and Fairhurst, 1971). A value of 3 times the blast hole radius was used in this dissertation. This will result in the load being applied in the transition zone shown in Figure 6.1.

The method of using an equivalent cavity allows the behaviour of the material in the seismic zone to be modelled without the need to model the cracking that occurs around the blast hole. For large scale models such as those used in this work, this method dramatically reduces the solving time of the models, as complex material models and cracking models are not required. As the paste fill is not in the area immediately surrounding the blast hole where cracks are expected to occur, the development of the cracks surrounding the blast hole does not need to be modelled. It is the shockwave travelling through the ore and into the paste fill which causes the damage to the paste fill and threatens the stability of the stope. In ABAQUS, if a sufficient load is applied to the model, the program will model the transmission of the shock wave through the material. Hence, an initial load is required that will transmit an equivalent shock wave through the model as that measured in the field. Since the purpose of this work is to model the behaviour of paste fill rather than the behaviour of the rock in the immediate vicinity of the blast hole, the use of an equivalent cavity is appropriate. However, the use of an equivalent cavity would not be suitable if the behaviour of the rock in the vicinity of the blast hole was required.

### ***6.7. Explosives Being Modelled***

The loading function applied to the numerical model will be dependent on the explosive used in the given application. Emulsion type explosives were used in both the field tests and the production blasts at Cannington Mine. In the test blasts in paste fill, cartridges of the explosive Powergel Powerfrag were used, and in the production blasting that was monitored, the explosive Powerbulk VE, at a density of approximately  $1.0 \text{ g/cm}^3$  was used. Both explosives were supplied by Orica. Information about these explosives is given in the Tables 3.1 (Powerbulk VE) and 4.2 (Powergel Powerfrag).

Powergel Powerfrag is a high strength, detonator sensitive packaged explosive. It is designed for priming applications, such as the initiation of explosive columns, and for use as a medium density column explosive in mining and general explosive work. Powergel Powerfrag is supplied in cartridges. Powerbulk VE is a primer sensitive bulk emulsion explosive that has been designed for

used in underground blasting applications. Powerbulk VE is a fluid with a viscosity similar to that of heavy grease. It is pumped into boreholes and can be used for boreholes of up to 35 m length. The explosive can be detonated using either a primer or a Powergel packaged explosive cartridge in conjunction with a detonator.

### **6.8. Form of the Loading Function**

As discussed in section 6.2, the pressure from an explosive blast is expected to increase to maximum pressure quickly, and slowly dissipate as the gasses penetrate the cracked region. In ABAQUS, a time-varying pressure is applied using the *\*DSLOAD* function in conjunction with the *\*AMPLITUDE* function. When the load is applied, the data lines on the *\*DSLOAD* function include the name of the amplitude function, and the maximum pressure. The maximum pressure is then multiplied by the amplitude function. Therefore, a 'unit' amplitude function is required.

The literature was consulted at this point of the development of the blast loading function to determine the expected shape for a blast loading function, or the functions used in numerical models by other researchers. A summary of loading functions used to model explosive materials is given in Table 6.3. These loading functions were used to model a variety of scenarios. Only the functions used to model blasting in a mine were considered as a possible loading function for use in this dissertation. Jiang et al. (1995) used the function given as equation 2.10 to model an emulsion explosive in rock, by applying the pressure to the walls of an equivalent cavity. Emulsion type explosives are also used at Cannington Mine. Therefore, the loading function represented by equation 2.10 was used to apply blast loads to the numerical models. The unit function is shown in Figure 6.2 for  $n = 1$  and  $\beta = 2000$  used by Jiang et al. (1995). These values for  $n$  and  $\beta$  were adopted for this work. The calculation of the initial peak pressure is discussed in section 6.8.1.

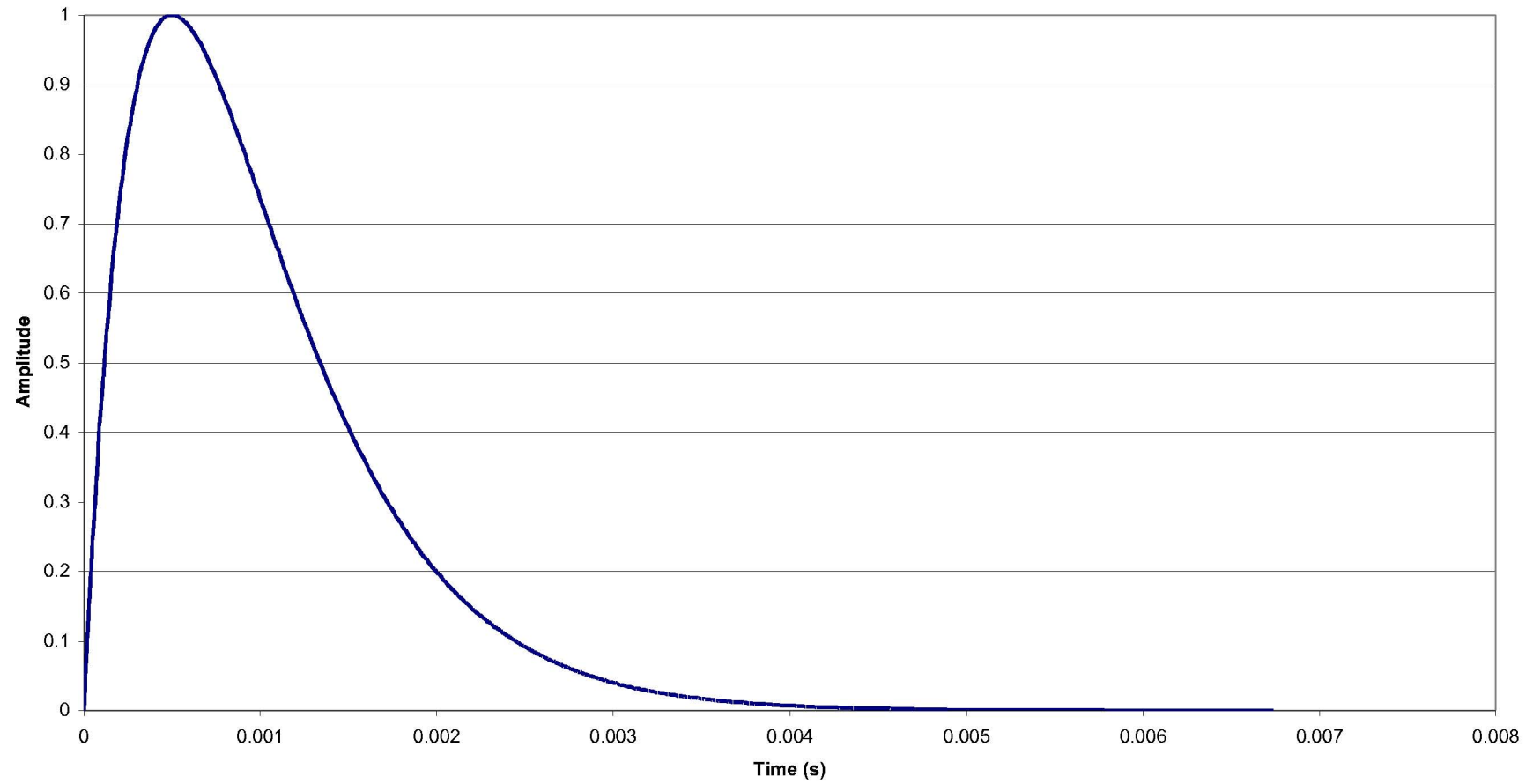
**Table 6.3 Loading Functions found in Literature**

Loading Function	Description	Reference
$p(t) = p_0 \left( 1 - \frac{t}{t_0} \right)$ <p>where <math>p_0</math> = initial peak pressure <math>t_0</math> = duration of blast loading</p>	Modelled the loading from a spherical source in air on aluminium cladding using LS-DYNA.	Hanssen et al. (2002)
$p(t) = p_0 \left( \frac{t}{t_0} \right) e^{-t/t_0}$ <p>where <math>p_0</math> = initial peak pressure <math>t_0</math> = duration of blast loading</p>	Modelled a cylindrical blast by applying the pressure to the blast hole wall. Interested in the explosive fracture in oil shale.	Grady and Kipp (1980)
$p(t) = p_0 t^n e^{-\varphi t}$ <p>where <math>p</math> = pressure <math>p_0</math> = initial peak pressure <math>t</math> = time <math>n</math> = constant <math>\varphi</math> = constant</p>	Modelled explosive in rock, applying pressure load to walls on an equivalent cavity. Some authors used a spherical source, others a cylindrical source.	Jiang et al. (1995)  Minchinton and Lynch (1996)  Blair and Minchinton (1996)  Blair and Jiang (1995)

Loading Function	Description	Reference
$p(t) = p_{ra} \left[ 1 - (t - t_a) \right] e^{-\frac{t-t_a}{b/T_s}}$ <p>where <math>p_{ra}</math> = resulting peak overpressure  <math>t_a</math> = arrival time  <math>b</math> = waveform parameter  <math>T_s</math> = positive phase duration</p>	<p>Modelled the explosion of a bomb in a city street using small-scale experiments and numerical simulation. This was a spherical source from an air blast.</p>	Smith et al. (2000)
$v_r(t) = 0 \quad 0 \leq t \leq t_a$ $v_r(t) = \frac{v_r^{\max}}{0.1t_a} (t - t_a) \quad t_a \leq t \leq 1.1t_a$ $v_r(t) = v_r^{\max} \left[ 1 - 0.4 \left( \frac{t - t_a}{t_a} \right) \right] e^{-0.4 \left( \frac{t - t_a}{t_a} \right)} \quad 1.1t_a \leq t$ <p>where <math>v_r</math> = radial velocity relative to the centre of charge  <math>v_r^{\max}</math> = peak radial velocity  <math>t_a</math> = arrival time of ground shock time, <math>t_a = \frac{r}{c_p}</math>  <math>r</math> = distance from centre of charge  <math>c_p</math> = longitudinal seismic velocity  <math>t</math> = time after explosion</p>	<p>Modelled ground shock wave propagation using FLAC to consider the effect of explosive loads in the design of underground civil defence structures. A spherical explosive source was assumed.</p>	Olofsson et al. (1999)

Loading Function	Description	Reference	
$p(t) = p_m \frac{t}{t_r}$	$t < t_r$	Applied a time-varying pressure to the outer surface of a cylinder three times the diameter of the actual blast hole, avoiding simulation of the crushed zone. A cylindrical source was used.	Potyondy et al. (1996)
$p(t) = p_m$	$t_r \leq t < t_f$		
$p(t) = p_m (0.76 + 2000t)^{-2}$	$t \geq t_f$		
<p>where <math>p_m</math> = maximum pressure  <math>t_r</math> = rise time  <math>t_f</math> = fall-off time</p>			
$p(t) = p_0 \sin(\omega t)$	Modelled a sill mat in a mine which was subjected to seismic loads	O'Hearn and Swan (1989)	
	Modelled structural response to sinusoidal excitation and real blast vibration transients	Todo and Dowding (1984)	

Loading Function	Description	Reference
Linear Pressure Pulse  maximum pressure at $t = 0$ s  zero pressure at $t = 0.00108$ s	Modelled sacrificial claddings under blast loading from an air blast explosion (spherical source)  Noted the spherical pressure front can be approximated as a plane pressure front if the distance of explosion is high compared to the dimensions of the plane surface that is subjected to the blast loading.	Guruprasad and Mukherjee (2000)
JWL Equation of State	Modelled cratering due to an explosive charge, using a new damage model for rock.	Yang et al. (1996)  Liu and Katsabanis (1996)  Thorne et al. (1990)



*Figure 6.2 – Unit Loading Amplitude Applied to ABAQUS/Explicit Models*

### 6.8.1. Calculating the Initial Peak Pressure

The calculation of the initial peak pressure used in the loading function (equation 2.10) is discussed in this section. The initial peak pressure was calculated for two cases, the explosion of a Powergel Powerfrag cartridge in paste fill, and the explosion of Powerbulk VE in rock (see Tables 4.2 and 3.1). The method used in this calculation is outlined below. The finite element models created for this dissertation were created through a three stage modelling process. The first stage of the modelling process involved validating the numerical model results of the transmission of blast waves through paste fill against data from the field instrumentation tests. The models created for stage 1 consisted of a single blast hole located in paste fill. Since the stage 1 model was based on the field instrumentation tests in which one cartridge of explosive was loaded into the blast hole, the pressure blast calculated for the explosion of a Powergel Powerfrage cartridge was applied to the model.

The second stage of the process involved validating the numerical model results of the transmission of blast waves through rock against the peak particle velocity predictions obtained from equation 6.3 and the stage 2 model consisted of a single blast hole located in a body of rock. The third and final stage of the modelling process involved modelling blast holes located in rock at various distances from a paste fill stope. The blast pressure calculated for a column of Powerbulk VE was applied to both the stage 2 and stage 3 models. The problem definition and geometry of the models from all three stages are discussed in section 7.3.

1. The following numerical models of a single blast hole were used:
  - a. Paste Fill: The stage 1 model, described in section 7.3.2, was used to model the detonation of a cartridge of explosive located in paste fill. This model was based on the field instrumentation tests described in chapter 4. The axisymmetric model consisted of a 3 m deep borehole, which was assumed to contain a 0.2 m long cartridge of explosive material. An area 15 m wide and 6 m deep was modelled, with infinite elements along the side and base of the model in order to provide a non-reflecting boundary. The mesh for the stage 1 model is shown in Figure 7.3.
  - b. Rock: Model 2, described in section 7.3.3, as used to model an explosive column in rock. The axisymmetric model consisted of a 3 m deep borehole, which was assumed to consist of 2 m of explosive material and 1 m of stemming material. An area 15 m wide and 6 m deep was modelled, with infinite elements along the side and base of the model in order to provide a



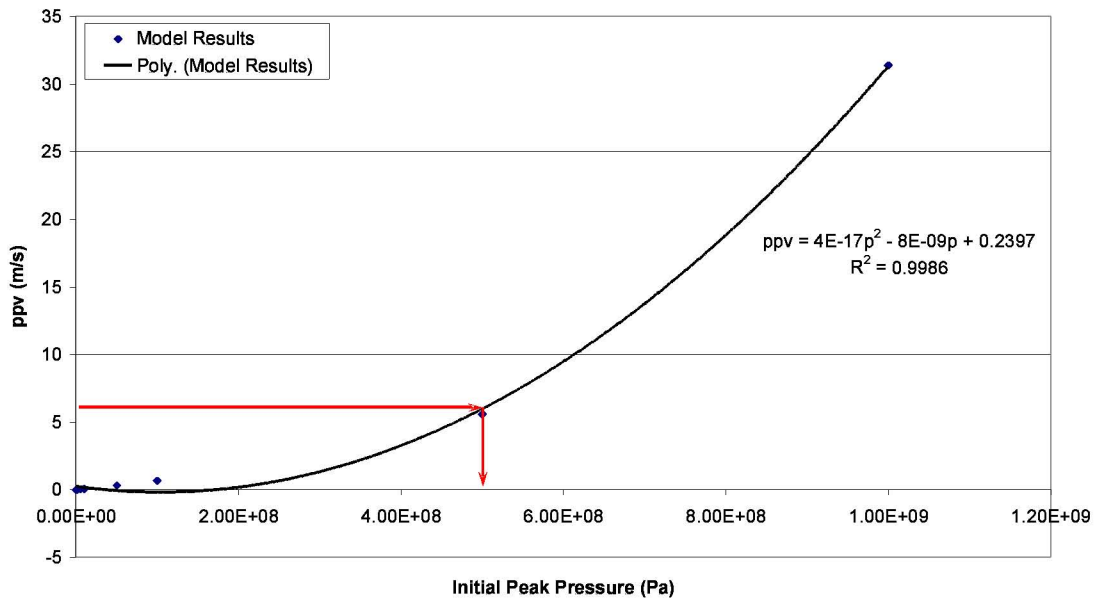
non-reflecting boundary. The mesh for the stage 2 model is shown in Figure 7.5.

2. The model was solved for a variety of blast loads using the time varying amplitude specified by equation 6.5 and initial peak pressures ranging between 100 kPa and 1000 MPa. For each loading case, the peak particle velocity (ppv) was computed at a number of points in the model that were located between 0.5 m and 14.0 m from the centreline of the blast hole.
3. The results from all of the different loading cases were collated. For each point at which the ppv was calculated, the ppv calculated by the model was plotted against the initial peak pressure applied to the model. This created a separate plot for each point of interest which showed the effect of the peak initial pressure on the ppv induced in the surrounding material. Trend lines were fitted to the model results. The plots for the points located 2.0 m and 5.0 m from the centreline of the blast hole in rock can be seen in Figure 6.3. The plots created in this step were used in steps 4 and 5 to estimate the peak initial pressure that should be applied to the model to produce the peak particle velocities shown in the experimental data.
4. For each plot created in step 3, the ppv was predicted using the formulae presented in section 6.4. The initial peak pressure to be applied to the model to calculate this ppv was then read from the plot as shown in Figure 6.3.
5. The initial peak pressure value to apply to the models was the average of the values obtained in step 4.

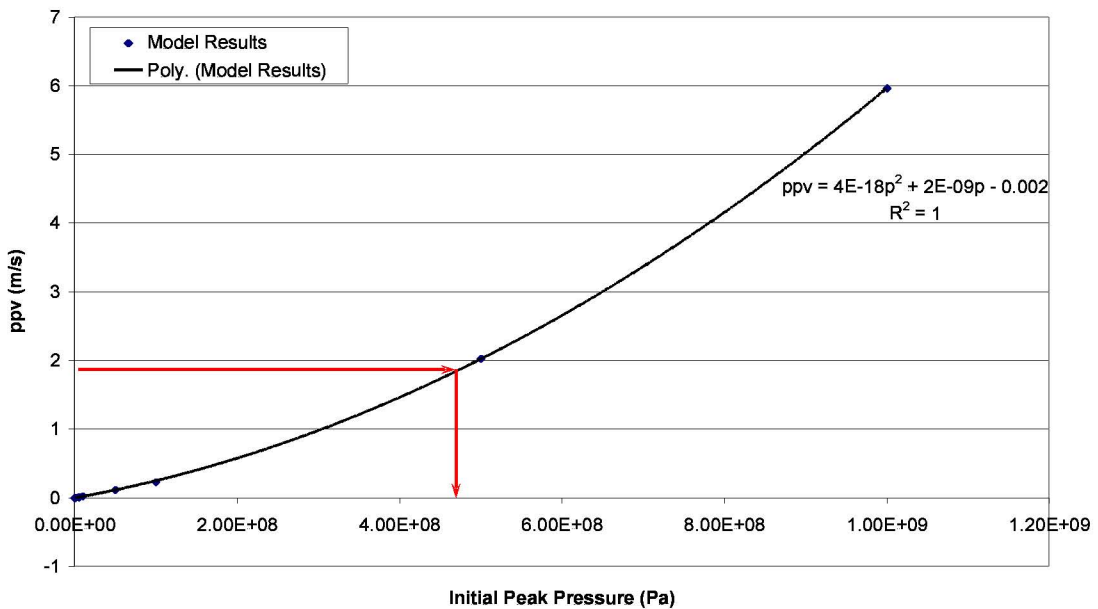
A pressure of 502 MPa was used for explosions in rock, and 45.1 MPa was used for explosions in paste fill.

### ***6.9. Validation of the Loading Function***

In order to validate the loading function, the model of the explosive cartridge in paste fill and the model of the explosive column in rock were run with the blast loads described in Section 6.8 applied. The results of these models were compared against the predicted ppv values for these scenarios. The results of the explosive cartridge in paste fill are shown in Figure 6.4 and the results of the explosive column in rock are shown in Figure 6.5.



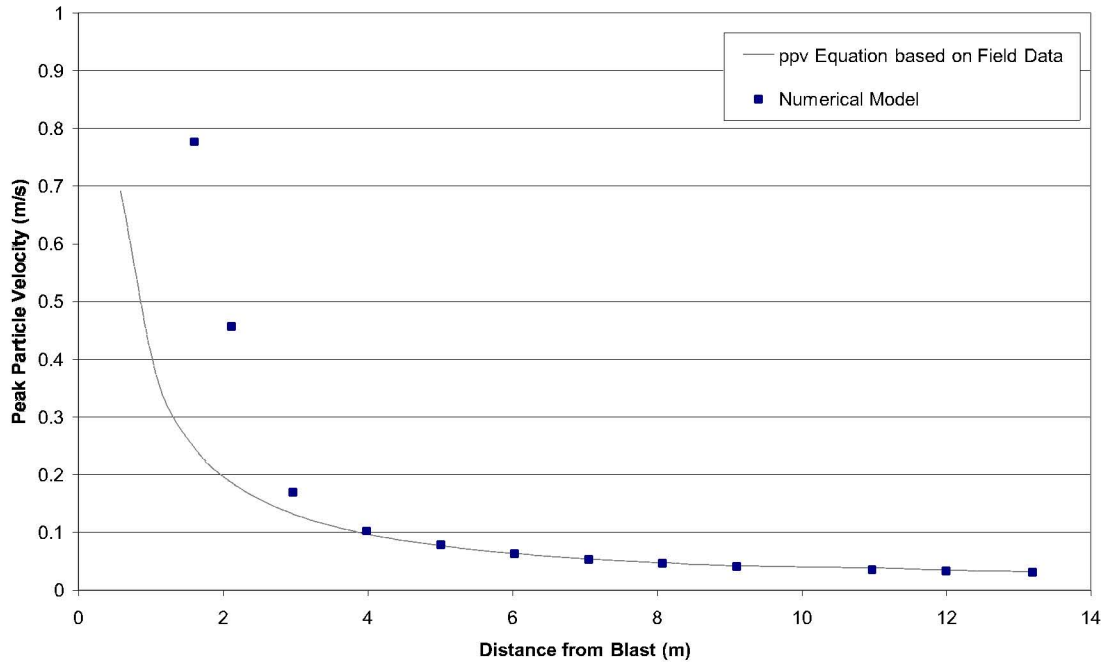
(a)



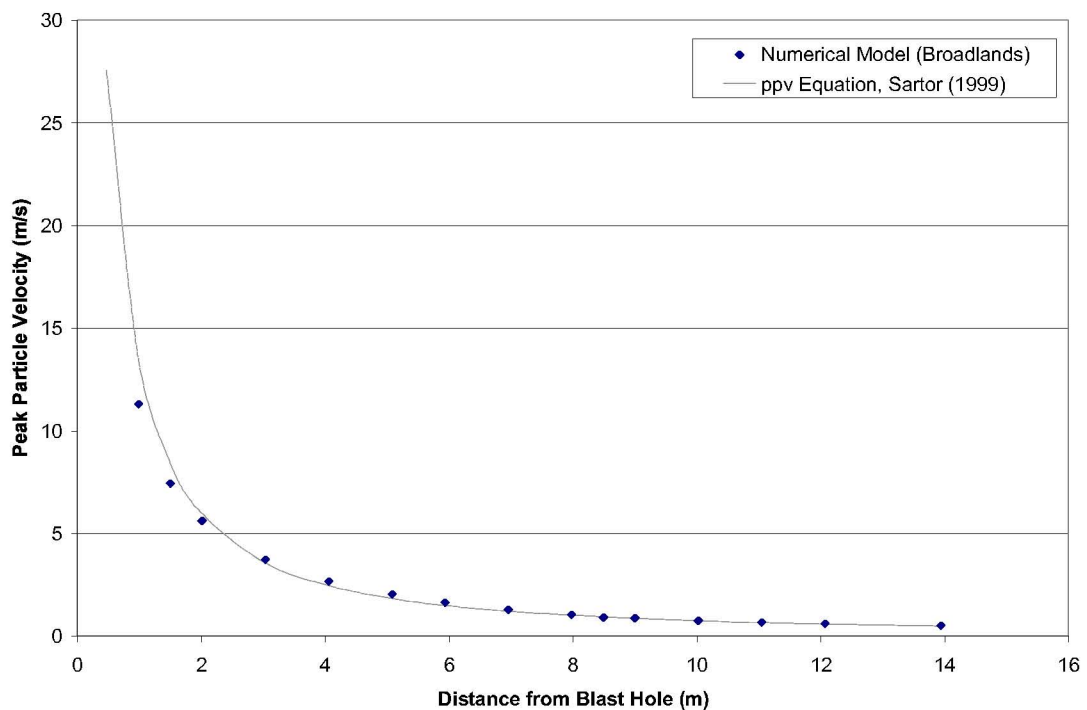
(b)

**Figure 6.3 – ppv Versus Pressure for 2 m Long Explosive Column in Rock**  
 (a) 2 m from Blast Column (b) 5 m from Blast Column

As seen in Figure 6.4, for distances greater than or equal to 2 m from the explosive in paste fill the model matches the predicted ppv quite closely, although the ppv are overestimated at distances less than 2 m from the source. Similar results are seen in rock.



**Figure 6.4 – Validation of the Stage 1 Model - Cartridge of Explosive in Paste Fill**



**Figure 6.5 – Validation of Stage 2 Model - Explosive Column in Rock**

The model overestimates the ppv close to the explosive source as the crushing and cracking mechanisms that occur in the vicinity surrounding the borehole are not considered in the numerical model. As discussed in section 6.5.5, since the purpose of the modelling for this

dissertation is to predict the ppv in paste fill as a result of blasting in adjacent rock, the effect of the stress wave is of interest rather than the crushing and fracturing which occurs around the blast hole. Since the paste fill is not within 2 m of the blast hole in the stage 3 model of blast holes in rock adjacent to paste fill, the results shown these models were found to produce acceptable results.

### ***6.10. Variables Which Affect Blast Loading***

The models discussed previously in this chapter consisted of a single explosive in a rock or paste fill mass. However, the production blast for the extraction of a stope in an underground mine consists of multiple blast holes which are detonated with millisecond delays between the detonation of each blast hole. There are many variables that can exist for a production blast, including the type of explosive used, the size of the blast, the blast hole pattern and the properties of the rock mass. These variables affect the stresses and peak particle velocities induced in a rock mass due to the blasting that occurs during the extraction of a stope. Some of these variables are discussed in the following sections.

#### **6.10.1. Types of Explosives**

The properties of explosives vary depending on the type of explosive. Commercial explosives used for mining applications can be broken into two groups, low and high explosives. Low explosives, such as black powder (or gun powder), are explosives that can be initiated by a flame, while high explosives are explosives which require shock or impact for detonation. High explosives consist of the following four main groups:

- Ammonium Nitrate-Fuel Oil (ANFO): As the name suggests, ANFO explosives consists of a mixture of ammonium nitrate and fuel oil. The performance of ANFO decreases when the explosive is exposed to water and mixtures containing more than 10 % water may fail to initiate. ANFO explosives have a velocity of detonation in the range of 2200 – 4000 m/s (Sen, 1995).
- Watergels: Watergels consist of a mixture of a gel base with ammonium nitrate and sometimes aluminium powder. These explosives have a gelatinous consistency which makes them suitable for use in wet conditions. Watergel explosives have a velocity of detonation in the range of 3500 – 5000 m/s (Sen, 1995).
- Emulsions: Emulsion explosives consist of fine microscopic droplets of oxidiser salts, finely dispersed into the continuous phase of fuel oil. These explosives have excellent

water resistance and can be detonated in deep wet blast holes. Emulsion explosives have a velocity of detonation in the range of 4500 – 6100 m/s (Sen, 1995).

- Gelignites: Gelignites are explosives which are based on nitroglycerine. They can be manufactured in gelatinous or semigelatinous form depending on the power, density and waterproofing requirements. Gelignite explosives have a velocity of detonation in the range of 3500 – 5500 m/s (Sen, 1995).

Emulsion type explosives were used at Cannington Mine for the field tests, and the production blasts which were instrumented and monitored for this project.

### **6.10.2. Rock Properties**

The rock structure and material properties will generally have a greater effect on the performance of blasting than the explosive properties. For the purpose of this modelling, it has been assumed that the rock mass is an isotropic and homogenous body, however, this is generally not the case. Rock masses contain joints and bedding planes which effect the transmission of the blast wave through the rock. These joints and beddings complicate the prediction of peak particle velocities and stresses in a rock mass due to the reflections of the blast wave which occur.

Rock material properties such as dynamic compressive strength, elastic modulus, density, porosity, internal friction, water content and in situ static stress effect the transmission of the blast wave through the rock and the subsequent damage to the rock mass.

### **6.10.3. Mining Methods**

The mining method which is used in a particular ore body depends on the type of rock and the geometry of the ore body. The various underground mining methods include longwall, open stope (also known as long hole stoping), cut and fill, room and pillar, shrinkage, sublevel caving and vertical crater retreat. The blasting pattern used for a particular mine will be dependent on the mining method.

At BHP Billiton's Cannington Mine, the open stope mining method is used with post placed back fill, where the ore is mined in blocks referred to as stopes. In open stope mining, access to the top and bottom of the ore block is set up with tunnels and a vertical hole is excavated from the top to the bottom of the stope. Blast holes are then drilled in order to excavate vertical slabs off the ore block (e-Gold Prospecting & Mining n.d.). The broken ore from the stope is then loaded into trucks from draw points at the bottom of the stope and hauled to the surface (BHP Billiton n.d.). Once the stope has been extracted, the void is filled with paste fill.

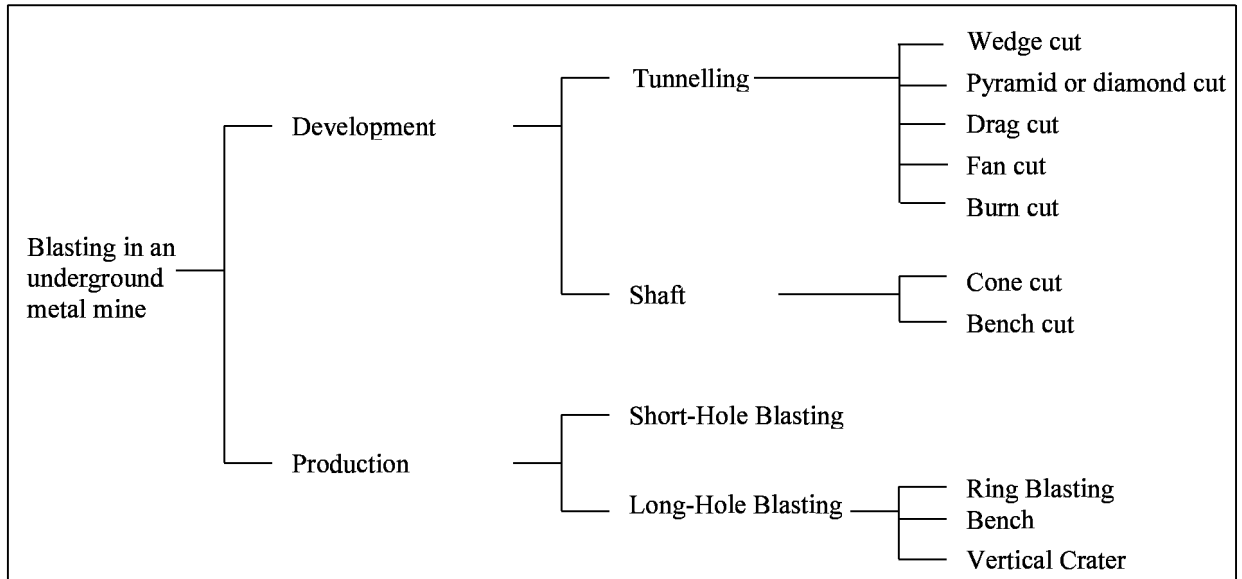
#### 6.10.4. Blasting Pattern

The blast load applied to a rock mass is dependent on many factors including the geometry of the ore body, the number of blast holes, the placement of the blast holes and the detonation order and delay timing. The blast pattern chosen for an ore body depends on the application of the blasting, the mining method being employed, the shape of the ore body, the depth and geological characteristics of the ore body.

The following definitions are useful for the discussion of blast hole patterns.

- Burden: The distance from the blast hole to the nearest free face
- Spacing: The distance between adjacent blast holes, measured perpendicular to the burden
- Charge length: The length of explosive in a blast hole
- Stemming: An inert substance, such as sand, filled between the explosive charge and the collar of the blast hole to confine the explosion gases. Materials such as water, drill cuttings, sand, mud and crushed rock are often used as stemming
- Decking: A technique of dividing the explosive column into two or more charges in the same blast hole, separated by stemming material.
- Charge density: The charge mass distributed in the column of a blast hole, measured in kg/m

A number of mining methods used in underground metal mines are shown in Figure 6.6, categorised by mining application. The blasting methods shown in the figure are broadly categorised into development and production blasts. Development blasts are the blasts required to access the ore body and transport the material after excavation. This type of mining includes tunnelling, shaft sinking, cross cutting and raising. Descriptions of the blasting patterns used in development blasts are given in Sen (1995).



**Figure 6.6 – Blasting Methods Used in Underground Metal Mines**

Production blasts are the blasts used in mining of the ore body. The long-hole blasting methods are of interest to this work. The three long-hole blasting systems are:

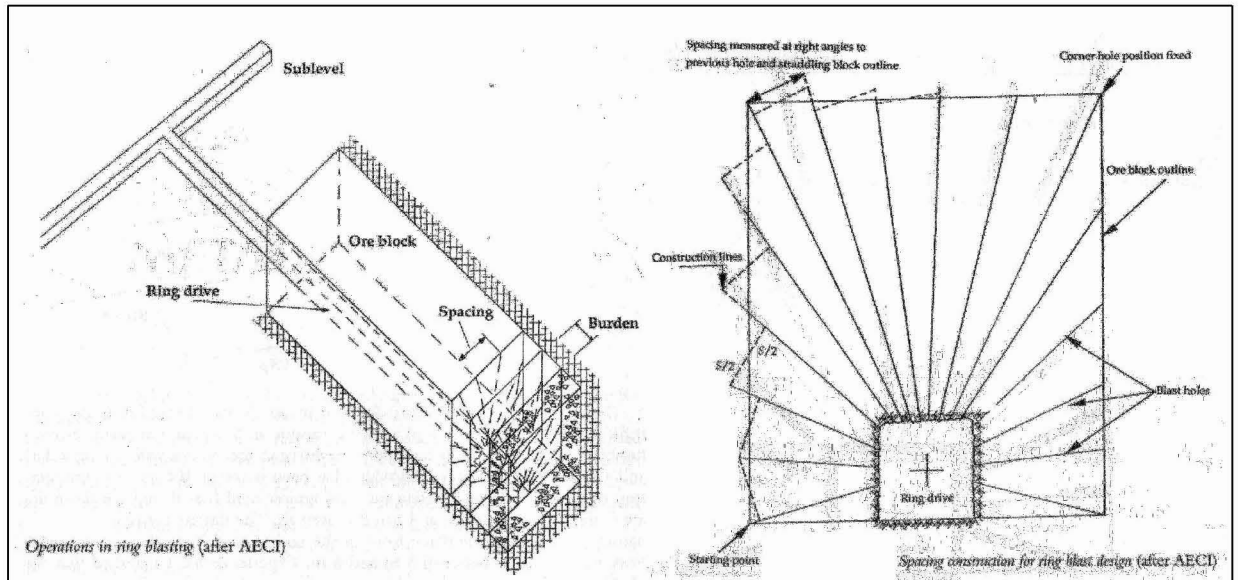
1. Ring Blasting

Ring blasting is the name given to the mining method that involves radial patterns of blast holes. It is used in the mining of massive ore bodies. Ring blasting involves the three steps listed below. These steps can be seen in Figure 6.7.

- a. Excavation of the “ring drive”, which is a tunnel running the full length of the stope
- b. Excavation of the “slot”, which is an empty space located at the end of the ring drive
- c. Drilling of sets of “rings” parallel to the slot

In ring blasting, the burden is defined as the distance between two consecutive rings, while the spacing is defined as the distance between the ends of adjacent holes in the same ring, measured as shown in Figure 6.7.

The collars of the blast holes are close together in ring blasting. As a result, a variable stemming length is used to avoid overcharging the ore body in this region.



**Figure 6.7 – Ring Blasting (Sen, 1995)**

## 2. Bench Blasting

Bench blasting involves the use of a series of parallel blast holes, and consists of the following steps:

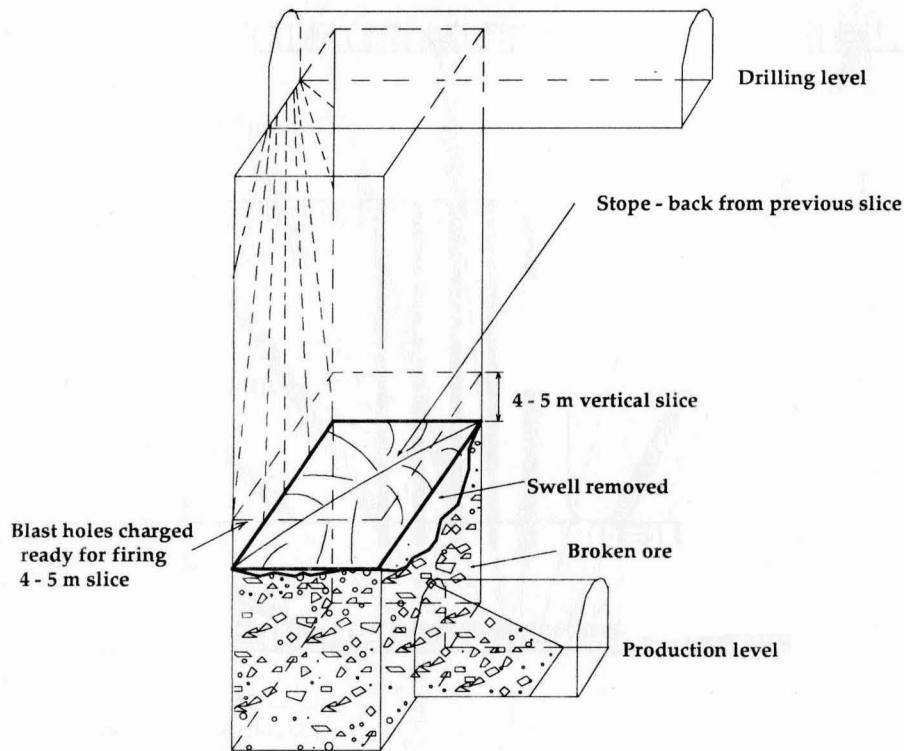
- a. Excavation of a development heading at the top of the sublevel to provide drilling space; and
- b. Drilling of blast holes. The blast holes can be horizontal, vertical, or inclined.

Either square drill patterns or staggered drill patterns can be utilised with bench blasting. Staggered patterns produce a more uniform blasting effect through the rock mass than square patterns. The effectiveness of a particular blasting pattern is dependent on the order of detonation.

## 3. Vertical Crater Retreat

In the vertical crater retreat method, the stope is mined from the bottom up. Blast holes are drilled downward from the top level to the bottom level. A slice of ore body is excavated from the lower level upward using the same blast holes for the different levels. Spherical charges are used in this method, and gravity assists the excavation process. The vertical crater retreat method is shown in Figure 6.8.





*Vertical crater retreat method (after Agnew Nickel)*

**Figure 6.8 – Vertical Crater Retreat Blasting (Sen, 1995)**

A combination of bench blasts and ring blasts were used in the production blasts monitored at Cannington Mine.

### 6.10.5. Initiation Patterns

Initiation patterns can vary greatly, with the optimal initiation depending on the blasting application, and geology. Initiation patterns are chosen to ensure that the blasting pattern is always working towards a free face.

### 6.10.6. Delay Intervals

Delay intervals between the detonation of blast holes in a blast round are used to reduce the ground vibrations and to increase fragmentation. The short delays are designed to allow the rock of previous blasts to move away and the free face of the next blast hole to be uncovered so that the blasting pattern is always working towards a free face. The delays are kept short enough that the rock from previous rows is still hanging in the air at the time of detonation of the next row, and is able to stop rock fragments from the second row from moving with greater speeds than average. The optimal delay time for a blast is dependent on the burden.

### **6.10.7. Blast Size**

The prediction of ppv from an explosive blast was discussed in section 6.4 and equations were presented from which to predict ppv based on the mass of explosive and the distance from the source. From equation 6.1 and 6.3 it can be seen that an increase in the linear charge density (mass per unit length) of explosive will result in a corresponding increase in ppv. Therefore, the ppv and consequently damage to the surrounding material can be decreased by reducing the mass of explosive detonated at any one time. This is achieved through the use of delay intervals.

### **6.10.8. Velocity of Detonation**

When an explosive detonates, the detonation is initiated at a point in the explosive material and a detonation wave travels through the explosive material. The rate at which this wave travels through the explosive is known as the velocity of detonation. The velocity of detonation is used in determining explosive performance, and often depends on both the explosive type and the blast hole diameter. Explosives with lower velocities of detonation tend to release gas energy over a longer period of time than explosives with higher velocities of detonation. This results in less fracturing around the blast hole and more heaving action. Therefore, the velocity of detonation of a given type of explosive can be used to determine which explosive is required for a given application.

## ***6.11. Summary***

A blast loading function was identified in this chapter. In order to identify a method of applying a blast load to the numerical model, the methods used by other authors and the mechanics of a blast were investigated. The typical use and the advantages and disadvantages of the different methods was considered along with the intent of the models created for this dissertation to determine the most appropriate method of load application for this work. The blast load was applied to the numerical model by applying a time-varying pressure pulse to the walls of an “equivalent cavity”. The form of the time-varying pressure pulse was based on the function used by Jiang et al. (1995) to model the detonation of the same type of explosive. The initial peak pressure for the time-varying pressure was set to the value required to produce peak particle velocities similar to those observed in field tests. At the end of the chapter, variables which affect the stresses and peak particle velocities induced in a rock mass due to the blasting were discussed.

## **7. Development of the Finite Element Model**

The finite element modelling package ABAQUS was used to model the effect of blasting on adjacent paste fill in an underground mine. This chapter describes the modelling package used, the problem definition and the input data for the numerical models created for this project.

### ***7.1. Finite Element Analysis***

This section outlines the finite element analysis process used for this project.

#### **7.1.1. General**

Finite element analysis is a computer technique which is commonly used in engineering analysis to study complex systems where it is difficult or expensive to use field experiments and where the solution to a problem cannot be solved using closed-form analytical solutions. In finite element analysis, a numerical technique known as the finite element method is used to solve a system of simultaneous equations. The system being modelled is represented by a geometrically similar model which consists of finite elements. The solution of a finite element model is approximate and the accuracy of a model depends on the quality of the finite element mesh. The system of simultaneous equations are produced by applying physical characteristics to the model such as constitutive models, equations of equilibrium and loads.

The modelling process generally includes three steps: pre-processing, analysis and visualisation. The pre-processing step is the step in which the finite element model is created. Most modelling packages provide built-in codes to create the finite element model. The analysis step is where a solution is computed, and the visualisation step is where the results are analysed. Finite element packages generally provide visualisation tools for the display of the model results in different formats.

A number of finite element software packages are available for different applications. ABAQUS/Explicit was determined to be the finite element modelling package that was most suitable for modelling blasting out of those available at the James Cook University School of Engineering. The other alternatives include ANSYS, PLAXIS and FLAC.

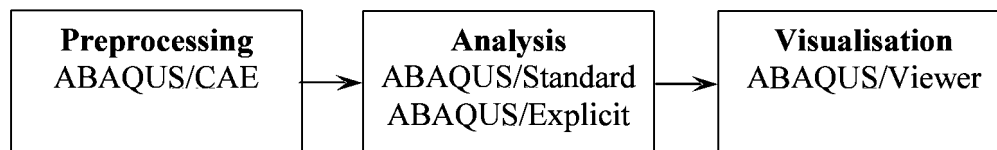
#### **7.1.2. ABAQUS**

ABAQUS is a finite element modelling package where the entire suite includes the following components:

- ABAQUS/Standard: A general-purpose finite element program;

- ABAQUS/Explicit: An explicit dynamics finite element program;
- ABAQUS/CAE: An interactive environment used to create models, submit and monitor jobs and evaluate model results; and
- ABAQUS/Viewer: A subset of ABAQUS/CAE (the Visualization module) used to evaluate model results.

The modelling process using ABAQUS is shown schematically in Figure 7.1. A brief description of each component is given in the following sections.



**Figure 7.1 – ABAQUS Modelling Process**

### **7.1.2.1. ABAQUS/Standard**

ABAQUS/Standard is a general-purpose solver. It uses traditional implicit integration scheme to solve a system of equations implicitly at each solution “increment”. ABAQUS/Standard can be used for a number of different analysis procedures including:

- Static analysis;
- Eigenvalue buckling analysis;
- Unstable collapse and postbuckling analysis;
- Quasi-static analysis;
- Direct cyclic analysis;
- Implicit dynamic analysis; and
- Complex eigenvalue extraction.

The transmission of blast waves through rock and backfill material is a dynamic analysis. Since ABAQUS/Explicit provides a more economical solution to this style of analysis than the solution methods used in ABAQUS/Standard, ABAQUS/Explicit was used for this project. ABAQUS/Standard was only used for the natural frequency extraction described in section 7.5.1.6.

### 7.1.2.2. ABAQUS/Explicit

ABAQUS/Explicit is a finite element program designed for solving highly nonlinear transient dynamic problems. The explicit dynamic procedure performs a large number of small time increments using a central-difference time integration rule. The solution for a set of simultaneous equations is not computed at each increment, making each increment relatively inexpensive. The explicit central-difference operator satisfies the dynamic equilibrium equations at the beginning of the increment,  $t$ , and the accelerations calculated at time  $t$  are used to advance the velocity solution to time  $t + \Delta t/2$  and the displacement solution to  $t + \Delta t$ . Therefore, the explicit method is efficient for the analysis of large models with a relative short dynamic response time (ABAQUS version 6.4 Documentation, 2003).

In the explicit dynamic analysis procedure, the equations of motion for the body are integrated using the explicit central-difference integration rule as follows (ABAQUS version 6.4 Documentation, 2003):

$$\dot{u}_{\left(i+\frac{1}{2}\right)}^N = \dot{u}_{\left(i-\frac{1}{2}\right)}^N + \frac{\Delta t_{(i+1)} + \Delta t_{(i)}}{2} \ddot{u}_{(i)}^N \quad (7.1)$$

$$u_{(i+1)}^N = u_{(i)}^N + \Delta t_{(i+1)} \dot{u}_{\left(i+\frac{1}{2}\right)}^N \quad (7.2)$$

where  $u^N$  is a degree of freedom (displacement or rotation component)

$\dot{u}$  is velocity

$\ddot{u}$  is acceleration

$i$  refers to the increment number in an explicit dynamic step.

The accelerations at the beginning of the increment are computed by:

$$\ddot{u}_{(i)}^N = \left(M^{NJ}\right)^{-1} \left(P_{(i)}^J - I_{(i)}^J\right) \quad (7.3)$$

where  $M^{NJ}$  is the mass matrix

$P^J$  is the applied load vector

$I^J$  is the internal force vector

A lumped mass matrix is used in this calculation. This is because the inverse of the matrix is simple to calculate and the vector multiplication of the mass inverse by the inertial force requires a limited number of operations (the number of degrees of freedom in the system) (ABAQUS version 6.4 Documentation, 2003).

An analysis in ABAQUS/Explicit may require an extremely large number of increments. However, as the increments are relatively expensive ABAQUS/Explicit often results in an economical solution. ABAQUS/Explicit has been used in the past to model blast induced damage in rock (Liu and Katsabanis 1997; Yang and Turcotte 1994), and has been shown to be capable of generating acceptable results. Therefore, ABAQUS/Explicit was chosen as the most suitable program in which to conduct the modelling for this project.

### ***7.1.2.3. ABAQUS/CAE***

ABAQUS/CAE is an interactive environment from which models can be created, run and the results analysed. It is broken up into modules, each of which is used to define a step in the modelling process. ABAQUS/CAE contains the following modules:

- The Part module: used to create parts which are used as building blocks to build a model;
- The Property module: used to define material properties and assign sections to parts;
- The Assembly module: used to create an assembly using the parts defined in the part module;
- The Step module: used to create analysis steps, specify output requests and specify solution controls;
- The Interaction module: used to define interactions between regions in the model. These reactions include mechanical and thermal interactions, analysis constraints and connections between two points;
- The Load module: used to define loads, boundary conditions and fields;
- The Mesh module: used to define node spacing, element types and create a mesh of the assembly;
- The Job module: used to create input files and to submit and monitor jobs; and
- The Visualisation module: used to analyse the results of the model.

ABAQUS/CAE was used to create and mesh basic input files for this project. The input files created by ABAQUS/CAE were then edited to use infinite elements which are not available in ABAQUS/CAE, but are available in ABAQUS/Explicit.

#### **7.1.2.4. ABAQUS/Viewer**

The Visualization module from ABAQUS/CAE is also licenced separately as ABAQUS/Viewer. This module allows the results of a model to be displayed in several formats including the ability to plot x-y data, view the deformed shape of a model and to plot contours of components for which field data was calculated. ABAQUS/Viewer was not used for this project as ABAQUS/CAE was used to view model results.

### **7.2. The ABAQUS input file**

Both ABAQUS/Standard and ABAQUS/Explicit are run as batch applications. The main input to these modules is an input file which contains the model definition and the steps to be processed. The input file is usually created by a preprocessor such as ABAQUS/CAE, although it can be written manually using the keywords given in the ABAQUS manuals. For this project, ABAQUS/CAE was used to create a basic input file for each model type which was then edited manually to include elements not available in ABAQUS/CAE and to run the analysis for different scenarios.

ABAQUS Input files contain the following two types of data defined in two separate sections:

- Model data
- History data

#### **7.2.1. Model Data**

The first section of the input file contains the model data which are used to define the model. The model data includes the following required data:

- Geometry of model defined as nodes and elements; and
- Material definitions.

In addition to the required data, the following optional model data can be defined:

- Parts and an Assembly;
- Initial Conditions;

- Boundary Conditions;
- Kinematic Constraints;
- Interactions;
- Amplitude Definitions;
- Output Control options for controlling the model definition data to be written to the output file;
- Environmental Properties; and
- Analysis Continuation information if the analysis is being continued from a previous model run.

The model data used in this project are defined in section 7.5.

### **7.2.2. History Data**

The second section of the input file contains the history data which are used to define the steps to be applied to the model. The history data are broken up into steps, which are individual components of an analysis. A new step can be used to define changes such as a different type of analysis, a change in the magnitude of a load or a change in output requests. Multiple steps can be used and there is no limit on the number of steps in a model. The required history data for a step includes the analysis type. The optional history data for a step depends on the type of step and can include the following:

- Loading;
- Boundary Conditions;
- Output Requests including components to be output and the time steps at which the output data are written;
- Contact; and
- Auxiliary Controls.

The history data used in each different analysis for this project are discussed in section 7.5.



### 7.2.3. Data Definitions

All data definitions in ABAQUS, whether model data or history data are written as option blocks, which are sets of data which describe part of the problem definition. Only the options that are relevant to the particular application are used. The options blocks are defined using three types of input lines in an ABAQUS input file, namely keyword lines, data lines and comment lines. Keyword lines are used to introduce options and have an asterisk preceding them. Keyword lines often have parameters, which are words or phrases which appear on the keyword line. Some parameters are required for a given keyword while others are optional. Parameters may also be assigned a value. An example of a keyword line is as follows:

*\*ELEMENT, type=CPE4, elset=Paste*

Data lines follow most keyword lines and are used to provide information that cannot adequately be defined using parameters. Comment lines are used to provide comments for users reading the input file and are ignored by ABAQUS. These lines must start with two asterisks (\*\*) and can be placed anywhere in the input file. An example of a keyword line, data line and comment line is as follows:

*Comment line       \*\* Surface Load. Name: Blast\_side2   Type: Pressure*

*Keyword line       \*Dload, amplitude=JIANG*

*Data line           Blast5\_surf2, P, 4.5e+07*

Where applicable, the keywords and parameters used for each option for the models created for this project are given in section 7.5.

## 7.3. Problem Definition

The problem definition for each model developed for this dissertation is described in the following section.

### 7.3.1. General

The finite element model for this dissertation was developed through a three stage modelling process. A set of models was developed for each stage as follows:

- Stage 1: A single column of explosive in paste fill;
- Stage 2: A single column of explosive in rock; and

- Stage 3: Columns of explosive in rock adjacent to paste fill.

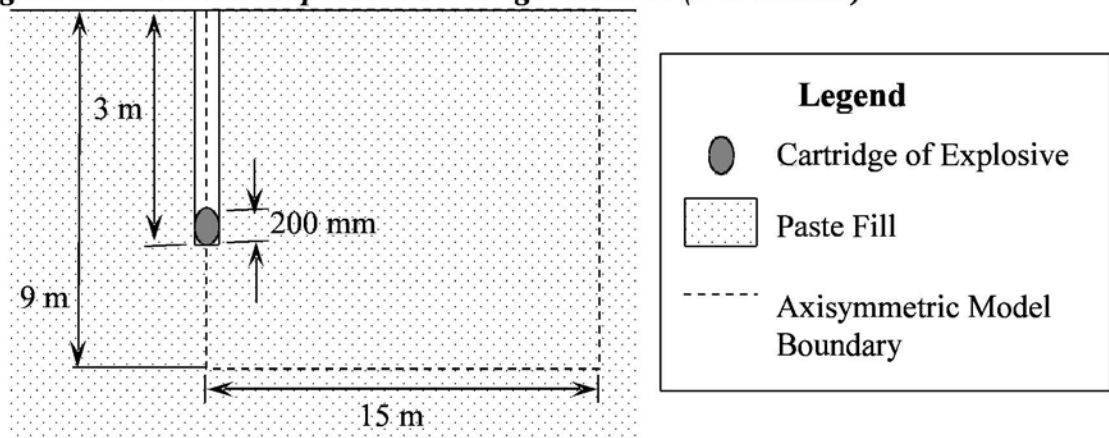
The stage 1 models were used to validate the model results of the transmission of blast waves through paste fill against the data obtained in the field instrumentation tests discussed in chapter 4. Once validated, these models were then used to compare the transmission of blast waves through different mixes of paste fill. Similarly, the stage 2 models were used to validate the model results of the transmission of blast waves through rock. The stage 3 models were then used to model blasts in rock adjacent to paste fill. The problem definition and geometry of each model are given in the following sections.

### 7.3.2. Stage 1 Model: Single Column of Explosive in Paste Fill

The stage 1 model was based on the scenario encountered in the field tests discussed in chapter 4. The purpose of this model was to validate the numerical model against the field instrumentation tests and to predict the effect of cement and solids content of the paste fill on the propagation of the blast wave. Once the model for stage 1 was validated, the material model developed for this stage was used for the stage 3 model.

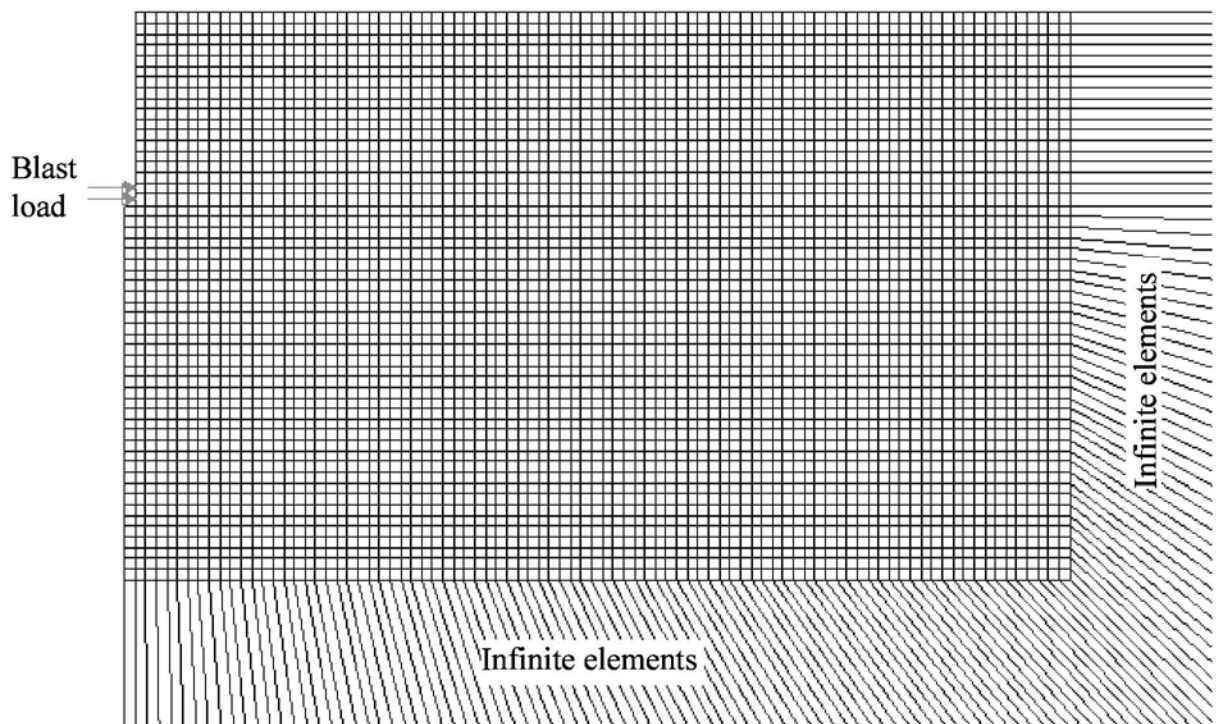
This scenario consisted of a blast hole in a mass of paste fill containing a single cartridge of emulsion explosive, as shown in Figure 7.2. The blast hole was 3 m deep and 44 mm in diameter. The cartridge of explosive was 200 mm long and had a diameter of 32 mm. For the purpose of this modelling, it was assumed that the rock/paste fill interface was at a sufficient distance from the explosive column to not affect the model results. In this situation, a line of symmetry exists down the centre line of the blast hole. Therefore, only the region outlined in Figure 7.2 had to be included in the model. Due to the symmetry of the geometry, an axisymmetric model was used.

**Figure 7.2 – Scenario Represented in Stage 1 Models (Not to Scale)**



The 15 m wide and 9 m high finite element model mesh is shown in Figure 7.3. The blast load was applied to the walls of an “equivalent cavity” with a radius of 66 mm, which is three times

the blast hole radius. The concept of an “equivalent cavity” was used in order to model the transmission of blast waves through the fill without modelling the cracking immediately surrounding the blast hole. This method allows the propagation of the blast wave within the material to be modelled without the need to use complex material models and cracking models. For large scale models such as those used in this work, the use of an “equivalent cavity” dramatically reduces the time required to solve the model. This concept is discussed further in section 6.6. Infinite elements were placed along the side and base of the model in order to provide a non-reflecting boundary. The blast load applied to this model is discussed in chapter 6, and the remainder of the model parameters are discussed later in this chapter.



**Figure 7.3 – Finite Element Mesh for the Stage 1 Model**

This model was initially solved for a paste fill mix of 76 % solids and 4 % cement, representative of the 76 % solids and 3.8 % paste fill mix of the stope used for the field tests. The model results were compared against the prediction of the ppv using the parameters obtained from the field tests in order to validate the model. The validation of this model is discussed in Chapter 8.

This model was then run for the different mixes of paste fill given in Table 7.1 in order to assess the wave propagation in different mixes of paste fill. The material properties for these mixes of paste fill are given in Table 7.2. The results of this assessment are discussed in Chapter 8.

**Table 7.1 Paste Fill Mixes used in the Stage 1 Model**

<b>Solids Content (%)</b>	76	76	76	78	78	78	80	80	80
<b>Cement Content (%)</b>	2	4	6	2	4	6	2	4	6

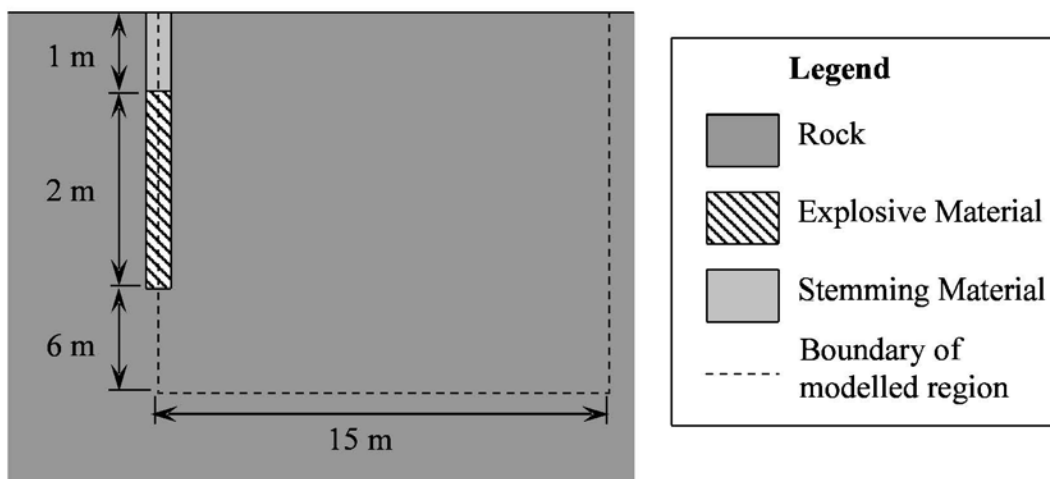
**Table 7.2 Material Properties used for Paste Fill**

<b>Paste Fill Mix</b>	<b>Elastic Parameters</b>			<b>Drucker-Prager Model Parameters</b>				<b>Damping</b>	
	$\rho$ (kg/m <sup>3</sup> )	<b>E</b> MPa	$\nu$	$\tan \beta$	<b>K</b>	$\psi$ (deg)	$\sigma_c$ kPa	$\varepsilon$	$\alpha$
74% S 2% C	2056	4	0.2	1.066	0.778	0	81.2	0	0.000567
74% S 4% C	2021	23.0	0.2	1.001	0.778	0	396.3	0	0.000567
74% S 6% C	2021	81.0	0.2	0.9185	0.778	0	621.6	0	0.000567
76% S 2% C	2130	23.0	0.2	0.9963	0.778	0	204.6	0	0.000567
76% S 4% C	2003	56.0	0.2	0.9614	0.778	0	692.5	0	0.000567
76% S 6% C	2003	98.0	0.2	0.9225	0.778	0	1176	0	0.000567
78% S 2% C	2182	17.0	0.2	0.9054	0.778	0	252.1	0	0.000567
78% S 4% C	2008	74.0	0.2	0.9160	0.778	0	959.4	0	0.000567
78% S 6% C	2088	140.0	0.2	0.9264	0.778	0	1747	0	0.000567
80% S 2% C	2057	25.0	0.2	0.9054	0.778	0	358.6	0	0.000567
80% S 4% C	2057	121.0	0.2	0.9160	0.778	0	1272	0	0.000567
80% S 6% C	2057	233	0.2	0.9224	0.778	0	2290	0	0.000567

S = solid content; C = cement content

### 7.3.3. Stage 2 Model: Single Column of Explosive in Rock

The stage 2 model was based on the scenario of a single column of emulsion explosive in a rock mass, as shown in Figure 7.4. The blast hole was 89 mm in diameter, with the diameter of the explosive based on the diameter of blast holes used in the production blasts monitored and discussed in Chapter 3. The blast hole was 3 m deep in this model, out of which a 2 m length is explosive material and a 1 m length is stemming material. The stemming material is used to ensure that the gases provide a load to the walls of the blast hole rather than escaping from the blast hole, and does not provide any strength to the system. Therefore, the stemming material was not modelled. For the purpose of this modelling, it was assumed that there was no paste fill in the vicinity of the explosive column. In this situation, a line of symmetry exists down the centre line of the blast hole. Therefore, only the region outlined in Figure 7.4 had to be included in the model. Due to the symmetry of the geometry, an axisymmetric model was used.

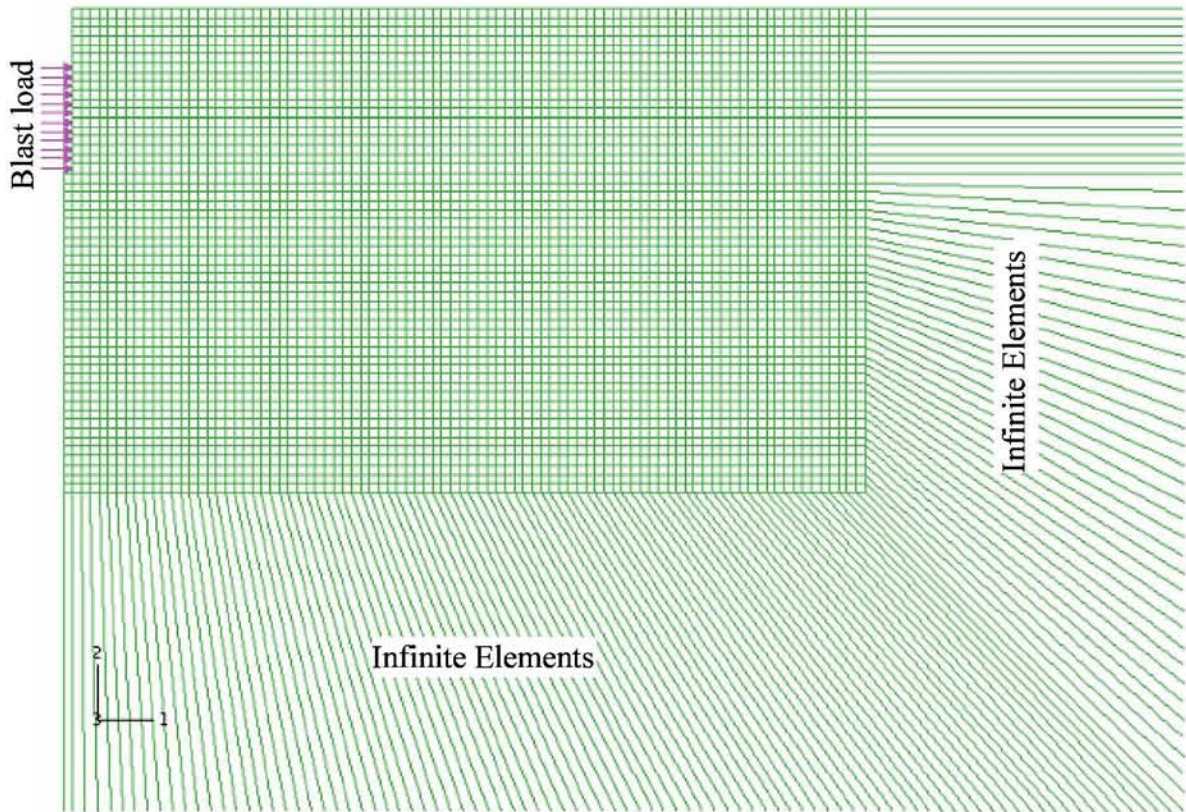


**Figure 7.4 – Scenario Represented in Stage 2 Model (Not to Scale)**

This model was similar to the stage 1 model and consisted of a 15 m wide and 9 m high finite element mesh, as shown in Figure 7.5. As for the stage 1 model, infinite elements were placed along the side and base of the model to provide a non-reflecting boundary and the blast load was applied to the walls of an “equivalent cavity”. A radius of 134 mm, which is three times the blast hole radius used in the production blasts, was used for the “equivalent cavity”. The blast load applied to this model is discussed in chapter 6, and the remainder of the model parameters are discussed later in this chapter.

This model was solved for the rock types listed in Table 7.3 in order to assess the effect of rock type on wave propagation. The material properties for these rock types are given in Table 7.4. The results of this assessment are discussed in Chapter 8. The model results when Broadlands rock type was used were compared against the prediction of the ppv using the parameters

obtained from the Sartor’s (1999) work in order to validate the model. The validation of this model is discussed in section 6.9.



**Figure 7.5 – Finite Element Mesh for Stage 2 Model**

**Table 7.3 Rock Types Used in the Stage 2 Model**

Symbol	Rock Type
BL	Broadlands
BM	Burnham
GH	Glenholme
HDMT	Magnetite bearing hedenbergite rock
PXAM	Pyrobole Rock
QZGA/IT	QZGA: garnetiferous quartzite/arkose QZIT: meta quartzite/arkose
QZHD	Hedenbergite quartzite rock

**Table 7.4 Material Properties used for Rock**

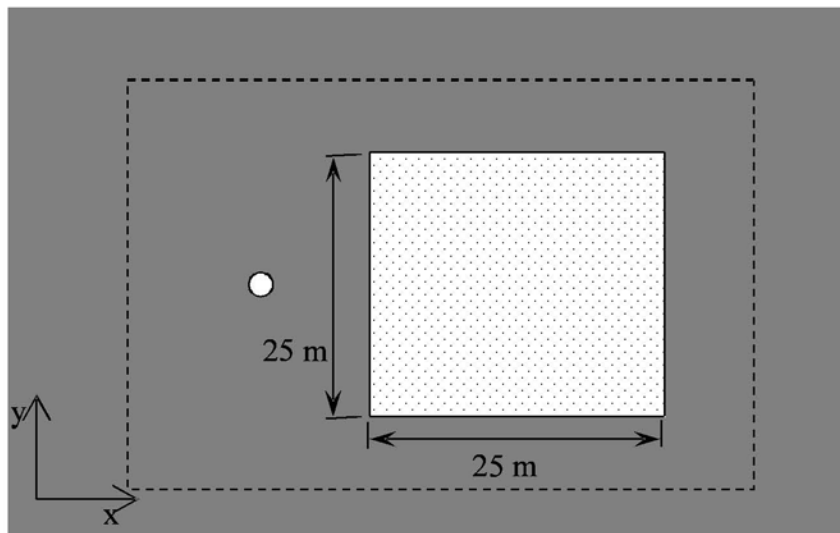
Rock Type	Elastic Parameters			Drucker-Prager Model Parameters				Damping	
	$\rho$ (kg/m <sup>3</sup> )	E GPa	$\nu$	$\tan \beta$	K	$\psi$ (deg)	$\sigma_c$ MPa	$\varepsilon$	$\alpha$
BL	3950	19.3	0.2	0.876	0.778	0	216.8	0	9.6102
BM	4440	20.9	0.2	0.876	0.778	0	220.0	0	9.4326
GH	3480	10.3	0.2	0.876	0.778	0	44.3	0	6.7008
HDMT	4060	11.7	0.2	0.876	0.778	0	142.7	0	7.3806
PXAM	3670	12.1	0.2	0.876	0.778	0	162.0	0	7.8942
QZGA	2930	16.0	0.2	0.876	0.778	0	189.3	0	10.1598
QZHD	2870	18.9	0.2	0.876	0.778	0	222.1	0	11.1570

### 7.3.4. Stage 3 Model: Columns of Explosive in Rock Adjacent to Paste Fill

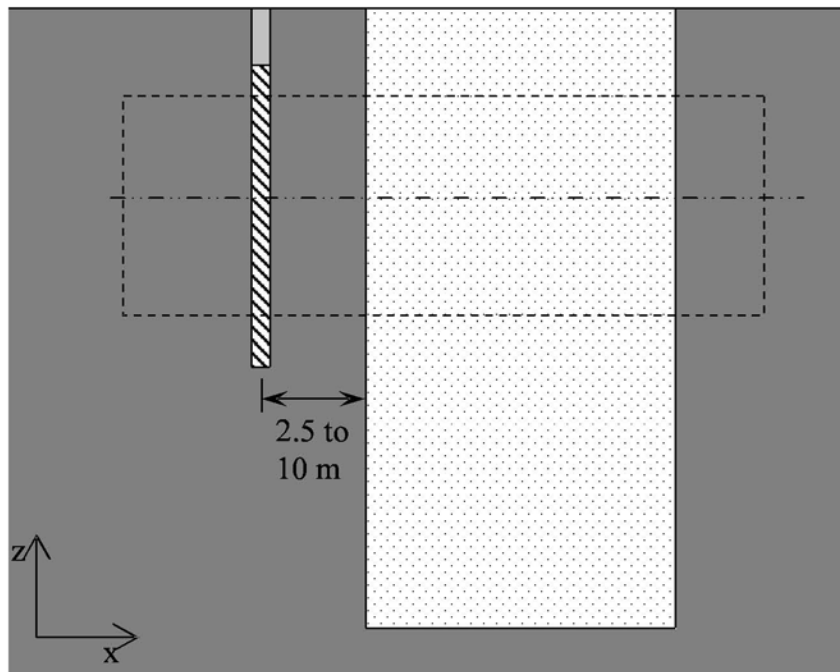
The stage 3 model was based on the scenario of columns of emulsion explosive in a rock mass adjacent to a stope which has been previously mined and filled with paste fill, as shown in Figure 7.6. Two different stage 3 models were created, one using a blast hole diameter of 89 mm and the other using a blast hole diameter of 76 mm. These diameters were based on the diameter of blast holes used in the production blasts monitored and discussed in Chapter 3.

The paste fill stope in this model was 25 m by 25 m in plan view, representative of the average dimensions of a stope. Several models were run with the column of explosive at 2.5, 5, 7.5 and 10 metres from the paste fill.

Figure 7.6 shows the geometry of this model. Many attempts were made to create and run a three-dimensional model of this scenario in ABAQUS/Explicit, however these attempts were unsuccessful due to the large numbers of elements required. Therefore, this system was modelled using plane strain elements to model the system in plan view. This scenario was approximated using a two-dimensional, plane strain model. Plane strain elements are used



(a) Plan View



(b) Elevation

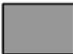
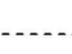



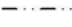

Legend		
	Rock	 Boundary of modelled region
	Explosive Material	 Blast Hole (plan view)
	Paste Fill	 Line of Symmetry
	Stemming Material	

Figure 7.6 – Scenario Represented in the Stage 3 Model

when it can be assumed that the normal and shear strain in the z-direction are zero. This generally applies in cases when the body is very thick in comparison to the dimensions in the x- and y-directions. The rock and paste stopes and the blast hole may be represented with plane strain elements as they are thick in the z-direction compared to the x- and y-directions. The



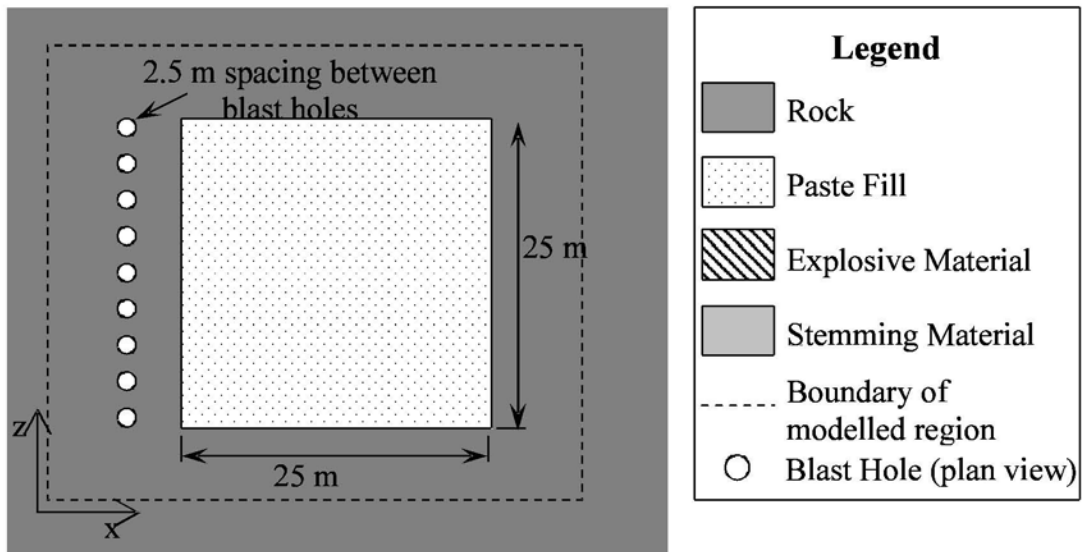
representation of the blast hole with plane strain models provides realistic results in the region surrounding the middle of the blast hole.

There are some limitations to representing a blast hole with a plane strain model. In the region surrounding the ends of the blast hole column there is no symmetry to enable the system to be modelled with a two dimensional model when the blast hole is located in rock adjacent to paste fill and a three-dimensional model would be required to provide accurate results. As discussed in section 2.5.2, the peak particle velocity experienced from the detonation of a column of a given diameter with a given type of explosive does not increase as the length of the column increases, as the charge weight in the blast hole is proportional to the charge length. Therefore, the peak particle velocities experienced at the ends of the blast hole are not expected to be greater than those in the centre of the blast hole column. As a result, the results obtained in a plane strain model are expected to be representative of the maximum peak particle velocities which would be experienced from a given blast hole.

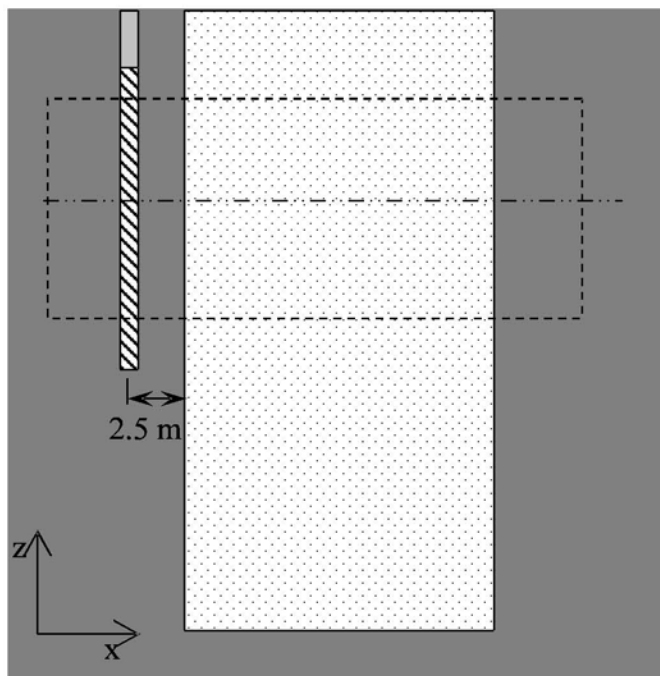
In addition to the scenario shown in Figure 7.5, a version of the stage 3 model was set up with loading applied to by a line of blast holes with a geometry shown in Figure 7.6. This model was run for several detonation patterns including the simultaneous detonation of the blast holes and detonation delays between each blast. Production blasts in mines generally consist of many blast holes, and the arrangement shown in Figure 7.7 is not uncommon. This arrangement was used for the vertical blast holes referred to as COS blast holes in the production blasts discussed in Chapter 3. In a production blast, these blast holes are generally detonated with a delay time of several milliseconds between blast holes.

The finite element model mesh of the plane strain model is shown in Figure 7.8. The model was run for a variety of loading patterns. The location of all blast hole locations modelled is shown in the figure. These blast holes were not all applied in one model run. The stage 3 modelling was run for three different loading scenarios which are described as follows:

- Scenario 1: A single blast hole was detonated adjacent to the centreline of the paste fill stope. This scenario was run for blast holes located at 2.5, 5.0, 7.5 and 10.0 m from the rock/paste fill interface.
- Scenario 2: A single blast hole was detonated at a location offset from the centreline of the paste fill stope. This scenario was run for blast holes located at an offset of 2.5, 5.0, 7.5 and 10.0 m from the centreline of the paste fill stope. All blast holes modelled in this scenario were located 2.5 m from the rock/paste fill interface.



(a) Plan View



(b) Elevation

**Figure 7.7 – Scenario Represented by Stage 3 Model (Plan View)**

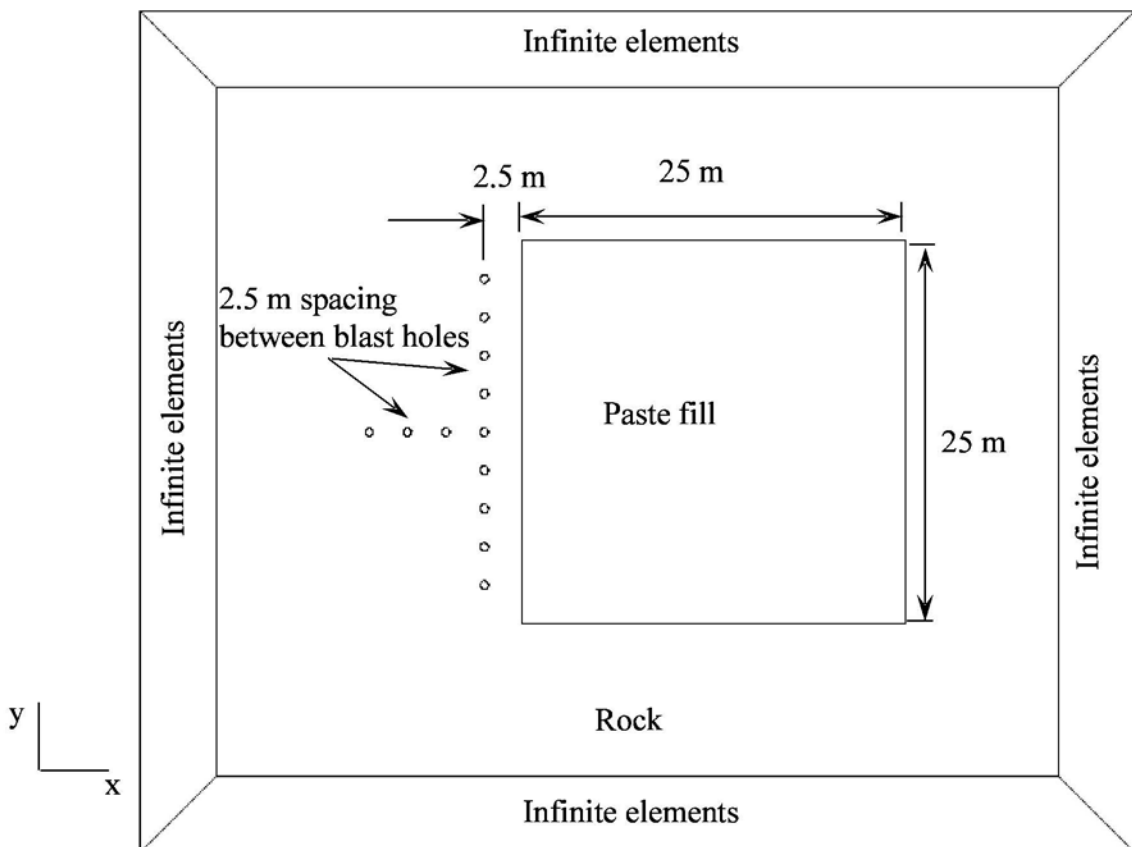
- Scenario 3: A row of blast holes located parallel to the face of the paste fill stope was detonated. These blast holes were located 2.5 m from the rock/paste fill interface and were spaced 2.5 m apart. The following three detonation patterns were modelled:
  - The detonation of all blast holes simultaneously;
  - The detonation of the blast holes one at a time starting from one end and working towards the other end; and

- The detonation of the centre blast hole followed by the blast holes to each side systematically until all blast holes have been detonated.

The models for scenario 3 were modelled with delays between the detonation of each blast hole of 100 ms, 200 ms and 400 ms.

The loading scenarios and the detonation patterns for the stage 3 modelling are discussed further in section 8.3.

Similar to the stage 1 and stage 2 models, the blast load was applied to the walls of an “equivalent cavity” with a radius of three times the blast hole radius and infinite elements were placed along the sides of the model in order to provide a non-reflecting boundary. The blast load applied to this model is discussed in chapter 6, and the remainder of the model parameters are discussed later in this chapter. This model was solved for the Broadlands rock type, and a paste fill mix of 76 % solids and 4 % cement. The results of this assessment are discussed in Chapter 8.



**Figure 7.8 – Finite Element Mesh for Stage 3 Model**

#### ***7.4. Simplifications and Assumptions***

The numerical models for this project were created based on the following assumptions and simplifications:

- Velocity of detonation will have negligible impact on the peak particle velocity and therefore can be ignored. The pressure from the detonation is applied over the entire length of the blast hole instantaneously.
- The rock material is homogeneous and does not contain any joints or faults. This is considered to be a conservative assumption, as it is likely that joints and faults in the rock do exist within the ore body. The presence of a joint or fault between the location of a blast hole in rock and the paste fill would result in the reflection of part of the stress wave from the explosive, reducing the impact of the stress wave on the paste fill. Therefore, the absence of joints and faults in this model is representative of the greatest load that would be expected to occur on the paste fill material as a result of nearby blasting in rock.

#### ***7.5. Model Parameters***

The model parameters for all modelling undertaken for this dissertation are discussed in the following section.

##### **7.5.1. Material Properties**

The material properties for both paste fill and rock are discussed in this section.

##### ***7.5.1.1. Constitutive Models***

The output of the finite element model is highly dependent on the material behaviour applied to the model. Soils consist of an accumulation of mineral particles, with the voids between the particles filled with water and/or air. The behaviour of such particulate materials is complex due to the various interactions between the particles. However, when considered at the macroscale, the behaviour of soils may be idealised as behaving like continua (Prevost and Popescu, 1996). Constitutive models are used to describe such soil behaviour, and many models exist. Previous research on the material behaviour of both paste fill and ore from Cannington Mine indicate that both materials can be adequately described using the Mohr-Coulomb material model (Rankine, 2004).

**7.5.1.2. Mohr Coulomb Material Model**

The Mohr-Coulomb failure criterion is widely used for materials such as soils and rock. The shear strength of a soil at a point is expressed as a function of the effective normal stress at the same point by the following equation:

$$\tau_f = d' + \sigma'_f \tan \phi \tag{7.4}$$

where  $\tau_f$  = shear strength

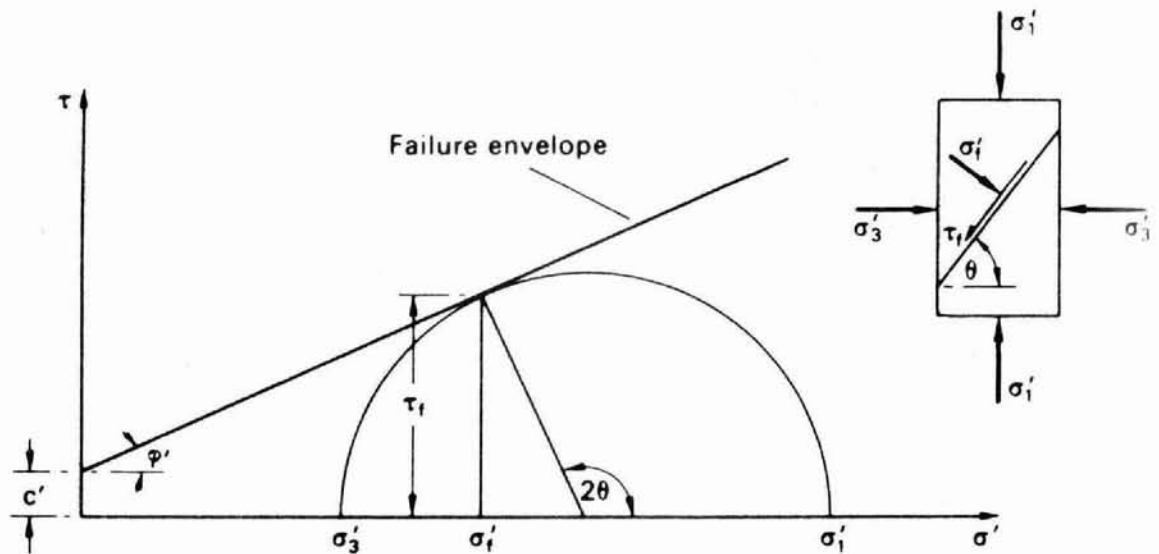
$d'$  = cohesion intercept in terms of effective stress

$\sigma'_f$  = effective normal stress

$\phi$  = angle of shearing resistance in terms of effective stress

The shear strength of a soil can also be expressed by Mohr's circle, which is defined by the effective major and minor principal stresses  $\sigma'_1$  and  $\sigma'_3$  at failure. At failure, the line represented by equation 7.4 will be tangential to the Mohr Circle as shown in Figure 7.9. From Figure 7.9, the Mohr-Coulomb failure criterion given below can be obtained. This failure criterion is independent of the effective intermediate principal stress.

Laboratory tests of both paste fill and rock from Cannington Mine indicated that both materials can be described by the Mohr-Coulomb failure criterion (Rankine, 2004).



**Figure 7.9 – Mohr Coulomb Stress Conditions at Failure (Craig 1997)**

### 7.5.1.3. *Material Models to apply in ABAQUS/Explicit*

Both paste fill and ore are best described using the Mohr-Coulomb Material Model. However, this material model is not available in ABAQUS/Explicit. Out of the material models available in ABAQUS/Explicit, the modified Drucker-Prager models were found to be the closest model to the Mohr-Coulomb material model. Therefore, the paste fill and rock were both modelled using the Drucker-Prager material model.

### 7.5.1.4. *Drucker Prager Plasticity Model*

The Drucker-Prager plasticity models (Drucker & Prager, 1952) are used to model materials which exhibit pressure-dependent yield (ABAQUS, 2003). Drucker-Prager materials are typically granular, like soils and rock. The Drucker-Prager plasticity models available in ABAQUS/Explicit can be used in conjunction with the elastic material model.

The yield criteria is described by equation 7.5 and the yield surface for the Drucker-Prager material model is given in Figure 7.10. The yield surface is shown in the meridional plane.

$$G = g - m \tan \eta - d = 0 \quad (7.5)$$

where  $G$  = yield criteria

$$g = \text{a deviatoric stress measure} = \frac{1}{2} q \left[ 1 + \frac{1}{K} - \left( 1 - \frac{1}{K} \right) \left( \frac{j}{q} \right)^3 \right]$$

$j$  = the third invariant of deviatoric stress

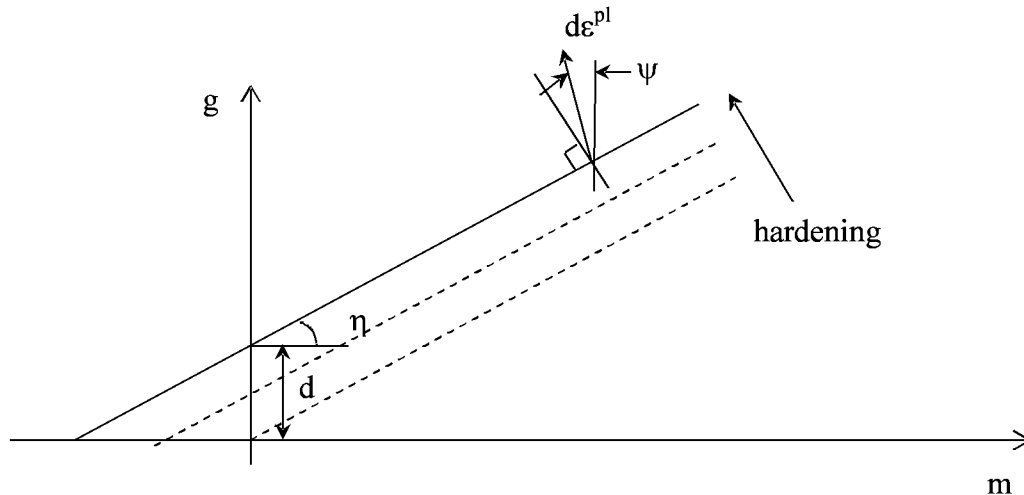
$q$  = the Mises equivalent stress

$K$  = is the ratio of the yield stress in triaxial tension to the yield stress in triaxial compression

$p$  = the equivalent pressure stress

$\eta$  = the slope of the linear yield surface in the  $p$ - $t$  stress plane commonly referred to as the friction angle of the material

$d$  = the cohesion of the material



**Figure 7.10 – Drucker-Prager Yield Surface in the Meridional Plane**

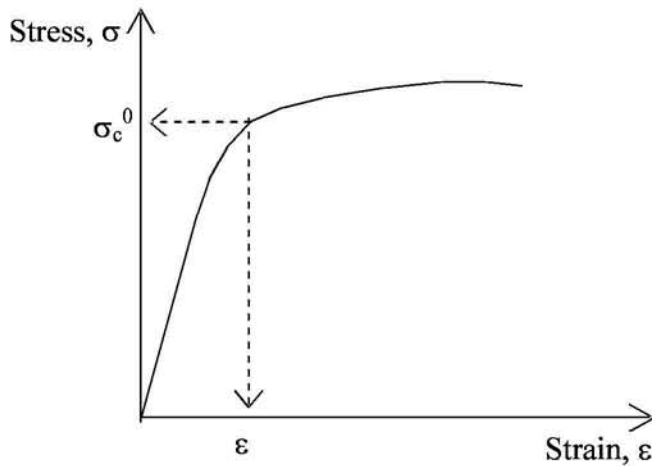
The Drucker Prager plasticity model is specified using the `*DRUCKER PRAGER` and the `*DRUCKER PRAGER HARDENING` keywords.

The `*DRUCKER PRAGER` keyword is used to define the yield surface and flow potential parameters for elastic-plastic material models that use one of the Drucker-Prager plasticity models. The data lines for the `*DRUCKER PRAGER` keyword are as follows:

1. The material angle of friction,  $\eta$ , in the p-t plane, given in degrees.
2. The ratio of the yield stress in triaxial tension to the yield stress in triaxial compression, K. K must be between 0.778 and 1.0 to ensure that the yield surface remains convex (ABAQUS, 2003).
3. The dilation angle,  $\psi$ , in the p-t plane, given in degrees.

The `*DRUCKER PRAGER HARDENING` keyword is used to define the hardening data for elastic-plastic material models that use one of the Drucker-Prager plasticity models. The data lines for the `*DRUCKER PRAGER HARDENING` keyword are as follows:

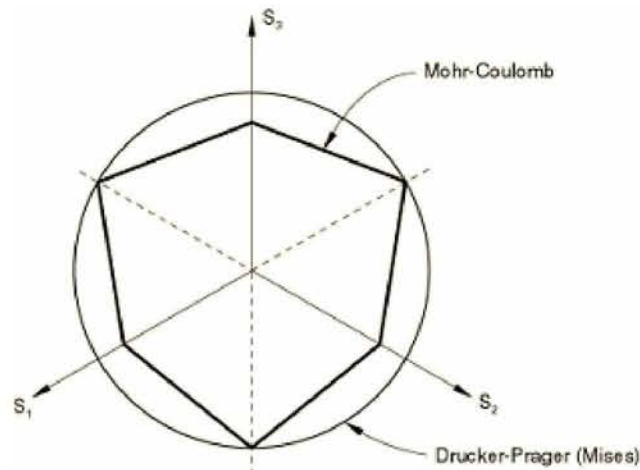
1. Yield Stress,  $\sigma_c^0$ . The yield stress is the stress which must be exceeded in the material to cause plastic deformation to the material. Prior to reaching the yield stress, elastic deformation will occur. The yield stress is shown on the typical stress-strain curve for a ductile material shown in Figure 7.11.
2. Absolute value of the corresponding plastic strain,  $\epsilon$ .



**Figure 7.11 – Typical Stress-Strain Curve for a Ductile Material**

### 7.5.1.5. Matching Mohr-Coulomb Parameters to the Drucker-Prager Model

The Mohr-Coulomb theory assumes a linear relationship between the deviatoric and pressure stress, and can therefore be matched by the linear Drucker-Prager model (ABAQUS 2003). Unlike the Mohr-Coulomb model, the Drucker-Prager model does not assume that failure is independent of the value of intermediate principal stress. The Mohr-Coulomb is generally considered to be accurate for most geotechnical applications, although the failure of typical geotechnical materials generally includes a small dependence on the intermediate principal stress. A comparison between the Drucker-Prager material model and the Mohr-Coulomb material model is given in Figure 7.12. In this figure, the Drucker-Prager and the Mohr-Coulomb yield surfaces are shown on the deviatoric plane where  $S_1$ ,  $S_2$  and  $S_3$  are the principal stresses. The Mohr-Coulomb model has vertices, while the Drucker-Prager model doesn't.



**Figure 7.12 – Comparison of Mohr-Coulomb and Drucker-Prager Models in the Deviatoric Plane (ABAQUS 2003)**



The Drucker-Prager parameters were obtained from the Mohr-Coulomb model by matching the triaxial test response. Using this method, the Drucker-Prager material properties can be obtained from the following equations:

$$\tan \beta = \frac{6 \sin \phi}{3 - \sin \phi} \quad (7.6)$$

$$\sigma_c^o = 2c \frac{\cos \phi}{1 - \sin \phi} \quad (7.7)$$

$$K = \frac{3 - \sin \phi}{3 + \sin \phi} \quad (7.8)$$

#### 7.5.1.6. Damping

Damping was applied to the numerical model in two formats: bulk viscosity and Rayleigh damping.

##### **Bulk Viscosity**

Bulk viscosity is used to introduce damping associated with volumetric straining to the model, and improve the modelling of high speed dynamic events. There are two forms of bulk viscosity that can be applied in ABAQUS:

1. Damping of the “ringing” in the highest element frequency. This form of bulk viscosity generates a bulk viscosity pressure which has the following linear relationship with volumetric strain:

$$p_{bv1} = b_1 \rho c_d l_e \dot{\epsilon}_{vol} \quad (7.9)$$

where  $p_{bv1}$  = bulk viscosity pressure

$b_1$  = damping coefficient

$\rho$  = density

$c_d$  = wave velocity

$l_e$  = an element characteristic length

$\dot{\epsilon}_{vol}$  = volumetric strain

The default value of  $b_1 = 0.06$  was used in this analysis.

2. Damping in solid continuum elements which has the following quadratic relationship with volumetric strain rate:

$$p_{bv2} = \rho(b_2 l_e \dot{\epsilon}_{vol})^2 \quad (7.10)$$

where  $p_{bv2}$  = bulk viscosity pressure

$b_2$  = damping coefficient

This form of damping smears a shock front across several elements, and is introduced to prevent elements from collapsing under extremely high velocity gradients. The default value of  $b_2 = 1.2$  was used in this analysis.

### Rayleigh Damping

Rayleigh damping is damping which is proportional to the stiffness and mass of the material. It can be expressed in terms of the fraction of critical damping by the following relationship:

$$\xi = \frac{\chi_R}{2\omega_i} + \frac{\delta_R \omega_i}{2} \quad (7.11)$$

where  $\xi$  = fraction of critical damping

$\chi_R$  = factor for *mass* proportional damping

$\delta_R$  = factor for *stiffness* proportional damping

$\omega_i$  = natural frequency at this mode

The mass proportional damping factor introduces damping forces caused by the absolute velocities of the model, which the stiffness proportional damping introduces damping forces caused by the elastic material stiffness. Rayleigh damping is applied to ABAQUS models by specifying the  $\chi_R$ , and  $\delta_R$  factors. Mass proportional damping was applied to the models produced for this project.

The mass proportional damping factor,  $\chi_R$ , was calculated using the following method:

1. Calculation of the fraction of critical damping

The fraction of critical damping in paste fill was calculated from velocity versus times curves obtained during the field tests described in Chapter 4. Such data was not available to calculate the fraction critical damping in rock, so a search of literature was conducted. According to (ABAQUS, 2003), rock generally has a fraction of critical damping of 2 to 5 % and 3 % fraction of critical damping (i.e.  $\xi = 0.03$ ) is suitable for analysis. This value was used for rock in the absence of suitable waveforms from which to calculate the fraction.

### 2. Natural Frequency extraction

A natural frequency extraction analysis was conducted to extract the natural frequencies for different nodes. This extraction was run on a version of model 1 to obtain the frequencies for paste fill and on a version of model 2 to obtain the frequencies for rock. The models were run using the \*STEP, TYPE=FREQUENCY keyword. The natural frequency obtained for each material for mode 1 was used in the calculation of the mass proportional damping factor.

### 3. Calculation of $\chi_R$

Once the fraction of critical damping and the natural frequency are known, the mass proportional damping factor is calculated from Equation 7.11 by setting  $\delta_R$  equal to 0.0.

## 7.5.2. Interface between Paste Fill and Rock

A tunnel was excavated into a paste fill stope at Cannington Mine to conduct the field tests discussed in Chapter 4. The interface between the rock and the paste fill was visible within the tunnel wall. Observations of the interface between the paste fill and rock showed that the paste fill had completely filled the void in the mine, and no gaps between the rock and paste were visible. The rock face had a rough surface, so that it is likely any failure would occur within the paste fill adjacent to the interface rather than at the interface.

In order to model the transmission of the stress wave across the interface, the reflection and refraction of the wave need to be predicted. The amount of energy that is transmitted through the interface depends on the impedance of the rock and the paste. The impedance is calculated from the density of the material and the velocity of the wave in the material, both of which can be calculated from the material properties. Since the wave transmission is dependent on the material properties of the rock and the paste, contact definitions were not used to define the interface. Contact definitions would not make any difference to the transmission of the wave

across the boundary, but will add to the solution time of the problem. The interface was specified by assigning different material properties to elements on each side of the interface.

This method of modelling the interface was applicable as the intent of the model is to model the transmission of a blast wave through the material, and blast damage is measured using ppv. If the removal of the ore and the stability of the nearby paste fill material were to be modelled, contact definitions would be necessary to define the interface, as the behaviour of the material at the interface becomes important.

### **7.5.3. Boundaries**

Infinite elements were located at the boundaries of the models to avoid provide a non-reflecting boundary. The infinite elements were used on the base and side of the axisymmetric models, and on the all sides of the plane strain model to provide a “quiet” boundary to the model. The infinite elements introduce additional boundary damping which minimise the reflection of dilatational and shear wave energy back into the finite element mesh.

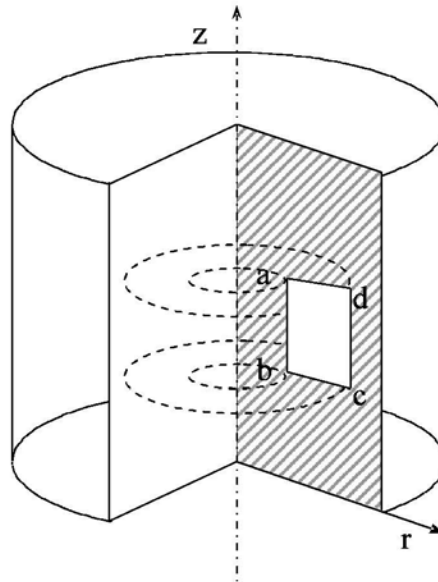
### **7.5.4. Element Definitions**

#### ***7.5.4.1. Element Types***

A wide variety of element types are available in ABAQUS, which enable the modelling package to be used for a wide variety of analysis types. These element types are broken up into families based on the different geometry types. The element families which are useful for the analysis of soil and rock are continuum (solid) elements and infinite elements. Within the continuum elements and infinite elements families, the elements are further classed within groups based on the dimensions of the problem. Since axisymmetric models and two-dimensional models were used for this project, discussion of elements available will be limited to these classes.

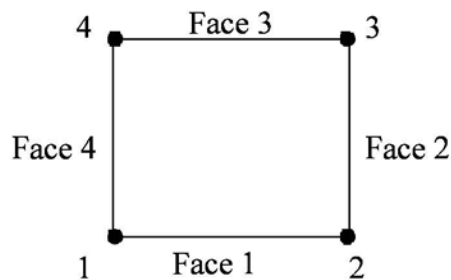
#### ***Axisymmetric Elements***

Axisymmetric elements are used when the system being modelled can be described using polar coordinates ( $r$ ,  $z$  and  $\theta$ ) and the loading is symmetrical about the axis. A model of a single blast hole is an example of such a case. If the loading and material properties are independent of  $\theta$ , the solution can be described completely in the  $r$ - $z$  plane. A typical axisymmetric element is shown in Figure 7.13.



**Figure 7.13 – Typical Axisymmetric Element (ABAQUS 2003)**

Four node, bilinear axisymmetric elements (CAX4) were used in the stage 1 and 2 models discussed previously in this chapter. The active degrees of freedom for these elements are  $u_r$  and  $u_z$ , displacement degrees of freedom in the  $r$  and  $z$ -directions. The elements are specified by providing the  $r$ - $z$  coordinates of the nodes and defining the nodes that make up the elements. The nodes are specified in the order shown in Figure 7.14.



**Figure 7.14 – Node Numbering on 4 node Axisymmetric Element (ABAQUS 2003)**

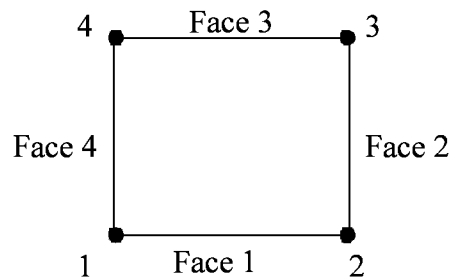
### **Two-Dimensional Elements**

Two types of two-dimensional elements are available within ABAQUS, plane stress and plane strain elements. Plane stress elements are used when the thickness of a body is small relative to its in-plane dimensions. This type of element is typically used for thin, flat bodies. The elements are defined in the  $X$ - $Y$  plane, as are all loadings and deformation. Plane strain elements are used when it can be assumed that the strains in a loaded body are functions of the planar coordinates and the out-of-plane normal and shear strains are equal to zero. Plane strain elements are typically used for bodies that are very thick relative to their lateral dimensions.

The elements are defined in the X-Y plane and all loading and deformation also occur in this plane. Plane strain elements were used for the two-dimensional models created for this project.

Four node, bilinear plane strain elements (CPE4) were used in model 3. The active degrees of freedom for these elements are  $u_x$  and  $u_y$ , displacement degrees of freedom in the x and y-directions.

The elements are specified by providing the X-Y coordinates of the nodes and defining the nodes that make up the elements. The nodes are specified in the order shown in Figure 7.15.



**Figure 7.15 – Node Numbering on 4 node Plane Strain Element (ABAQUS 2003I)**

### ***Infinite Elements***

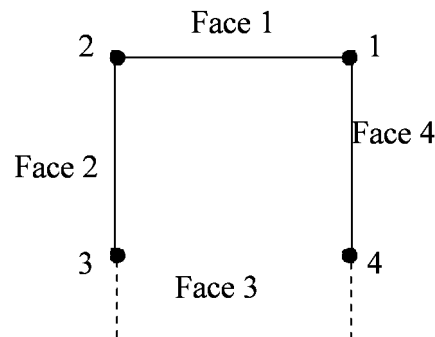
Infinite elements were used in all three models to provide a non-reflecting boundary. These elements are often used in cases where the region of interest is small compared to the surrounding medium and they provide a “quiet” boundary to the finite element model in dynamic analyses. Infinite elements are designed to be used in conjunction with planar, axisymmetric or three-dimensional finite elements and are available as plane stress, plane strain, three-dimensional or axisymmetric infinite elements. The standard finite elements are used to model the region of interest and the infinite elements are used to model the far field.

The material properties assigned to infinite elements must match the material properties assigned to the elements adjacent to the infinite elements. Since the solution in the far field is assumed to be linear, only linear material properties can be applied to infinite elements. The material response is assumed to be isotropic in infinite elements.

Four-node, axisymmetric infinite elements (CINAX4) were used in models 1 and 2, while four-node, plane strain infinite elements (CINPE4) were used in model 3.

Infinite elements are specified in a similar manner to the type of elements they are to be used in conjunction with. However, the node numbers must be specified in such a way that the first face is the face that is connected to the finite element mesh, as shown in Figure 7.16. The

location of the nodes located away from the finite element mesh in the infinite direction (nodes 3 and 4 in Figure 7.16) is not meaningful for an explicit dynamic analysis as these nodes are not used in explicit dynamic analyses.



**Figure 7.16 – Node Numbering on 4 Infinite Element (ABAQUS 2003)**

The infinite elements introduce additional normal and shear transactions on the boundary that are proportional to the normal and shear components of the velocity at the boundary during dynamic steps. The boundary damping constants are chosen to minimise the reflection of dilatational and shear energy back into the mesh. While this formulation does not provide perfect transmission of energy out of the mesh, it usually provides acceptable modelling for most practical cases (ABAQUS 2003).

#### **7.5.4.2. Element types used in Models**

The following element types were used in the numerical models:

- The stage 1 model in paste fill (section 7.3.2) and the stage 2 model in rock (section 7.3.3): 4 node, bilinear elements (CAX4) were used for the body and 4 node linear, one-way infinite elements (CINAX4) were used for the side and base of the axisymmetric models.
- The stage 3 Model (section 7.3.4): 4 node, bilinear plane strain elements (CPE4) were used for the body and 4 node linear, one-way infinite elements (CINPE4) were used for the sides of the plane strain model.

The blast load was applied as a surface based distributed load using the \*DSLOAD keyword. This type of loading is available to all elements which have displacement degrees of freedom, and was able to be applied to both the axisymmetric and plane strain elements. In the case of axisymmetric elements, the distributed load is the load applied per unit area.

### 7.5.5. Loading of Model

The blast load was applied to the models for all three stages as a surface load applied to the surface of an equivalent cavity of the blast hole. The load is applied using the \*DSLOAD keyword, using the AMPLITUDE parameter to specify the name of the amplitude curve that specifies the variation of the load with time. The name of the surface and the pressure is specified in the datalines. The loads applied to the models are calculated by multiplying the pressure by the amplitude curve. The amplitude curve is specified in the model data using the \*AMPLITUDE keyword. For more information on the loading of the models, refer to Chapter 6.

### 7.5.6. Outputs

ABAQUS/Explicit creates the following output files during an analysis:

- Data file (*job-name.dat*): a text file that is generated by the analysis input file processor and contains printed output of the model definition, the history definition and any error or warning messages that were detected while processing the input file;
- Output database file (*job-name.odb*): a binary file used to store results for postprocessing with the Visualization module of ABAQUS/CAE (ABAQUS/Viewer);
- Selected results file (*job-name.sel*): a file which stores user-selected results which are converted into the results file;
- Results file (*job-name.fil*): a file containing results which can be read by external postprocessors;
- Message file (*job-name.msg*): a text file containing diagnostic messages about the progress of the solution; and
- Status file (*job-name.sta*): a text file containing information about the status of the analysis, diagnostic messages and information about the stable time increment.

The results of an analysis were analysed using ABAQUS/CAE to analyse an output database file in the Visualization module. From ABAQUS/CAE, the deformed mesh can be plotted and results can be viewed as contour plots on the mesh or as graphs.

Two types of output data are available in ABAQUS, field output and history output, which are defined as follows:



- Field output: output data used for infrequent requests for a large portion of the model. This data is used to generate contour plots, animations, displaced shape plots and x-y plots. This data is requested as complete sets of basic variables.
- History output: output data used for frequent requests for a small portion of the model. This data is used to generate x-y plots. This data can be requested as individual sets of basic variables, such as a particular stress component.

The output data is controlled by the \*OUTPUT option. Field output data is requested by using the FIELD parameter on the \*OUTPUT option, in conjunction with the \*CONTACT OUTPUT, \*ELEMENT OUTPUT, \*NODE OUTPUT, or \*RADIATION OUTPUT option, depending on the type of output required. History output data is requested by using the HISTORY parameter on the \*OUTPUT option, in conjunction with the command for the type of output required. The number of history output requests is important as more than 1000 requests causes the performance to degrade. As each component of a variable is considered a separate request, typically only the components of interest are specified. The output frequency is also specified with the output request.

The following output requests were specified in the numerical models for all three stages:

- Field Data: The VARIABLE=PRESELECT parameter was specified to indicate that the default output variables for the procedure type should be written to the output database.
- History Data: Acceleration, Velocity and Displacement in directions 1 and 2

Field output data was requested for the entire model in all three models. History data was specified for the following:

- Stage 1 Model (section 7.3.2): Output was specified at nodes level with the explosive cartridge, at 1.0 m intervals.
- Stage 2 Model (section 7.3.3): Output was specified at nodes at mid height of the section of the blast hole containing explosive, at 1.0 m intervals.
- Stage 3 Model (section 7.3.4): Output was specified at nodes in both paste fill and rock at mid height of the section of the blast hole containing explosive, at 1.0 m intervals.

The analysis of the numerical models is discussed in Chapter 8.

## **8. Numerical Model Results and Discussion**

The results of the numerical models are presented in the following chapter. A description of each model is given in Chapter 7. As discussed in section 7.3, the numerical modelling was conducted in a three stage process, with a set of models created for each stage. The stages were as follows:

- Stage 1: A single column of explosive in paste fill;
- Stage 2: A single column of explosive in rock; and
- Stage 3: Columns of explosive in rock adjacent to paste fill.

### ***8.1. Stage 1 Model: Single Column of Explosive in Paste Fill***

#### **8.1.1. Stage 1 Model Scenarios**

As discussed in section 7.3.2, the stage 1 model was based on the field instrumentation tests discussed in chapter 4. In these tests, blast holes within the paste fill were detonated and monitored in order to obtain a representative equation for predicting peak particle velocity within paste fill. The purpose of the stage 1 model was to validate the numerical model against data obtained in the field instrumentation tests, and to model the effects of the cement and solids content of paste fill on the transmission of blast waves within the material. The field instrumentation test data was used for validation of the model as it ensured that the transmission of blast waves within paste fill was being modelled correctly. Although blasting within the paste fill would not normally occur, it was considered necessary to conduct the field instrumentation tests and model this scenario to ensure that the transmission of the blast wave through the paste fill could be correctly modelled. The transmission of blast waves through rock and across the rock/paste fill interface were modelled in stages 2 and 3. The scenario modelled in this case can be defined as follows:

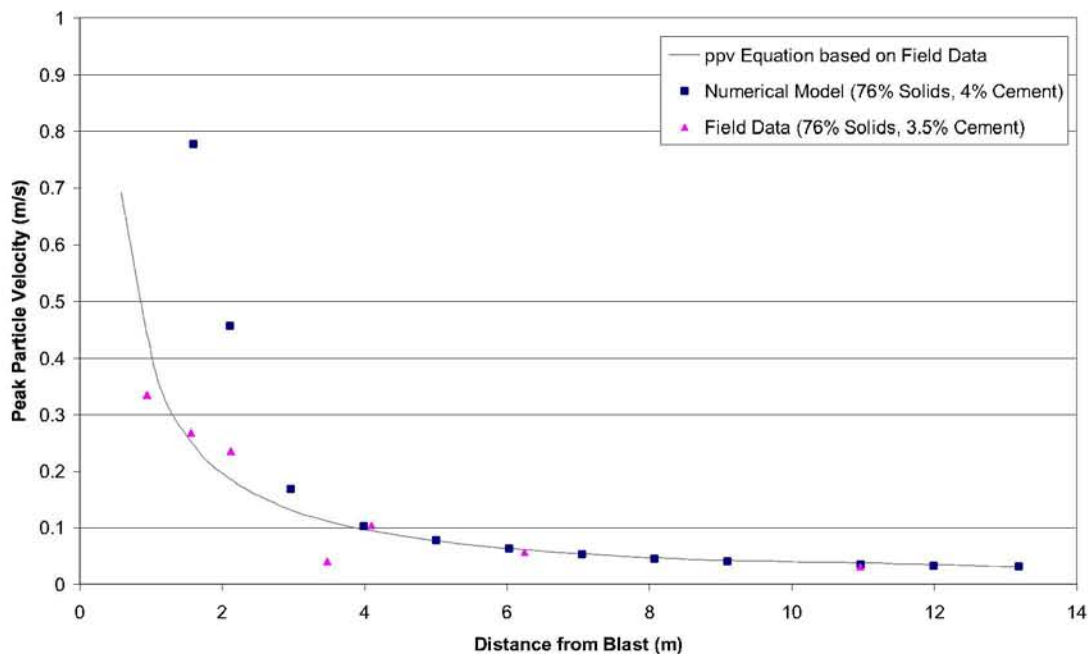
- The blast is through one 3 m long, 44 mm diameter borehole containing one cartridge of emulsion explosive;
- The borehole is located in a uniform mass of paste fill;
- The paste fill/rock interface is located at a sufficient distance from the blast hole that effects of the reflection of the blast wave from the interface are negligible; and
- The borehole is drilled perpendicular to the floor of the tunnel.

The stage 1 model was run for the mixes of paste fill shown in Table 7.1. An input file for a stage 1 model with a solids content of 76 % and a cement content of 4 % is given in Appendix F.

## 8.1.2. Stage 1 Model Results and Discussion

### 8.1.2.1. Comparison of Model Results and Field Data

The results from the run of model 1 for a paste fill mix of 76 % solids and 4 % cement content was compared against the data obtained during the field instrumentation tests as shown in Figure 8.1. The model results are also compared against the peak particle velocity predicted by the ppv equation and the constants obtained for paste fill from the field instrumentation tests. The form of the ppv equation is given in Equation 4.5. The charge weight for the field instrumentation tests was 170 g.



**Figure 8.1 – Stage 1 Model Results and Field Instrumentation Test Data**

As can be seen, for distances greater than or equal to 2 m from the explosive in paste fill the model matches the field data and the predicted peak particle velocity quite closely. For distances less than 2 m from the explosive source the model overestimates the peak particle velocity. The model overestimates the peak particle velocities close to the explosive source as the crushing and cracking mechanisms that occur in the vicinity surrounding the borehole are not considered in the numerical model.

As discussed in section 6.6, the blast pressure was applied to the walls of a cylindrical “equivalent cavity” in order to model only the seismic zone around the borehole, in which elastic wave propagation is expected to occur. This method avoids modelling the region where new cracks in the material are initiated from the shock wave during an explosion as the blast is applied at a point where the strength of the material is greater than the stresses experienced from the shock wave. This allows the propagation of the blast wave within the material to be modelled without the need to use complex material models and cracking models. For large scale models such as those used in this work, the use of an “equivalent cavity” dramatically reduces the time required to solve the model. In production blasts, the blast holes are located within the rock and the rock/paste fill interface is generally located beyond the region where cracks are initiated. Since the purpose of this project is to predict the behaviour of the paste fill adjacent to blasting, the ability to model the cracking mechanism in paste fill was not considered necessary.

The velocity waveforms produced by the numerical model were also compared against field data. The shape of the velocity profile predicted by the numerical model is similar to the field data.

### ***8.1.2.2. Damage to Paste Fill***

Figure 8.2 shows the deformed mesh and the stress experienced in the model in the area the blast was applied. As can be seen, the numerical model predicts localized deformation only, which agrees with observations during the field tests.

### ***8.1.2.3. Effect of Cement Content on Peak Particle Velocity***

The stage 1 model was run for mixes of paste fill with different cement contents and solid contents to observe the effect these changes have on peak particle velocity. A comparison of fill mixes with 76 % solids and 2 %, 4 % and 6 % cement content is shown in Figure 8.3. Figures 8.4 and 8.5 show similar comparisons for mixtures with 78 % and 80 % solids respectively. The results show that the peak particle velocity in the paste fill decreases as the strength of the paste fill is increased by increasing the cement content. This in turn means that the damage caused to the paste fill by blasting decreases as the cement content is increased.

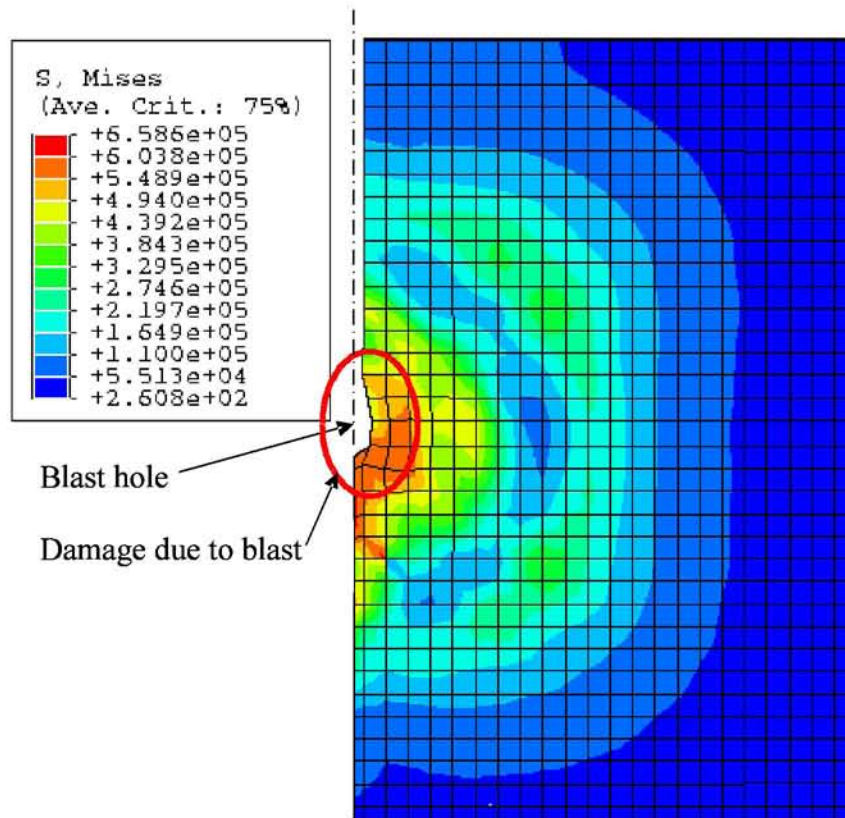


Figure 8.2 – Stress in the Region of the Blast Load

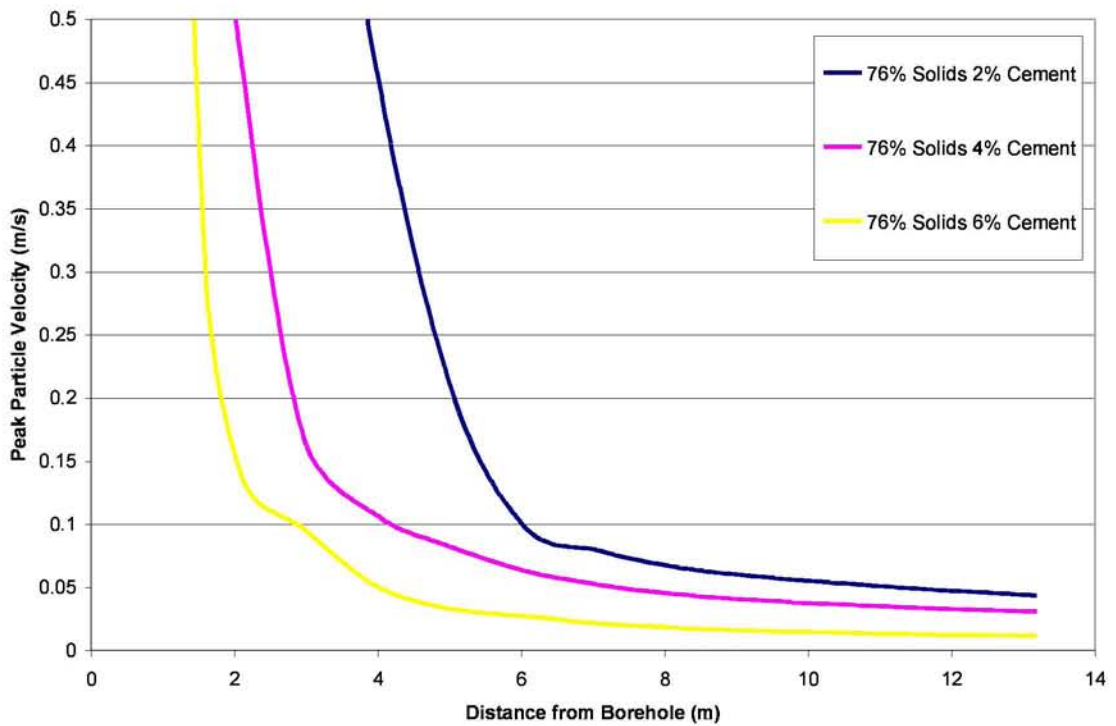
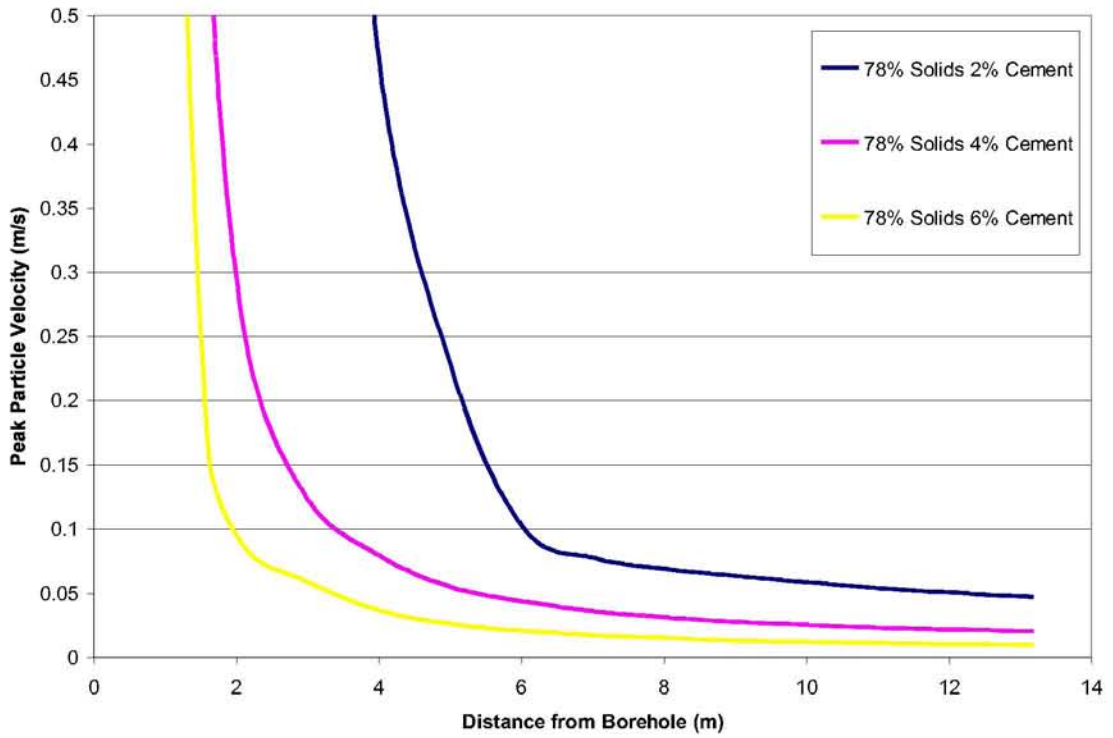
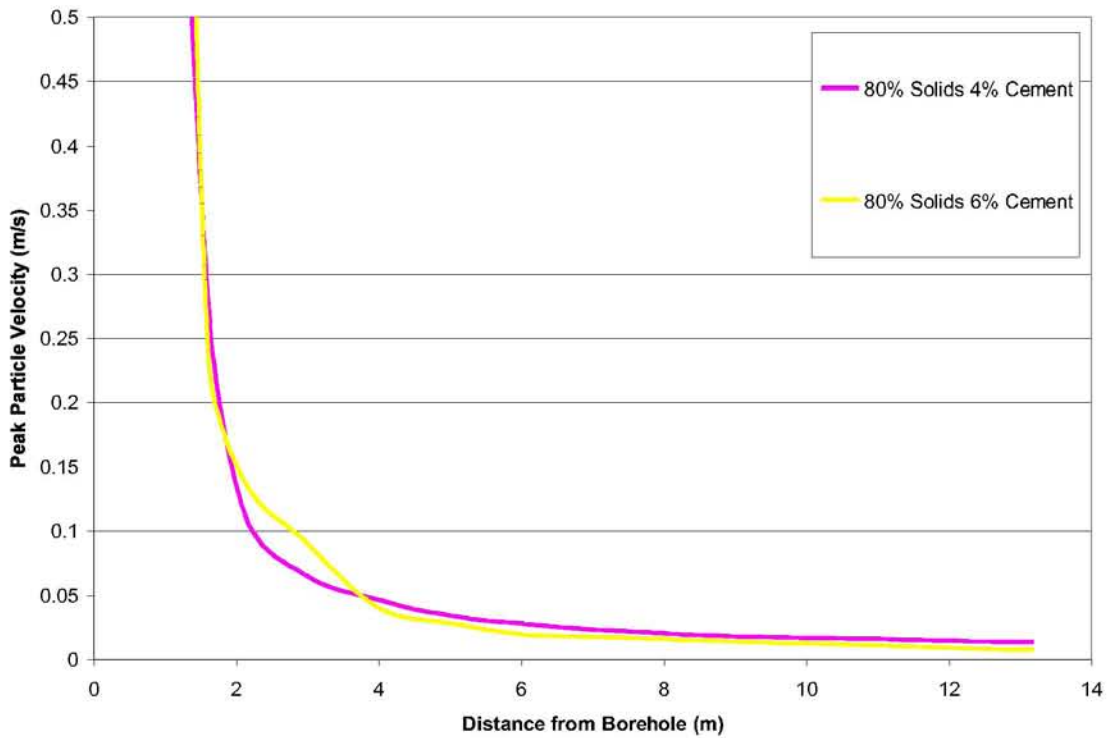


Figure 8.3 – Stage 1 Model Results for Paste Fill with 76% Solids Content



**Figure 8.4 – Stage 1 Model Results for Paste Fill with 78% Solids Content**



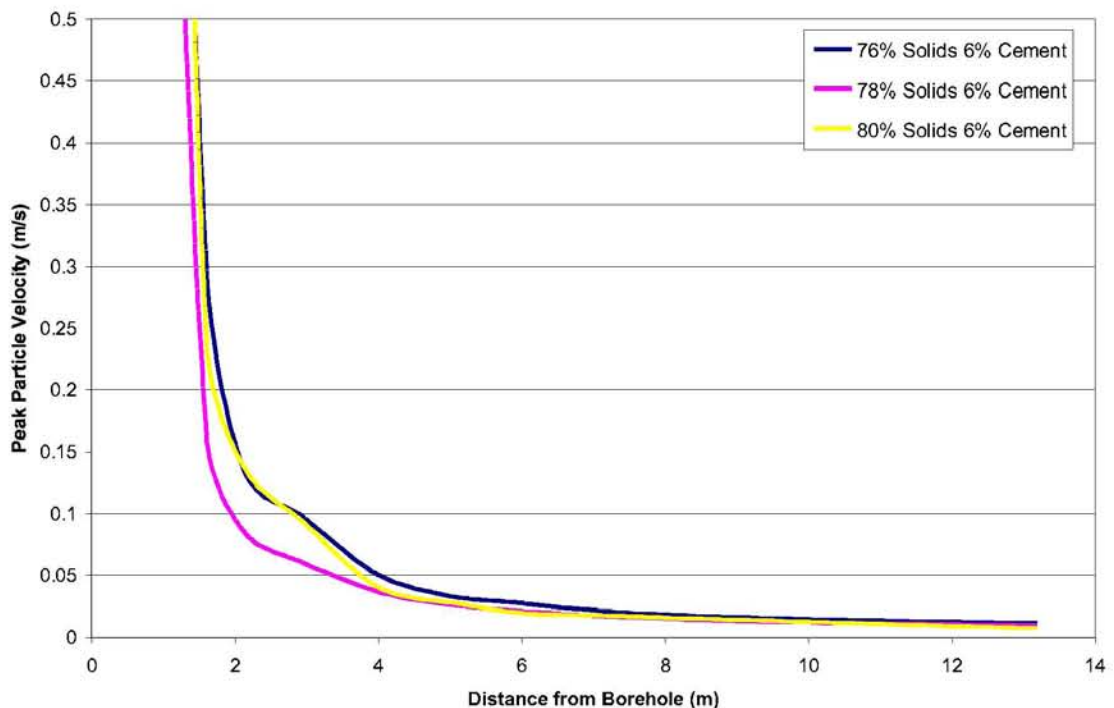
**Figure 8.5 – Stage 1 Model Results for Paste Fill with 80% Solids Content**

#### 8.1.2.4. *Effect of Solids Content on Peak Particle Velocity*

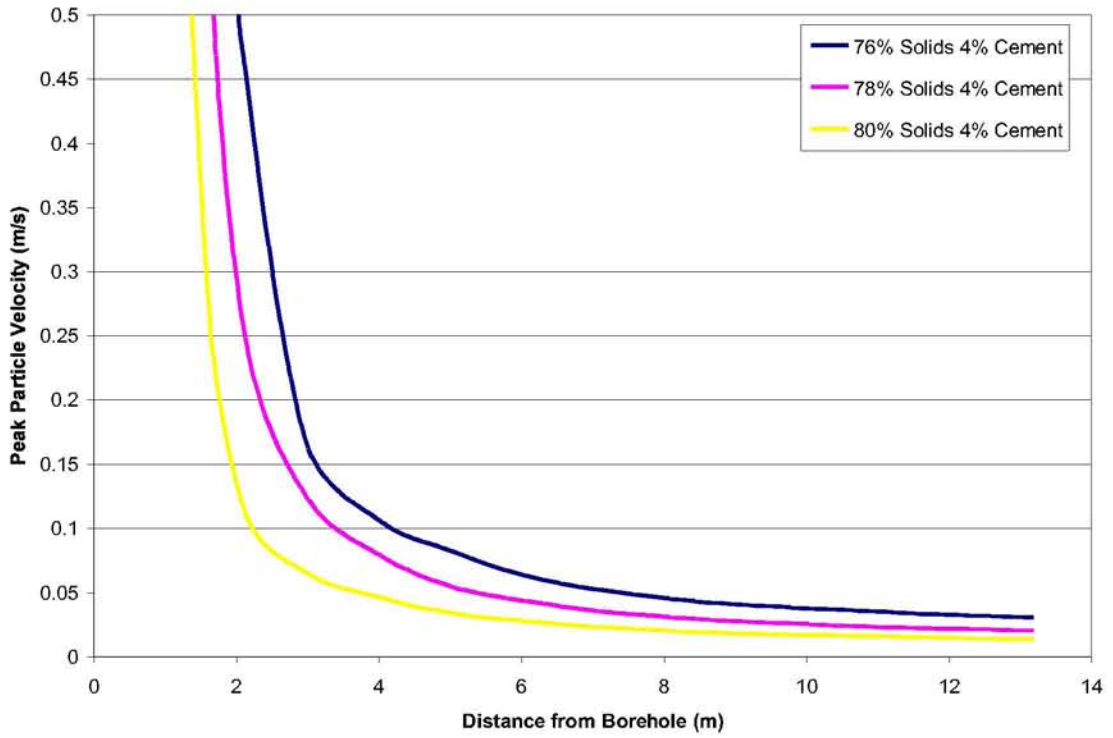
The stage 1 model was run for mixes of paste fill with different cement contents and solid contents to observe the effect these changes have on peak particle velocity. A comparison of fill mixes with 6 % cement and 76 %, 78 % and 80 % solids content is shown in Figure 8.6. Figures 8.7 and 8.8 show similar comparisons for mixtures with 4 % and 2 % cement respectively. The results show that the peak particle velocity in the paste fill decreases as the strength of the paste fill is increased by increasing the solids content, when the cement content is low. For a cement content of 6 %, the results were similar for all solids contents. This in turn means that the damage caused to the paste fill by blasting decreases as the solids content is increased when the cement content is low.

#### 8.1.2.5. *Comparison between Effect of Cement and Solids Content*

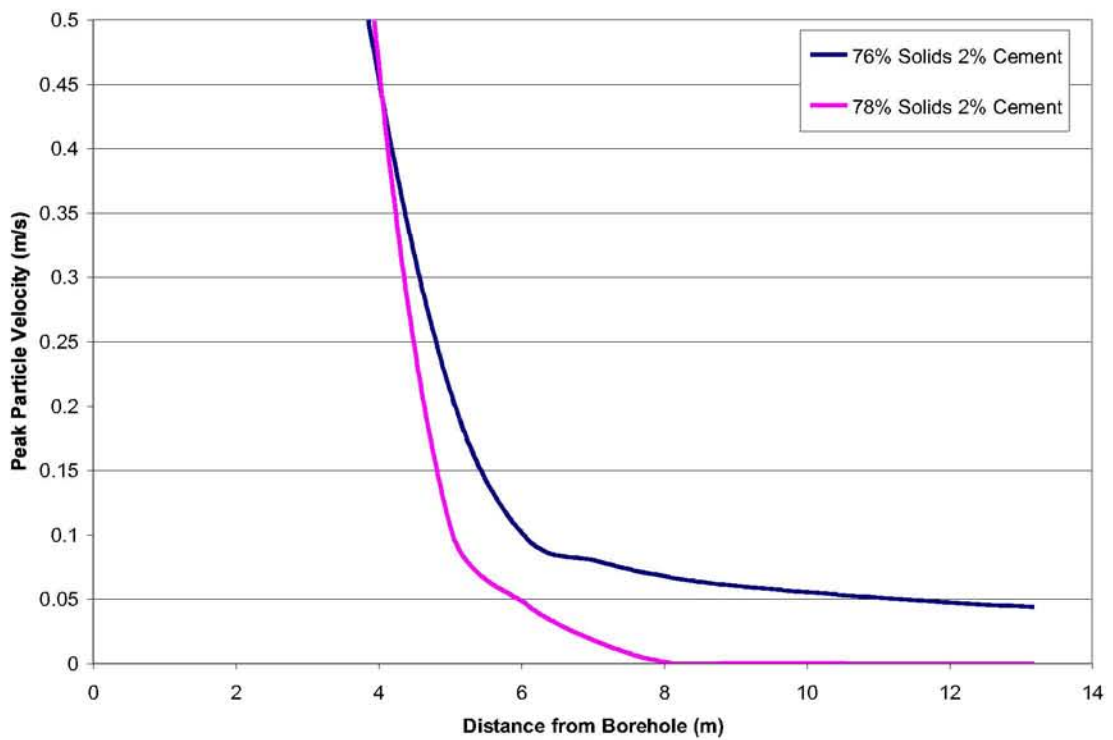
Figure 8.9 shows a comparison between the results from all paste fill mixes that were run in the stage 1 model. This graph shows that an increase in cement content produces a larger reduction in peak particle velocity in the paste fill than a corresponding increase in solids content does. These results indicate that a small decrease in cement content can be offset by an increase in solids content without increasing the volume of paste fill that fails, as reported in van Gool et al. (2006). For example, a 76 % solids and 6 % cement mixture of paste fill results in peak particle velocities in the fill of the same magnitude as an 80 % solids and 4 % cement paste fill.



**Figure 8.6 – Stage 1 Model Results for Paste Fill with 6% Cement Content**

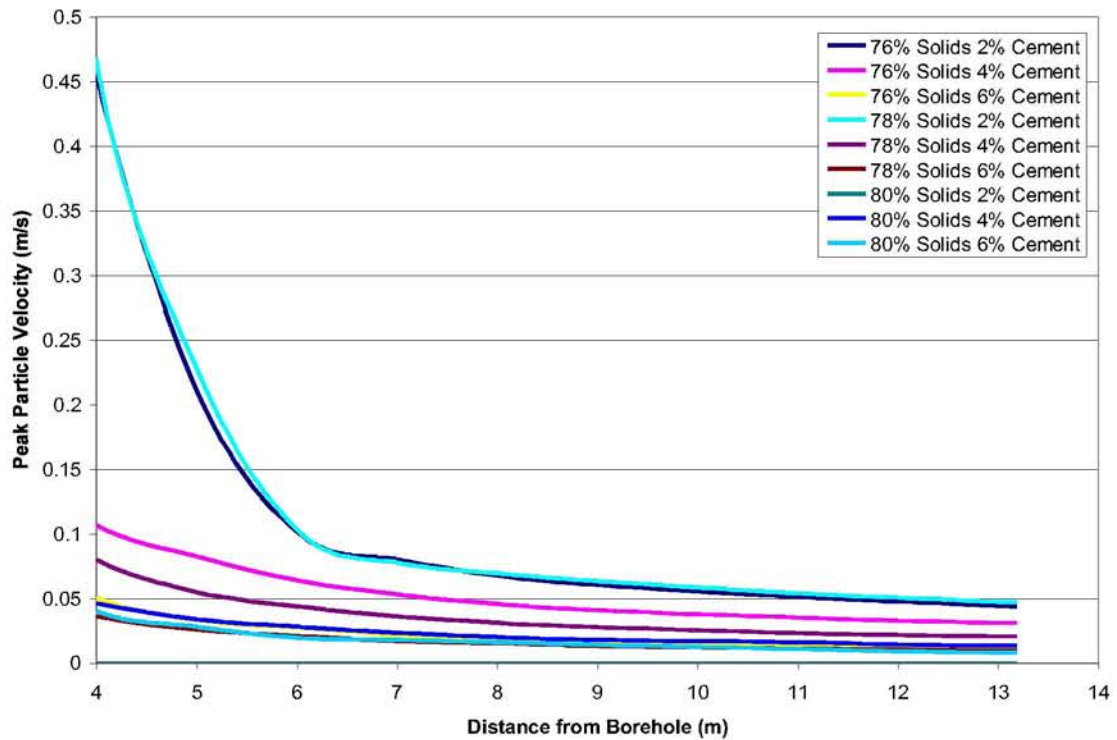


**Figure 8.7 – Stage 1 Model Results for Paste Fill with 4% Cement Content**



**Figure 8.8 – Stage 1 Model Results for Paste Fill with 2% Cement Content**





**Figure 8.9 –Stage 1 Model Results for Different Paste Fill Mixes**

## 8.2. Stage 2 Model: Single Column of Explosive in Rock

### 8.2.1. Scenarios Modelled

As discussed in section 7.3.3, the stage 2 model was based on the scenario of a single column of emulsion explosive in a rock mass. The scenario modelled in this case can be defined as follows:

- 89 mm diameter borehole, as used in the production blasts at Cannington Mine;
- One 3 m long borehole containing a 2 m length of emulsion explosive and 1 m of stemming;
- The borehole is located in a uniform mass of rock;
- The rock/paste fill interface is located at a sufficient distance from the blast hole that effects of the reflection of the blast wave from the interface are negligible i.e. the entire blast and the effects are confined within the rock; and
- The borehole is drilled perpendicular to the floor of the tunnel.

The stage 2 model was run for the following rock types found at Cannington Mine in order to assess the effect of rock type on wave propagation:

- Broadlands (BL)
- Burnham (BM)
- Glenholme (GH)
- Magnetite bearing hedenbergite rock (HDMT)
- Pyrobole Rock (PXAM)
- Garnetiferous quartzite/arkose and meta Meta quartzite/arkose (QZGA/IT)
- Hedenbergite quartzite rock (QZHD)

An input file for a stage 2 model of an explosive column in Broadlands rock type is given in Appendix F.

### **8.2.2. Results and Discussion**

#### ***8.2.2.1. Comparison of Results against Peak Particle Velocity Prediction Equation***

A site specific peak particle velocity equation for Cannington Mine rock developed by Sartor (1999) was used to validate the stage 2 model. As discussed in section 2.3.2, Sartor used equation 2.5 to model the vibration induced damage from blasting in rock at Cannington Mine. Data such as the timing and amplitude of the peak particle velocity were measured, using a set of geophones, to develop a site-specific vibration equation for Cannington Mine rock. The constants in the equation were found to be:  $K = 2938$ ,  $\alpha = \frac{1}{2}$   $\beta = 0.66$ .

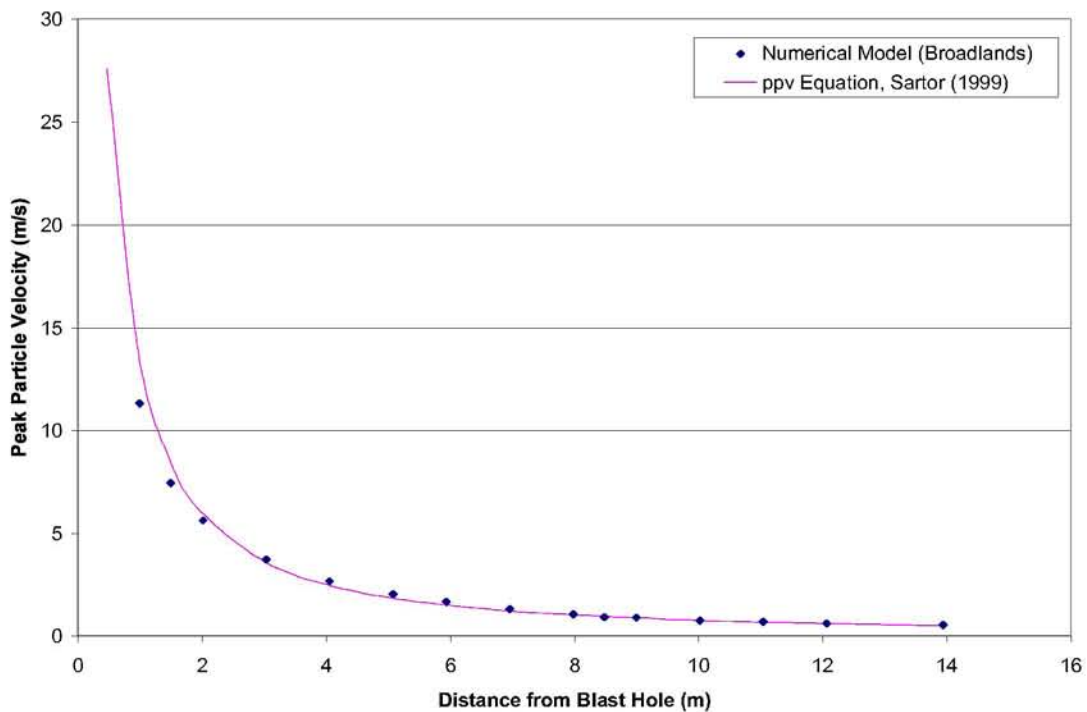
The model results when Broadlands rock type was used were compared against the prediction of the peak particle velocity using the parameters obtained from the Sartor's work in order to validate the model. The results of the explosive column in rock are shown in Figure 8.10. As can be seen, for distances greater than or equal to 1.0 m from the explosive in rock the model matches the predicted ppv quite closely, although the ppv are overestimated at distances less than 1.0 m from the source. The model overestimates the peak particle velocities close to the explosive source as the crushing and cracking mechanisms that occur in the vicinity surrounding the borehole are not considered in the numerical model. Since the purpose of this project is to predict the behaviour of the paste fill adjacent to blasting, and the closest borehole modelled

was located 2.5 m from the rock/paste fill boundary, the ability to model the cracking mechanism in rock was not considered necessary.

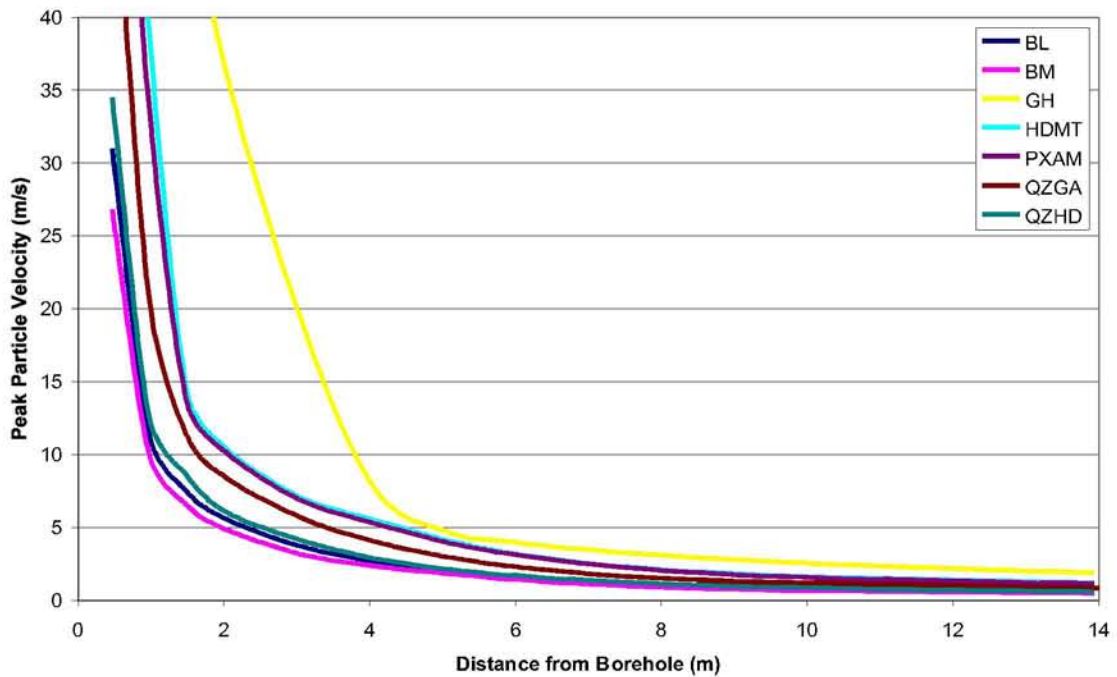
### 8.2.2.2. *Effect of Rock Parameters on Peak Particle Velocity*

Figure 8.11 shows a comparison between the results from the different rock types that were run in the stage 2 model. As can be seen, the majority of rock types yield similar results in the model. The exception is the Glenholme (GH), which is the weakest rock type that was modelled. Peak particle velocity predictions for the other 6 rock types will yield similar results. The Broadlands (BL) rock type was used for the stage 3 model.

The peak particle velocities predicted for the Glenholme are much higher than those predicted for the other rock types, as expected for the weaker rock. Peak particle velocity predictions for this rock type are likely to be overestimated in the steep region of the curve. Therefore, peak particle velocity predictions for Glenholme are likely to only be accurate for distances greater than 4 m from the rock.



**Figure 8.10 – Stage 2 Model Results Versus Peak Particle Velocity Predictions**



*Figure 8.11 – Stage 2 Model Peak Particle Velocities for Different Rock Types*

### **8.3. Stage 3 Model: Column of Explosive in Rock Adjacent to Paste Fill**

#### **8.3.1. General**

As discussed in section 7.3.4, the stage 3 model was based on the scenario of columns of emulsion explosive in a rock mass adjacent to a paste fill stope. The system was modelled in plan view using plane strain elements. The Broadlands rock type and a paste fill mix of 76 % solids and 4 % cement were used for this analysis. The paste fill stope in this model was 25 m by 25 m in plan view, representative of the average dimensions of a stope. Several scenarios were modelled, with the difference between the scenarios being the number and location of the boreholes.

#### **8.3.2. Scenario 1: Single Borehole Detonated Adjacent to the Centreline of a Paste Fill Stope**

The stage 3 model scenario 1 consisted of modelling a single column of explosive adjacent to a paste fill stope. The column of explosive was located adjacent at the centreline of the paste fill stope as shown in Figure 7.6. The following variations were included in scenario 1:

- Two different borehole diameters were used, 89 mm and 76 mm. The majority of the boreholes in the production blasts monitored and discussed in Chapter 3 were 89 mm diameter boreholes, however, some boreholes adjacent to the paste fill had a diameter of 76 mm.
- The model was solved for the detonation of a single blast hole. Four different models were solved with the blast hole located at a distance of 2.5, 5, 7.5 and 10 m between the rock/paste fill interface and the blast hole.

An input file for a stage 3 scenario 1 model of an explosive column located 2.5 m from the paste fill stope is given in Appendix F.

### ***8.3.2.1. Effect of Rock/Paste Fill Interface***

Figures 8.12 to 8.15 show the particle velocity in the rock and the paste fill at 5, 20, 45 and 90 ms respectively after the detonation of an 89 mm diameter blast hole located 2.5 m from the rock/paste fill interface. Together, these figures show the transmission of the wave across the rock/paste fill interface. The boundary between the rock and the paste fill is shown with a red line and the location of the blast hole is shown with a red circle. The following observations were made from the models:

- A portion of the wave was reflected back into the rock at the rock/paste fill interface. This resulted in some high velocities being observed at the boundary wall in Figure 8.12.
- The refracted wave travelled through the paste fill much slower than the reflected wave travelled through the rock. The reflected wave can be seen leaving the system in Figure 8.13 prior to the refracted wave in the paste fill has moved a significant distance from the rock/paste fill boundary. In Figures 8.14 and 8.15, it can be seen that as the refracted wave begins to cross the paste fill, the reflected waves has left modelled region of the rock.

The much slower velocity of the wave in the paste fill in comparison to the rock is due to the different p-wave velocities in the different materials. As shown in Table 3.10, the p-wave velocity in the rock is 2330 m/s while the p-wave velocity in paste fill is 176 m/s. These model observations agree with observations made from the field monitoring program discussed in Chapter 3.

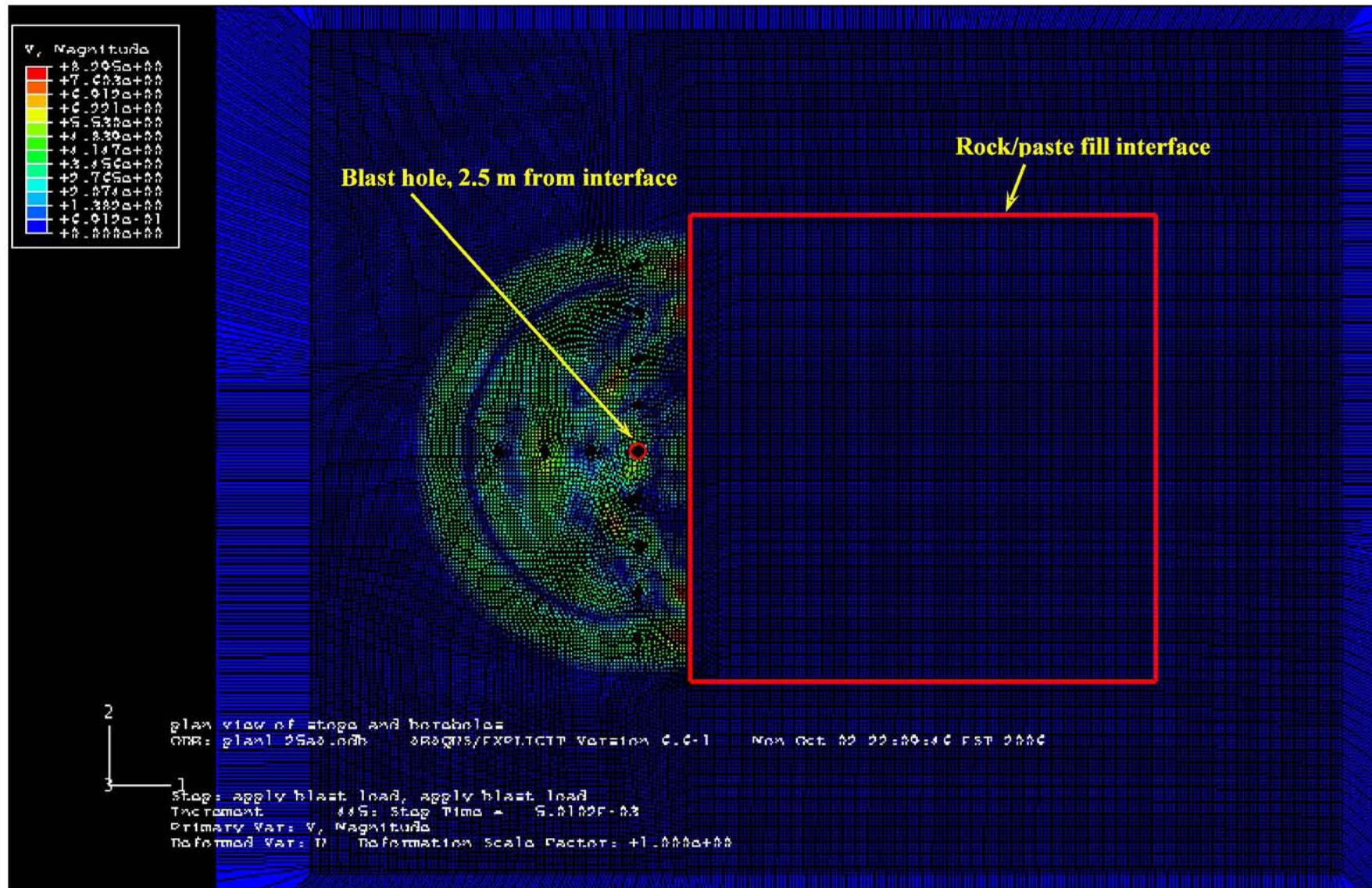


Figure 8.12 – Particle Velocity 0.005 s After Detonation

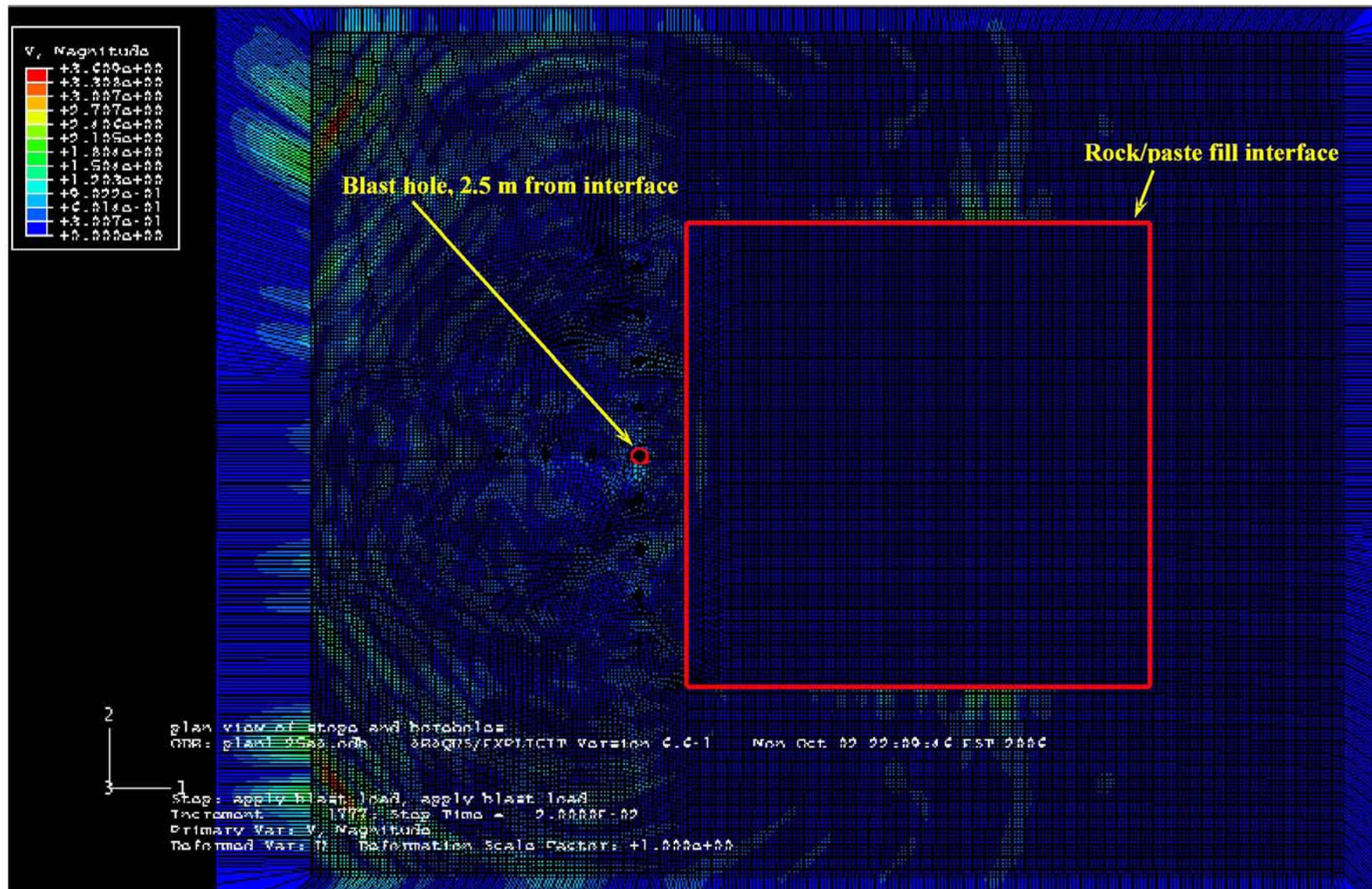


Figure 8.13 – Particle Velocity 0.020 s After Detonation

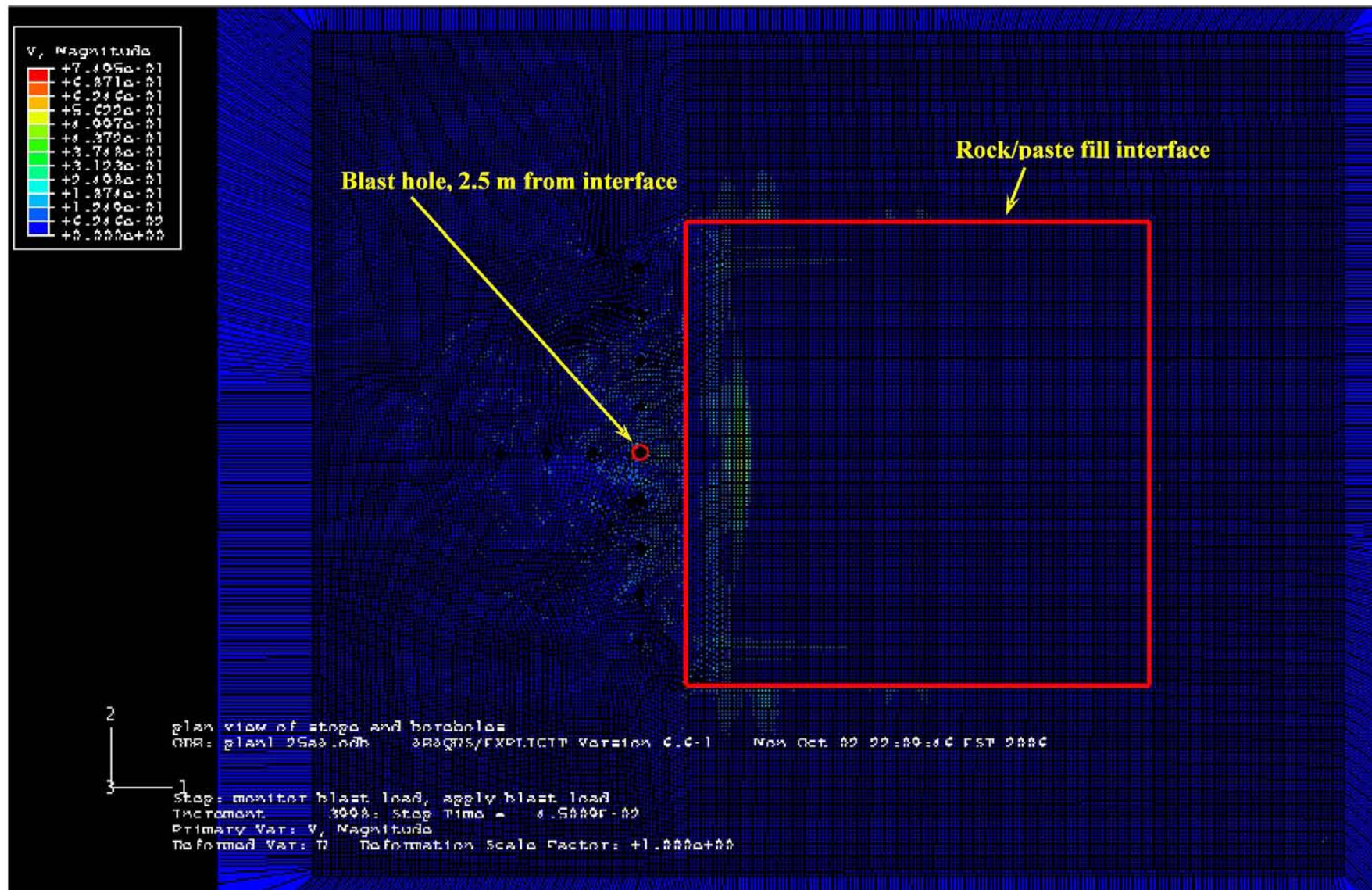


Figure 8.14 – Particle Velocity 0.045 s After Detonation



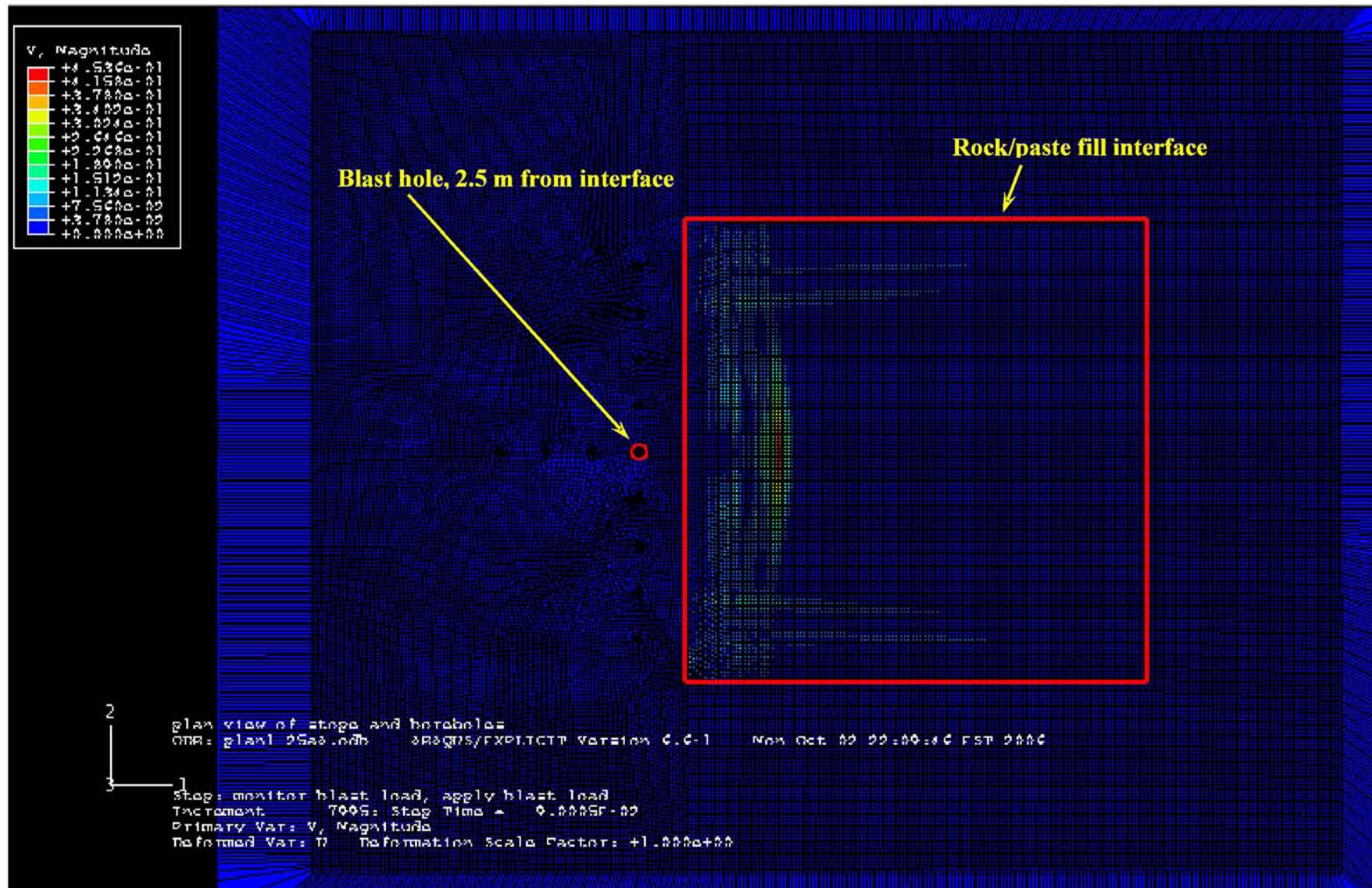


Figure 8.15 – Particle Velocity 0.090 s After Detonation

### **8.3.2.2. *Internal Reflections Within Paste Fill***

Figures 8.16 to 8.21 show the particle velocity in the rock and the paste fill at 49, 98, 147, 196, 245 and 294 ms respectively after the detonation of an 89 mm diameter blast hole located 5.0 m from the rock/paste fill interface. Together, these figures show the transmission of the wave across the paste fill stope. These figures show the internal reflections of the blast wave within the paste fill after the wave has crossed the rock/paste fill interface (shown in Figures 8.12 to 8.15 for an explosive column located 2.5 m from the rock/paste fill interface). The boundary between the rock and the paste fill is shown with a red line and the location of the blast hole is shown with a red circle. The following observations were made from the models:

- The wave is observed to travel across the stope (Figures 8.16 and 8.17), reflect back into the stope at the paste fill/rock boundary on the right hand side (Figure 8.18), travel back across the stope (Figures 8.19 and 8.20) and reflect back into the paste fill at the paste fill/rock boundary on the left hand side (Figure 8.21).
- Some refraction of the wave is seen at the paste fill/rock boundary opposite the side of the stope that the blasting occurred on (Figure 8.18).
- Reflection of the wave is also observed at the paste fill/rock boundary to the top and bottom of the figure.

The velocity profiles within the stope show the presence of a second wave arrival. The velocity profiles at a point on the centreline of the stope and 3.5 m from the rock/paste fill boundary are shown in Figures 8.22 and 8.23 and the location of the point is shown in Figure 8.24. The second wave arrival in the velocity profile is the arrival of the reflected wave at that point. The reflection of the wave back and forward within the paste fill was observed in the monitoring of the production blasts discussed in Chapter 3 and in the field instrumentation tests discussed in Chapter 4. Both the field data and the numerical model indicate that once a wave enters a paste fill stope, it stays within that stope and attenuates within the paste fill.

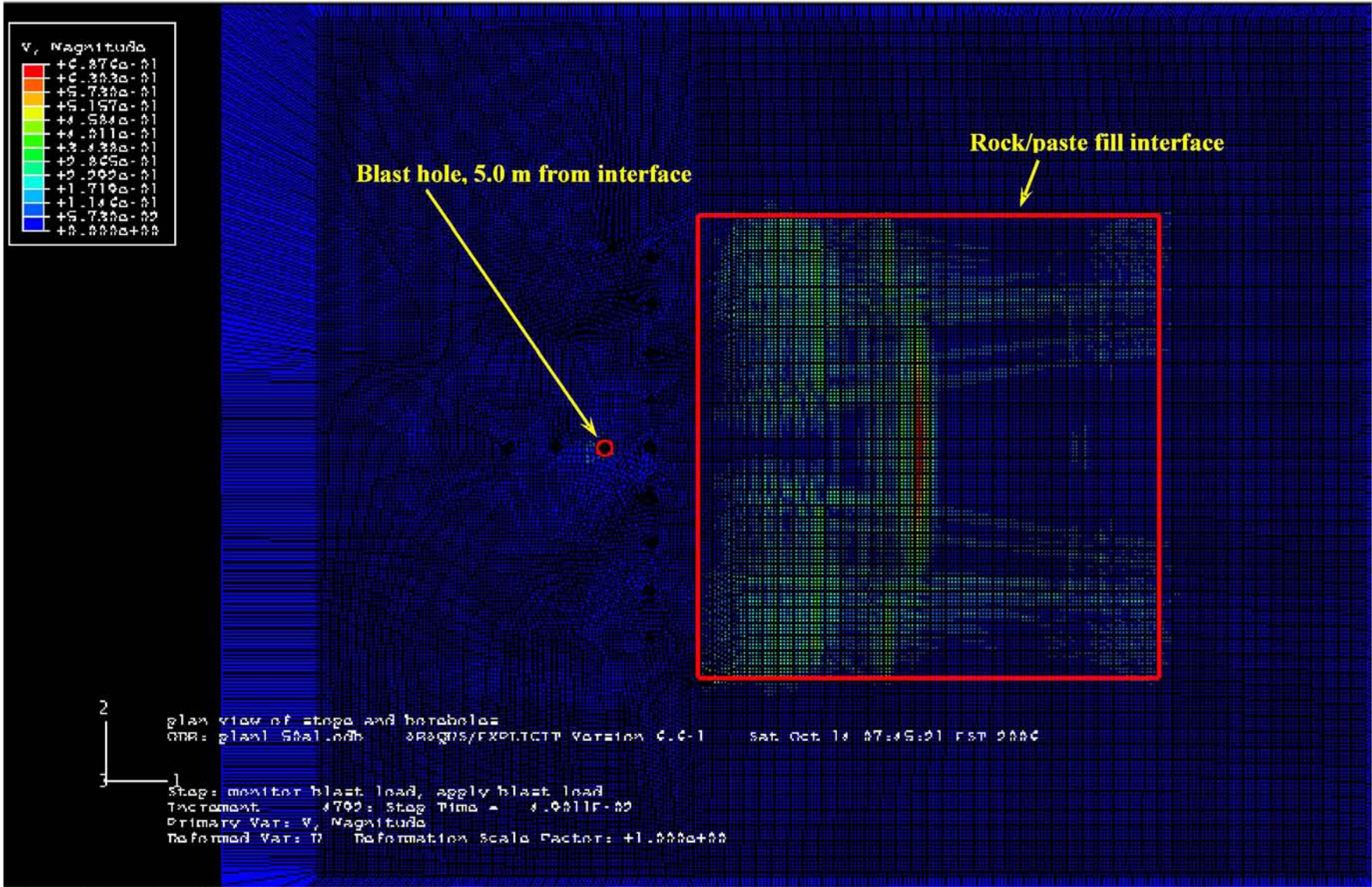


Figure 8.16 – Particle Velocity 0.049 s After Detonation

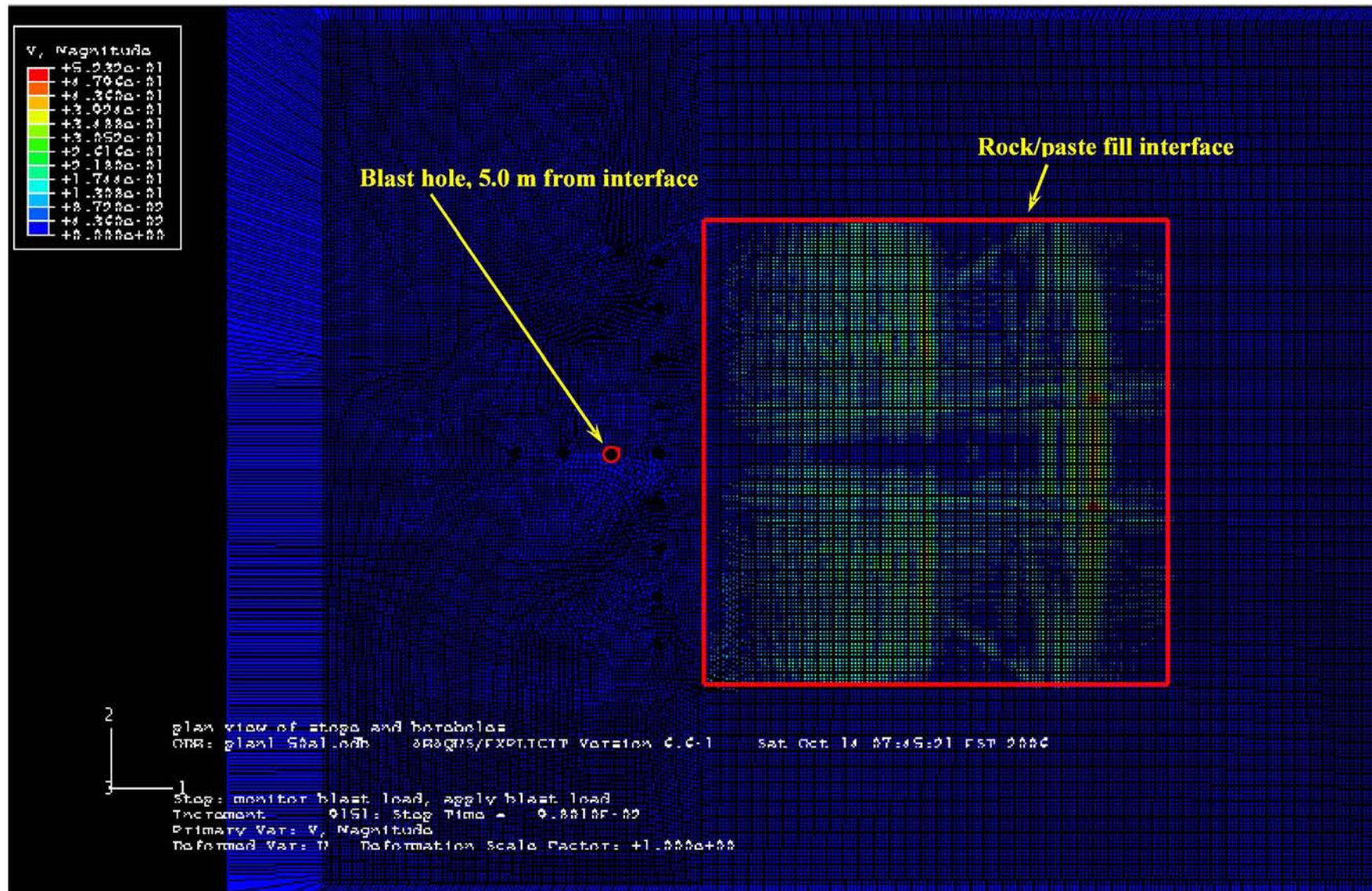


Figure 8.17 – Particle Velocity 0.098 s After Detonation

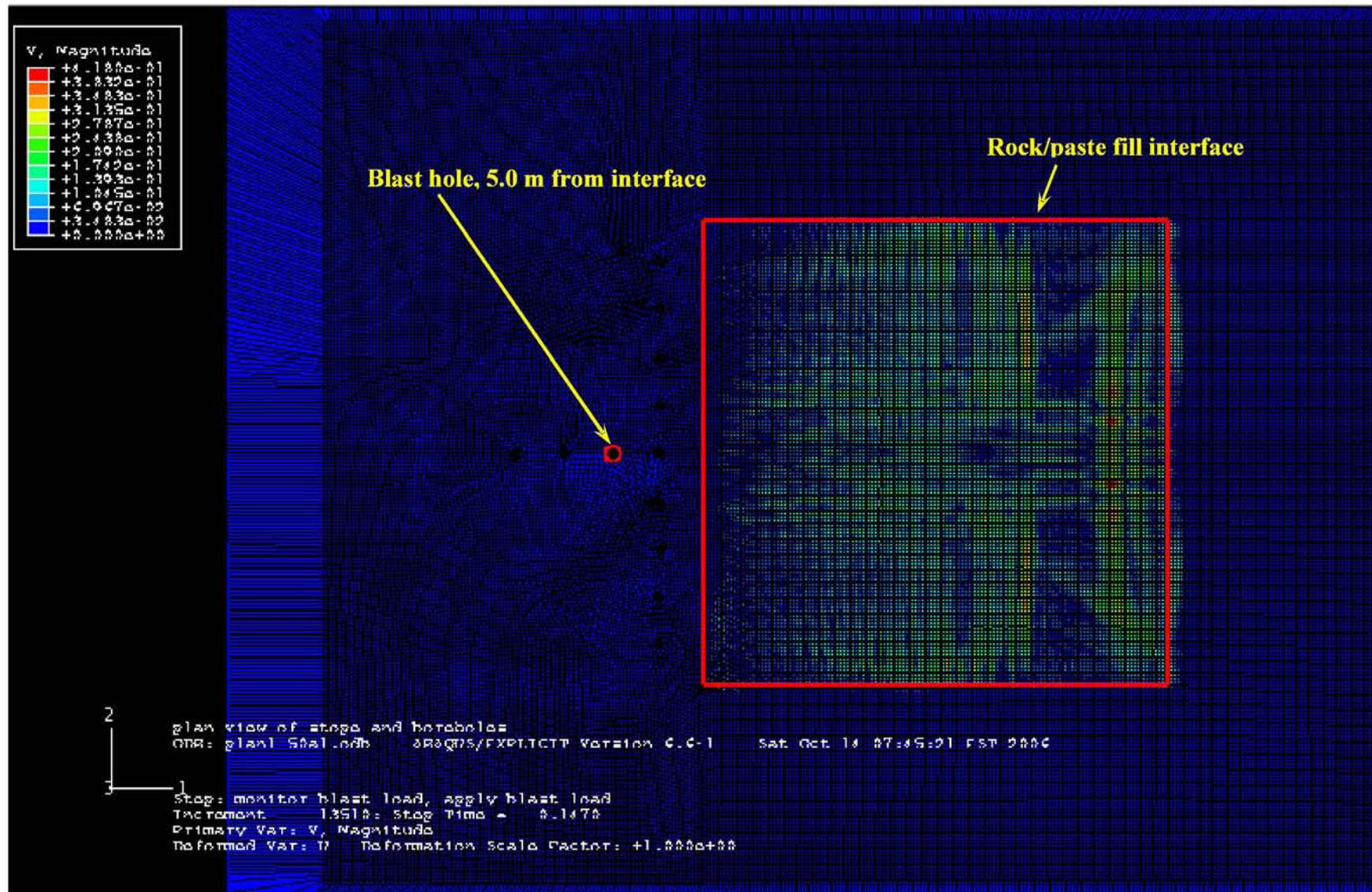


Figure 8.18 – Particle Velocity 0.147 s After Detonation

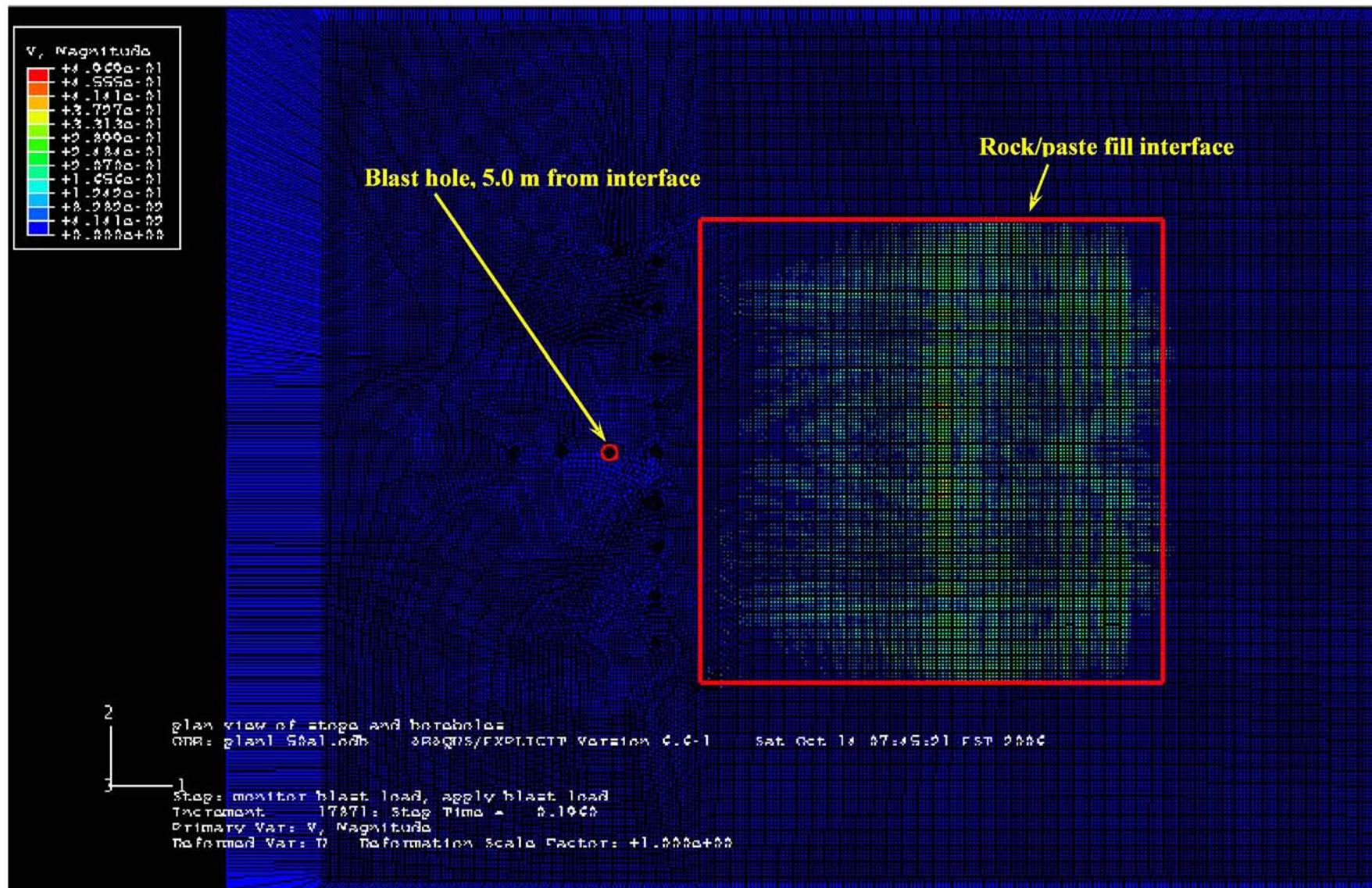


Figure 8.19 – Particle Velocity 0.196 s After Detonation

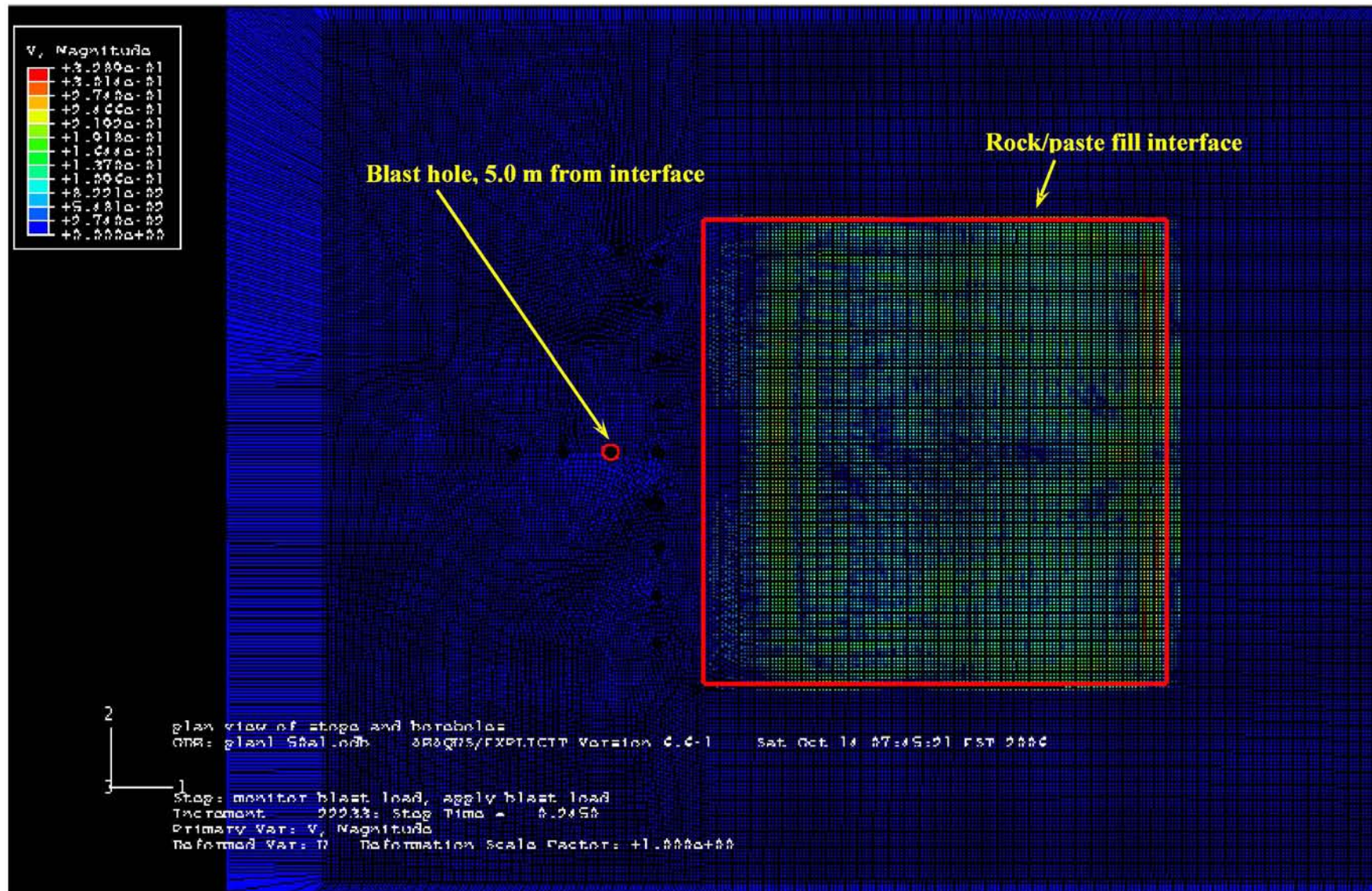


Figure 8.20 – Particle Velocity 0.245 s After Detonation

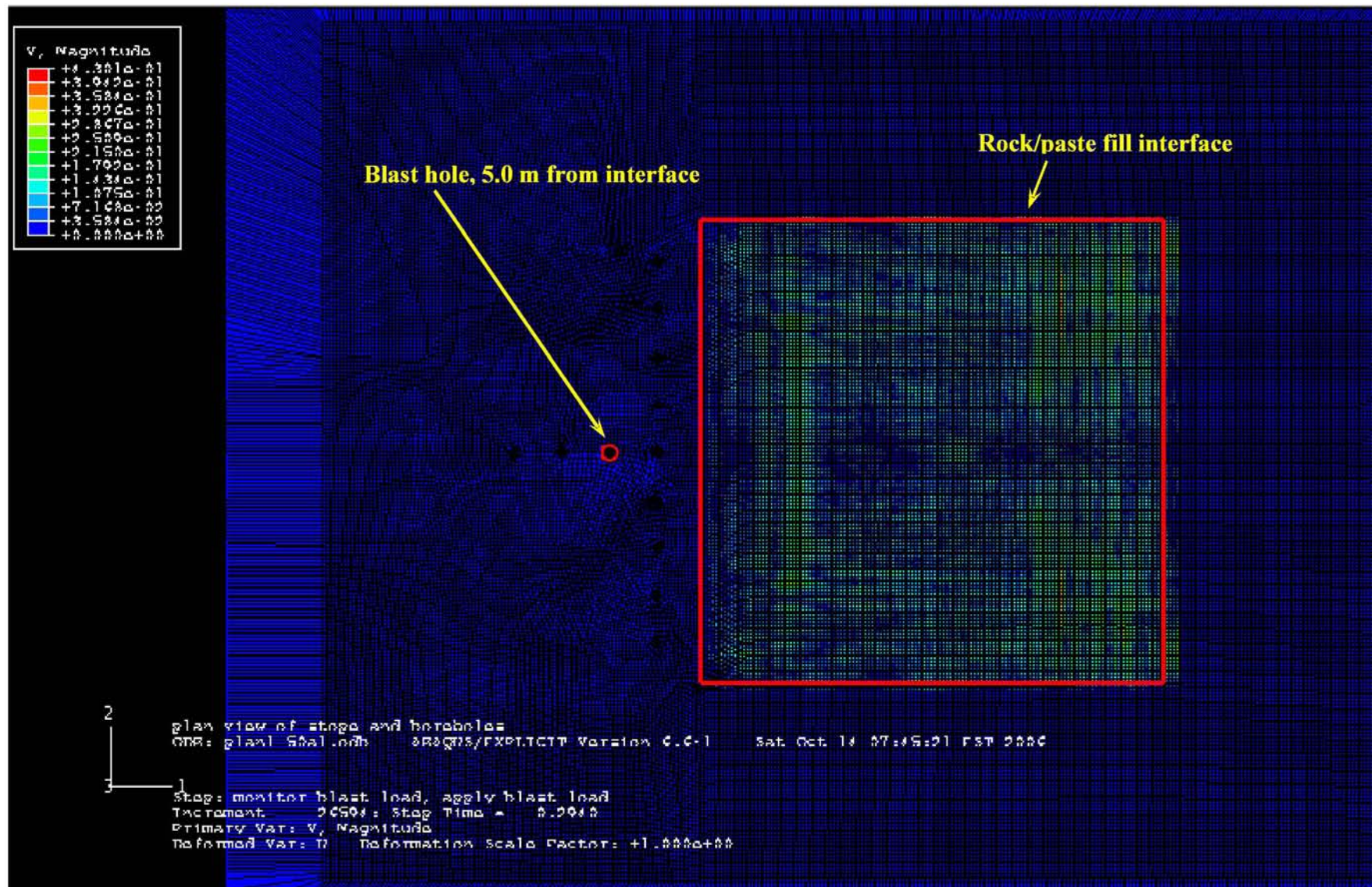
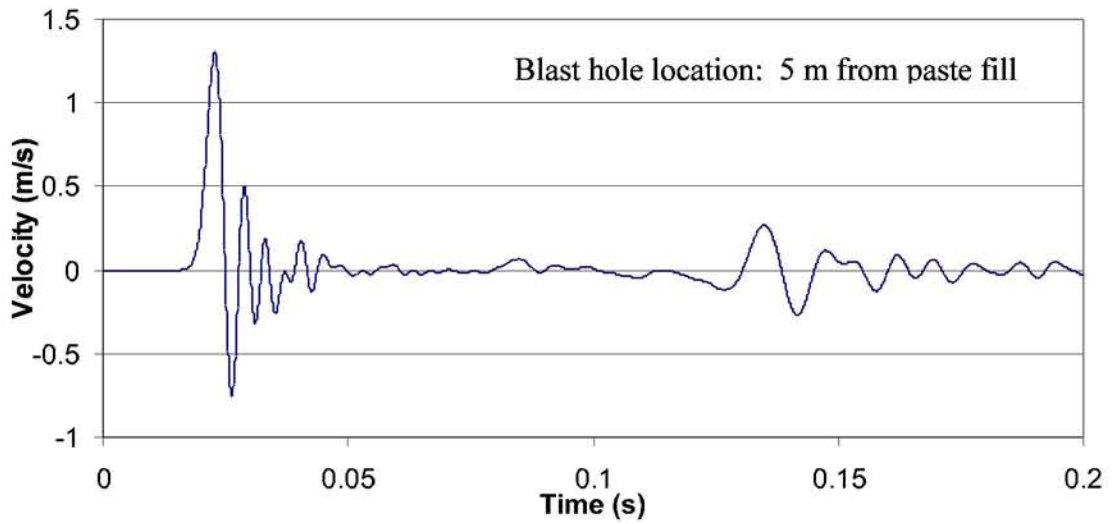
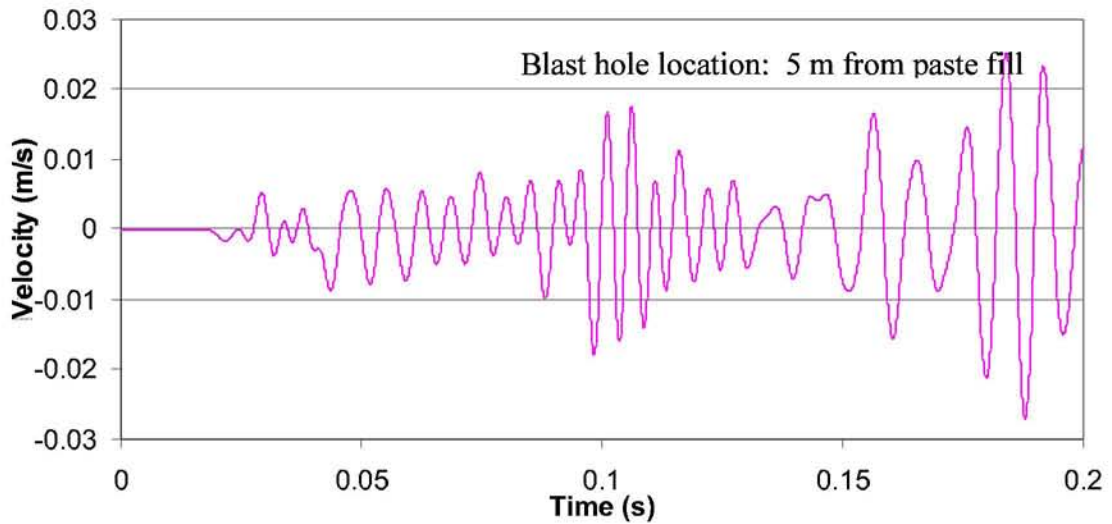


Figure 8.21 – Particle Velocity 0.294 s After Detonation





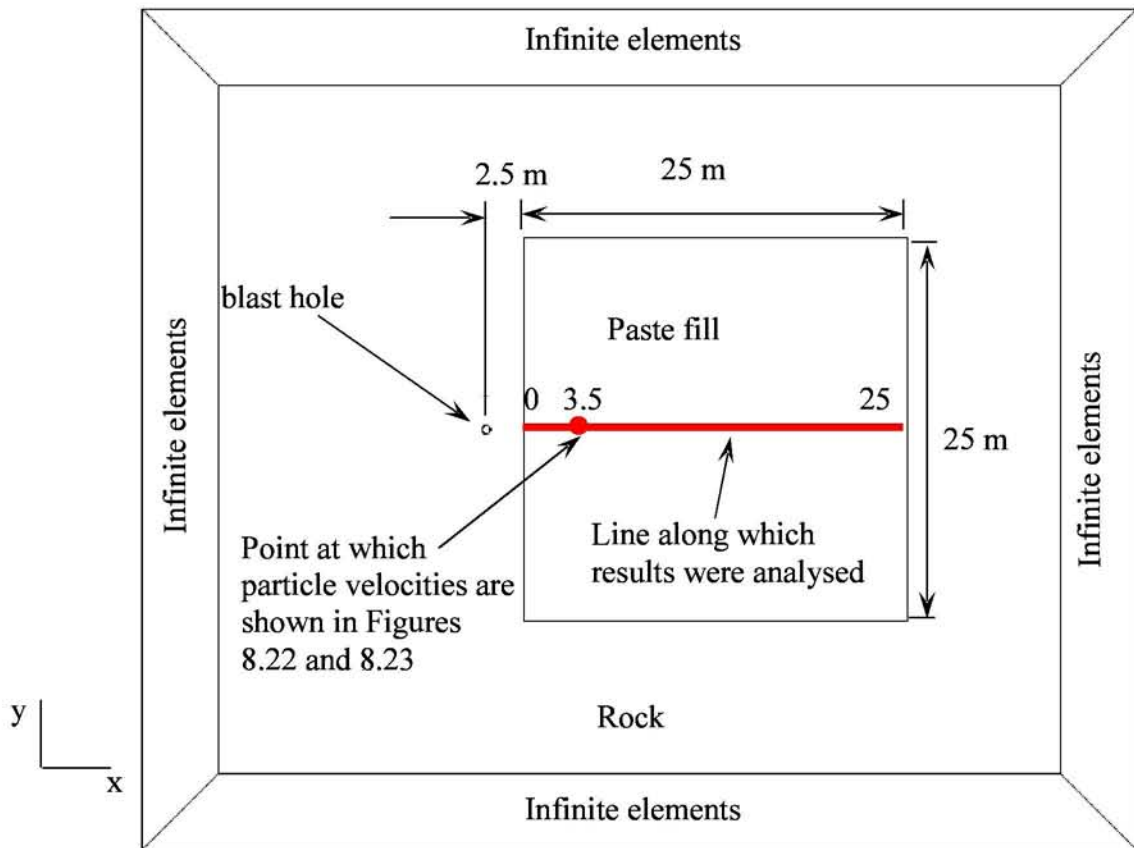
**Figure 8.22 – Particle Velocity in the x-Direction**



**Figure 8.23 – Velocity in the y-Direction**

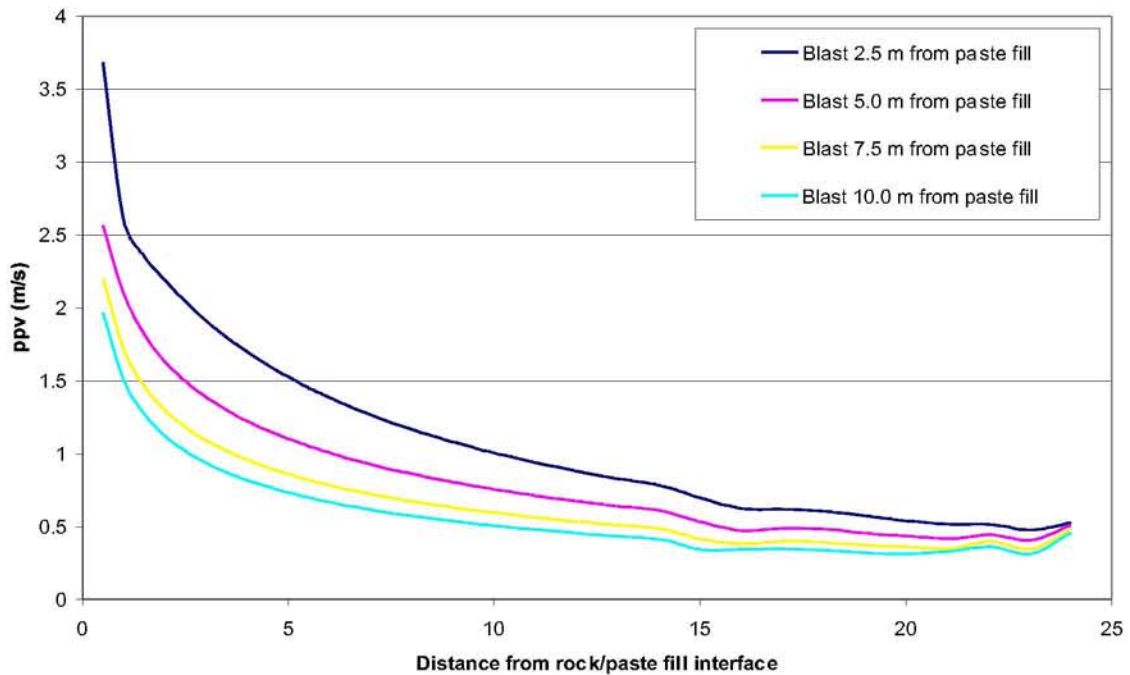
### **8.3.2.3. Effect of Distance of Borehole from Paste Fill on Peak Particle Velocity**

In order to analyse the model, the peak particle velocities along the centreline of the paste fill stope were compared. The peak particle velocity was plotted against distance from the rock/paste fill boundary so that the boundary closest to the borehole was at 0 m and the opposite boundary was at 25 m as shown in Figure 8.24.



**Figure 8.24 – Centreline of Paste Fill Along Which the Results Have Been Analysed**

The peak particle velocities predicted for the detonation of boreholes located at 2.5, 5.0, 7.5 and 10.0 m from the rock/paste fill boundary are shown in Figure 8.25. From this figure it can be seen that as the distance between the borehole and the paste fill is increased, the peak particle velocities generated in the paste fill decreased and therefore the damage to the paste fill is reduced. The distance into the paste fill of the expected failure plane is given in Table 8.1. These distances are based on failure to paste fill occurring when peak particle velocities of 2.5 m/s or greater is experienced in the paste fill for a mix of 76 % solids and 4 % cement as discussed in Chapter 3.



**Figure 8.25 – Comparison of results from a Single Borehole at Various Locations Relative to the Paste Fill**

#### 8.3.2.4. Effect of Borehole Diameter on Peak Particle Velocity

The production blasts monitored for this project consisted of mainly 89 mm diameter boreholes with 76 mm diameter boreholes in the set of blast holes located adjacent to one of the paste fill faces. The location of the 76 mm diameter blast holes is shown in Figure 8.26. The smaller diameter boreholes have a smaller linear charge density and therefore apply a smaller load to the surrounding material. The load for the 76 mm diameter boreholes was determined using the method presented in section 6.8.1.

The peak particle velocities predicted for 76 mm diameter boreholes was compared against those predicted for 89 mm diameter boreholes as shown in Figure 8.27. From this figure it can be seen that the smaller diameter boreholes result in lower peak particle velocities generated in the paste fill and therefore the damage to the paste fill is reduced. The distance into the paste fill of the expected failure plane is given in Table 8.1. These distances are based on failure to paste fill occurring when peak particle velocities of 2.5 m/s or greater are experienced in the paste fill as discussed in Chapter 3. The results show that 89 mm boreholes located 7.5 m or more from the paste fill are likely to cause damage to less than 0.5 m into the paste fill stope, while 76 mm diameter boreholes located 5 m or more from the paste fill are likely to cause damage to less than 0.5 m into the paste fill stope. Therefore, smaller diameter boreholes should be used for boreholes 5 m or closer to paste fill.

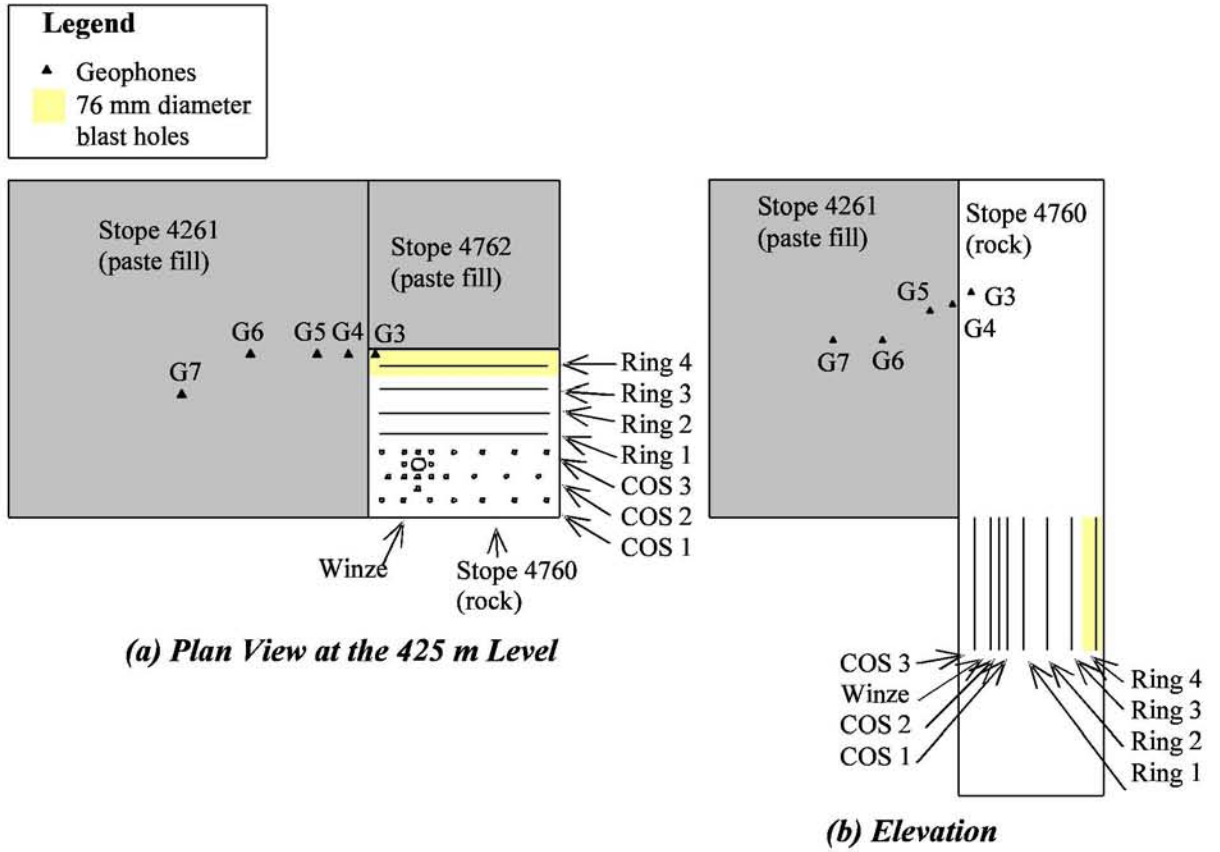


Figure 8.26 – Location of 76 mm Diameter Blast Holes, Blast 904064

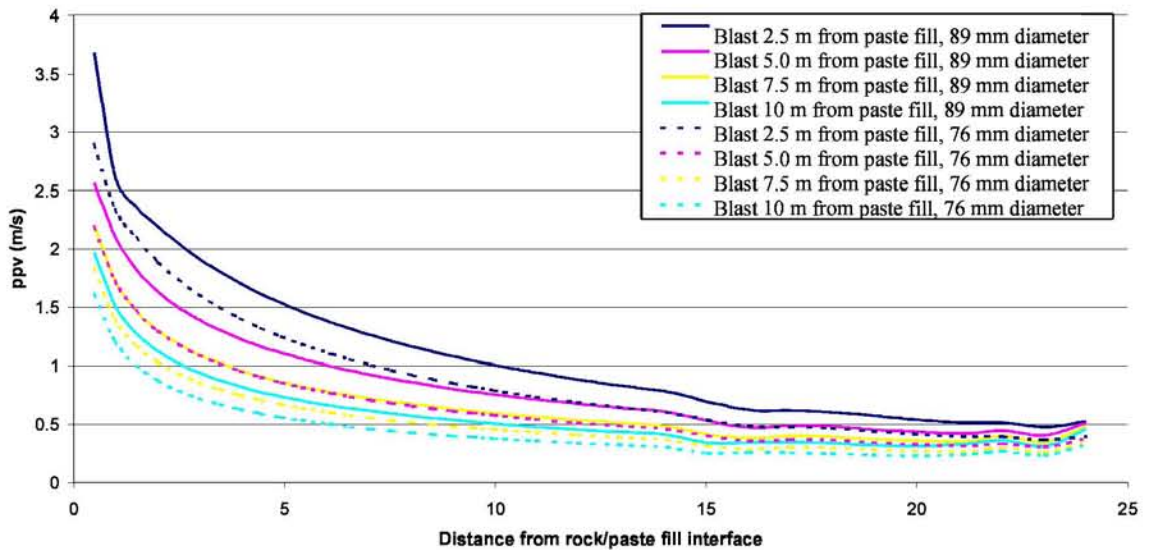


Figure 8.27 – Comparison of Results from a 89 mm and 76 mm Diameter Blast Holes

**Table 8.1 Expected Failure of Paste Fill from Single Column of Explosive in Nearby Rock**

Distance Between Borehole and Paste Fill (m)	Location of Failure Plane: Distance into the Paste Fill from Rock/Paste Fill Interface (m)	
	89 mm Diameter Borehole	76 mm Diameter Borehole
2.5	1.25	0.90
5.0	0.5	< 0.5
7.5	< 0.5	< 0.5
10.0	< 0.5	< 0.5

### **8.3.3. Scenario 2: Single Borehole Offset from the Centreline of the Paste Fill Stope**

The stage 3 model, scenario 2 consisted of a plane strain model of a single column of explosive adjacent to a paste fill stope. The column of explosive was offset from the centreline of the paste fill stope as shown in Figure 8.28. Offset distances of 2.5, 5.0, 7.5 and 10.0 m were used. An input file for a stage 3 scenario 2 model of an explosive column located 2.5 m from the paste fill stope with an offset of 2.5 m is given in Appendix F.

#### **8.3.3.1. Effect of Location of Borehole Relative to Paste Fill**

In order to analyse the model, the peak particle velocities along the face of the paste fill stope were compared. The peak particle velocity was plotted against offset of the point from the centreline of the paste fill stope as shown in Figure 8.29.

The peak particle velocities predicted for the detonation of boreholes located at offsets of 0, 2.5, 5.0, 7.5 and 10.0 m from the centreline of the paste fill stope are shown in Figure 8.30. From this figure it can be seen that a single column of explosive produces a high peak particle velocity in the area near the borehole site, and produces reasonably constant peak particle velocities across the rest of the paste fill face. Typically, the peak particle velocities would be expected to reduce with distance from the explosive source, however the constant peak particle velocity predicted across the entire paste fill face can be explained by the reflections of the wave which have been observed to occur within the paste fill.

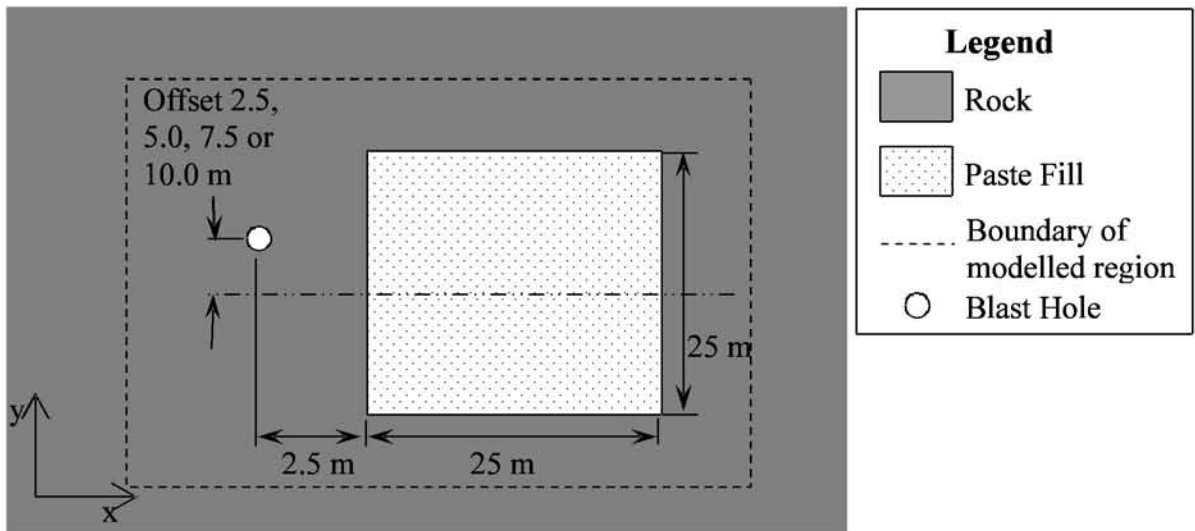


Figure 8.28 – Stage 3 Model, Scenario 2

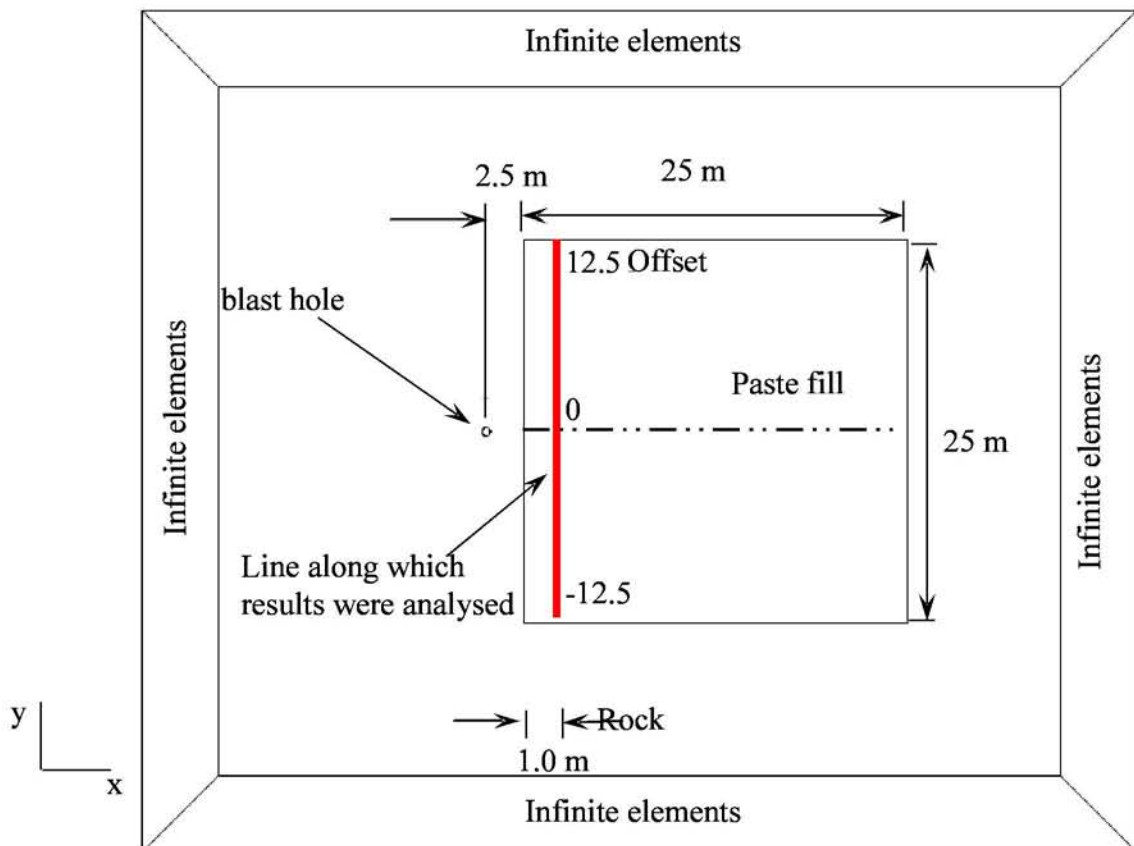
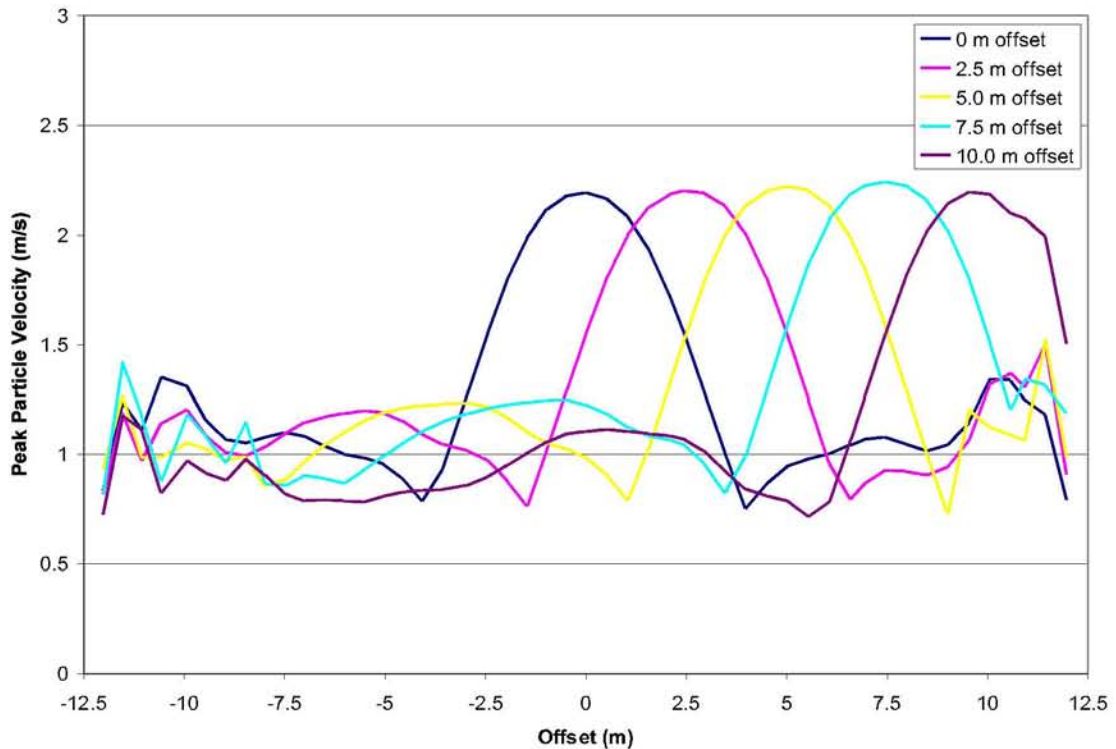


Figure 8.29 – Line Along which Results were Analysed for Stage 3 Model, Scenario 2



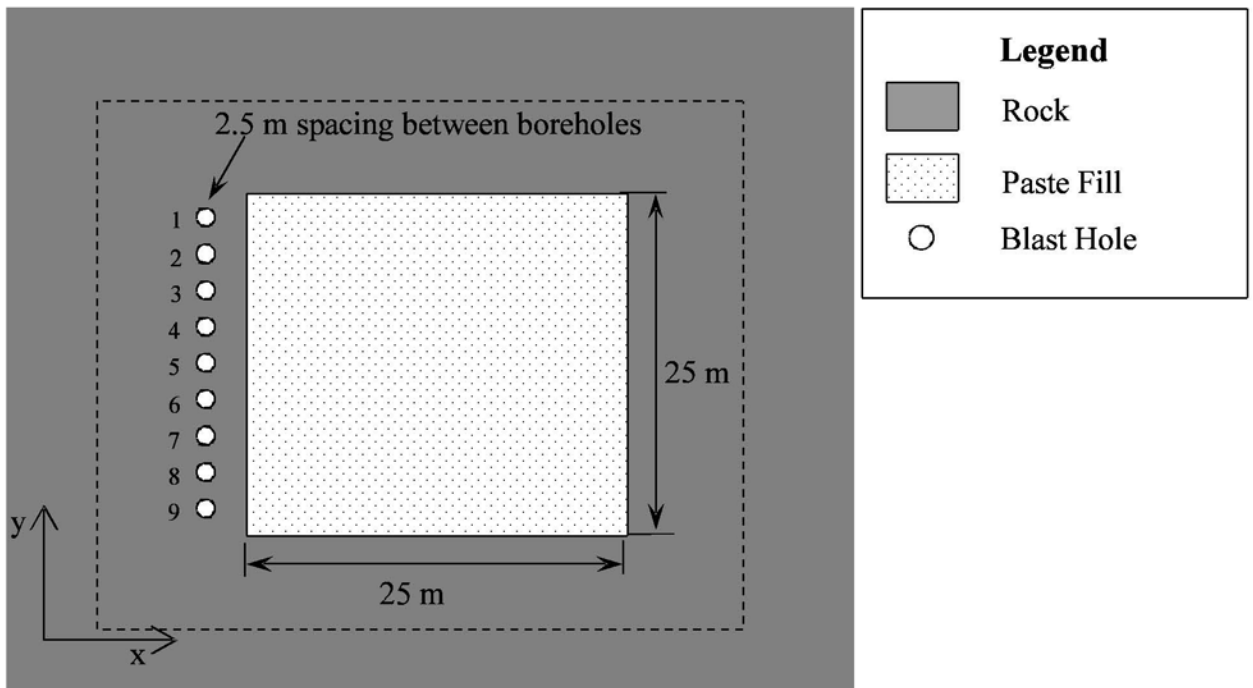
**Figure 8.30 – Peak Particle Velocities Along Paste Fill Face Due to a Single Column of Explosive**

#### **8.3.4. Scenario 3: Detonation of a Row of Boreholes Parallel to a Face of the Paste Fill Stop**

The above model analyses were all based on the detonation of a single borehole. However, in practice, production blasts consist of the detonation of multiple boreholes with small delays between each detonation. Therefore, a cumulative effect from the multiple boreholes will be observed, and the damage to paste fill will be much greater than that caused by a single borehole. The stage 3 model, scenario 3 consisted of a plane strain model of a row of explosive boreholes 2.5 m from a paste fill stop. The boreholes were spaced 2.5 m apart. The boreholes were numbered as shown in Figure 8.31. The analysis was run for detonation delays of 100 ms, 200 ms and 400 ms, where the delay is the time between two blasts. The following blast patterns were modelled:

- Blast Pattern 1. Simultaneous detonation of all 9 boreholes
- Blast Pattern 2. Detonation of the boreholes in the following order: 1, 2, 3, 4, 5, 6, 7, 8, 9.
- Blast Pattern 3: Detonation of the boreholes in the following order: 5, 4 and 6, 3 and 7, 2 and 8, 1 and 9.

Input files for stage 3 models of the blast patterns described above are given in Appendix F.



**Figure 8.31 – Borehole Numbering for Stage 3 Model, Scenario 3**

#### **8.3.4.1. Comparison of Single Borehole Versus Multiple Boreholes**

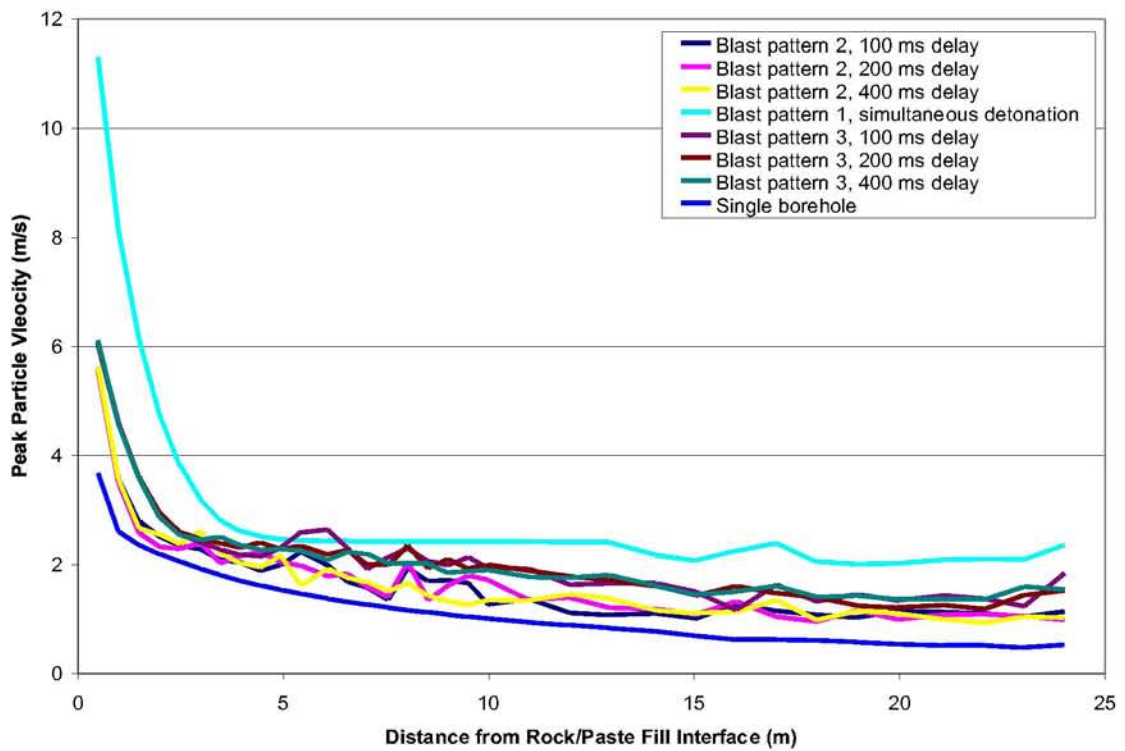
The peak particle velocities in paste fill predicted for multiple boreholes were compared against the peak particle velocities predicted for a single borehole. A comparison of the peak particle velocities along the centreline of the paste fill stope is shown in Figure 8.32 while the comparison along the face of the paste fill stope is shown in Figure 8.33. As expected, multiple boreholes result in higher peak particle velocities that are approximately constant across the face of the paste fill stope, except for the ends. The detonation of all boreholes simultaneously results in much higher peak particle velocities along the face of the paste fill face. The use of delays between boreholes results in the wave from earlier boreholes being allowed to propagate for a short distance before the next detonation. This produces a more uniformly crushed product in the crushed zone while reducing the peak particle velocities and damage to material in the far field.

The velocities along the centreline of the stope are higher for multiple boreholes throughout the length of the stope. The curve for a single borehole is much smoother than the curves for multiple boreholes with delays between the boreholes. This is due to the interaction of the reflected waves from the earlier blasts with the waves from later blasts. The predicted failure plane in the paste fill is given in Table 8.2 for multiple boreholes located 2.5 m from a paste fill stope. These distances are based on failure to paste fill occurring when peak particle velocities of 2.5 m/s or greater is experienced in the paste fill for a mix of 76 % solids and 4 % cement as discussed in Chapter 3.

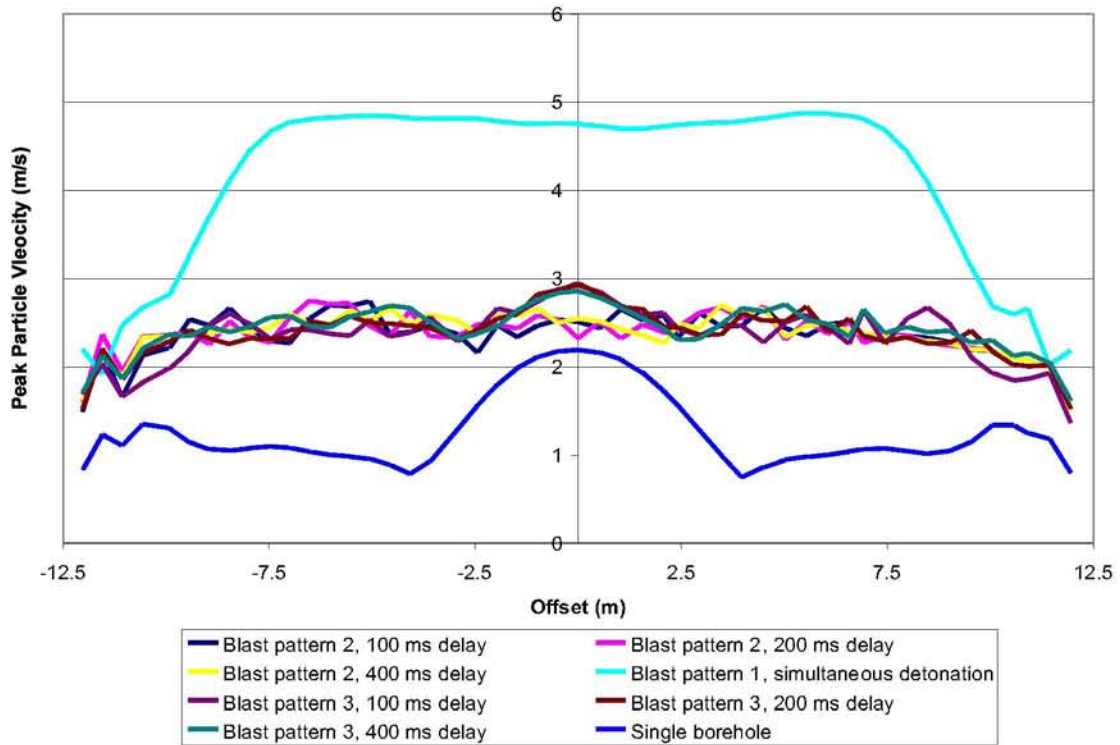


**Table 8.2 Expected Failure of Paste Fill from Multiple Boreholes in 2.5 m from Paste Fill**

Blast Pattern	Delay (ms)	Location of Failure Plane: Distance from Rock/Paste Fill Boundary (m)
1	0	4.5
2	100	2.0
2	200	2.0
2	400	2.0
3	100	2.5
3	200	2.5
3	400	2.5



*Figure 8.32 – ppv Predicted along the Centreline of a Paste Fill Stop*



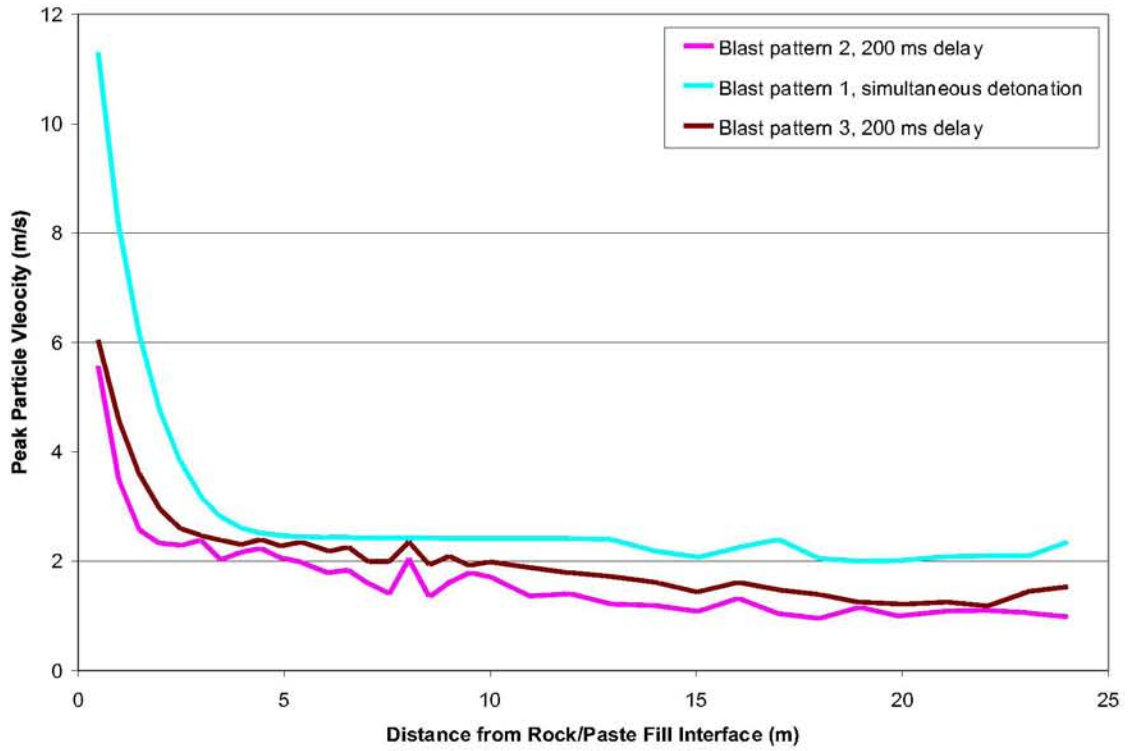
**Figure 8.33 – ppv Predicted Along the Face of a Paste Fill Stope**

### 8.3.4.2. Comparison of Detonation Patterns

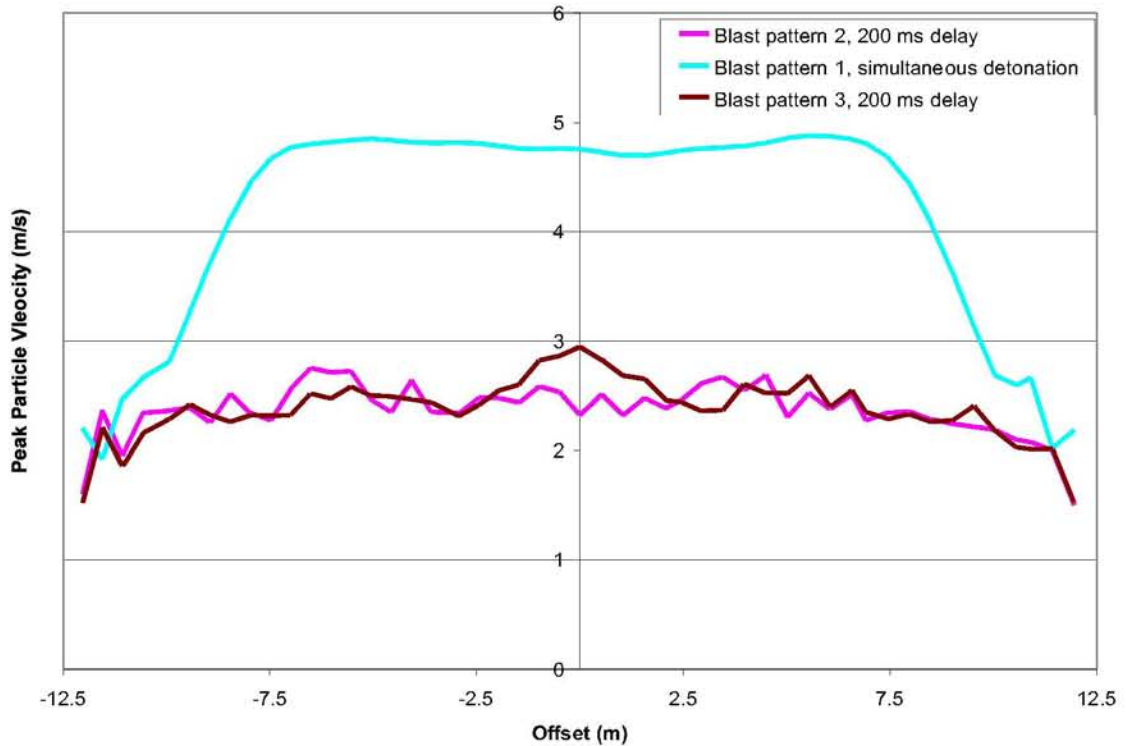
A comparison of peak particle velocities predicted along the centreline of the stope is shown in Figure 8.34 for the three detonation patterns modelled, with a delay time of 200 ms. The graph shows that blast pattern 1 where, the detonation of all boreholes occurs simultaneously, produces higher peak particle velocities throughout the full length of the stope. The peak particle velocities near the rock/paste fill boundary are much larger than those predicted for the other two blast patterns, and the failure zone of paste fill is predicted to be approximately twice as wide as those for blast patterns 2 and 3. The failure zone is predicted to be 4.5 m wide failure zone for blast pattern 1, 2.0 and 2.5 m wide failure zone for blast patterns 2 and 3 respectively.

Blast pattern 3, the detonation of the boreholes starting in the middle and working out to the ends of the stope is shown to produce slightly higher peak particle velocities across the paste fill stope when compared to blast pattern 2. However, a comparison of the peak particle velocities predicted across the face of the stope (Figure 8.35) shows that these higher velocities only occur along the centreline of the stope and that similar peak particle velocities are predicted across the rest of the paste fill. Similar results were observed for delays of 100 ms and 400 ms. These results show that from the point of view of reducing damage to nearby paste fill, a delay between the detonation of multiple boreholes is necessary, however the actual order of

detonation has little effect on the damage to the paste fill. The detonation order does play a large role in the resulting material in the crushed zone and should be designed accordingly.



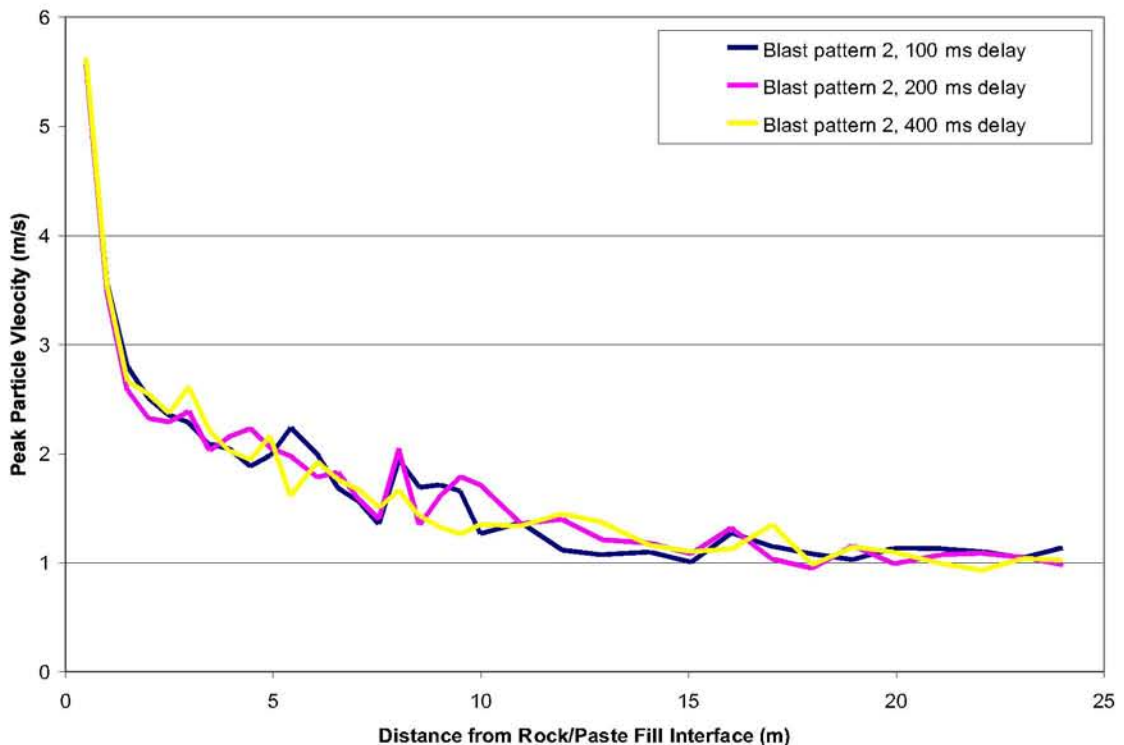
**Figure 8.34 – ppv Predicted Along the Centreline of a Paste Fill Stope for Different Detonation Patterns**



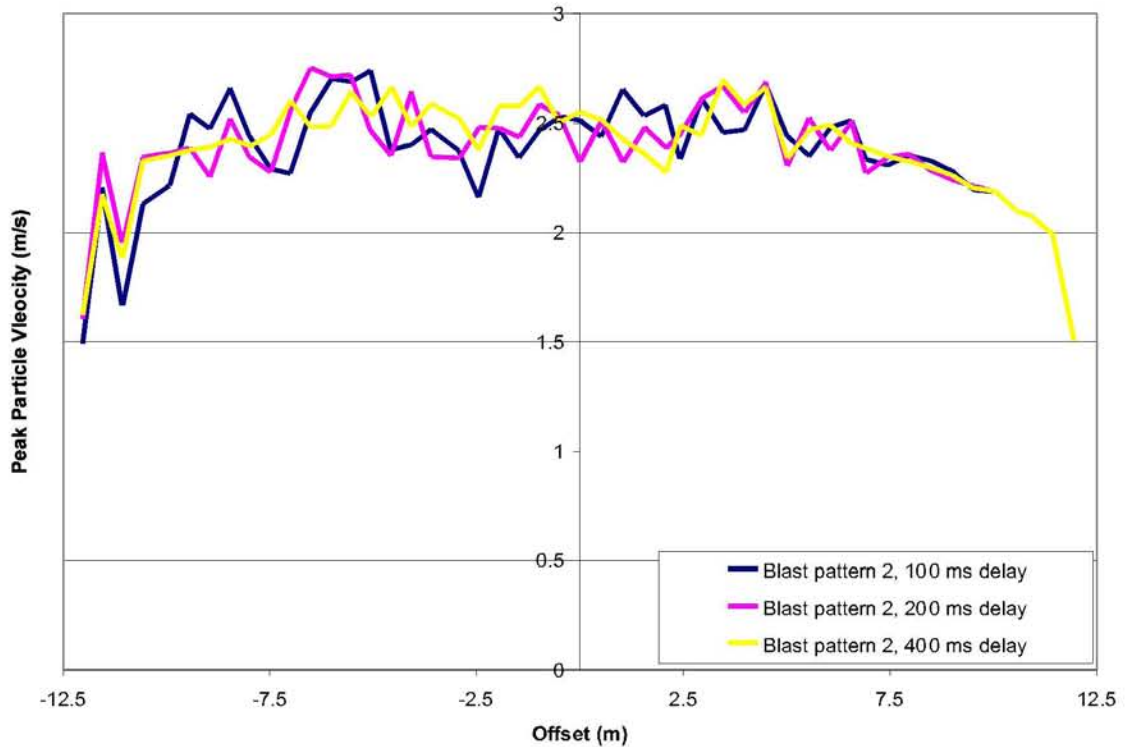
**Figure 8.35 – ppv Predicted Along the Face of a Paste Fill Stope for Different Detonation Patterns**

### 8.3.4.3. Effect of Delay Time on Peak Particle Velocity

A comparison of peak particle velocities predicted along the centreline of the stope for different detonation times is shown in Figure 8.36 for blast pattern 2. The graph shows that there is no significant difference between the magnitude of the peak particle velocities experienced in the paste fill due to the different detonation times. The peak particle velocities in the region near the rock/paste fill boundary are due to the initial wave travelling in the paste fill. These peak particle velocities do not vary with the different detonation times. The peak particle velocities throughout the rest of the paste fill are the result of the waves from each blast being transmitted through the paste fill and the reflections of these waves on the paste fill/rock boundary. Due to the different delay times, the times when these waves interact with each other varies, resulting in the slight variation of peak particle velocity at a given point throughout the majority of the paste fill. A comparison of the peak particle velocities across the face of the paste fill stope (Figure 8.37) shows no significant difference between the peak particle velocities predicted from different delay times.



**Figure 8.36 – ppv Predicted Along the Centreline of a Paste Fill Stope for Different Delay Times**



**Figure 8.37 – ppv Predicted Along the Face of a Paste Fill Stop for Different Delay Times**

These results show that from the point of view of reducing damage to nearby paste fill, the actual delay between the detonation of boreholes has little effect on the damage to nearby paste fill, although results presented above show that a delay between the detonation of multiple boreholes is necessary. Like the detonation order, the delay time between boreholes plays a large role in the resulting material in the crushed zone and should be designed accordingly.

## 8.4. Summary

### 8.4.1. Stage 1 Model

The stage 1 model was run for a paste fill mix of 76 % solids and 4 % cement, which corresponded to the mixture of paste fill the field instrumentation tests were conducted in. Comparison between the model results and the field data showed that the model correctly predicts the peak particle velocity in the paste fill at distances equal or greater than 2 m from the explosive source. Comparison between velocity waveforms between the model and the field data showed similar patterns.

The stage 1 model was run for a number of different mixes of paste fill to study the effect of solids content and cement content on the peak particle velocities experienced in paste fill during nearby blasting. The model results showed the following:

- A decrease in cement content of the paste fill results in a higher peak particle velocity in the paste fill, and in turn a larger volume of paste fill that is likely to be damaged during nearby blasting.
- For low cement contents, a decrease in solids content of the paste fill results in a higher peak particle velocity in the paste fill, and in turn a larger volume of paste fill that is likely to be damaged during nearby blasting. For a cement content of 6 %, the results were similar for all solids contents.
- A small decrease in cement content can be partially compensated for by an increase in solid content of the paste fill. For example, a 76 % solids and 6 % cement content mixture of paste fill results in peak particle velocities in the fill of the same magnitude as an 80 % solids and 4 % cement content of paste fill.

#### **8.4.2. Stage 2 Model**

The stage 2 model was created to validate the model against the peak particle velocities predicted by the peak particle velocity prediction equation. Once the model was validated, it was run for a number of different rock types to study the effect of rock type on the peak particle velocities experienced in rock mass during nearby blasting. The model results showed that the majority of rock types at Cannington Mine yield similar results in the model. The exception is the Glenholme which is the weakest rock type and for which much high peak particle velocities were predicted.

#### **8.4.3. Stage 3 Model**

Model 3, scenario 1 modelled the detonation of a single borehole located adjacent to the centreline of a paste fill stope. The model was run for a paste fill mix of 76 % solids and 4 % cement and the broadlands rock type. The model results showed the following:

- A portion of the wave was reflected back into the rock at the rock/paste fill interface. This resulted in some high velocities being observed in the rock at the rock/paste interface as shown in Figures 8.12 to 8.15.
- The wave refracted from the rock/paste fill interface travelled through the paste fill much slower than the reflected wave travelled through the rock.
- Once the wave entered the paste fill it was observed to reflect back into the paste fill at the boundaries of the paste fill. This reflection was observed to continue until the wave attenuated within the paste fill.

- The damage to paste fill is reduced as the distance between the borehole and the paste fill is increased. For boreholes located at distances greater than 5 m from the paste fill, the thickness of the failure zone from a single borehole is predicted to be less than 0.5 m.
- The damage to paste fill is reduced as the diameter of the borehole is reduced. For boreholes located at distances greater than 2.5 m from the paste fill, the thickness of failure from a single borehole is predicted to be less than 0.5 m.
- In order to reduce the damage to paste fill, smaller diameter boreholes should be used for boreholes located within 5 m of paste fill.

Model 3, scenario 2 modelled the detonation of a single borehole located adjacent a paste fill stope and offset from the centreline. The model was run for a paste fill mix of 76 % solids and 4 % cement and the Broadlands rock type. The model results showed that a single column of explosive produces a high peak particle velocity in the area near the borehole site, and produces reasonably constant peak particle velocities across the rest of the paste fill face. The constant peak particle velocity predicted across the entire paste fill face is due to the reflections which have been observed to occur within the paste fill.

The detonation of a row of boreholes was modelled with model 3, scenario 3. The results showed the following:

- The detonation of all boreholes simultaneously results in much higher peak particle velocities and damage than the detonation of multiple boreholes with small delays (100 ms to 400 ms delays were modelled). Therefore, delays are necessary to reduce damage to the nearby paste fill during blasting. Delays are typically used in mining applications to produce a more uniformly crushed product in the crushed zone.
- A comparison between results from the different blast patterns modelled showed that the order of detonation has little effect on the damage to the paste fill. The detonation order does play a large role in the resulting material in the crushed zone and should be designed accordingly.
- A comparison between the results from the same blast patterns with different delay times showed that the delay time between the detonation of boreholes has little effect on the damage to nearby paste fill. However, a delay between the detonation of multiple boreholes is necessary. Like the detonation order, the delay time between boreholes plays a large role in the resulting material in the crushed zone and should be designed accordingly.

## **9. Summary, Conclusions and Recommendation for Future Work**

### ***9.1. Summary and Conclusions***

The following gives a summary of the work conducted for this dissertation and the conclusions that were drawn from it.

#### **Field Monitoring**

- Production blasts were monitored in order to measure ppv experienced in paste fill due to blasting of a secondary stope, to provide field data on the transmission of a blast through the rock/paste fill interface and to estimate the ppv at which damage occurs in paste fill.
- Site observations indicated that once the wave entered the paste fill, it appeared to remain in the paste fill, reflecting on the paste fill/rock boundary.
- Analysis of the data on each side of the paste fill interface indicated that a large portion of the wave energy is reflected at the boundary. The ppv in the paste fill is between 55 % and 85 % of the wave in the rock.
- Fourier analysis of the waveforms indicate that the higher frequencies attenuate earlier than the lower frequencies.
- Based on observations from the field monitoring, the field tests and work by others, the ppv at which damage to paste fill begins to occur is estimated to be in the vicinity of 2.5 to 3.5 m/s.

#### **Field Tests**

- Field tests were undertaken in paste fill in order to study the transmission of a wave in paste fill without any effects of the rock or the rock/paste fill boundary.
- Peak particle velocities were obtained from the field test waveforms and used to calculate the parameters for the ppv prediction equation.
- The parameters for the ppv prediction equation are:
  - $k = 1000$



- $\beta = 1.02$
- The field data was used to validate the paste fill numerical model.

### **Laboratory Tests**

- Laboratory tests were used to study the attenuation of longitudinal waves in a paste column.
- Peak particle velocity was observed to decrease with distance from the source.
- Wavelength was observed to increase with distance from the source.
- Higher frequencies were observed to attenuate faster than lower frequencies.
- The wave attenuated faster in the paste fill once it had fully cured and reached its full strength. Therefore, in order to reduce the damage observed in paste fill during blasting, the paste fill should be allowed to fully cure before it is exposed to nearby blasting.
- As the strength of the material increases, waves attenuate faster within the material.

### **Numerical Models**

ABAQUS/Explicit was used to model effect of blasting on paste fill, using ppv as a measure of damage. Numerical models were created and calibrated against data obtained during field tests and the field monitoring.

A single blast hole in a paste fill mass was modelled with the stage 1 model. The results showed the following:

- A decrease in cement content of the paste fill results in a higher peak particle velocity in the paste fill, and in turn a larger volume of paste fill that is likely to be damaged during nearby blasting.
- A decrease in solids content of the paste fill results in a higher peak particle velocity in the paste fill, and in turn a larger volume of paste fill that is likely to be damaged during nearby blasting, when the cement content is low. For a cement content of 6 %, the results were similar for all solids contents.

- A small decrease in cement content can be partially compensated for by an increase in solid content of the paste fill. For example, a 76 % solids and 6 % cement content mixture of paste fill results in peak particle velocities in the fill of the same magnitude as an 80 % solids and 4 % cement content of paste fill.

A single blast hole in a rock mass was modelled with the stage 2 model in order to validate the loading in the rock. The results showed the following:

- The majority of rock types at Cannington Mine yielded similar results in the numerical model. The exception is the Glenholme which is the weakest rock type and for which much high peak particle velocities were predicted.

The detonation of a single borehole located adjacent to the centreline of a paste fill stope was modelled with model 3, scenario 1. The model was run for a paste fill mix of 76 % solids and 4 % cement and the broadlands rock type. The model results showed the following:

- A portion of the wave was reflected back into the rock at the rock/paste fill interface. This resulted in some high velocities being observed in the rock at the rock/paste interface as shown in Figures 8.13 to 8.16.
- The wave refracted from the rock/paste fill interface travelled through the paste fill much slower than the reflected wave travelled through the rock.
- Once the wave entered the paste fill it was observed to reflect back into the paste fill at the boundaries of the paste fill. This reflection was observed to continue until the wave attenuated within the paste fill.
- The damage to paste fill is reduced as the distance between the borehole and the paste fill is increased. For boreholes located at distances greater than 5 m from the paste fill, the thickness of the failure zone from a single borehole is predicted to be less than 0.5 m.
- The damage to paste fill is reduced as the diameter of the borehole is reduced. For boreholes located at distances greater than 2.5 m from the paste fill, the thickness of failure from a single borehole is predicted to be less than 0.5 m.
- In order to reduce the damage to paste fill, smaller diameter boreholes should be used for boreholes located within 5 m of paste fill.

The detonation of a single borehole located adjacent to a paste fill stope and offset from the centreline was modelled with model 3, scenario 2. The results showed the following:

- A single column of explosive produces a high peak particle velocity in the area near the borehole site, and produces reasonably constant peak particle velocities across the rest of the paste fill face. The constant peak particle velocity predicted across the entire paste fill face is due to the reflections which have been observed to occur within the paste fill.

The detonation of a row of boreholes was modelled with model 3, scenario 3. The results showed the following:

- The detonation of all boreholes simultaneously results in much higher peak particle velocities and damage than the detonation of multiple boreholes with small delays (100 ms to 400 ms delays were modelled). Therefore, delays are necessary to reduce damage to the nearby paste fill during blasting. Delays are typically used in mining applications to produce a more uniformly crushed product in the crushed zone.
- A comparison between results from the different blast patterns modelled showed that the order of detonation has little effect on the damage to the paste fill. The detonation order does play a large role in the resulting material in the crushed zone and should be designed accordingly.
- A comparison between the results from the same blast patterns with different delay times showed that the delay time between the detonation of boreholes has little effect on the damage to nearby paste fill. However, a delay between the detonation of multiple boreholes is necessary. Like the detonation order, the delay time between boreholes plays a large role in the resulting material in the crushed zone and should be designed accordingly.

## ***9.2. Recommendations for Future Work***

The following recommendations for future work were drawn from this study:

### **Monitoring**

Undertake a monitoring program in which ppv are measured for blasting occurring adjacent to the section of the paste fill in which the monitoring equipment is installed in order to confirm the estimation of the ppv at which damage to paste fill occurs.

### **Numerical Modelling**

Run the stage 3 model for an extended period of time to study how long the stress wave in the paste fill continues to reflect internally within the paste fill.

## 10. References

- ABAQUS, Inc. (2003). "ABAQUS online documentation: Version 6.4-1." ABAQUS, Inc.
- Atchison, T. C. (1968). "Fragmentation principles." Surface mining, E. P. Pfeleider, ed., American Institute of Mining and Metallurgical Engineers, AIME, 355-372.
- Baylot, J. T. (1993). "Loads on structures buried in low-shear-strength soils subjected to localized blast effects," PhD, University of Illinois at Urbana-champaign.
- BHP Billiton (n.d.). "Mining" retrieved August 28, 2007 from [http://cannington.bhpbilliton.com/production\\_process/mining.asp](http://cannington.bhpbilliton.com/production_process/mining.asp)
- Blair, D., and Minchinton, A. (1996). "On the damage zone surrounding a single blasthole." *Rock Fragmentation by Blasting*, Rotterdam, 121-130.
- Blair, D. P., and Jiang, J. J. (1995). "Surface vibrations due to a vertical column of explosive." *International Journal of Rock Mechanics and Mining Science and Geomechanics Abstracts*, 32(2), 149-154.
- Bloss, M. L., Cowling, R., and Meek, J. L. (1993). "A procedure for the design of stable cemented fill exposures." *MINEFILL'93 5th International Symposium on Mining with Backfill*, Johannesburg, 3-8.
- Bloss, M. L., and Greenwood, A. G. (1998). "Cemented rock fill research at Mount Isa Mines Limited 1992 - 1997." *Minefill98 6th International Symposium on Mining with Backfill*, Brisbane, 207-215.
- Brady, B. H. G., and Brown, E. T. (1993). *Rock mechanics : For underground mining*, Chapman & Hall, London.
- Criag, R. F. (1997). *Soil mechanics*, 6<sup>th</sup> Edition, E & FN Spon an imprint of Chapman & Hall, London.
- Cowling, R., Auld, G. J., and Meek, J. L. (1983). "Experience with cemented fill stability at Mount Isa Mines." *proceedings of the International Symposium on Mining with Backfill*, Lulea, 329-340.
- Daehnke, A., Rossmannith, H. P., and Knasmillner, R. E. (1996). "Blast-induced dynamic fracture propagation." *Rock Fragmentation by Blasting*, Rotterdam, 13-19.

- Drucker, D. C., and Prager, W. (1952). "Soil Mechanics and Plastic Analysis or Limit Design." *Quarterly of Applied Mathematics*, 10, 157-165.
- e-Gold Prospecting & Mining (n.d.). "Mining Methods" retrieved August 28, 2007 from [http://www.e-goldprospecting.com/html/mining\\_methods.html](http://www.e-goldprospecting.com/html/mining_methods.html)
- Grady, D. E., and Kipp, M. E. (1980). "Continuum modelling of explosive fracture in oil shale." *International Journal of Rock Mechanics and Mining Sciences and Geomechanic Abstracts*, 17, 147-157.
- Guruprasad, S., and Mukherjee, A. (2000). "Layered sacrificial claddings under blast loading. Part 1 - analytical studies." *International Journal of Impact Engineering*, 24, 957-973.
- Hanssen, A. G., Enstock, L., and Langseth, M. (2002). "Close-range blast loading of aluminium foam panels." *International Journal of Impact Engineering*, 27, 593-618.
- Harries, G. (1990). "Development of a dynamic blasting simulation." *The Third International Symposium on Rock Fragmentation by Blasting*, Brisbane, Australia, 175 -179.
- Holmberg, R., and Persson, P.A. (1979). "Design of tunnel perimeter blasthole patterns to prevent rock damage." *Tunnelling '79*, London, 280-283.
- ISO 16063-1:1998. "Methods for the calibration of vibration and shock transducers - Part 1: Basic concepts."
- Jiang, J. J., Blair, D. P., and Baird, G. R. (1995). "Dynamic response of an elastic and viscoelastic full-space to a spherical source." *International Journal for Numerical and Analytical Methods in Geomechanics*, 19, 181-193.
- Kjartansson, E. (1979). "Constant Q-wave propagation and attenuation." *Journal of Geophysical Research*, 84(B9), 4737-4748.
- Kolsky, H. (1963). *Stress waves in solids*, Dover Publications, Inc., New York.
- Kutter, H. K., and Fairhurst, C. (1971). "On the fracture process in blasting." *International Journal of Rock Mechanics and Mining Science*, 8, 181-202.
- Lee, E., Finger, M., and Collins, W. (1973). "JWL equation of state coefficients for high explosives." Technical Report UCID-16189, Lawrence Livermore National Laboratory, Livermore, CA.

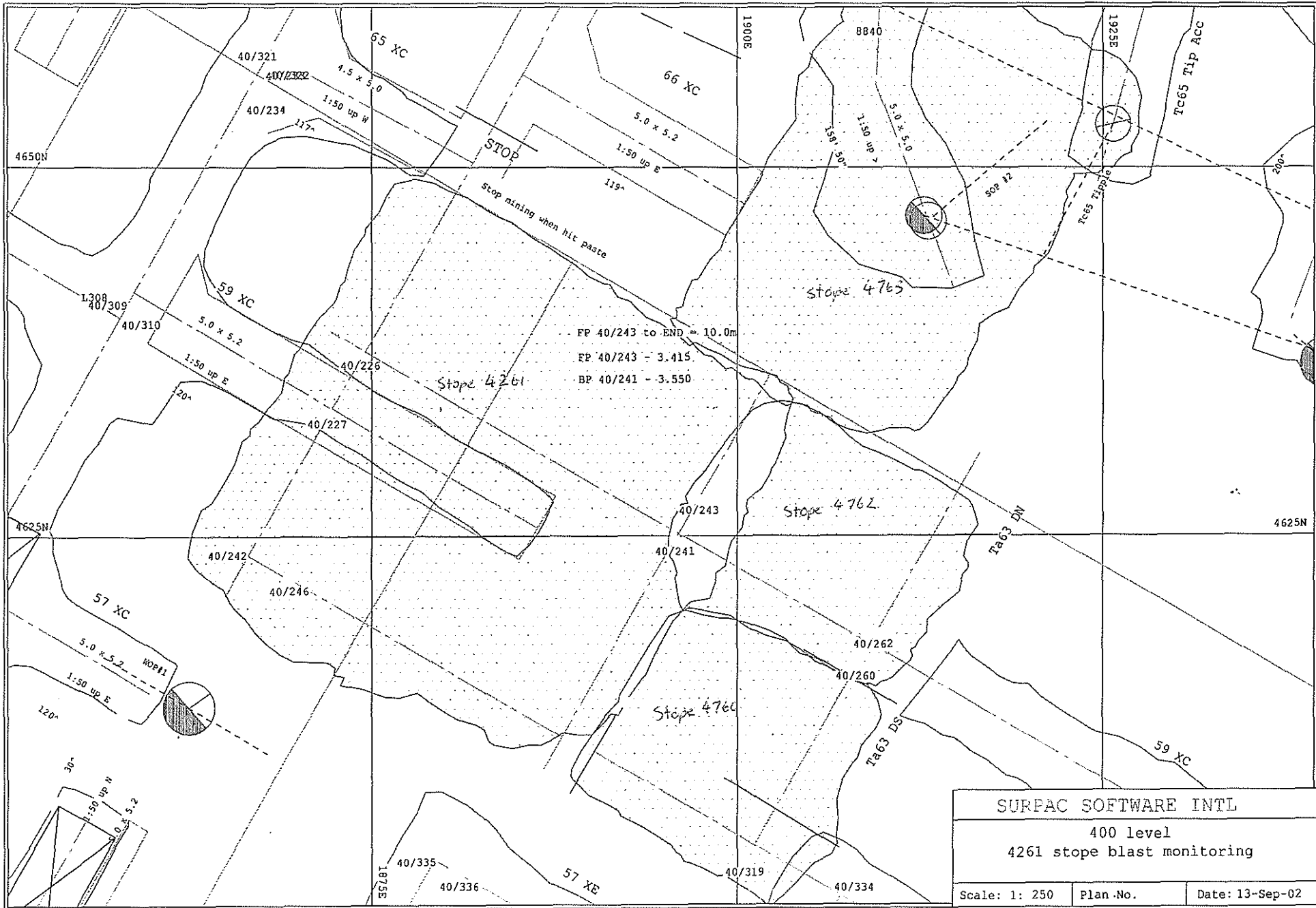
- Lilley, C. R. (1994). "The likelihood of blast induced near field damage in cemented hydraulic fill," Undergraduate Thesis, The University of Queensland, Brisbane.
- Lilley, C. R., and Chitombo, G. P. F. (1998). "Development of a near field damage model for cemented hydraulic fill." *Minefill'98*, Brisbane, 191-196.
- Liu, L., and Katsabanis, P. D. (1996). "Numerical modelling of the effects of air decking/decoupling in production and controlled blasting." *Rock Fragmentation by Blasting*, Rotterdam, 319-330.
- Liu, L., and Katsabanis, P. D. (1997). "Development of a continuum damage model for blasting analysis." *International Journal of Rock Mechanics and Mining Science*, 34(2), 217-231.
- Minchinton, A., and Lynch, P. M. (1996). "Fragmentation and heave modelling using a coupled discrete element gas flow code." *Rock Fragmentation by Blasting*, Rotterdam, 71-80.
- Mitchell, R. J., and Nnadi, G. N. (1994). "Centrifuge models of underground mine backfill blast damage." *Dynamic Geotechnical Testing II, ASTM STP 1213*, Philadelphia, 360-369.
- Mitchell, R. J., Olsen, R. S., and Smith, J. D. (1982). "Model studies on cemented tailings used in mine backfill." *Canadian Geotechnical Journal*, 19(3), 289-295.
- Nnadi, G. N. (1990). "Dynamic behaviour of cemented mine backfill," PhD Thesis, Queen's University, Kingston, Ontario, Canada.
- Nnadi, G. N., and Mitchell, R. J. (1991). "Use of centrifuge models to study simulated blast loadings on backfills." *Rock Mechanics*, 84, 58-63.
- O'Hearn, B., and Swan, G. (1989). "The use of models in sill mat design at Falconbridge." *Innovations in Mining Backfill Technology, Proceedings of the 4th International Symposium on Mining with Backfill*, Montreal, 139-146.
- Olofsson, S.-O., Rosengren, L., and Svedbjork, G. (1999). "Modeling of ground-shock wave propagation in soil using FLAC." *FLAC and Numerical Modeling in Geomechanics*, Rotterdam, 401-405.
- Persson, P.-A., Holmberg, R., and Lee, J. (1994). *Rock blasting and explosives engineering*, CRC Press, Inc., Boca Raton, Florida.
- Pierce, M. E. (2001). "Assessment of the liquefaction potential of saturated hydraulic fill in the 3ES stope at Osborne Mine." Itasca Consulting Group, Inc., Minneapolis.

- Pierce, M. E., Bawden, W. F., and Paynter, J. T. (1998). "Laboratory testing and stability analysis of paste backfill at the Golden Giant Mine." *MINEFILL '98 6th International Symposium on Mining with Backfill*, Brisbane, 159-165.
- Potyondy, D. O., Cundall, P. A., and Sarracino, R. S. (1996). "Modeling of shock- and gas-driven fractures induced by a blast using bonded assemblies of spherical particles." *Rock Fragmentation by Blasting*, Rotterdam, 55-62.
- Preece, D. S., and Taylor, L. M. (1990). "Spherical element bulking mechanisms for modeling blasting induced rock motion." *The Third International Symposium on Rock Fragmentation by Blasting*, Brisbane, Australia, 189-194.
- Preece, D. S., and Thorne, B. J. (1996). "A study of detonation timing and fragmentation using 3-D finite element techniques and a damage constitutive model." *Rock Fragmentation by Blasting*, Rotterdam, 147-156.
- Prevost, J. H., and Popescu, R. (1996). "Constitutive relations for soil materials." *Electronic Journal of Geotechnical Engineering*. <http://geotech.civen.okstate.edu/ejge/ppr9609/part11.htm>. [March 2007]
- Rankine, K. J. (2000). "Geotechnical characterisation and stability analysis of BHP Cannington paste backfill," Undergraduate Thesis, James Cook University, Townsville.
- Rankine, R. (2004). "The geotechnical characterisation and stability analysis of BHP Billiton's Cannington Mine paste fill," PhD Thesis, James Cook University, Townsville.
- Rankine, R. M., Rankine, K. J., Sivakugan, N., Karunasena, W., and Bloss, M. (2001). "Geotechnical characterisation and stability analysis of BHP Cannington paste backfill." *Proceedings of 15th ISSMGE*, Istanbul, Turkey, 1241-1244.
- Sarracino, R. S., and Brinkmann, J. R. (1990). "The modelling of shock effects in blasthole liner experiments." *The Third International Symposium on Rock Fragmentation by Blasting*, Brisbane, Australia, 199-203.
- Sartor, T. (1999). "Modelling vibration induced damage from blasting at the Cannington Mine," Undergraduate Thesis, The University of Queensland, Brisbane.
- Sen, G. C. (1995). *Blasting technology: For mining and civil engineers*, UNSW Press, Sydney.
- Sharma, P. V. (1997). *Environmental and engineering geophysics*, Cambridge University Press, Cambridge.

- Sharpe, J. A. (1942). "The production of elastic waves by explosion pressures. I. Theory and empirical field observations." *Geophysics*, 7(2), 144-154.
- Smith, P. D., Whalen, G. P., Feng, L. J., and Rose, T. A. (2000). "Blast loading on buildings from explosions in city streets." *Structures and Buildings*, 146(1), 47-55.
- Starfield, A. M., and Pugliese, J. M. (1968). "Compression waves generated in rock by cylindrical explosive charge: A comparison between a computer model and field measurements." *International Journal of Rock Mechanics and Mining Science*, 5, 65-77.
- Thorne, B. J., Hommert, P. J., and Brown, B. (1990). "Experimental and computational investigation of the fundamental mechanisms of cratering." *The Third International Symposium on Rock Fragmentation by Blasting*, Brisbane, 117-124.
- Todo, H., and Dowding, C. H. (1984). "One and two support models for blast response." *Journal of Geotechnical Engineering*, 110(6), 675-683.
- van Gool, B. S., Karunasena, W., and Sivakugan, N. (2006). "Modelling the effects of blasting on paste fill." *Computational Methods*, Singapore, 695-700.
- Yang, R. L., Bawden, W. F., and Katsabanis, P. D. (1996). "A new constitutive model for blast damage." *International Journal of Rock Mechanics and Mining Sciences and Geomechanic Abstracts*, 33(3), 245-254.
- Yang, R. L., Rocque, P., Katsabanis, P., and Bawden, W. F. (1994). "Measurement and analysis of near-field blast vibration and damage." *Geotechnical and Geological Engineering*, 12, 169-182.
- Yang, R. L., and Turcotte, R. (1994). "Blast damage modelling using abaqus/explicit." *ABAQUS Users Conference Proceedings*, Newport Rhode Island, 629-647.
- Zou, D. (1990). "Experimental study of computer simulation of bench blasting in production scale." *The Third International Symposium on Rock Fragmentation by Blasting*, Brisbane, Australia, 171-174.



**Appendix A - Plan of Stopes in Monitoring Program**



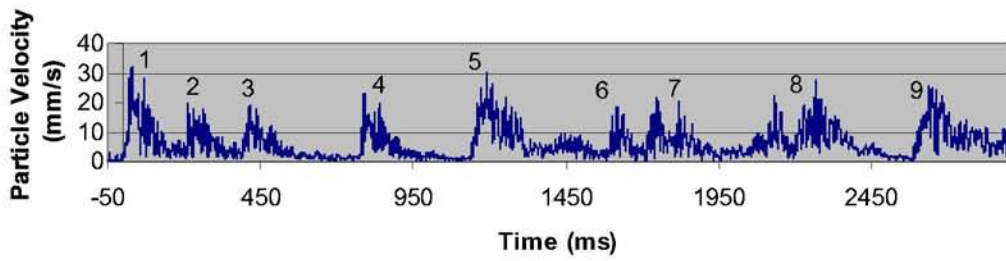
SURPAC SOFTWARE INTL		
400 level		
4261 stope blast monitoring		
Scale: 1: 250	Plan No.	Date: 13-Sep-02

400mapd.pf

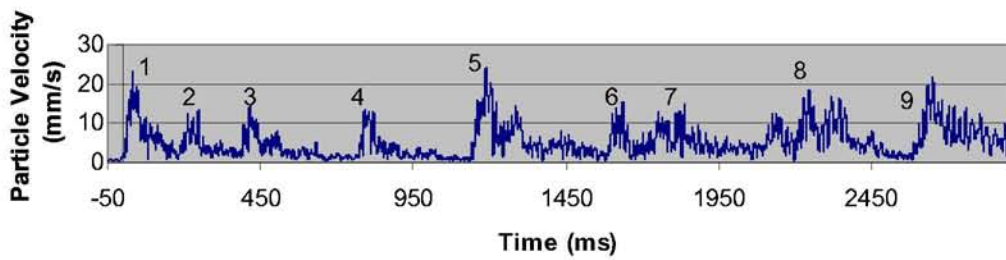
**Appendix B - Stope 4760**

***Waveforms Recorded - 904064***

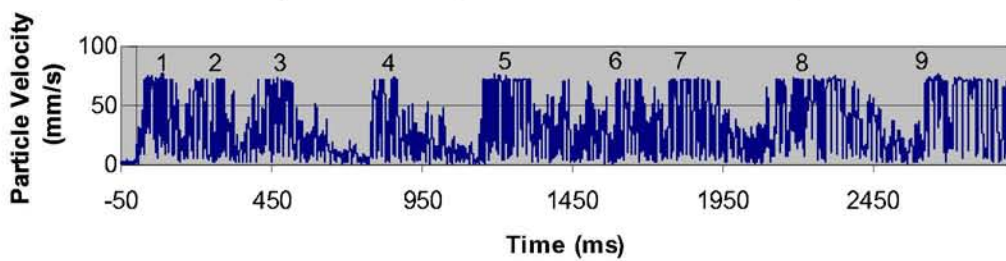
**Geophone G3 - Magnitude of Resultant Velocity**



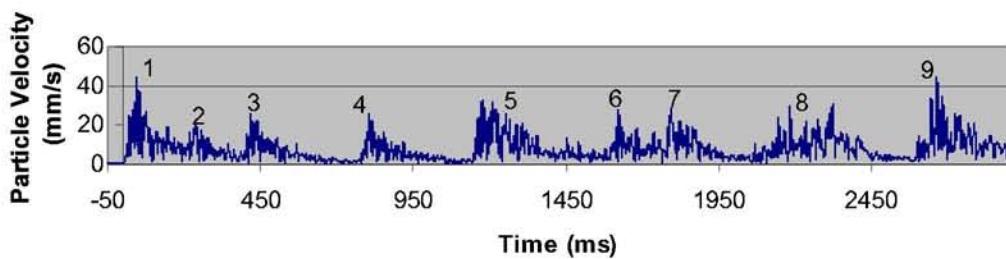
**Geophone G4 - Magnitude of Resultant Velocity**



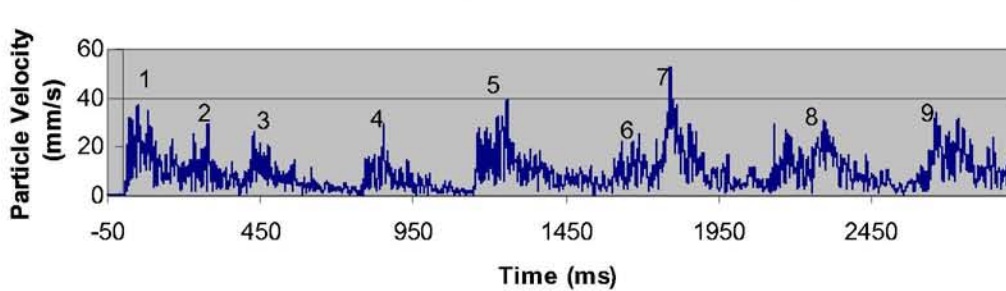
**Geophone G5 - Magnitude of Resultant Velocity**



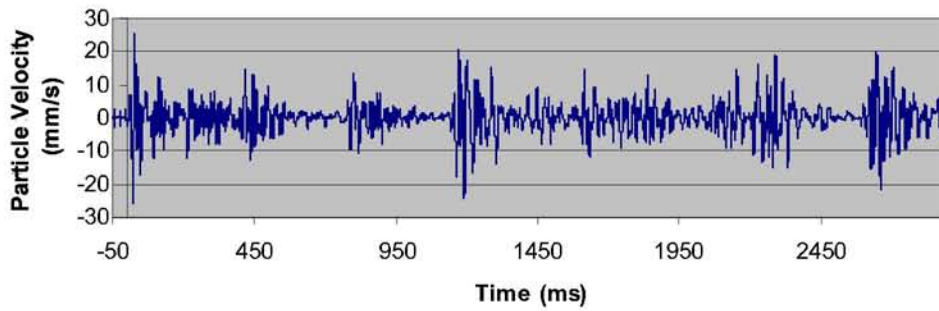
**Geophone G6 - Magnitude of Resultant Velocity**



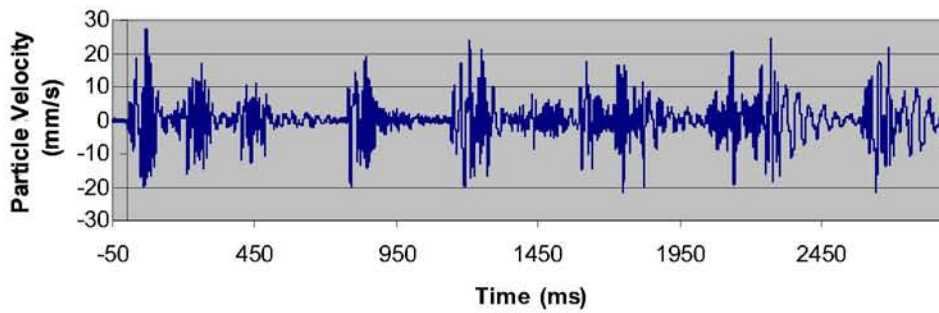
**Geophone G7 - Magnitude of Resultant Velocity**



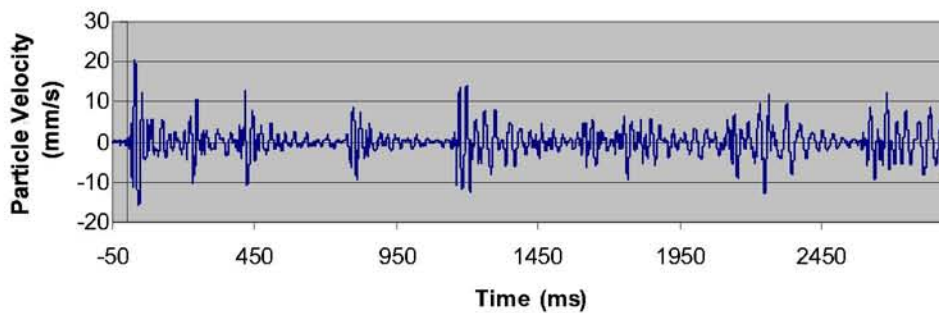
**Geophone G3 - Radial Direction**



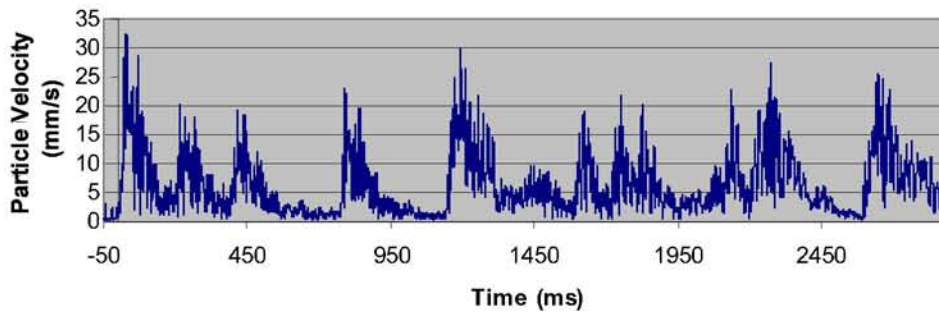
**Geophone G3 - Transverse Direction**



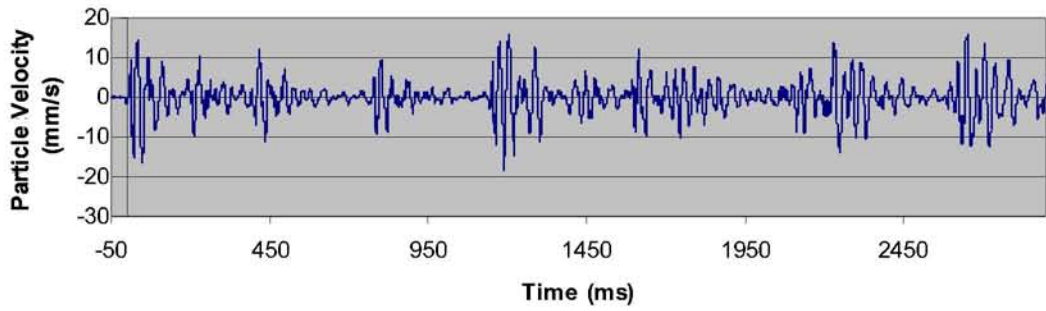
**Geophone G3 - Vertical Direction**



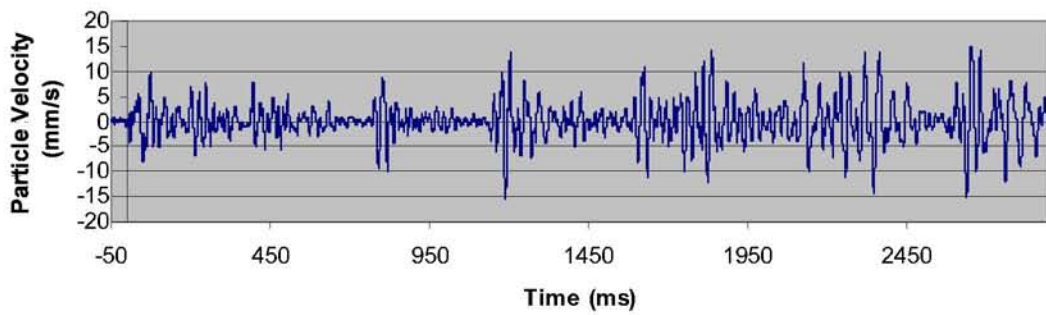
**Geophone G3 - Magnitude of Resultant Velocity**



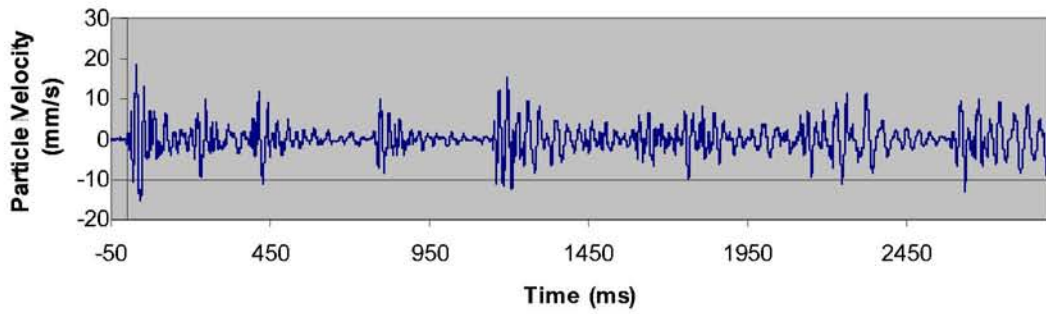
**Geophone G4 - Radial Direction**



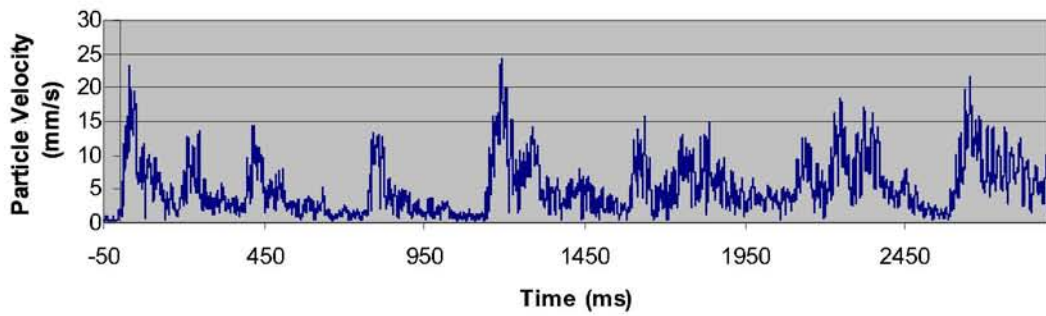
**Geophone G4 - Transverse Direction**



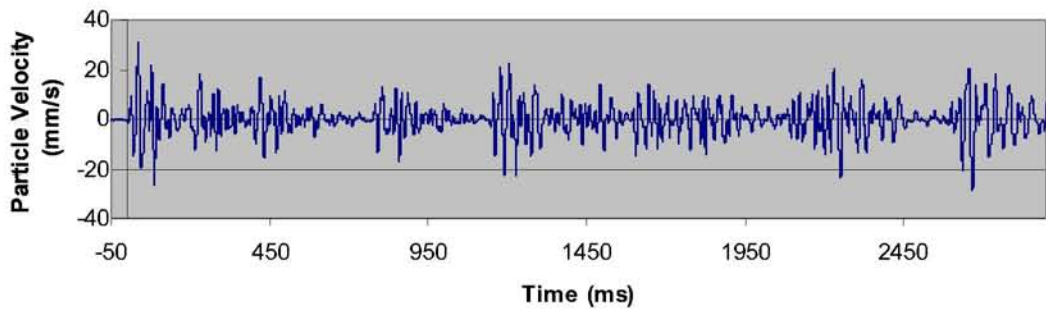
**Geophone G4 - Vertical Direction**



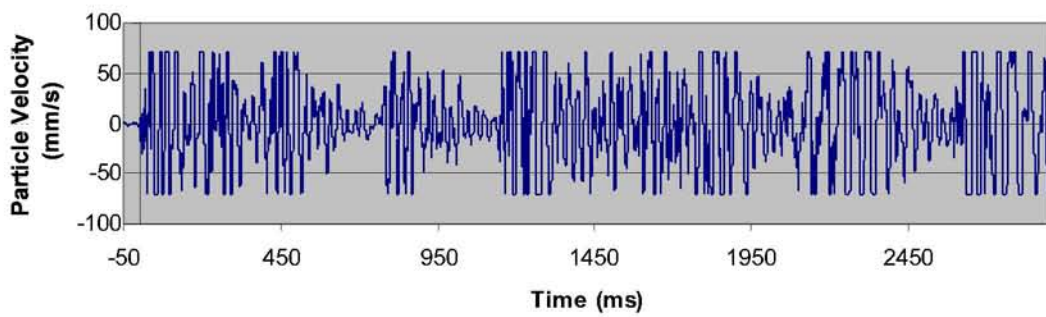
**Geophone G4 - Magnitude of Resultant Velocity**



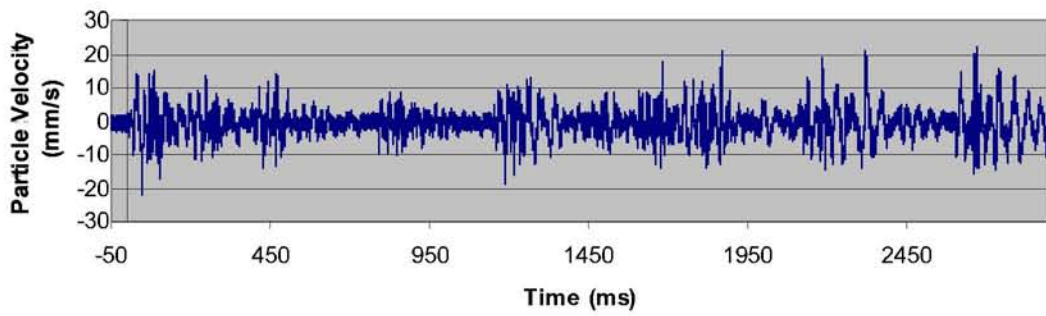
**Geophone G5 - Radial Direction**



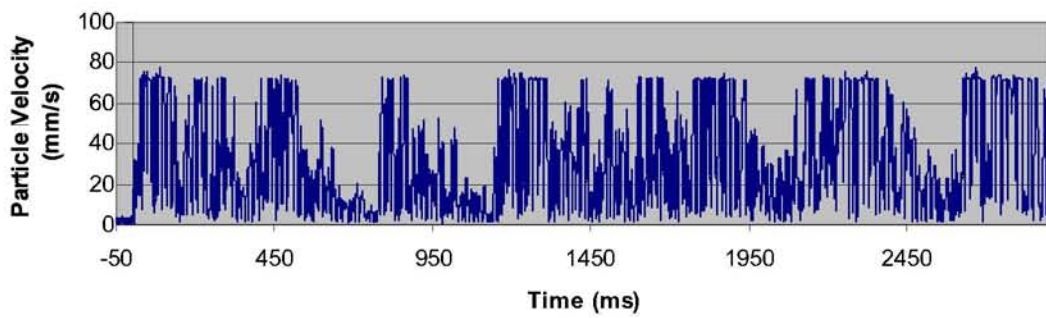
**Geophone G5 - Transverse Direction**



**Geophone G5 - Vertical Direction**

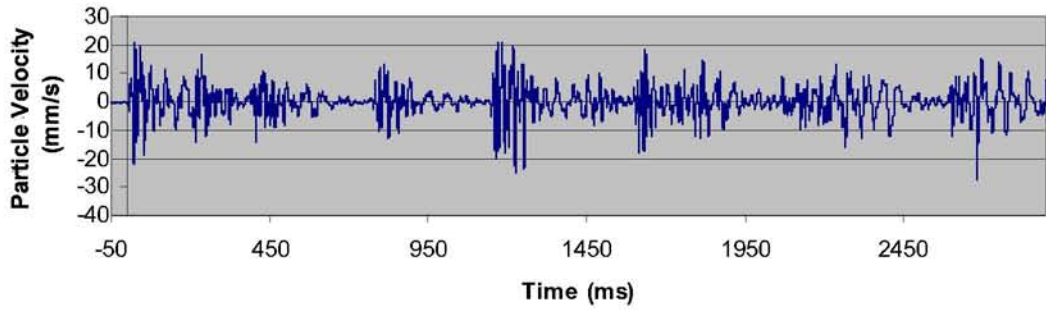


**Geophone G5 - Magnitude of Resultant Velocity**

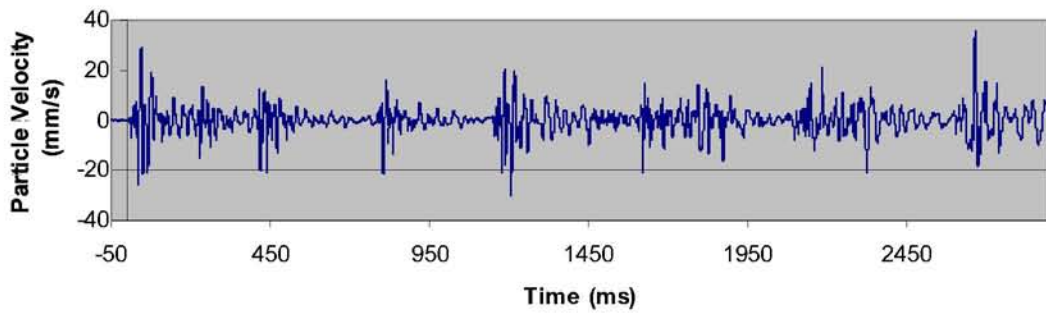




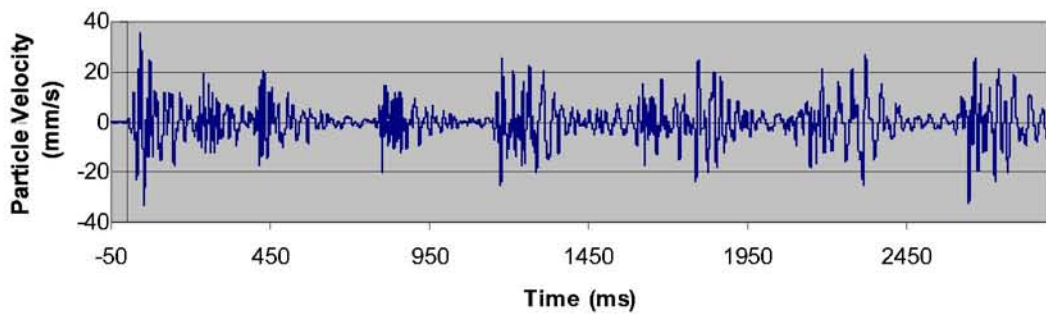
**Geophone G6 - Radial Direction**



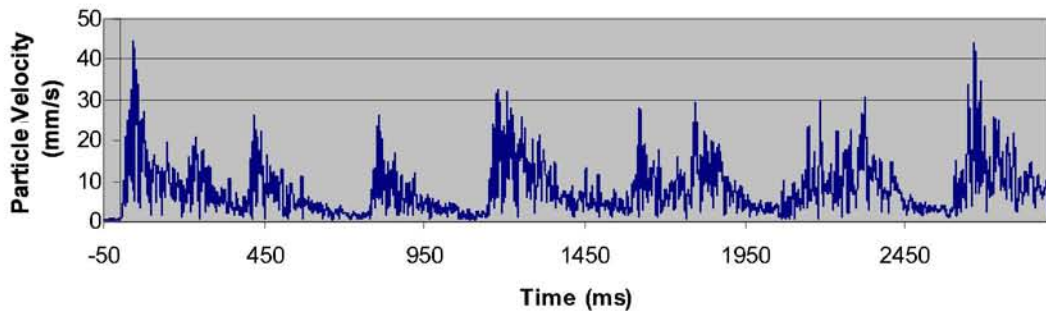
**Geophone G6 - Transverse Direction**



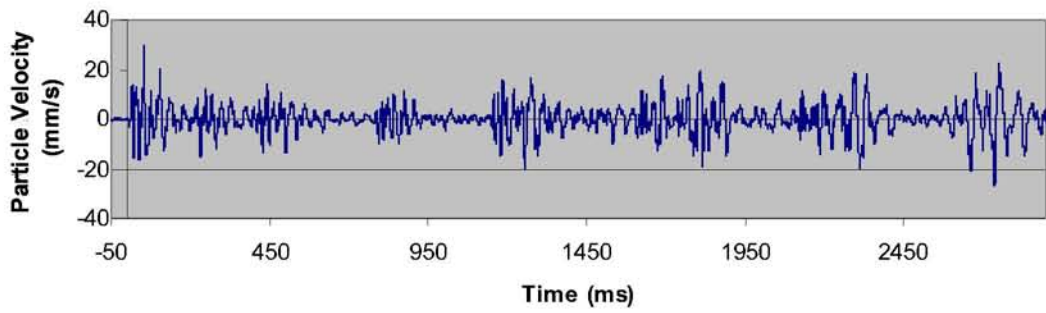
**Geophone G6 - Vertical Direction**



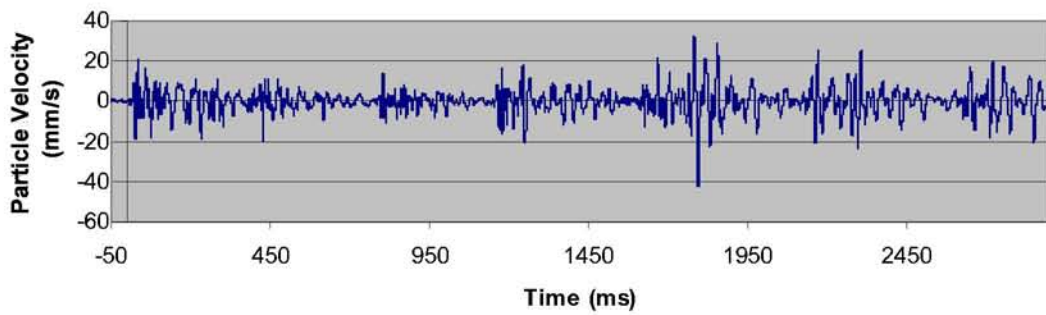
**Geophone G6 - Magnitude of Resultant Velocity**



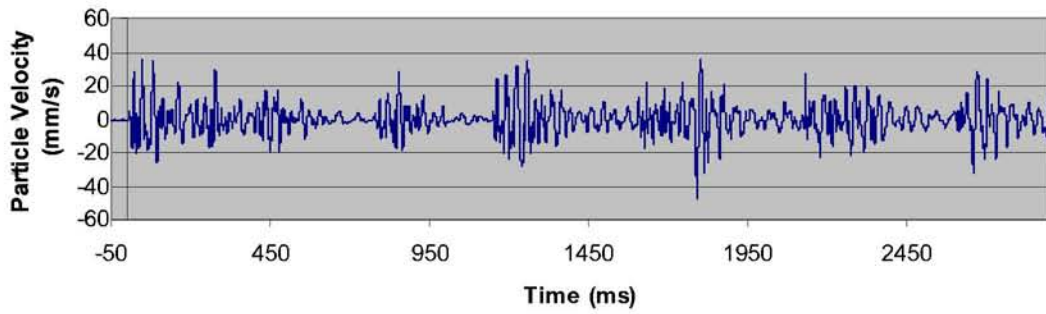
**Geophone G7 - Radial Direction**



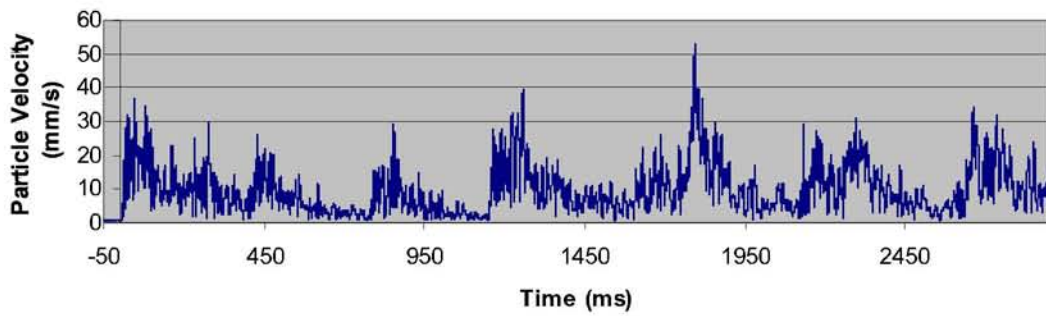
**Geophone G7 - Transverse Direction**



**Geophone G7 - Vertical Direction**

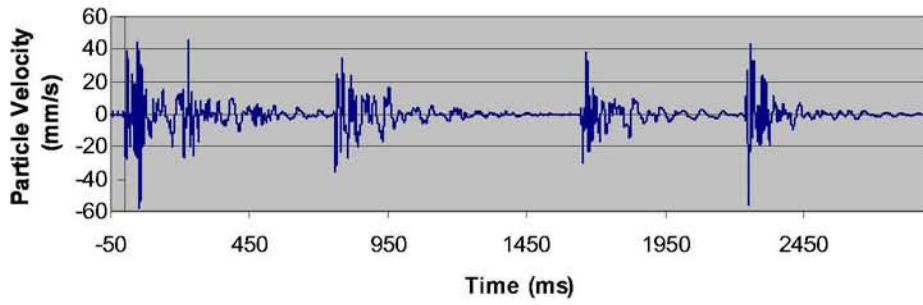


**Geophone G7 - Magnitude of Resultant Velocity**

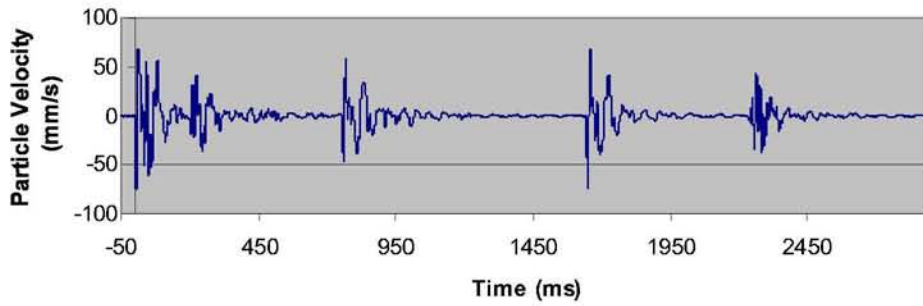


***Waveforms Recorded - 904068***

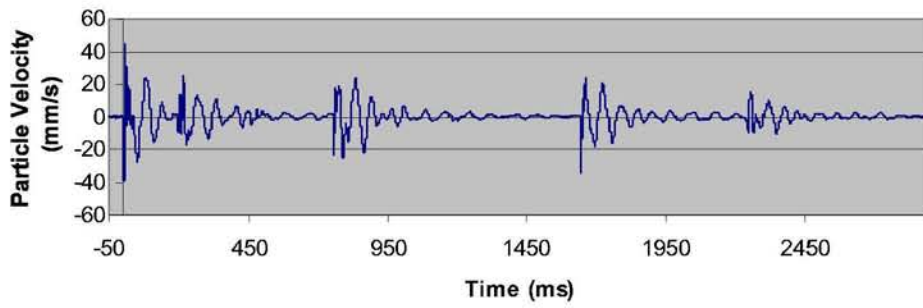
**Geophone G3 - Radial Direction**



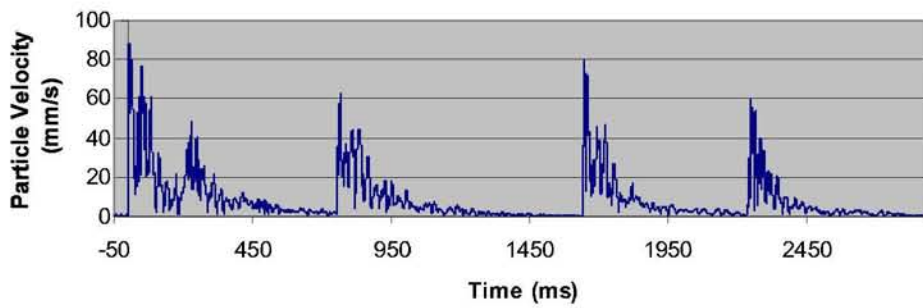
**Geophone G3 - Transverse Direction**



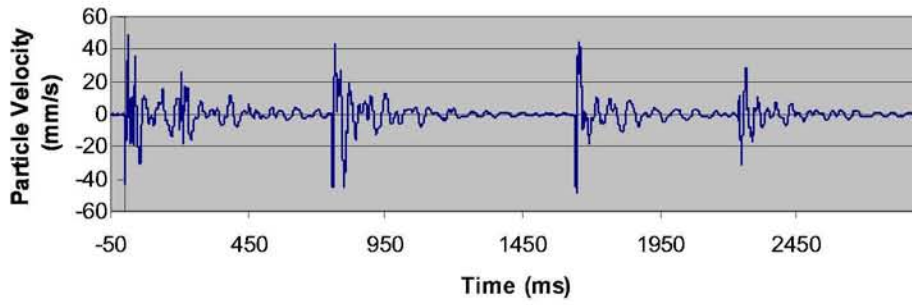
**Geophone G3 - Vertical Direction**



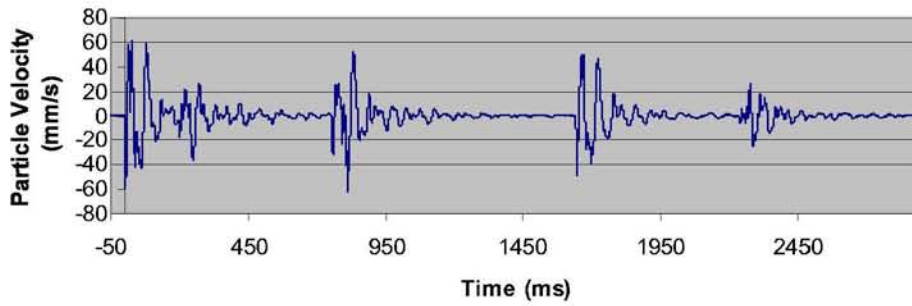
**Geophone G3 - Magnitude of Resultant Velocity**



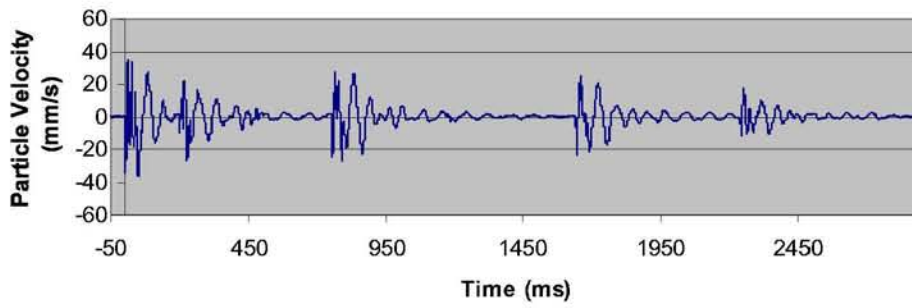
**Geophone G4 - Radial Direction**



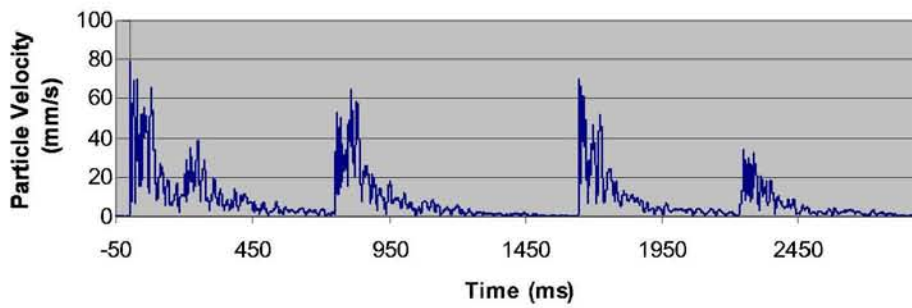
**Geophone G4 - Transverse Direction**



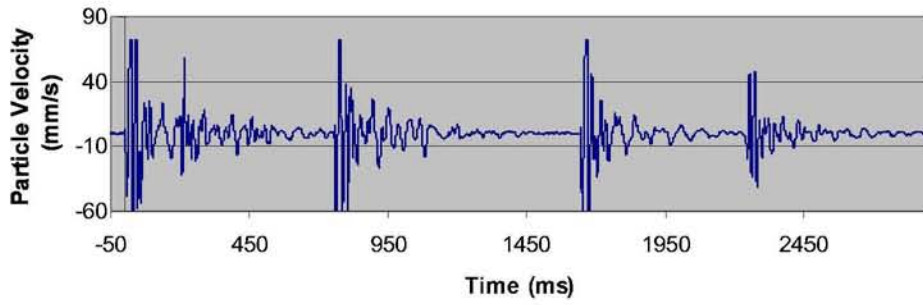
**Geophone G4 - Vertical Direction**



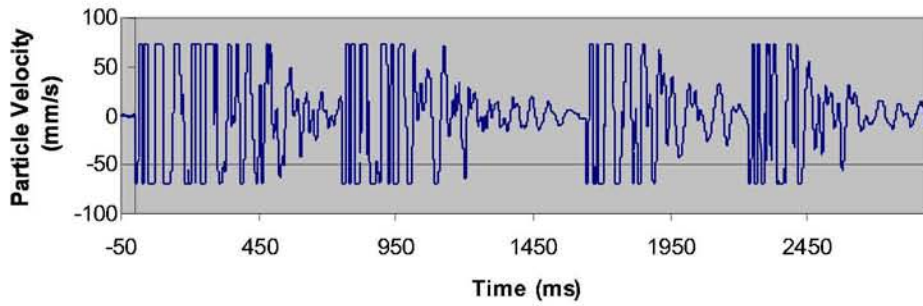
**Geophone G4 - Magnitude of Resultant Velocity**



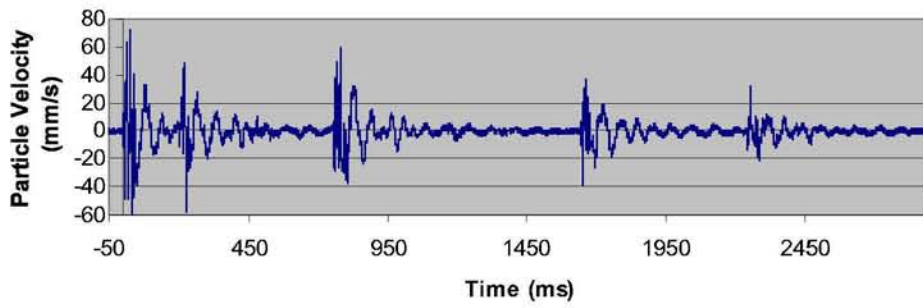
**Geophone G5 - Radial Direction**



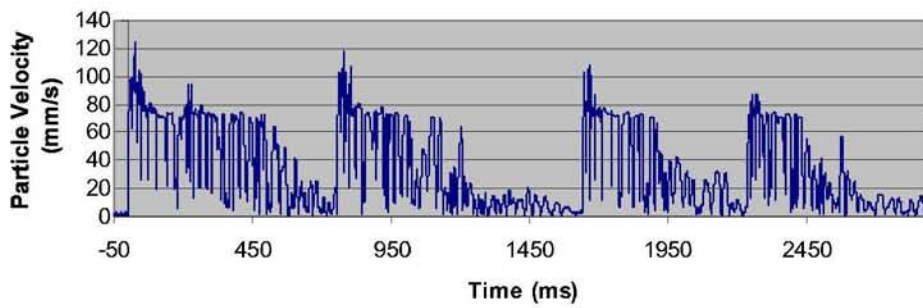
**Geophone G5 - Transverse Direction**



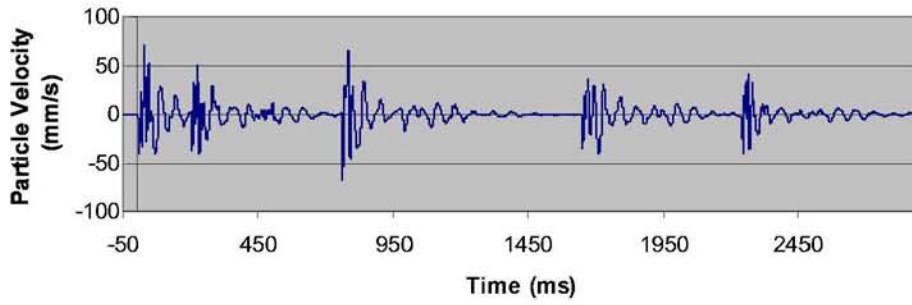
**Geophone G5 - Vertical Direction**



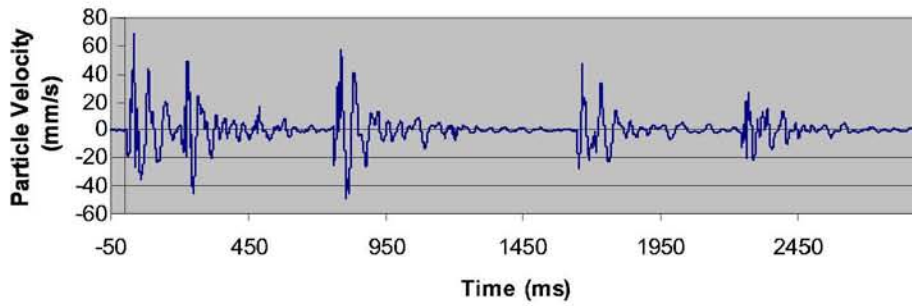
**Geophone G5 - Magnitude of Resultant Velocity**



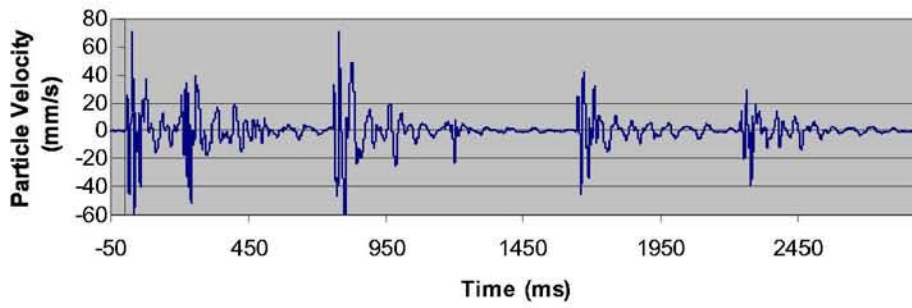
**Geophone G6 - Radial Direction**



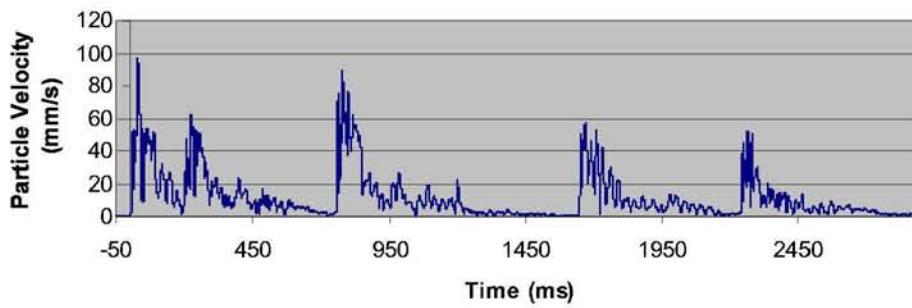
**Geophone G6 - Transverse Direction**



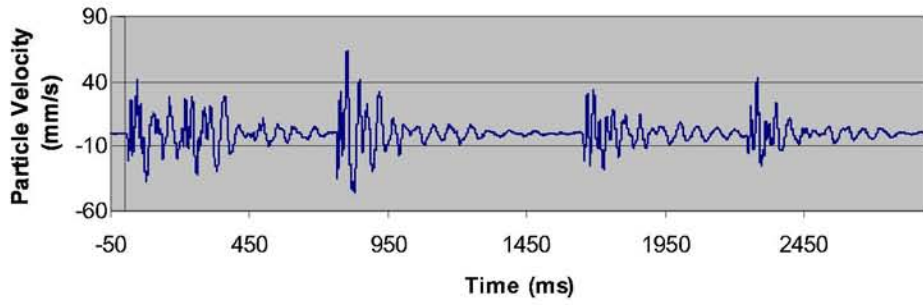
**Geophone G6 - Vertical Direction**



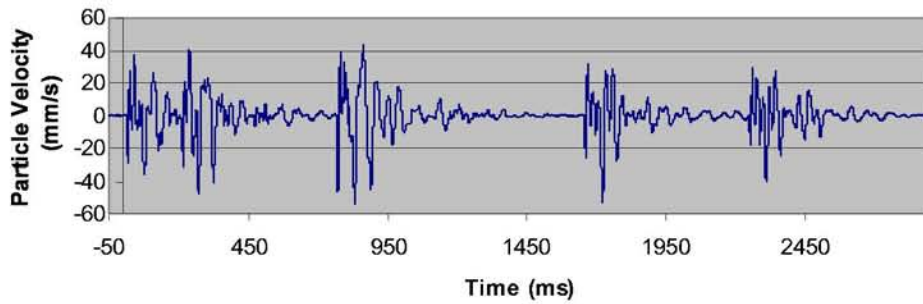
**Geophone G6 - Magnitude of Resultant Velocity**



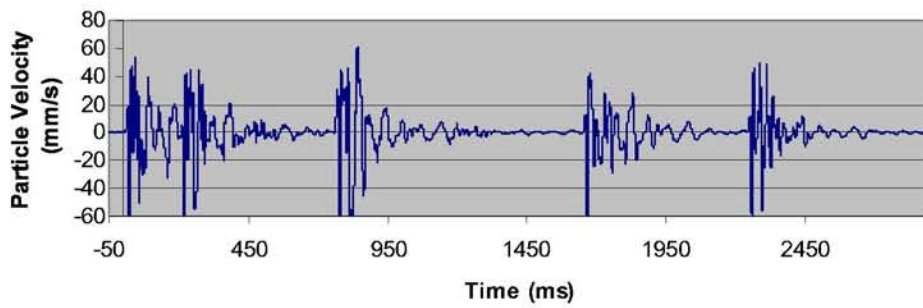
**Geophone G7 - Radial Direction**



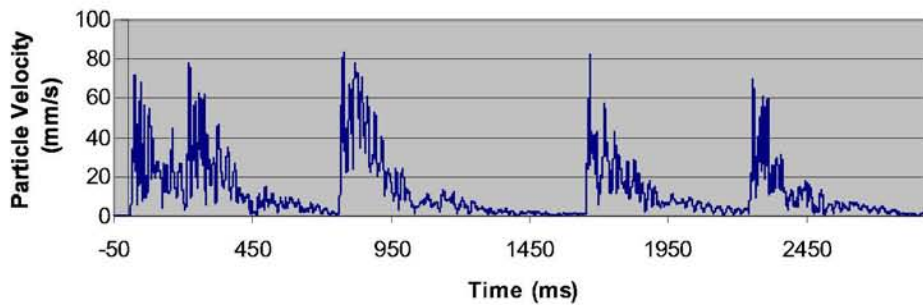
**Geophone G7 - Transverse Direction**



**Geophone G7 - Vertical Direction**

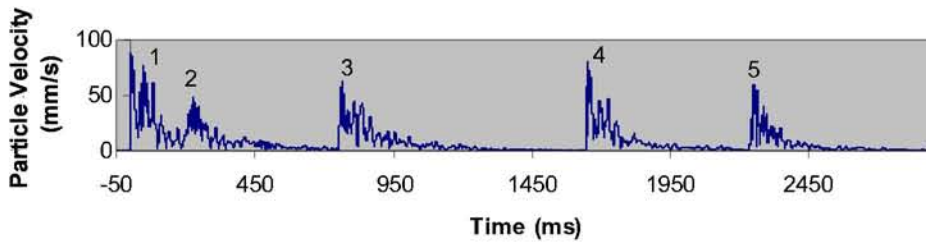


**Geophone G7 - Magnitude of Resultant Velocity**

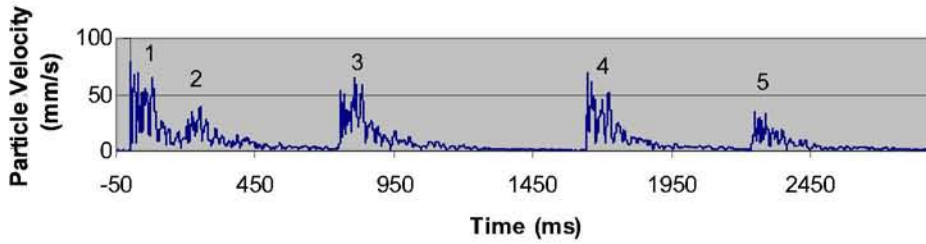




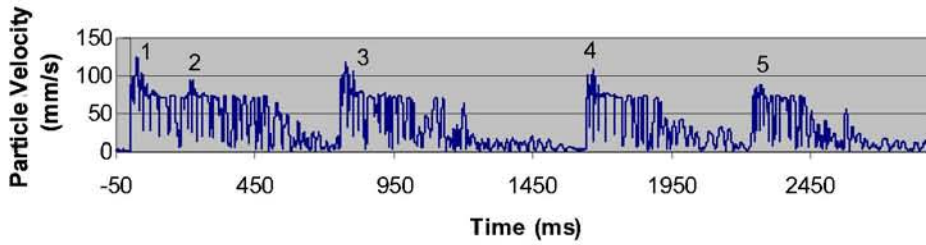
**Geophone G3 - Magnitude of Resultant Velocity**



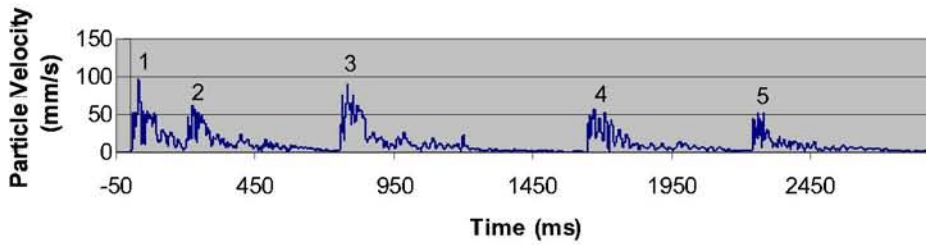
**Geophone G4 - Magnitude of Resultant Velocity**



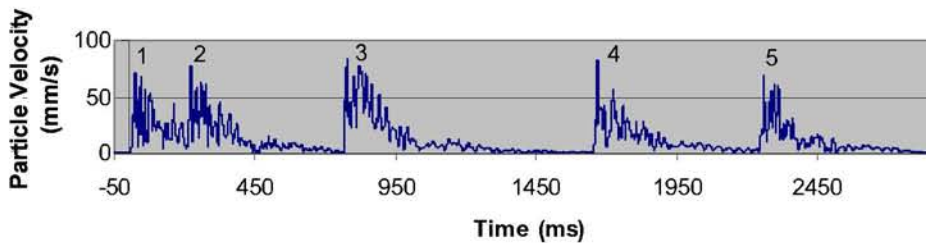
**Geophone G5 - Magnitude of Resultant Velocity**



**Geophone G6 - Magnitude of Resultant Velocity**

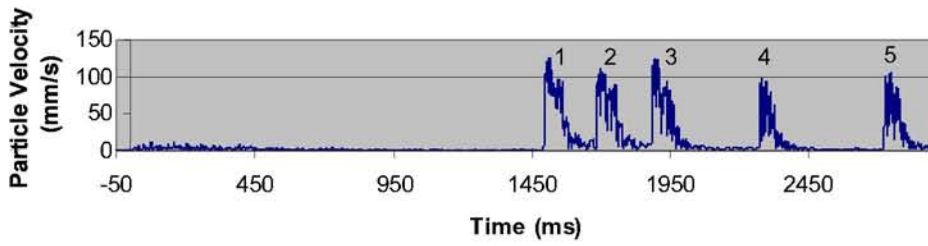


**Geophone G7 - Magnitude of Resultant Velocity**

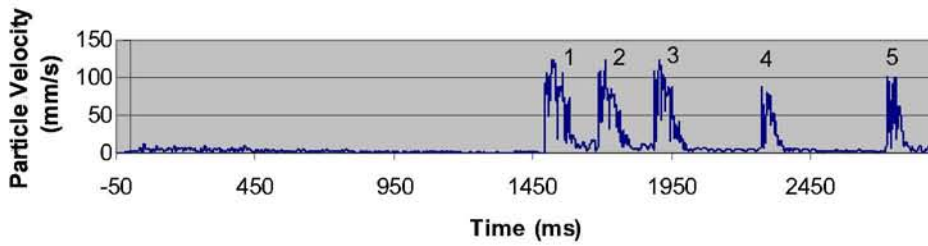


***Waveforms Recorded - 904072***

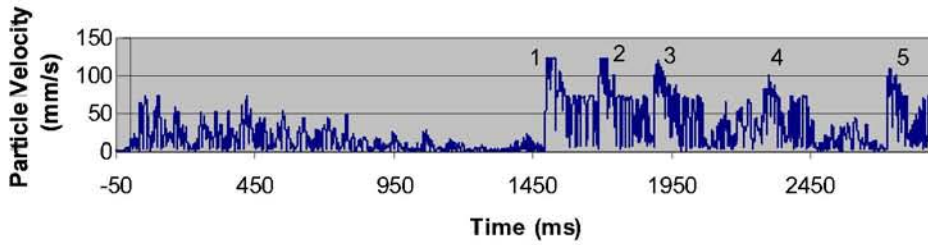
**Geophone G3 - Magnitude of Resultant Velocity**



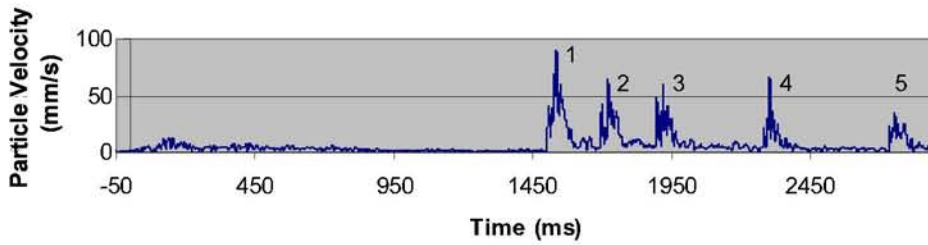
**Geophone G4 - Magnitude of Resultant Velocity**



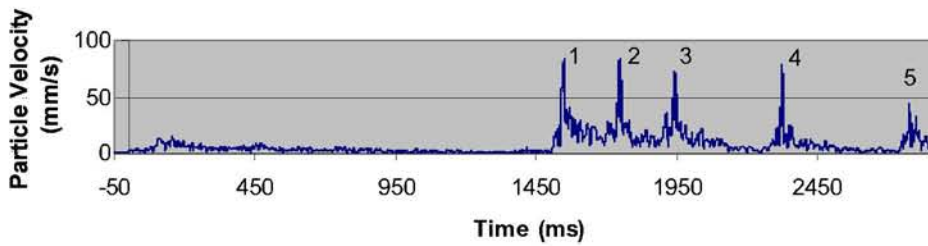
**Geophone G5 - Magnitude of Resultant Velocity**



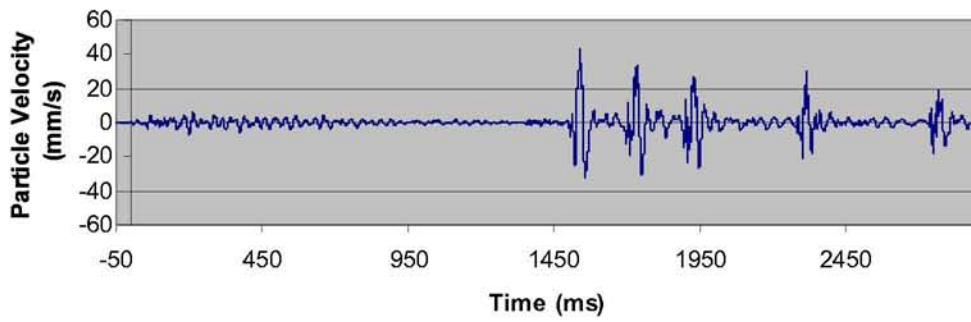
**Geophone G6 - Magnitude of Resultant Velocity**



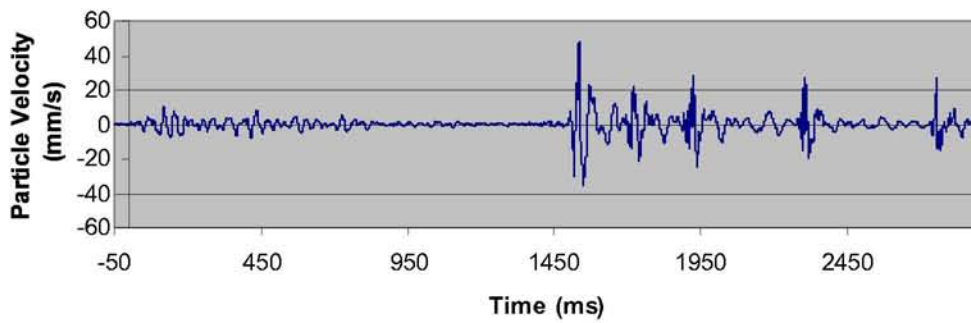
**Geophone G7 - Magnitude of Resultant Velocity**



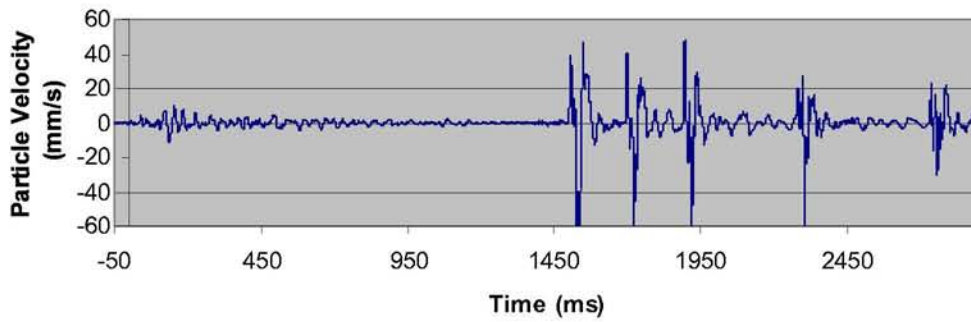
**Geophone G6 - Radial Direction**



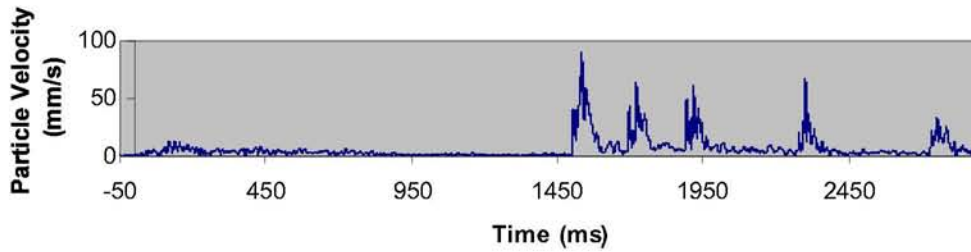
**Geophone G6 - Transverse Direction**



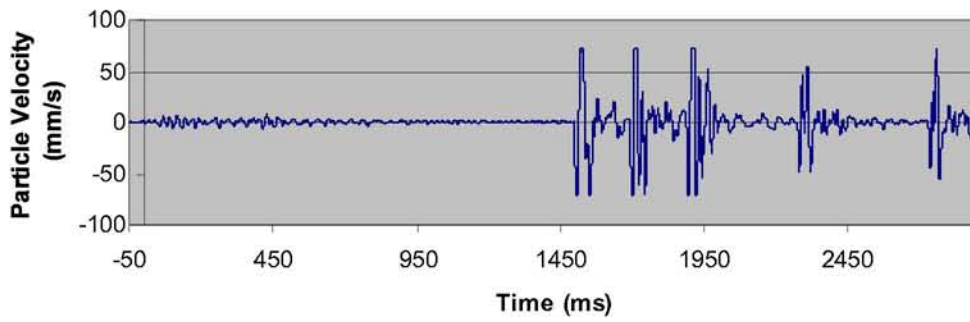
**Geophone G6 - Vertical Direction**



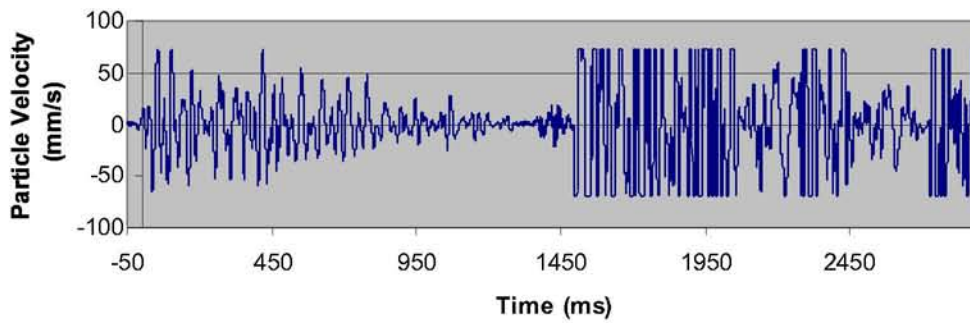
**Geophone G6 - Magnitude of Resultant Velocity**



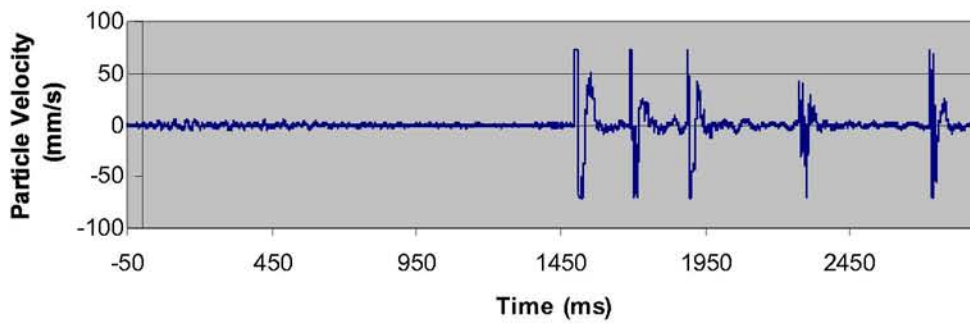
**Geophone G5 - Radial Direction**



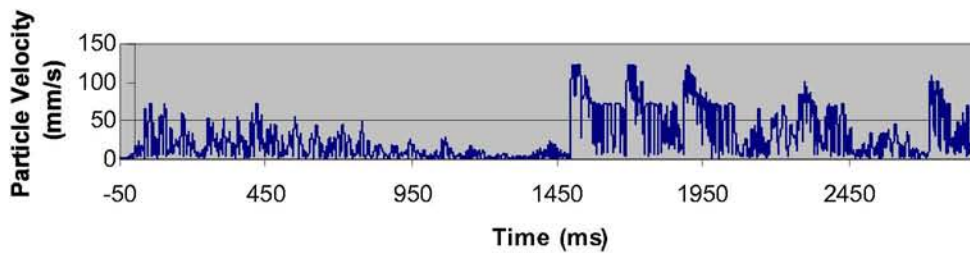
**Geophone G5 - Transverse Direction**



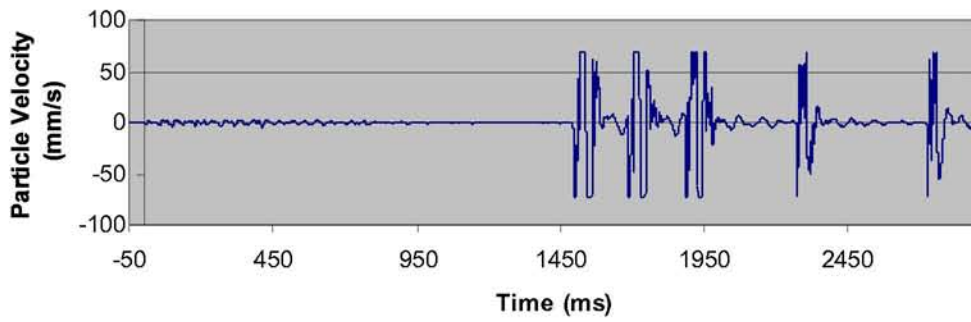
**Geophone G5 - Vertical Direction**



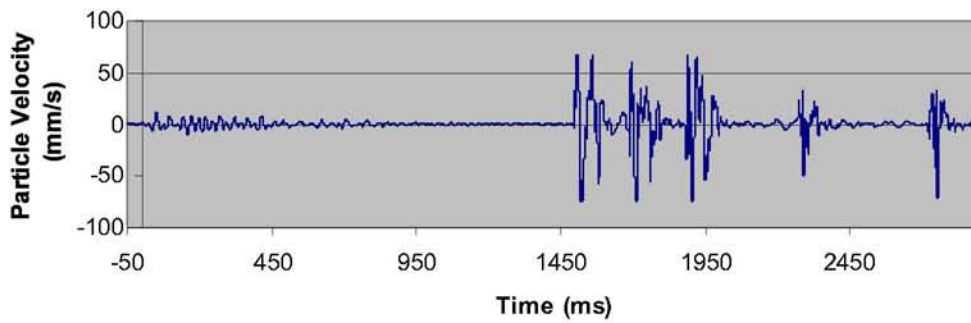
**Geophone G5 - Magnitude of Resultant Velocity**



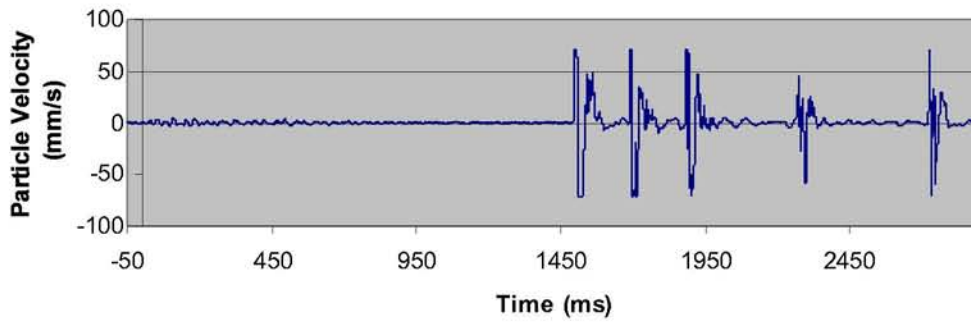
**Geophone G4 - Radial Direction**



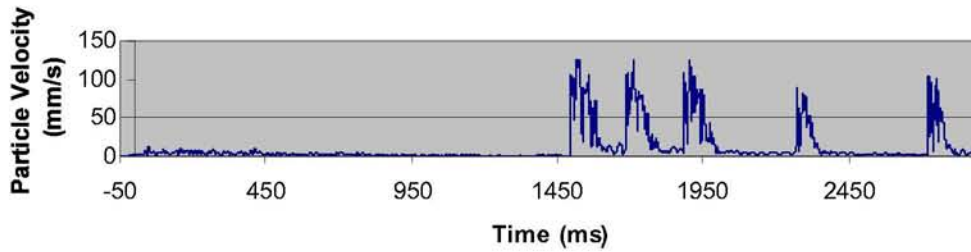
**Geophone G4 - Transverse Direction**



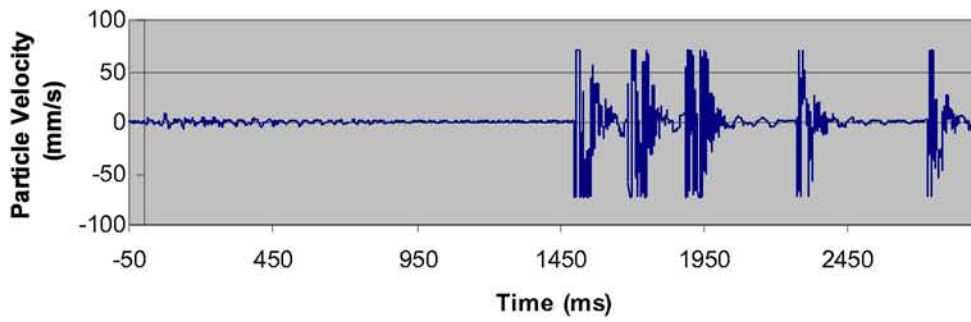
**Geophone G4 - Vertical Direction**



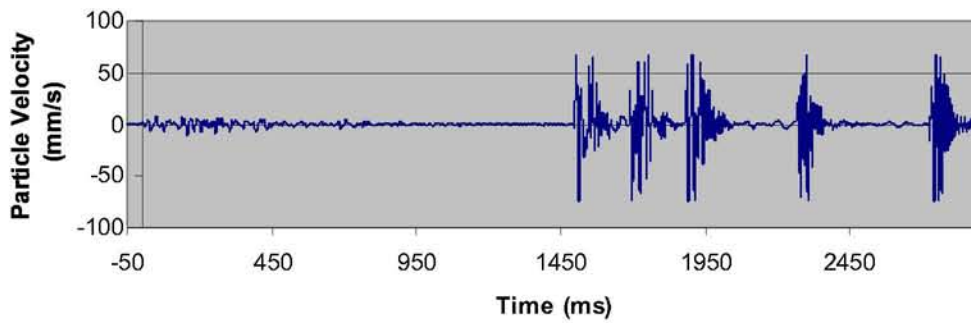
**Geophone G4 - Magnitude of Resultant Velocity**



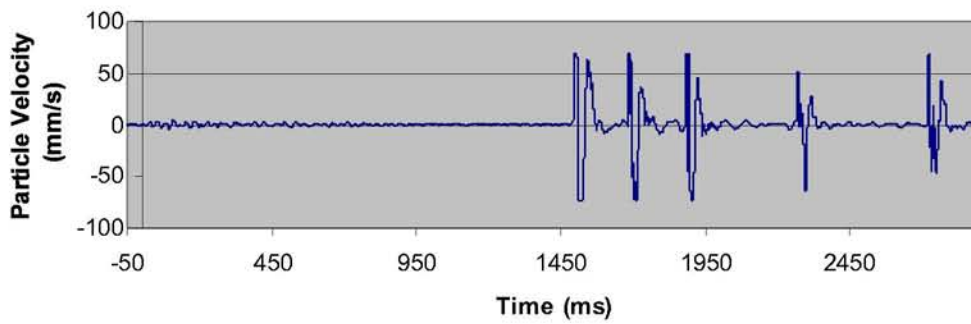
**Geophone G3 - Radial Direction**



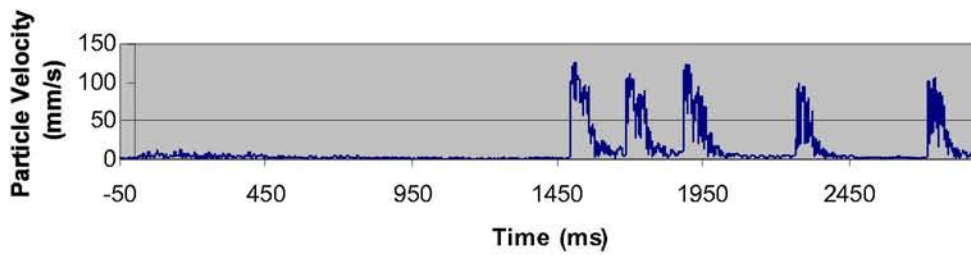
**Geophone G3 - Transverse Direction**



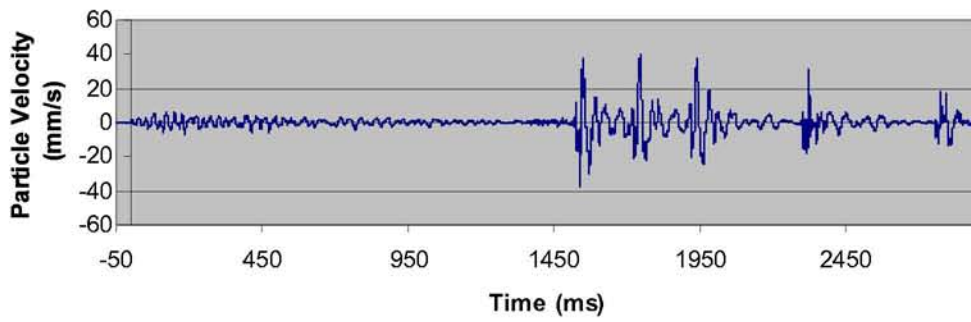
**Geophone G3 - Vertical Direction**



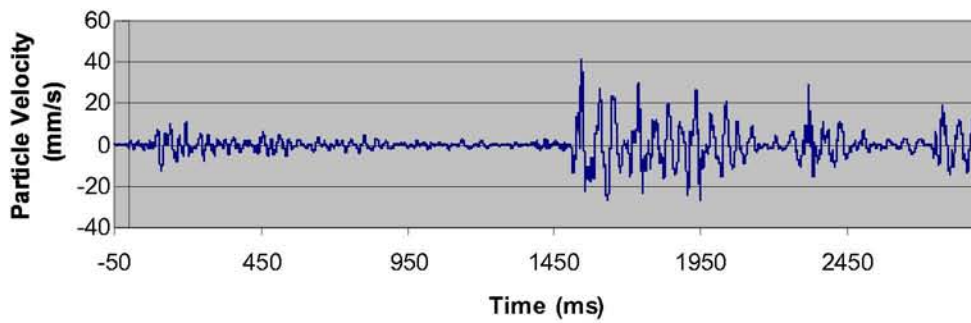
**Geophone G3 - Magnitude of Resultant Velocity**



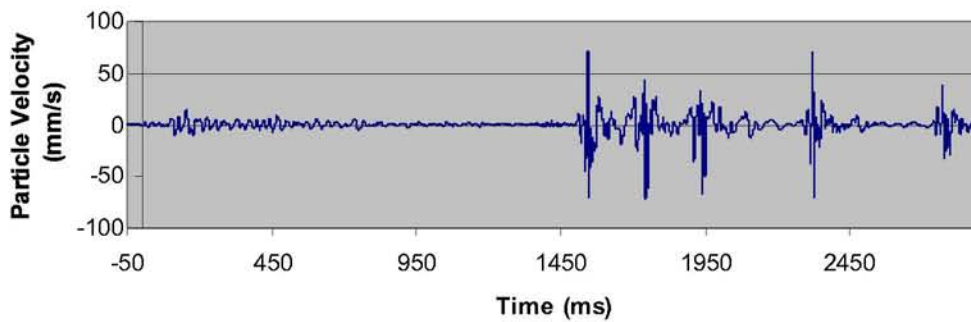
**Geophone G7 - Radial Direction**



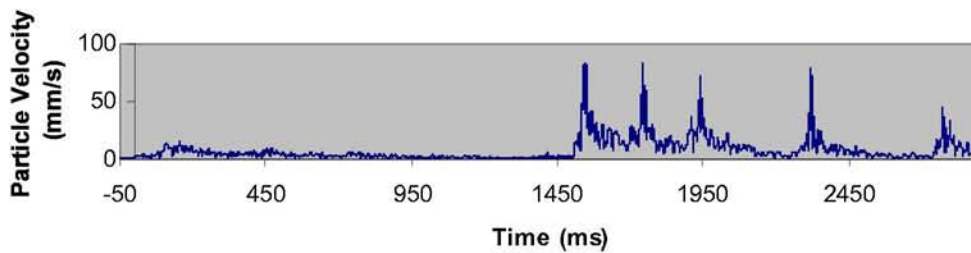
**Geophone G7 - Transverse Direction**



**Geophone G7 - Vertical Direction**



**Geophone G7 - Magnitude of Resultant Velocity**

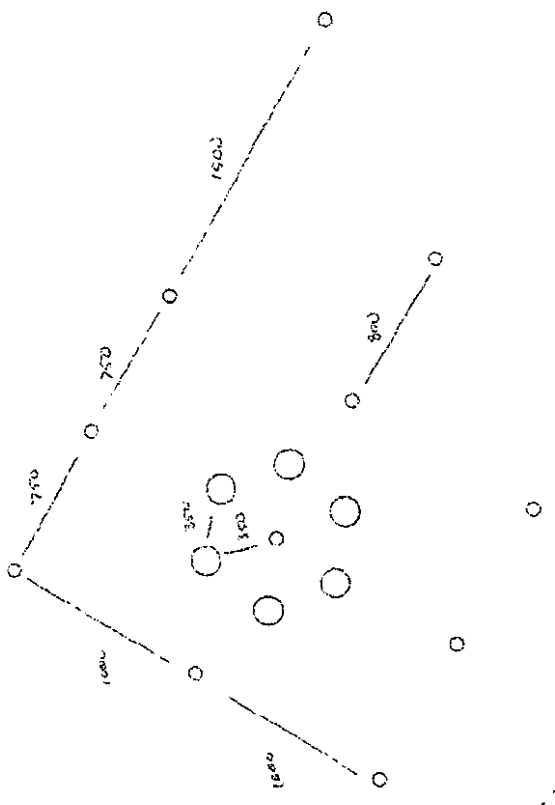




***Blasting Plans - 904064***

# Blast 904064

← NORTH

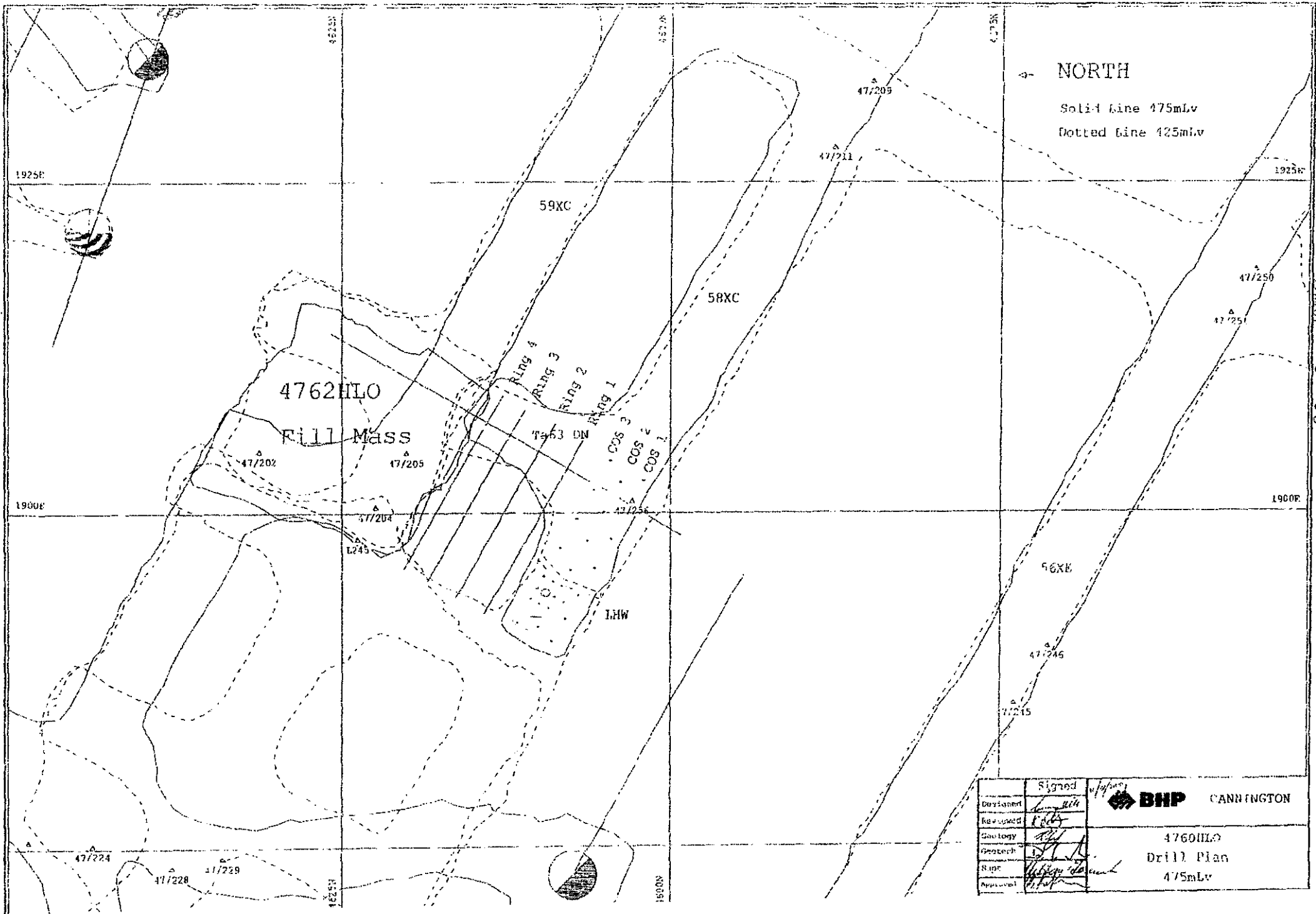


Wentz Detonator  
 12 Packets 200 Holes 68mm  
 6 Cables 152mm  
 Heli. Lumber 21mm  
 General Construction Bombs.

\* Drill All Holes to B/T  
 NINE Holes B/T in 400mm 68xc.

Signed		BNP CONNINGTON	
Designed	1/2/80	4766HNO	
Reviewed	J.B.E.	Blis Plan	
Geology	[Signature]	3/5/80	
Research	[Signature]		
Dept	[Signature]		
Approved	[Signature]		
Supervisor	[Signature]	Scale: 1:25	Sheet: 11 of 11

***Blasting Plans - 904068***



East 4704068

← NORTH  
 Solid Line 175mLv  
 Dotted line 125mLv

Designed	Signed	 <b>BHP</b> CANNINGTON
Reviewed	<i>[Signature]</i>	
Geology	<i>[Signature]</i>	
Geotech	<i>[Signature]</i>	
Approved	<i>[Signature]</i>	
		4760HLO Drill Plan 475mLv

Ring Section Drilling Report.

Date: 10-Aug-01

Ring: COS 1

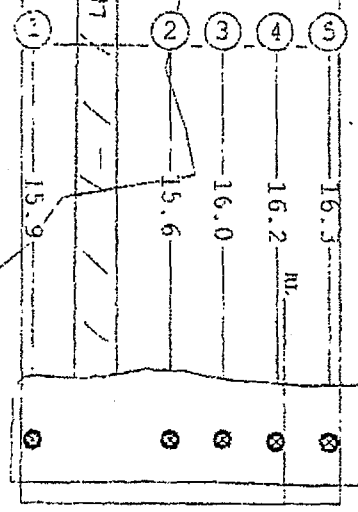
No.	Rt. OS	Collar OS	Dip	Dump	Length	b/t
11	8W	11.97	0	90	15	3000
12	4W	11.97	0	90	15	3000
13	9W	11.97	0	90	15	3000
14	14	11.97	0	90	15	3000
15	7	11.97	0	90	15	3000
						50.0

COS 1

400 58XC

← WEST  
Section  
looks North

425 58XC



Ring Burden 1.5m  
Toe Spacing 2.5m  
Hole diameter: 89mm

475 58XC

	Signed	<b>BHP</b> CARRINGTON 476GHLO COS 1, 475 mlv Looking Looking NORTH
Designed	<i>[Signature]</i>	
Reviewed	<i>[Signature]</i>	
Geology	<i>[Signature]</i>	
Geotech	<i>[Signature]</i>	
Approved	<i>[Signature]</i>	Scale: 1:250
Surveyor		Date: 11-Aug-01

INSTRATA.NI

Ring Border drilling report:

Date: 10-Aug-01

Ring: COS 2

No.	PL	OS	Collar	GE	Dip	Dump	length	b/t
1	11.4W		11.4W	0	90		15.4	N
2	6.4W		6.4W	0	90		15.4	N
3	3.9W		3.9W	0	90		15.4	N
4	1.4W		1.4W	0	90		15.6	N
5	1.1E		1.1E	0	90		15.6	N
							77.3	

COS 2

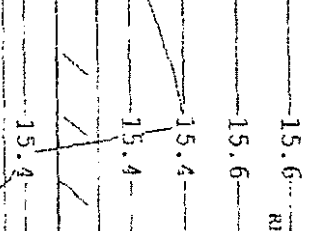
400 58XC

← WEST

Section  
looks North

425 58XC

① ② ③ ④ ⑤



Ring Border: 1.5m

Toe Spacing: 2.5m

Hole diameter: 89mm

475 58XC



	Signed	<i>u/a/see</i>	<b>BHP</b> CANNINGTON
Designed	<i>[Signature]</i>		
Reviewed	<i>[Signature]</i>		
Geology	<i>[Signature]</i>	4760HLC	
Geotech	<i>[Signature]</i>	COS 2, 475 mLv	
Supt	<i>[Signature]</i>	Looking Looking NORTH	
Approved	<i>[Signature]</i>		
Surveyor		Scale: 1:250	Date: 11-Aug-01

Vertical text on the left margin: 10/08/01

Ring Design Drilling report:

Date: 15-Aug-01

Ring COS 3

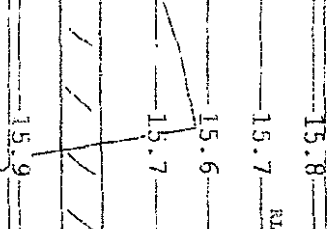
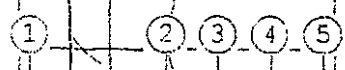
No	Bl. OS	Collar OS	Dip	Dump	length	b/t
1	2W	1.9W	90	1.5	15.9	N
2	4W	5.4W	90	1.5	15.9	N
3	4W	5.4W	90	1.5	15.7	N
4	4W	5.4W	90	1.5	15.6	N
5	4W	5.4W	90	1.5	15.7	N
6	4W	5.4W	90	1.5	15.8	N
						7# 6

COS 3

400 58XC

← WEST  
Section  
looks North

425 58XC



Ring Burden 1.5m

Toe Spacing 2.5m

Hole diameter: 89mm

475 58XC

	Signed		CANNINGTON
Designed	<i>[Signature]</i>		
Reviewed	<i>[Signature]</i>	4760H10	
Geology	<i>[Signature]</i>	COS 3, 475 mLv	
Checked	<i>[Signature]</i>	Looking Looking NORTH	
Supt	<i>[Signature]</i>	Scale: 1:250	Date: 11-Aug-01
Approved	<i>[Signature]</i>		
Surveyor			

K:\00100001.ppt

Ring Design drilling report:  
 Date: 12-Aug-01  
 Ring: 1

No.	RI	DS	Collar DS	Dip	Ramp	Length	b/t
1	1	1W	3.6W	242	90	3.6	N
2	1	2W	6W	256	90	4.4	N
3	1	3W	6W	267	90	5.3	N
4	1	4W	6W	283	90	6.3	N
5	1	5W	6W	297	90	7.1	N
6	1	6W	6W	310	90	8.1	N
7	1	7W	6W	318	90	9.1	N
8	1	8W	6W	324	90	10.1	N
9	1	9W	6W	335	90	11.1	N
10	1	10W	6W	348	90	12.1	N
11	1	11W	6W	363	90	13.1	N
12	1	12W	6W	381	90	14.1	N
13	1	13W	6W	402	90	15.1	N
14	1	14W	6W	426	90	16.1	N
15	1	15W	6W	453	90	17.1	N
16	1	16W	6W	483	90	18.1	N
17	1	17W	6W	516	90	19.1	N
18	1	18W	6W	553	90	20.1	N
19	1	19W	6W	594	90	21.1	N
20	1	20W	6W	639	90	22.1	N
21	1	21W	6W	687	90	23.1	N
22	1	22W	6W	738	90	24.1	N
23	1	23W	6W	792	90	25.1	N
24	1	24W	6W	849	90	26.1	N
25	1	25W	6W	909	90	27.1	N
26	1	26W	6W	972	90	28.1	N
27	1	27W	6W	1038	90	29.1	N
28	1	28W	6W	1106	90	30.1	N
29	1	29W	6W	1176	90	31.1	N
30	1	30W	6W	1248	90	32.1	N
31	1	31W	6W	1321	90	33.1	N
32	1	32W	6W	1396	90	34.1	N
33	1	33W	6W	1473	90	35.1	N
34	1	34W	6W	1551	90	36.1	N
35	1	35W	6W	1631	90	37.1	N
36	1	36W	6W	1712	90	38.1	N
37	1	37W	6W	1795	90	39.1	N
38	1	38W	6W	1880	90	40.1	N
39	1	39W	6W	1967	90	41.1	N
40	1	40W	6W	2056	90	42.1	N
41	1	41W	6W	2147	90	43.1	N
42	1	42W	6W	2240	90	44.1	N
43	1	43W	6W	2335	90	45.1	N
44	1	44W	6W	2432	90	46.1	N
45	1	45W	6W	2531	90	47.1	N
46	1	46W	6W	2631	90	48.1	N
47	1	47W	6W	2733	90	49.1	N
48	1	48W	6W	2837	90	50.1	N
49	1	49W	6W	2943	90	51.1	N
50	1	50W	6W	3051	90	52.1	N
51	1	51W	6W	3161	90	53.1	N
52	1	52W	6W	3273	90	54.1	N
53	1	53W	6W	3387	90	55.1	N
54	1	54W	6W	3503	90	56.1	N
55	1	55W	6W	3621	90	57.1	N
56	1	56W	6W	3741	90	58.1	N
57	1	57W	6W	3863	90	59.1	N
58	1	58W	6W	3987	90	60.1	N
59	1	59W	6W	4113	90	61.1	N
60	1	60W	6W	4241	90	62.1	N
61	1	61W	6W	4371	90	63.1	N
62	1	62W	6W	4503	90	64.1	N
63	1	63W	6W	4637	90	65.1	N
64	1	64W	6W	4773	90	66.1	N
65	1	65W	6W	4911	90	67.1	N
66	1	66W	6W	5051	90	68.1	N
67	1	67W	6W	5193	90	69.1	N
68	1	68W	6W	5337	90	70.1	N
69	1	69W	6W	5483	90	71.1	N
70	1	70W	6W	5631	90	72.1	N
71	1	71W	6W	5781	90	73.1	N
72	1	72W	6W	5933	90	74.1	N
73	1	73W	6W	6087	90	75.1	N
74	1	74W	6W	6243	90	76.1	N
75	1	75W	6W	6401	90	77.1	N
76	1	76W	6W	6561	90	78.1	N
77	1	77W	6W	6723	90	79.1	N
78	1	78W	6W	6887	90	80.1	N
79	1	79W	6W	7053	90	81.1	N
80	1	80W	6W	7221	90	82.1	N
81	1	81W	6W	7391	90	83.1	N
82	1	82W	6W	7563	90	84.1	N
83	1	83W	6W	7737	90	85.1	N
84	1	84W	6W	7913	90	86.1	N
85	1	85W	6W	8091	90	87.1	N
86	1	86W	6W	8271	90	88.1	N
87	1	87W	6W	8453	90	89.1	N
88	1	88W	6W	8637	90	90.1	N
89	1	89W	6W	8823	90	91.1	N
90	1	90W	6W	9011	90	92.1	N
91	1	91W	6W	9201	90	93.1	N
92	1	92W	6W	9393	90	94.1	N
93	1	93W	6W	9587	90	95.1	N
94	1	94W	6W	9783	90	96.1	N
95	1	95W	6W	9981	90	97.1	N
96	1	96W	6W	10181	90	98.1	N
97	1	97W	6W	10383	90	99.1	N
98	1	98W	6W	10587	90	100.1	N
99	1	99W	6W	10793	90	101.1	N
100	1	100W	6W	11001	90	102.1	N
101	1	101W	6W	11211	90	103.1	N
102	1	102W	6W	11423	90	104.1	N
103	1	103W	6W	11637	90	105.1	N
104	1	104W	6W	11853	90	106.1	N
105	1	105W	6W	12071	90	107.1	N
106	1	106W	6W	12291	90	108.1	N
107	1	107W	6W	12513	90	109.1	N
108	1	108W	6W	12737	90	110.1	N
109	1	109W	6W	12963	90	111.1	N
110	1	110W	6W	13191	90	112.1	N
111	1	111W	6W	13421	90	113.1	N
112	1	112W	6W	13653	90	114.1	N
113	1	113W	6W	13887	90	115.1	N
114	1	114W	6W	14123	90	116.1	N
115	1	115W	6W	14361	90	117.1	N
116	1	116W	6W	14601	90	118.1	N
117	1	117W	6W	14843	90	119.1	N
118	1	118W	6W	15087	90	120.1	N
119	1	119W	6W	15333	90	121.1	N
120	1	120W	6W	15581	90	122.1	N
121	1	121W	6W	15831	90	123.1	N
122	1	122W	6W	16083	90	124.1	N
123	1	123W	6W	16337	90	125.1	N
124	1	124W	6W	16593	90	126.1	N
125	1	125W	6W	16851	90	127.1	N
126	1	126W	6W	17111	90	128.1	N
127	1	127W	6W	17373	90	129.1	N
128	1	128W	6W	17637	90	130.1	N
129	1	129W	6W	17903	90	131.1	N
130	1	130W	6W	18171	90	132.1	N
131	1	131W	6W	18441	90	133.1	N
132	1	132W	6W	18713	90	134.1	N
133	1	133W	6W	18987	90	135.1	N
134	1	134W	6W	19263	90	136.1	N
135	1	135W	6W	19541	90	137.1	N
136	1	136W	6W	19821	90	138.1	N
137	1	137W	6W	20103	90	139.1	N
138	1	138W	6W	20387	90	140.1	N
139	1	139W	6W	20673	90	141.1	N
140	1	140W	6W	20961	90	142.1	N
141	1	141W	6W	21251	90	143.1	N
142	1	142W	6W	21543	90	144.1	N
143	1	143W	6W	21837	90	145.1	N
144	1	144W	6W	22133	90	146.1	N
145	1	145W	6W	22431	90	147.1	N
146	1	146W	6W	22731	90	148.1	N
147	1	147W	6W	23033	90	149.1	N
148	1	148W	6W	23337	90	150.1	N
149	1	149W	6W	23643	90	151.1	N
150	1	150W	6W	23951	90	152.1	N
151	1	151W	6W	24261	90	153.1	N
152	1	152W	6W	24573	90	154.1	N
153	1	153W	6W	24887	90	155.1	N
154	1	154W	6W	25203	90	156.1	N
155	1	155W	6W	25521	90	157.1	N
156	1	156W	6W	25841	90	158.1	N
157	1	157W	6W	26163	90	159.1	N
158	1	158W	6W	26487	90	160.1	N
159	1	159W	6W	26813	90	161.1	N
160	1	160W	6W	27141	90	162.1	N
161	1	161W	6W	27471	90	163.1	N
162	1	162W	6W	27803	90	164.1	N
163	1	163W	6W	28137	90	165.1	N
164	1	164W	6W	28473	90	166.1	N
165	1	165W	6W	28811	90	167.1	N
166	1	166W	6W	29151	90	168.1	N
167	1	167W	6W	29493	90	169.1	N
168	1	168W	6W	29837	90	170.1	N
169	1	169W	6W	30183	90	171.1	N
170	1	170W	6W	30531	90	172.1	N
171	1	171W	6W	30881	90	173.1	N
172	1	172W	6W	31233	90	174.1	N
173	1	173W	6W	31587	90	175.1	N
174	1	174W	6W	31943	90	176.1	N
175	1	175W	6W	32301	90	177.1	N
176	1	176W	6W	32661	90	178.1	N
177	1	177W	6W	33023	90	179.1	N
178	1	178W	6W	33387	90	180.1	N
179	1	179W	6W	33753	90	181.1	N
180	1	180W	6W	34121	90	182.1	N
181	1	181W	6W	34491	90	183.1	N
182	1	182W	6W	34863	90	184.1	N
183	1	183W	6W	35237	90	185.1	N
184	1	184W	6W	35613	90	186.1	N
185	1	185W	6W	35991	90	187.1	N
186	1	186W	6W	36371	90	188.1	N
187	1	187W	6W	36753	90	189.1	N
188	1	188W	6W	37137	90	190.1	N
189	1	189W	6W	37523</			



Drill Design drilling report:

Date: 12-Aug-01

Ring: 2

Loc	R#	OS	Collar	OS	Dip	Dump	Length	b/t
1	0	0W		0W	22.0	0.0	11.5	0.0
2	0	0W		0W	22.0	0.0	11.5	0.0
3	0	0W		0W	22.0	0.0	11.5	0.0
4	0	0W		0W	22.0	0.0	11.5	0.0
5	0	0W		0W	22.0	0.0	11.5	0.0
6	0	0W		0W	22.0	0.0	11.5	0.0
7	0	0W		0W	22.0	0.0	11.5	0.0
8	0	0W		0W	22.0	0.0	11.5	0.0
9	0	0W		0W	22.0	0.0	11.5	0.0
10	0	0W		0W	22.0	0.0	11.5	0.0
11	0	0W		0W	22.0	0.0	11.5	0.0
12	0	0W		0W	22.0	0.0	11.5	0.0
13	0	0W		0W	22.0	0.0	11.5	0.0
							148.5	

# Ring 2

400 Ta63 DS

← WEST Section looks North

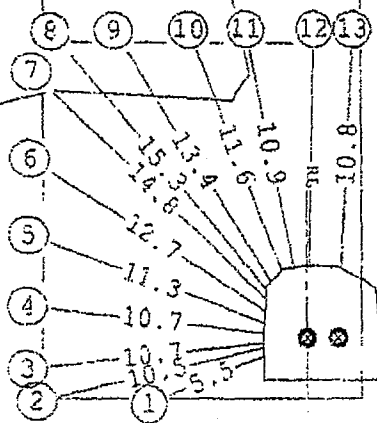
425 Ta63 DS

Ring Burden 2.5m

Toe Spacing 3.1m

Hole diameter: 89mm

475 Ta63 DS



Signed	<i>[Signature]</i>	BHP CANNINGTON
Designed	<i>[Signature]</i>	
Surveyed	<i>[Signature]</i>	
Geology	<i>[Signature]</i>	
Geotech	<i>[Signature]</i>	475CH10
Supt	<i>[Signature]</i>	Ring 2, 475 mLv
Approved	<i>[Signature]</i>	Looking Looking NORTH
Surveyor		Scale: 1:250 Date: 12-Aug-01

0101221.RP

Ring Design Drilling report:

Date: 12-Aug-01

Ring: 3

No	AL	OS	Collar	OS	Dip	Dump	Length	b/c
1	0	0	1.7W	247	90	0	5.6	V
2	0	0	1.7W	258	90	0	11.2	M
3	0	0	1.7W	267	90	0	12.0	M
4	0	0	1.7W	281	90	0	11.1	M
5	0	0	1.7W	294	90	0	11.1	M
6	0	0	1.7W	307	90	0	13.6	M
7	0	0	1.7W	321	90	0	14.2	M
8	0	0	1.7W	334	90	0	12.1	M
9	0	0	1.7W	347	90	0	11.0	M
10	0	0	1.7W	360	90	0	10.6	M
11	0	0	1.7W	373	90	0	10.5	M
12	0	0	1.7W	386	90	0	10.6	M
							138.9	

# Ring 3

400 Ta63 DS

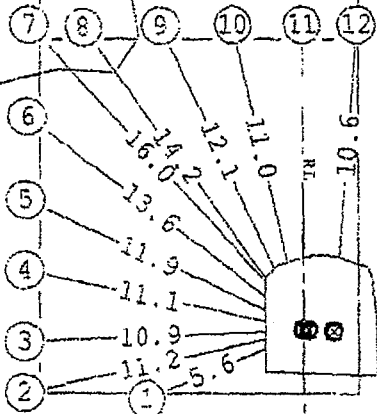
← WEST  
Section  
looks North

425 Ta63 DS

Ring Burden 2.5m

Toe Spacing 3.1m

Hole diameter: 69mm



475 Ta63 DS

	Signed	<i>[Signature]</i>	<b>BHP</b> CANNINGTON
Designed	<i>[Signature]</i>		
Reviewed	<i>[Signature]</i>		
GeoLog	<i>[Signature]</i>		4760HLO
Geotech	<i>[Signature]</i>		Ring 3, 475 mLv
Supr	<i>[Signature]</i>		Looking Looking NORTH
Approved	<i>[Signature]</i>		
Surveor			Scale: 1:250 Date: 12-Aug-01

-delcom.pl

Ring Design Drilling report:  
Date: 12-Aug-01  
Ring 4

No.	RL	CS	Collar OS	Dip	Dmg	Length	b/t
1	1.6W	33	90	11.7	N		
2	1.6W	35	90	11.2	N		
3	1.6W	35	90	11.2	N		
4	1.6W	35	90	11.1	N		
5	1.6W	35	90	11.4	N		
6	1.6W	35	90	12.1	N		
7	1.6W	35	90	12.4	N		
8	1.6W	35	90	12.8	N		
9	1.6W	35	90	14.9	N		
10	1.6W	35	90	12.8	N		
11	1.6W	35	90	11.5	N		
12	1.6W	35	90	11.0	N		
13	1.6W	35	90	10.5	N		
14	1.6W	35	90	10.5	N		
15	1.6W	35	90	10.5	N		
16	1.6W	35	90	10.5	N		
17	1.6W	35	90	10.5	N		
18	1.6W	35	90	10.5	N		
19	1.6W	35	90	10.5	N		
20	1.6W	35	90	10.5	N		
21	1.6W	35	90	10.5	N		
22	1.6W	35	90	10.5	N		
23	1.6W	35	90	10.5	N		
24	1.6W	35	90	10.5	N		
25	1.6W	35	90	10.5	N		
26	1.6W	35	90	10.5	N		
27	1.6W	35	90	10.5	N		
28	1.6W	35	90	10.5	N		
29	1.6W	35	90	10.5	N		
30	1.6W	35	90	10.5	N		
31	1.6W	35	90	10.5	N		
32	1.6W	35	90	10.5	N		
33	1.6W	35	90	10.5	N		
34	1.6W	35	90	10.5	N		
35	1.6W	35	90	10.5	N		
36	1.6W	35	90	10.5	N		
37	1.6W	35	90	10.5	N		
38	1.6W	35	90	10.5	N		
39	1.6W	35	90	10.5	N		
40	1.6W	35	90	10.5	N		
41	1.6W	35	90	10.5	N		
42	1.6W	35	90	10.5	N		
43	1.6W	35	90	10.5	N		
44	1.6W	35	90	10.5	N		
45	1.6W	35	90	10.5	N		
46	1.6W	35	90	10.5	N		
47	1.6W	35	90	10.5	N		
48	1.6W	35	90	10.5	N		
49	1.6W	35	90	10.5	N		
50	1.6W	35	90	10.5	N		
51	1.6W	35	90	10.5	N		
52	1.6W	35	90	10.5	N		
53	1.6W	35	90	10.5	N		
54	1.6W	35	90	10.5	N		
55	1.6W	35	90	10.5	N		
56	1.6W	35	90	10.5	N		
57	1.6W	35	90	10.5	N		
58	1.6W	35	90	10.5	N		
59	1.6W	35	90	10.5	N		
60	1.6W	35	90	10.5	N		
61	1.6W	35	90	10.5	N		
62	1.6W	35	90	10.5	N		
63	1.6W	35	90	10.5	N		
64	1.6W	35	90	10.5	N		
65	1.6W	35	90	10.5	N		
66	1.6W	35	90	10.5	N		
67	1.6W	35	90	10.5	N		
68	1.6W	35	90	10.5	N		
69	1.6W	35	90	10.5	N		
70	1.6W	35	90	10.5	N		
71	1.6W	35	90	10.5	N		
72	1.6W	35	90	10.5	N		
73	1.6W	35	90	10.5	N		
74	1.6W	35	90	10.5	N		
75	1.6W	35	90	10.5	N		
76	1.6W	35	90	10.5	N		
77	1.6W	35	90	10.5	N		
78	1.6W	35	90	10.5	N		
79	1.6W	35	90	10.5	N		
80	1.6W	35	90	10.5	N		
81	1.6W	35	90	10.5	N		
82	1.6W	35	90	10.5	N		
83	1.6W	35	90	10.5	N		
84	1.6W	35	90	10.5	N		
85	1.6W	35	90	10.5	N		
86	1.6W	35	90	10.5	N		
87	1.6W	35	90	10.5	N		
88	1.6W	35	90	10.5	N		
89	1.6W	35	90	10.5	N		
90	1.6W	35	90	10.5	N		
91	1.6W	35	90	10.5	N		
92	1.6W	35	90	10.5	N		
93	1.6W	35	90	10.5	N		
94	1.6W	35	90	10.5	N		
95	1.6W	35	90	10.5	N		
96	1.6W	35	90	10.5	N		
97	1.6W	35	90	10.5	N		
98	1.6W	35	90	10.5	N		
99	1.6W	35	90	10.5	N		
100	1.6W	35	90	10.5	N		

# Ring 4

400 Ta63 DS

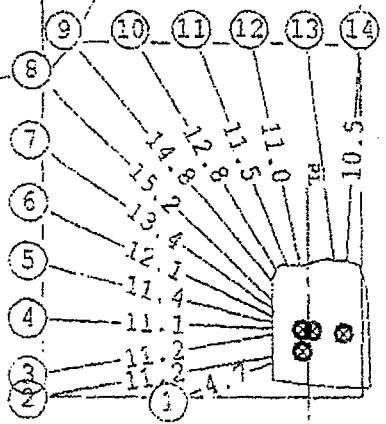
← WEST  
Section  
looks North

425 Ta63 DS

620 Drilling Only

Ring Burden 2.0m  
Toe Spacing 2.5m  
Hole diameter: 76mm

475 Ta63 DS

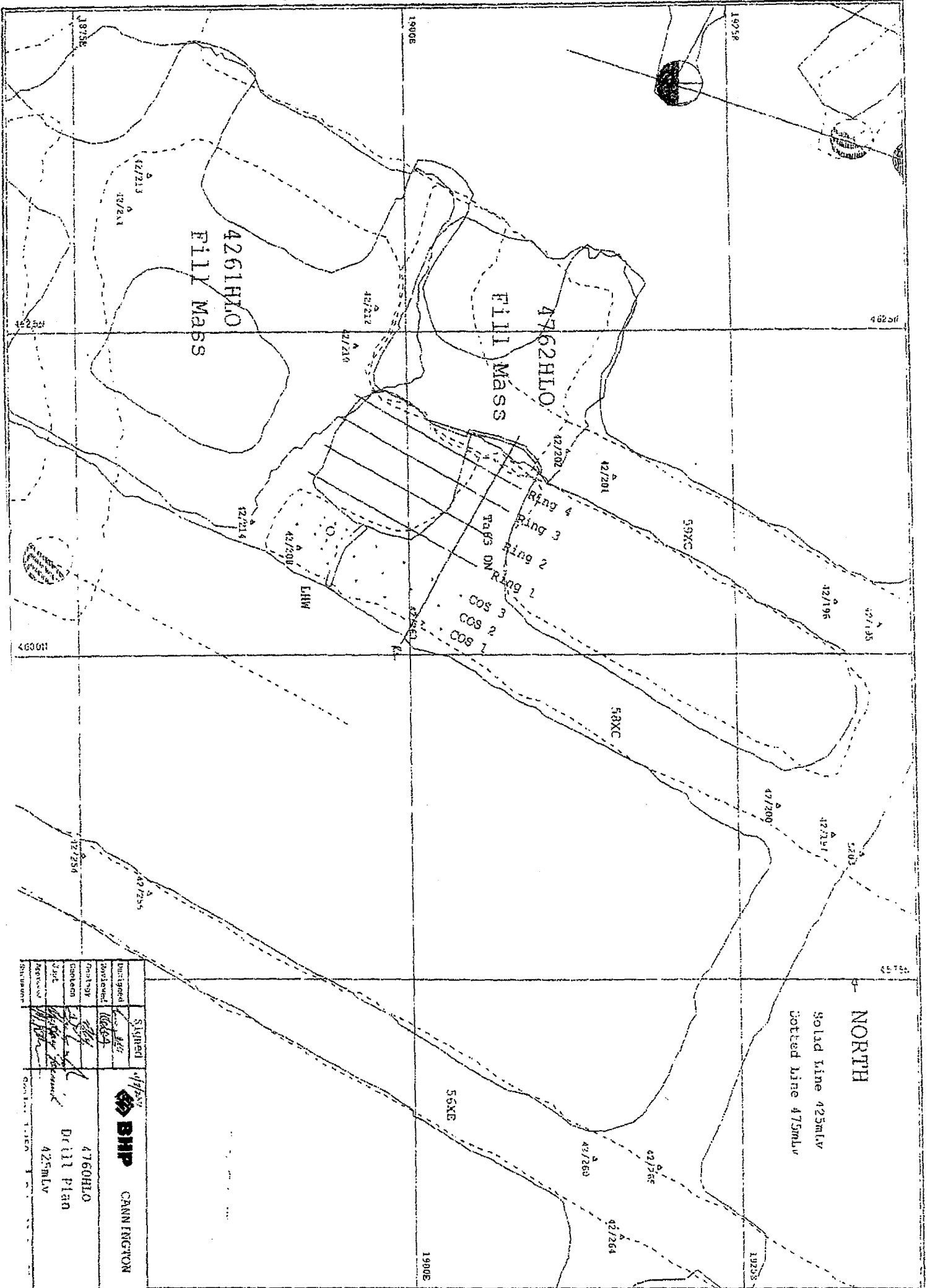


Designed	Signed	12/8/01	<b>BHP</b> CANNINGTON
Reviewed			
Geology			1760H10
Geotech			Ring 4, 475 mlv
Subst			Looking Looking NORTH
Approver			
Surveyor			Scale: 1:250 Date: 12-Aug-01

topofearth.pc

***Blasting Plans - 904072***

Blast 904072



NORTH

Solid line 425mLV  
Dotted line 475mLV

Designed	Signed	 <b>BHP</b> CANNINGTON 4760HLO Drill Plan 425mLV
Checked		
Drawn		
Reviewed		
Approved		

Ring design drilling report

Date: 11-Aug-01

Ring: COS 1

No	RL OS	Cellar OS	Dip	Dump	Length	b/t
1	11.9W	11.9W	180	90	21.9	N
2	3.4W	3.4W	180	90	21.8	N
3	2.9W	2.9W	180	90	21.7	N
4	2.4W	2.4W	180	90	21.7	N
5	2.1E	2.1E	180	90	21.7	N
					108.9	

COS 1

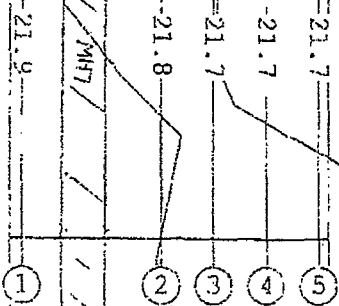
400 58XC

WEST  
Section  
looks North

+21114  
Fall Mass

425 58XC

Ring Burden 1.5m  
Toe Spacing 2.5m  
Hole diameter: 89mm



475 58XC

Signed	<i>[Signature]</i>	 BHP CANNINGTON
Designed	<i>[Signature]</i>	
Revised	<i>[Signature]</i>	
Geology	<i>[Signature]</i>	
Geotech	<i>[Signature]</i>	
Supt	<i>[Signature]</i>	4760HLC COS 1, 425 mlv Looking Looking NORTH
Approved	<i>[Signature]</i>	Scale: 1:250
Supervisor		Date: 11-Aug-01

K

Blast 904072

Final Design drilling report:

Date: 11-Aug-01

Ring COS 2

No.	RL	OS	Collar	OS	Dip	Damp	Length	b/t
1	11.4W	11.4R	1.20	90	22.0	N		
2	10.4W	10.4R	1.20	90	21.9	N		
3	10.9W	10.9R	1.20	90	21.7	N		
4	1.4W	1.4R	1.20	90	21.6	N		
5	1.1E	1.1E	1.20	90	21.7	N		
							109.9	

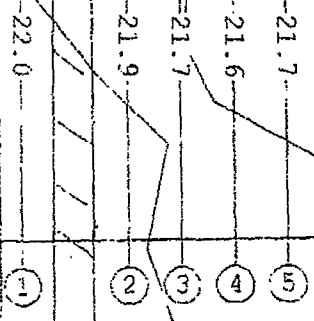
COS 2

400 58XC

WEST  
Section  
looks North

426142  
Date 07/05/01

425 58XC



Ring Burden 1.5m  
Toe Spacing 2.5m  
Hole diameter: 89mm

475 58XC

	Signed	 CANNINGTON
Designed	<i>[Signature]</i>	
Reviewed	<i>[Signature]</i>	
Geology	<i>[Signature]</i>	
Geotech	<i>[Signature]</i>	
Supr	<i>[Signature]</i>	
Approved	<i>[Signature]</i>	476CHIO COS 2, 425 mlv Looking Looking NORTH
Surveyor		Scale: 1:250 Date: 11-Aug-01

10/1/01/003

Blast Design Drilling Report:

Date: 11-Aug-01

Proj: COS 3

No.	R1	OS	Collar	OS	Dip	Dump	Length	b/t
1	11.84		11.84		130	90	22.0	N
2	11.84		11.84		130	90	21.9	N
3	11.84		11.84		130	90	21.9	N
4	11.84		11.84		130	90	21.9	N
5	11.84		11.84		130	90	21.9	N
109.7								

COS 3

400 58XC

← WEST  
Section  
looks North


426/46  
Fall MASS

425 58XC

Ring Burden 1.5m  
Toe Spacing 2.5m  
Hole diameter: 89mm

① ② ③ ④ ⑤

475 58XC

Signed		 <b>BHP</b> CANNINGTON
Designed	<i>[Signature]</i>	
Reviewed	<i>[Signature]</i>	4760HLO
Geology	<i>[Signature]</i>	COS 3, 425 mLv
Geotech	<i>[Signature]</i>	Looking Looking NORTH
Supt	<i>[Signature]</i>	
Approved	<i>[Signature]</i>	
Supervisor		Scale: 1:250 Date: 11-Aug-01

10-1-01-01



Design drilling report:

Date: 12-Aug-01

Ring: 1

No.	EL OS	Collar OS	Dip	Dump	Length	b/c
1	252.9	252.9	0	0	0	0
2	252.9	252.9	0	0	0	0
3	252.9	252.9	0	0	0	0
4	252.9	252.9	0	0	0	0
5	252.9	252.9	0	0	0	0
6	252.9	252.9	0	0	0	0
7	252.9	252.9	0	0	0	0
8	252.9	252.9	0	0	0	0
9	252.9	252.9	0	0	0	0
10	252.9	252.9	0	0	0	0
11	252.9	252.9	0	0	0	0
12	252.9	252.9	0	0	0	0
13	252.9	252.9	0	0	0	0

# Ring 1

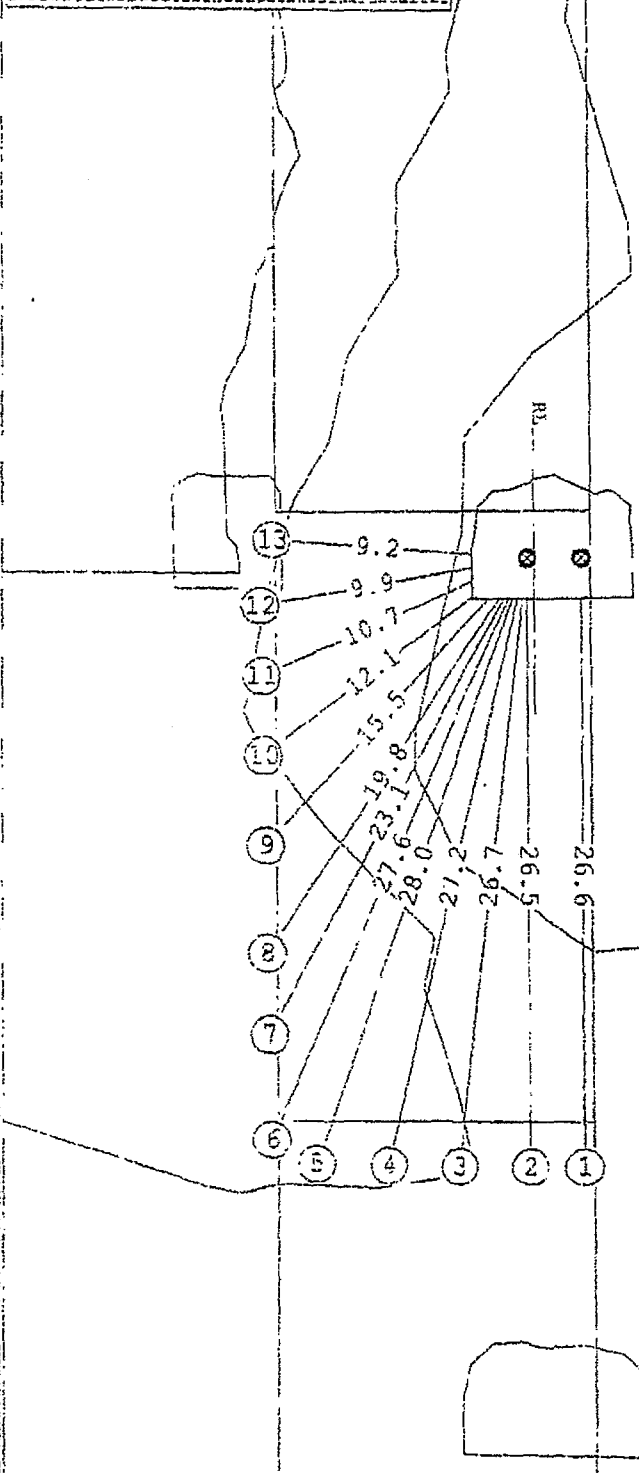
400 Ta63 DS

WEST  
Section  
looks North

425 Ta63 DS

Ring Burden 2.5m  
Toe Spacing 3.1m  
Hole diameter: 89mm

475 Ta63 DS



Designed	Signed		CANNINGTON
Reviewed			
Geotech		4760HLO	
Surveyor		Ring 1, 425 mLv	
		Looking Looking NORTH	
		Scale: 1:250	Date: 12-Aug-01

T0824.000.rpt

Design Drilling report:  
 Date: 12-Aug-01  
 Ring: 2

No.	RL OS	Collar OS	Dip	Dmp	Length	b/t
1	1.5E	1.6E	178	90	26.6	N
2	0.9E	1.1W	183	90	26.7	N
3	0.3W	1.8E	90	90	27.3	N
4	0.3W	1.9E	90	90	27.6	N
5	0.8W	2.0E	90	90	28.6	N
6	1.0W	2.0E	90	90	28.8	N
7	1.2W	2.1E	90	90	29.7	N
8	1.5W	2.1E	90	90	30.5	N
9	2.0W	2.2E	90	90	31.3	N
10	2.0W	2.3E	90	90	32.3	N
11	2.0W	2.5E	90	90	33.3	N
12	2.0W	2.5E	90	90	34.3	N
13	2.0W	2.7E	90	90	35.3	N
					261.6	

# Ring 2

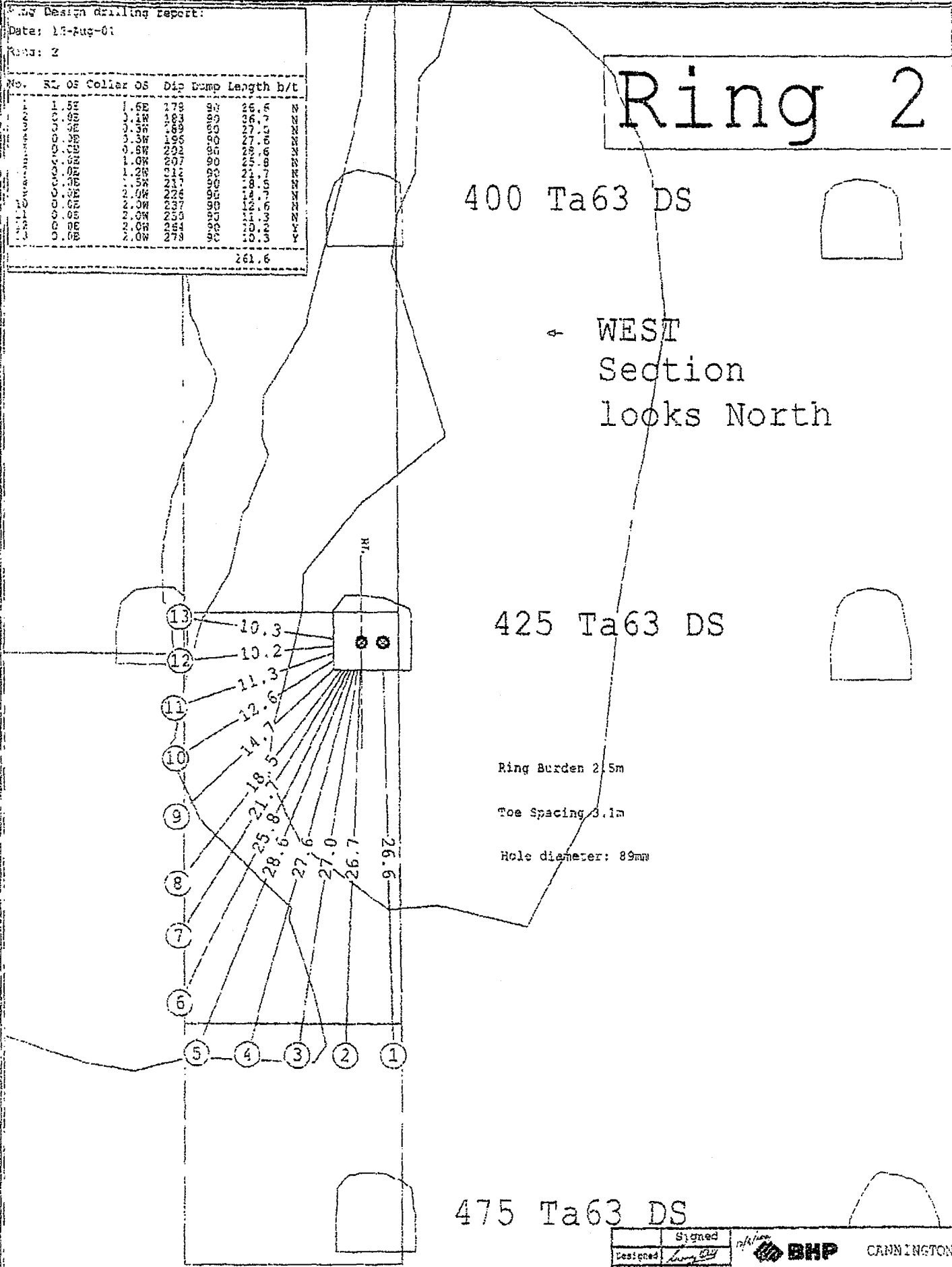
400 Ta63 DS

← WEST  
Section  
looks North

425 Ta63 DS

Ring Burden 2.5m  
 Toe Spacing 3.1m  
 Hole diameter: 89mm

475 Ta63 DS



Signed		BHP CANNINGTON
Designed	<i>[Signature]</i>	
Revised	<i>[Signature]</i>	
Geology	<i>[Signature]</i>	4760H20
Geotech	<i>[Signature]</i>	Ring 2, 425 RLW
Subst	<i>[Signature]</i>	Looking Looking NORTH
Approver	<i>[Signature]</i>	
Surveyor		Scale: 1:250 Date: 12-Aug-01

t 40 Lead 24

Ring Design Drawing Report:

Date: 12-Aug-01

Ring: 3

No.	RL	DS	Collar	DS	Diag	Dump	Length	b/t
1	27000	000	000	000	000	000	000	000
2	27000	000	000	000	000	000	000	000
3	27000	000	000	000	000	000	000	000
4	27000	000	000	000	000	000	000	000
5	27000	000	000	000	000	000	000	000
6	27000	000	000	000	000	000	000	000
7	27000	000	000	000	000	000	000	000
8	27000	000	000	000	000	000	000	000
9	27000	000	000	000	000	000	000	000
10	27000	000	000	000	000	000	000	000
11	27000	000	000	000	000	000	000	000
12	27000	000	000	000	000	000	000	000
13	27000	000	000	000	000	000	000	000
							268.4	

# Ring 3

400 Ta63 DS

← WEST  
Section  
looks North

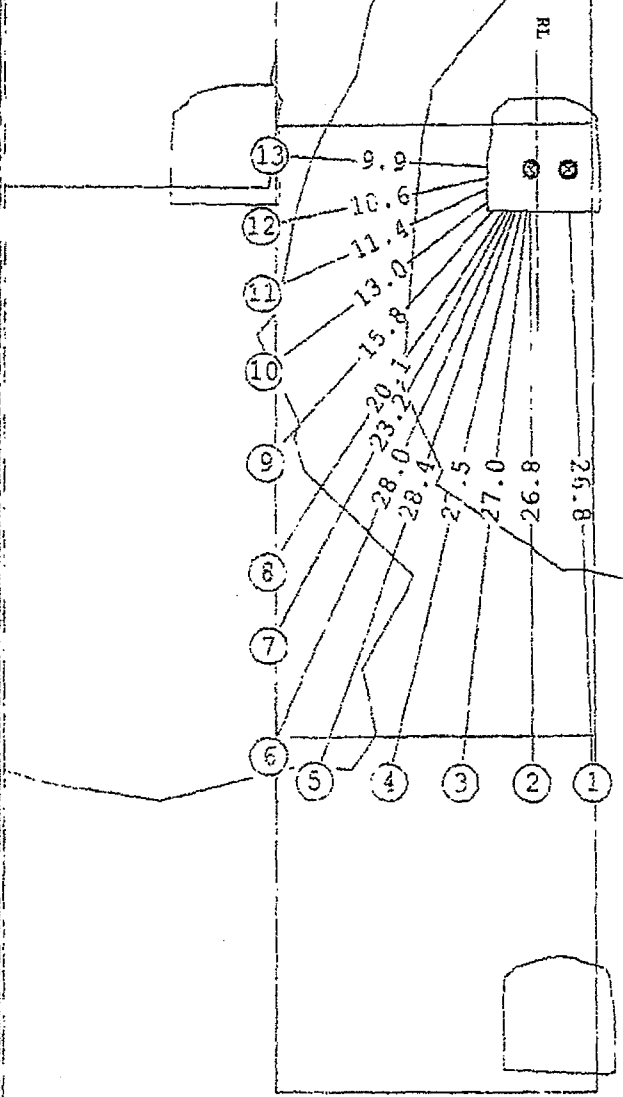
425 Ta63 DS

Ring Burden 2.5m

Toe Spacing 3.1m

Hole diameter: 88mm

475 Ta63 DS



	Signed	12/1/01	<b>BHP</b> CANNINGTON
Designed	<i>[Signature]</i>		
Reviewed	<i>[Signature]</i>		
Geology	<i>[Signature]</i>		
Geotech	<i>[Signature]</i>		
Supt	<i>[Signature]</i>		
Approved	<i>[Signature]</i>		
Surveyor			
			4760HLO
			Ring 3, 425 mlv
			Looking Looking NORTH
		Scale: 1:250	Date: 12-Aug-01

S:\022222\13

Ring design drilling report.

Date: 12-Aug-01

Ring: 4

NO	FL	OS	Collar OS	Big Dump	Length	b/t
1	22	7W	4E	268	60	26.9
2	22	7W	4E	268	60	26.8
3	22	7W	4E	268	60	26.9
4	22	7W	4E	268	60	26.8
5	22	7W	4E	268	60	26.9
6	22	7W	4E	268	60	26.8
7	22	7W	4E	268	60	26.9
8	22	7W	4E	268	60	26.8
9	22	7W	4E	268	60	26.9
10	22	7W	4E	268	60	26.8
11	22	7W	4E	268	60	26.9
12	22	7W	4E	268	60	26.8
13	22	7W	4E	268	60	26.9
14	22	7W	4E	268	60	26.8
15	22	7W	4E	268	60	26.9
16	22	7W	4E	268	60	26.8

# Ring 4

400 Ta63 DS

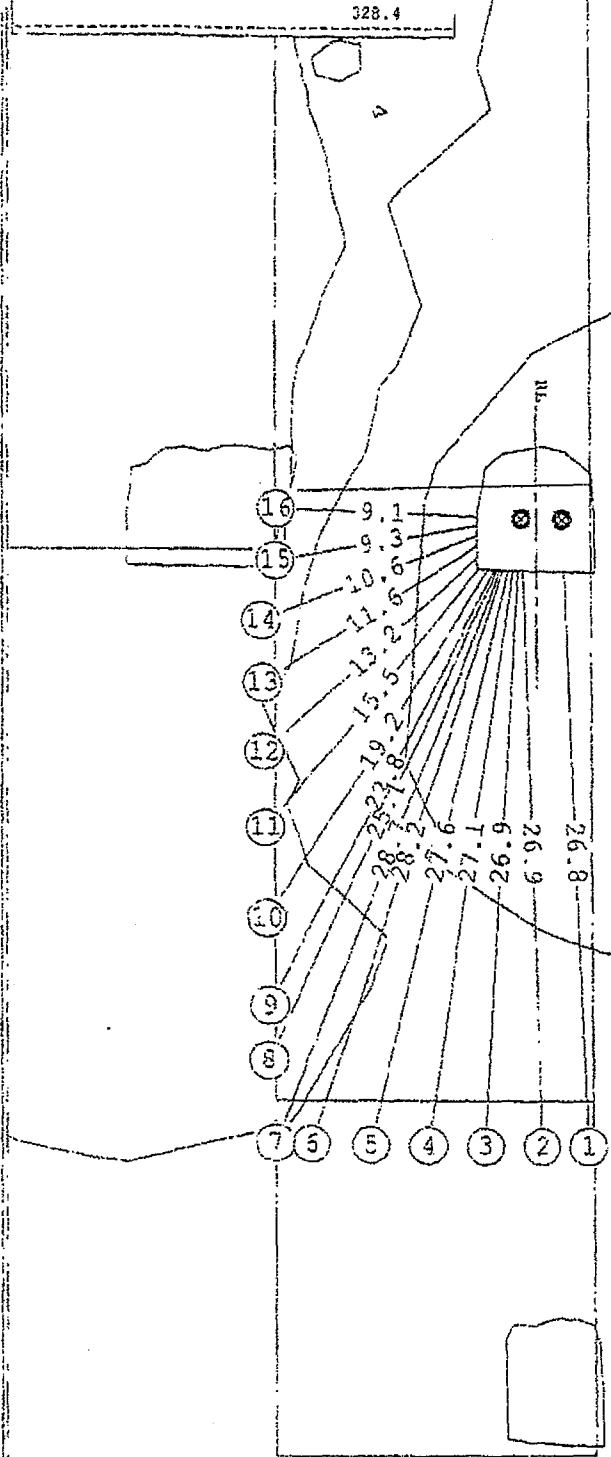
← WEST  
Section  
looks North

425 Ta63 DS

620 Drilling Only

Ring Burden 7.0m  
Toe Spacing 2.5m  
Hole diameter: 76mm

475 Ta63 DS



Designed	Signed	<b>BHP</b> CANNINGTON
Reviewed		
Geology		4750HL0
Geotech		Ring 4, 425 MLV
Sept		Looking Looking NORTH
Approved		
Surveyor		Scale: 1:250 Date: 12-Aug-01

bdr-fuj.nf

*Blasting Records*

	<b>Blast</b>	<b>Stope</b>	<b>Level</b>	<b>Ring</b>	<b>Kilos</b>	<b>Date</b>	<b>Metres</b>	<b>Ring no.</b>	<b>Length</b>	<b>Delay Time (ms)</b>
425mLv COS 1	904064	4760HL	425	Winze	893	18/09/2001	143.5	1	21.9	
425mLv COS 2	904064	4760HL	425	Winze	893	18/09/2001	143.5	1	22	
425mLv COS 3	904064	4760HL	425	Winze	893	18/09/2001	143.5	1	22	
475mLv COS 1	904068	4760HL	475	COS, 1, 2, 3, 4	3204	22/09/2001	576	3	16	200
475mLv COS 1	904068	4760HL	475	COS, 1, 2, 3, 4	3204	22/09/2001	576	4	16.2	600
475mLv COS 1	904068	4760HL	475	COS, 1, 2, 3, 4	3204	22/09/2001	576	5	16.3	1400
475mLv COS 2	904068	4760HL	475	COS, 1, 2, 3, 4	3204	22/09/2001	576	4	15.6	400
475mLv COS 2	904068	4760HL	475	COS, 1, 2, 3, 4	3204	22/09/2001	576	5	15.6	1000
475mLv COS 3	904068	4760HL	475	COS, 1, 2, 3, 4	3204	22/09/2001	576	3	15.6	200
475mLv COS 3	904068	4760HL	475	COS, 1, 2, 3, 4	3204	22/09/2001	576	4	15.7	600
475mLv COS 3	904068	4760HL	475	COS, 1, 2, 3, 4	3204	22/09/2001	576	5	15.8	1400
475mLv Ring 1	904068	4760HL	475	COS, 1, 2, 3, 4	3204	22/09/2001	576	1	3.6	3000
475mLv Ring 1	904068	4760HL	475	COS, 1, 2, 3, 4	3204	22/09/2001	576	2	9.4	2650
475mLv Ring 1	904068	4760HL	475	COS, 1, 2, 3, 4	3204	22/09/2001	576	3	9.1	2400
475mLv Ring 1	904068	4760HL	475	COS, 1, 2, 3, 4	3204	22/09/2001	576	4	9.3	2275
475mLv Ring 1	904068	4760HL	475	COS, 1, 2, 3, 4	3204	22/09/2001	576	5	10.3	1950

475mLv Ring 1	904068	4760HL	475	COS, 1, 2, 3, 4	3204	22/09/2001	576	6	12.1	1800
475mLv Ring 1	904068	4760HL	475	COS, 1, 2, 3, 4	3204	22/09/2001	576	7	14.1	1675
475mLv Ring 1	904068	4760HL	475	COS, 1, 2, 3, 4	3204	22/09/2001	576	8	13.4	1400
475mLv Ring 1	904068	4760HL	475	COS, 1, 2, 3, 4	3204	22/09/2001	576	9	11.8	1675
475mLv Ring 1	904068	4760HL	475	COS, 1, 2, 3, 4	3204	22/09/2001	576	10	10.9	1800
475mLv Ring 1	904068	4760HL	475	COS, 1, 2, 3, 4	3204	22/09/2001	576	11	10.8	1950
475mLv Ring 1	904068	4760HL	475	COS, 1, 2, 3, 4	3204	22/09/2001	576	12	10.8	2275
475mLv Ring 2	904068	4760HL	475	COS, 1, 2, 3, 4	3204	22/09/2001	576	1	5.5	4350
475mLv Ring 2	904068	4760HL	475	COS, 1, 2, 3, 4	3204	22/09/2001	576	2	10.5	3900
475mLv Ring 2	904068	4760HL	475	COS, 1, 2, 3, 4	3204	22/09/2001	576	3	10.7	3800
475mLv Ring 2	904068	4760HL	475	COS, 1, 2, 3, 4	3204	22/09/2001	576	4	10.7	3450
475mLv Ring 2	904068	4760HL	475	COS, 1, 2, 3, 4	3204	22/09/2001	576	5	11.3	3050
475mLv Ring 2	904068	4760HL	475	COS, 1, 2, 3, 4	3204	22/09/2001	576	6	12.7	3000
475mLv Ring 2	904068	4760HL	475	COS, 1, 2, 3, 4	3204	22/09/2001	576	7	14.8	2650
475mLv Ring 2	904068	4760HL	475	COS, 1, 2, 3, 4	3204	22/09/2001	576	8	15.3	2400
475mLv Ring 2	904068	4760HL	475	COS, 1, 2, 3, 4	3204	22/09/2001	576	9	13.4	2650
475mLv Ring 2	904068	4760HL	475	COS, 1, 2, 3, 4	3204	22/09/2001	576	10	11.6	3000

475mLv Ring 2	904068	4760HL	475	COS, 1, 2, 3, 4	3204	22/09/2001	576	11	10.9	3050
475mLv Ring 2	904068	4760HL	475	COS, 1, 2, 3, 4	3204	22/09/2001	576	12	10.6	3450
475mLv Ring 2	904068	4760HL	475	COS, 1, 2, 3, 4	3204	22/09/2001	576	13	10.8	3800
475mLv Ring 3	904068	4760HL	475	COS, 1, 2, 3, 4	3204	22/09/2001	576	1	5.6	5600
475mLv Ring 3	904068	4760HL	475	COS, 1, 2, 3, 4	3204	22/09/2001	576	2	11.2	5500
475mLv Ring 3	904068	4760HL	475	COS, 1, 2, 3, 4	3204	22/09/2001	576	3	10.9	4700
475mLv Ring 3	904068	4760HL	475	COS, 1, 2, 3, 4	3204	22/09/2001	576	4	11.1	4600
475mLv Ring 3	904068	4760HL	475	COS, 1, 2, 3, 4	3204	22/09/2001	576	5	11.9	4350
475mLv Ring 3	904068	4760HL	475	COS, 1, 2, 3, 4	3204	22/09/2001	576	6	13.6	3900
475mLv Ring 3	904068	4760HL	475	COS, 1, 2, 3, 4	3204	22/09/2001	576	7	16	3800
475mLv Ring 3	904068	4760HL	475	COS, 1, 2, 3, 4	3204	22/09/2001	576	8	14.2	3450
475mLv Ring 3	904068	4760HL	475	COS, 1, 2, 3, 4	3204	22/09/2001	576	9	12.1	3800
475mLv Ring 3	904068	4760HL	475	COS, 1, 2, 3, 4	3204	22/09/2001	576	10	11	3900
475mLv Ring 3	904068	4760HL	475	COS, 1, 2, 3, 4	3204	22/09/2001	576	11	10.5	4350
475mLv Ring 3	904068	4760HL	475	COS, 1, 2, 3, 4	3204	22/09/2001	576	12	10.6	4600
475mLv Ring 4	904068	4760HL	475	COS, 1, 2, 3, 4	3204	22/09/2001	576	1	4.7	9700
475mLv Ring 4	904068	4760HL	475	COS, 1, 2, 3, 4	3204	22/09/2001	576	2	11.2	9600



475mLv Ring 4	904068	4760HL	475	COS, 1, 2, 3, 4	3204	22/09/2001	576	3	11.2	8600
475mLv Ring 4	904068	4760HL	475	COS, 1, 2, 3, 4	3204	22/09/2001	576	4	11.1	8500
475mLv Ring 4	904068	4760HL	475	COS, 1, 2, 3, 4	3204	22/09/2001	576	5	11.4	7400
475mLv Ring 4	904068	4760HL	475	COS, 1, 2, 3, 4	3204	22/09/2001	576	6	12.1	6400
475mLv Ring 4	904068	4760HL	475	COS, 1, 2, 3, 4	3204	22/09/2001	576	7	13.4	5500
475mLv Ring 4	904068	4760HL	475	COS, 1, 2, 3, 4	3204	22/09/2001	576	8	15.2	4600
475mLv Ring 4	904068	4760HL	475	COS, 1, 2, 3, 4	3204	22/09/2001	576	9	14.8	4350
475mLv Ring 4	904068	4760HL	475	COS, 1, 2, 3, 4	3204	22/09/2001	576	10	12.8	4600
475mLv Ring 4	904068	4760HL	475	COS, 1, 2, 3, 4	3204	22/09/2001	576	11	11.5	5500
475mLv Ring 4	904068	4760HL	475	COS, 1, 2, 3, 4	3204	22/09/2001	576	12	11	6400
475mLv Ring 4	904068	4760HL	475	COS, 1, 2, 3, 4	3204	22/09/2001	576	13	10.6	7400
475mLv Ring 4	904068	4760HL	475	COS, 1, 2, 3, 4	3204	22/09/2001	576	14	10.5	8500
425mLv COS 1	904072	4760HL	425	COS, 1, 2, 3, 4	3902	25/09/2001	727	3	21.7	200
425mLv COS 1	904072	4760HL	425	COS, 1, 2, 3, 4	3902	25/09/2001	727	4	21.7	400
425mLv COS 1	904072	4760HL	425	COS, 1, 2, 3, 4	3902	25/09/2001	727	5	21.7	600
425mLv COS 2	904072	4760HL	425	COS, 1, 2, 3, 4	3902	25/09/2001	727	4	21.6	400
425mLv COS 2	904072	4760HL	425	COS, 1, 2, 3, 4	3902	25/09/2001	727	5	21.7	1000

425mLv COS 3	904072	4760HL	425	COS, 1, 2, 3, 4	3902	25/09/2001	727	3	21.6	200
425mLv COS 3	904072	4760HL	425	COS, 1, 2, 3, 4	3902	25/09/2001	727	4	21.6	600
425mLv COS 3	904072	4760HL	425	COS, 1, 2, 3, 4	3902	25/09/2001	727	5	21.6	1400
425mLv ring 1	904072	4760HL	425	COS, 1, 2, 3, 4	3902	25/09/2001	727	1	26.6	1800
425mLv ring 1	904072	4760HL	425	COS, 1, 2, 3, 4	3902	25/09/2001	727	2	26.5	1675
425mLv ring 1	904072	4760HL	425	COS, 1, 2, 3, 4	3902	25/09/2001	727	3	26.7	1400
425mLv ring 1	904072	4760HL	425	COS, 1, 2, 3, 4	3902	25/09/2001	727	4	27.2	1400
425mLv ring 1	904072	4760HL	425	COS, 1, 2, 3, 4	3902	25/09/2001	727	5	28	1400
425mLv ring 1	904072	4760HL	425	COS, 1, 2, 3, 4	3902	25/09/2001	727	6	27.6	1675
425mLv ring 1	904072	4760HL	425	COS, 1, 2, 3, 4	3902	25/09/2001	727	7	23.1	1800
425mLv ring 1	904072	4760HL	425	COS, 1, 2, 3, 4	3902	25/09/2001	727	8	19.8	1950
425mLv ring 1	904072	4760HL	425	COS, 1, 2, 3, 4	3902	25/09/2001	727	9	15.5	2275
425mLv ring 1	904072	4760HL	425	COS, 1, 2, 3, 4	3902	25/09/2001	727	10	12.1	2400
425mLv ring 1	904072	4760HL	425	COS, 1, 2, 3, 4	3902	25/09/2001	727	11	10.7	2650
425mLv ring 1	904072	4760HL	425	COS, 1, 2, 3, 4	3902	25/09/2001	727	12	9.9	3000
425mLv ring 1	904072	4760HL	425	COS, 1, 2, 3, 4	3902	25/09/2001	727	13	9.2	3050
425mLv ring 2	904072	4760HL	425	COS, 1, 2, 3, 4	3902	25/09/2001	727	1	26.6	2650

425mLv ring 2	904072	4760HL	425	COS, 1, 2, 3, 4	3902	25/09/2001	727	2	26.7	2400
425mLv ring 2	904072	4760HL	425	COS, 1, 2, 3, 4	3902	25/09/2001	727	3	27	2275
425mLv ring 2	904072	4760HL	425	COS, 1, 2, 3, 4	3902	25/09/2001	727	4	27.6	1950
425mLv ring 2	904072	4760HL	425	COS, 1, 2, 3, 4	3902	25/09/2001	727	5	28.6	2275
425mLv ring 2	904072	4760HL	425	COS, 1, 2, 3, 4	3902	25/09/2001	727	6	25.8	2400
425mLv ring 2	904072	4760HL	425	COS, 1, 2, 3, 4	3902	25/09/2001	727	7	21.7	2650
425mLv ring 2	904072	4760HL	425	COS, 1, 2, 3, 4	3902	25/09/2001	727	8	18.5	3000
425mLv ring 2	904072	4760HL	425	COS, 1, 2, 3, 4	3902	25/09/2001	727	9	14.7	3050
425mLv ring 2	904072	4760HL	425	COS, 1, 2, 3, 4	3902	25/09/2001	727	10	12.6	3450
425mLv ring 2	904072	4760HL	425	COS, 1, 2, 3, 4	3902	25/09/2001	727	11	11.3	3800
425mLv ring 2	904072	4760HL	425	COS, 1, 2, 3, 4	3902	25/09/2001	727	12	10.2	3900
425mLv ring 2	904072	4760HL	425	COS, 1, 2, 3, 4	3902	25/09/2001	727	13	10.3	4350
425mLv ring 3	904072	4760HL	425	COS, 1, 2, 3, 4	3902	25/09/2001	727	1	26.8	3800
425mLv ring 3	904072	4760HL	425	COS, 1, 2, 3, 4	3902	25/09/2001	727	2	26.8	3450
425mLv ring 3	904072	4760HL	425	COS, 1, 2, 3, 4	3902	25/09/2001	727	3	27	3050
425mLv ring 3	904072	4760HL	425	COS, 1, 2, 3, 4	3902	25/09/2001	727	4	27.5	3000
425mLv ring 3	904072	4760HL	425	COS, 1, 2, 3, 4	3902	25/09/2001	727	5	28.4	3050

425mLv ring 3	904072	4760HL	425	COS, 1, 2, 3, 4	3902	25/09/2001	727	6	28	3450
425mLv ring 3	904072	4760HL	425	COS, 1, 2, 3, 4	3902	25/09/2001	727	7	23.2	3800
425mLv ring 3	904072	4760HL	425	COS, 1, 2, 3, 4	3902	25/09/2001	727	8	20.1	3900
425mLv ring 3	904072	4760HL	425	COS, 1, 2, 3, 4	3902	25/09/2001	727	9	15.8	4350
425mLv ring 3	904072	4760HL	425	COS, 1, 2, 3, 4	3902	25/09/2001	727	10	13	4600
425mLv ring 3	904072	4760HL	425	COS, 1, 2, 3, 4	3902	25/09/2001	727	11	11.4	4700
425mLv ring 3	904072	4760HL	425	COS, 1, 2, 3, 4	3902	25/09/2001	727	12	10.6	5500
425mLv ring 3	904072	4760HL	425	COS, 1, 2, 3, 4	3902	25/09/2001	727	13	9.9	5600
425mLv ring 4	904072	4760HL	425	COS, 1, 2, 3, 4	3902	25/09/2001	727	1	26.8	6400
425mLv ring 4	904072	4760HL	425	COS, 1, 2, 3, 4	3902	25/09/2001	727	2	26.9	5500
425mLv ring 4	904072	4760HL	425	COS, 1, 2, 3, 4	3902	25/09/2001	727	3	26.9	4600
425mLv ring 4	904072	4760HL	425	COS, 1, 2, 3, 4	3902	25/09/2001	727	4	27.1	4350
425mLv ring 4	904072	4760HL	425	COS, 1, 2, 3, 4	3902	25/09/2001	727	5	27.6	3900
425mLv ring 4	904072	4760HL	425	COS, 1, 2, 3, 4	3902	25/09/2001	727	6	28.2	4350
425mLv ring 4	904072	4760HL	425	COS, 1, 2, 3, 4	3902	25/09/2001	727	7	28.7	4450
425mLv ring 4	904072	4760HL	425	COS, 1, 2, 3, 4	3902	25/09/2001	727	8	25.1	4600
425mLv ring 4	904072	4760HL	425	COS, 1, 2, 3, 4	3902	25/09/2001	727	9	22.8	4700

425mLv ring 4	904072	4760HL	425	COS, 1, 2, 3, 4	3902	25/09/2001	727	10	19.2	5500
425mLv ring 4	904072	4760HL	425	COS, 1, 2, 3, 4	3902	25/09/2001	727	11	15.5	5600
425mLv ring 4	904072	4760HL	425	COS, 1, 2, 3, 4	3902	25/09/2001	727	12	13.2	6400
425mLv ring 4	904072	4760HL	425	COS, 1, 2, 3, 4	3902	25/09/2001	727	13	11.6	6500
425mLv ring 4	904072	4760HL	425	COS, 1, 2, 3, 4	3902	25/09/2001	727	14	10.6	7400
425mLv ring 4	904072	4760HL	425	COS, 1, 2, 3, 4	3902	25/09/2001	727	15	9.3	8400
425mLv ring 4	904072	4760HL	425	COS, 1, 2, 3, 4	3902	25/09/2001	727	16	9.1	9600

**Appendix C - Stope 4763**

***Blasting Records***

**ORICA**

**CANNINGTON**

PARTNERS FOR PERFORMANCE

DATE	6/05/2002	OPERATOR	NK	LEVEL	375
DELIVERY NO.	904186			STOPE	47 63
				RING	6

HOLE	Diam	Design	Actual	Collar	Charge	80%	Delay	COMMENTS
RING 6								
1	89	5.8	5.8	1	4.8	4.00	720	
2	89	13.9	13.9	4	9.9	8.26	680	
3	89	13.6	13.6	1	12.6	10.51	640	
4	89	13.4	13.4	5	8.4	7.01	620	
5	89	13.7	13.7	1	12.7	10.59	600	
6	89	14.5	14.5	6	8.5	7.09	580	
7	89	15.8	15.8	2	13.8	11.51	560	
8	89	17.6	17.6	8	9.6	8.01	540	
9	89	20.2	20.2	1	19.2	16.01	520	DP
10	89	24.6	24.6	13	11.6	9.67	500	
11	89	27.8	27.8	4	23.8	19.85	495	DP
12	89	26.7	26.7	14	12.7	10.59	515	
13	89	26.1	26.1	1	25.1	20.93	535	DP
14	89	22.7	22.7	11	11.7	9.76	555	
15	89	22.1	22.1	6	16.1	13.43	575	DP
16	89	21.9	21.9	2	19.9	16.60	590	DP
17	89	23.9	23.9	1	22.9	19.10	610	DP
18	89	24	24	9	15	12.51	630	DP
19	89	10.2	10.2	3	7.2	6.00	650	
20	89	3.5	3.5	1	2.5	2.09	670	
Total					268	223.51		

**METRES CHARGED** 268

EMULSION BATCH NO.		KGs	1666.96
GASSER BATCH NO.			

CALIBRATIONS	
EP PUMP	OK
GASSER PUMP	
5 kg SCALES	OK
25 kg SCALES	OK

TIME	TIME
CUP WEIGHT	CUP WEIGHT
TEMPERATURE	TEMPERATURE

Density delivered



**ORICA**

**CANNINGTON**

PARTNERS FOR PERFORMANCE

DATE	8/05/2002	OPERATOR	NK	LEVEL	425
DELIVERY NO.	904187			STOPE	47 63
				RING	5

HOLE	Diam	Design	Actual	Collar	Charge	80%	Delay	COMMENTS
RING 5								
1	89	27.9	27.9	1	26.9	22.43	550	DP
2	89	28.3	28.3	13	15.3	12.76	510	DP
3	89	26.6	26.6	2	24.6	20.52	490	DP
4	89	27.1	27.1	1	26.1	21.77	470	DP
5	89	27.9	27.9	10	17.9	14.93	450	DP
6	89	28.9	28.9	16	12.9	10.76	430	
7	89	32	32	3	29	24.19	410	DP
8	89	32.7	32.7	18	14.7	12.26	390	
9	89	28.3	28.3	9	19.3	16.10	370	DP
10	89	23.8	23.8	1	22.8	19.02	350	DP
11	89	20.5	20.5	8	12.5	10.43	330	
12	89	18.3	18.3	2	16.3	13.59	310	
13	89	16.6	16.6	6	10.6	8.84	290	
14	89	15.5	15.5	1	14.5	12.09	270	
15	89	14.9	14.9	6	8.9	7.42	250	
16	89	15	15	2	13	10.84	230	
17	89	15.5	15.5	6	9.5	7.92	210	
18	89	16.5	16.5	1	15.5	12.93	190	DP
19	89	18.4	18.4	8	10.4	8.67	170	
20	89	20	20	3	17	14.18	150	DP
21	89	18.5	18.5	8	10.5	8.76	160	
22	89	16.4	16.4	1	15.4	12.84	180	DP
23	89	15	15	5	10	8.34	200	
24	89	14.2	14.2	1	13.2	11.01	220	
25	89	12.5	12.5	3	9.5	7.92	240	
26	89	13.4	13.4	1	12.4	10.34	280	
Total					408.7	340.86		

**METRES CHARGED**

408.7

EMULSION BATCH NO.	73
GASSER BATCH NO.	A27

KGs 2542.114

CALIBRATIONS	
EP PUMP	OK
GASSER PUMP	310
5 kg SCALES	OK
25 kg SCALES	OK

TIME	11.00am	TIME	12.00pm
CUP WEIGHT	1999	CUP WEIGHT	1597
TEMPERATURE	35	TEMPERATURE	35

Density delivered 1.0

**ORICA**

**CANNINGTON**

PARTNERS FOR PERFORMANCE

DATE	8/05/2002	OPERATOR	Gary	LEVEL	450
DELIVERY NO.	904188			STOPE	47 63
				RING	5

HOLE	Diam	Design	Actual	Collar	Charge	80%	Delay	COMMENTS
RING 5								
2	89	14.7	8	3	5	4.17	130	
3	89	15.1	6	2	4	3.34	110	
4	89	16.1	6	3	3	2.50	90	
5	89	17.5	5	1	4	3.34	70	
6	89	19.6	5	3	2	1.67	50	
7	89	22.6	5	1	4	3.34	30	
8	89	21.9	5					
9	89	20.9	8	1	7	5.84	0	
10	89	22.7	11	2	9	7.51	20	
11	89	23.5	16	4	12	10.01	40	
12	89	22.8	22.8	11	11.8	9.84	60	
13	89	22.1	22.1	1	21.1	17.60	80	DP
14	89	22.1	22.1	9	13.1	10.93	100	
15	89	22.2	22.2	1	21.2	17.68	150	DP
Total					117.2	97.74		

<b>METRES CHARGED</b>	117.2
-----------------------	-------

EMULSION	
BATCH NO.	73
GASSER	
BATCH NO.	A27

KGs	728.984
-----	---------

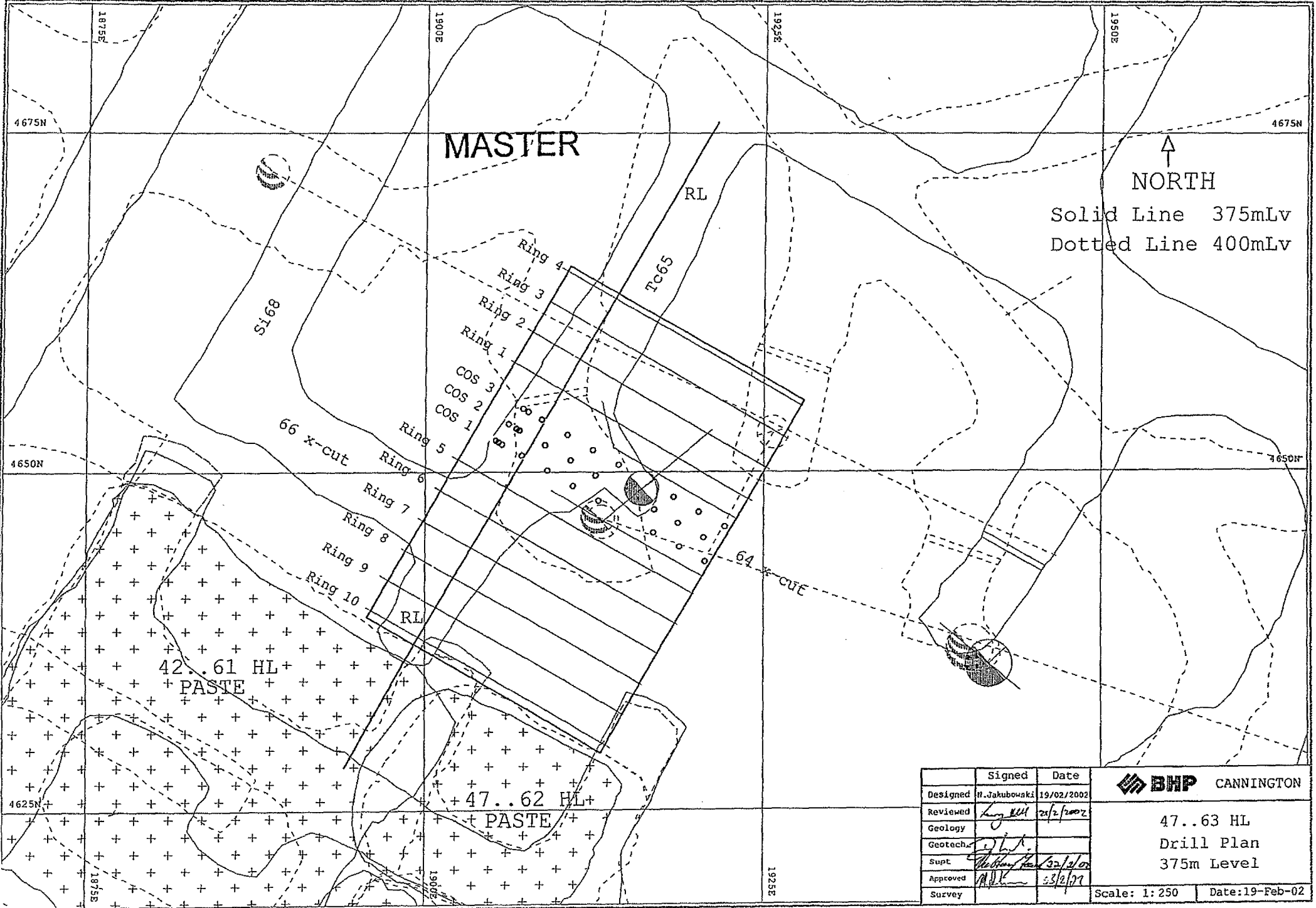
<b>CALIBRATIONS</b>	
EP PUMP	OK
GASSER PUMP	310
5 kg SCALES	OK
25 kg SCALES	OK

TIME	8.00pm	TIME	9.00pm
CUP WEIGHT	1988	CUP WEIGHT	1568
TEMPERATURE	35	TEMPERATURE	35

Density delivered	1.0
-------------------	-----

Sheet I.d 24/7/98 V1

## ***Blasting Plans***



	Signed	Date
Designed	N. Jakubowski	19/02/2002
Reviewed	<i>[Signature]</i>	20/2/2002
Geology		
Geotech	<i>[Signature]</i>	
Supt	<i>[Signature]</i>	22/2/02
Approved	<i>[Signature]</i>	23/2/02
Survey		

**BHP CANNINGTON**

47..63 HL  
Drill Plan  
375m Level

Scale: 1:250 Date: 19-Feb-02

Ring Design drilling report:

Date: 11-Feb-02

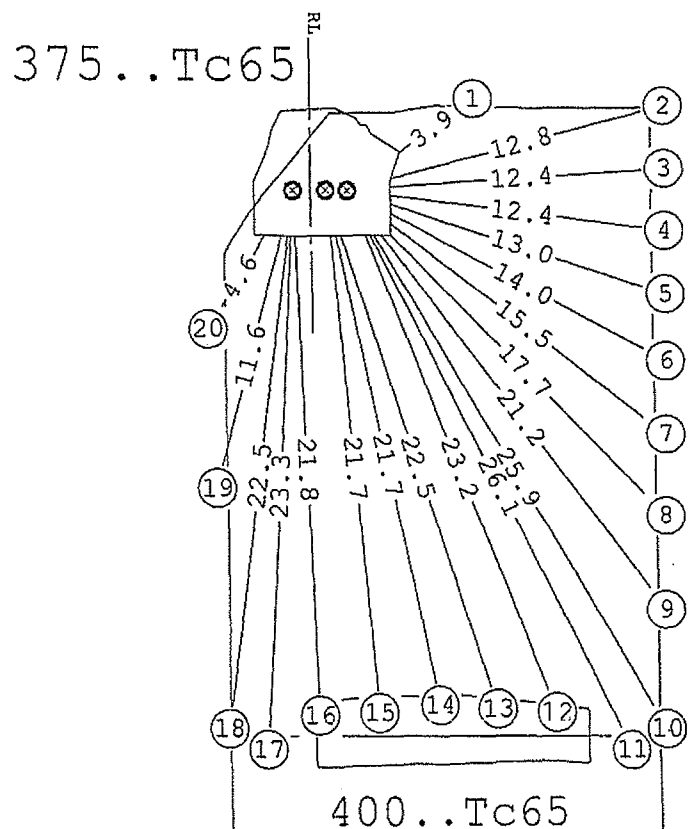
Ring: 5

No.	RL	OS	Collar	OS	Dip	Dump	Length	b/t
1	1.7E		4.1E		144	90	3.9	N
2	1.7E		165		165	90	12.8	N
3	1.7E		177		177	90	12.4	N
4	1.7E		187		187	90	12.4	N
5	1.7E		198		198	90	13.0	N
6	1.7E		200		200	90	14.0	N
7	1.7E		211		211	90	15.5	N
8	1.7E		222		222	90	17.7	N
9	1.7E		233		233	90	21.2	N
10	1.7E		244		244	90	25.1	N
11	1.7E		255		255	90	26.1	N
12	1.7E		266		266	90	23.3	Y
13	1.7E		277		277	90	21.7	Y
14	0.0		1.4E		255	90	21.7	Y
15	0.0		1.2E		255	90	21.7	Y
16	0.0		0.0		266	90	21.7	Y
17	0.0		0.0		266	90	21.7	Y
18	0.0		0.0		277	90	21.7	Y
19	0.0		1.1W		277	90	22.5	N
20	0.0		1.4W		280	90	11.6	N
21	0.0		2.1W		302	90	4.6	N
							347.9	

# Ring 5

MASTER

← WEST  
Section  
Looks North



Hole diameter: 89mm  
Ring Burden: 2.6m  
Toe Spacing: 3.0m

Ensure all down holes  
are bagged off



425mLv



	Signed	Date	<b>BHP CANNINGTON</b>  47..63 HL Ring 5, 375 mLv Looking North
Designed	<i>N J</i>		
Reviewed	<i>Long</i>	21/2/02	
Geology			
Geotech			
Supt	<i>W. H. ...</i>	22/2/02	
Approved	<i>W. H. ...</i>	23/2/02	
Survey			

Scale: 1:250 | Date: 11-Feb-02

todelep.pf

Ring Design drilling report;  
 Date: 11-Feb-02  
 Ring: 6

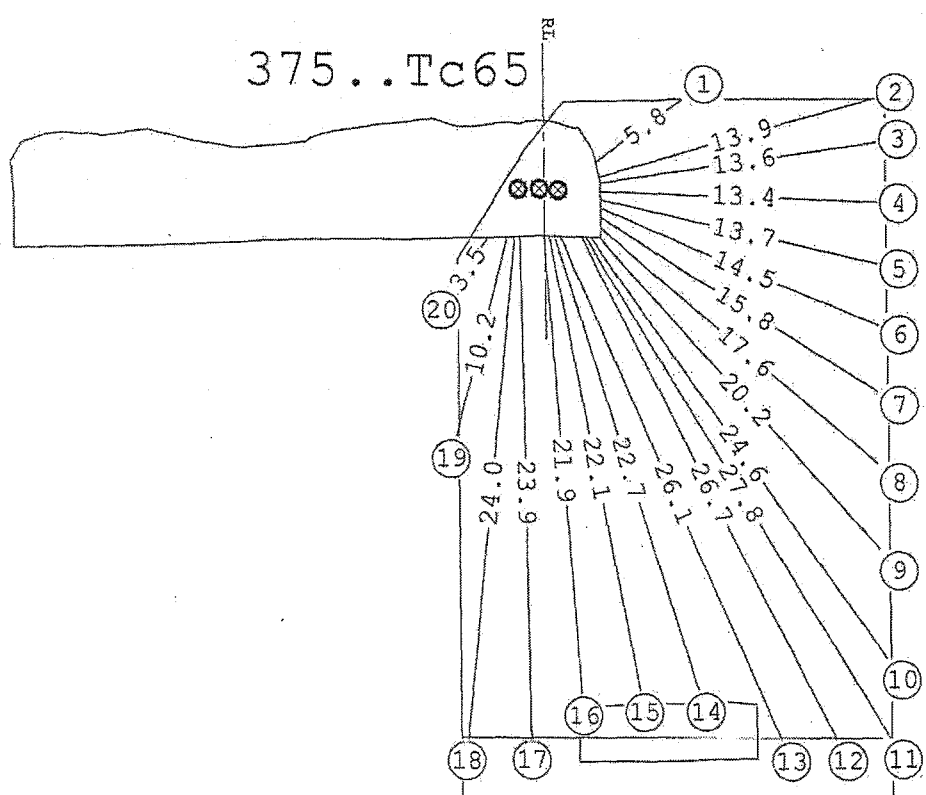
No.	RL OS	Collar OS	Dip	Dump	Length b/t	
1	0.7E	2.4E	144	90	5.8	N
2	0.7E	2.6E	164	90	13.9	N
3	0.7E	2.7E	172	90	13.6	N
4	0.7E	2.7E	182	90	13.4	N
5	0.7E	2.7E	193	90	13.7	N
6	0.7E	2.7E	203	90	14.5	N
7	0.7E	2.7E	212	90	15.8	N
8	0.7E	2.7E	221	90	17.6	N
9	0.7E	2.6E	228	90	20.2	N
10	0.7E	2.2E	235	90	24.6	N
11	0.7E	1.9E	239	90	27.8	N
12	0.7E	1.7E	244	90	26.7	N
13	0.2W	0.7E	247	90	26.1	Y
14	0.2W	0.5E	253	90	22.7	Y
15	0.2W	0.2E	259	90	22.1	Y
16	0.2W	0.0W	266	90	21.0	Y
17	1.2W	1.2W	269	90	23.9	N
18	1.2W	1.4W	275	90	24.0	N
19	1.2W	1.8W	284	90	10.2	N
20	1.2W	2.7W	303	90	3.5	N

362.2

# Ring 6

MASTER

← WEST  
 Section  
 Looks North



Hole diameter: 89mm  
 Ring Burden: 2.6m  
 Toe Spacing: 3.0m

Ensure all down holes  
are bagged off

425mLv

	Signed	Date	<b>BHP</b> CANNINGTON
Designed	NJ		
Reviewed	<i>[Signature]</i>	21/2/2002	47..63 HL Ring 6, 375 mLv Looking North
Geology			
Geotec	<i>[Signature]</i>		
Supt	<i>[Signature]</i>	22/2/02	
Approved	<i>[Signature]</i>	23/2/02	
Survey			Scale: 1:250    Date: 11-Feb-02

todeletg.pl

Ring Design drilling report:

Date: 11-Feb-02

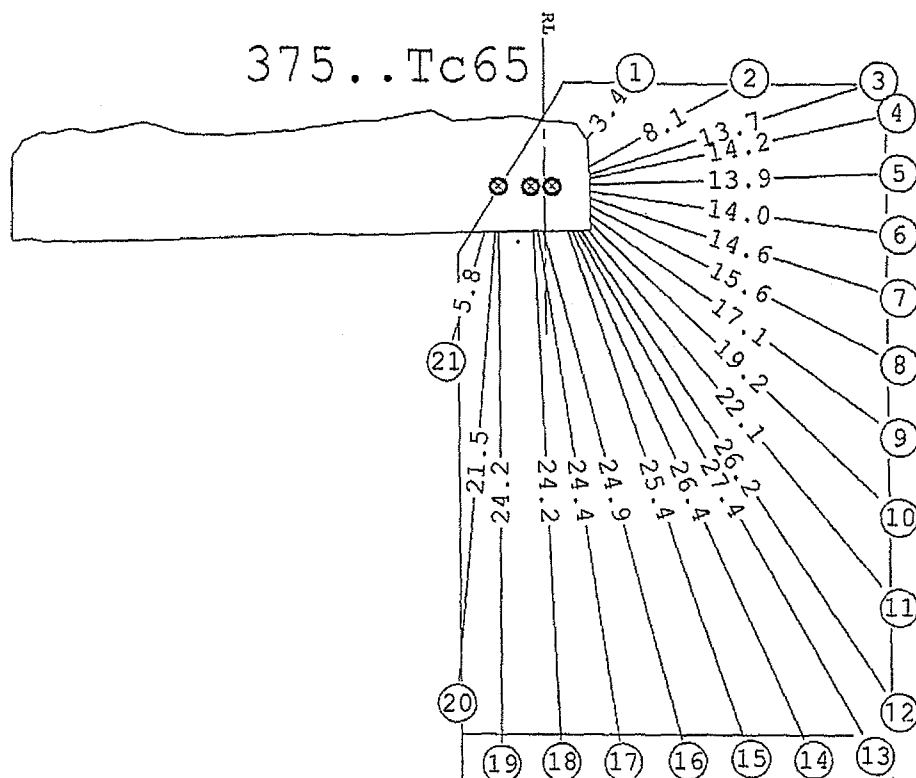
Ring: 7

No.	RL	OS	Collar	OS	Dip	Dump	Length	b/t
1	0.4E	2.0E	127	90	3.4	N		
2	0.4E	2.1E	152	90	8.1	N		
3	0.4E	2.2E	162	90	13.7	N		
4	0.4E	2.2E	168	90	14.2	N		
5	0.4E	2.2E	178	90	13.9	N		
6	0.4E	2.2E	188	90	14.0	N		
7	0.4E	2.2E	198	90	14.6	N		
8	0.4E	2.2E	207	90	15.6	N		
9	0.4E	2.2E	216	90	17.1	N		
10	0.4E	2.2E	224	90	19.2	N		
11	0.4E	2.1E	231	90	22.1	N		
12	0.4E	1.7E	237	90	26.2	N		
13	0.4E	1.5E	241	90	27.4	N		
14	0.4E	1.3E	246	90	26.4	N		
15	0.4E	1.1E	251	90	25.4	N		
16	0.6W	0.1W	255	90	24.9	N		
17	0.6W	0.3W	261	90	24.4	N		
18	0.6W	0.5W	267	90	24.2	N		
19	2.1W	2.1W	270	90	24.2	N		
20	2.1W	2.3W	275	90	21.5	N		
21	2.1W	2.8W	287	90	5.8	N		
							386.2	

# Ring 7

MASTER

← WEST  
Section  
Looks North



Hole diameter: 89mm  
Ring Burden: 2.6m  
Toe Spacing: 3.0m

Ensure all down holes  
are bagged off

425mLv

	Signed	Date	
Designed	<i>[Signature]</i>		
Reviewed	<i>[Signature]</i>	21/2/02	
Geology			
Geotechnical	<i>[Signature]</i>		
Supt	<i>[Signature]</i>	23/2/02	
Approved	<i>[Signature]</i>	23/2/02	
Survey			

47.63 HL  
Ring 7, 375 mLv  
Looking North

Scale: 1:250 Date: 11-Feb-02

todelet.pl

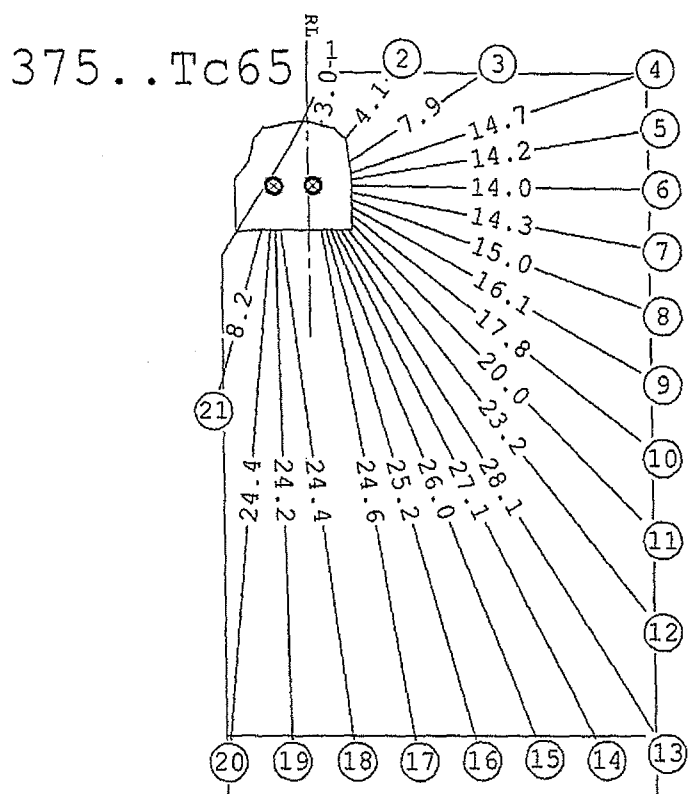
Ring Design drilling report:  
 Date: 11-Feb-02  
 Ring: 8

No.	RL	OS	Collar	OS	Dip	Dump	Length	b/t
1	0	0	0	0	99	90	3.0	N
2	11.8	0	0	0	126.6	90	4.1	N
3	11.8	0	0	0	147	90	7.9	N
4	11.8	0	0	0	161	90	14.7	N
5	11.8	0	0	0	171	90	14.2	N
6	11.8	0	0	0	181	90	14.0	N
7	11.8	0	0	0	191	90	14.3	N
8	11.8	0	0	0	201	90	15.0	N
9	11.8	0	0	0	210	90	16.1	N
10	11.8	0	0	0	218	90	17.8	N
11	11.8	0	0	0	222	90	20.0	N
12	11.8	0	0	0	233	90	23.2	N
13	11.8	0	0	0	243	90	24.4	N
14	11.8	0	0	0	249	90	24.2	N
15	11.8	0	0	0	255	90	24.6	N
16	11.8	0	0	0	260	90	25.2	N
17	11.8	0	0	0	266	90	26.0	N
18	11.8	0	0	0	273	90	27.1	N
19	11.8	0	0	0	279	90	28.1	N
20	11.8	0	0	0	286	90	28.2	N
21	11.8	0	0	0	288	90	28.2	N
							376.5	

# Ring 8

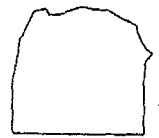
MASTER

← WEST  
 Section  
 Looks North

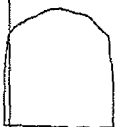


Hole diameter: 89mm  
 Ring Burden: 2.6m  
 Toe Spacing: 3.0m

Ensure all down holes  
 are bagged off



425mLv



	Signed	Date	BWP CANNINGTON
Designed	NJ		
Reviewed	<i>[Signature]</i>	21/2/2002	
Geology			
Geotech	<i>[Signature]</i>		
Supt	<i>[Signature]</i>	20/2/02	
Approved	<i>[Signature]</i>	23/2/02	Scale: 1:250    Date: 11-Feb-02
Survey			

toelets.pl



Ring Design drilling report:

Date: 14-Feb-02

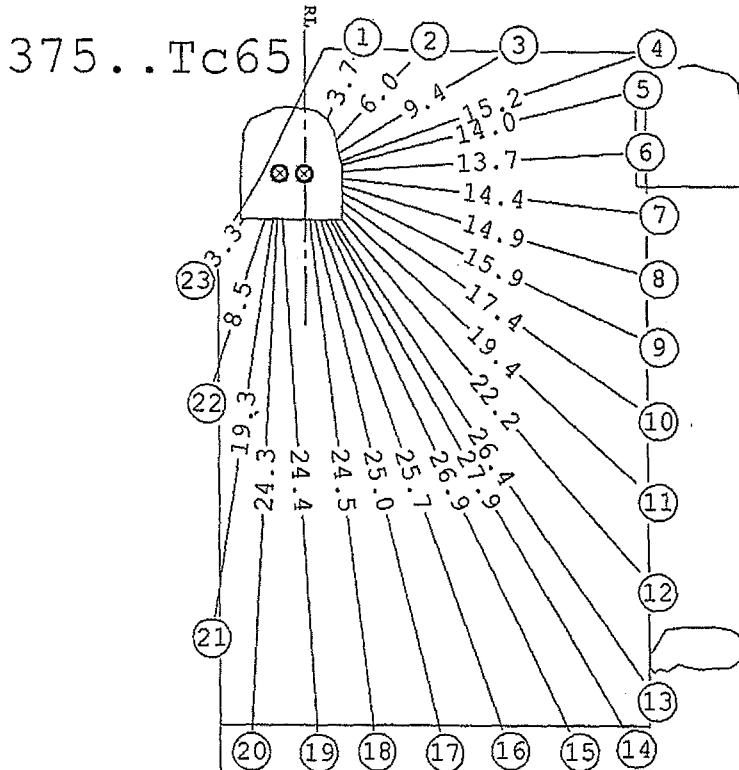
Ring: 9

No.	RL	OS	Collar OS	Dip	Dump	Length	b/t
1	0.0W	1.1E	114	90	3.7	N	
2	0.0W	1.5E	134	90	6.0	N	
3	0.0W	1.6E	149	90	9.4	N	
4	0.0W	1.7E	160	90	15.2	N	
5	0.0W	1.7E	166	90	14.0	N	
6	0.0W	1.8E	176	90	13.7	N	
7	0.0W	1.8E	186	90	14.4	N	
8	0.0W	1.8E	196	90	14.9	N	
9	0.0W	1.8E	206	90	15.9	N	
10	0.0W	1.8E	215	90	17.4	N	
11	0.0W	1.8E	223	90	19.4	N	
12	0.0W	1.8E	230	90	22.2	N	
13	0.0W	1.4E	236	90	26.4	N	
14	0.0W	1.2E	240	90	27.9	N	
15	0.0W	1.0E	245	90	26.9	N	
16	0.0W	0.7E	250	90	25.7	N	
17	0.0W	0.5E	256	90	25.0	N	
18	0.0W	0.2E	263	90	24.5	N	
19	1.2W	1.1W	266	90	24.4	N	
20	1.2W	1.3W	273	90	24.3	N	
21	1.2W	1.5W	278	90	19.3	N	
22	1.2W	1.9W	288	90	8.5	N	
23	1.2W	2.8W	308	90	3.3	N	
402.6							

# Ring 9

MASTER

← WEST  
Section  
Looks North



Hole diameter: 89mm

Ring Burden: 2.6m

Toe Spacing: 3.0m

Ensure all down holes  
are bagged off

425mLv

	Signed	Date	<b>BHP</b> CANNINGTON  47..63 HL Ring 9, 375 mLv Looking North
Designed	<i>NJ</i>		
Reviewed	<i>Long</i>	<i>21/2/02</i>	
Geology			
Geotech			
Supt	<i>W. G. ...</i>	<i>22/2/02</i>	
Approved	<i>M. ...</i>	<i>23/2/02</i>	
Survey			Scale: 1:250

todelety.pl

Ring Design drilling report:

Date: 11-Feb-02

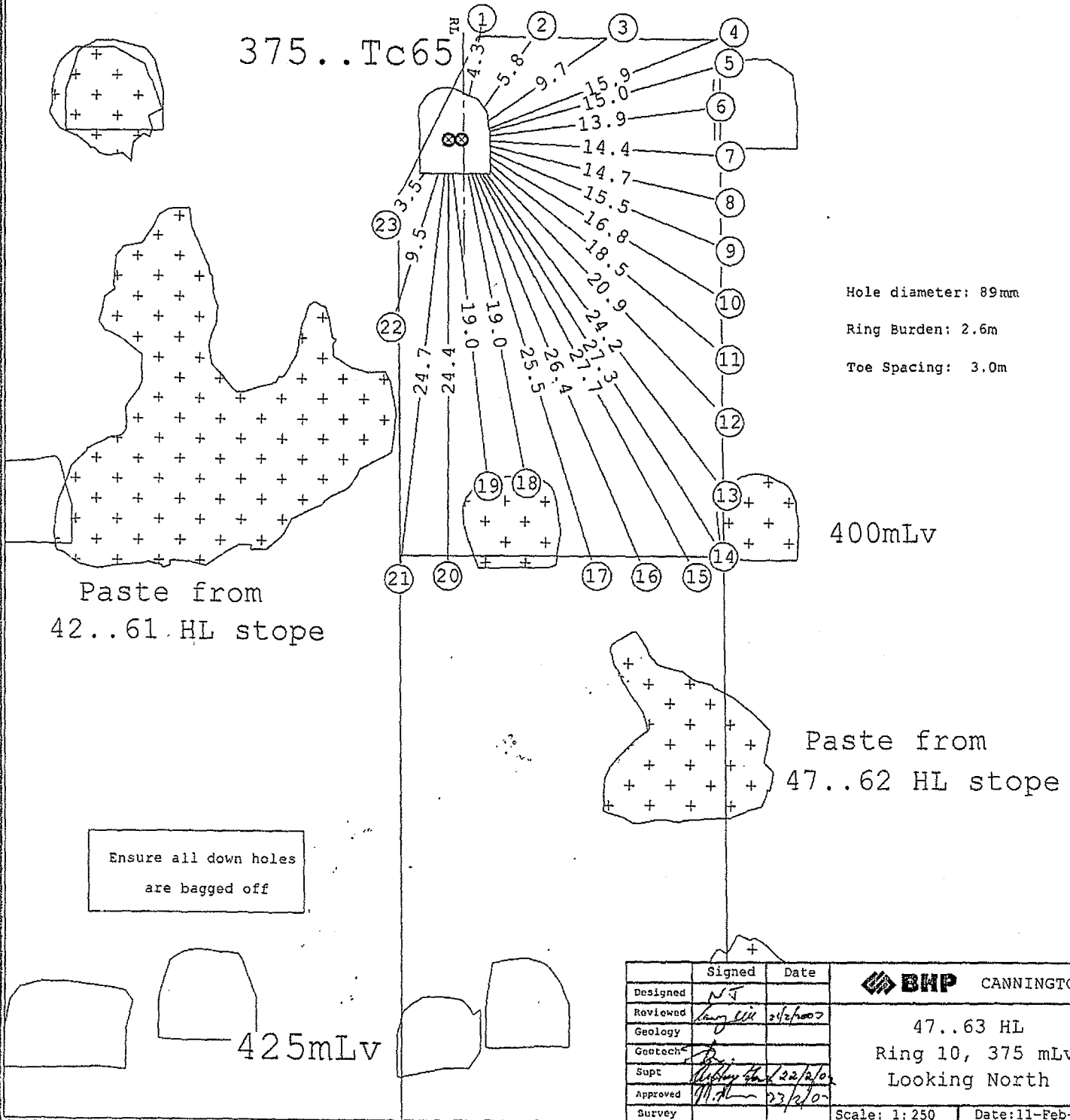
Ring: 10

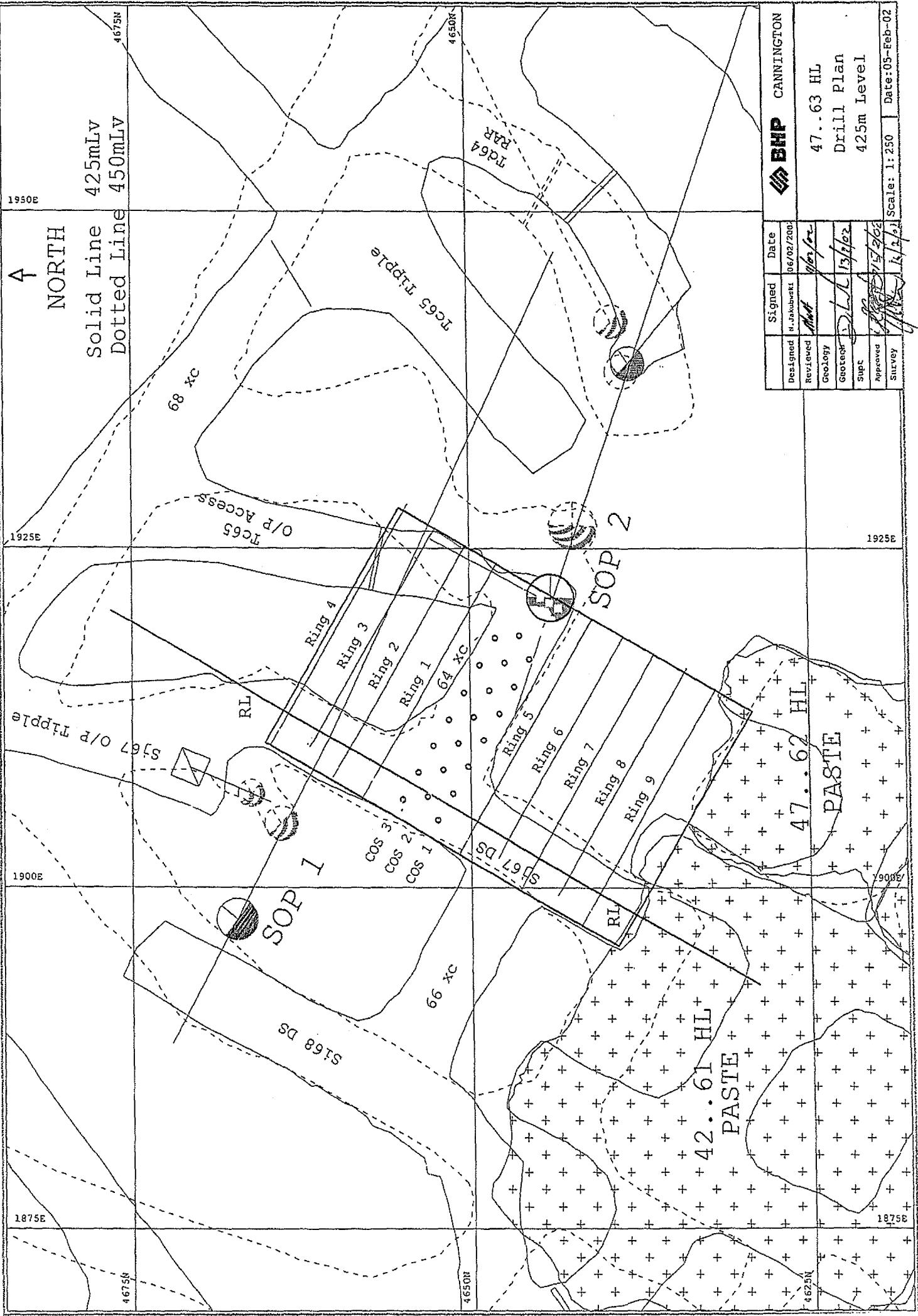
# Ring 10

No.	RL	OS	Collar	OS	Dip	Dump	Length	b/t
1	0.1W	0.4E	100	90	4.3	N		
2	0.1W	1.3E	126	90	5.8	N		
3	0.1W	1.6E	145	90	9.7	N		
4	0.1W	1.6E	158	90	15.0	N		
5	0.1W	1.7E	164	90	15.9	N		
6	0.1W	1.7E	172	90	13.9	N		
7	0.1W	1.7E	183	90	14.4	N		
8	0.1W	1.7E	193	90	14.7	N		
9	0.1W	1.7E	202	90	15.5	N		
10	0.1W	1.7E	211	90	16.8	N		
11	0.1W	1.7E	219	90	18.5	N		
12	0.1W	1.7E	227	90	19.0	N		
13	0.1W	1.5E	233	90	20.9	N		
14	0.1W	1.2E	238	90	24.4	N		
15	0.1W	1.0E	242	90	27.7	N		
16	0.1W	0.8E	247	90	26.4	N		
17	0.1W	0.0E	253	90	25.5	N		
18	0.1W	0.0E	259	90	19.0	N		
19	0.1W	0.0E	264	90	24.4	N		
20	0.1W	0.0E	270	90	24.7	N		
21	0.1W	1.2W	277	90	9.5	N		
22	0.1W	1.6W	287	90	3.5	N		
23	0.1W	2.5W	306	90		N		
396.4								

MASTER

← WEST  
Section  
Looks North





<b>BHP</b> CANNINGTON	
Designed	N. Jakubowski
Reviewed	<i>[Signature]</i>
Geology	<i>[Signature]</i>
Geotech	<i>[Signature]</i>
Supt	<i>[Signature]</i>
Approved	<i>[Signature]</i>
Survey	<i>[Signature]</i>
Signed	Date
	06/02/2008
47..63 HL	
Drill Plan	
425m Level	
Scale: 1:250	Date: 05-Feb-02

Ring Design drilling report:

Date: 11-Feb-02

Ring: 5

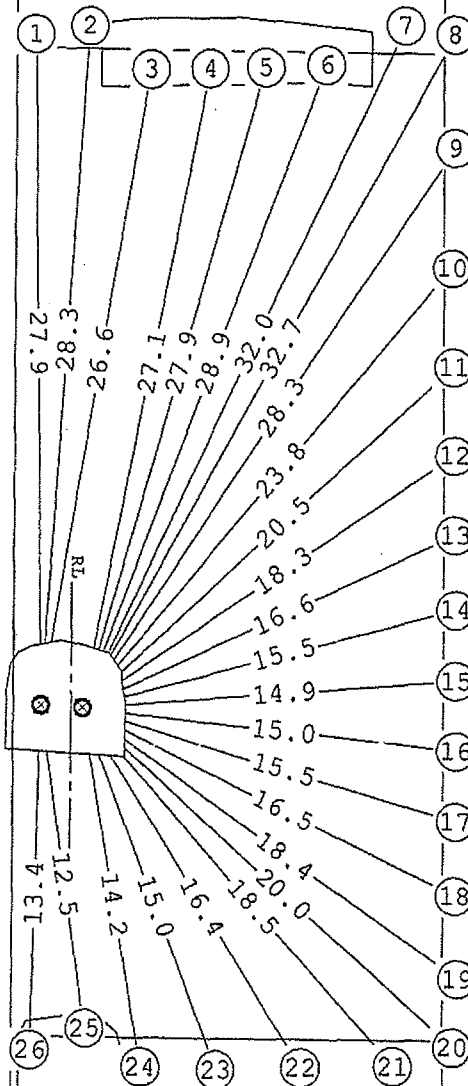
No.	RL	OS	Collar OS	Dip	Dump	Length	b/t
1	1.4W		1.5W	89	90	27.9	N
2	1.4W		1.2W	94	90	28.3	N
3	1.4W		0.9W	100	90	26.6	Y
4	0.5E		1.1E	101	90	27.1	Y
5	0.5E		1.3E	106	90	27.9	Y
6	0.5E		1.5E	111	90	28.9	Y
7	0.5E		1.7E	115	90	32.0	N
8	0.5E		1.9E	119	90	32.7	N
9	0.5E		2.0E	123	90	28.3	N
10	0.5E		2.2E	130	90	23.8	N
11	0.5E		2.4E	137	90	20.5	N
12	0.5E		2.4E	145	90	18.3	N
13	0.5E		2.4E	155	90	16.6	N
14	0.5E		2.5E	164	90	15.5	N
15	0.5E		2.5E	175	90	14.9	N
16	0.5E		2.5E	186	90	15.0	N
17	0.5E		2.5E	196	90	15.5	N
18	0.5E		2.5E	206	90	16.5	N
19	0.5E		2.5E	215	90	18.4	N
20	0.5E		2.5E	222	90	20.0	N
21	0.5E		2.5E	228	90	18.5	N
22	0.5E		1.9E	238	90	16.4	Y
23	0.5E		1.3E	249	90	15.0	N
24	0.5E		0.9E	260	90	14.2	N
25	1.4W		1.1W	262	90	12.5	Y
26	1.4W		1.5W	271	90	13.4	Y

544.8

# Ring 5

← WEST  
Section  
Looks North

400..Tc65



Hole diameter: 89mm

Ring Burden: 2.6m

Toe Spacing: 3.0m

425..Sj67

450..Sj67

Ensure all down holes  
are bagged off

	Signed	Date		
Designed	<i>N.S.</i>			
Reviewed	<i>[Signature]</i>	11/2/02		
Geology	<i>[Signature]</i>	17/2/02		
Supt	<i>[Signature]</i>	15/2/02		
Approved	<i>[Signature]</i>		47..63 HL Ring 5, 425 mLv Looking North	
Survey			Scale: 1:250	Date: 11-Feb-02

codelete.pf

Ring Design drilling report:

Date: 11-Feb-02

Ring: 6

No.	RL	OS	Collar OS	Dip	Dump	Length	b/t
1	1.5W	1.5W	90	90	28.8	N	
2	1.5W	1.2W	95	90	28.7	N	
3	0.5W	0.0W	99	90	26.4	Y	
4	0.1E	0.8E	104	90	27.3	Y	
5	0.1E	1.0E	108	90	28.1	Y	
6	0.1E	1.3E	113	90	31.5	N	
7	0.1E	1.5E	117	90	32.6	N	
8	0.1E	1.6E	121	90	30.5	N	
9	0.1E	1.8E	127	90	25.8	N	
10	0.1E	2.0E	134	90	22.2	N	
11	0.1E	2.1E	142	90	19.5	N	
12	0.1E	2.1E	151	90	17.6	N	
13	0.1E	2.1E	160	90	16.3	N	
14	0.1E	2.1E	170	90	15.5	N	
15	0.1E	2.1E	181	90	15.3	N	
16	0.1E	2.1E	191	90	15.6	N	
17	0.1E	2.1E	202	90	16.5	N	
18	0.1E	2.1E	212	90	17.9	N	
19	0.1E	2.1E	220	90	19.9	N	
20	0.1E	2.1E	225	90	20.7	N	
21	0.1E	1.8E	233	90	17.8	N	
22	0.1E	1.2E	243	90	16.0	N	
23	1.5W	0.6W	248	90	15.4	N	
24	1.5W	1.1W	258	90	12.6	Y	
25	1.5W	1.5W	271	90	12.5	N	

531.1

# Ring 6

← WEST  
Section  
Looks North

400..Tc65

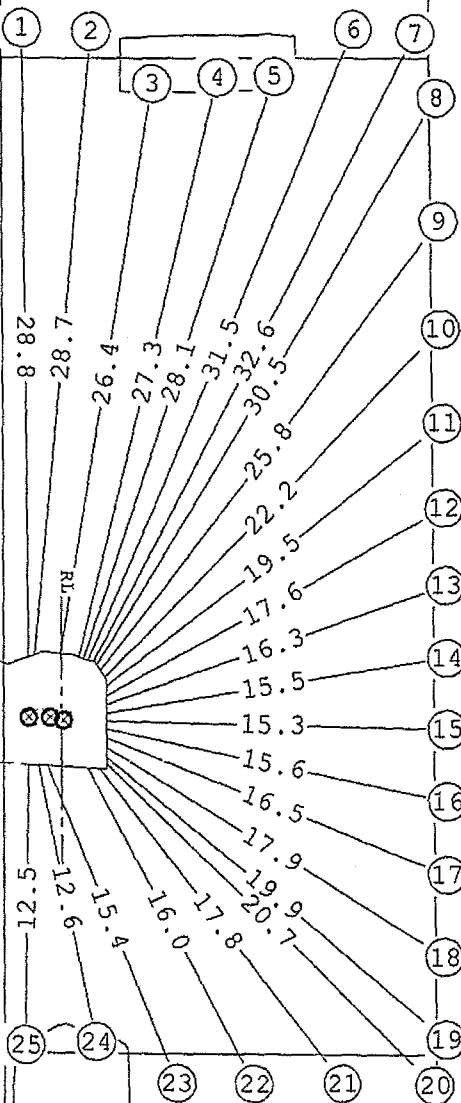
Hole diameter: 89mm

Ring Burden: 2.6m

Toe Spacing: 3.0m

425..Sj67

450..Sj67



Ensure all down holes  
are bagged off

	Signed	Date	
Designed	M. J.		
Reviewed	M.H.	11/2/02	
Geology			
Geotech.	D. D.	13/2/02	
Supt			47..63 HL
Approved			Ring 6, 425 mLv
Survey			Looking North
			Scale: 1:250
			Date: 11-Feb-02

todeletf.pf

Ring Design drilling report:

Date: 11-Feb-02

Ring: 7

No.	RL	OS	Collar OS	Dip	Dump	Length b/t	
1	1.8W	1.8W	90	90	28.8	N	N
2	1.8W	1.6W	94	90	28.7	N	N
3	1.1W	0.7W	98	90	28.6	N	N
4	1.1W	0.4W	103	90	29.3	N	N
5	1.1W	0.1W	108	90	30.0	N	N
6	0.1E	1.1E	110	90	30.8	N	N
7	0.1E	1.4E	115	90	32.2	N	N
8	0.1E	1.6E	119	90	32.6	N	N
9	0.1E	1.7E	123	90	28.7	N	N
10	0.1E	1.9E	130	90	24.3	N	N
11	0.1E	2.0E	137	90	21.1	N	N
12	0.1E	2.0E	145	90	18.7	N	N
13	0.1E	2.0E	155	90	17.0	N	N
14	0.1E	2.1E	165	90	15.9	N	N
15	0.1E	2.1E	175	90	15.4	N	N
16	0.1E	2.1E	186	90	15.4	N	N
17	0.1E	2.1E	197	90	16.0	N	N
18	0.1E	2.1E	206	90	17.1	N	N
19	0.1E	2.1E	216	90	19.3	N	N
20	0.1E	2.1E	221	90	20.9	N	N
21	0.1E	2.1E	227	90	18.9	N	N
22	0.1E	1.7E	233	90	17.1	N	N
23	0.1E	1.2E	242	90	15.6	N	N
24	1.1W	0.2W	246	90	15.2	N	N
25	1.1W	0.6W	256	90	14.2	N	N
26	1.8W	1.5W	261	90	12.0	Y	Y
27	1.8W	1.8W	270	90	12.3	N	N

576.0

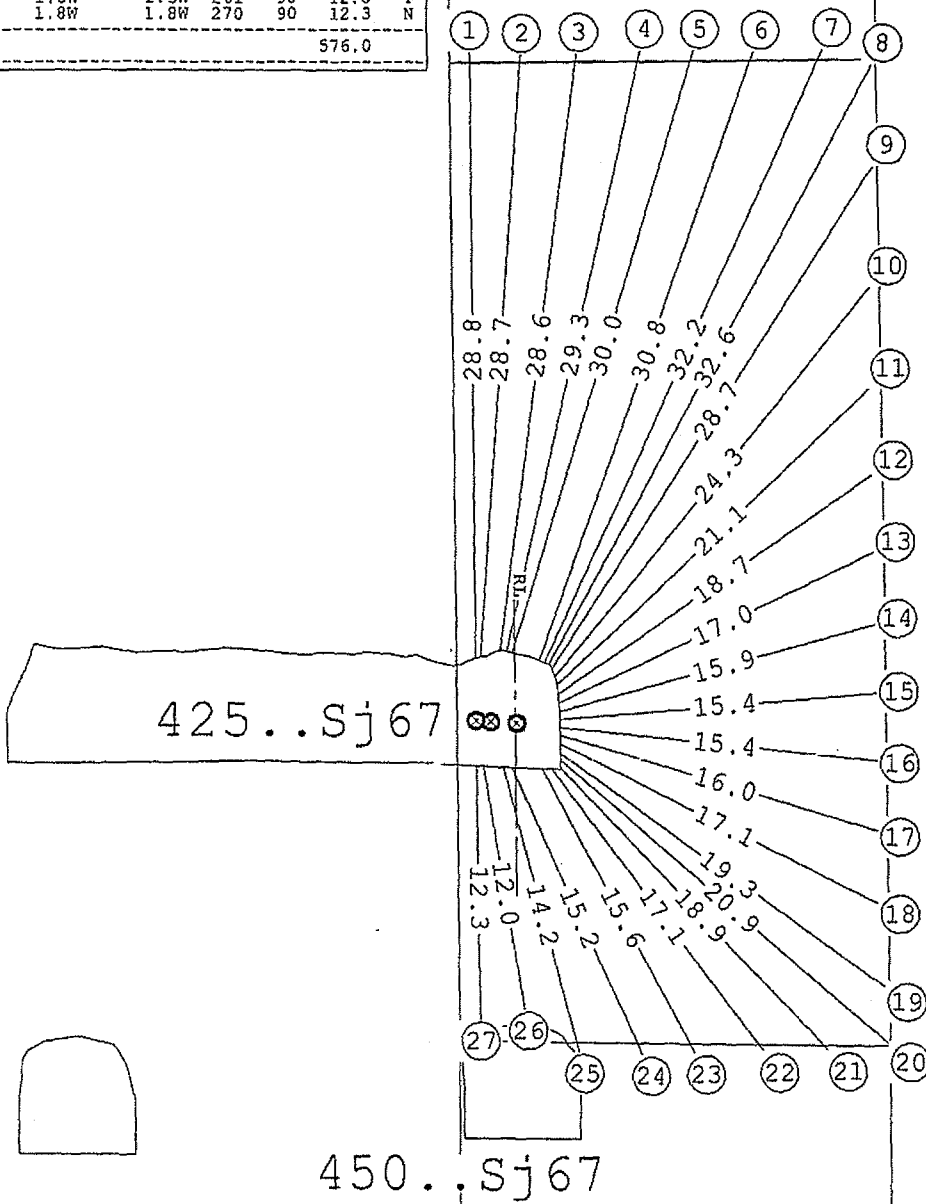
# Ring 7

← WEST  
Section  
Looks North

Hole diameter: 89mm

Ring Burden: 2.6m

Toe Spacing: 3.0m



425..Sj67

450..Sj67

Ensure all down holes  
are bagged off

	Signed	Date	
Designed	N.S.		
Reviewed	Matt	11/2/02	
Geology			
Geotech			
Supt			47..63 HL
Approved			Ring 7, 425 mLv
Survey			Looking North

Scale: 1:250 Date: 11-Feb-02

todeletg.pf

Ring Design drilling report:

Date: 11-Feb-02

Ring: 8

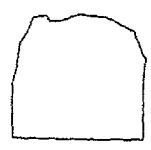
No.	RL	OS	Collar	OS	Dip	Dump	Length	b/t
1	1.3W	1.4W	89	90	28.8	N		
2	1.3W	1.0W	95	90	28.9	N		
3	1.3W	0.7W	101	90	29.1	N		
4	0.1E	0.8E	103	90	29.7	N		
5	0.1E	1.0E	107	90	30.3	N		
6	0.1E	1.2E	112	90	31.5	N		
7	0.1E	1.4E	117	90	32.9	N		
8	0.1E	1.5E	121	90	31.3	N		
9	0.1E	1.7E	126	90	26.5	N		
10	0.1E	1.9E	133	90	22.8	N		
11	0.1E	1.9E	140	90	20.1	N		
12	0.1E	2.0E	149	90	16.0	N		
13	0.1E	2.0E	158	90	16.5	N		
14	0.1E	2.1E	168	90	15.6	N		
15	0.1E	2.1E	179	90	15.3	N		
16	0.1E	2.1E	189	90	15.5	N		
17	0.1E	2.1E	199	90	16.2	N		
18	0.1E	2.1E	209	90	17.5	N		
19	0.1E	2.1E	218	90	19.7	N		
20	0.1E	2.1E	224	90	20.7	N		
21	0.1E	1.8E	231	90	18.8	N		
22	0.1E	1.4E	239	90	17.2	N		
23	0.1E	1.0E	247	90	16.0	N		
24	1.3W	0.6W	251	90	15.3	N		
25	1.3W	1.0W	260	90	12.2	N		
26	1.3W	1.4W	272	90	12.9	Y		

559.4

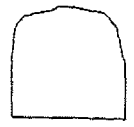
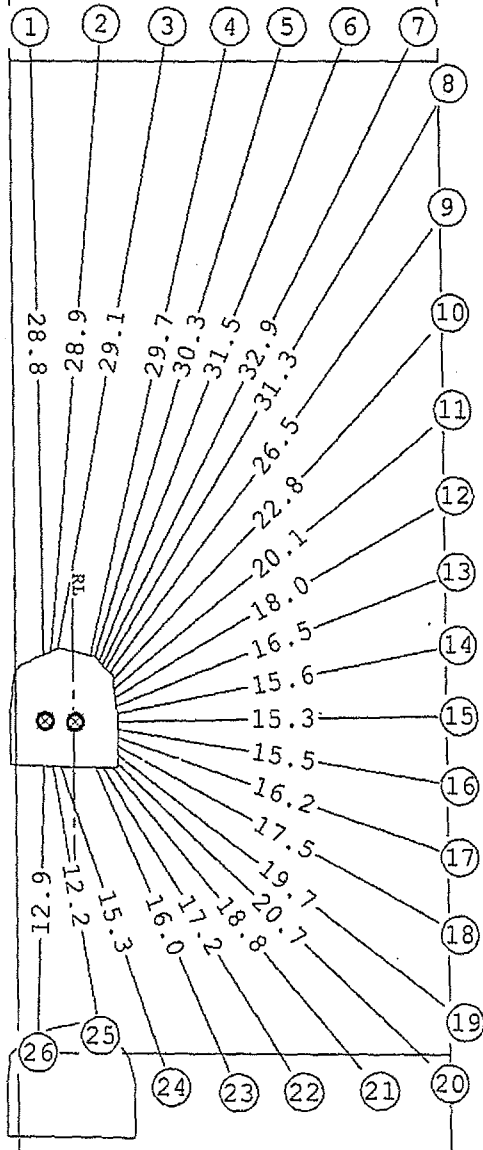
# Ring 8

← WEST  
Section  
Looks North

Hole diameter: 89mm  
Ring Burden: 2.6m  
Toe Spacing: 3.0m



425..Sj67



450..Sj67

Ensure all down holes  
are bagged off

	Signed	Date	<b>BHP CANNINGTON</b>  47..63 HL Ring 8, 425 mLv Looking North
Designed	N.G.		
Reviewed	<i>[Signature]</i>	11/02/02	
Geotech	<i>[Signature]</i>	13/02/02	
Supt	<i>[Signature]</i>	15/02/02	
Approved	<i>[Signature]</i>	15/02/02	
Survey			Scale: 1:250
			Date: 11-Feb-02

todeleth.pf

Ring Design drilling report:

Date: 11-Feb-02

Ring: 9

No.	RL	OS	Collar OS	Dip	Dump	Length b/t	
1	1.3W	1.4W	89	90	28.5	N	
2	0.6W	0.5W	92	90	28.5	N	
3	0.6W	0.2W	97	90	28.6	N	
4	0.6W	0.1E	102	90	29.1	N	
5	0.0W	0.8E	106	90	29.7	N	
6	0.0W	1.1E	111	90	30.7	N	
7	0.0W	1.3E	116	90	32.1	N	
8	0.0W	1.5E	120	90	32.9	N	
9	0.0W	1.6E	124	90	29.5	N	
10	0.0W	1.7E	130	90	24.4	N	
11	0.0W	1.8E	137	90	21.2	N	
12	0.0W	1.9E	146	90	18.8	N	
13	0.0W	2.0E	155	90	17.1	N	
14	0.0W	2.0E	165	90	16.0	N	
15	0.0W	2.0E	175	90	15.5	N	
16	0.0W	2.0E	186	90	15.5	N	
17	0.0W	2.0E	196	90	16.1	N	
18	0.0W	2.0E	206	90	17.2	N	
19	0.0W	1.9E	215	90	18.6	N	
20	0.0W	1.9E	222	90	20.9	N	
21	0.0W	1.9E	228	90	20.3	N	
22	0.0W	1.5E	235	90	18.3	N	
23	0.6W	0.5E	241	90	17.0	N	
24	0.6W	0.2E	249	90	15.9	N	
25	0.6W	0.2W	259	90	14.9	N	
26	0.6W	0.6W	268	90	12.3	N	
27	1.3W	1.4W	272	90	13.5	Y	

583.0

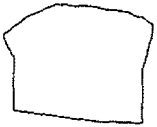
# Ring 9

← WEST  
Section  
Looks North

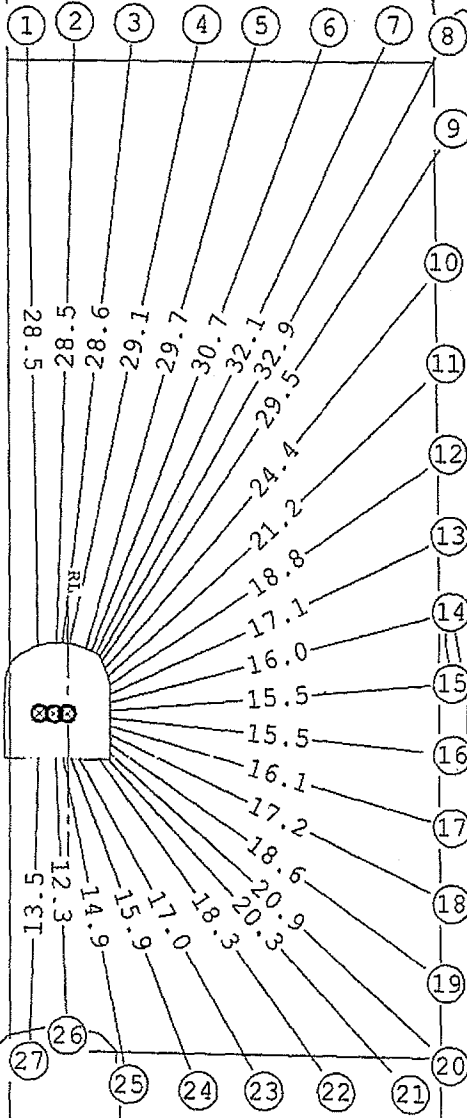
Hole diameter: 89mm

Ring Burden: 2.6m

Toe Spacing: 3.0m



425..Sj67



450..Sj67

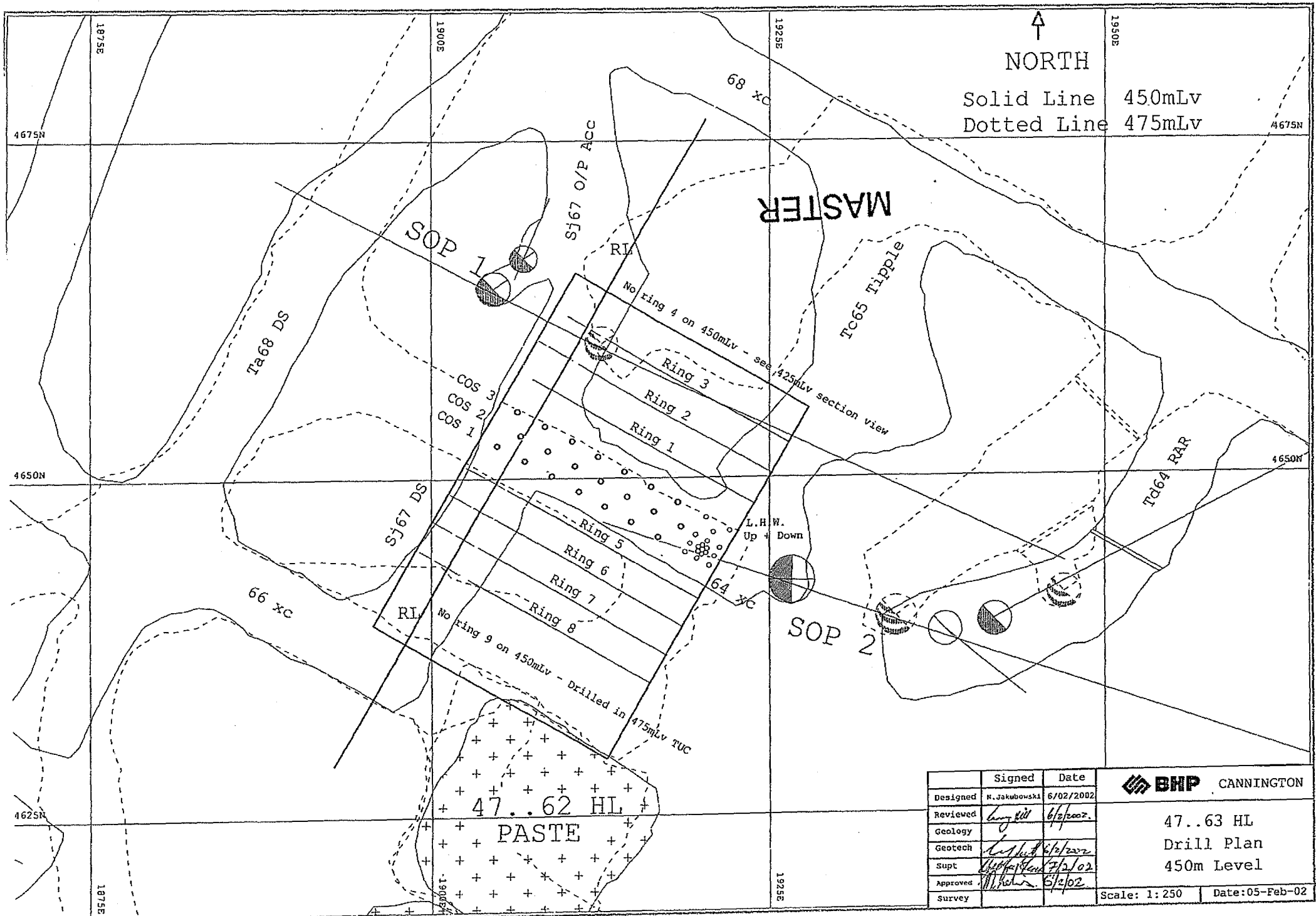
Ensure all down holes  
are bagged off

	Signed	Date	<b>BHP CANNINGTON</b>  47..63 HL Ring 9, 425 mLv Looking North
Designed	N-J		
Reviewed	<i>[Signature]</i>	11/2/02	
Geology	<i>[Signature]</i>	11/2/02	
Geotech	<i>[Signature]</i>	11/2/02	
Supt	<i>[Signature]</i>	11/2/02	
Approved	<i>[Signature]</i>	11/2/02	
Survey	<i>[Signature]</i>	11/2/02	

Scale: 1:250 Date: 11-Feb-02

codelet1.pf





	Signed	Date	<b>BHP</b> CANNINGTON 47..63 HL Drill Plan 450m Level
Designed	N. Jakubowski	6/02/2002	
Reviewed	<i>[Signature]</i>	6/2/2002	
Geology	<i>[Signature]</i>	6/2/2002	
Geotech	<i>[Signature]</i>	6/2/2002	
Supt	<i>[Signature]</i>	7/2/02	
Approved	<i>[Signature]</i>	6/2/02	Scale: 1:250
Survey			Date: 05-Feb-02

Ring Design drilling report:

Date: 06-Feb-02

Ring: 5

No.	RL	OS	Collar OS	Dip	Dump	Length	b/t
1	0.7E	2.7E	172	90	14.8	N	
2	0.7E	2.7E	183	90	14.7	NN	
3	0.7E	2.7E	194	90	15.1	NN	
4	0.7E	2.7E	204	90	16.1	NN	
5	0.7E	2.7E	213	90	17.5	NN	
6	0.7E	2.7E	222	90	19.6	NN	
7	0.7E	2.5E	229	90	22.6	NN	
8	0.7E	2.2E	234	90	21.9	NN	
9	0.7E	1.9E	240	90	20.9	NN	
10	0.7E	1.6E	246	90	22.7	NN	
11	0.7E	1.4E	253	90	23.5	NN	
12	0.7E	1.1E	260	90	22.8	NN	
13	0.7E	0.8E	266	90	22.1	NN	
14	0.6W	0.5W	270	90	22.1	NN	
15	0.6W	0.7W	275	90	22.2	NN	

298.8

400..Tc65

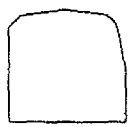
# Ring 5

MASTER

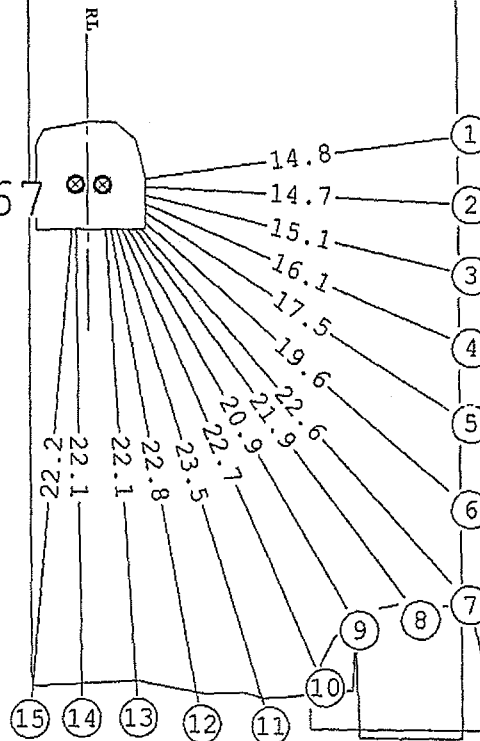
← WEST  
Section  
Looks North



425..Sj67



450..Sj67



Hole diameter: 89mm

Ring Burden: 2.6m

Toe Spacing: 3.1m

475..Ta64

Ensure all down holes  
are bagged off

	Signed	Date	<b>BHP</b> CANNINGTON  47..63 HL Ring 5, 450 mLv Looking North
Designed	N.J		
Reviewed	<i>[Signature]</i>	11/2/02	
Geology	<i>[Signature]</i>	11/2/02	
Geotech	<i>[Signature]</i>	11/2/02	
Supt	<i>[Signature]</i>	11/2/02	
Approved	<i>[Signature]</i>	11/2/02	
Survey			Scale: 1:250
			Date: 06-Feb-02

todelet.L.Pf

Ring Design drilling report:

Date: 05-Feb-02

Ring: 6

No.	RL	OS	Collar OS	Dip	Dump	Length b/t	
1	1.1E	3.1E	176	90	14.4	N	
2	1.1E	3.1E	186	90	14.4	NN	
3	1.1E	3.1E	194	90	14.6	NN	
4	1.1E	3.1E	204	90	15.7	NN	
5	1.1E	3.1E	214	90	17.3	NN	
6	1.1E	3.1E	223	90	19.6	NN	
7	1.1E	2.7E	231	90	23.2	NY	
8	1.1E	2.4E	237	90	21.0	Y	
9	1.1E	2.1E	242	90	20.5	NN	
10	1.1E	1.8E	249	90	19.3	NN	
11	1.1E	1.5E	258	90	17.7	NN	
12	1.1E	1.2E	266	90	16.8	NN	
13	0.6W	0.5W	268	90	16.8	NN	
14	0.6W	0.8W	276	90	16.5	NN	
						247.8	

400..Tc65

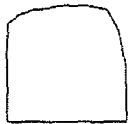
# Ring 6

MASTER

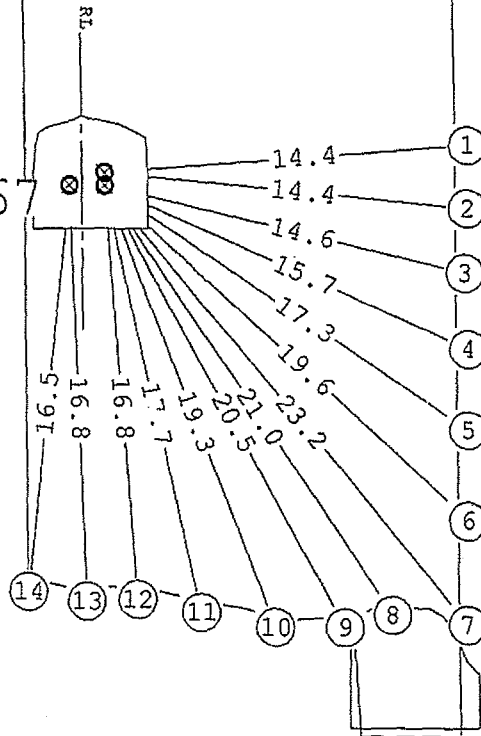
← WEST  
Section  
Looks North



425..Sj67



450..Sj67



Hole diameter: 89mm

Ring Burden: 2.6m

Toe Spacing: 3.1m

475..Ta64

Ensure all down holes  
are bagged off

	Signed	Date	<b>BHP</b> CANNINGTON  47..63 HL Ring 6, 450 mLv Looking North
Designed	N.J		
Reviewed	<i>[Signature]</i>	6/2/2002	
Geology	<i>[Signature]</i>	6/2/2002	
Supt	<i>[Signature]</i>	6/2/2002	
Approved	<i>[Signature]</i>	6/2/02	
Survey			Scale: 1:250
			Date: 06-Feb-02

codelet1.pf

Ring Design drilling report:

Date: 06-Feb-02

Ring: 7

No.	RL	OS	Collar OS	Dip	Dump	Length	b/t
1	0.9E	2.9E	176	90	14.5	N	
2	0.9E	2.9E	186	90	14.6	NN	
3	0.9E	2.9E	197	90	15.1	NN	
4	0.9E	2.9E	206	90	16.1	NN	
5	0.9E	2.9E	214	90	17.4	NN	
6	0.9E	2.9E	219	90	18.7	NN	
7	0.9E	2.9E	226	90	20.5	NN	
8	0.9E	2.5E	233	90	18.3	NN	
9	0.9E	2.1E	241	90	16.7	NN	
10	0.9E	1.6E	251	90	14.6	NN	
11	0.9E	1.2E	261	90	13.4	NN	
12	0.7W	0.6W	256	90	12.7	NN	
13	0.7W	1.0W	278	90	12.1	N	

204.6

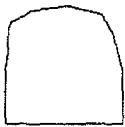
# Ring 7

MASTER

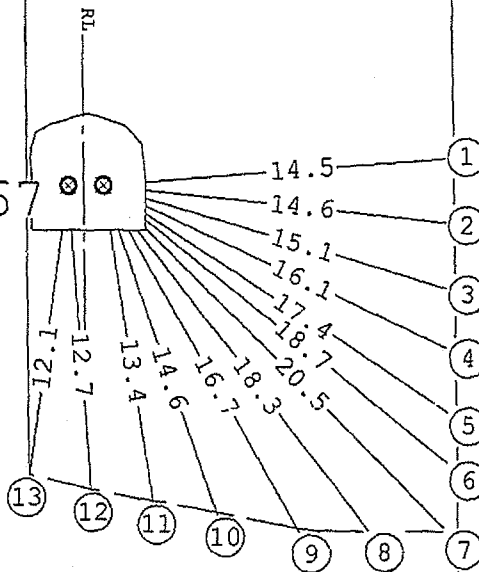
← WEST  
Section  
Looks North



425..Sj67



450..Sj67



Hole diameter: 89mm

Ring Burden: 2.6m

Toe Spacing: 3.1m



475..Ta64

T.U.C.

Ensure all down holes  
are bagged off

	Signed	Date	
Designed	<i>N.J.</i>		
Reviewed	<i>Longhill</i>	4/2/02	
Geology			
Geotech	<i>John Hall</i>	6/2/02	
Supt	<i>Walter King</i>	7/2/02	
Approved	<i>M. King</i>	6/2/02	
Survey			

47..63 HL  
Ring 7, 450 mLv  
Looking North

Scale: 1:250 Date:06-Feb-02

Ring Design drilling report:

Date: 06-Feb-02

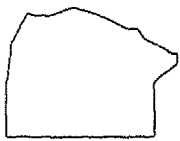
Ring: 8

No.	RL	OS	Collar	OS	Dip	Dump	Length	b/t
1	0.8E	2.8E	175	90	14.7	N		
2	0.8E	2.8E	185	90	14.6	N		
3	0.8E	2.8E	196	90	15.1	N		
4	0.8E	2.8E	205	90	16.1	N		
5	0.8E	2.8E	214	90	17.7	N		
6	0.8E	2.8E	222	90	15.2	N		
7	0.8E	2.8E	232	90	11.7	N		
8	0.8E	2.1E	244	90	9.6	N		
9	0.8E	1.4E	257	90	7.8	N		
10	0.8E	0.7E	273	90	7.4	N		
11	1.1W	1.5W	278	90	7.3	N		
							137.4	

# Ring 8

← WEST  
Section  
Looks North

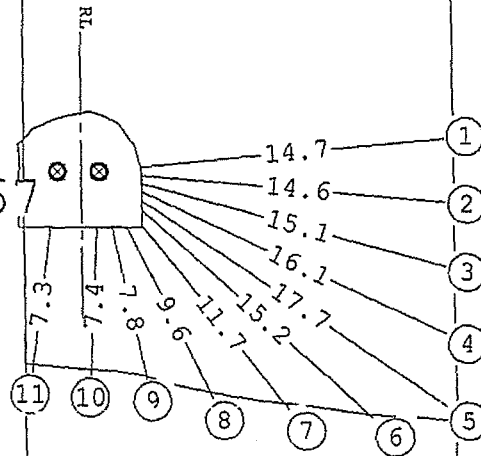
MASTER



425..Sj67



450..Sj67



Hole diameter: 89mm

Ring Burden: 2.6m

Toe Spacing: 3.1m

T.U.C.

475..Ta64

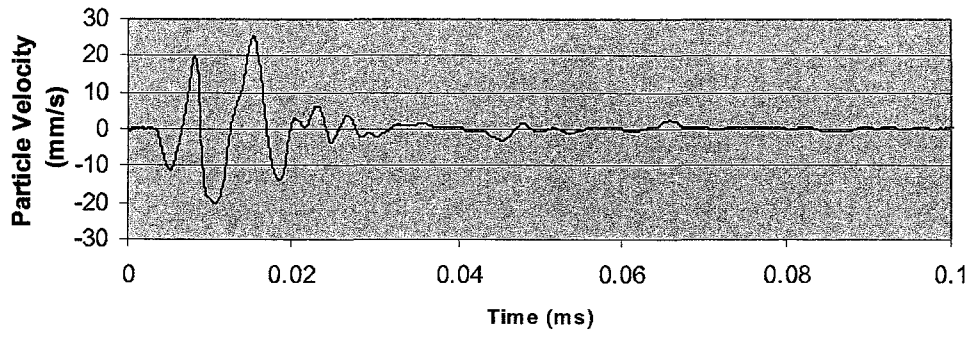
Ensure all down holes  
are bagged off

	Signed	Date	<b>BHP</b> CANNINGTON  47..63 HL Ring 8, 450 mLv Looking North
Designed	M.J.		
Reviewed	<i>[Signature]</i>	6/2/2002	
Geology			
Geotech	<i>[Signature]</i>	6/2/2002	
Supt	<i>[Signature]</i>	6/2/2002	
Approved	<i>[Signature]</i>	2/2/02	
Survey			

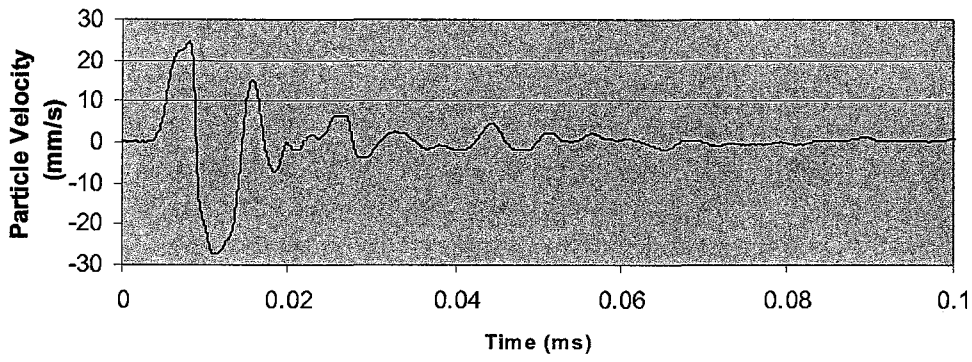
Scale: 1:250 Date:06-Feb-02

**Appendix D – Field Instrumentation Tests**

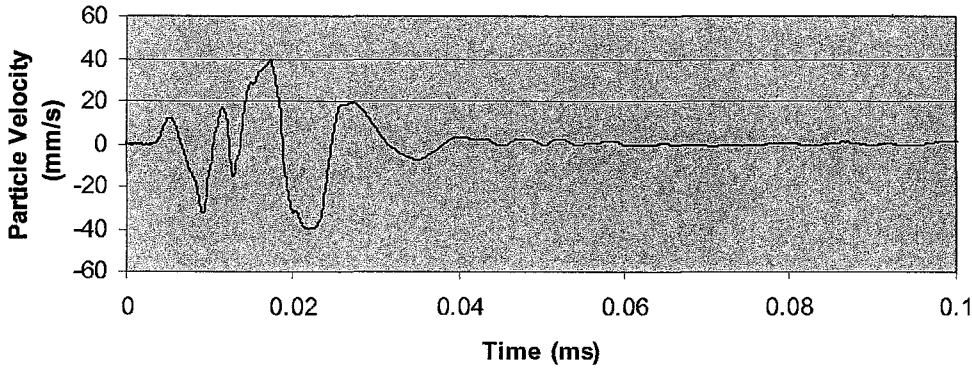
**Radial Direction**



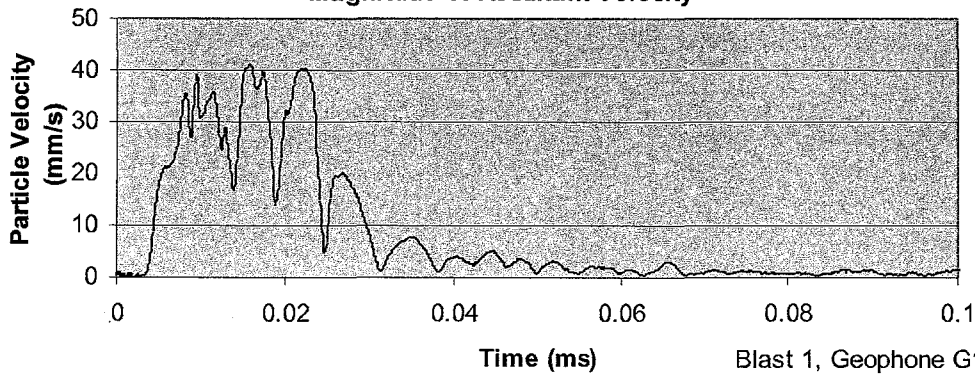
**Transverse Direction**



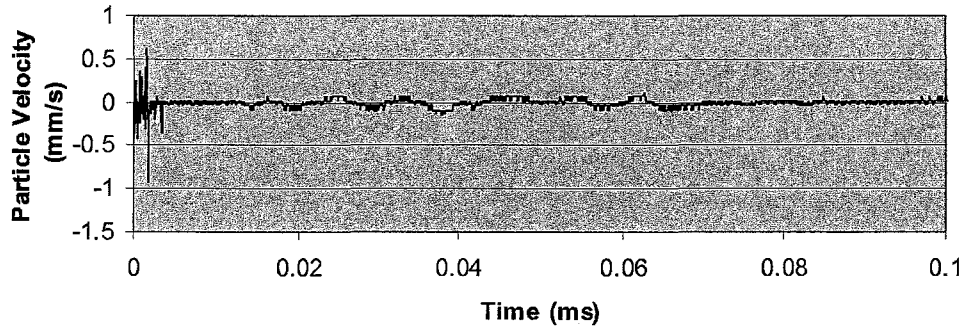
**Vertical Direction**



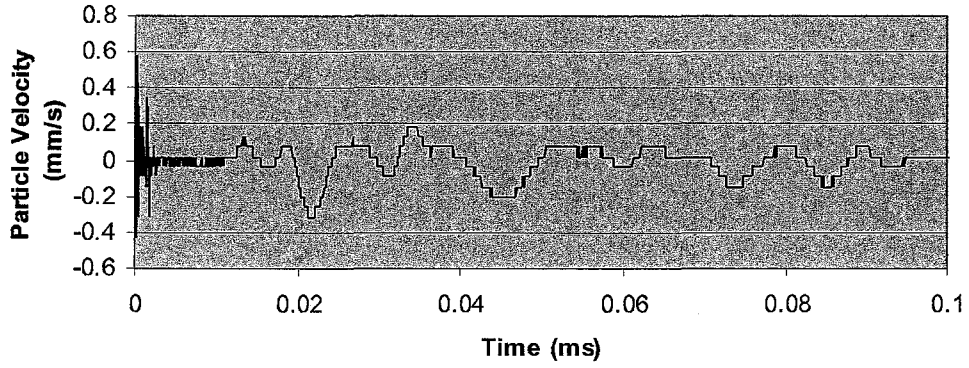
**Magnitude of Resultant Velocity**



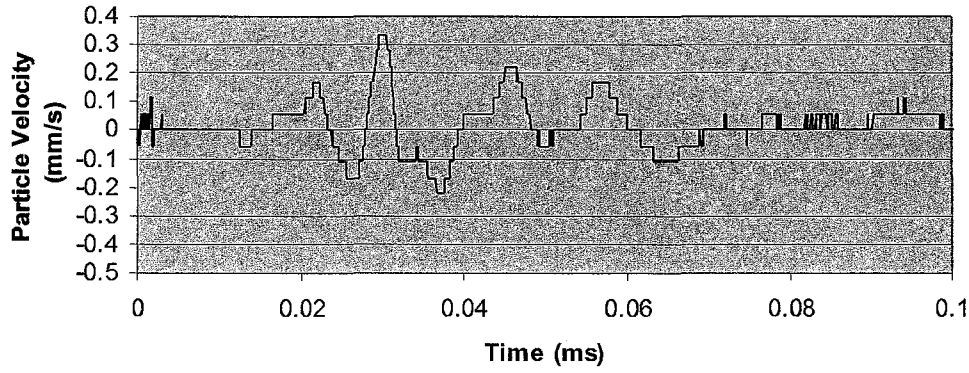
**Radial Direction**



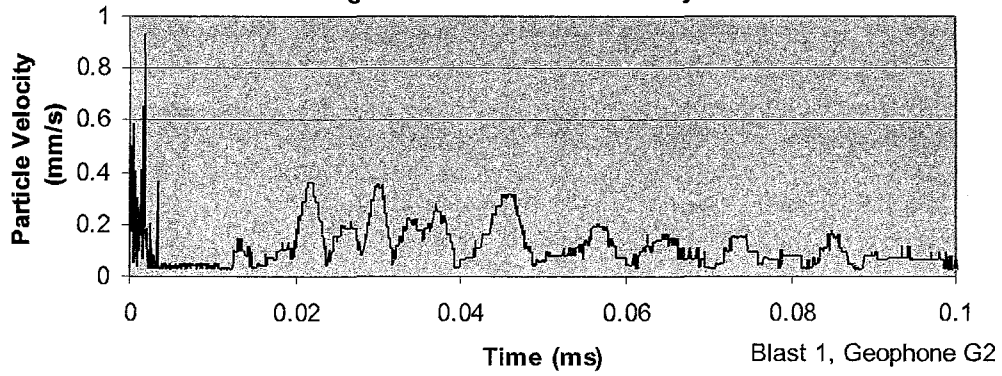
**Transverse Direction**



**Vertical Direction**



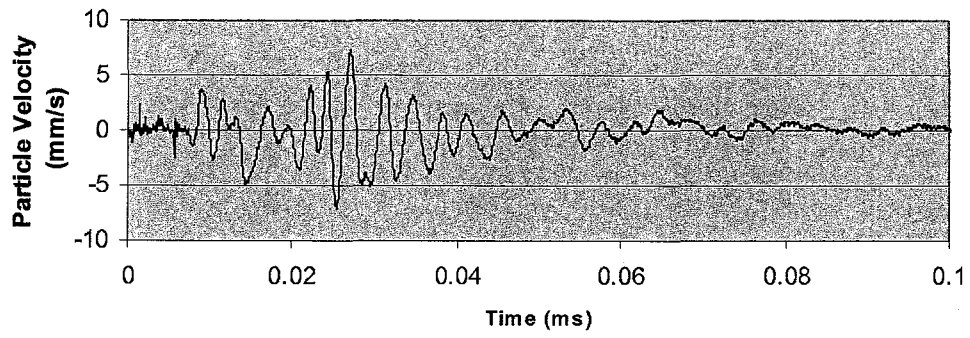
**Magnitude of Resultant Velocity**



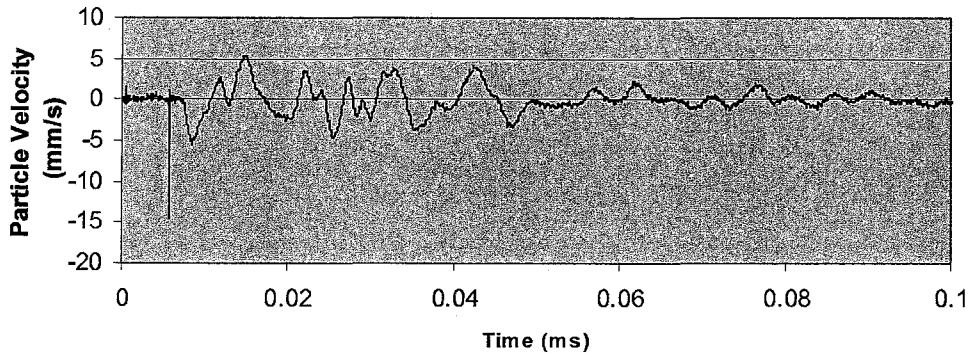
Blast 1, Geophone G2



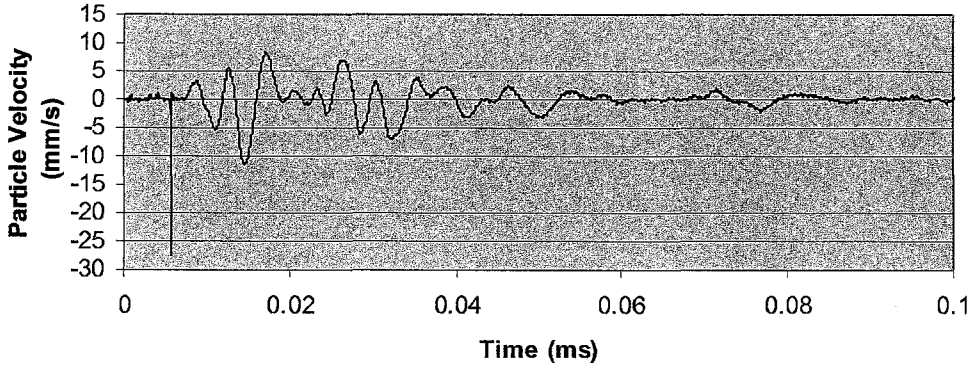
**Radial Direction**



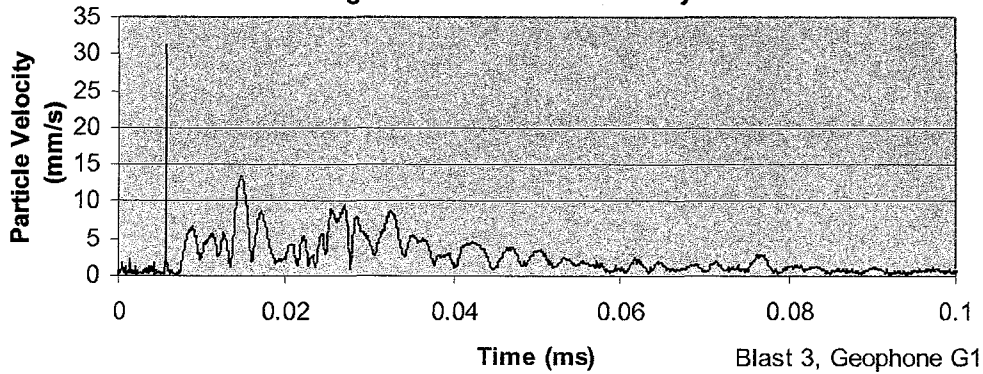
**Transverse Direction**



**Vertical Direction**

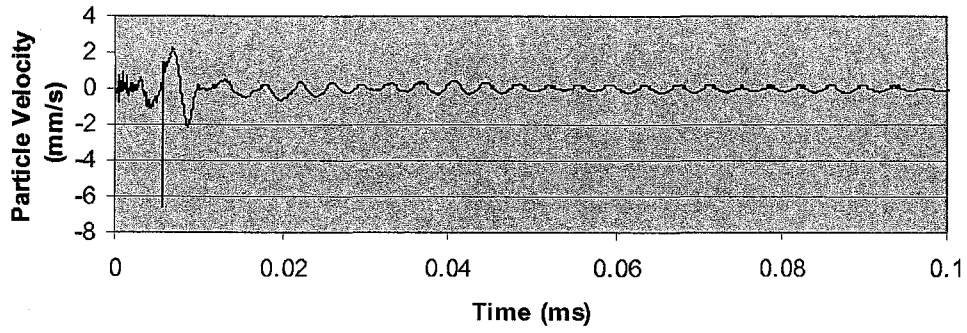


**Magnitude of Resultant Velocity**

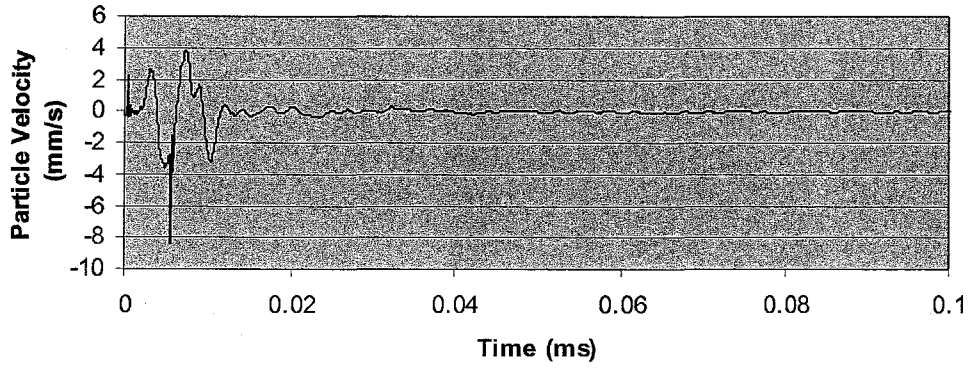


Blast 3, Geophone G1

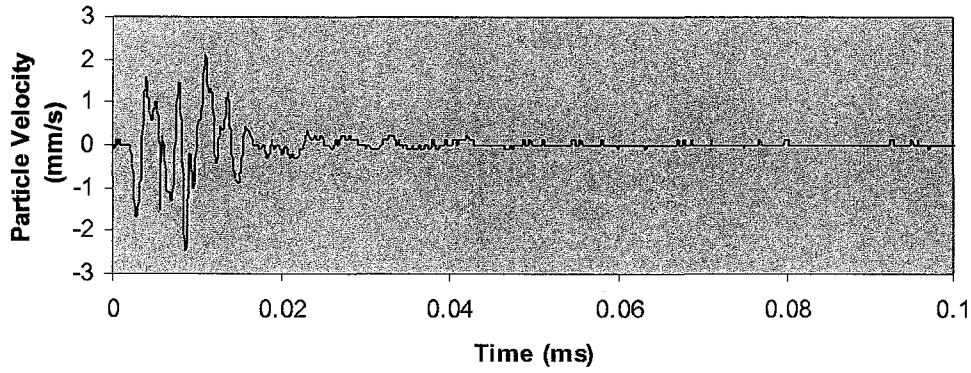
Radial Direction



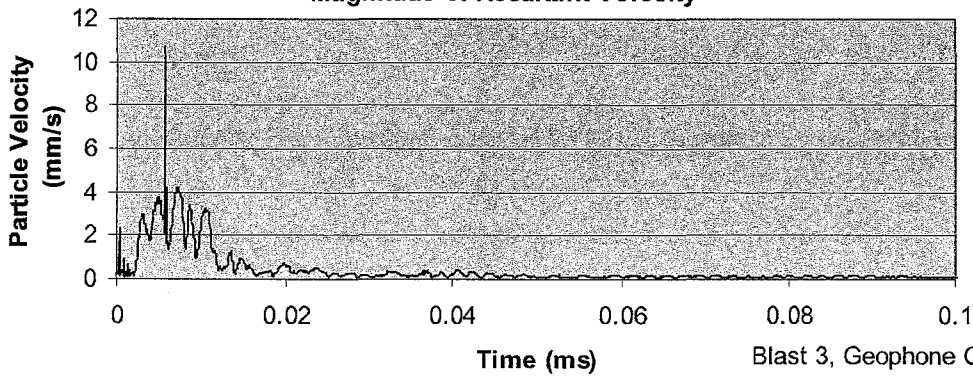
Transverse Direction



Vertical Direction

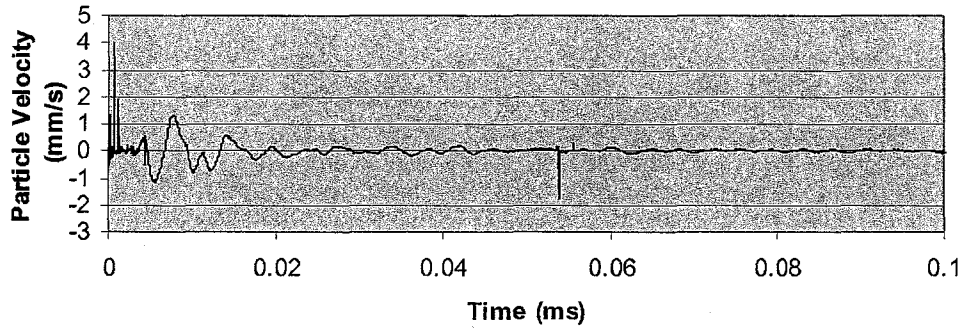


Magnitude of Resultant Velocity

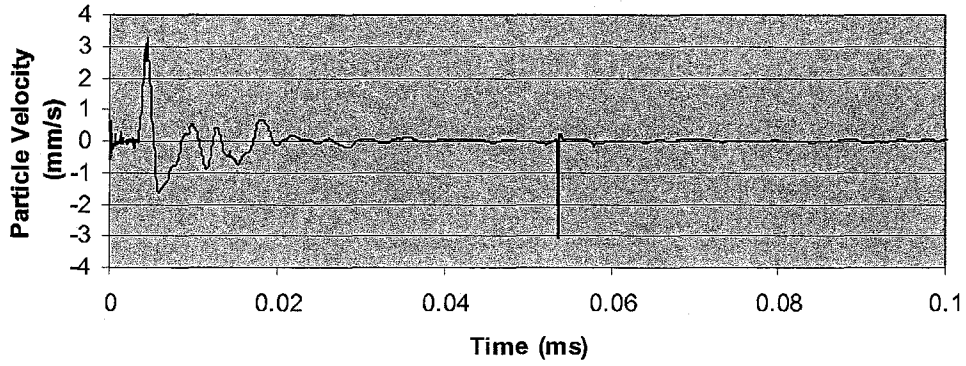


Blast 3, Geophone G2

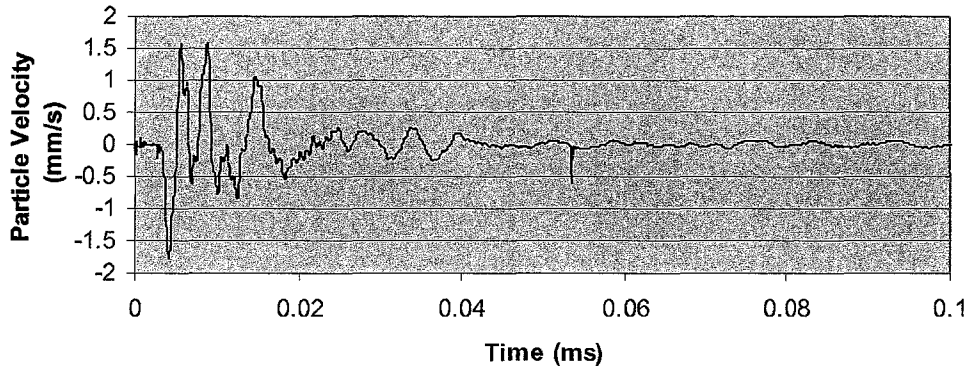
Radial Direction



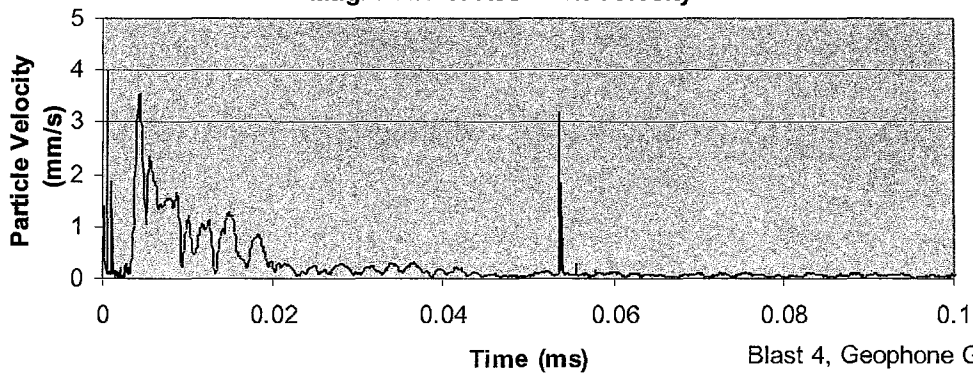
Transverse Direction



Vertical Direction

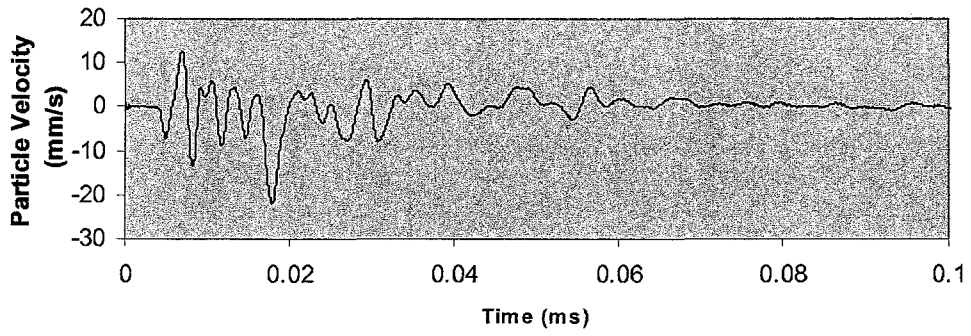


Magnitude of Resultant Velocity

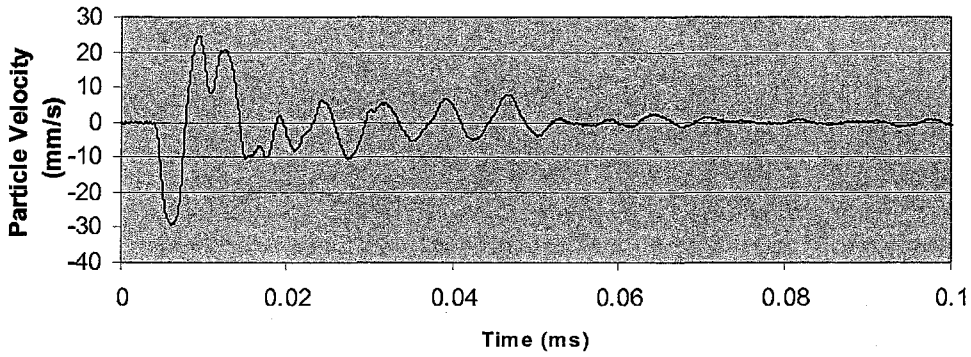


Blast 4, Geophone G2

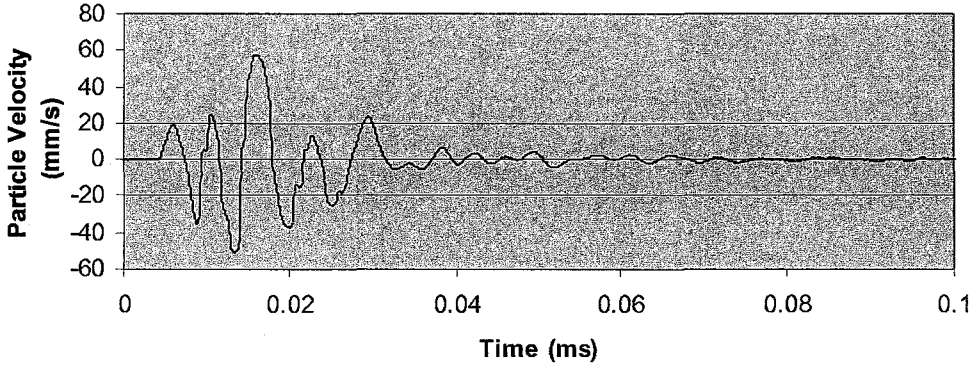
**Radial Direction**



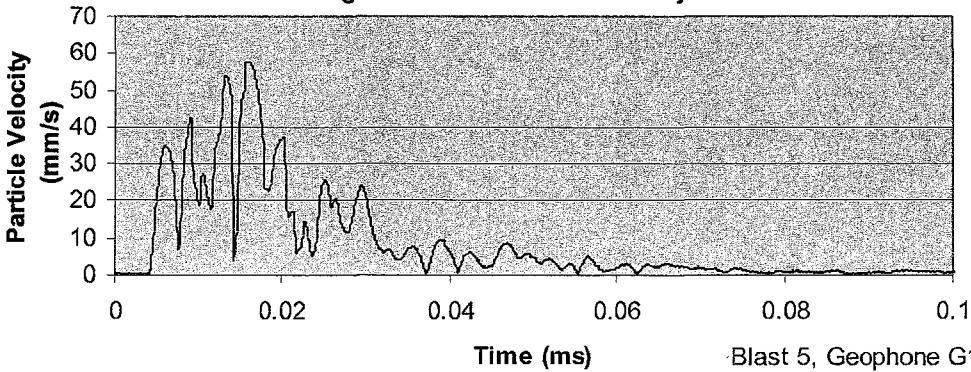
**Transverse Direction**



**Vertical Direction**

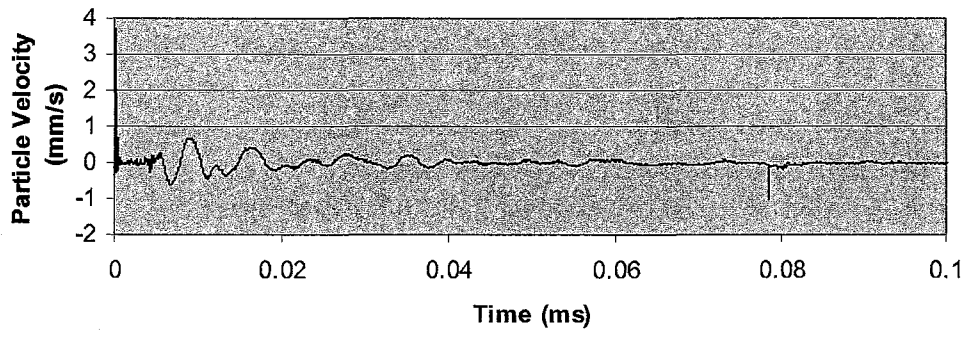


**Magnitude of Resultant Velocity**

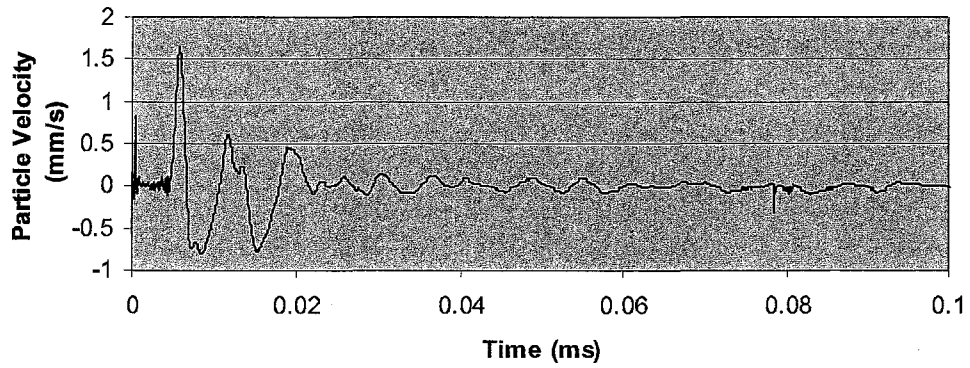


Blast 5, Geophone G1

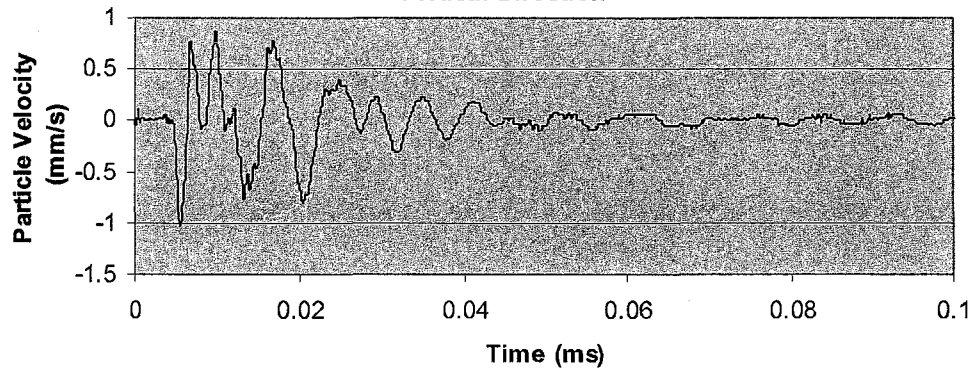
### Radial Direction



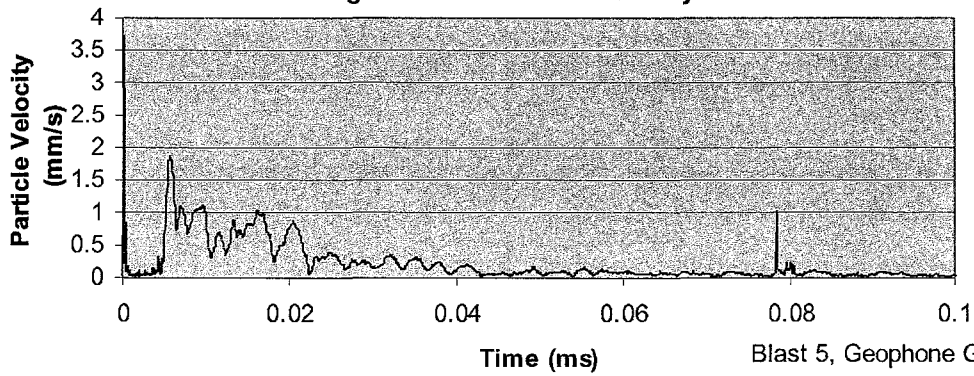
### Transverse Direction



### Vertical Direction

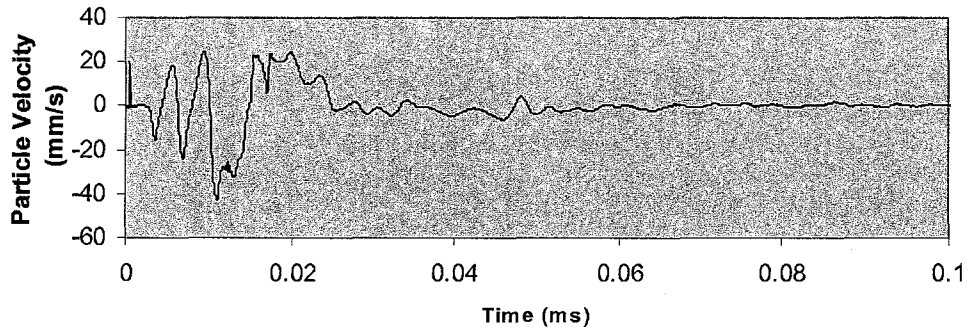


### Magnitude of Resultant Velocity

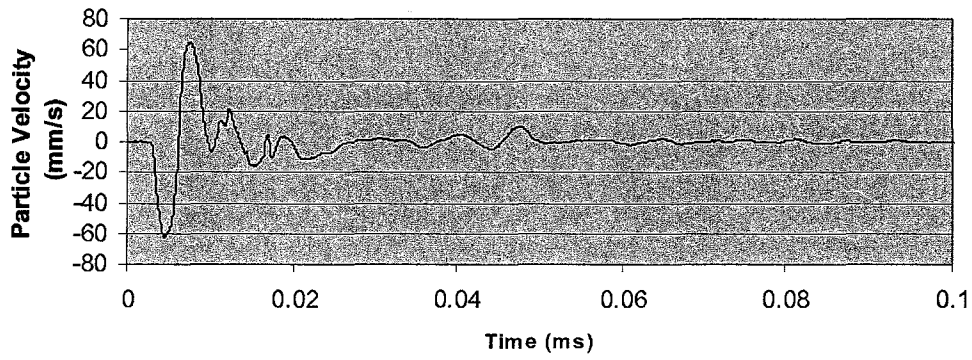


Blast 5, Geophone G2

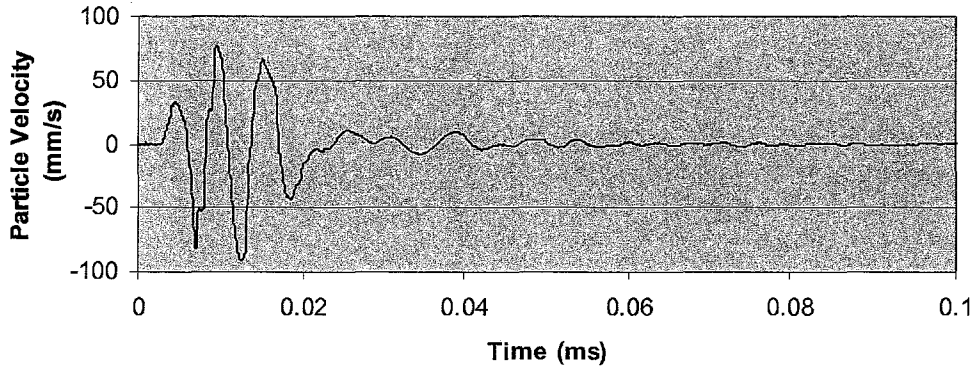
**Radial Direction**



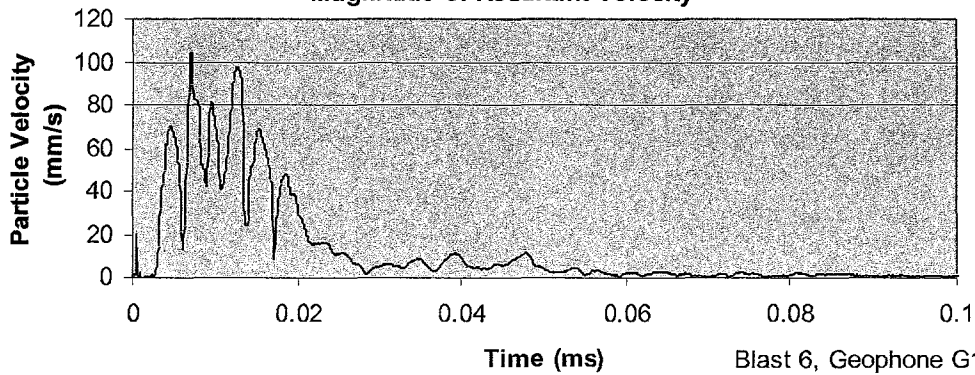
**Transverse Direction**



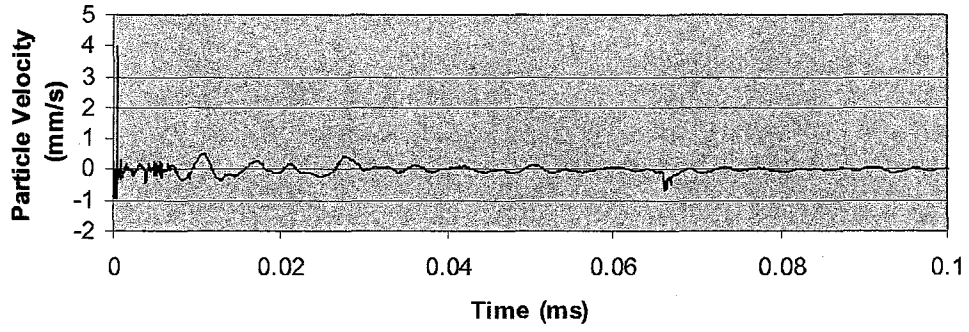
**Vertical Direction**



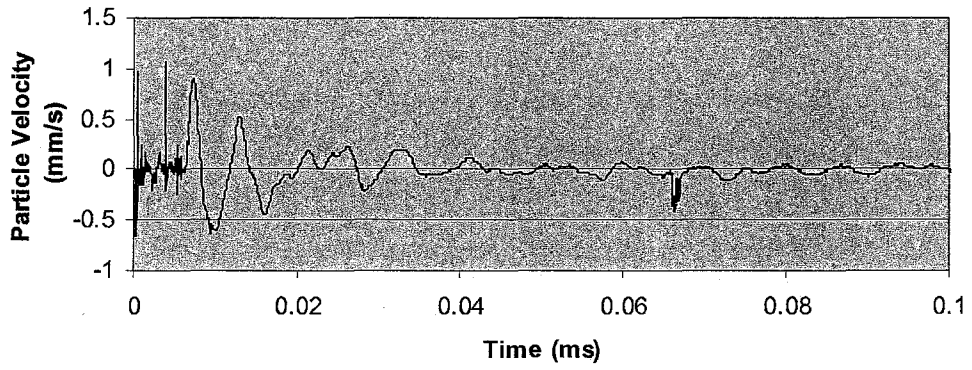
**Magnitude of Resultant Velocity**



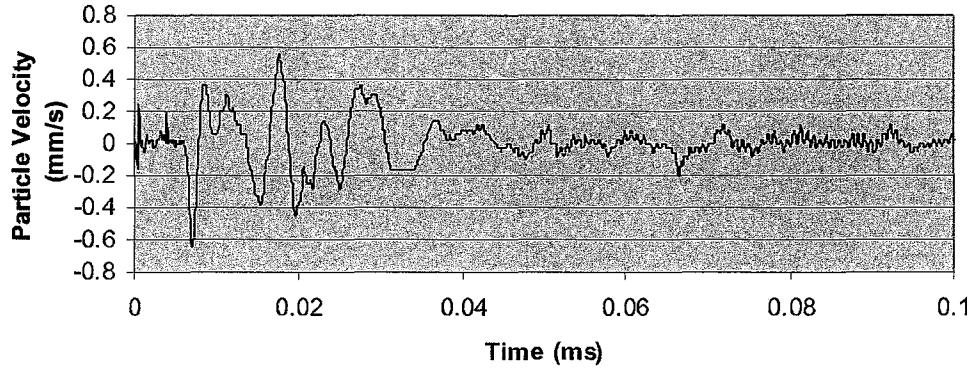
**Radial Direction**



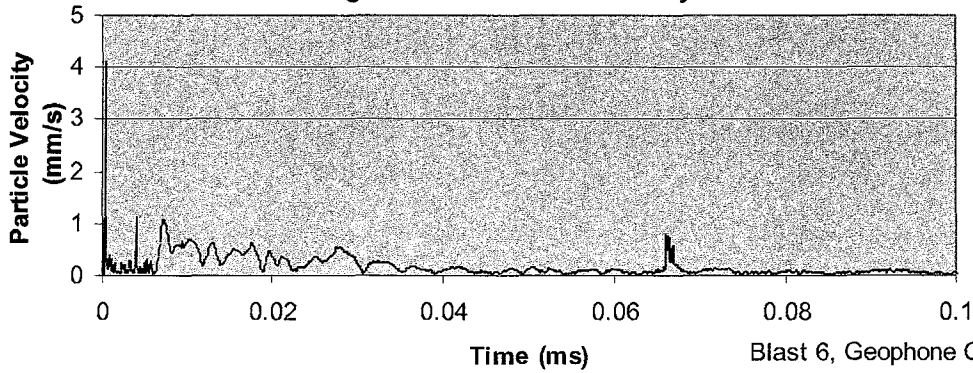
**Transverse Direction**



**Vertical Direction**

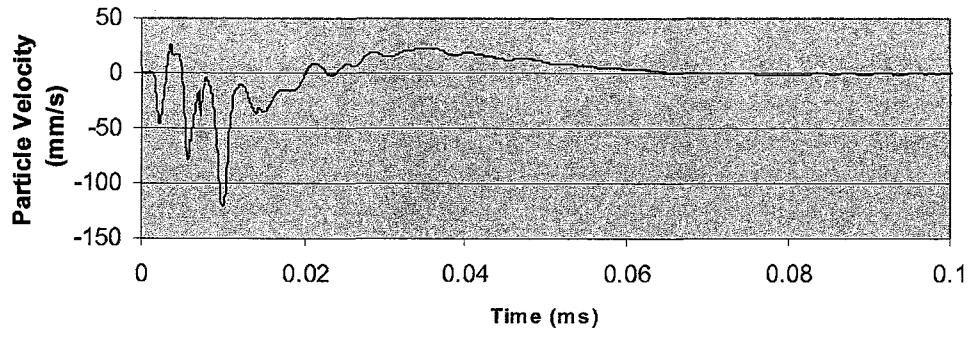


**Magnitude of Resultant Velocity**

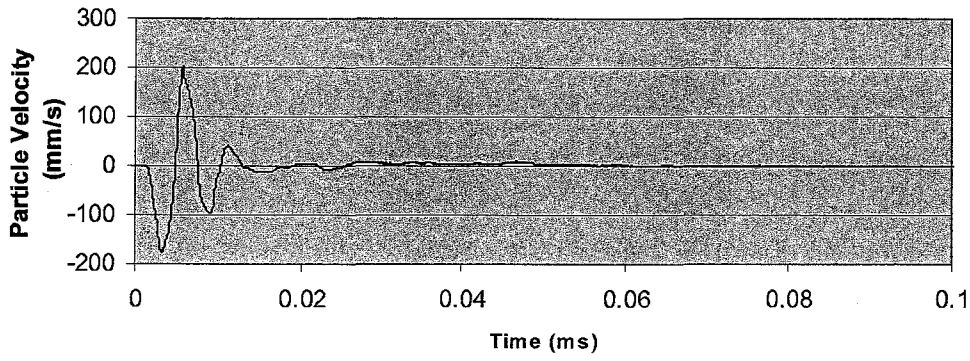


Blast 6, Geophone G2

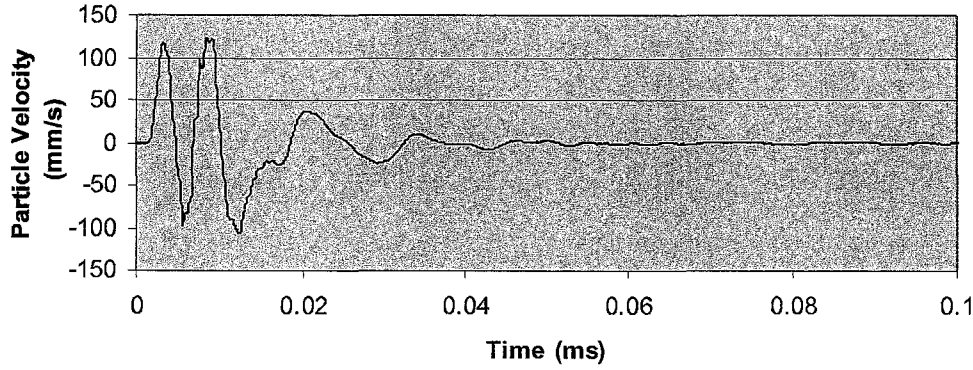
Radial Direction



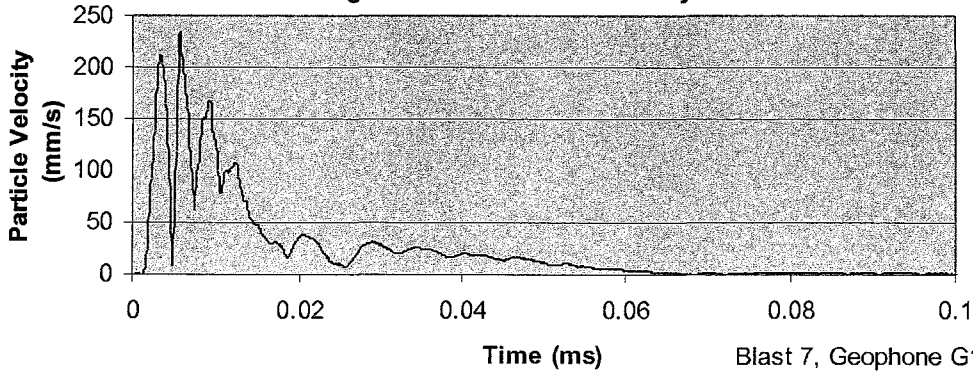
Transverse Direction



Vertical Direction



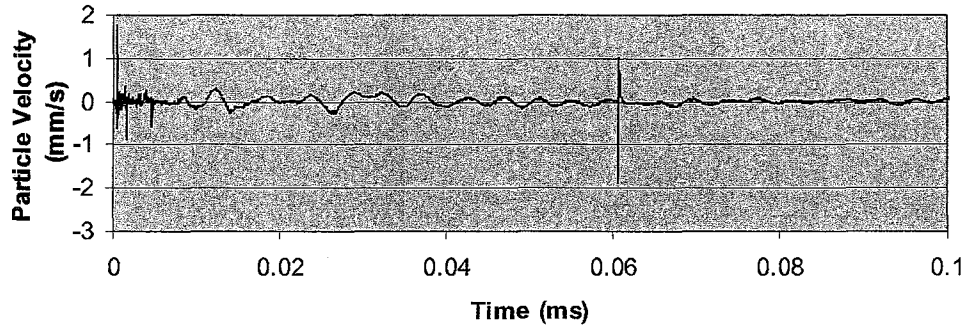
Magnitude of Resultant Velocity



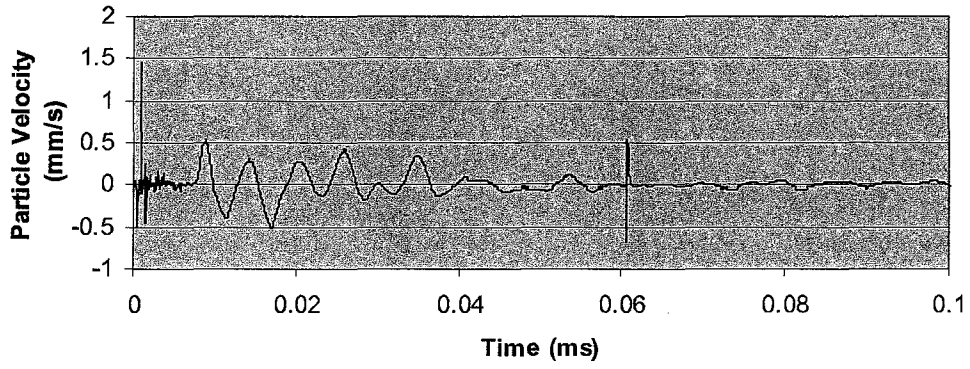
Blast 7, Geophone G1



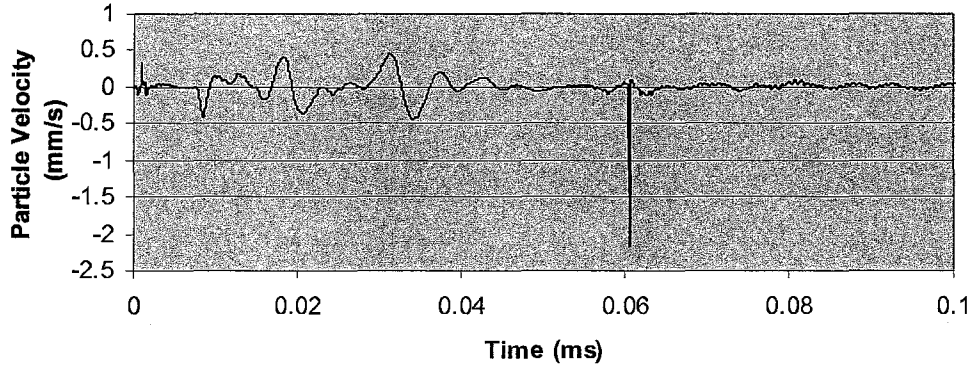
Radial Direction



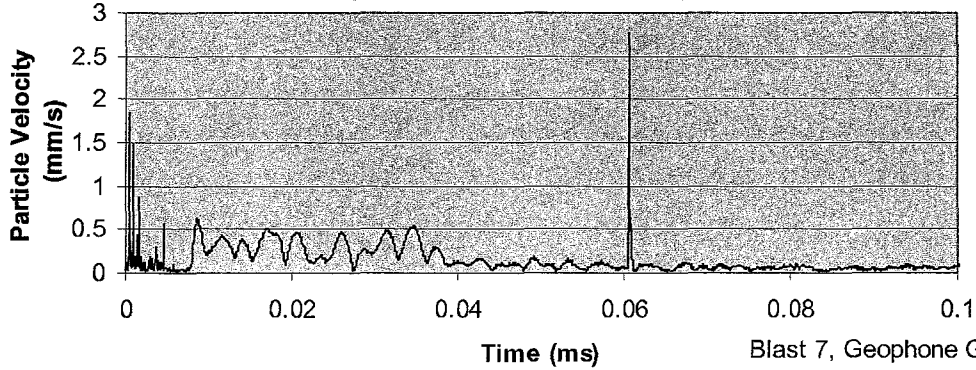
Transverse Direction



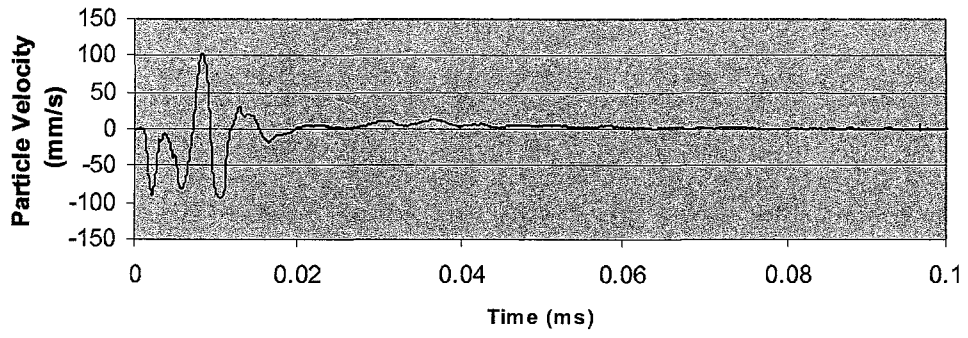
Vertical Direction



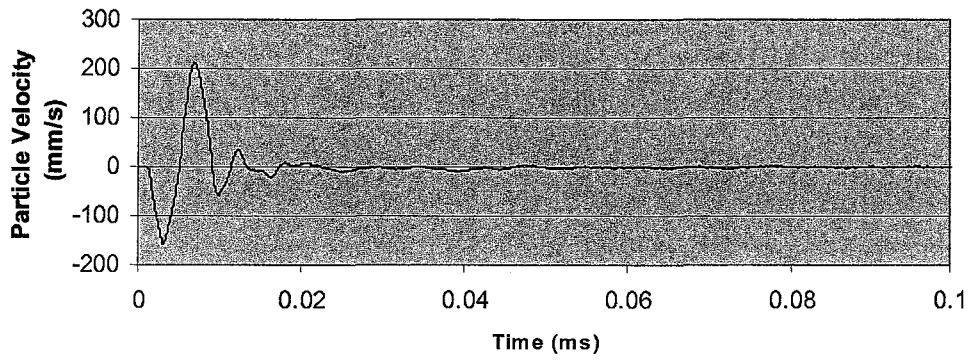
Magnitude of Resultant Velocity



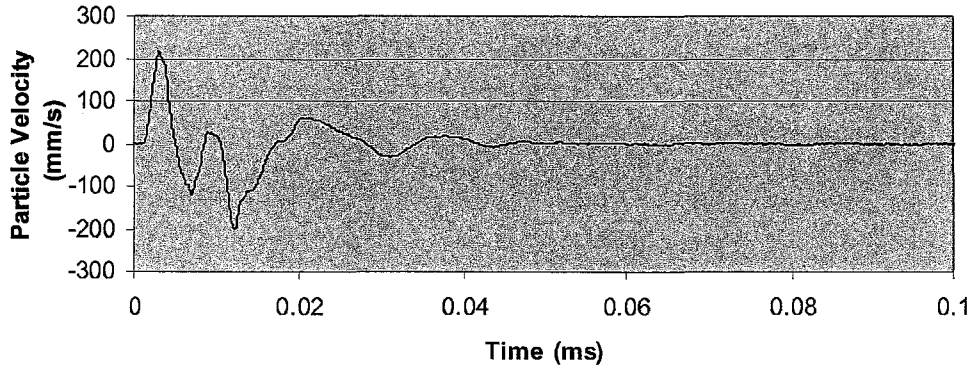
**Radial Direction**



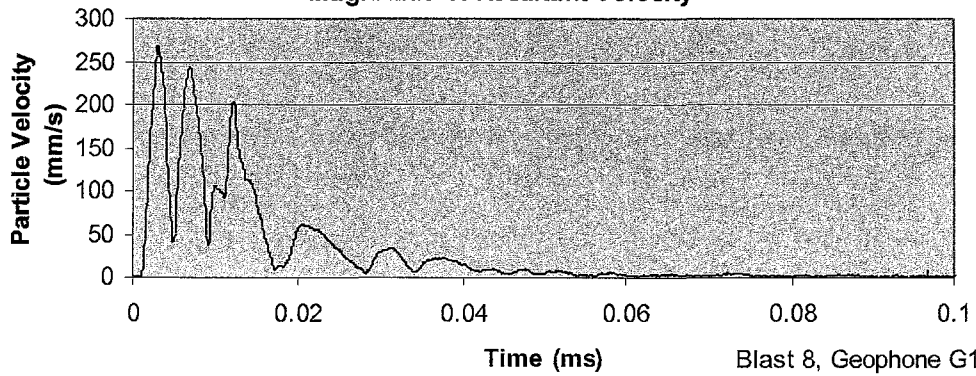
**Transverse Direction**



**Vertical Direction**

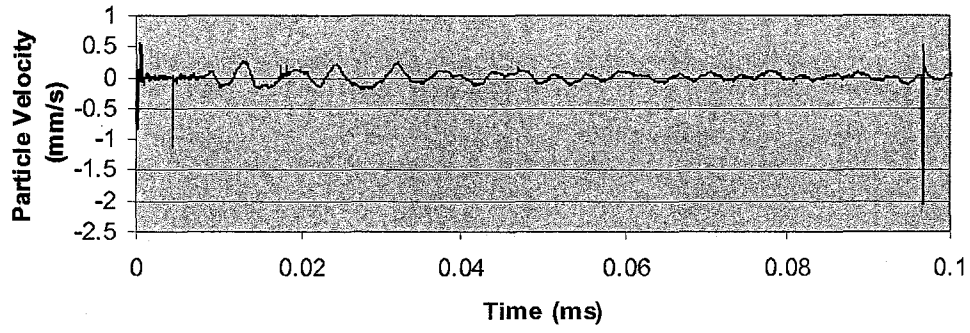


**Magnitude of Resultant Velocity**

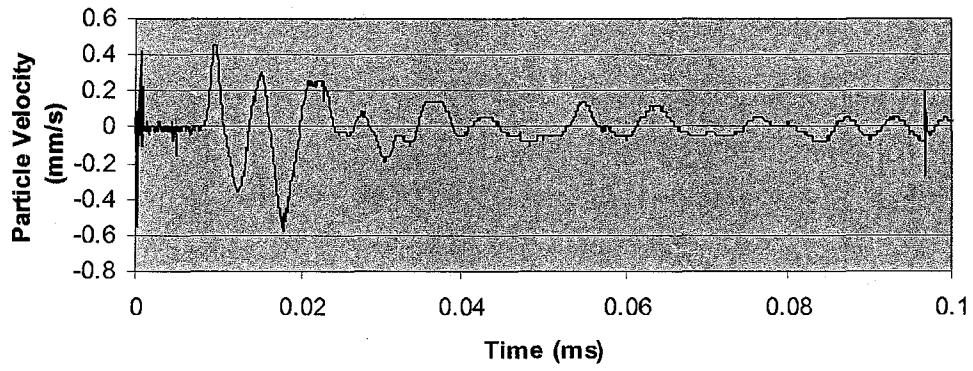


Blast 8, Geophone G1

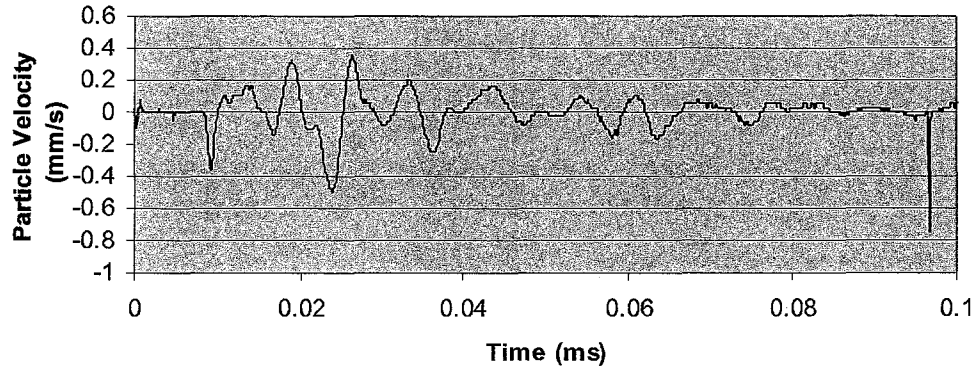
Radial Direction



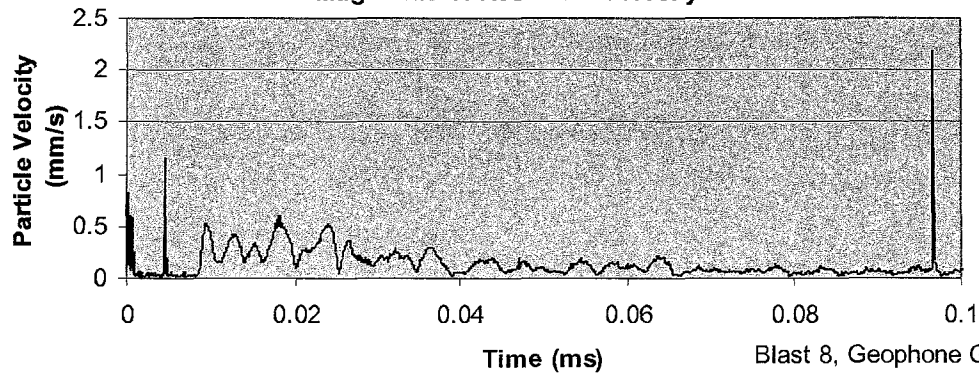
Transverse Direction



Vertical Direction

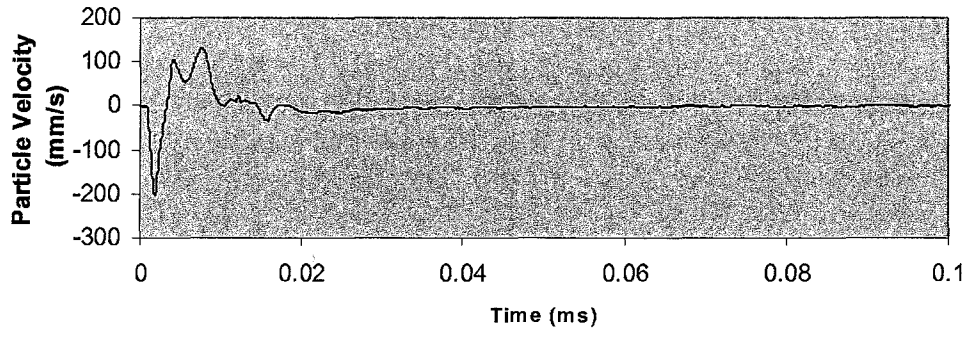


Magnitude of Resultant Velocity

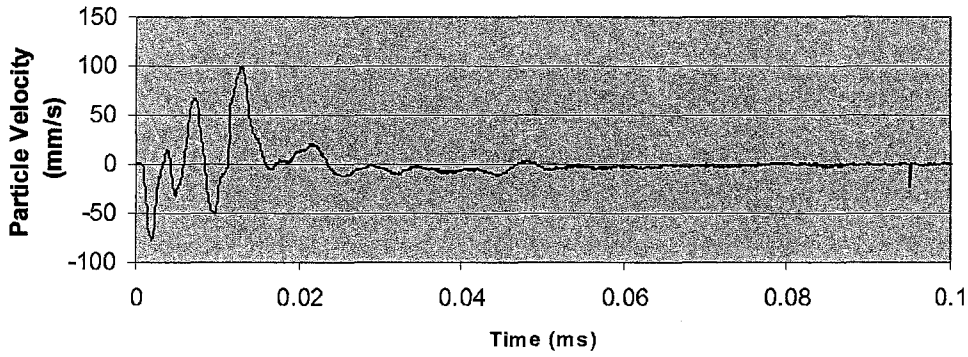


Blast 8, Geophone G2

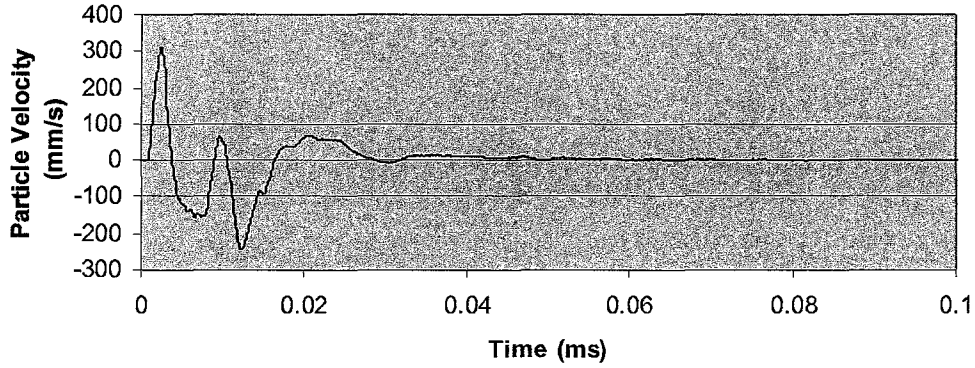
**Radial Direction**



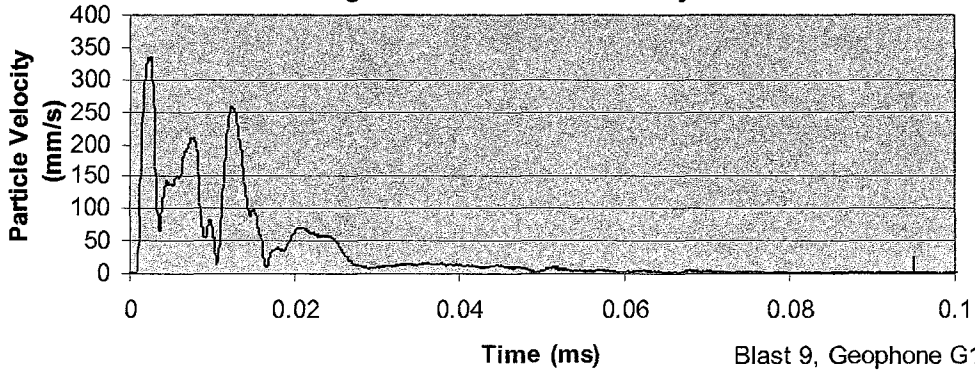
**Transverse Direction**



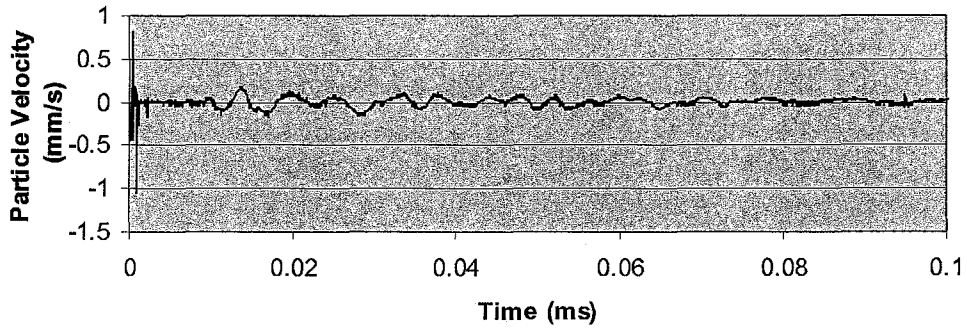
**Vertical Direction**



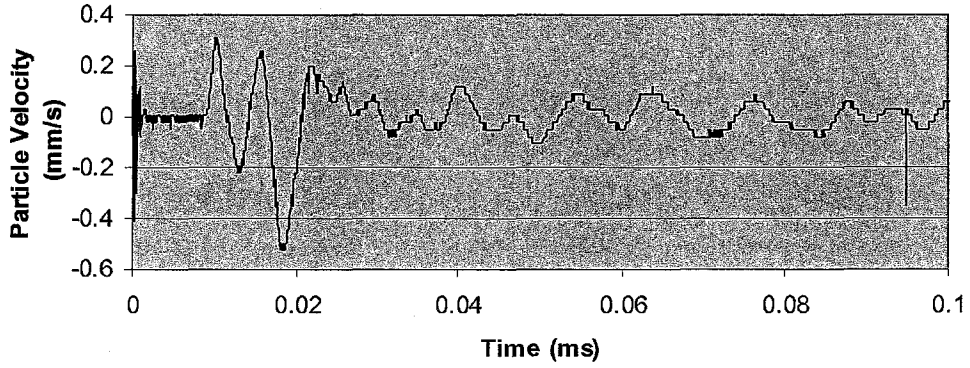
**Magnitude of Resultant Velocity**



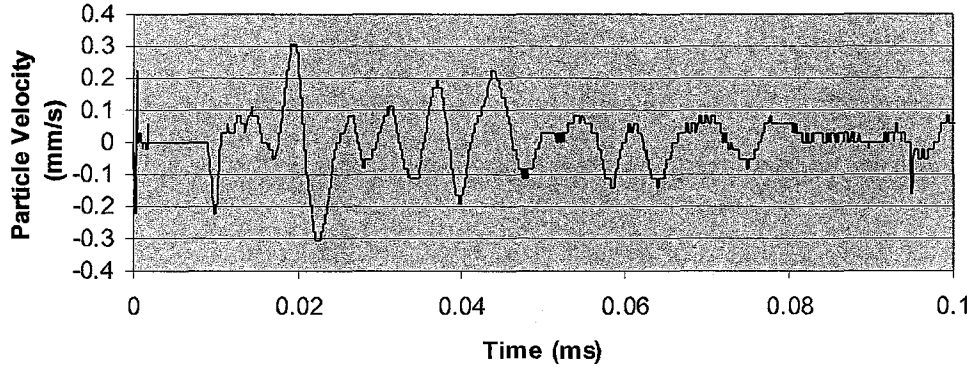
### Radial Direction



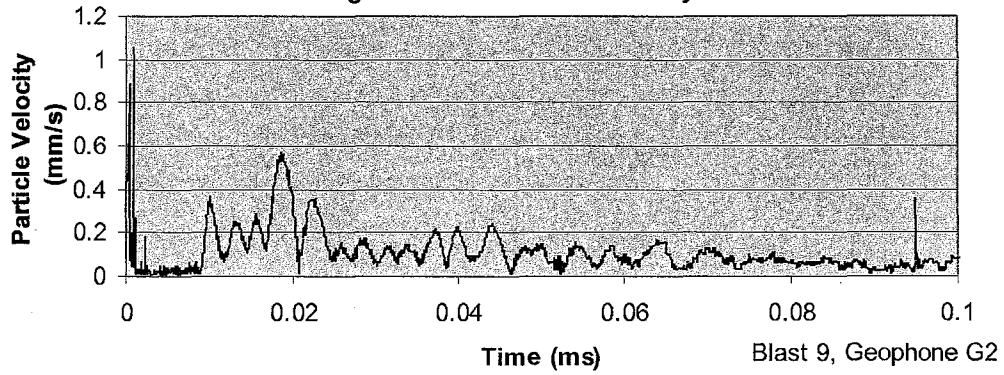
### Transverse Direction



### Vertical Direction



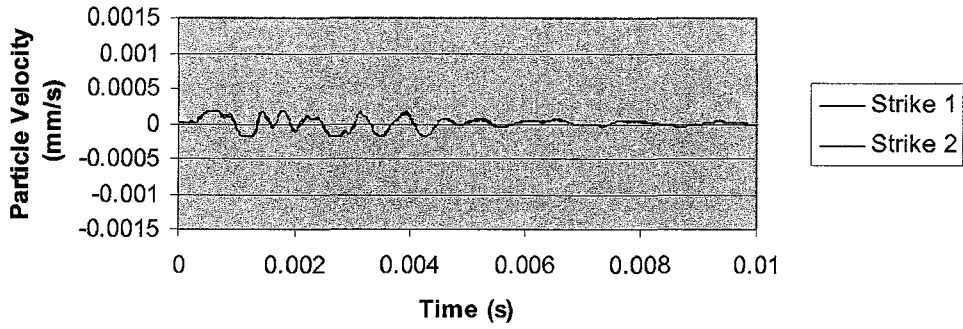
### Magnitude of Resultant Velocity



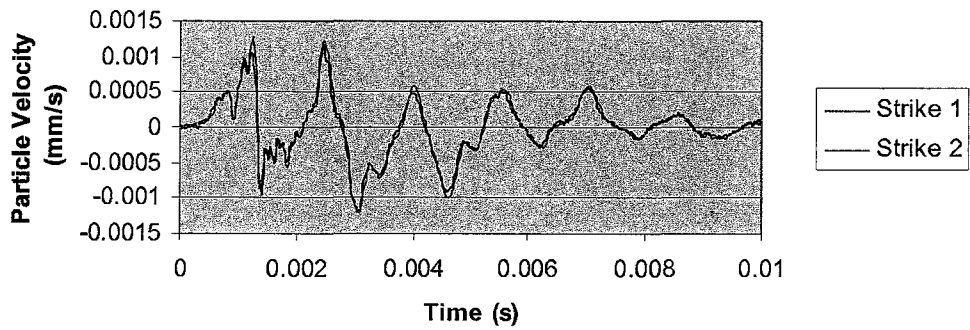
Blast 9, Geophone G2

**Appendix E – Waveforms Recorded in Laboratory Tests**

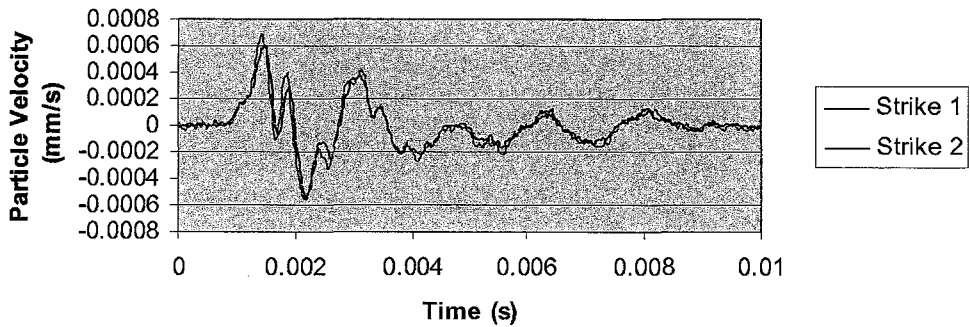
0.5 m from Hammer Strike



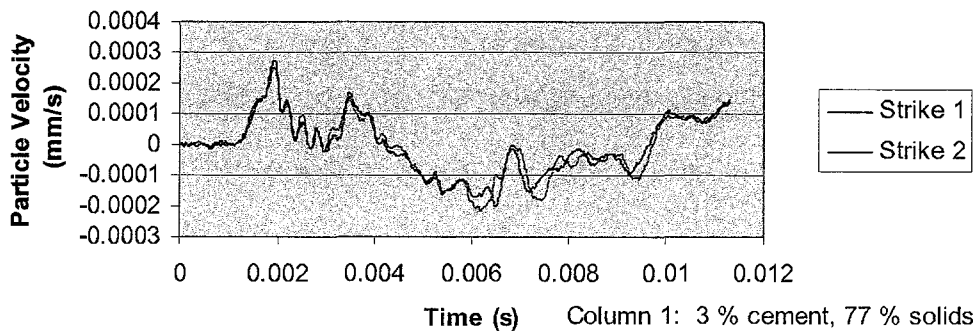
1.0 m from Hammer Strike



1.5 m from Hammer Strike



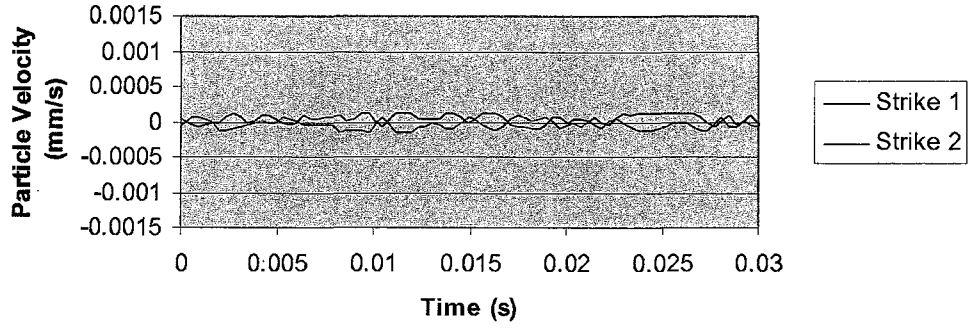
2.0 m from Hammer Strike



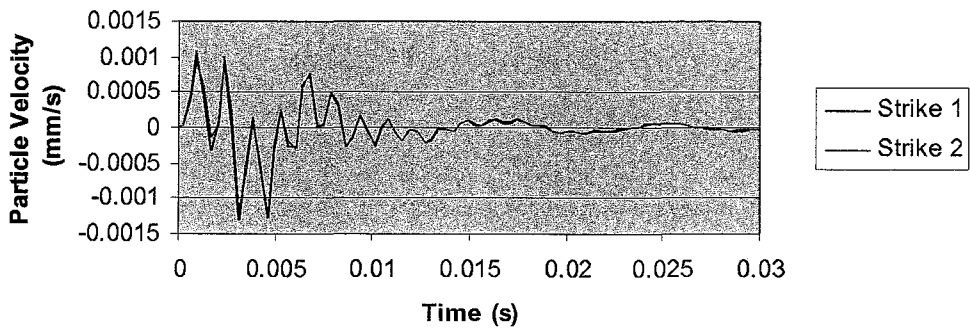
Column 1: 3 % cement, 77 % solids  
Curing age: 7 days

*Waveforms Recorded for Column 1 After 7 Days Curing Time*

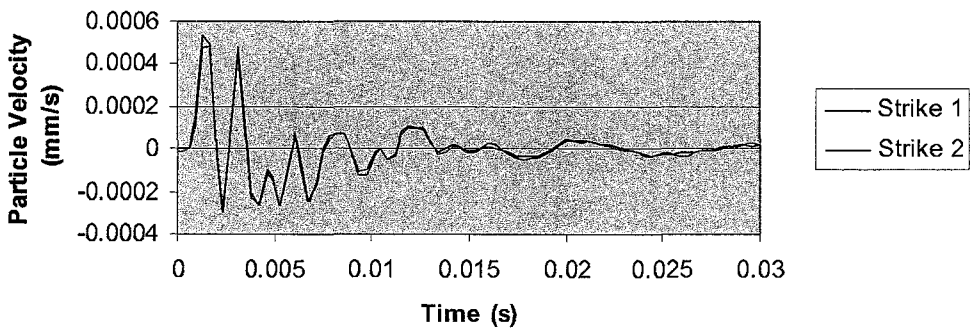
0.5 m from Hammer Strike



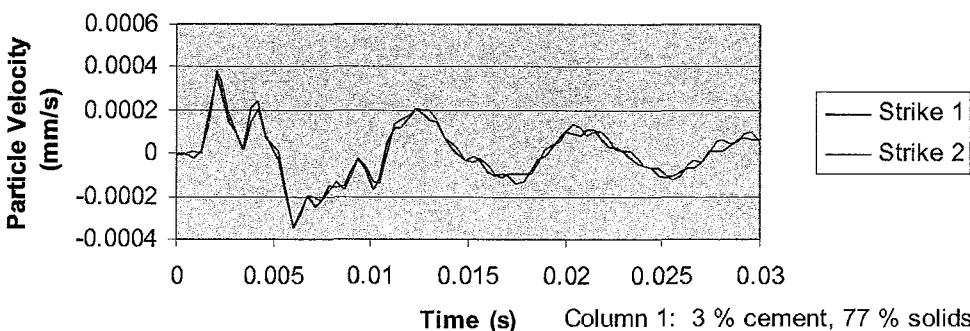
1.0 m from Hammer Strike



1.5 m from Hammer Strike



2.0 m from Hammer Strike

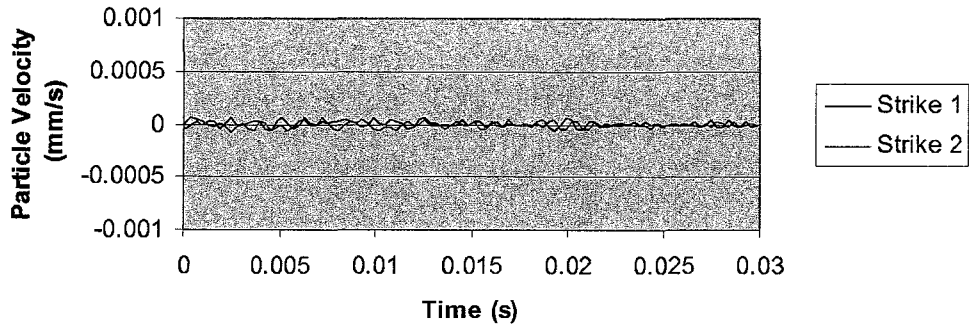


Column 1: 3 % cement, 77 % solids  
Curing age: 14 days

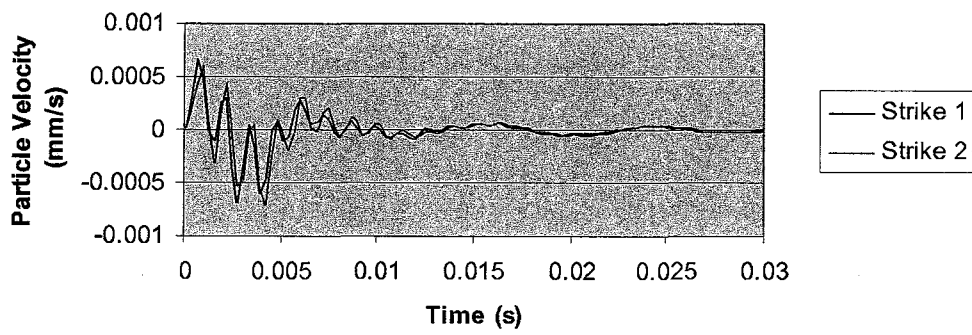
*Waveforms Recorded for Column 1 After 14 Days Curing Time*



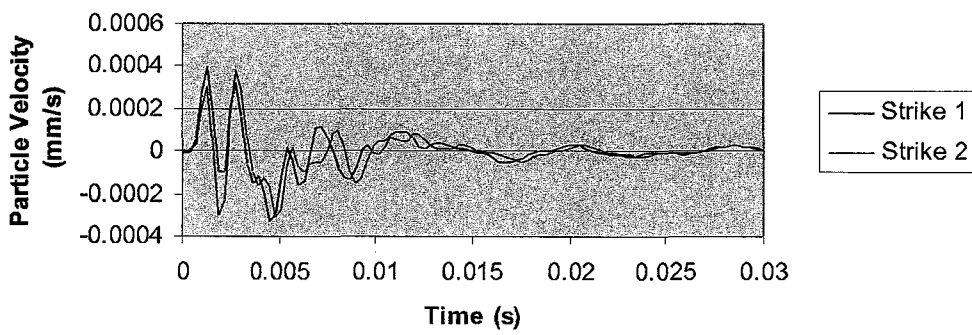
0.5 m from Hammer Strike



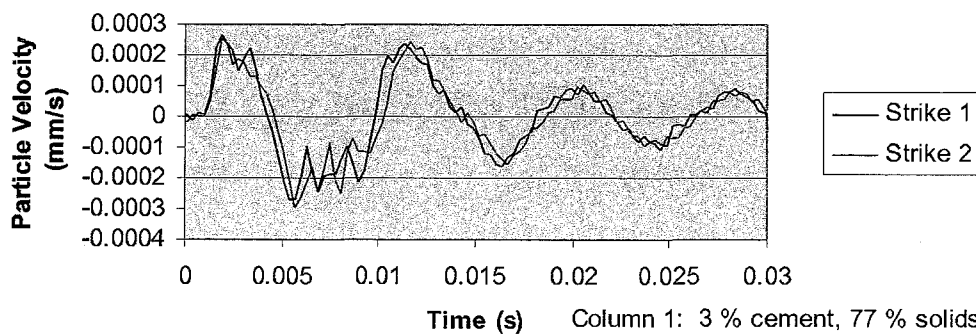
1.0 m from Hammer Strike



1.5 m from Hammer Strike



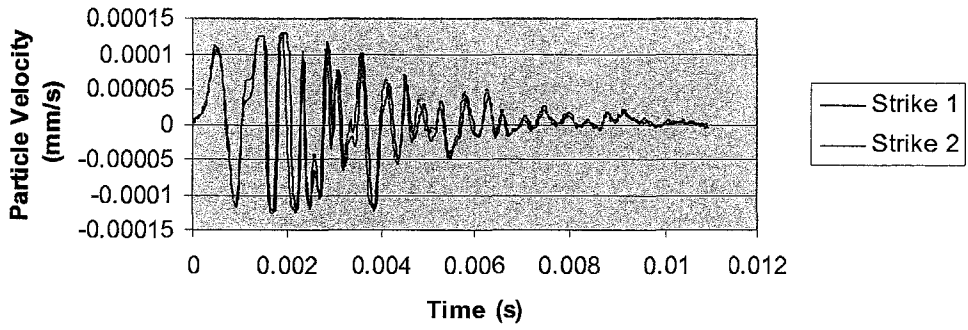
2.0 m from Hammer Strike



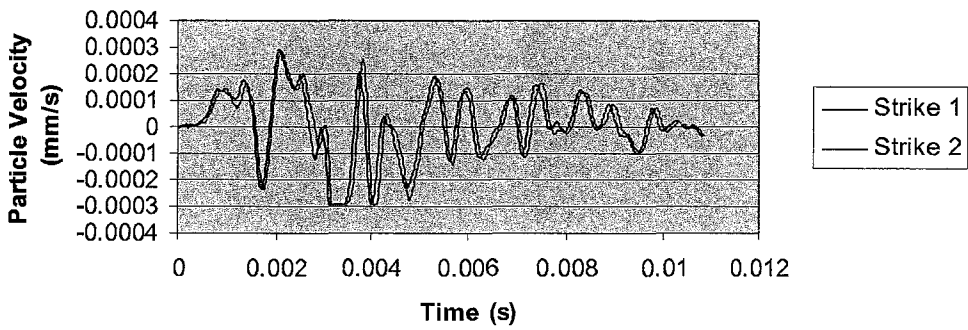
Column 1: 3 % cement, 77 % solids  
Curing age: 28 days

*Waveforms Recorded for Column 1 After 28 Days Curing Time*

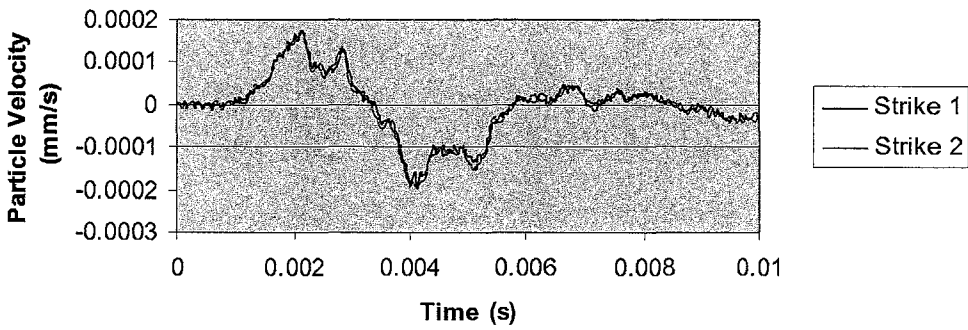
0.5 m from Hammer Strike



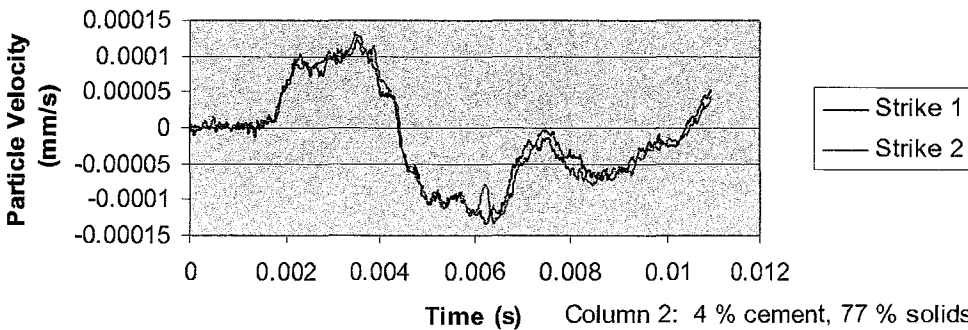
1.0 m from Hammer Strike



1.5 m from Hammer Strike



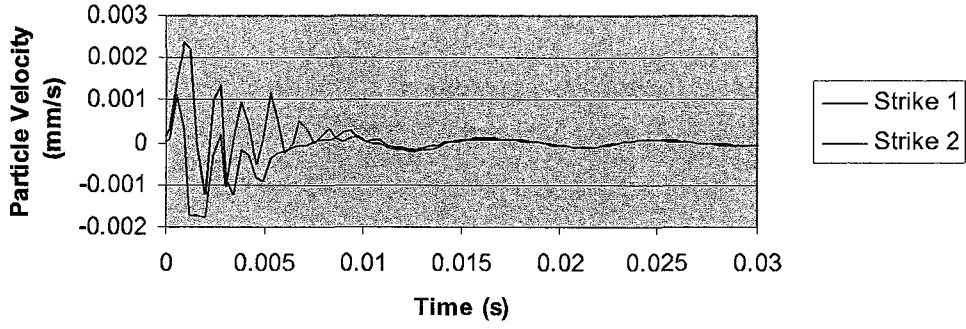
2.0 m from Hammer Strike



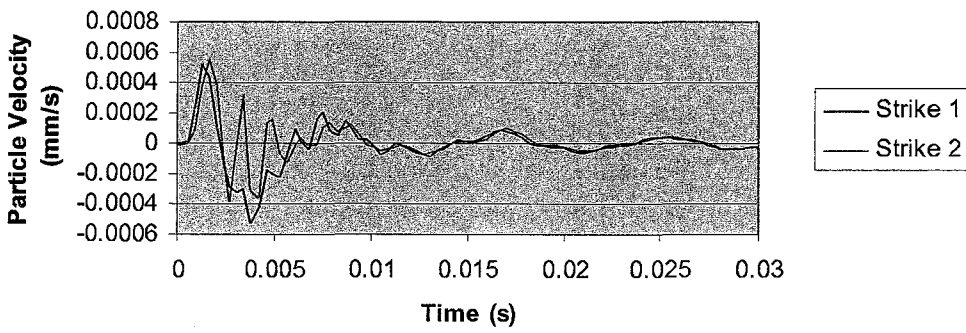
Column 2: 4 % cement, 77 % solids  
Curing age: 7 days

*Waveforms Recorded for Column 2 After 7 Days Curing Time*

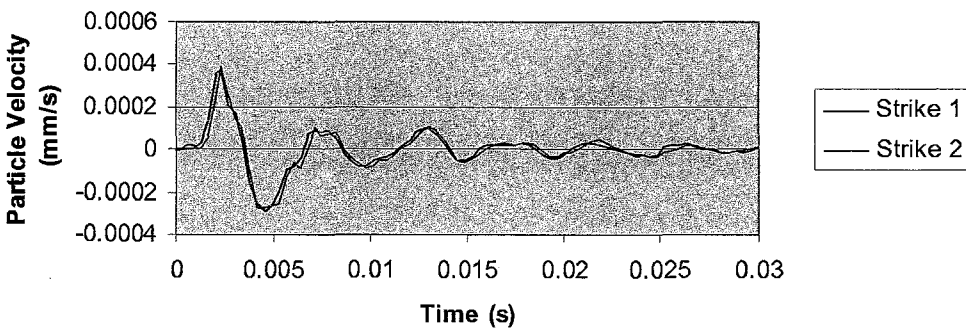
0.5 m from Hammer Strike



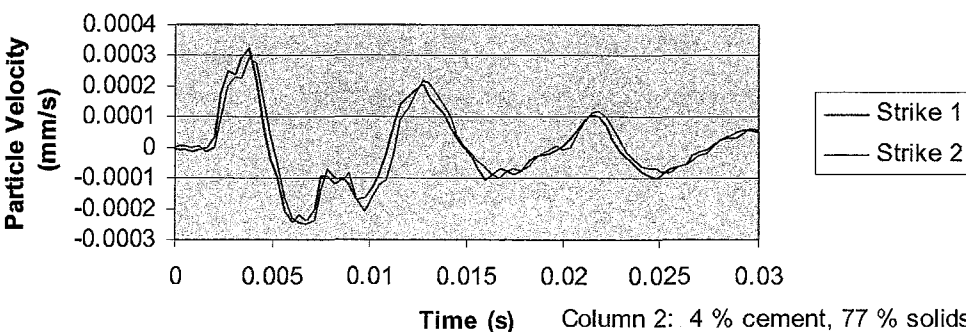
1.0 m from Hammer Strike



1.5 m from Hammer Strike



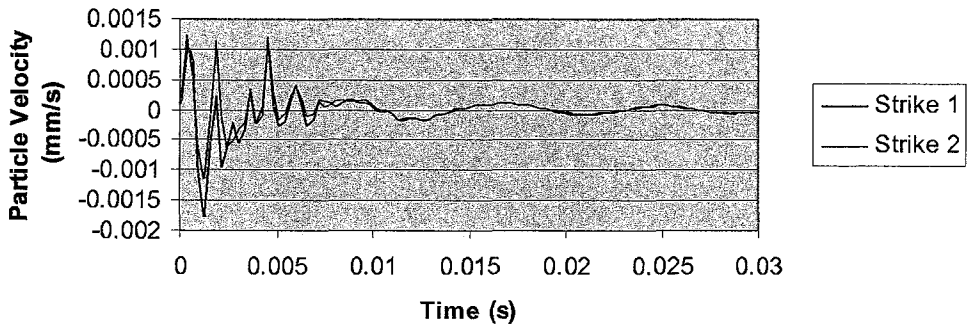
2.0 m from Hammer Strike



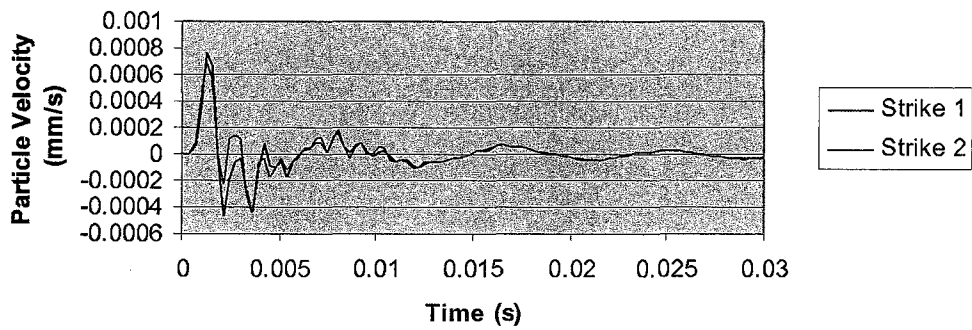
Column 2: 4 % cement, 77 % solids  
Curing age: 14 days

*Waveforms Recorded for Column 2 After 14 Days Curing Time*

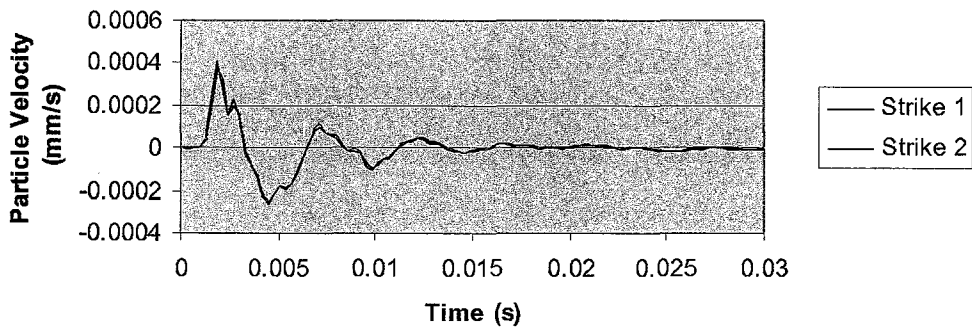
0.5 m from Hammer Strike



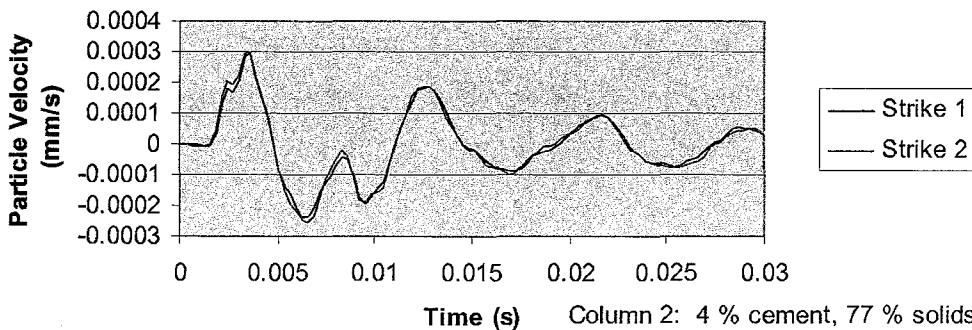
1.0 m from Hammer Strike



1.5 m from Hammer Strike



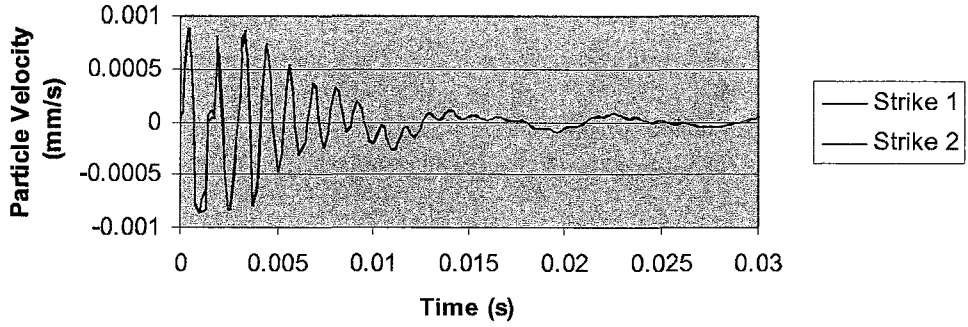
2.0 m from Hammer Strike



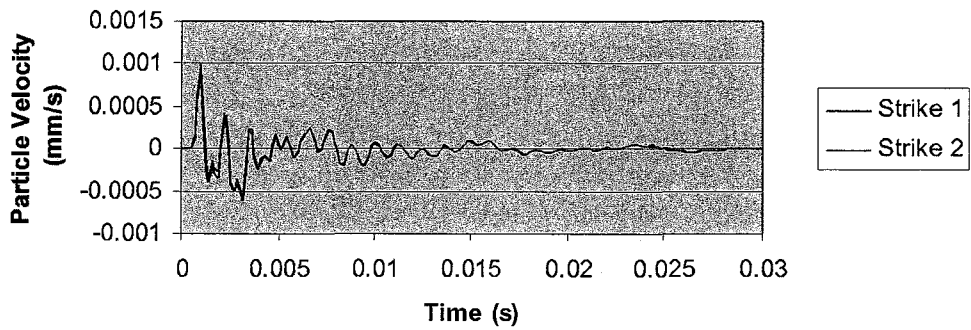
Column 2: 4 % cement, 77 % solids  
Curing age: 28 days

*Waveforms Recorded for Column 2 After 28 Days Curing Time*

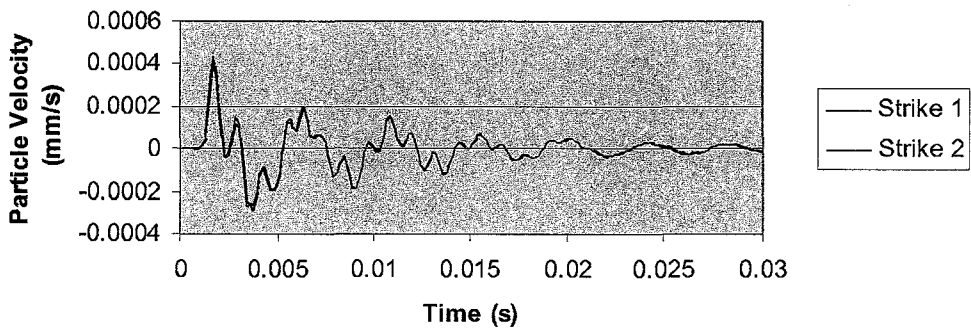
0.5 m from Hammer Strike



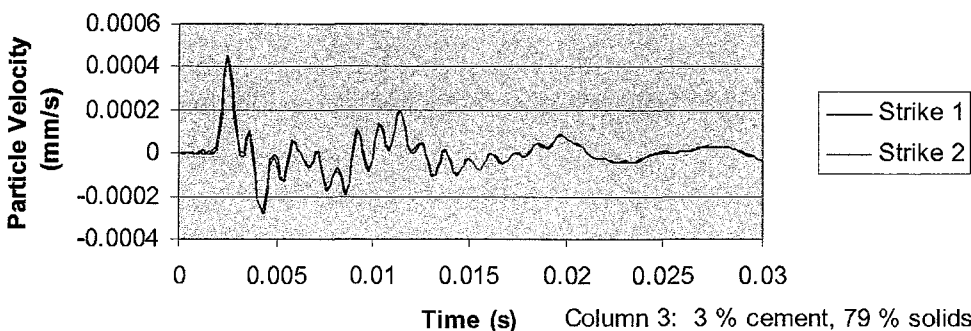
1.0 m from Hammer Strike



1.5 m from Hammer Strike



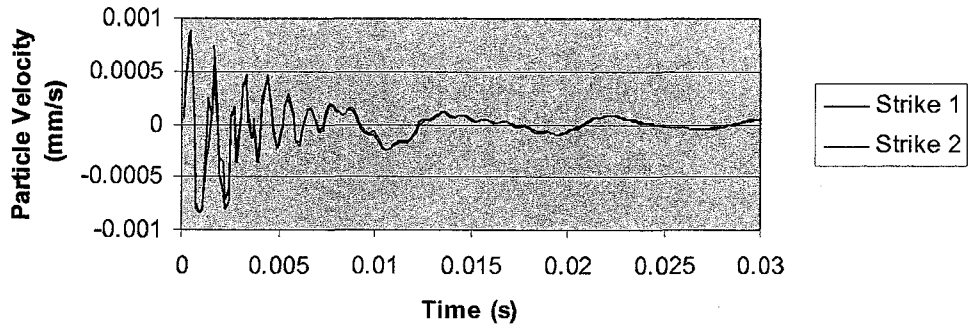
2.0 m from Hammer Strike



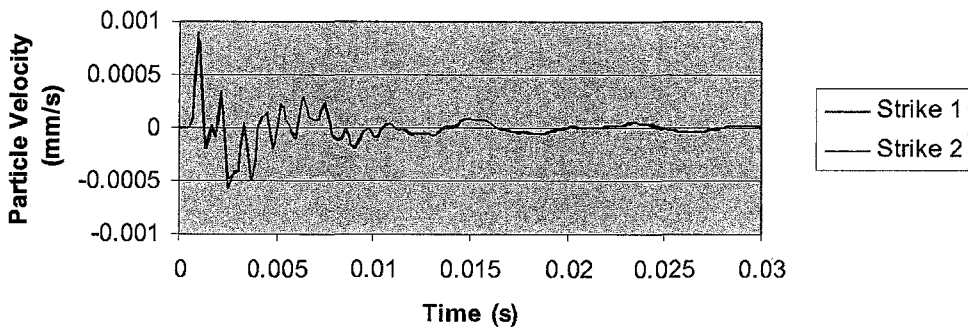
Column 3: 3 % cement, 79 % solids  
Curing age: 7 days

*Waveforms Recorded for Column 3 After 7 Days Curing Time*

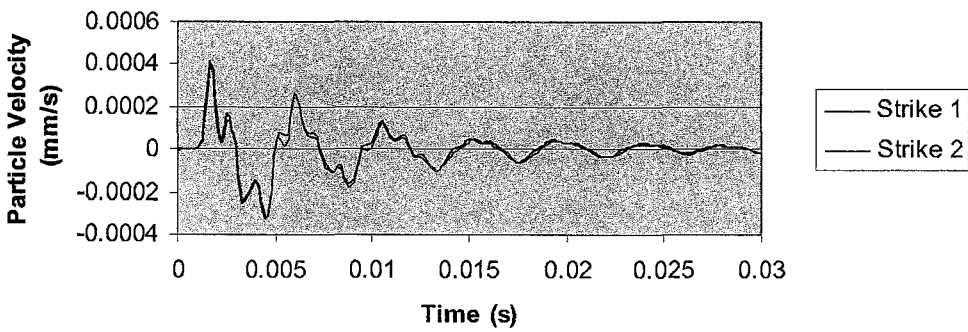
0.5 m from Hammer Strike



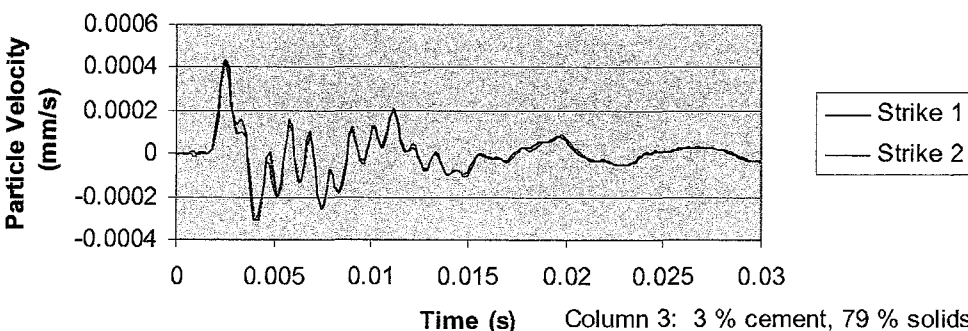
1.0 m from Hammer Strike



1.5 m from Hammer Strike



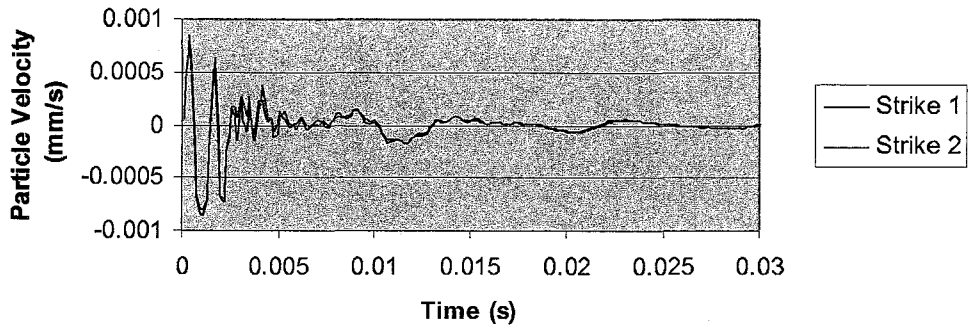
2.0 m from Hammer Strike



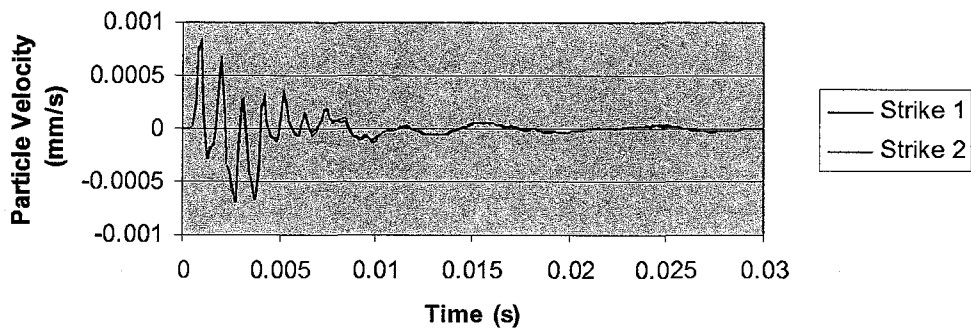
Column 3: 3 % cement, 79 % solids  
Curing age: 14 days

*Waveforms Recorded for Column 3 After 14 Days Curing Time*

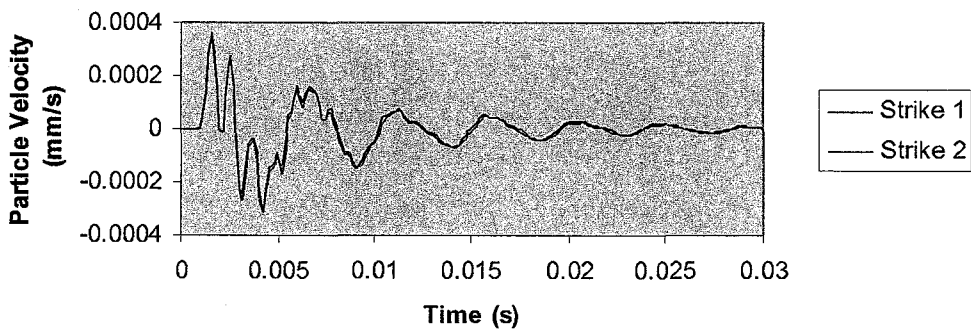
0.5 m from Hammer Strike



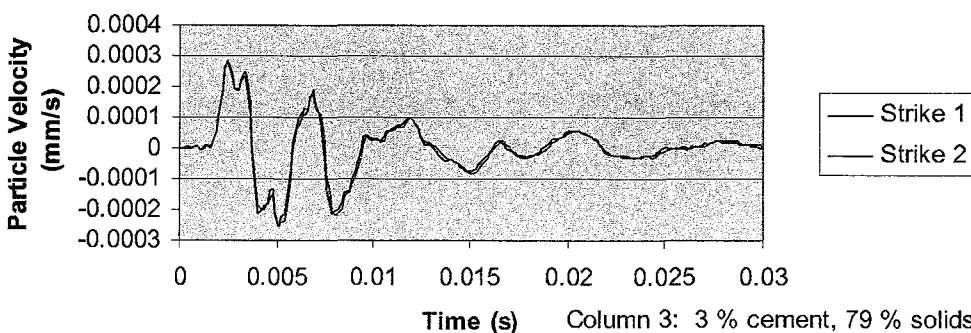
1.0 m from Hammer Strike



1.5 m from Hammer Strike



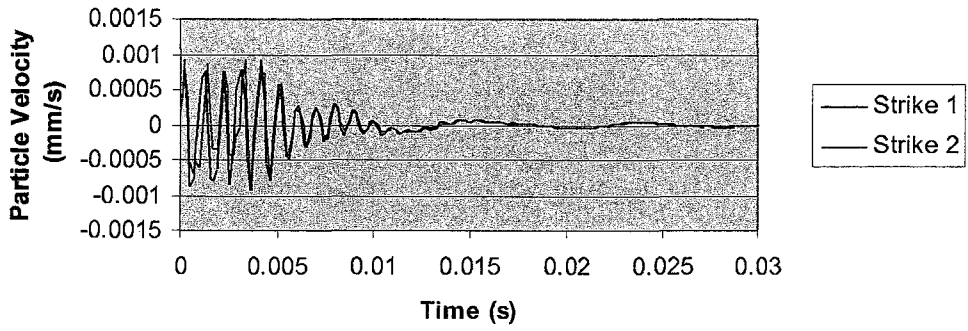
2.0 m from Hammer Strike



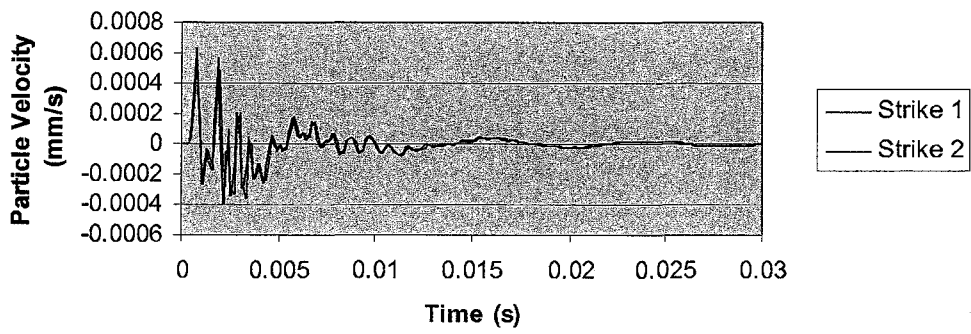
Column 3: 3 % cement, 79 % solids  
Curing age: 28 days

*Waveforms Recorded for Column 3 After 28 Days Curing Time*

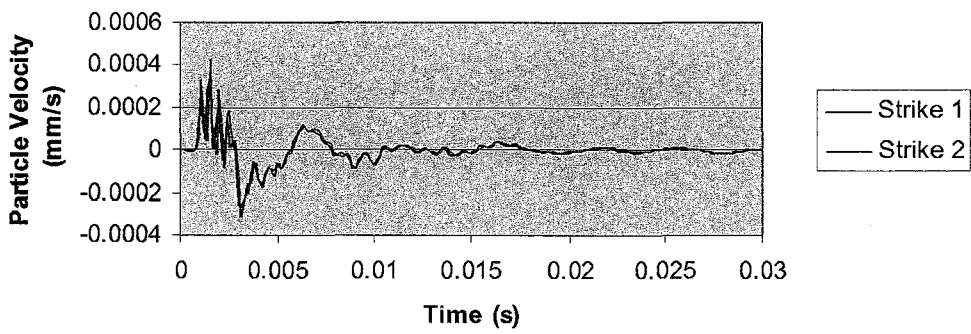
0.5 m from Hammer Strike



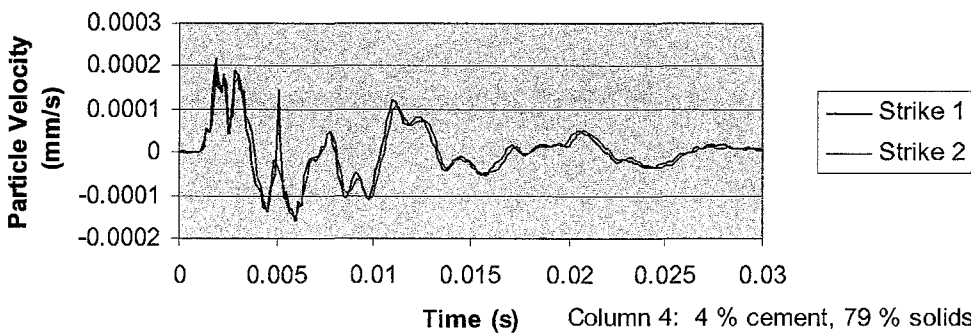
1.0 m from Hammer Strike



1.5 m from Hammer Strike



2.0 m from Hammer Strike

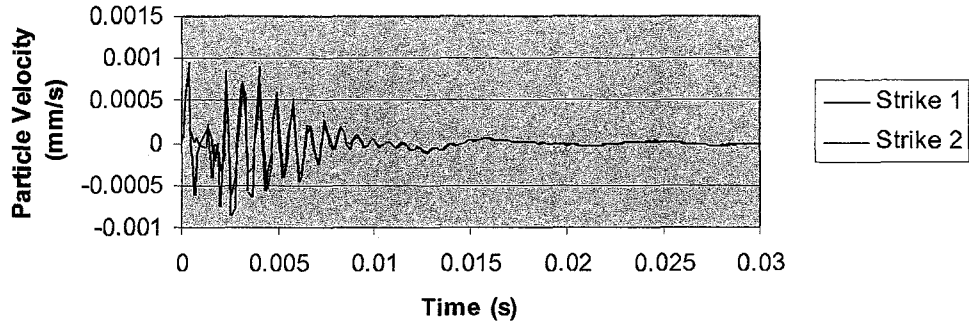


Column 4: 4 % cement, 79 % solids  
Curing age: 7 days

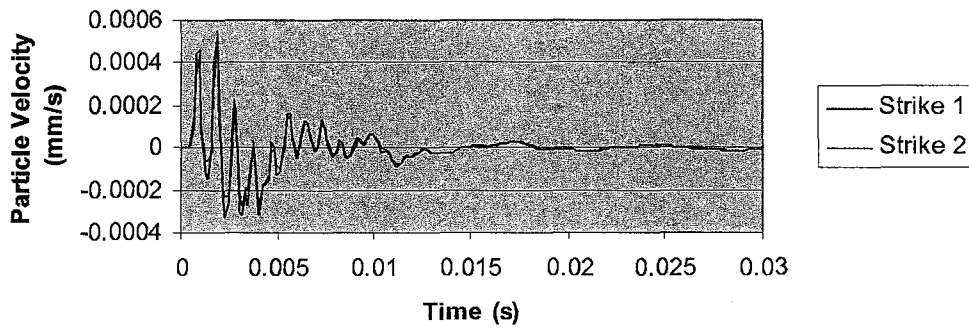
*Waveforms Recorded for Column 4 After 7 Days Curing Time*



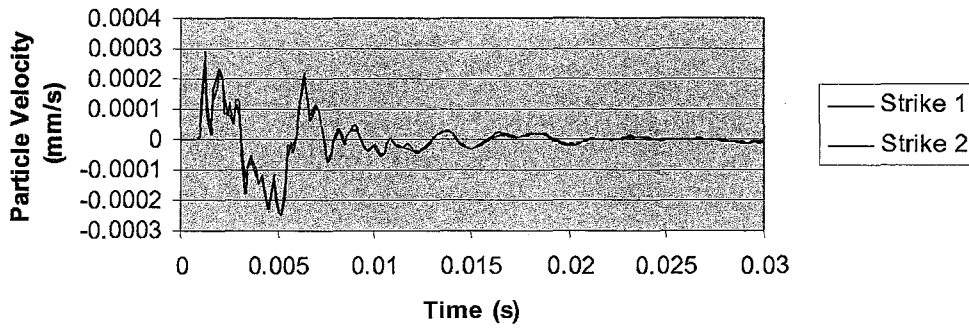
0.5 m from Hammer Strike



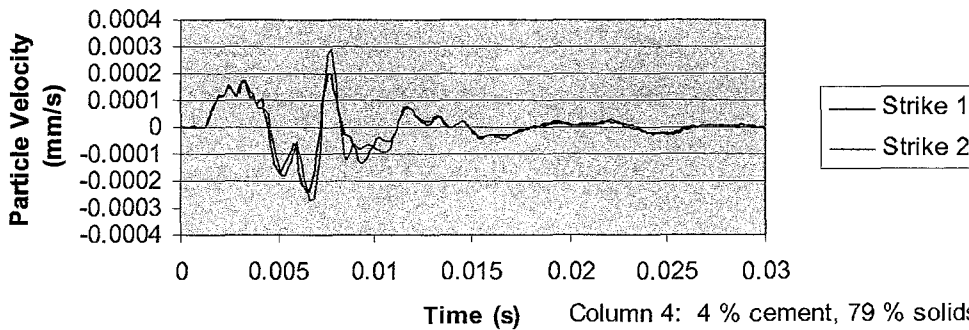
1.0 m from Hammer Strike



1.5 m from Hammer Strike



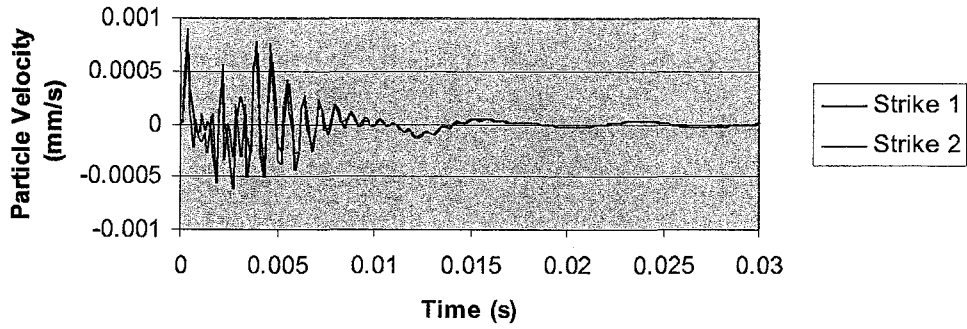
2.0 m from Hammer Strike



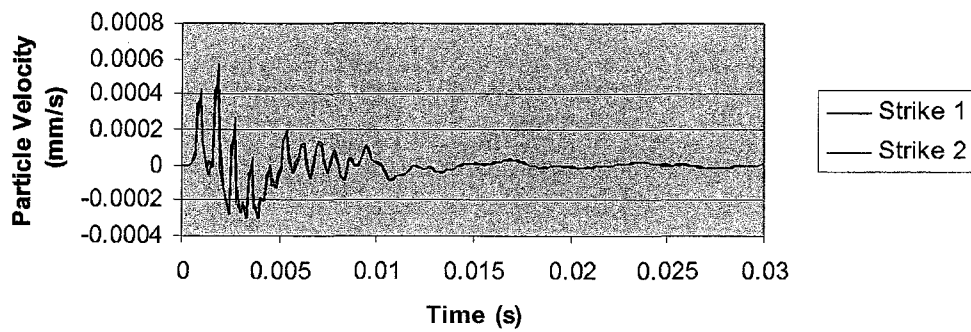
Column 4: 4 % cement, 79 % solids  
Curing age: 14 days

*Waveforms Recorded for Column 4 After 14 Days Curing Time*

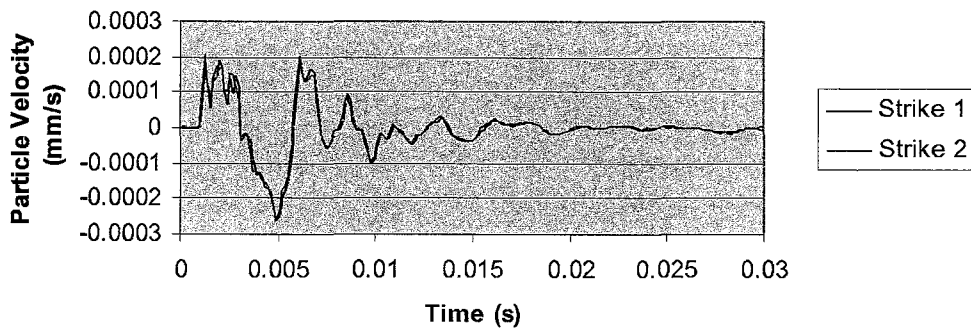
0.5 m from Hammer Strike



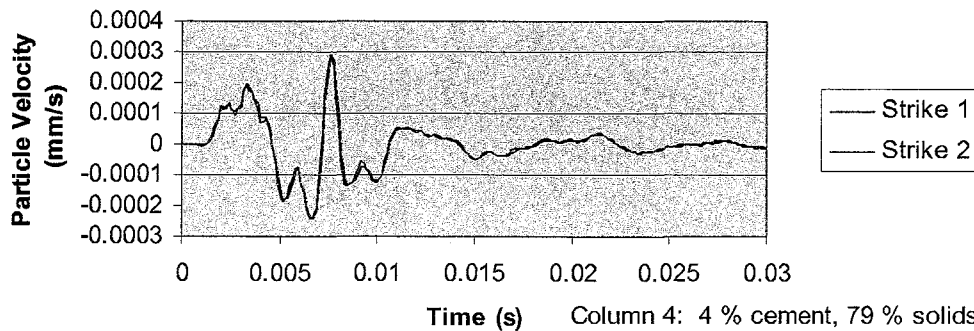
1.0 m from Hammer Strike



1.5 m from Hammer Strike



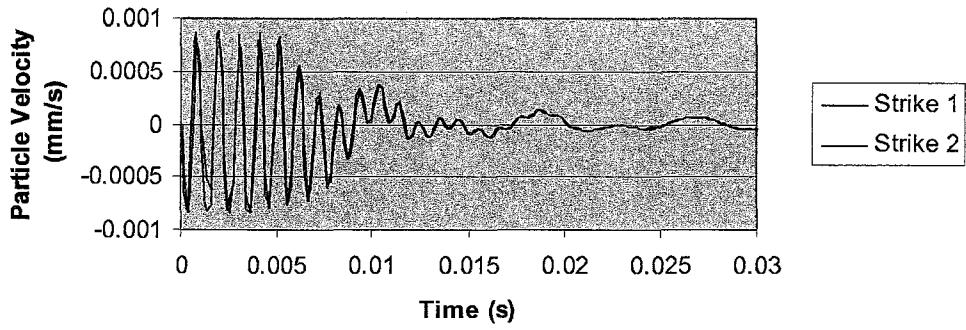
2.0 m from Hammer Strike



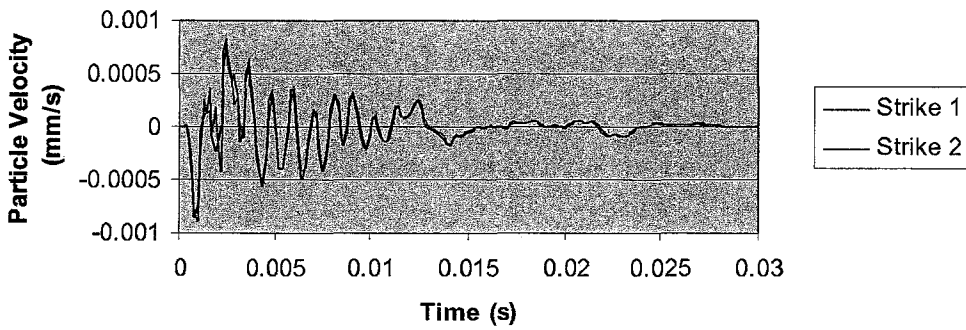
Column 4: 4 % cement, 79 % solids  
Curing age: 28 days

*Waveforms Recorded for Column 4 After 28 Days Curing Time*

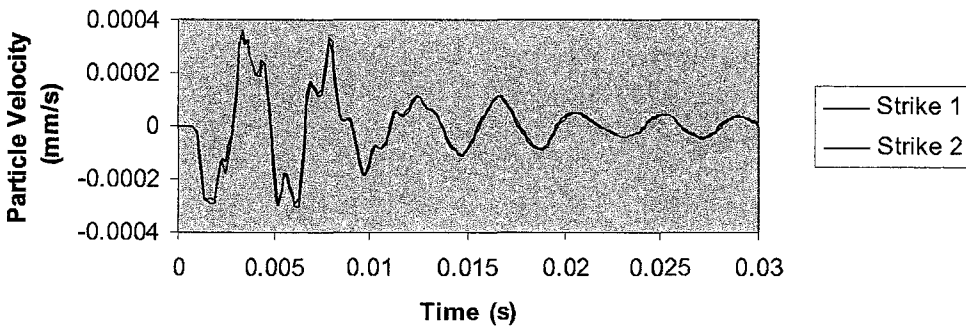
0.5 m from Hammer Strike



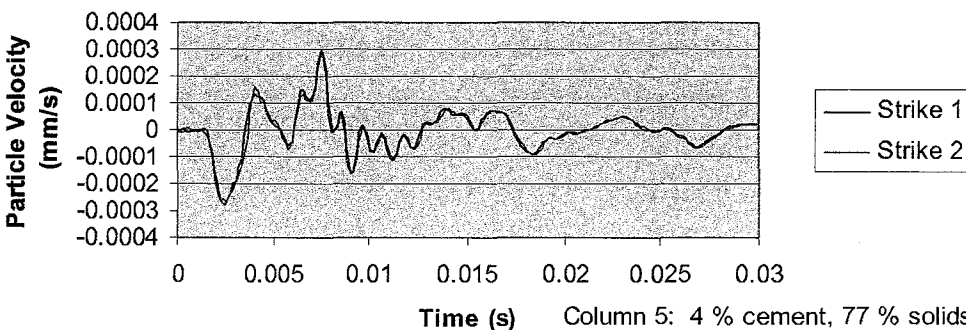
1.0 m from Hammer Strike



1.5 m from Hammer Strike



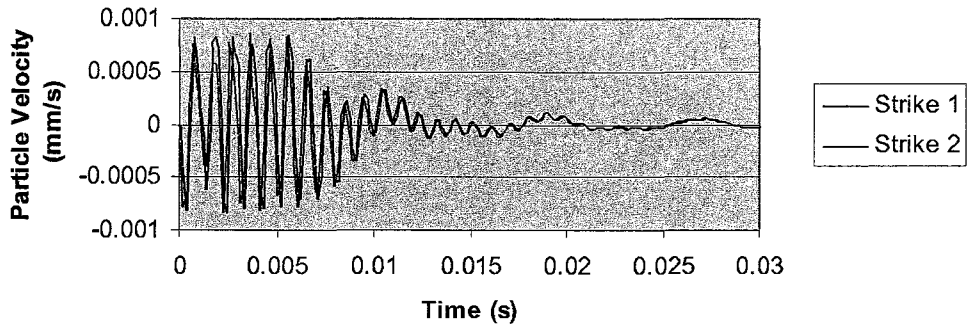
2.0 m from Hammer Strike



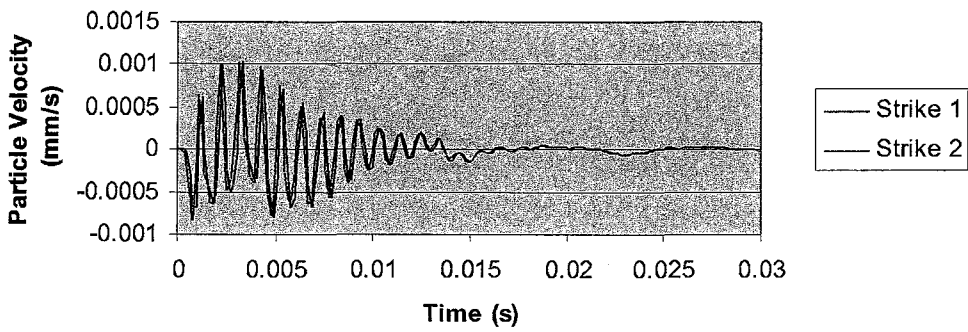
Column 5: 4 % cement, 77 % solids  
Curing age: 7 days

*Waveforms Recorded for Column 5 After 7 Days Curing Time*

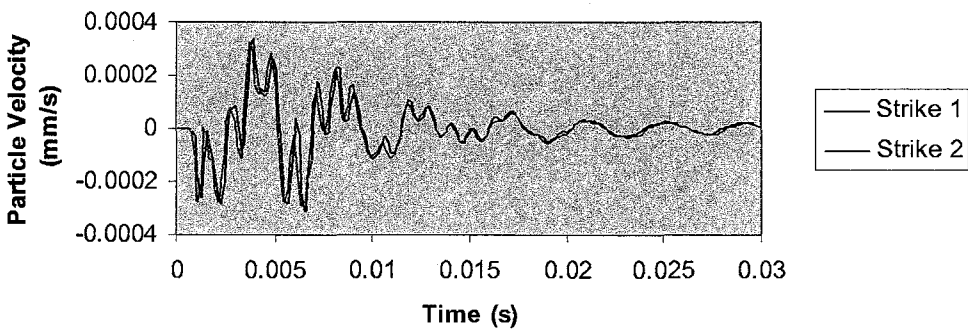
0.5 m from Hammer Strike



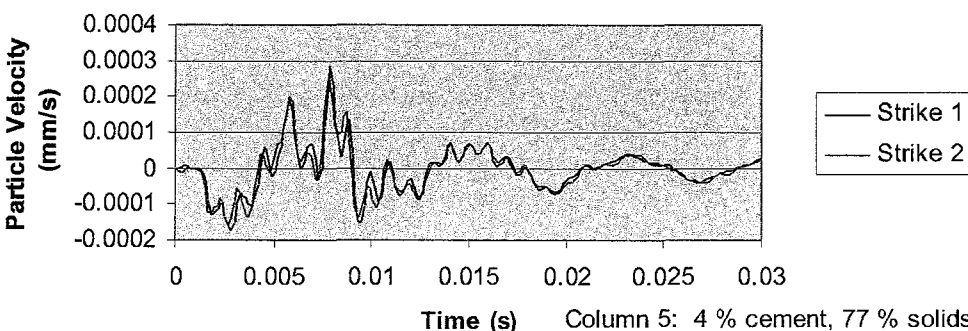
1.0 m from Hammer Strike



1.5 m from Hammer Strike



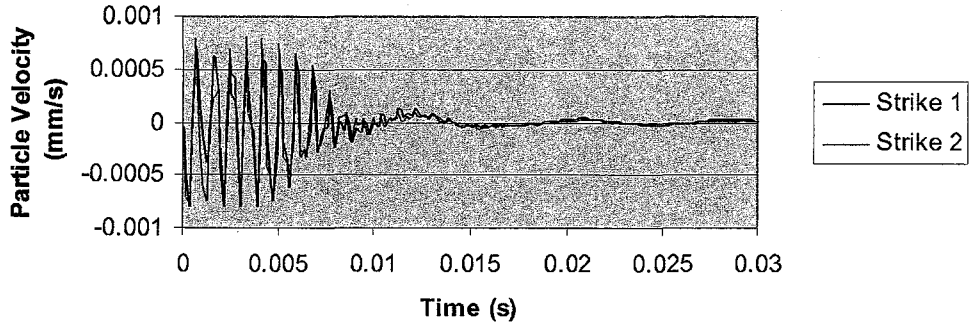
2.0 m from Hammer Strike



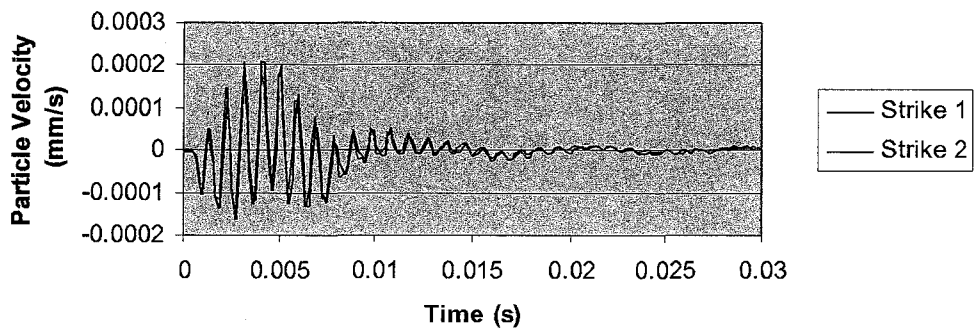
Column 5: 4 % cement, 77 % solids  
Curing age: 2 weeks

*Waveforms Recorded for Column 5 After 14 Days Curing Time*

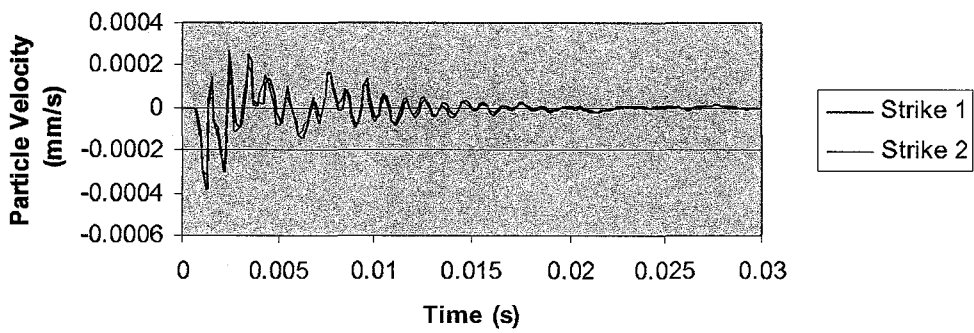
0.5 m from Hammer Strike



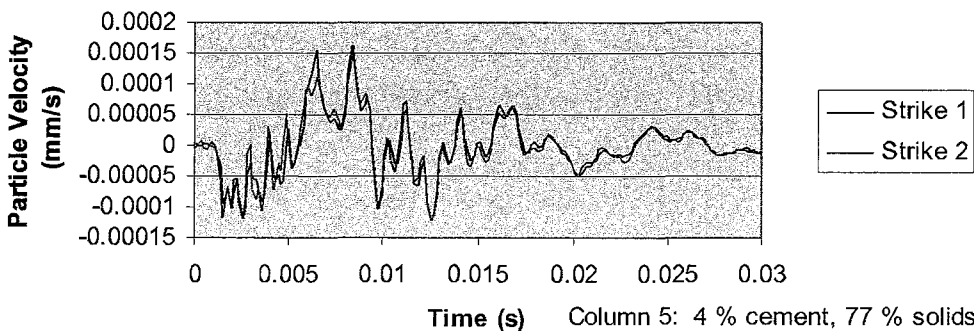
1.0 m from Hammer Strike



1.5 m from Hammer Strike



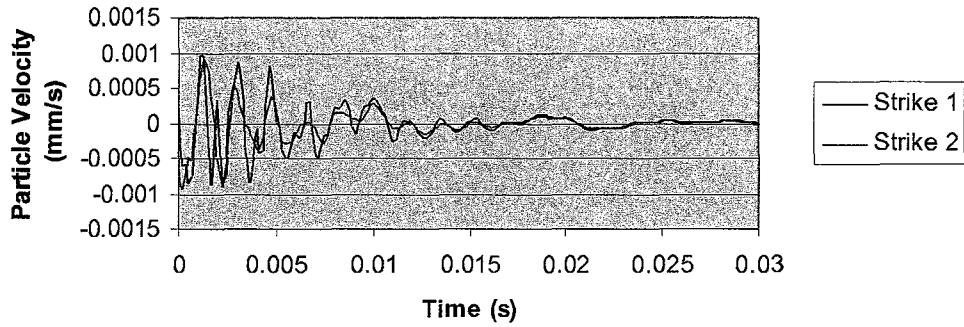
2.0 m from Hammer Strike



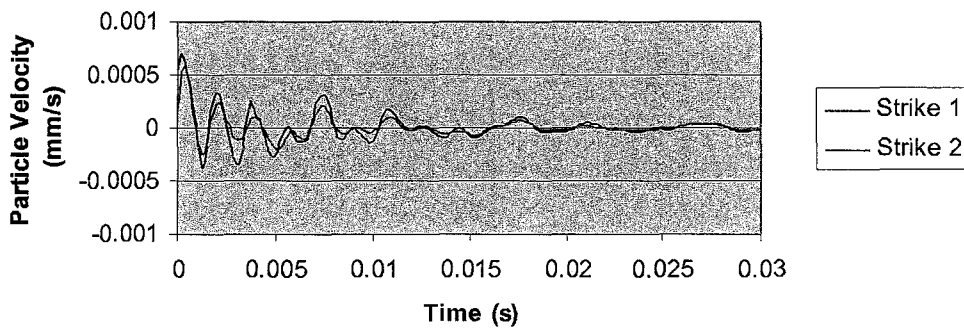
Column 5: 4 % cement, 77 % solids  
Curing age: 28 days

*Waveforms Recorded for Column 5 After 28 Days Curing Time*

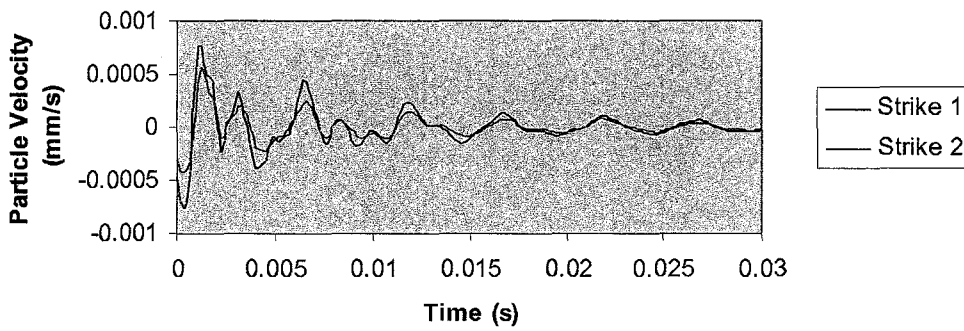
0.5 m from Hammer Strike



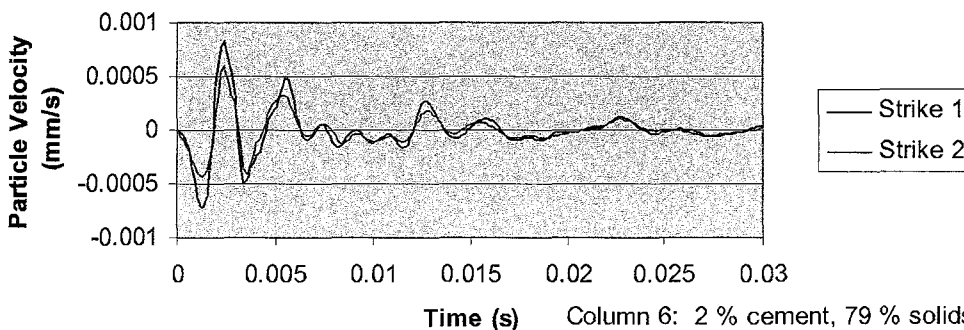
1.0 m from Hammer Strike



1.5 m from Hammer Strike



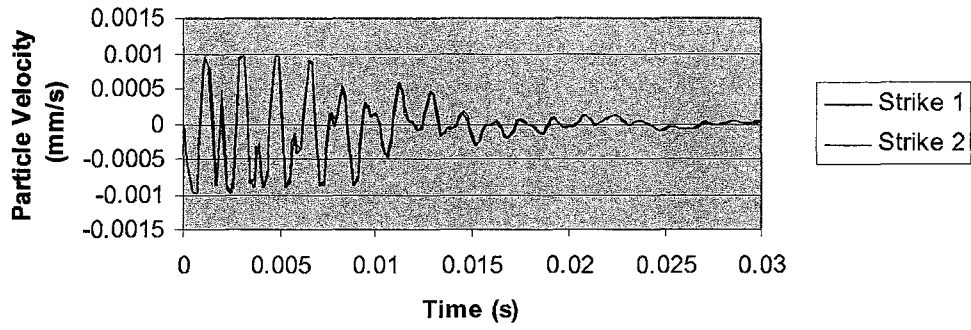
2.0 m from Hammer Strike



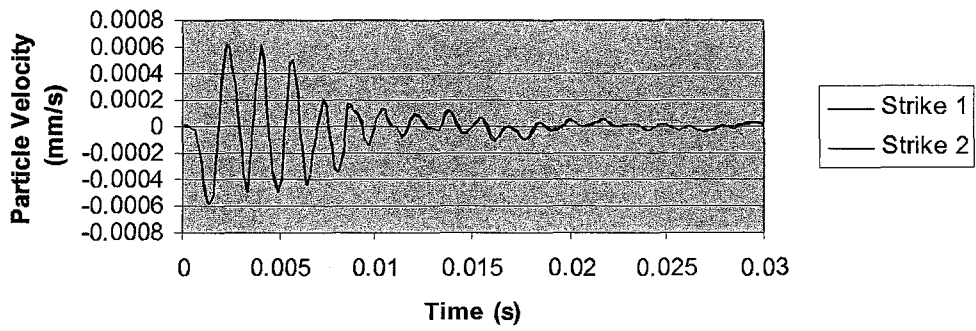
Column 6: 2 % cement, 79 % solids  
Curing age: 7 days

*Waveforms Recorded for Column 6 After 7 Days Curing Time*

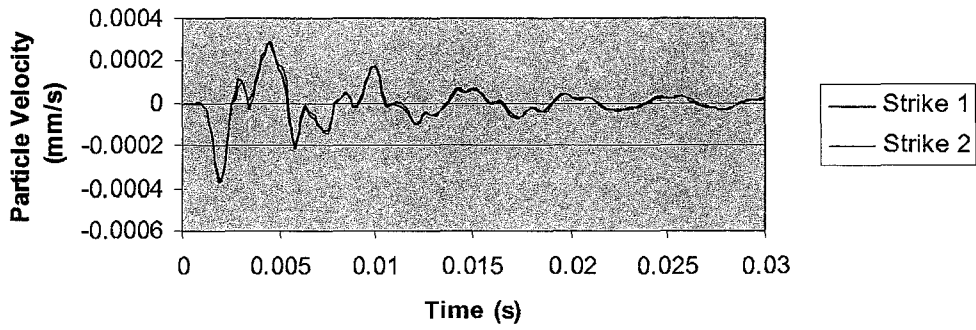
0.5 m from Hammer Strike



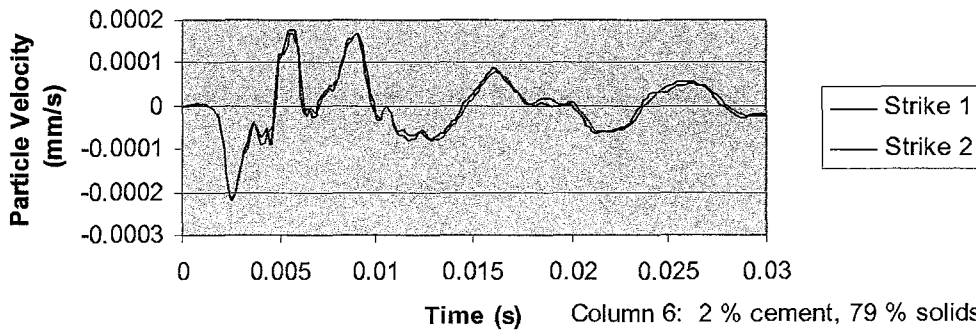
1.0 m from Hammer Strike



1.5 m from Hammer Strike



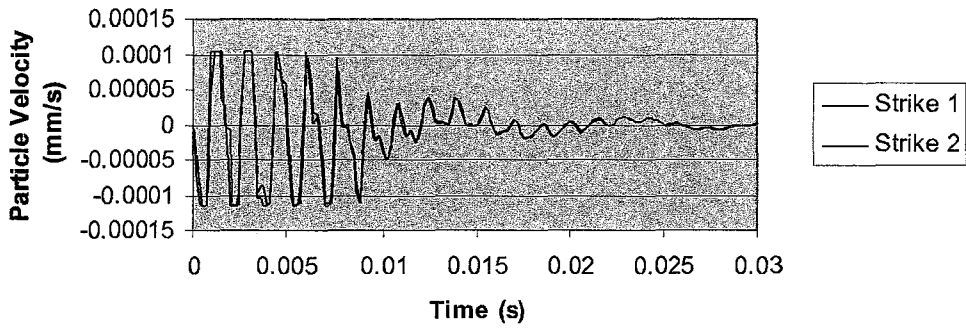
2.0 m from Hammer Strike



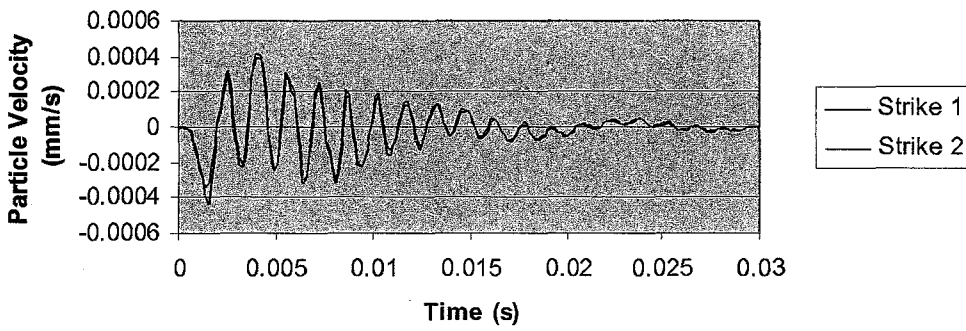
Column 6: 2 % cement, 79 % solids  
Curing age: 14 days

*Waveforms Recorded for Column 6 After 14 Days Curing Time*

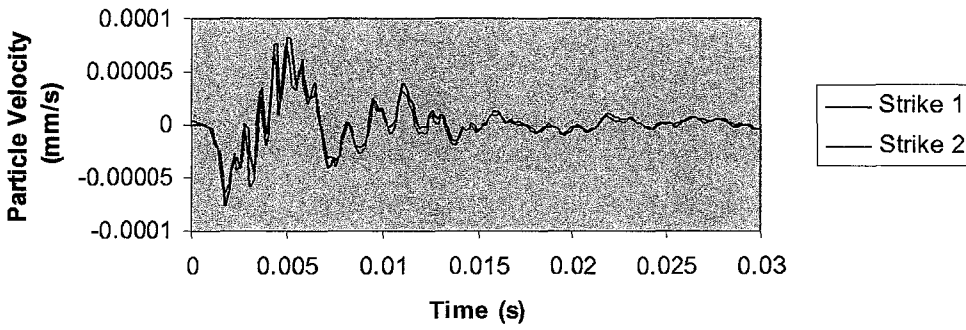
0.5 m from Hammer Strike



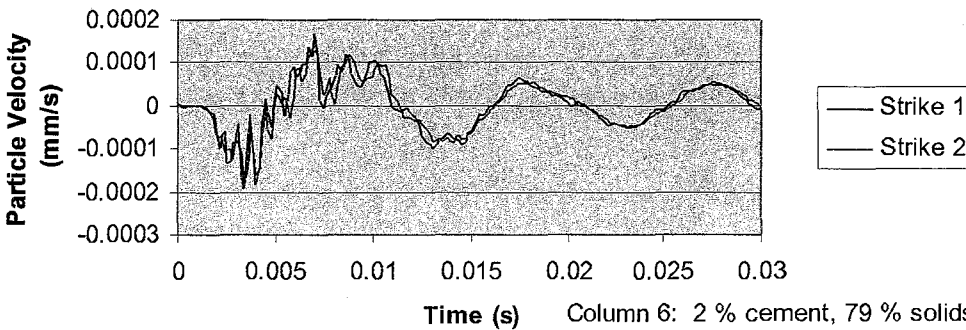
1.0 m from Hammer Strike



1.5 m from Hammer Strike



2.0 m from Hammer Strike



Column 6: 2 % cement, 79 % solids  
Curing age: 28 days

*Waveforms Recorded for Column 6 After 28 Days Curing Time*



**Appendix F – Electronic Copy of Finite Element Model Input  
Files**

The attached disc contains the following input files:

<b>File Name</b>	<b>Stage</b>	<b>Description</b>
stage1_764	Stage 1	Single column of explosive in paste fill. Paste fill mix of 76 % solids and 4 % cement
stage2kBL	Stage 2	Single column of explosive in rock. Broadlands rock type
stage3s1	Stage 3, Scenario 1	Single column of explosive in rock adjacent to the centerline of an adjacent paste fill stope. Blast hole located 2.5 m from paste fill
stage3s2	Stage 3, Scenario 2	Single column of explosive in rock offset from the centerline of an adjacent paste fill stope. Blast hole located 2.5 m from paste fill, offset 2.5 m.
st3s3bp1	Stage 3, Scenario 3	Multiple columns of explosive in rock adjacent to a paste fill stope. Blast holes located 2.5 m from paste fill. All blast holes detonated simultaneously.
st3s3bp2	Stage 3, Scenario 3	Multiple columns of explosive in rock adjacent to a paste fill stope. Blast holes located 2.5 m from paste fill. Detonation pattern 2.
st3s3bp3	Stage 3, Scenario 3	Multiple columns of explosive in rock adjacent to a paste fill stope. Blast holes located 2.5 m from paste fill. Detonation pattern 3.